
Abstract

Uncontrolled segregation in particulate mixtures has long been considered as an annoying, and costly, feature encountered in many materials handling operations and although the onset is not clear, many believe it to be driven by the differences in particulate physical properties. An increasing number of usefully scaled laboratory and computer simulation investigations are being carried, particularly by the physics community, to help our understanding of this phenomenon. Physicists at the University of Nottingham have identified that through careful control of frequency and acceleration during vertical vibration, different types of particles can be positioned and/or segregated in a small rectangular cell. An extension of this work resulted in the design of a new small scale batch separator capable of recovering at least one separated particle layer in a different chamber.

This work has explored the scale up of the small particle separator to operate in a semi-continuous mode. Since complete experimental know how of particle segregation phenomena is still deficient an empirical design strategy was used. This scaled up particle separator was driven by a pneumatically powered vertical vibration bench in which dry, non-cohesive particulate mixtures of varying densities and sizes ($<1000\mu\text{m}$) were vertically vibrated under different conditions to assess their separation behaviours. Experiments with regular (e.g. glass and bronze) and irregular shaped particle mixtures (e.g. comminuted glass and bronze) showed that lower magnitudes of vertical vibration frequency ($30\pm 10\%$), dimensionless acceleration ($3\pm 10\%$), particle bed heights (20 and 40mm in majority of the investigated cases) and partition gap sizes (5 and 10mm) were important for separation. Finally, the technique was employed to separate various industrially

relevant particle mixtures (shredded printed circuit boards, iridium and aluminium oxide and shredded personal computer wires).

Two-dimensional Discrete Element Modelling (DEM) with interstitial fluid interactions simulated with a maximum of 1000 virtual glass and bronze particles showed some important aspects of particle segregation such as; layered particle separation, high density particles ending on top and bottom of the particle bed, convection currents, particle bed tilting and partitioned particle separation.

The application of Positron Emission Particle Tracking (PEPT) to glass, bronze, ilmenite and sand particles showed distinct trajectory maps in three dimension (X,Y and Z) with varying particle speeds in the vertically vibrated particle mixtures. The low density particles were mostly observed to move in the middle while the high density particles patrolled in the outer periphery of the separation cell. These distinct particle motions suggested that convection currents played an important role in controlling segregation. Furthermore, the application of a smoke blanket visualization technique showed the existence of air convection currents on top of the vertically vibrating particle mixtures.

The experiments on the scaled up semi-continuous particle separator confirmed what was identified previously in that good particle separation could be achieved through careful control of the frequency and acceleration during vertical vibration. This information lays the foundations for a new breed of low cost, dry separator for fine particulate mixtures.

Key Words: Vertical vibration, particle separator, fine particle mixtures, dry separation, PEPT, DEM, smoke visualizations.

Statement of Authentication

I certify that the work presented in this thesis is, to the best of my knowledge and belief, original and my own work except as acknowledged in the thesis. I hereby declare that I have not submitted this material, either in whole or part, for a degree at this or any other institution.

Acknowledgements

First and foremost I owe my deepest gratitude to my Ph.D. supervisor, Prof. Nick J. Miles, who has always supported me throughout my research with his wise advice, penetrating criticism, experience, enthusiasm, inspiration, patience and knowledge which has been invaluable to me from the initial to the final levels whilst allowing me the room to work in my own way. Without his encouragement and effort this subject understanding, research and thesis would not have been completed. It is a pleasure to work and interact with such a formidable person.

I would like to take this opportunity to thank all those people who spent their time and shared their knowledge for helping me to complete my research and thesis with the best possible results that I regard as so important. The help and support of Dr. Paul Langston, Dr. Nusruth B.M., Dr. Philip Hall, Dr. Yun Chen, Dr. Risa Lui, Helena Webster and all other Colleagues in the Faculty of Engineering, cannot be forgotten.

I wish to thank all academics, staff and the Faculty of Engineering for allowing me the use of facilities and laboratories, which enabled this experimental work to be carried out. Special thanks go to Mr. Tony Gospel, Dave Mee, Christopher Somerfield, David Clift, Sue Richards, Terry Cullinan, Phil Bennett and all laboratory and library staff who were always ready to help.

Special thanks go to the Overseas Research Student Scholarship and The University of Nottingham Award, for their financial support, without which I would not have seen my dreams come true.

I would like to thank the many people who have taught me in the School, College and University. I am especially grateful to my M.Sc research supervisor in Loughborough University, Prof. Chris D.

Rielly, for introducing me to the wonderful world of knowledge by research about half a decade ago.

I am indebted to my many student colleagues who deserve a special mention for providing a stimulating and fun environment in which to learn and grow. I am especially grateful to Mr. Mohammad Ali Bek, Dr. Osama Farid, Abdur Rehman, Dr. Anand, Laura and Aimaro for helping me get through the difficult times, and for all the emotional support, camaraderie, entertainment, and caring they provided.

I wish to thank all my friends in Nottingham who were exceptionally caring for all the time we spent together. Mr. Saqib, Zahid, Adil, Saeed, Wajahat, Shahid, Sajid, Majid, Zeshan, Usman, Dr. Masami Kunata, Dr. Abubakar and Rizwan deserve a special mention. I would also like to say a big thank you to all those who visited me during my time in Nottingham and made me feel less far from my family and friends.

I wish to thank my entire extended family for providing a loving and caring environment to me. My brother and sisters were particularly supportive and my grandmother was a constant source of encouragement. Lastly, and most importantly, I wish to thank my parents, Mr. and Mrs. Abdul Habib. They bore me, raised me, taught me, love me and have been a constant source of emotional and moral support. To them I dedicate this thesis.

Table of Contents

Abstract -----	i
Statement of Authentication -----	iii
Acknowledgements -----	iv
Table of Contents -----	vi
List of Figures -----	xvi
List of Tables -----	xxxii
List of Equations -----	xxxiv
Nomenclature -----	xxxvii

Chapter-1

1 Introduction -----	1
1.1 Particle properties-----	6
1.2 Particle segregation -----	9
1.3 Particle segregation and separation-----	12
1.4 Aim and Objectives -----	17
1.5 Thesis structure -----	18

Chapter-2

2 Particle separation: A review -----	19
2.1 Introduction -----	19
2.2 Particle separation techniques-----	21
2.2.1 Size based physical separation techniques -----	21
2.2.1.1 Hand sorting-----	21
2.2.1.2 Automated sorting -----	22

2.2.1.3	Differential melting based sorting -----	24
2.2.1.4	Screening -----	25
2.2.2	Size and density based physical separation techniques -----	26
2.2.2.1	Air classification -----	26
2.2.2.2	Dry jigging -----	28
2.2.2.3	Elutriation -----	30
2.2.2.4	Ballistic separation -----	30
2.2.2.5	Nail roll separator -----	32
2.2.3	Gravity/density based physical separation techniques -----	33
2.2.3.1	Dense medium separation -----	33
2.2.3.2	Dry heavy medium separation -----	34
2.2.3.3	Cyclone separation -----	35
2.2.3.4	Wet and dry shaking table -----	35
2.2.3.5	Spiral Separation -----	37
2.2.3.6	Centrifugal separation -----	37
2.2.4	Magnetic and electrostatic separation techniques -----	38
2.2.4.1	Magnetic separation -----	38
2.2.4.2	Electrostatic separation -----	39
2.2.5	Eddy current separation -----	40
2.2.6	Froth flotation -----	41
2.3	Particle size and physical separation -----	42

2.4	Vibrated particle mixtures -----	45
2.4.1	Vibrated particle flows -----	45
2.5	Vibrated particle beds -----	49
2.6	Segregation in vibrated particle beds -----	51
2.6.1	Vibration driven size segregation -----	51
2.6.1.1	The rise of coarse particles on vibration -----	52
2.6.2	Vertical vibration driven density segregation -----	60
2.6.3	Vertical vibration induced particle segregation and the surrounding fluid -----	75
2.6.4	Particle bed tilting and distinct convective motions -----	81
2.6.5	Vertical vibration induced separation of fine size particles -----	84
2.7	Concluding remarks -----	91

Chapter-3

3	Materials and methods -----	93
3.1	Introduction -----	93
3.2	Materials -----	96
3.2.1	Rig-1 design -----	96
3.2.2	Rig-2 design -----	100
3.2.3	Separation cell designs -----	103
3.3	Methods -----	106
3.3.1	Preparation of test mixtures -----	106
3.3.1.1	Retsch cutting mill (SM2000/750) -----	107
3.3.1.2	Retsch jaw crusher -----	108
3.3.2	Sampling techniques -----	108
3.3.3	Quantitative means of sample analysis -----	110

3.3.3.1	Sieve analysis -----	110
3.3.3.2	Dense media separation (DMS) and/or sink-float analysis -----	111
3.3.3.3	Density measurement-----	113
3.3.3.4	Inductively Coupled Plasma-Atomic Emission Spectroscopy (ICP-AES) -----	114
3.3.3.4.1	Sample Preparation-----	115
3.3.3.4.2	ICP-AES analysis system -----	117
3.3.3.5	Positron Emission Tomography (PET) -----	119
3.3.3.5.1	: Radioactive labelling of a tracer particle ----	121
3.3.3.5.2	Positron Emission Particle Tracking (PEPT) setup - -----	123
3.3.4	Qualitative means of analysis -----	124
3.3.4.1	Visual estimation of particle separation -----	124
3.3.4.2	Digital imaging technique-----	125
3.3.4.3	Scanning Electron Microscope (SEM) imaging ----	125
3.4	Concluding remarks-----	127

Chapter-4

4	Discrete element modelling of the vertically vibrated particle bed -----	128
4.1	Introduction -----	128
4.2	Background to DEM simulations-----	130

4.2.1	Soft particle based DEM simulations -----	133
4.3	The applied DEM model-----	136
4.3.1	Construction of a discrete geometry -----	137
4.3.2	Particle contact models-----	140
4.3.3	Particle contact forces -----	142
4.3.3.1	Normal elastic force -----	145
4.3.3.2	Normal damping force -----	145
4.3.3.3	Friction force -----	146
4.3.3.4	Tangential damping force-----	147
4.3.3.5	Particle-wall contacts -----	148
4.3.4	DEM simulation parameters-----	148
4.3.5	Modelling of external forces in DEM -----	149
4.3.5.1	Gravitational force -----	149
4.3.5.2	Vibration force-----	149
4.3.6	Air drag calculation -----	150
4.3.7	Integration of Particle motion in DEM -----	152
4.3.7.1	Translational particle motion -----	153
4.3.7.2	Rotational particle motion -----	154
4.3.8	DEM input parameters-----	155
4.3.8.1	Group-1 input variables-----	155
4.3.8.2	Group-2 input variables-----	155
4.3.8.3	Group-3 output variables -----	155
4.3.9	The DEM implementation code -----	156

4.3.9.1	DEM validation tests -----	157
4.3.10	DEM simulation setup-----	158
4.4	DEM simulation of the vertically vibrating particle mixtures -- -----	160
4.4.1	Preliminary density segregation simulations-----	160
4.4.2	DEM simulation of density segregation in the glass and bronze particle mixture -----	163
4.4.2.1	DEM simulation of density segregation in the glass and bronzer particle mixture-A -----	164
4.4.2.2	DEM simulation of density segregation in the glass and bronzer particle mixture-B -----	171
4.4.2.3	DEM simulation of density segregation in glass and bronzer particle mixture-C-----	173
4.4.2.4	DEM simulation of density segregation in the partitioned separation cell -----	175
4.5	Concluding remarks-----	178

Chapter-5

5	Separation of particle mixtures in the scaled up vertical vibration separator-----	180
5.1	Introduction -----	180
5.2	The scaled up design development of a new vertical vibration induced particle separator -----	182
5.2.1	The development of scaled up vertical vibration bench-----	183
5.2.2	The development of scaled up separation cell design -----	184
5.2.3	Particle segregation in the L-type separation cell geometry -----	192
5.2.4	Particle segregation in the T-type separation cell geometry -----	201

5.2.4.1	Separation of a glass and bronze particle mixture	201
5.2.4.2	Separation of shredded electrical cable particles	-204
5.3	Detailed particle segregation assessment in the T-type separation cell	-----211
5.3.1	Segregation of the glass and bronze particle mixtures	----- 211
5.3.1.1	The effect of vertical vibration frequency on particle separation	-----213
5.3.1.2	The effect of partition gap size on particle separation	-----218
5.3.1.3	The effect of varying particle bed height on vertical vibration induced particle separation	-----219
5.3.1.3.1	Separation at 20 and 40 mm bed heights	-----222
5.3.1.3.2	Separation at 60 mm bed height	-----225
5.3.1.3.3	Separation at 80 and 100 mm bed heights	---226
5.3.2	Separation of the shredded glass and bronze particle mixtures	---- 226
5.3.3	Separation of the sand and bronze particle mixtures	----- 230
5.3.4	Interstitial fluid visualisation via smoke blanket motions	----- 233
5.4	Concluding remarks	-----241

Chapter-6

6	Tracking particle dynamics in the vibration separator	-----242
6.1	Introduction	-----242
6.2	Particle tracking: A review	-----244
6.3	Positron Emission Particle Tracking (PEPT) experiments	--248

6.3.1	Glass and bronze particle tracking-----	250
6.3.1.1	Bronze tracer in a 20 mm width separation cell, C-1 - -----	253
6.3.1.2	Glass tracer in a 20 mm width separation cell, C-1--- -----	261
6.3.1.3	Bronze tracer in a 40 mm width separation cell, C-2 - -----	266
6.3.1.4	Glass tracer in a 40 mm width separation cell, C-2--- -----	271
6.3.2	Glass (53-150 μ m) and glass (300-600 μ m) particle tracking -----	276
6.3.2.1	PEPT of the large glass tracer particle in a 20 mm width separation cell, C-1-----	278
6.3.2.2	PEPT of the small glass tracer particle in a 20 mm width separation cell, C-1-----	282
6.3.2.3	PEPT of the large glass tracer particle in a 40 mm width separation cell, C-2-----	285
6.3.2.4	PEPT of the small glass tracer particle in a 40 mm width separation cell, C-2-----	288
6.3.3	Sand and ilmenite particle tracking-----	291
6.3.3.1	PEPT of the ilmenite tracer particle in a 20 mm width separation cell, C-1 -----	293
6.3.3.2	PEPT of the sand tracer particle in a 20 mm width separation cell, C-1 -----	296
6.3.3.3	PEPT of the ilmenite tracer particle in a 40 mm width separation cell, C-2 -----	299

6.3.3.4	PEPT of the sand tracer particle in a 40 mm width separation cell, C-2 -----	302
6.4	Concluding remarks-----	305

Chapter-7

7	Dry separation of solid waste mixtures -----	306
7.1	Introduction -----	306
7.2	Solid waste WEEE mixtures -----	307
7.3	Current practices to separate PCB -----	317
7.3.1	Application-1: Vibration induced separation of WEEE mixtures-----	323
7.3.1.1	WEEE sample-1: waste electrical cables -----	323
7.3.1.1.1	Sample preparation-----	324
7.3.1.1.2	Initial experiments on the separation of waste electrical cables -----	327
7.3.1.1.3	Separation of -1.5 mm Retsch mill cut electrical cables in separation cell C-1 & 2 -----	331
7.3.1.1.4	Separation of -0.75 mm Retsch mill cut electrical cables in separation cell C-1 & 2. -----	332
7.3.1.2	WEEE sample-2: printed circuit boards (PCBs) ---	337
7.3.1.2.1	Sample preparation-----	339
7.3.2	Application-2: Dry separation of iridium and aluminium oxide mixtures -----	352
7.3.2.1	Introduction -----	352

7.3.2.1.1	Separation of iridium/aluminium oxide sample-1 -	354
7.3.2.1.2	Separation of iridium/aluminium oxide sample-2 -	357
7.3.2.1.3	Separation of iridium/aluminium oxide sample-3 -	359
7.3.2.1.4	Separation of iridium/aluminium oxide sample-4 -	361
7.4	Concluding remarks-----	363

Chapter-8

8	Conclusions and future work-----	364
8.1	Conclusions-----	364
8.2	New scientific contributions -----	371
8.3	Future work -----	372

References -----	373
-------------------------	-----

Appendix-A (Figures)-----	I
----------------------------------	---

Appendix-B (Calibration graphs)-----	XIII
---	------

Appendix-C (PCB metal concentration graph)-----	XV
--	----

Appendix-D (PEPT and Smoke blanket videos)-----	XVII
--	------

List of Figures

- Figure 1.1: A change in particle bed behaviour with increasing the magnitude of vertical vibration acceleration in a rectangular geometry box (Adapted from Tai and Hsiau, 2009).----- 2
- Figure 1.2: The important physical properties of particles at various description levels and/or size length scales (Jaeger, 1997). ----- 6
- Figure 1.3: Sand grains originating from different global locations and as seen under a microscope (Adapted from Modderman collections, 2009). ----- 7
- Figure 1.4: Time averaged progression of particle segregation in a vertically vibrated particle bed. The intruder particles can rise in the bed against gravity to exhibit a Brazil Nut Effect, BNE (a) or can sink to show a Reverse Brazil Nut Effect, RBNE (b) (Adapted from Kurdrolli, 2004). ----- 9
- Figure 1.5:- Segregation in a stony desert, Panawonica (Adapted from David and Janet’s Collection).----- 10
- Figure 1.6: The catalogue of segregation investigations carried out to date.----- 14
- Figure 2.1: Side view of an automated colour based sorting system (Adapted from Steinert systems, 2009). ----- 23
- Figure 2.2: Sorting distinct plastics by melting point differences (Adapted from Delgado and Stenmark, 2005). ----- 24
- Figure 2.3: Various screen separation ranges (Adapted from Perry and Green 1999).----- 25
- Figure 2.4: Air Separator types:- (a) gravitational, (b) gravitational-cross-flow or expansion chamber, (c) centrifugal-

counter-flow, (d) centrifugal-cross-flow (Adapted from Shapiro & Galperin, 2004). ----- 27

Figure 2.5: Principle of a continuous pneumatic jigging (Adapted from De Jong *et al.*, 2005). ----- 28

Figure 2.6: Principle of ballistic separator (Adapted from Density Separation, 2009). ----- 31

Figure 2.7: Nail-roll separator (Adapted from Tohka and Lehto, 2005). ----- 32

Figure 2.8: Dry sand (as a heavy medium) fluidised bed separation principle (Adapted from De Jong *et al.*, 2005). ----- 34

Figure 2.9: Dry shaking table (Adapted from Density Separation, 2009). ----- 36

Figure 2.10: Knelson[®] Concentrator ring (Adapted from Knelson, 2009). ----- 38

Figure 2.11: Electrostatic particle separation (Adapted from Perry and Green, 1999). ----- 39

Figure 2.12: The rise of coarse particle on vibration and convection trends. "a" shows a single global convection current, "b & c" binary convection rolls and "d & e" multiple convection rolls in the vibrated particle bed. ----- 52

Figure 2.13: Rise time vs particle diameter to density ratio in a fixed size ratio binary particle mixture (Adapted from Liffman *et al.*, 2001). ----- 61

Figure 2.14: Solid-solid extraction (Adapted from Akiyama *et al.*, 2000). ----- 61

Figure 2.15: Particle bed behaviour under vertical vibration of increasing accelerations (a-c) (Adapted from Akiyama *et al.*, 2000).

----- 63

Figure 2.16: Apparatus used by Klein *et al.*, 2006. ----- 66

Figure 2.17: Particle bed behaviours under vertical vibration. P_{N_2} , represents the nitrogen gas pressure in the vibrating cell (Klein *et al.*, 2006).----- 67

Figure 2.18: Vertical vibration setup, where, (a) is the particle segregation box, (b) accelerometers, (c) double transducer assembly and (d) is the connecting frame.----- 69

Figure 2.19: Visualized behaviour of mixture B1 in air, as a function of f & Γ showing the onset of bronze on top (α), sandwich separation (β), the transition boundary between the two (γ), onset of slow (δ) and rapid (ϵ) asymmetric inversion oscillation. Also (A) & (C) represents bronze on top, particle throwing and interface thrashing (A), tilt formation (B), sandwich formation (D), Oscillation between bronze on top and sandwich configurations (E) and continuous asymmetric oscillations (F) and the area of continuous symmetric oscillations (G) (Adapted from Burtally *et al.*, 2003). ----- 71

Figure 2.20: An initially well mixed bed of 90-125 μ m glass and bronze spheres separating into the bronze on top regime when vibrated at $f = 40\text{Hz}$, $\Gamma = 3.0$, in an 80mm high x 80mm wide x 10mm thick, glass lined cell with bronze at 25% and glass 75% by volume (B1). (N.B. S = seconds) (Adapted from Burtally *et al.*, 2003). ----- 72

Figure 2.21: The behaviour of 50:50 volume percentage mixture of 300-355 μ m glass-bronze particles submerged in water. (A) Represent a tilted bronze on top configuration, (B) tilted bronze on top via tilted sandwich configuration, (C) symmetric bronze on top

via symmetric sandwich configuration, (D) represents the incomplete separation region and the line " α " represents the f value where cluster formation was seen in two minutes of vertical vibration. The light and dark gray colours in (a), (b) and (c) represents the low and high density materials (Adapted from Leaper *et al.*, 2005).----- 79

Figure 2.22: Particle convection currents in glass and bronze rich regions in the presence of water at different frequency and acceleration values (a, b & c) as reported by Leaper *et al.*, (2005). ----- 82

Figure 2.23: Partition cell separator (Adapted from Mohabuth, 2007).----- 85

Figure 2.24: Visualized f and α phase diagrams for 75% (volume) glass and 25% (volume) bronze (90-125 μ m) mixture at various bed heights. Where, A, B & C represent the good, poor and no separation zones (Adapted from Mohabuth, 2007). ----- 87

Figure 2.25: Separation behaviour of printed circuit board (PCB) fractions (150-212 μ m) (Adapted from Mohabuth, 2007). ----- 89

Figure 2.26: Scaled up vibration driven dry based particle separator (Adapted from Mohabuth, 2007).----- 90

Figure 3.1: Rig-1, (a) separation cell and (b) pneumatic vibrator assembly. ----- 97

Figure 3.2: Air supply and control to the pneumatic vibrator. ----- 99

Figure 3.3: Rig-2. Scaled up vertical vibration separator. -----101

Figure 3.4: L-type particle separation cell. -----103

Figure 3.5: T-type particle separation cell. -----104

Figure 3.6: Final separation cell designs used in vibration induced particle separation experiments.-----	105
Figure 3.7: Cutting mill (Adapted from Retsch, 2009). -----	107
Figure 3.8: (a) He pycnometer, Accpvc 1330 model, (b) working principle. -----	113
Figure 3.9: Positron Emission Particle Tracking (PEPT) setup.-----	120
Figure 3.10: Gamma (γ) photons emission mechanism and its scanning by PEPT. -----	122
Figure 3.11: Scanning Electron Microscope (SEM), Quanta 600 (FEI company). -----	126
Figure 4.1: The coordinate system used in the DEM simulation. -	134
Figure 4.2: Geometric constructs/grids which are used to speed up the detection of the interacting particle pairs (Adapted from Fazekas, 2007).-----	138
Figure 4.3: Schematic diagram of contact forces that are modelled by using a soft sphere based linear spring-dashpot model (Fazekas, 2007; Asmar <i>et al.</i> , 2002; Wassgren, 1997). -----	141
Figure 4.4: The DEM simulation flowchart. -----	156
Figure 4.5: DEM simulation setup. -----	158
Figure 4.6: DEM simulation of segregation progression in the 70:30% high and low density particle mixture (Table 4.2). -----	161
Figure 4.7: DEM simulation of time averaged (from a to l, ~ 10 second) segregation progression in an 80:20 % number glass and bronze particle mixture-A (Table 4.3). -----	166

Figure 4.8: DEM simulation of time averaged (from a to l, ~7.8 second) segregation progression in an 80:20 % number glass and bronze particle mixture-A (Table 4.3). -----	170
Figure 4.9: DEM simulation of time averaged (from a to f, ~5.0 second) segregation progression in a 70:30 % number glass and bronze particle mixture-B (Table 4.3). -----	172
Figure 4.10: DEM simulation of particle mixture-C (Table 4.3). --	174
Figure 4.11: DEM simulated segregation in a glass (40 % by number) and bronze (60 % by number) working particle mixture. -----	176
Figure 5.1: Design of a semi-continuous vertical vibration induced particle separation cell with an open end in one direction. -----	184
Figure 5.2: SEM images of the spherical glass and bronze working particles. -----	186
Figure 5.3: Particle size characterisation of glass and bronze particles used in the preliminary investigations. -----	186
Figure 5.4: Grade and recovery of the separated bronze particles in the first scaled up separation cell geometry. -----	190
Figure 5.5: % Grade of the separated bronze particles in product-1 in relation to the average particle separation time. -----	191
Figure 5.6: Particle size distribution of the glass particles (mixture A and B combined) used in the size segregation experiments. -----	193
Figure 5.7: Size segregation behaviour of mixture-A in the L-type particle separation cell.-----	196
Figure 5.8: Size segregation behaviour of mixture-B in the L-type particle separation cell.-----	198

Figure 5.9: Separation grades of big size particles in product-1 in relation to an average particle separation time. -----199

Figure 5.10: Grades and recoveries of the big size particles in mixture A and B at a particle bed height of 60 mm in the L-type particle separator. -----200

Figure 5.11: Density segregation behaviour of a finely sized 80:20%wt glass and bronze particle mixture at a particle bed height of 100 mm in the 40 mm width T-type separation cell. -----202

Figure 5.12: SEM image of the shredded electrical cable particles. -----205

Figure 5.13: Particle size characterisation of the shredded electrical cable particles used in the T-type cell. -----206

Figure 5.14: Particle separation behaviour of the shredded electrical cable particles in a 20 mm width T-type separation cell. -----207

Figure 5.15: Grades of the separated shredded electrical cable particles in a 20 mm width T-type separation cell. -----209

Figure 5.16: Grades of separated copper in product-1 at different intervals of an average particle separation time. -----209

Figure 5.17: Particle throwing from the tilted bed surface at a vertical vibration frequency value of $40 \pm 10\%$ Hz in a 20 mm width separation cell. Initial particle bed height of 60 mm, glass and bronze concentration of 70:30%wt (mixture-C) and a partition gap size of ~ 5 mm were used in this investigation. -----215

Figure 5.18: Inverted tilt formation at a vertical vibration frequency value of 35 ± 10 Hz. The image shown here shows a glass and bronze (70:30%wt) working mixture-C with an initial particle bed

height of 40 mm in separation cell C-1 and with a partition gap size of ~5 mm. -----216

Figure 5.19: Bronze separation efficiency vs particle bed height in separation cells C-1 and C-2. A partition gap size of 5 mm and the vertical vibration frequency and dimensionless acceleration magnitudes of $30 \pm 10\%$ Hz and $3 \pm 10\%$ were used in this investigation. -----221

Figure 5.20: Bronze separation efficiency vs particle bed height in separation cells C-1 and C-2. A partition gap size of 10 mm and the vertical vibration frequency and dimensionless acceleration magnitudes of $30 \pm 10\%$ Hz and $3 \pm 10\%$ were used in this investigation. -----221

Figure 5.21: The size characterisation of the shredded glass and bronze particles. -----227

Figure 5.22: Scanning Electron Microscope (SEM) images of the shredded glass and bronze particles. -----228

Figure 5.23: Bronze separation efficiency vs particle bed height in separation cells C-1 and C-2. A partition gap size of ~5 mm and the vertical vibration frequency and dimensionless acceleration magnitudes of $30 \pm 10\%$ Hz and $3 \pm 10\%$ were used in this investigation. -----229

Figure 5.24: The size characterisation of the white beach sand and bronze particles. -----231

Figure 5.25: SEM image of the working sand and bronze particles. -----231

Figure 5.26: Bronze separation efficiency vs particle bed height in separation cells C-1 and C-2. A partition gap size of 5 mm and the vertical vibration frequency and dimensionless acceleration

magnitudes of $30\pm 10\%$ Hz and $3\pm 10\%$ were used in this investigation. -----	232
Figure 5.27: A simplified design assembly of the smoke/aerosol generator.-----	235
Figure 5.28: Experimental setup for the smoke blanket visualization investigations. -----	236
Figure 5.29: Visualized smoke blanket movements in the main working chamber of C-1 with closed partition gap sizes (a and b) and with a partition gap size of 5 mm in one direction (c and d). The recorded observations are presented as Smoke-Video-D15 in the provided Compact Disk (CD), No.15 in Appendix-D. -----	237
Figure 5.30: Visualized smoke blanket displacements in the main working chamber of C-1 with a partition gap size of 5 mm in one direction. The recorded observations are presented as Smoke-Video-D13 and D14 in the provided CD, No.13 and 14 in Appendix-D -----	240
Figure 6.1: Particle size characterisation of the glass and bronze particles used in the PEPT investigations. -----	250
Figure 6.2: The real time change in the position of a bronze tracer particle with respect to X (horizontal), Y(Vertical) and Z-axis in separation cell, C-1. -----	253
Figure 6.3: The three dimensional bronze tracer location and average speed at the end of the PEPT experiment when time, $t=980$ sec. The recorded real time observations are presented as PEPT-Video-D01 at 10X speed in the provided CD (No.1 in Appendix-D). -----	255
Figure 6.4: The occupancy and velocity field vectors of a bronze tracer particle in relation to the separation cell (C-1) geometry. -	257

Figure 6.5: The three dimensional motion and occupancy mapping of a bronze tracer particle in separation cell, C-1. -----258

Figure 6.6: The real time change in the position of a glass tracer particle with respect to X (horizontal), Y(Vertical) and Z-axis in separation cell, C-1. -----261

Figure 6.7: The three dimensional glass tracer location and average speed from the start to the end of the PEPT experiment. The recorded real time observations are presented as PEPT-Video-D02 at 10X speed in the provided CD (No.2 in Appendix-D). -----262

Figure 6.8: The occupancy and velocity field vectors of the glass tracer particle in relation to the separation cell (C-1) geometry. -264

Figure 6.9: The three dimensional motion and occupancy mapping of a glass tracer particle in separation cell, C-1. -----264

Figure 6.10: The real time change in the position of a bronze tracer particle with respect to X (horizontal), Y (vertical) and Z-axis in separation cell, C-2. -----266

Figure 6.11: The three dimensional bronze tracer location and average speed from start to the end of the PEPT experiment in a 40 mm width separation cell, C-2. The recorded real time observations are presented as PEPT-Video-D03 at 10X speed in the provided CD (No.3 in Appendix-D). -----268

Figure 6.12: The occupancy and velocity field vectors of a bronze tracer particle in relation to the separation cell (C-2) geometry. -269

Figure 6.13: The three dimensional motion and occupancy mapping of a bronze tracer particle in separation cell, C-2. -----270

Figure 6.14: The real time change in the position of a glass tracer particle with respect to X(horizontal), Y(Vertical) and Z-axis in separation cell, C-2. -----271

Figure 6.15: The three dimensional glass tracer location and average speed from start to the end of the PEPT experiment in a 40 mm width separation cell, C-2. The recorded real time observations are presented as PEPT-Video-D04 at 10X speed in the provided CD (No.4 in Appendix-D). -----272

Figure 6.16: The occupancy and velocity field vectors of a glass tracer particle in relation to the separation cell (C-2) geometry. -274

Figure 6.17: The three dimensional motion and occupancy mapping of a bronze tracer particle in separation cell, C-2. -----275

Figure 6.18: Particle size characterisation of two distinctly sized glass particles used in the PEPT investigations. -----277

Figure 6.19: The three dimensional large glass tracer location and average speed from start to the end of PEPT experiment in a 20 mm width separation cell, C-1. The recorded real time observations are presented as PEPT-Video-D05 at 10X speed in the provided CD (No.5 in Appendix-D). -----278

Figure 6.20: The three dimensional motion and occupancy mapping of a large glass tracer particle in separation cell, C-1. -----280

Figure 6.21: The three dimensional small glass tracer location and average speed from start to the end of PEPT experiment in a 20 mm width separation cell, C-1. The recorded real time observations are presented as PEPT-Video-D06 at 10X speed in the provided CD (No.6 in Appendix-D). -----282

Figure 6.22: The three dimensional motion and occupancy mapping of a small glass tracer particle in separation cell, C-1. -----284

Figure 6.23: The three dimensional large glass tracer location and average speed from start to the end of PEPT experiment in a 40 mm width separation cell, C-2. The recorded real time observations are presented as PEPT-Video-D07 at 10X speed in the provided CD (No.7 in Appendix-D). -----285

Figure 6.24: The three dimensional motion and occupancy mapping of a large glass tracer particle in separation cell, C-2. -----287

Figure 6.25: The three dimensional small glass tracer location and average speed from start to the end of PEPT experiment in a 40 mm width separation cell, C-2. The recorded real time observations are presented as PEPT-Video-D08 at 10X speed in the provided CD (No.8 in Appendix-D). -----288

Figure 6.26: The three dimensional motion and occupancy mapping of a small glass tracer particle in separation cell, C-2. -----290

Figure 6.27: Particle size characterisation of the ilmenite and sand particles used in the PEPT investigations. -----292

Figure 6.28: The three dimensional ilmenite tracer location and average speed from start to the end of PEPT experiment in a 20 mm width separation cell, C-1. The recorded real time observations are presented as PEPT-Video-D09 at 10X speed in the provided CD (No.9 in Appendix-D). -----293

Figure 6.29: The three dimensional motion and occupancy mapping of an ilmenite tracer particle in separation cell, C-1. -----295

Figure 6.30: The three dimensional sand tracer location and average speed from start to the end of PEPT experiment in a 20 mm width separation cell, C-1. The recorded real time observations are presented as PEPT-Video-D10 at 10X speed in the provided CD (No.10 in Appendix-D). -----296

Figure 6.31: The three dimensional motion and occupancy mapping of a sand tracer particle in separation cell, C-1. -----	298
Figure 6.32: The three dimensional ilmenite tracer location and average speed from start to the end of PEPT experiment in a 40 mm width separation cell, C-2. The recorded real time observations are presented as PEPT-Video-D11 at 10X speed in the provided CD (No.11 in Appendix-D).-----	299
Figure 6.33: The three dimensional motion and occupancy mapping of an ilmenite tracer particle in separation cell, C-2. -----	301
Figure 6.34: The three dimensional sand tracer location and average speed from start to the end of PEPT experiment in a 40 mm width separation cell, C-2. The recorded real time observations are presented as PEPT-Video-D12 at 10X speed in the provided CD (No.12 in Appendix-D).-----	302
Figure 6.35: The three dimensional motion and occupancy mapping of a sand tracer particle in separation cell, C-2. -----	304
Figure 7.1: Breakdown of EC WEEE arising in 2005 (Adapted from Huisman <i>et al.</i> , 2008). -----	309
Figure 7.2: Feed preparation steps for vibration separation of waste PC electrical cables. -----	325
Figure 7.3: Size characterisation of waste electrical cables from - 0.75 and -1.5 mm Retsch mill cut. -----	327
Figure 7.4: Separation 250-425µm shredded electrical cables in a L-type separation cell (Bed height = 150 mm and Partition gap size = 5 mm). -----	330

Figure 7.5: Copper grade (wt%) vs particle bed height (mm) of the separated electrical cables in a 20 mm width separation cell (C-1). -----	333
Figure 7.6: True density (g.cm^{-3}) vs particle bed height (mm) of the separated electrical cables in a 20 mm width separation cell (C-1). -----	334
Figure 7.7: Visually assessed separation time (min.) vs particle bed height (mm) in a 20 mm width separation cell (C-1). -----	335
Figure 7.8: Copper grade (%) vs particle bed height (mm) in a 40 mm width separation cell (C-2). -----	336
Figure 7.9: True density (g.cm^{-3}) vs particle bed height (mm) of the separated electrical cables in a 40 mm width separation cell (C-2). -----	336
Figure 7.10: Visually assessed separation time (min.) vs particle bed height (mm) in 40 mm width separation cell (C-2). -----	337
Figure 7.11: PCB feed preparation for cutting in Retsch mill. ----	340
Figure 7.12: Particle size characterisation of PCB -0.75 and -1.5 mm Retsch mill cut. -----	341
Figure 7.13: Scanning electron microscope (SEM) images of -0.75 mm PCB feed and separated fractions. -----	342
Figure 7.14: Scanning electron microscope (SEM) images of -1.5 mm PCB feed and separated fractions. -----	343
Figure 7.15: Particle size characterisation of -0.75 mm PCB cut separated products. -----	345
Figure 7.16: Particle size characterisation of -1.5 mm PCB cut separated products. -----	345

Figure 7.17: Sink-float analysis of the separated PCB fractions.	-346
Figure 7.18: Helium pycnometer density measurements of the separated PCB fractions.	-----347
Figure 7.19: Particle size characterisation of iridium and aluminium oxide mixtures.	-----354
Figure 7.20: Grades of the separated Ir/Al ₂ O ₃ fractions (sample-1).	-----355
Figure 7.21: SEM Images of the feed and separated 150-300µm Ir and Al ₂ O ₃ fractions (sample-1).	-----357
Figure 7.22: Grades of the separated Ir/Al ₂ O ₃ fractions (sample-2).	-----358
Figure 7.23: SEM Images of the feed and separated 75-425µm Ir and Al ₂ O ₃ separated fractions (sample-2).	-----358
Figure 7.24: Grades of the separated Ir/Al ₂ O ₃ fractions (sample-3).	-----359
Figure 7.25: SEM Images of the feed and separated 150-300µm Ir and Al ₂ O ₃ separated fractions (sample-3).	-----360
Figure 7.26: SEM Image of 300-425µm Ir/Al ₂ O ₃ mixture.	-----360
Figure 7.27: Grades of the separated Ir/Al ₂ O ₃ fractions (sample-4).	-----361
Figure 7.28: SEM Images of the feed and separated 53-425µm Ir and Al ₂ O ₃ separated fractions (sample-4).	-----362
Figure 7.29: 38-53µm and <38 µm Ir and Al ₂ O ₃ grinding mixture (sample-4).	-----362

List of Tables

Table 2.1: Physical separation techniques and their recommended particle size ranges (Adapted from Xing and Hendriks, 2004).-----	43
Table 2.2: Four distinct working particle mixtures (A, B, C & D) with three different compositions (1, 2 & 3) as used by Burtally <i>et al.</i> , (2003 & 2004) and Burtally, (2004) (Adapted from Mohabuth, 2007). -----	70
Table 3.1: Reliability of various sampling techniques (Adapted from ParticlesCIC, 2009). -----	109
Table 3.2: Commonly used particle size analysis methods (Adapted from BSI 1796-1, 1989 and ISO 2591-1, 1988). -----	111
Table 4.1: The parameters used in the DEM-fluid simulations. ---	159
Table 4.2: The size and density of the simulated working particle mixture used in the preliminary density segregation investigation. -----	160
Table 4.3: The size and composition of the simulated working particle mixtures used in the DEM simulations. -----	163
Table 5.1: Composition of the synthetic glass and bronze particle mixture used in the preliminary investigations. -----	185
Table 5.2: Composition of the spherical glass particle mixtures A and B used in the size segregation investigations carried in an L-type particle separator. (* dia.= diameter) -----	194
Table 5.3: Experimental parameters and their ranges used in the vertical vibration induced separation of a glass and bronze particle mixture. -----	212

Table 5.4: Synthetic glass and bronze particle mixtures used in the detailed vertical vibration induced particle separation assessment. -----	212
Table 5.5: Particle separation behaviour at different frequency and dimensionless acceleration values in the separation cells C-1 and 2. (N.B: *χ represent poor and *√ represent good particle separation). -----	217
Table 5.6: Synthetic shredded glass and bronze particle mixtures used in the detailed vertical vibration induced particle separation assessment.-----	227
Table 5.7: Synthetic sand and bronze particle mixtures used in the detailed vertical vibration induced particle separation assessment. (*N.B. the density of particles used in this work was measured by Helium Pycnometer (Section 3.3.3.3)). -----	230
Table 6.1: Operating parameters used in the PEPT experiments.	251
Table 7.1: Banned compounds in the RoHS (Restriction of Hazardous Substances) directive, 2002 (Adapted from Bigum and Brogaard, 2009). -----	311
Table 7.2: Change in elemental concentrations (mg.kg ⁻¹) of CED with time (Adapted from Dimitrakakis, <i>et al.</i> , 2009).-----	313
Table 7.3: Comparison of average metal contents of some valuable metals in high grade WEEE and ore (Adapted from Bigum and Brogaard, 2009). -----	314
Table 7.4: Typical composition of printed circuit boards from EOL computers (Adapted from Guo <i>et al.</i> , 2003). -----	315
Table 7.5: PCB metal fraction enrichment values as reported by Viet <i>et al.</i> , (2005).-----	318

Table 7.6: Average metal content in PCBs disassembled from obsolete printers (Adapted from Yoo *et al.*, 2009). -----319

Table 7.7: Chemical analysis of the two concentrates with feed for the EOL-PCBs generated from the obsolete computers (Adapted from Das *et al.*, 2009). -----320

Table 7.8: Elemental composition of PCB sourced from EOL computers (Adapted from Goosey and Kellner, 2002). -----320

Table 7.9: Specific gravity of different materials in PCBs obtained from EOL computers (Adapted from Goosey and Kellner, 2002). -321

Table 7.10: Chemical composition of PCB originating from EOL computers (Adapted from Mohabuth, 2007). -----321

Table 7.11: Major elements in -0.75 mm PCB feed as analysed by ICP-AES alongside their corresponding wavelengths and CVs. All elements digested in aqua-regia except silver Ag, which was digested in nitric acid. -----348

Table 7.12: Major elements in -1.5 mm PCB feed as analysed by ICP-AES alongside their corresponding wavelengths and CVs. All elements digested in aqua-regia except silver Ag, which was digested in nitric acid. -----349

Table 7.13: Elemental composition change in complete vibration separation cycle for -0.75 mm PCB cut. -----350

Table 7.14: Elemental composition change in complete vibration separation cycle for -1.5 mm PCB cut. -----350

List of Equations

Equation 2.1	50
Equation 2.2	56
Equation 2.3	57
Equation 2.4	58
Equation 2.5	64
Equation 3.1	119
Equation 3.2	119
Equation 4.1	136
Equation 4.2	142
Equation 4.3	142
Equation 4.4	142
Equation 4.5	143
Equation 4.6	143
Equation 4.7	144
Equation 4.8	144
Equation 4.9	144
Equation 4.10	145
Equation 4.11	145

Equation 4.12	146
Equation 4.13	146
Equation 4.14	146
Equation 4.15	146
Equation 4.16	147
Equation 4.17	147
Equation 4.18	147
Equation 4.19	147
Equation 4.20	148
Equation 4.21	148
Equation 4.22	150
Equation 4.23	150
Equation 4.24	150
Equation 4.25	150
Equation 4.26	151
Equation 4.27	151
Equation 4.28	152
Equation 4.29	152
Equation 4.30	152
Equation 4.31	153

Equation 4.32	154
Equation 4.33	154
Equation 4.34	154
Equation 5.1	190
Equation 5.2	190
Equation 5.3	199
Equation 5.4	199
Equation 5.5	220

Nomenclature

Symbol	Description
Γ_c	Critical vibration acceleration, (dimensionless)
C_d	Coefficient of drag acting on a single particle
$\ F\ $	Friction force, (N)
F_c	Cohesion force, (N)
$F_{n,t}$	Normal and tangential contact force, (N).
F_{nd}	Normal damping force, (N)
F_{ne}	Normal elastic force, (N)
F_s	Force exerted by particles on the interstitial fluid (N)
$K_{n,t}$	Normal and tangential stiffness coefficients, (N.m ⁻¹)
R_r	Spheres' radii, (m)
S_d	Particle density separation parameter, (dimensionless)
T_c	Critical particle temperature, (K)
T_k	Kinetic particle temperature, (K)
a_p	Particle acceleration, (m.s ⁻²)
r_c	Centre point of the sphere
$u_{n,t}$	Normal and tangential particle displacement, (m)
v_f	Interstitial fluid velocity, (m.s ⁻¹)
$v_{n,t}$	Normal and tangential particle velocity, (m.s ⁻¹)
ν_p	Poisson's ratio
γ_c	Coefficient of critical damping
$\gamma_{n,t}$	Normal and tangential damping coefficients
ε_{cond}	Control parameter, (dimensionless)
ε_r	Coefficient of restitution
ε_v	Particle void fraction
μ_f	Coefficient of friction
μ_{fv}	Fluid Viscosity, (Pa.s = kg.m ⁻¹ .s ⁻¹)
ω_a	Angular velocity (rad.s ⁻¹)
$\langle \rangle$	Average value

Δx	Length of the particle container, (m)
10X	Ten times faster than the normal speed
h	Fill height, (m)
h	Particle fill height, (m)
Γ	Vibration acceleration parameter, (dimensionless)
ΔP	Fluid pressure drop, (Pa=N.m ⁻¹)
F	Force, (N)
I	Moment of inertia, (N.m.s)
M	Particle momentum (Kg.m.s ⁻¹)
N	Total number of particles, (dimensionless)
T	Temperature, (K)
a	Oscillation amplitude, (m)
d	Particle diameter, (m)
f	Vibration frequency, (Hz)
g	Gravitational acceleration, (m.s ⁻²)
k	Spring constant
m	Mass, (g)
r	Radius, (m)
t	Time, (second)
ε	Ratio of normal component of relative velocities before and after collision
π	Mathematical constant, (3.141593)
ρ	Density, (kg.m ⁻³)
ω	Angular frequency, (Hz)

Abbreviations

2D	Two Dimensions
3D	Three Dimensions
BNE	Brazil Nut Effect
CA	Cellular Automata
CED	Consumer Electronic Devices
Defra	Department of Environment, Food and Rural Affairs, UK.
DEM	Discrete Element Modelling
DM	Dense Medium
DMS	Dense Medium Separation
DVD	Digital Video Drive
EC	European Commission
ECM	Environmentally Conscious Manufacturing
ECMPRO	Product Recovery Obligation
EEE	Electrical and Electronic Equipment
EOL	End of life
EU	European Union
E-waste	Electronic Waste
ICP-AES	Inductively Coupled Plasma-Atomic Emission Spectroscopy
IT	Information Technology
MC	Monte Carlo
MD	Molecular Dynamics
PBB	Poly-Brominated Biphenyls
PBDE	Poly-Brominated Di-phenyl Ethers
PC	Personnel Computer
PCB	Printed Circuit Board
PD	Particle Dynamics
PEPT	Positron Emission Particle Tracking
PET	Positron Emission Tomography
PIV	Particle Image Velocimetry
PTV	Particle Tracking Velocimetry
RBNE	Reverse Brazil Nut Effect

RoHS	Restriction of Hazardous Substances
SEM	Scanning Electron Microscope
SPT	Sodium Poly-Tungstate
TDS	Total Dissolved Solids
USB	Universal Serial Port
WEEE	Waste Electrical and Electronic Equipment
WFD	Waste Framework Directive
ZW	Zero Waste

Introduction

It is customary to divide matter into gases, liquids and solids (Klein *et al.*, 2006). However, there are many examples of dual particle nature and astounding particle properties such as segregation, arching and heaping that form the basis to enable particulate materials to be distinguished from the other states of matter (Tai and Hsiau, 2009; Klein *et al.*, 2006; Jaeger and Nagel, 1992; Pak and Behringer, 1993; Jaeger *et al.*, 1996). Particulate matter can be defined as large assemblies of discrete, macroscopic, solid particles that can originate from the same and/or distinct particle species (Campbell, 1990; Majid and Walzel, 2009; Jaeger *et al.*, 1996; Neederman, 1992; Liao and Hsiau, 2010). These particles generally have a size larger than one micron to offset their Brownian motions in the surrounding fluid (Aranson and Tsimring, 2006; de Gennes, 1999). Dynamic particles can be normally characterised by hard inelastic contacts between their elementary constituents and by their inter particle and solid boundary frictional effects (Tai and Hsiau, 2009). Non-cohesive particles are known to exist in varying sizes and shapes which, in the absence of any cohesive forces, are supposed to be held together by gravity only (Aoki *et al.*, 1996;

Serero *et al.*, 2006). Particulate matter is considered to embody the properties of solids, liquids and gases (Tai and Hsiau, 2009; Klein *et al.*, 2006; Jaeger and Nagel, 1992; Pak and Behringer, 1993; Ford *et al.*, 2009; de Gennes, 1999; Kadanoff, 1999). An example of a particle bed behaviour under the influence of external excitations such as vertical vibration is shown in Figure 1.1 to demonstrate some solid and fluid like analogies.

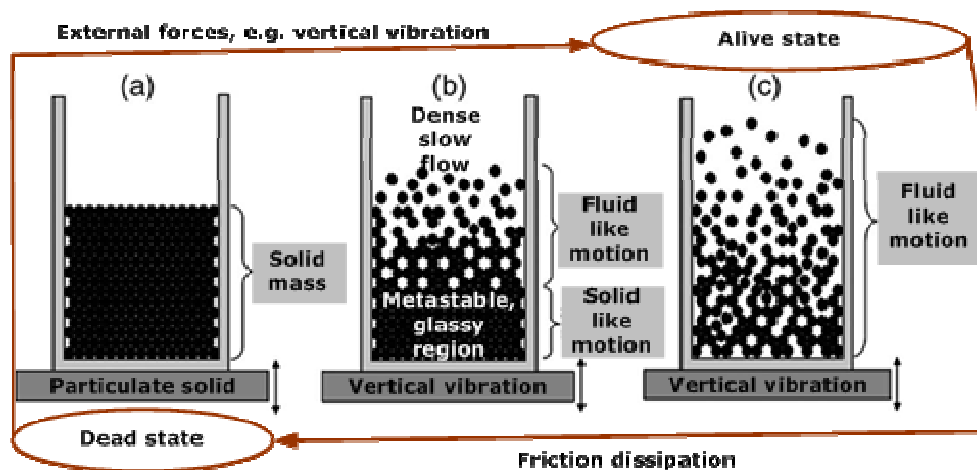


Figure 1.1: A change in particle bed behaviour with increasing the magnitude of vertical vibration acceleration in a rectangular geometry box (Adapted from Tai and Hsiau, 2009).

Figure 1.1 shows three different particle bed stages in a confined rectangular geometry. The absence of any external disturbances is marked by the particles behaviour as a solid mass (Figure 1.1 (a)). However, as an external excitation such as vertical vibration is induced on the stationary particles, a mobile particle phase resembling somewhat fluid-like dynamics as shown in Figure 1.1 (b & c) can be readily observed. The intensity of particles mobility in the mobile phase is strongly dependent on the magnitude of external excitation as represented in Figure 1.1 (b & c). Nevertheless, continuing research in the field of particulate matter has demonstrated some easy to observe but difficult to analyse, diverse, complex, surprising/astonishing, rich, and interesting

phenomena such as, particle segregation (Hsiau *et al.*, 2002; Duran *et al.*, 1993; Baumann *et al.*, 1994; Ristow, 1994; Jullien *et al.*, 1992; Rosato *et al.*, 1987; Knight *et al.*, 1993), dissipative interactions (Luding *et al.*, 1994), density waves (Lee and Leibig, 1994), dilatancy (Coniglio and Herrmann, 1996), friction (Poschel and Buchholtz, 1993; Ulrich *et al.*, 2007), cohesion (Hopkins and Louge, 1991), fluidization (Clement and Rajchenbach, 1991; Tsuji *et al.*, 1992; Ichiki and Hayakawa, 1995), fragmentation (Ishii and Matsushita, 1992; Herrmann, 1995), attrition (Ning and Ghadiri, 1996; Ghadiri *et al.*, 1991), surface waves (Wassgren *et al.*, 1996; Pak and Behringer, 1993), heaping (Wassgren *et al.*, 1996; Evesque and Rajchenbach, 1989; Clément *et al.*, 1992; Lee, 1994; Thomas and Squires, 1998), clustering (Akoi *et al.*, 1996; Mullin, 2000; Mullin, 202), dissipative interactions (Luding *et al.*, 1994), dilatancy (Coniglio and Herrmann, 1996), friction (Poschel and Buchholtz, 1993; Ulrich *et al.*, 2007), fluidisation (Ichiki and Hayakawa, 1995; Götzendorfer *et al.*, 2006), convection (Taguchi, 1992), Brazil Nut Effect (BNE) (Hsiau *et al.*, 2002; Arason and Tsimring, 2006), Reverse Brazil Nut Effect (RBNE) (Breu *et al.*, 2003; Ulrich *et al.*, 2007) and arching (Wassgren *et al.*, 1996). These intrinsic particle phenomena are considered unique to the versatile state of particulate matter (Jaeger and Nagel, 1992; Jaeger *et al.*, 1996; Knight *et al.*, 1993; Kadanoff, 1999; de Gennes, 1999).

The unique, practically important and scientifically rich domain of particulate matter has attracted the attention of many researchers from a broad range of scientific and engineering disciplines (Serero, *et al.*, 2006; Kakalios, 2005; Zeilstra *et al.*, 2008; Kudrolli, 2004). The research investigations in this field have come from areas as diverse as process and chemical engineering, physics, astronomy, pharmacy, agriculture and earth sciences (Aranson and Tsimring, 2006; de Gennes, 1999; Kakalios, 2005). The research interest in particulate matter is mainly sparked by their natural omnipresence and widespread industrial use (Qingfan *et al.*, 2003; Kuo and Chen,

2008), which is considered second only to water in their importance to human activities (Goldhirsch, 2001; Kakalios, 2004; de Gennes, 1999). Examples of particulate matter include, but are not limited to, sand, ores, grains, dry chemicals, plastic pellets, toner, pharmaceuticals, solid waste, agrochemicals, fertilizers, mineral processing, munitions, debris flow, food and ceramics (Rosato *et al.*, 2002; de Gennes, 1999). The importance of particulate matter becomes more evident by considering that an estimated 50% of all products and at least 75% of all raw materials in industry are particulate in nature (Nedderman, 1992; Thomas, 2005). In chemical industry, alone, an estimated one half of the products and nearly three quarters of the raw materials (weight basis) are handled in particulate form (Nedderman, 1992). It has been estimated that in USA alone, nearly 80% of everything that is produced industrially and/or agriculturally is in particulate form at some stage of its processing and/or manufacture (Kakalios, 2005). The choice of processing materials in their particulate form is generally favoured due to their relative ease of handling and transportation in comparison to the other forms of matter (Jaeger, 1997; Chou, 2000). It is mainly due to the self evident importance of particulate matter in almost every aspect of our daily life that considerable research interest in this field is being demonstrated over a long period of time.

Early 18th century contributions in the field of particulate matter included the work of Charles-Augustin de Coulomb (1736-1806) who introduced the law of friction for particulate materials followed by Michael Faraday's (1791-1867) explanation of particle heaping phenomena. Other early known contributors include Ernst Florens Friedrich Chladni (1756-1827), who observed particulate behaviours on the vibrating plates and Osborne Reynolds (1842-1912), who explained the principle of particle dilatancy (Fazekas, 2007; Wieghardt, 1975).

In comparison to the other research fields (e.g. fluid dynamics), the hard, inelegant, messy and peculiar behaviour of the particulate matter has resulted in limited progress in its understanding during most of the 19th and 20th century. However, renewed interest in developing a deeper understanding about particulate media has been sparked notably in the physics community during last quarter of the 20th century (Aranson and Tsimring, 2006; de Gennes, 1999; Goldhirsch, 2003). Ever since, explorations of the intrigued particle bed behaviours in somewhat simplified vertical or horizontal planes using fast performance computer simulations and experimentations have gained momentum and are continuing to thrive at a substantial pace (Ottino and Khakar, 2000; Rosato *et al.*, 2002; de Gennes, 1999; Goldhirsch, 2003). As a result, a great deal of research to-date has been focused on gaining an insight into the vertically and horizontally vibrated particle beds. However, despite this our understanding of the physics of particle media remains in infancy and much more remains to be done (Götzendorfer, 2007; Goldhirsch, 2003). At this stage, even a common approach explaining any particulate phenomenon is far from agreement (Ottino and Khakar, 2000). In the absence of any consensus based equations describing simple particle behaviours, many different descriptions such as continuum, discrete, particle dynamics (PD), lattice Boltzmann, Monte Carlo (MC) and Cellular Automata calculations (CA) are currently in use to explain the diverse particle phenomena (Ottino and Khakar, 2000; Ottino, 2006). A single fit-all particle description approach has proved imperfect to explain the whole range of diverse particle phenomena (Ottino, 2006).

1.1 Particle properties

Particulate matter can show complex internal/external physical conditions and interactions at different size length scales (Sun *et al.*, 2009). Properties of a single particle (Lehon *et al.*, 2003) and that of bulk as well as the nature and type of the interstitial fluids (e.g. air, water) can significantly influence the overall behaviour of particles in many different particle processing unit operations such as, size reduction, separation, fluidisation, conveying and transportation (Klein *et al.*, 2006; Richardson *et al.*, 2002; Castellanos, 2005). The classification of particles at different size length scales is important to understand their basic physical properties and to predict their communal collective behaviours in any particle handling unit operation (Rosato *et al.*, 2002). The general classification of particles at different description levels and/or size length scales along with their important physical properties are summarised and listed in Figure 1.2.

Microscopic level	Mesoscopic level	Macroscopic level
● Single grain level	●●●●● Several grains	 Material as a whole
Mass Shape Size Volume Density Stiffness Terminal velocity Hardness Surface energy Topography Chemical properties Mechanical properties Electrical properties	Interfaces Forces Torques Conservation laws Volume constraints	Size distribution Void fraction Static charge Mass Bulk density Cohesiveness Moisture content Stress/Strain relation Bulk modulus Boundary conditions

Figure 1.2: The important physical properties of particles at various description levels and/or size length scales (Jaeger, 1997).

Figure 1.2 demonstrates that particle physical properties that may be central at a single particle scale could be of less significance in particle processing at macroscopic levels. Nevertheless, naturally occurring grains are usually non-spherical and poly-dispersed. While flowing or otherwise forced they are prone to attrition or break-up and their properties may therefore be time dependent (Serero, *et al.*, 2006). In nature, sand is probably the most common noncohesive particle system (Jaeger *et al.*, 1996; de Gennes, 1999). Some of the size and shape variations associated with dry sand are shown in Figure 1.3, where many different particle shapes such as round, elongated, regular, irregular, polyhedral, ellipsoidal and spherical can be seen.



Figure 1.3: Sand grains originating from different global locations and as seen under a microscope (Adapted from Modderman collections, 2009).

Even in case of the same particulate material (e.g. sand in this case) the variation in particle composition and properties as a function of

source location is clearly evident in Figure 1.3, an observation which was also identified in the work of Kadanoff, (1999). Considering the particle size and shape variations presented in Figure 1.3 as an example, one can presume that a greater flexibility is generally required in designing any new particle processing system. Nevertheless, in case of any particle processing unit operation the particle size characterisation is of immense importance. The size of an industrial particle can vary on a wide scale, ranging from very large to very small (Ottino and Khakhar, 2002). At micron and submicron levels the attractive van der Waals forces can result in cohesion which can lead to a loose particle packing (Castellanos, 2005). However, as the particle size increases these attractive forces are offset by other more complex particle interactions. Industrial particles of diameters $<1\mu\text{m}$ are generally classified as hyper-powders, $<10\mu\text{m}$ as superfine powders, $<100\mu\text{m}$ as powders and $\geq 3000\mu\text{m}$ as pebbles, aggregates or a rock depending on the size increment (Kakalios, 2005). In this work anything between $1\mu\text{m}$ and $1000\mu\text{m}$ was classified as finely sized particles.

Particulate matter of different types, shapes and size ratios are persistently used in many different industrial unit operations due to their ease of production and storage (Thornton *et al.*, 2006; de Gennes, 1999; Chou, 2000). The industrial processing of particles results in quite undefined and complicated particle behaviours (de Gennes, 1999). One such example is particle size segregation under the influence of external excitations such as vertical vibration (Kurdrolli, 2004; Kakalios, 2005) whereby, large intruder particles can rise against gravity to exhibit BNE or sink to show RBNE in a predominantly finely sized particle bed as shown in Figure 1.4.

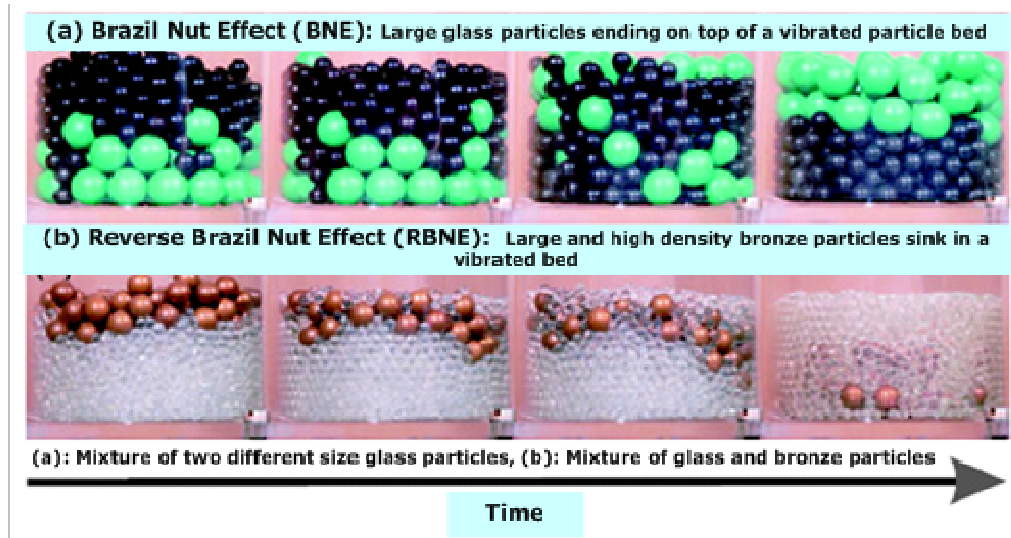


Figure 1.4: Time averaged progression of particle segregation in a vertically vibrated particle bed. The intruder particles can rise in the bed against gravity to exhibit a Brazil Nut Effect, BNE (a) or can sink to show a Reverse Brazil Nut Effect, RBNE (b) (Adapted from Kurdrolli, 2004).

1.2 Particle segregation

Segregation in bulk solid particles with different constituent properties can be defined as spontaneous de-mixing of particles under the influence of external disturbances (Sarkar and Khakhar, 2008; Ottino, 2006). The segregation phenomenon generally represents a spatially non-uniform state (Jha and Puri, 2009). Bulk particle assemblies subjected to external excitations such as vibration, shear, shaking, gravity, an electromagnetic field and even simple interstitial fluid motions can result in particle segregation (Aranson and Tsimring, 2006; Kakalios, 2005). It is normally considered as a distinct particle phenomenon without parallel in solid, liquid and gaseous states (de Gennes, 1999). Different forms of particle segregation (e.g. density segregation, size segregation) can be commonly observed in many different particle processing

unit operations such as mixing, fluidisation, transportation, storing and conveying (Rosato *et al.*, 2002). The size length scale of a segregation phenomenon can range from few millimetres, e.g. BNE in a box (Figure 1.4), to several tens of kilometres, e.g. stony desert as shown in Figure 1.5.



Figure 1.5:- Segregation in a stony desert, Panawonica (Adapted from David and Janet's Collection).

Williams (1963, 1976) proposed three different segregation mechanisms (trajectory, percolation and rise of coarse particle) and discussed the influence of particle properties (e.g. size, shape, density and elasticity) on segregation (Rosato *et al.*, 2002). However, further investigations have shown that in addition to the properties reported by Williams (1963, 1976), other particle properties such as rigidity, friction, boundary conditions, brittleness, size distributions, chemical affinity, magnetic properties, interstitial fluid and the ability to absorb moisture can also have a significant influence on particle segregation (Kurdrolli, 2004).

“Brazil Nut Effect” (BNE) is a classic example of particle size segregation, where shaking small and large size nuts in a jar can result in large Brazil nuts ending up on top of the smaller ones (Hsiau *et al.*, 2002; Arason and Tsimring, 2006). Many different

mechanisms are proposed behind the Brazil Nut Effect, some of them include filling of voids by smaller particles directly beneath the larger ones during particle bed flights and distinct particle convective motions which can drag large sized particles against gravity to end up on top of the particle bed surface (Kurdrolli, 2004). It has been shown that there are conditions where the influence of container geometry and wall roughness can actually reverse the BNE (Naylor *et al.*, 2003; Breu *et al.*, 2003; Hsiau *et al.*, 2002), causing the large particles to sink in the predominantly finely sized particle bed as shown in Figure 1.4(b).

The control of particle size distribution can be of immense importance in unit operations like pharmaceutical mixing via shaking, where the segregated particles might be of an active ingredient in a poly-dispersed formulation (Jaeger *et al.*, 1996). Similar particle segregation examples can be seen in other industrial mixers which result in an exact opposite to what is actually required from that unit operation (Jain *et al.*, 2005; Bridgwater, 2003; Jaeger *et al.*, 1996; Ottino, 2006). Nevertheless, BNE, RBNE and many other particle segregation mechanisms are a continuing source of major concern in many different industrial processes that require a tight quality control in their final particulate products (Ford *et al.*, 2009; Jha and Puri, 2009; Rosato *et al.*, 2002).

Density segregation is another type of segregation where particulate matter tends to segregate out as a result of density differences (Akiyama *et al.*, 2000; Ohtsuki *et al.*, 1995). Whereas size segregation is believed to be predominantly driven by percolation and/or due to the particle convection currents, differences in particle buoyant forces and/or momentum may well be the prime cause for density segregation in a vertically vibrated particle bed (Jain *et al.*, 2005).

1.3 Particle segregation and separation

Engineers from mineral, chemical, civil, mechanical and process professions have long been striving to improve their basic knowledge about particulate materials (Götzendorfer *et al.*, 2006). This is mainly because bulk particle quantities are often manipulated in their industries (Aranson and Tsimring, 2006; de Gennes, 1999). Particulate materials find widespread industrial use mainly due to their ease of production and storage. Sales of powdered metals alone have exceeded €6 billion in Europe and \$5 billion in North America (Thornton *et al.*, 2005). Industrially relevant particulate materials are often present in the form of mixtures and their separation is an important unit operation in many different particle processing industries. The purpose of any industrial particle separation operation is to partition the original material into two or more products.

The industrial relevance of particulate materials and their separation is believed to be as old as engineering itself (Ottino, 2006). This could make one believe that a well developed theoretical and experimental framework in the field of particle separation was in place. However, many different factors (Section-1.1 and Section-1.2) have resulted in disproportionately little attention being given to this field and a consistent picture is still far from clear (Kurdrolli, 2004). A small improvement in any particle handling technology including fine particle separation thus has the potential to result in a big impact (Jaeger *et al.*, 1996).

A number of particle separation techniques are readily available with the majority of the macro sized particle separation techniques operating on a dry basis. The dry based term used in this work actually refers to any particle separation operation being carried in the presence of an interstitial gas such as air. Nevertheless, the well developed micro sized particle separation techniques on the

other hand are mostly based on wet processing, examples include jigging, pinched sluices, spiral, shaking wet table, high gravity separators, hydrocyclone, settling tank, heavy media, and froth flotation (Falconer, 2003; Richardson *et al.*, 2002). The use of a wet based particle separation process such as flotation is generally dictated by the size limitations of very fine particles (Miettinen *et al.*, 2010). Nevertheless, only a limited number of dry based techniques exist for separating micro size particles and any new development in this field is seldomly reported in literature. The latest work in the field of fine particle separation is reported by Weitkämper *et al.*, (2009); Walton *et al.*, (2010), Hirajima *et al.*, (2010); and Oshitani *et al.*, (2010).

Recent years have seen a substantial and renewed interest in the investigations of dynamic particle bed behaviours in the Physics and Engineering communities (Aranson and Tsimring, 2006; Ottino and Khakhar, 2000; Kurdrolli, 2004; Kakalios, 2005). It is mainly due to the complex particle nature that these investigations have mainly looked into rather simplified particle systems such as the vertically and horizontally vibrated particle beds in different geometries (Kurdrolli, 2004; Kakalios, 2005). Both experimental and computer simulation studies have been carried out, mostly based on the idealised spherical particles such as glass, bronze, polystyrene and steel beads (Campbell, 1990; Jaeger and Nagel 1992; Jaeger *et al.*, 1996; de Gennes, 1999; Kadanoff, 1999; Kurdrolli, 2004; and Julio, 2005). Nevertheless, the continuing investigations in this field have resulted in our improved understanding of particulate materials and their relevant processes such as fluidisation, compaction, heaping, surface waves, particle convection and segregation of fine particles (Aranson and Tsimring, 2006). The particle segregation investigations carried out to date can be summarised and fall in one or more of the categories listed in Figure 1.6.

Container shape		
Circular	Non-circular	
Degree of filling		
Less than half	Exactly half	More than half
Regime		
Avalanching	Continuous	
Particulate material		
Identical particles	Density differences	Size differences
Particle interactions		
Non-segregating	Segregating	
Particle shapes		
Regular shapes e.g., spherical	Irregular shapes e.g., needle like	
Vibration dynamics		
By imposed cyclic displacements of a wall or the container (shaking).	By cyclic modulation of a confined stress	

Figure 1.6: The catalogue of segregation investigations carried out to date.

Figure 1.6 highlights some of the complex and inherent variables related to a particle segregation system. Nevertheless, recent investigations by Burtally *et al.*, (2002, 2003), and Burtally, (2004) have shown the use of vertical vibration to separate different size and composition mixtures of finely sized glass and bronze spheres into two different layers in a rectangular shaped prototype cell (dimensions 50mm height and 40X10mm in the horizontal plane). The results from these investigations showed tilting of the particle bed; sharp separation boundaries and distinctive convection rolls in each glass and bronze phases for a wide range of mixtures. In addition to the low vibration frequency and acceleration, experiments carried out in vacuum showed that density segregation in air was the prime factor behind such behaviours. Moreover, Leaper *et al.*, (2005) discussed the importance of the surrounding medium on particle separation in a vertically vibrated bed of glass and bronze particle mixtures.

The investigations reported by Burtally *et al.*, (2002, 2003) and Burtally, (2004) have thus sparked the need to explore and develop a new breed of dry based, vibration driven, fine particle separators.

This work was further extended by Mohabuth and Miles, (2005), Mohabuth *et al.*, (2007) and Mohabuth, (2007); and they reported a new prototype scale partition cell separator that was capable of recovering the separated fine particle layers in two separate chambers. This prototype partition cell separator was used to separate a wide variety of regular and irregular shaped particle mixtures. Different high grade particle components were reported to be recovered on a prototype scale of only a few grams. Despite our limited understanding of vibration induced particle segregation, this work can be considered as a promising step forward towards developing a new scaled up vibration driven particle separator capable of separating finely sized particle mixtures on a dry basis.

Dry based particle separation techniques for separating finely sized particle mixtures are gaining importance due to their decreased economic and environmental loads (Vasconcelos *et al.*, 2009; Macpherson *et al.*, 2009; Weitkämper *et al.*, 2009; Hirajima *et al.*, 2010). Foreseeing an increasing interest in the dry based processing of finely sized particles, a novel, scaled up vertical vibration driven dry based particle separation technique that can separate finely sized particle mixtures in the presence of air only is presented here. The development of this technique is mainly based on the previously reported work of Mohabuth and Miles (2005), Mohabuth, (2007) and Mohabuth *et al.*, (2007) on a prototype scale.

In many particle separation systems scale up is undermined by the unpredictable nature of particle behaviour and unlike classical fluid dynamics, general constitutive laws are largely unknown (Ottino and Khakhar, 2000). Therefore, the design decisions in particle processing are routinely made without complete understanding of the true phenomenon. It is mainly due to this reason that industrial particle processing facilities often operate inefficiently. Despite a large body of work on separating particle mixtures, size length scales, theories and related governing equations are still deficient

and are subject to a great deal of debate (Ford *et al.*, 2009). Absence of even simple design correlations and experimental data therefore dictates the use of experience and heuristics derived from empirical testing and tuning prototypes in designing a new scaled up vertical vibration driven fine particle separation system.

The work presented here covers the scaled up vibration driven particle separator design, separation of different binary particle mixtures on dry basis, particle motion tracking by Positron Emission Particle Tracking (PEPT), surrounding fluid behaviour visualisation, industrial applications and an attempt at Discreet Element Modelling (DEM) with fluid interactions. This work can be used to help identify any operational difficulties, which can be avoided in any future applications.

1.4 Aim and Objectives

The main aim of this research project was to develop a scaled up vertical vibration driven particle separation system and to assess its potential for dry based separation of a range of particle mixtures.

The objectives were to:

- ❖ Design and construct a scaled up industrially relevant vertical vibration driven particle separation system.
- ❖ Assess and analyse the rich and complex particle separation behaviours in various binary synthetic particle mixtures.
- ❖ Identify the optimised particle separation configurations in the scaled up vertical vibration induced particle separation system.
- ❖ Track the real time motions of solo particles during the vertical vibration driven particle separations in various mixtures.
- ❖ Visualise the interstitial fluid behaviours during the vertical vibration induced particle separation.
- ❖ Simulate particle segregation by using Discrete Element Modelling (DEM) with fluid interactions.
- ❖ Extend the application of newly developed separator design to separate the finely size solid waste multi-component particle mixtures.

1.5 Thesis structure

This thesis is organized as follows.

- | | |
|-----------|---|
| Chapter-1 | Introduces the research area and gives the aim and objectives of this research. |
| Chapter-2 | Background literature on particle separation and a perspective on vertical vibration induced particle bed behaviours. |
| Chapter-3 | Presents a description of the apparatus and experimental methods used in this research. |
| Chapter-4 | Presents an effort at Discrete Element Modelling (DEM) with fluid interactions of a vertically vibrated binary particle segregation system. |
| Chapter-5 | Results on initial particle separation investigations and visualisation of interstitial fluid behaviour during the vertical vibration treatment of a glass and bronze particle mixture. |
| Chapter-6 | Results on real time Positron Emission Particle Tracking (PEPT) of solo particles in parallel mixtures. |
| Chapter-7 | Application of vertical vibration induced particle separation technique to separate the industrially relevant complex shaped particle mixtures. |
| Chapter-8 | Concludes all the presented work and presents the future work based on the above investigations. |

Particle separation: A review

2.1 Introduction

An increasing amount of research to date has been focused on understanding particulate materials (Kakalios, 2004). This is mainly due to the fact that particle properties and their behaviours under different static and mobile conditions are fundamental to understanding of many manmade processes and natural phenomena (de Gennes, 1999). Since the majority of industrially relevant particles are usually present in the form of mixtures, the deliberate separation of particle mixtures according to their distinct physical properties is an important unit operation which is encountered in many systems involving industrial handling of particulate materials (Macpherson *et al.*, 2009; Thornton *et al.*, 2006). Separation incorporates a series of physical processes to separate particle mixtures into the desired fractions. This is accomplished based on their distinct physical properties such as particle size, shape, colour, texture, electrical, electrostatic, magnetic, optical, infrared,

permeability, solubility, wettability, X-ray sensing, pneumatics, and density (Richardson *et al.*, 2002;). A range of industrial devices have been developed to accomplish particle separations (Richardson *et al.*, 2002; Thornton *et al.*, 2006). Regardless of the technology used, the main purpose of any particle separator is always the same: to split/divide original feed material into two or more products along a certain distinct boundary so as to obtain the greatest possible extent of separation (Barsky, 2004).

The development history of many well-established industrial and commercially available physical separation techniques can be related back to the mining and mineral industries where they find common use (Richardson *et al.*, 2002; Veasey, 1997). Recent emphasis in new particle separation design developments has been on automated, dry (Vasconcelos *et al.*, 2009; Hirajima *et al.*, 2010; Macpherson *et al.*, 2009) and continuous operations (Richardson *et al.*, 2002). Almost all physical separation techniques work on the principles of coding and separation. A particular particle property such as large/small, high density/low density and magnetic/non-magnetic is identified as a recognising code, once coded these particulate materials can then be separated according to that code (Richardson *et al.*, 2002; Barsky, 2004; Veasey, 1997). The majority of particle separation techniques are binary coded with only a few producing more than two streams of product (Veasey, 1997).

The presence of a large number of particle separation designs and techniques therefore necessitates the selection for a particular application to be governed by several factors. In addition to the distinct particle properties, other design factors such as separation efficiency, dry versus wet operation and the potential for downstream waste processing receive due consideration in selecting any new particle separation process (Oshitani *et al.*, 2010; Hirajima *et al.*, 2010). High product yields and simultaneous washing may be an advantage in certain applications where the feed material is

already wet however, the deliberate use of wet particle separation operations are often associated with high costs, due to maintaining a water circuit, corrosion, fines treatment, water treatment after use, filtering, drying and sludge disposal (Macpherson *et al.*, 2009; Richardson *et al.*, 2002; Hirajima *et al.*, 2010; Oshitani *et al.*, 2010). For fine particle separations, wet concentration techniques are generally considered more effective; this is largely due to the limited available alternative choices for dry separation in this particle size range (Hirajima *et al.*, 2010; Macpherson *et al.*, 2009; Oshitani *et al.*, 2010). Furthermore, for an efficient particle separation each physical separation process incorporate an effective feed size and size range of the final products (Xing and Hendriks, 2006; Perry and Green, 1999).

In the following section some of the commonly used physical particle separation techniques are reviewed. The principal emphasis will be on dry based particle separation techniques as they require less energy than wet and no pre- and post- chemical treatments unlike some wet physical separation techniques such as froth flotation and dense media separation are generally required.

2.2 Particle separation techniques

2.2.1 Size based physical separation techniques

2.2.1.1 Hand sorting

Manual sorting is probably one of the oldest forms of physical separation. The theory behind this technique is based on the

identification of different working particles by legions of hand sorters with an exceptionally “trained eye” while the working particles pass by them on a moving conveyer belt (Delgado and Stenmark, 2005).

The processing application of a manual sorting operation generally needs to be justified against time, throughput and with other major involved efforts. This is mainly because of its labour intensiveness, costs, greater possibility of human errors and the frequently entailed bad working environment for workers (Delgado and Stenmark, 2005; Schlesinger, 2006). In comparison to the industrially developed countries many developing countries still preferably use hand sorting, mainly due to its low operational costs. The hand sorting technique can be effectively used to separate the visually distinguishable macro-size particles which are normally between 300 to 50 mm size ranges (Nwafor, 2009).

2.2.1.2 Automated sorting

In many industrially advanced countries an increasing trend is to use automated sorting techniques. This is mainly because of the current and foreseen environmental legislations, and the ever increasing handling tonnage (Deanne, 2004).

Many automated sorting systems, readily available in the market, take advantage of differences in particle physical properties (e.g. colour, size and shape) in their sorting operations (Deanne, 2004). The colour based sorting systems separate visually dissimilar constituents based on differences in colour, brightness and reflection (Steinert Systems, 2009). This technique employs a high quality colour camera, as a simulated “trained eye”, on a moving conveyer belt. A particular constituent’s moving position is visually identified with the help of this camera. An instant real time electronic signal is then sent to the ejection nozzles which, with an appropriate and

predetermined time lag, blow it away for collection into a separate chamber generally located just next to the conveyer end (Steinert Systems, 2009). An example of an automated sorting system is shown in Figure 2.1.

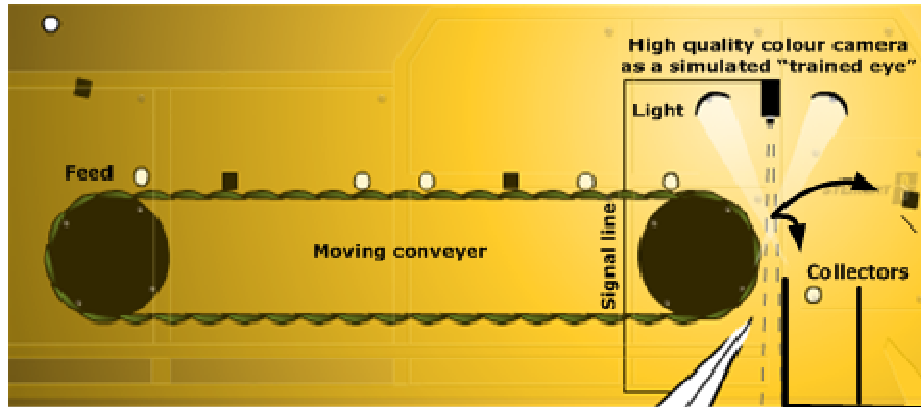


Figure 2.1: Side view of an automated colour based sorting system (Adapted from Steinert systems, 2009).

Other examples of automated sorting systems working on the same separation principle but each with a distinct simulated "trained eye" include; induction, X-ray, infrared, ultraviolet and radioactivity sensing sorters (Steinert Systems, 2009).

Automated sorters are predominantly run on a dry basis. The working particle size and its' liberation are important considerations for any visual sensing (Wills, 1997). In any automated sorting operation sensing limitations generally prevent the use of particles that are less than 10 mm in size. The use of an inconsistent feed size, multiple and dirty particle layers may result in conveying a poor visual signal to the "trained eye" (Steinert Systems, 2009). This will eventually affect the overall grade and recovery of the separated particle products, therefore feed preparation is of paramount importance in any sorting operation. Hence, washing, drying and particle sizing are commonly used in feed preparation,

adding to the overall operational costs of automated sorting systems (Wills, 1997).

2.2.1.3 Differential melting based sorting

Plastic fractions can be sorted based on their differences in melting temperatures. This is especially easy when their melting points are significantly different. Heated rolls, or belt separators, are generally used for this purpose (Figure 2.2). For any particle mixture the lowest melting point polymer will adhere to the heated belt and when this belt turns around, the un-melted ones will discharge on to the next high temperature belt and so on. To achieve a high grade separation by this technique, a contamination free monolayer chipped feed is generally used which flows on the differentially heated belts of the kind shown in Figure 2.2 (Delgado and Stenmark, 2005).

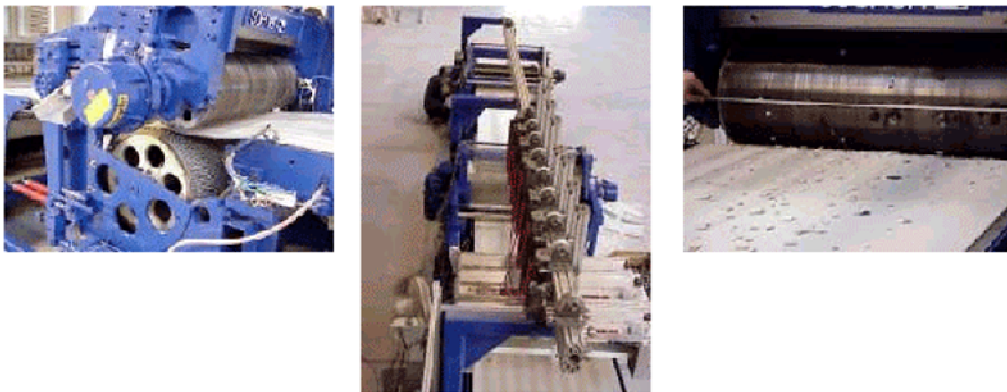


Figure 2.2: Sorting distinct plastics by melting point differences (Adapted from Delgado and Stenmark, 2005).

2.2.1.4 Screening

Screening is a physical separation process that separate particulate materials according to their individual particle sizes, both wet and dry screening can be used for this purpose (Wills, 1997). A particular motion is usually transmitted to the screening mediums which are mostly made up of wire mesh, bars and perforated plates. The screen motion promotes undersize working particles to pass through the screen openings as fines. At the same time, particles larger than the aperture size are carried over as oversize on the screen surface. Particle size is of paramount importance in any screening operation and as the amounts of near size particles increases so the screen separation efficiency decreases (Young, 2009; Wills, 1997; Perry and Green, 1997). The effective working particle size range of different screens is shown as a guide in Figure 2.3.

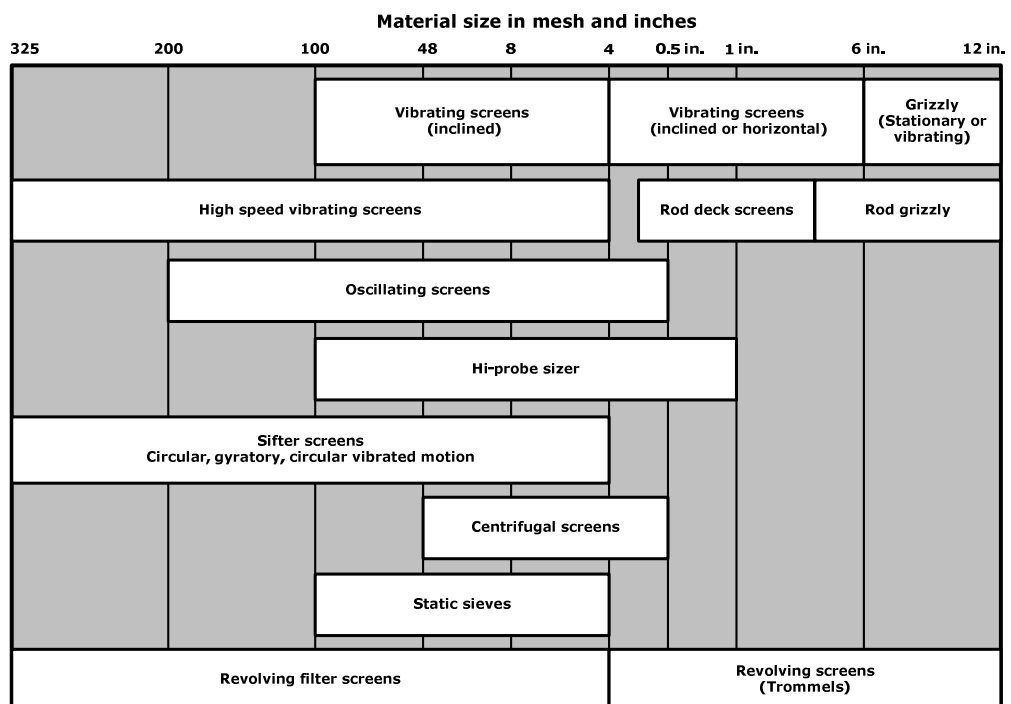


Figure 2.3: Various screen separation ranges (Adapted from Perry and Green 1999).

Distinct screen motion is of interest due to its influence on screening performance (Young, 2009). A variety of screen array motions which involve some variable magnitudes of speed and amplitude can be used for this purpose; examples include revolving, shaking, inclined vibratory, horizontal gyratory and circular vibratory (Young, 2009; Wills, 1997). The main objective of these screen motions are two-fold; first to evenly distribute working particulate materials over the full screen surface and second to assist stratified fine particles to pass through the screen openings. The speed and amplitude of these screen motions are controlled to prevent any violent agitation and hop (Young, 2009).

Screen blinding is any condition which reduces the screen opening areas by particle plugging and coatings (Wills, 1997). In practice any particle shape e.g. spherical, crystalline, flaky, cylindrical and irregular can lead to screen plugging. Cumulative blinding eventually results in total loss of the screening function, this can be controlled by using some anti-blinding devices such as bouncing balls, brushes, wiping rings and screen heaters (Wills, 1997; Perry and Green, 1999). In any industrial unit operation, the screening application is generally limited to a minimum working particle size of 40 μ m (325 mesh size) (Wills, 1997; Perry and Green, 1997) as shown in Figure 2.3.

2.2.2 Size and density based physical separation techniques

2.2.2.1 Air classification

Air classification can be used to separate working particle mixtures based on their differences in size and density (Wills, 1997; Perry

and Green, 1999; Buell, 2010). Air can be forced through the vertical, horizontal and inclined columns to blow up light and fine particles while the dense and oversize particles will fall (Shapiro & Galperin, 2004). The majority of the air separation columns are vertically mounted such as the one used in the work of Hirajima *et al.*, (2010). Like all other physical separation techniques, the selection of an air separator/classifier for a specific use is generally based on product requirements, technological and economic factors (Shapiro & Galperin, 2004). Some of the commonly used air classifier designs are shown in Figure 2.4.

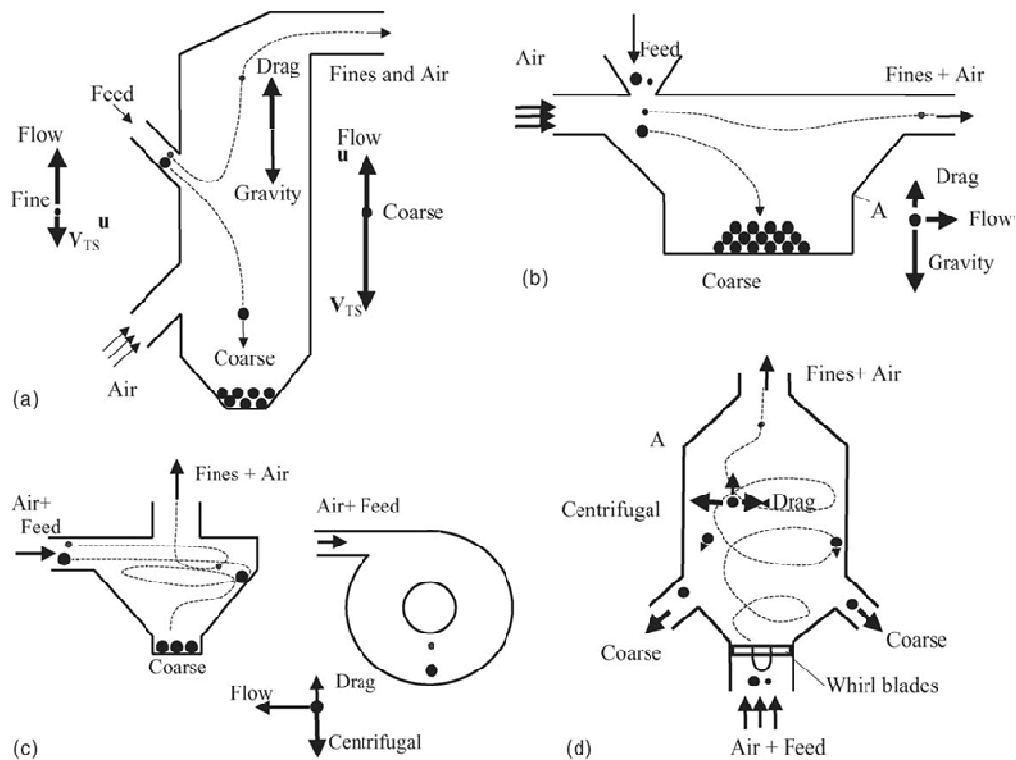


Figure 2.4: Air Separator types:- (a) gravitational, (b) gravitational-cross-flow or expansion chamber, (c) centrifugal-counter-flow, (d) centrifugal-cross-flow (Adapted from Shapiro & Galperin, 2004).

Among other things, the separation of a working particle mixture into light and heavy fractions by using the air classification technique is principally based on individual differences in particle

terminal velocities, drag and gravitational forces (Hirajima *et al.*, 2010). Other controlling parameters are; air to solid ratio, column air velocity, moisture content and column loading. The application of an air separator to separate particle sizes less than 500 μm is generally considered troublesome (Shapiro & Galperin, 2004). This is mainly due to the difficulty in achieving sharp separation cuts in the finally separated particle layers. Otherwise, this technique offers an added advantage of continuous separation with high throughputs (Shapiro & Galperin, 2004). Air classification is mostly used to separate different municipal solid waste fractions (Shapiro & Galperin, 2004). Recently, air classification has been used to explore the separation behaviour of comminuted printed circuit board fractions (Eswaraiah *et al.*, 2006).

2.2.2.2 Dry jigging

In dry jigging air is pulsated through the perforated bottom of a rectangular box which holds the working particle mixture (De Jong *et al.*, 2005). A continuous pneumatic jig is shown as an example in Figure 2.5.

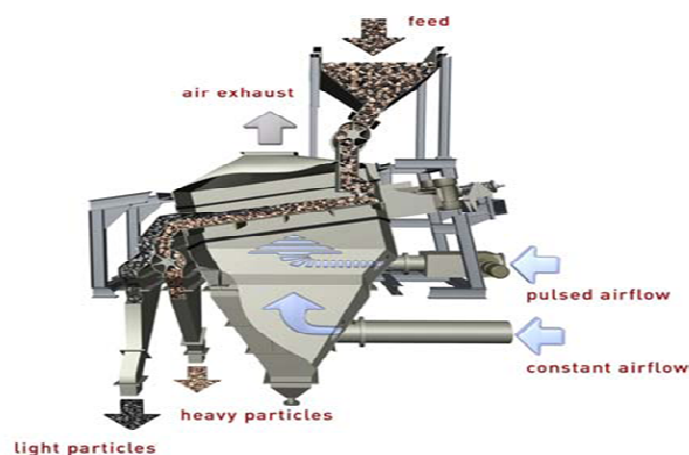


Figure 2.5: Principle of a continuous pneumatic jigging (Adapted from De Jong *et al.*, 2005).

During the course of a pneumatic jiggling operation, such as the one shown in Figure 2.5, the simple pulsating air action through the mixed particle bed causes stratification of the light (top) and heavy (bottom) fractions (De Jong *et al.*, 2005). Particle stratification probably results because of the differences in particulate terminal velocities, gravity effects, settling, buoyancy, acceleration and drag forces acting differently on distinct particle fractions (De Jong *et al.*, 2005). However, complete understanding of the dry jiggling operations is still lacking, this is primarily due to the vast array of control variables that need to be optimised for any specific particle separation application (Nwafor, 2009). Some of the most important particle separation control variables in pneumatic jiggling are air flow rate, frequency and amplitude of pulsation, particle feed properties, bed thickness, and the degree of bed inclination (Nwafor, 2009; Falconer, 2003). Furthermore, boundary walls also affect dry separation in a pneumatic jig (Nwafor, 2009; Falconer, 2003).

A novel batch dry jiggling system has been used at the University of Nottingham, UK, to separate a number of particle mixtures in the presence of air only (Nwafor, 2009). Particles of less than 3 mm size are generally recommended for use in dry jiggling (Cui and Forssberg, 2003). The potential application of a dry jiggling technique to separate finely sized (<500 μm) particles is still restricted. This is perhaps due to the difficulty in controlling the motion of very finely sized particles during pneumatic jiggling (Nwafor, 2009). The pulsating air action can easily make them airborne and they can be carried away from the separation box as dust particles, this affects the formation of clear separation cuts which are later recovered as separated products (Nwafor, 2009).

2.2.2.3 Elutriation

Elutriation is a process of separating working particle mixtures by an upward fluid current (Wills, 1997; Wen and Hashinger, 1960; Li *et al.*, 2004; Eisenmann, 2005). Water and air are the fluids generally used. Elutriation works on the reverse of the gravity sedimentation principle and normally takes place in a turbulent bed of distinct particle materials (Wills, 1997).

In elutriation, applications of fluid currents help stratify working particle mixtures, this leaves heavy and big size fractions at bottom whilst light and finely sized particles move to the top (Wills, 1997). Factors affecting particle separation in this class of separator are; magnitude of linear fluid velocity, particle's terminal velocity, particle bed dimensions, particle shape and size (Wen and Hashinger 1960; Hanesian and Rankell, 1968; Wills, 1997).

2.2.2.4 Ballistic separation

Ballistic separators make use of the kinetic energy of distinct particles to help separate divergent working particle mixtures (Density Separation, 2009). An example of ballistic separation is shown in Figure 2.6.

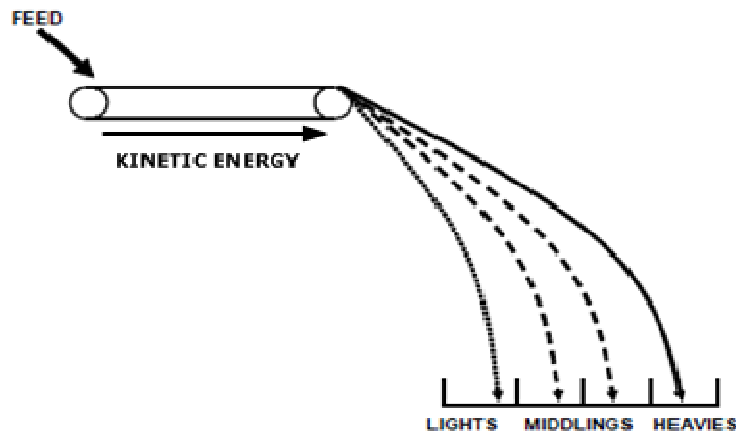


Figure 2.6: Principle of ballistic separator (Adapted from Density Separation, 2009).

The ballistic separation theory is based on the principle that dense particles will travel furthest away in the presence of a fluid in comparison to their light counterparts (Density Separation, 2009). The feed material is generally ejected into the standing air at high speeds (generally above 3 m.s^{-1}) from a sufficient height (several meters) so as to allow a separation to take effect between heavy and light particles (Figure 2.6). Some manufacturers have claimed a high separation precision of about 90% in separating three distinct material fractions with a high throughput at comparatively low energy consumption rates by using ballistic separators (Sort-O-Mat, 2009). These separators are commonly used in the solid waste industry to separate organic materials from contaminants such as plastic bottles, cans, glass and others (Density separation, 2009). The use of this technique to separate fine particle mixtures looks troublesome; this is mainly due to the involvement of a high kinetic energy force to impart particle separation (Sort-O-Mat, 2009).

2.2.2.5 Nail roll separator

Differences in shapes are rarely used as the main particle separation parameter. On the other hand, shape differences have been reported to affect almost all particle separation operations (e.g. eddy current separation) (Wills, 1997). Shape separations can be best accomplished by taking advantage of the particle roll-ability (e.g. on an inclined conveyer belt), passing (e.g. the use of varied screen openings) and catching (e.g. wire shapes).

The nail roll separator takes advantage of the wire shape catching mechanism as shown in Figure 2.7. It consists of a nailed cylindrical roll that also vibrates in the axial direction. The rotating nailed cylinder specifically targets for the wire shaped elements of the particle mixture for capturing and carrying to the other side of the cylinder with the help of rotation and vibration, while the spherical and stoned shaped materials will drop through the nail spacing (Figure 2.6) (Tohka and Lehto, 2005).

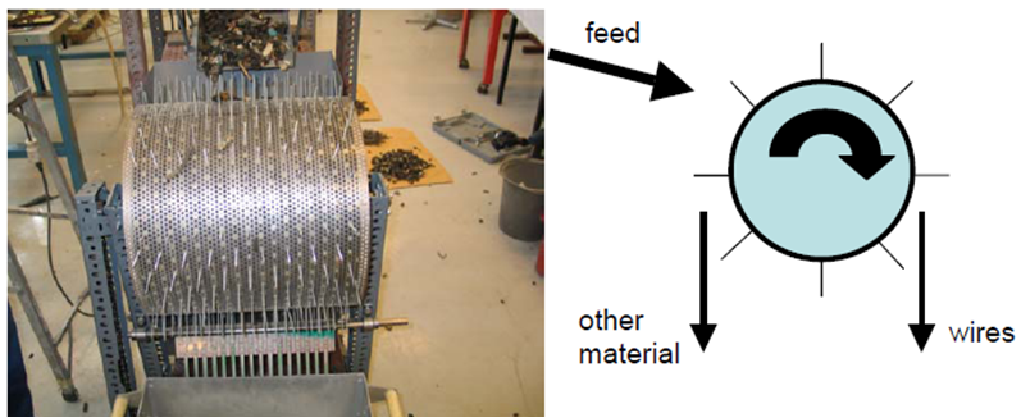


Figure 2.7: Nail-roll separator (Adapted from Tohka and Lehto, 2005).

2.2.3 Gravity/density based physical separation techniques

Density based physical separation techniques are generally based on the principle that when a fluid is added to a mixture of working particles, the material denser than the fluid will sink and those lighter will float (Wills, 1997, Perry and Green, 1999). Various density based wet separators are available for common industrial use; examples include settling tanks, sink-float, hydro-cyclones, wet jigging and froth flotation (Wills, 1997, Perry and Green, 1999). However, the use of density based wet physical separation techniques is considered troublesome in water scarce areas and the requirement of further downstream processing of the wet separated products generally adds to the environmental and economic loads of the physical separation operations (Macpherson *et al.*, 2009; Hirajima *et al.*, 2010; Oshitani *et al.*, 2010).

2.2.3.1 Dense medium separation

Dense medium (DM), sink-float or heavy medium separation is a commonly used technique for coal cleaning and mineral concentrations (Wills, 1997). Particulate materials of different specific gravities can be separated by immersing them in a heavy liquid of intermediate specific gravity; this causes the light particles to float while the heavies sink (Perry and Green, 1999). Industrial experience of working with dense medium separators have shown that the well liberated and coarse sized working particles can be easily separated with the help of this technique; this probably is due to the high settling rates of the large and dense particles. In industrial practice working particles of up to 3 mm diameter are generally preferred in the static dense medium separation units however anything down to 500 μ m can be separated in the dynamic

dense medium units (e.g. in dense medium cyclones) (Wills, 1997; Perry and Green, 1999).

2.2.3.2 Dry heavy medium separation

Large particles of sizes ≥ 20 mm can be separated by using a dry dense medium (DM) separation technique as shown in Figure 2.8.

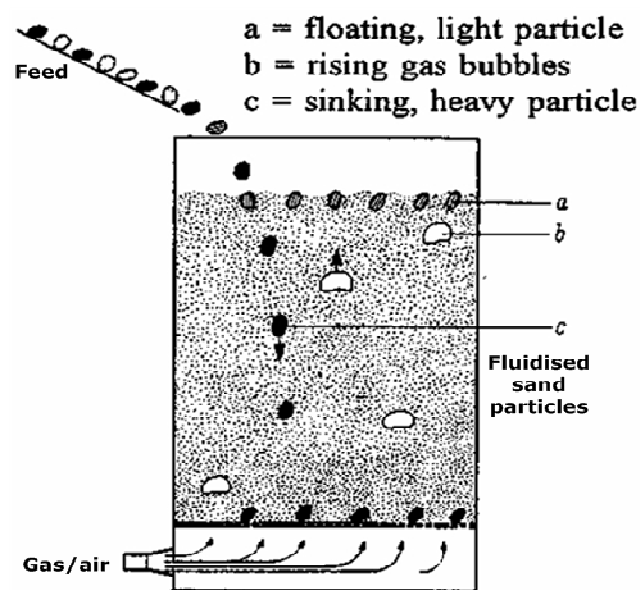


Figure 2.8: Dry sand (as a heavy medium) fluidised bed separation principle (Adapted from De Jong *et al.*, 2005).

Dry dense medium separation works by blowing a gas through the perforated bottom into a particle bed of dry sand (De Jong *et al.*, 2005; Oshitani *et al.*, 2010). Dry sand particles are fluidised when their weights are balanced by the drag force of the upward flowing gas (De Jong *et al.*, 2005; Oshitani *et al.*, 2010). If at this stage a feed consisting of a working particle mixture is introduced into this fluidised sand, the working particles with specific gravity greater than the density of the fluidised sand will settle down and vice versa (Figure 2.8) (Oshitani *et al.*, 2010; De Jong *et al.*, 2005). Some believe that the separation efficiency of a dry DM separator can be

compared in parallel to wet jigging and can be ranked highest among all the dry based density separation techniques (De Jong *et al.*, 2005). Minor disadvantages with dry DM particle separation include the loss of sand with floating working particles and flowing gas (De Jong *et al.*, 2005; Oshitani *et al.*, 2010).

2.2.3.3 Cyclone separation

Centrifugal force can be used to an advantage in separating the working particle mixtures according to their size, shape and density (Wills, 1997, Perry and Green, 1999). The rate of particle settling in a fluid increases if a predominantly centrifugal, instead of gravitational force, is used for separation (Wills, 1997, Perry and Green, 1999).

The feed mixture comprised working particles to the cyclone separator is usually introduced in slurry form (Wills, 1997, Perry and Green, 1999). Feed sizes in the range of 20 μ m to 300 μ m are generally separated by using this technique (Couper *et al.*, 2010).

2.2.3.4 Wet and dry shaking table

In wet tabling the separation of feed slurry comprised working particles is based on the principal that different constituents will follow slightly different streams on a riffled plane surface which is slightly inclined, differentially shaken and washed with an even flow of water at right angle to the direction of slurry motion (Wills, 1997, Perry and Green, 1999). In wet tabling the working particle's shape and size is less of a concern in comparison to their density (Wills, 1997, Perry and Green, 1999). The later property is widely considered to be the prime separation cause in these operations.

This is especially true in case of liberated finely sized particles which are the main use of this separation technology (Wills, 1997; Perry and Green, 1999).

Dry shaking tables separate light and heavy particle fractions by means of vibrations combined with an upward air flow (Density Separation, 2009; Wills, 1997, Perry and Green, 1999). The operation of a dry shaking table is shown as an example in Figure 2.9.

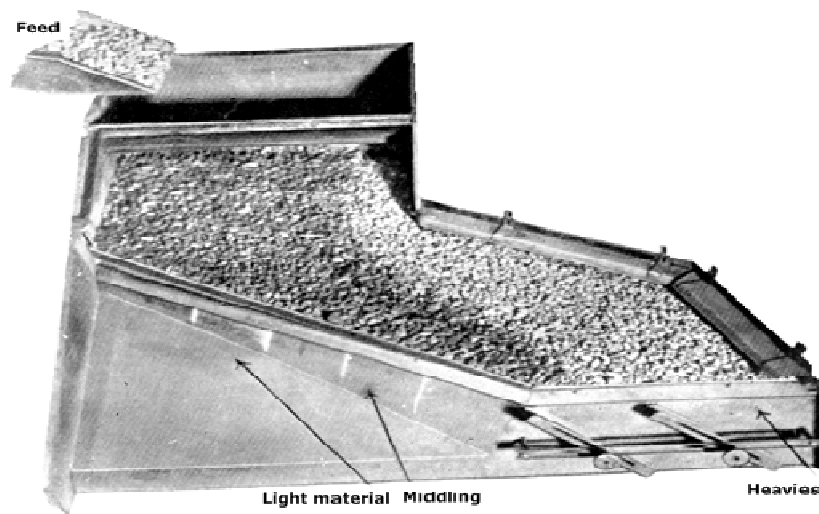


Figure 2.9: Dry shaking table (Adapted from Density Separation, 2009).

In a dry shaking table the direction of the vibration motion is generally inclined upward from a horizontal position and a gust of air is driven through the perforated deck. An upward air flow through the particulate material will make it partially fluidised. This fluidisation and the use of vibration are thought to make the heavy particles migrate vertically down near to the table surface, once there they experience a comparatively strong vibration force and hence start to migrate towards right side of the table, finally collected as a separate stream (Figure 2.9) (Density Separation, 2009). The light particles will follow an opposite path to the heavies. Being lighter they will float over the particle surface and

will be less sensitive to the vibrations and hence will not follow the same route as heavies. This results in their collection as a separate stream to the heavies (Figure 2.9). Coarse working particle sizes are generally preferred for dry air tabling; the feed size is usually between ≥ 2 mm to ≤ 20 mm with a bed thickness between 10 and 100 mm, depending on the type of materials (Density Separation, 2009; Perry and Green, 1999). Some particle examples that are normally separated by dry tabling include; coal, ilmenite, seeds, cork, wood chips and coffee.

2.2.3.5 Spiral Separation

The presence of density differentials in particle mixtures are the basis of separation in spiral separators, however shape and size factors can also be of equal importance (Perry and Green, 1999).

As the particle feed in slurry form flows down in the spiral channel heavy and/or larger size particles move to the inside of channel. This distinct fluid stream is recovered separately at various opening pores. The fines laden stream follows the outer trajectory in the spiral channel and is hence recovered separately. The separation action taking place in this piece of equipment is believed to be as a result of various complex force actions including centrifugal, friction, gravity and water drag. Generally, working particle mixtures with sizes from $2000\mu\text{m}$ to $75\mu\text{m}$ can be separated by this technique (Perry and Green, 1999).

2.2.3.6 Centrifugal separation

Many different centrifugal separator designs are used to separate finely sized particle mixtures; an example is the Knelson[®]

centrifugal separator which can separate distinct density particles in the sizes ranging from 10 μm to 6000 μm (Knelson, 2009). The Knelson[®] separator has distinct inner rings that help retain the centrifugally separated working particles (Figure 2.10). This technique is widely used in recovering precious metals such as gold and platinum and its use has also been extended to recover various finely sized solid waste fractions (Wang, 2006).



Figure 2.10: Knelson[®] Concentrator ring (Adapted from Knelson, 2009).

2.2.4 Magnetic and electrostatic separation techniques

2.2.4.1 Magnetic separation

The attraction and repulsion properties of an individual particle in a magnetic field are used to direct separation in this case. Ferrous metals such as iron and steel are commonly separated by magnetic separation. Magnetic separators are usually available in three

different configurations; magnetic head pulley, drum and magnetic belt (Steinert, 2009). Dry and wet magnetic separations are both commonly practiced. The working particle mixtures to be magnetically separated are sent along a conveyer belt where magnetic field is either directed from above or beneath the moving belt.

Particle size and liberation are both important considerations in any magnetic separation operation. Recent advances in this field include the use of strong magnetic field and magnetic field gradients to separate diamagnetic and paramagnetic particles (Catherall *et al.*, 2005).

2.2.4.2 Electrostatic separation

Electrostatic or high tension particle separation works on the principles of attraction and repulsion due to the difference in electrostatic charges (Taylor, 1988; Vesilind & Rimer, 1981; Perry and Green, 1999). Working particles with a positive electrical charge can be separated from particles with a negative electrical charge by merely placing them in an electric field as shown in Figure 2.11.

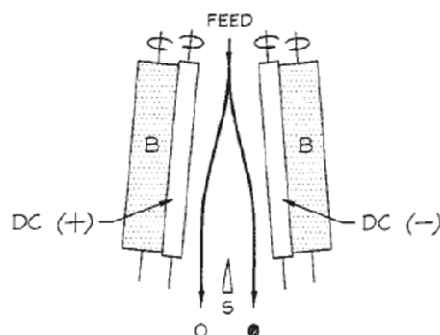


Figure 2.11: Electrostatic particle separation (Adapted from Perry and Green, 1999).

The conductive particles receive a surface charge and thus become attracted to the electrodes while dielectric particles don't and are therefore repelled (Taylor, 1988; Vesilind & Rimer, 1981; Perry and Green, 1999). Before using this technique, an electrostatic charge has to be applied to the working particles. Electrification, conductive induction and ion bombardment are the most commonly used techniques for this purpose. With any electrostatic charging technique, the amount of charge that can be deposited on a particle is strongly dependent on the particle charge density and surface area of the individual particle. Hence, very finely sized particles have greater probability for less charging. This results in their decreased capability to overcome drag resistance of the carrying fluid and subsequently move to the respective electrodes. This problem can potentially be solved by having a long separation area between the two opposite charged electrodes (Taylor, 1988; Vesilind & Rimer, 1981; Perry and Green, 1999).

2.2.5 Eddy current separation

The main principal behind eddy current separation is, "an electric charge can be induced in a conductor by changes in a magnetic flux cutting through it" (Poms, 2009). In an eddy current separator, feed particles are generally moved on a conveyer belt which passes on a rotating drum. The inside of this drum contains a fast rotating magnetic block that produces a strong and changing magnetic flux. When conducting particles move near to this changing flux, magnetic fields are induced; this is as a result of the metallic particulate's spiralling current. These magnetic fields then interact with magnetic fields of the rotating drum and these interactions result in an increased kinetic energy of the particle. The increased energy particulates tend to throw themselves away from the conveyer end and follow different trajectories depending on their

individual energy levels (Poms, 2009). Eddy current separators are widely used in separating different solid waste fractions. The particle size of the materials separated by this technique usually range between 5 to 100 mm. However, some workers have used less than 5 mm particle sizes in their separations using a reverse magnetic drum motion (Cui, 2005).

2.2.6 Froth flotation

If a sufficient wettability difference between mixed but liberated finely sized working particles exists, then they can be effectively separated by using a flotation technique (Perry and Green, 1999), examples include froth, ion and foam flotation. Froth flotation technique involves the relative interactions of solid, fluid and air. A particle-fluid suspension is generally subjected to a flock of air bubbles in a suitably designed vessel (Wills, 1997). The hydrophobic particles attach with air bubbles and are hence carried over to the top surface for recovery; the hydrophilic particles remain suspended in the fluid and are recovered separately. Differences in surface chemical properties are the basis of separation in this technique.

In a feed conditioning step before flotation, the relative wettability of the working particles can be enhanced with surface acting agents. The actual chemistry of this technique is quite complex and many different reagents such as polar and non-polar collectors, froths, modifiers, activators, pH regulators, depressants and flocculants are commonly used to enhance distinct particle-bubble attachments (Perry and Green, 1999).

2.3 Particle size and physical separation

The discussions presented in Section 2.2 have shown that the differences in bulk particle properties form the basis for any physical separation technique. It is rare for a single physical separation technique to be employed for a mineral concentration process; instead a combination of different techniques is commonly used. A high degree of component liberation is usually required prior to any physical separation process and often, the degree of liberation is in direct relation to the size range of the working particles. Physical separation is generally preferred for use with coarse size particles, mainly due to their ease of separation and handling. However, the liberation issues on numerous occasions dictates the use of fine (<1000 μm) size particles in many physical separation processes. Many different types of comminution devices such as crushing, grinding and cutting mills are commonly used for reducing the size of the working particle mixtures and to ease the liberation of desired component (Cleary *et al.*, 2008). The main role of a comminution unit operation is to liberate the valuable and desired particles from the bulk material, resulting in the production of a range of particle sizes from their operations (Wills, 1997; Perry and Green, 1999; Cleary *et al.*, 2008).

The well liberated particle size range resulting from the comminution unit operation necessitates the use of a range of physical separation techniques to best accomplish the final separation grades of the particulate products. This potentially is one of the main drivers for having a range of physical separation devices (Section 2.2) in common industrial use. All physical separation techniques have a distinct working size range of the particles, some of the commonly used techniques with their recommended working particle size range are summarised in Table 2.1.

	Physical separation techniques	Working particle size ranges
1	Manual sorting	>80 mm
2	Screening	>40 μ m
3	Cyclone	10-150 μ m (20-300 μ m reported by Couper <i>et al.</i> , 2010)
4	Sink Float	>1 mm
5	Shaking Table (wet) Shaking table (dry)	30 μ m-3.5 mm 2.0 mm -20 mm
6	Jig (wet) Jig (dry and continuous)	>75 μ m >1 mm (De Jong <i>et al.</i> , 2005)
7	Sedimentation	45 μ m-2 mm
8	Spiral	60 μ m-3.5 mm
9	Magnetic separation	>100 μ m
10	Electrostatic separation	>100 μ m
11	Eddy current separation	5-100 mm
12	Flotation	45 μ m-2 mm

Table 2.1: Physical separation techniques and their recommended particle size ranges (Adapted from Xing and Hendriks, 2004).

The physical separation technology for coarse sized particles is well developed. However, the majority of the physical separation operations in industrial mineral processes rely on the processing behaviours of finely sized particle mixtures. Dry based physical separation of fine particles has many advantages over wet processing, e.g., onsite concentration, less transportation costs, mobile operations, less physical degradation and so on (Oshitani *et al.*, 2010; Hirajima *et al.*, 2010). However, in the absence of many dry based processing alternatives, the majority of the finely sized particle separation techniques rely on wet processing in their operations (Hirajima *et al.*, 2010). This is despite the fact that majority of the mineral deposits are in arid (e.g. Africa, Australia, Asia and America) and near arctic (e.g. Russia, Europe, North America, Canada) regions (Density separation, 2009). The water scarcity and below freezing temperatures in these areas make it difficult, if not impossible, to use wet particle concentration processes. Furthermore, the consumption of water by quarrying operations is restricted by the UK Water Act (2003) which aims to ensure sustainable use of water resources, strengthen the voice of

consumers and promote water conservation (Wagner and Mitchell, 2007). Hence, the mineral, mining and recycling industry in UK is required to adopt 'water efficient' particle processing methods that include many physical particle separation processes.

The use of wet physical separation processes for fine size particle separations has the potential for adverse environmental impacts; therefore, an effluent treatment system is generally required to decrease the environmental load. However, this results in increased costs. Furthermore in a finely sized working particle separation operation, a large number of control variables are normally optimised for any single separation operation. Hence, process flexibility is an issue of great concern and a slight change in any particle property will result in an adverse effect on the final grade and recovery of the separated products (Wills, 1997; Perry and Green, 1999).

Although mineral processing continues to be in demand for supplying valuable virgin materials, "waste" is now widely considered as a valuable resource (Mohabuth, 2007). Many similarities can be found between mineral and solid waste resource recovery operations, examples include particle size, liberation and cohesiveness. Perhaps this is one of the main reasons that solid waste treatments in their recent developments have found an increasingly large use of mineral separation techniques to recover valuable components. Waste recycling has gained importance mainly as a result of the economic boost starting in the last quarter of the 21st century. The economic situation has especially boomed during the last two decades and thus has resulted in price hike of many virgin resources to a peak level. More recently the global credit crunch has forced many industrial operators to rely on recycled materials in an effort to cut on their import bills. Nevertheless, in addition to other commercial factors, better public understanding about the environment has also resulted in an

increased awareness about sustainable growth and resource efficiency. This has driven many industries to review their current processing operations in such a way so as to improve their resource utilization.

Dry based physical separation of fine particles is widely considered as an important unit operation. Any new developments in this area have the potential for greater overall economic and technical advancement impact. The next section will look into various new developments in dry based separation of finely sized, multi-component, particle mixtures under vertical vibration.

2.4 Vibrated particle mixtures

2.4.1 Vibrated particle flows

Particulate materials under certain conditions can show fluid like behaviours, they can flow and fill in any shapes imposed on them (Tai and Hsiau, 2009; Klein *et al.*, 2006; Jaeger and Nagel, 1992; Pak and Behringer, 1993; Ford *et al.*, 2009; de Gennes, 1999; Kadanoff, 1999; Campbell, 1990; Jaeger, Nagel and Behringer, 1996). On the other hand particulates are also capable of showing some distinct features such as forming piles (Clément *et al.*, 1992), heaping (Wassgren *et al.*, 1996; Faraday, 1831), surface waves (Wassgren *et al.*, 1996) and maintaining a stable inclined surface up to some degrees with the base of the container (Evesque and Rajchenbach, 1989). These bulk shape features, in the absence of any external forces, can stay stable for an infinite amount of time (Jaeger, 1997). The main motivations behind such behaviours are the balancing between different inter-particle and bulk particle forces, including friction, gravitation and fluid drag acting distinctly

on the individual particles (Castellanos, 2005; Jaeger *et al.*, 1996; de Gennes, 1999). The particle forces that normally act between two particles are known as adhesion and the ones that act tangentially are commonly termed as friction (Jaeger, 1997). Particle friction exists in many different forms, some of the best known are static, kinetic, molecular, deformation and rolling (School for Champions, 2009). Among all these friction types, the static and kinetic ones are considered dominant in the processing of dry particles.

Particle flows are encountered in many industrial processes and in comparison to fluid flow these distinct particle flows normally come across innumerable inter particle collisions which are widely believed to be dissipative in nature (Midi, 2004; Jaeger, 1997; de Gennes, 1999; Zivkovic *et al.*, 2008; Wassgren *et al.*, 1996; Ottino and Khakhar, 2002; Pak *et al.*, 1995; Majid and Walzel, 2009; Campbell, 2006). The dissipative nature of inter-particle collisions in any steady state particle flow system necessitates energy being continuously fed into the system (Tai and Hsiau, 2009; Campbell, 2006). The energy is often delivered in the form of shear, shaking; interstitial fluid motion and by the application of an electric or magnetic field (Aranson and Tsimring, 2006). Amongst the all mentioned particle driving forces, sinusoidal horizontal or vertical oscillations are commonly used in industry to enhance a range of particle flows (Wassgren *et al.*, 1996).

A number of pieces of particle processing equipment use vibration in one form, or another, to transport and handle various particle mixtures (Chou, 2000). The elementary understanding of a vibrated particle bed is therefore of interest because of many different practical reasons (Kudrolli, 2004). For example, vibration is widely used to control the flow of particulates from various hoppers and silos (Zivkovic *et al.*, 2008; Chou, 2000). Vibration is also used to avoid any flow obstructions and to limit the formation of plugs in

other particle flows (Zivkovic *et al.*, 2008). A recent investigation (Xu and Zhu, 2006) has shown that the use of a vibro-fluidised reactor can help improve the fluidisation potential of finely sized particles. The onset of vibro-fluidisation in a deep particle bed is also investigated in the work of Ford *et al.*, (2009). Beside other uses, vibro-fluidisation has also been used to separate finely sized coal particles from the other undesired mineral contaminants (Luo *et al.*, 2008). The importance of vibrated particle beds in the improved operational performances of reactors, combustion chambers and heat exchangers is highlighted in the work of Squires, (2004). Moreover, the use of vibration has also been reported in enhancing the quality of sintered products (Zivkovic *et al.*, 2008). Other examples of advantageous vibration use include particle sorting and tabling.

The industrial application of vibration is not just limited to particle conveying; other processes such as dry particle mixing also utilize it in their operations (Katayama *et al.*, 2003; Deng and Wang, 2003). However, the use of vibration often results in many complex particle behaviours (Section 1 in Chapter-1). On occasions the use of vibration in various particle processing unit operations results in an undesired separation, or segregation, of the particle mixtures (McCarthy, 2009; Jaeger *et al.*, 1996; Kudrolli, 2004). In addition to segregation, vibration of finely sized particles can also result in compaction (Azéma *et al.*, 2006). Nevertheless, uncontrolled particle segregation has continued to be a source of great industrial frustration and can be a costly problem (McCarthy, 2009; Kakalios, 2004). Hence, the control and avoidance of undesired particle segregation is of great importance to many industrial processes such as pharmaceutical processing where the proper proportions of all ingredients are expected to be present in whole the particle mixtures (Kakalios, 2004). The complexity of these particle behaviours becomes more evident by considering the length scales (Section 1.2 in Chapter 1) on which they happen (Rosato *et al.*,

2002; Jaeger, 1997; Goldshtein *et al.*, 1996). Other considerations include their sensitivity to varying external conditions as well as to minor changes in internal particle composition. Particle processing operations generally involve the control of a number of process variables (Wills, 1997, Perry and Green, 1999). The quantification of these dynamic and/or static variables is still lacking in many areas of vibrated particle studies. A unified theory regarding vibrated particle flows currently seems almost impossible, in many cases, conventional statistical physics concepts prove to be unsuitable for particulate materials (Midi, 2004; Ford *et al.*, 2009; Kurdrolli, 2004; Aranson and Tsimring, 2006; Kakalios, 2005).

Despite the importance of particulate materials in every aspect of our daily life, progress in understanding of their basic properties, underlying mechanics and essential physics still remains poor (Bridgwater, 2003; Ottino and Khakar, 2002; Aoki and Akiyama, 1995; Aranson and Tsimring, 2006; Kakalios, 2004). This knowledge is of core importance in order to design and operate an efficient particle processing and handling system. In the absence of any particle processing design equations, general approaches and even the consensus based basic equations of particle motion; the particle handling equipment has continued to be designed on an empirical basis (Ottino and Khakhar, 2002). It has been reported (Duran, 2000; Jaeger *et al.*, 1996) that many of the present day particle handling and processing techniques are severely out of date and haven't been changed since the 19th century. It is only recently that this subject has started to undergo a firm placement on numerical basis (Goldhirsch, 2003; Kakalios, 2004). However, technical hitches still exist and the tradition of empirical design development still prevails in many new designs of particle handling equipment. Hence it is generally difficult, if not impossible, to study and understand the particle behaviours on industrial length scales (Wassgren *et al.*, 1996). It is due to this that extensive laboratory scale studies are generally carried out to investigate the various

controlling parameters (Wassgren *et al.*, 1996; Midi, 2004; Pak *et al.*, 1995). Despite all these simplifications, particle behaviours are still complex. Many usefully scaled prototype studies are reported on vibrating bed of particles (Jaeger, 1997; Luding *et al.*, 1994; Mohabuth, 2007; Hsiau *et al.*, 2002; Pak *et al.*, 1995). These laboratory scale studies may not completely mimic the core particle flow problems but can result in generating new ideas and new solutions for processing particulate materials. The next section will therefore investigate some of the previously reported work on vibration driven particle beds in relation to the objectives of this research.

2.5 Vibrated particle beds

Controlled vibration driven particle beds are often employed as idealised systems for observing the fundamental mechanics of particle flows (Wassgren *et al.*, 1996; Ford *et al.*, 2009). An approximate fluid like behaviour can be observed by vibrating particle media with a sufficient magnitude of vibration (Campbell, 1990; Wassgren *et al.*, 1996; Ford *et al.*, 2009). To simplify the particle response, these vibrations are usually subjected in one vertical direction only. The application of vertical vibration to a shallow particle bed usually results in its transition from a static to a dynamic state. Most of the experimental shallow particle beds are only a few particle diameters deep. Vigorous vibration of these particle beds can result in vibrofluidization, a particle state which has some similarities to a gas fluidization (Clement and Rajchenbach, 1991; Tsuji *et al.*, 1992; Ichiki and Hayakawa, 1995; Tai and Hsiau, 2009; Kadanoff, 1999). This fluidised state is highly desirable in many particle mixing (Zivkovic *et al.*, 2008) and separation processes (Xu and Zhu, 2006). The main aim of particle fluidization is to mobilize the individual particles (Xu and Zhu,

2006). However, unlike gas fluidization, the onset of vibrofluidization is not very well characterised. Once under vibration, only particle momentum is considered to be conserved, the kinetic energy is lost through dissipation of energy into heat and collision deformations (Jaeger, 1997; de Gennes, 1999; Zivkovic *et al.*, 2008; Wassgren *et al.*, 1996; Ottino and Khakhar, 2002).

Typical of particulate materials, if sufficient differences in particle physical properties in a vibration driven particle bed exist then the energy dissipation can lead to a variety of well know particle phenomenon (Section 1 in Chapter-1). Suitable vibration conditions leading to segregation can result in the formation of two distinct component layers in a binary particle mixture; this could form the basis for exploring a new particle separation system based on vibration driven particle segregation.

In any vibration driven particle bed it is customary to define the overall bed motion by the dimensionless vibration acceleration parameter, Γ which by definition is the ratio of peak container acceleration to that of gravity and is generally defined by Equation 2.1.

$$\Gamma = \frac{a\omega^2}{g} \qquad \text{Equation 2.1}$$

where, a (m) is the oscillation/vibration amplitude, g (m.s⁻²) is the gravitational acceleration, $\omega = 2\pi f$, is the angular frequency, Hz, π is a mathematical constant ($\pi = 3.141593$) whose value is the ratio of any circle's area to the square of its radius and f is the vibration frequency, Hz.

2.6 Segregation in vibrated particle beds

In particle technology, segregation can be defined as the separation of particles with different physical properties during their handling, storage and transportation (Sarkar and Khakhar, 2008; Ottino, 2006). Particle segregation looks simple but has extremely diverse and complex mechanisms. The onset of segregation due to differences in particle size has been observed for many years and many mechanisms have been proposed to explain this phenomenon (Rosato *et al.*, 2002; Jaeger, 1997). Particles with parallel physical properties are not generally expected to show any segregation. Whenever a sufficient difference in individual particle properties exists, segregation is most likely to result in particle mixtures (Kurdrolli, 2004; Ford *et al.*, 2009; Jha and Puri, 2009; Rosato *et al.*, 2002). In addition to size, differences in other particle properties such as density, shape, modulus of elasticity, friction coefficients, surface texture, adhesion and cohesiveness can also lead to segregation (Kurdrolli, 2004). However, the presence of large size variations in many working particle mixtures makes size segregation more accountable in comparison to the other types (e.g. density segregation) of segregation. Total segregation prevention can hardly be practised; however, complete understanding of its underlying mechanisms can help moderate its adverse effects to an acceptable level.

2.6.1 Vibration driven size segregation

As discussed earlier, size segregation can result from many different particle processing operations. A well-known example of this is the so called "Brazil Nut Effect" (BNE); in BNE large nuts are alleged to rise to the top surface of a shaken container which mostly comprises mixed nuts of small sizes (Rosato *et al.*, 1987; Knight *et al.*, 1993;

Rosato *et al.*, 1991; Jullien *et al.*, 1992; Duran, 2000; Kurdrolli, 2004; Duran *et al.*, 1993). However, there are conditions where BNE can be reversed; this phenomenon is extensively reported in literature (Shinbrot and Muzzio, 1998; Breu *et al.*, 2003) as "Reverse Brazil Nut Effect" (RBNE).

In addition to shaking, there are other mechanisms such as sifting, repose angle, trajectory, percolation, and elutriation that can lead to size segregation (Dolgunin *et al.*, 2006). However due to the limitations of this research work, detailed discussions will only be presented on vibration driven particle segregation.

2.6.1.1 The rise of coarse particles on vibration

When a mixture of different size particles is vibrated, the rise of coarse particles can be easily observed (Kurdrolli, 2004). One such example is the rise of a steel ball in a vibrated particle bed of small glass beads as shown in Figure 2.12.

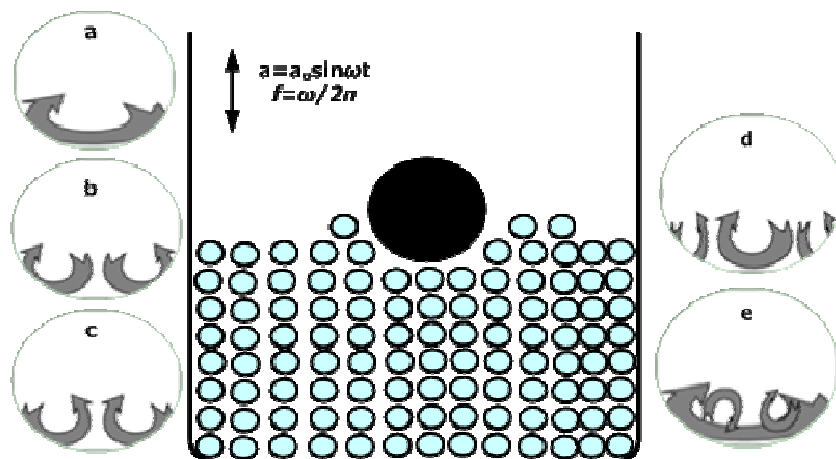


Figure 2.12: The rise of coarse particle on vibration and convection trends. "a" shows a single global convection current, "b & c" binary convection rolls and "d & e" multiple convection rolls in the vibrated particle bed.

Sufficient vibration acceleration and frequency will encourage the gradual rise of a large particle to reach the top particle bed surface (Kurdrolli, 2004). It is generally observed that this segregation effect will increase with increasing density of the large particle (Schröter *et al.*, 2006). The actual theory behind this effect is not very well understood, many mechanisms including void filling, static compressive force, convection, condensation, thermal diffusion, nonequipartition of energy, interstitial gas forcing, friction and buoyancy have been proposed to explain this (Schröter *et al.*, 2006; Serero *et al.*, 2006).

The action of container walls on fine particles will help in setting up convection currents (Knight, 1997; Knight *et al.*, 1996). The actual cause of this behaviour is still not clear (Serero *et al.*, 2006). However, one theory (Schröter *et al.*, 2006; Liffman *et al.*, 1997; Hsiau and chen, 2000) claims that the upward acceleration of particle bed during the vertical vibration cycle will result in particle bed compaction. This compaction will promote the induction of shear forces throughout the particle bed. As the particle bed moves down to complete the vertical vibration cycle it will experience a particle bed expansion. This bed expansion will result in boundary wall shear forces having a pronounced effect on the adjacent particles. The completion of these two phases will give rise to the development of convection rolls inside the vibrating particle bed (Schröter *et al.*, 2006; Liffman *et al.*, 1997; Hsiau and chen, 2000). The particle bed compaction and expansion effect during the course of vertical vibration has been proposed to increase with increasing wall friction (Knight, 1997). Taguchi (1992) proposed visco-elastic particle interactions as the prime cause for particle convection in a vibrated particle bed. The convection trend will depend on the type of particles and container geometry, amongst other some of the most commonly observed convection current trends are shown in Figure 2.12, where; (a) the whole container geometry is patrolled by a single convection current. The major convection current will

mostly follow the outer periphery which will be very close to the container wall boundaries. (b) Dual convection currents in an opposite direction to each other which will be falling in the centre and rising near to the wall boundaries of the vibrating container. These patterns resemble a valley shape as reported by Akoi *et al.*, (1996). (c) Dual convection currents in the opposite direction which will rise in the centre and fall near to the wall boundaries of the container and (d & e) distinct and multiple convection currents which will follow somewhat complex trajectories.

The convective particle motions inside the vibrated particle bed will result in lifting of large particles to the top particle bed surface (Knight *et al.*, 1993; Kurdrolli, 2004; Knight *et al.*, 1996). Once there, the large size of the intruder particles will prevent them from joining the overall convective motion of the predominantly small particles (Knight *et al.*, 1993; Kurdrolli, 2004). Hence, the position of large intruder particles will remain stable on top of the vibrating surface as long as no attempt is made to alter the other processing conditions (Knight *et al.*, 1993; Kurdrolli, 2004). A possible explanation of this trend is that, when a particle bed is shaken the particles enjoy the opportunity to rearrange themselves. This rearrangement is possible due to the particle bed expansion during bed flight. As the whole particle mixture is subjected to the gravitational and fluid drag forces (Figure 2.12), there is a great tendency for all particles to settle down. The majority of these particles are believed to settle down during their downward vibration phase. During the settling phase, the small particles generally wins in finding voids near edged up large intruder particles. Hence, the settling of small sized particles in vacant gaps near or directly beneath the surface of large intruder particles results in their gradual rise to the top surface (Rosato *et al.*, 1987; Duran *et al.*, 1993, Duran *et al.*, 1994; Rosato *et al.*, 2002; Thornton *et al.*, 2006).

Cooke *et al.*, (1996) proposed an equivalent slip plane and dislocation particle motion model for both particle bed and intruder particles in their BNE investigations. As the vibration amplitude was increased the inter particle voids became larger. These large voids were capable of accommodating big size particles. This can adversely affect the gradual rise of big particles to the top vibrating particle bed surface. Instead, a RBNE can be expected in this situation. In addition, the presence of an intermediate size particle can slow down the size segregation mechanism between large and small particles. Furthermore, it has been claimed (Rosato *et al.*, 1991) that the size segregation mechanism usually follows first order kinetics. This claim has been based on attainment of equilibrium states which are distinctly characterized by a balance between mixing and size separation (Rosato *et al.*, 1991). In the absence of any theoretical explanations about size segregation mechanisms Trujillo *et al.*, (2003), suggested that in the presence of gravity, the particle size differences will always give rise to a static compressive force that will lead to size segregation. Shishodia and Wassgren, (2001) have discussed the role of distinct particle buoyant forces on size segregation in a vibration driven size differential working particle mixture.

Some researchers (Yang, 2006; Campbell, 1990; Falcon *et al.*, 1999; Breu *et al.*, 2003; Tai and Hsiau, 2004) have proposed the introduction of a kinetic particle temperature " T_k " term that corresponds to the average kinetic energy of the random particle motion. Hsiau *et al.*, (2008) focused on relating particle temperatures with vibration acceleration and velocity in dry and wet particle systems by using a positron emission particle tracking (PEPT) system. They (Hsiau *et al.*, 2008) anticipated a rise of particle temperature with increasing vibration acceleration, this increase in vibration acceleration is also affected by the amount and viscosity of the surrounding fluid. Despite many reservations, many (Moon *et al.*, 2004; Soto *et al.*, 1999; Huan *et al.*, 2004; Wildman

and Huntley, 2003) have proposed the particle temperature in an analogy to a gaseous state. This is done by using the mean particle kinetic energy term of the type given in Equation 2.2;

$$T_k \propto \frac{1}{N} \sum_i \frac{m_i}{2} (v_i - \langle v \rangle)^2 \text{ where } \langle v \rangle = \frac{1}{N} \sum_i v_i \quad \text{Equation 2.2}$$

where, "N" is the total number of particles and "m_i" and "v_i" are the mass and the velocity of the ith particle and the symbol "<>" represent an average value.

The particulate materials have some distinguishing features that make them non analogous to a gaseous system, these aspects include rough particle surface, size, shape, mass and inelastic collisions (Herminghaus, 2005; Serero *et al.*, 2006). However despite this, various numerical (Moon *et al.*, 2004; Soto *et al.*, 1999; Serero *et al.*, 2006) and experimental studies (Huan *et al.*, 2004; Wildman and Huntley, 2003) have shown that "T_k" can be related to the particulate position, vertical vibration motion, acceleration and also to the number of particles in the container. In binary particle mixtures the heavy particles will generally have a high particle temperature in comparison to the lighter ones (Feitosa and Menon, 2002). Based on particle temperature theory, two different segregation mechanisms are recommended, which include phase transitions (Hong *et al.*, 2001) and momentum balance. Momentum balance is based on kinetic theory which makes use of the steady state Boltzmann equation (Trujillo *et al.*, 2003; Brey *et al.*, 2005; Garzó and Dufty, 2002; Galvin *et al.*, 2005; Garzó, 2008).

Hong *et al.*, (2001), proposed that when vibration acceleration is increased above a certain value, the whole particle bed of mono-dispersed particles will become vibrofluidized. They (Hong *et al.*, 2001) proposed a critical particle temperature term "T_c" for this fully vibrofluidized particle state based on the assumption that the initial particle mixture will be at spatially homogeneous temperature. Also for a binary particle mixture it was argued that the fluidised particles

will have a different critical temperature in comparison to those condensing at the bottom. Based on the differences in critical temperatures for binary species in a particle mixture the segregation relation shown as Equation 2.3 with control parameter, ε_{cond} , was proposed;

$$\varepsilon_{cond} = \frac{T_L^c}{T_S^c} = \left(\frac{d_L}{d_S}\right)^3 \frac{\rho_L h_L}{\rho_S h_S} \quad \text{Equation 2.3}$$

where, $\frac{T_L^c}{T_S^c}$ corresponds to the critical temperatures, $\frac{d_L}{d_S}$ to diameters, $\frac{\rho_L}{\rho_S}$ to the densities and $\frac{h_L}{h_S}$ to the fill heights of the large and small particles. The value $\varepsilon_{cond} = 1$, ($T_L^c < T_S^c$), will favour condensing of small particles while the large particles will fluidise, (BNE). However, when $\varepsilon_{cond} > 1$, RBNE will take place. This concept of critical temperature mapping of particle segregation is based on the condition that the driving regime temperature, "T" is an intermediate value between the two critical temperatures.

Hsiao and Hunt, (1996) proposed that in a gradient of temperature the heavy particles are expected to move to the places with low "T" value. Strong vertical temperature gradients were proposed in simulations (Bougie *et al.*, 2002; Moon *et al.*, 2004) and experiments (Huan *et al.*, 2004; Wildman and Huntley, 2003; Wildman and Parker, 2002; Losert *et al.*, 1999; Feitosa and Menon 2002). However, the complicated vibration temperature relationship generally fails to predict the type of segregation that can be expected at a particular particle temperature. In addition, nonequipartition particle issues have also been identified in particle size segregation (Galvin *et al.*, 2005; Brey *et al.*, 2005; Kurdrolli, 2004). Trujillo *et al.*, (2003), proposed a hydrodynamic model that introduced a pseudo-thermal buoyancy force which was proportional to the particle temperature ratio of two distinct particles. Sarkar and

Khakhar, (2008) recently reported experimental evidence from the effective particle temperature and size segregation approach.

Breu *et al.*, (2003) proposed that diameter ratios of the large and small particles in inverse relation to the corresponding density ratios will result in BNE and vice versa. Hence, in a binary particle mixture the probability of a particle species crossover to condense or fluidise can be predicted by the following simple relation, Equation 2.4;

$$\frac{d_l}{d_s} \approx \left(\frac{\rho_l}{\rho_s}\right)^{-1} \text{ where } \frac{d_l}{d_s} < \left(\frac{\rho_l}{\rho_s}\right)^{-1} = \text{BNE} \quad \text{Equation 2.4}$$

where, $\frac{d_l}{d_s}$ and $\frac{\rho_l}{\rho_s}$ are the respective diameter and density ratios of the large and small particles. Researchers (Nicodemi *et al.*, 2002; Tarzia *et al.*, 2004 and Tarzia *et al.*, 2005) have also demonstrated the use of a hard sphere lattice model approach to explain the particle size segregation phenomenon.

Different segregation forms in a particle mixture can be easily observed by driving the same particle mixture at different frequency levels. Consequently, at low frequency measurements, inertia and convective particle motion can lead to segregation (Huerta and Ruiz-Suárez, 2004). Also, in an equal sized binary particle mixture with a relative density difference >1 , convection mechanisms are considered as a predominant cause for segregation (Huerta and Ruiz-Suárez, 2004). At high vibration frequency levels, the subsequent increase in particle fluidization will generally result in suppressing the formation of particle convection currents. This situation may therefore lead to a buoyancy or sinkage mechanism to cause segregation (Huerta and Ruiz-Suárez, 2004).

In addition to focusing on particle size segregation mechanisms, Naylor *et al.*, (2003) also debated the role of interstitial fluid presence during segregation. They (Naylor *et al.*, 2003) proposed

that the presence of an interstitial fluid is not a necessary condition for size segregation. However, Möbius *et al.*, (2001); Akiyama *et al.*, (1998) and Kurdrolli, (2004) objected to this idea and highlighted the importance of interstitial fluid presence during size segregation. Sanders *et al.*, (2004) discussed the presence of an attractive force between multiple intruder particles, this inter-particle attractive force between identical particles may be the basis for observing strong collective particle bed behaviour during vertical vibration.

It is mainly due to the complex nature of the size segregation phenomenon that researchers (Kurdrolli, 2004) have focused on a narrow range of conditions in an effort to identify the dominant mechanisms. However, despite all these simplifications, contradictory results on the same phenomena are fairly common (Jaeger, 1997; Huerta and Ruiz-Suárez, 2004). Furthermore, a variety of investigation tools such as computer simulations and experimentation have been used to increase the body of knowledge on segregation mechanisms and other particulate phenomena (Campbell, 1990; Jaeger and Nagel 1992; Jaeger *et al.*, 1996; de Gennes, 1999; Kadanoff, 1999; Kudrolli, 2004; and Julio, 2005).

The underlying mechanisms of size segregation have also been observed to depend on driving conditions (e.g. vibration) and particle parameters. The interdependence of these two parameters is not known, for example, the relationship between particle size and density to promote segregation in a particle system is still unidentified. In gravity driven particle flows down inclined chutes, strong size segregation effects in comparison to the density segregation can be observed (Rosato *et al.*, 2002). This leads us to a somewhat more complex situation in our efforts to completely understand size segregation. As efforts continue to completely understand the particle segregation phenomena, some researchers (Akiyama *et al.*, 2000; Ohtsuki *et al.*, 1995; Jain *et al.*, 2005;

Mohabuth, 2007, Burtally *et al.*, 2002 & 2003) have looked into the effects of particle density on segregation.

2.6.2 Vertical vibration driven density segregation

External excitations such as vertical vibration can drive an equal size but different density particle mixture to segregate based on differences in particle buoyant forces (Jain *et al.*, 2005; Akiyama *et al.*, 2000; Ohtsuki *et al.*, 1995; Jain *et al.*, 2005; Mohabuth, 2007, Burtally *et al.*, 2002 & 2003). Only a limited amount of reported literature is available on density segregation when compared to size segregation (Akiyama *et al.*, 2000; Burtally *et al.*, 2003, Mohabuth and Miles, 2005; Mohabuth *et al.*, 2007 and Leaper *et al.*, 2005). In density segregation, equal size particles can separate into two different particle layers with denser particles appearing on the top in a vibrating particle bed (Shrinbot and Muzzio, 1998; Shishodia and Wassgren, 2001; Mohabuth and Miles, 2005). The situation becomes even more complex when the working particle mixtures differ both in size and density (Jain *et al.*, 2005).

Hong *et al.*, (2001) used hard particle simulations to study reverse buoyancy effects on high density particles. In their (Hong *et al.*, 2001) investigations, as the density ratio between the intruder particle and particle bed was increased, the dense intruder particle was observed to sink and vice versa. Liffman *et al.*, (2001) investigated the two dimensional motion of an intruder particle in a non-convective particle bed. Hollow steel discs with the aim to vary the relative particle density ratios by filling them with a high density material were used in a particle bed of glass particles. They (Liffman *et al.*, 2001) observed a drop in the intruder rise time, " t " (seconds) with increasing relative particle density ratios which followed a trend, shown in Figure 2.13.

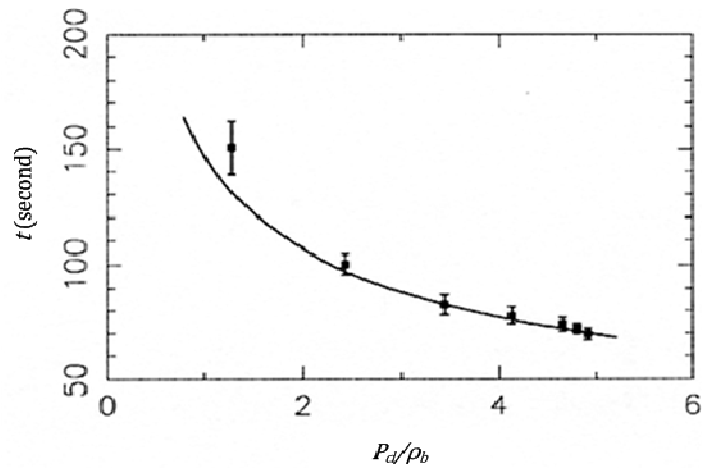


Figure 2.13: Rise time vs particle diameter to density ratio in a fixed size ratio binary particle mixture (Adapted from Liffman *et al.*, 2001).

Akiyama *et al.*, (2000) failed to show any particle layer separation of glass and steel particles in the range of vertical vibration they investigated (dimensionless acceleration between 0 and 10 at a fixed vertical vibration frequency of 50Hz). However, introduced the concept of solid-solid extraction by separating equal sized ($d=1290\mu\text{m}$) glass ($\rho=2500\text{kg.m}^{-3}$) particles from a mixture with lead ($\rho=11389\text{kg.m}^{-3}$) and steel ($\rho=7850\text{kg.m}^{-3}$) particles under vertical vibration as shown in Figure 2.14.

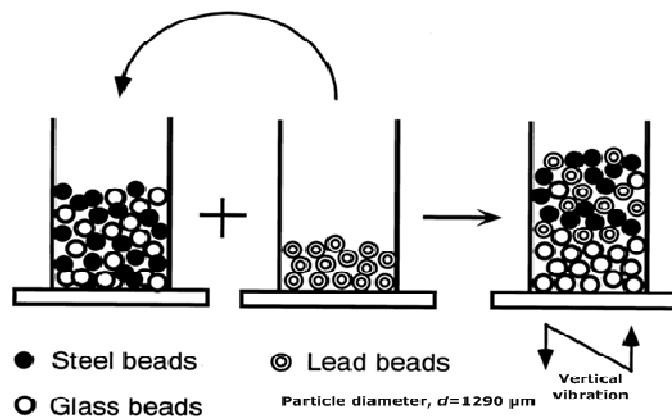


Figure 2.14: Solid-solid extraction (Adapted from Akiyama *et al.*, 2000).

Akiyama *et al.*, (2000) proposed that in a particle mixture of glass, steel and lead particles the individual differences in particle momentum can be the prime cause for high density lead and steel particles to appear on top of a vibrated particle bed surface. When a particle bed sets into motion with the vibration acceleration magnitude significantly greater than 1g, dense particles are expected to gain a high momentum value, mainly due to their high mass content. If the acceleration is only in one vertical direction, dense particles will travel furthest in this direction during their particle bed expansion cycle. This will result in an opportunity for low density and low momentum particles to settle down in their next compaction cycle during vertical vibration. These successive vertical vibration cycles will result in a particle bed stratification based on density effects. A further increase in vibration acceleration value above this point will eventually result in chaotic particle bed motions. This chaotic stage can be blamed to suppress the particle bed stratifications. Hence, for a layered particle separation to take place it is generally more desirable to vertically vibrate a particle bed at small frequency and higher amplitudes.

Figure 2.15 shows three different particle convection mechanisms as observed by Akiyama *et al.*, (2000) in experiments at different acceleration values.

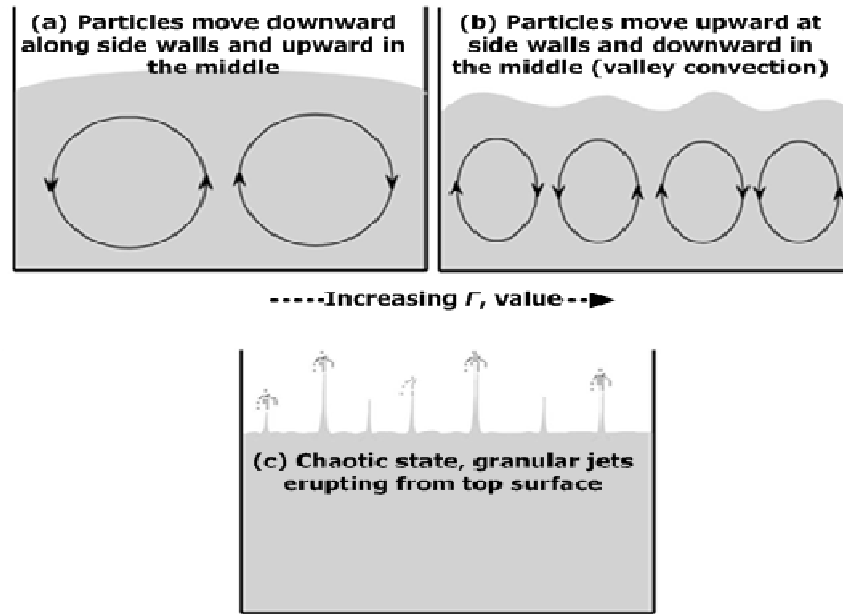


Figure 2.15: Particle bed behaviour under vertical vibration of increasing accelerations (a-c) (Adapted from Akiyama *et al.*, 2000).

In Figure 2.15 it can be seen that a lower acceleration value (a) resulted in a single convection heap rising in the middle and falling near to the walls. A further increase in acceleration showed valley convection currents (b) that eventually resulted in a chaotic particle bed state (c).

Scaling up and/or down has always been an issue with all particle handling systems (Ottino and Khakhar, 2002). Akiyama *et al.*, (2000) therefore used four different kinds of vessels that all comprised a 3 cm thickness and 3, 5, 7 and 10 cm widths to investigate scaling effects associated with the particle vibration system. An increase in vessel width to 7 cm resulted in a limited inverse density segregation. Under the experimental conditions of Akiyama *et al.*, (2000), the inverse density segregation finally diminished when their vessel width was increased to 10 cm. Best density segregation results were claimed with a small 3cm width vessel. Akiyama *et al.*, (2000) have also debated the relationship between particle size and critical vibration acceleration, Γ_c (a point

where bed stratification can be first observed). Comparison made in their work (Akiyama *et al.*, 2000) with others revealed an increase in dimensionless acceleration value with an incremental rise in particle size during vertical vibration. Other notable observations in their work (Akiyama *et al.*, 2000) included the less favourable conditions for convection current developments in high density particulate materials. Based on these observations they (Akiyama *et al.*, 2000) suggested the use of a low particle bed height for convection roll development in a vibrated particle bed of high density materials. One of the reasons for diminishing particle convection rolls in their work can be the use of big particle sizes which were hard to vibro-fluidize under their experimental conditions.

The particle size importance associated with particle processing operations (e.g. component liberation is in close association with particle size), possibly directed Burtally *et al.*, (2002 & 2003) to focus their attention on finely sized particles in their density segregation studies. They (Burtally *et al.*, 2002 & 2003) used various glass ($\rho_g=2500\text{kg.m}^{-3}$) and bronze ($\rho_b=8900\text{kg.m}^{-3}$) particle bed combinations in their experimental investigations. They proposed a new density separation parameter, " S_d " derived from Stokes' law and the equation of motion of two individual particles. General forces acting on a single particle in air are shown in Figure 2.12. The proposed new " S_d ", factor is defined by Equation 2.5 as;

$$S_d = \frac{\rho_2 d_2^2}{\rho_1 d_1^2} \quad \text{Equation 2.5}$$

where " d_1 & d_2 " and " ρ_1 & ρ_2 " with $\rho_2 > \rho_1$, are the diameters and densities of the respective segregating particles. The particle separation factor, " S_d " implies that when, $S_d \neq 1$, different particles will experience a different drag force in their surrounding fluids (Burtally, 2004; Biswas *et al.*, 2003). As a result, high density

particles will travel furthest and condense with a time lag in comparison to the light particles. A few vibration cycles will result in gradual density segregation and stratification of the particle bed. Furthermore, for an equal size particle mixture, the S_d -factor value reduces to density ratio of the particles. Many assumptions have been taken into consideration in deriving this relationship, for example, fluid drag was considered to be the only resistance force to the segregating particles. The value of this drag force was considered to be in a range where the introduction of a correction factor was not deemed necessary. This theory marked air drag to be the crucial factor for density separation behaviours of glass and bronze particles (Burtally, 2004).

Klein *et al.*, (2006) probably realised the importance of interstitial gas on density segregation and therefore investigated the surrounding fluid effects on a particle bed of equal size ($d=98\pm 8\mu\text{m}$) glass and bronze particles that were vertically vibrated. Their (Klein *et al.*, 2006) apparatus shown in Figure 2.16 was fairly similar to the one used by Burtally, (2004) which is shown in Figure 2.18.

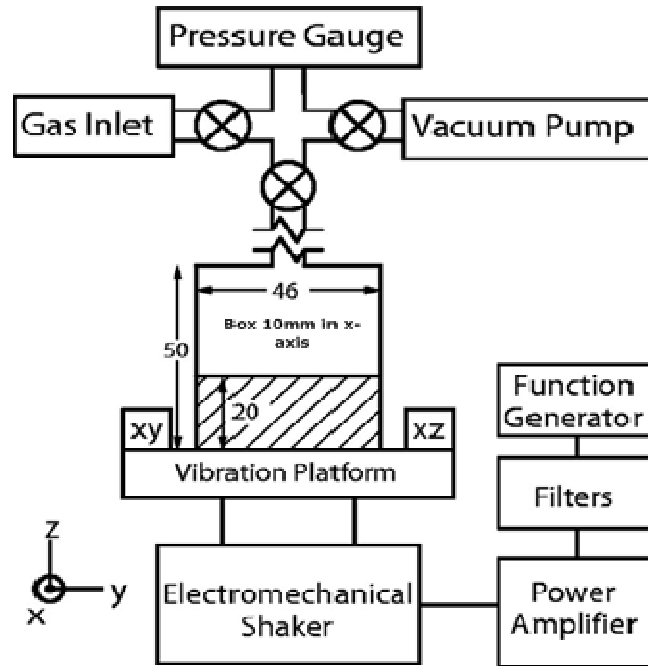


Figure 2.16: Apparatus used by Klein *et al.*, 2006.

Klein *et al.*, (2006) carried out their investigations in a frequency " f " range of 0 to 200Hz and with dimensionless acceleration, " Γ " of between 0 and 20. They used Nitrogen, N_2 (viscosity= $17.9\mu\text{Pa}\cdot\text{s}$) and neon, Ne (viscosity= $32.1\mu\text{Pa}\cdot\text{s}$) as their interstitial fluids. The experiments were carried out at room temperature in a vibration driven particle cell shown in Figure 2.16. In their investigations (Klein *et al.*, 2006), the fluid viscosity was supposed to be independent of gas pressure ($P > 25\text{Torr}$). The observed particle bed behaviours under different operating conditions are shown in Figure 2.17.

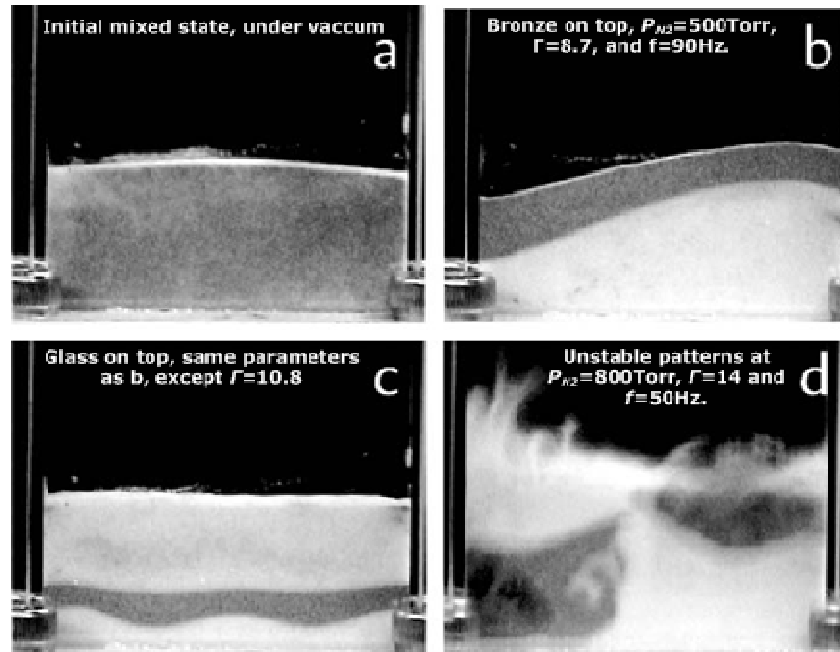


Figure 2.17: Particle bed behaviours under vertical vibration. P_{N_2} represents the nitrogen gas pressure in the vibrating cell (Klein *et al.*, 2006).

The observations revealed in Figure 2.17 were similar to the density segregation trends reported by Burtally *et al.*, (2002 & 2003) and Biswas *et al.*, (2003). It was observed that bronze particles were relatively more mobile in the chosen working fluids (Klein *et al.*, 2006). The bronze particles travelled a distance that was nearly three times longer than the glass particles. It is generally acknowledged that particle deceleration resistance in any interstitial fluid is inversely proportional to the particle mass content (Klein *et al.*, 2006). Further investigations reported by Klein *et al.*, (2006) revealed significantly different particle bed behaviours in the working fluids (N_2 and N_e). The dependence of density segregation behaviour on gas viscosity was more significant at low vibration frequency ($f=50\text{Hz}$) than in comparison to what was observed at high value ($f=90\text{Hz}$). Furthermore, as the gas pressure was reduced below 50Torr, bronze top layer behaviour was observed to diminish.

Klein *et al.*, (2006) suggested that the formation of a thick bronze top layer has the ability to suppress the low density glass particles to appear on top of the vibrating particle bed surface. However, at high values of vibration frequency and amplitude glass particles have the ability to overcome this resistance and appear on top as shown in Figure 2.17. In conclusion Klein *et al.*, (2006) proposed that in addition to vibration frequency and acceleration, density segregation is also a sensitive function of interstitial gas pressure and viscosity.

Burtally *et al.*, (2002) reported the spontaneous particle separation of similar size glass and bronze spheres driven by vertical vibration in the presence of air only. The experimental setup used by Burtally *et al.*, (2002 & 2003), Burtally, (2004) and later in the vibration separation work extended by Mohabuth and Miles (2005), Mohabuth *et al.*, (2007) and Mohabuth, (2007); is shown in Figure 2.18.

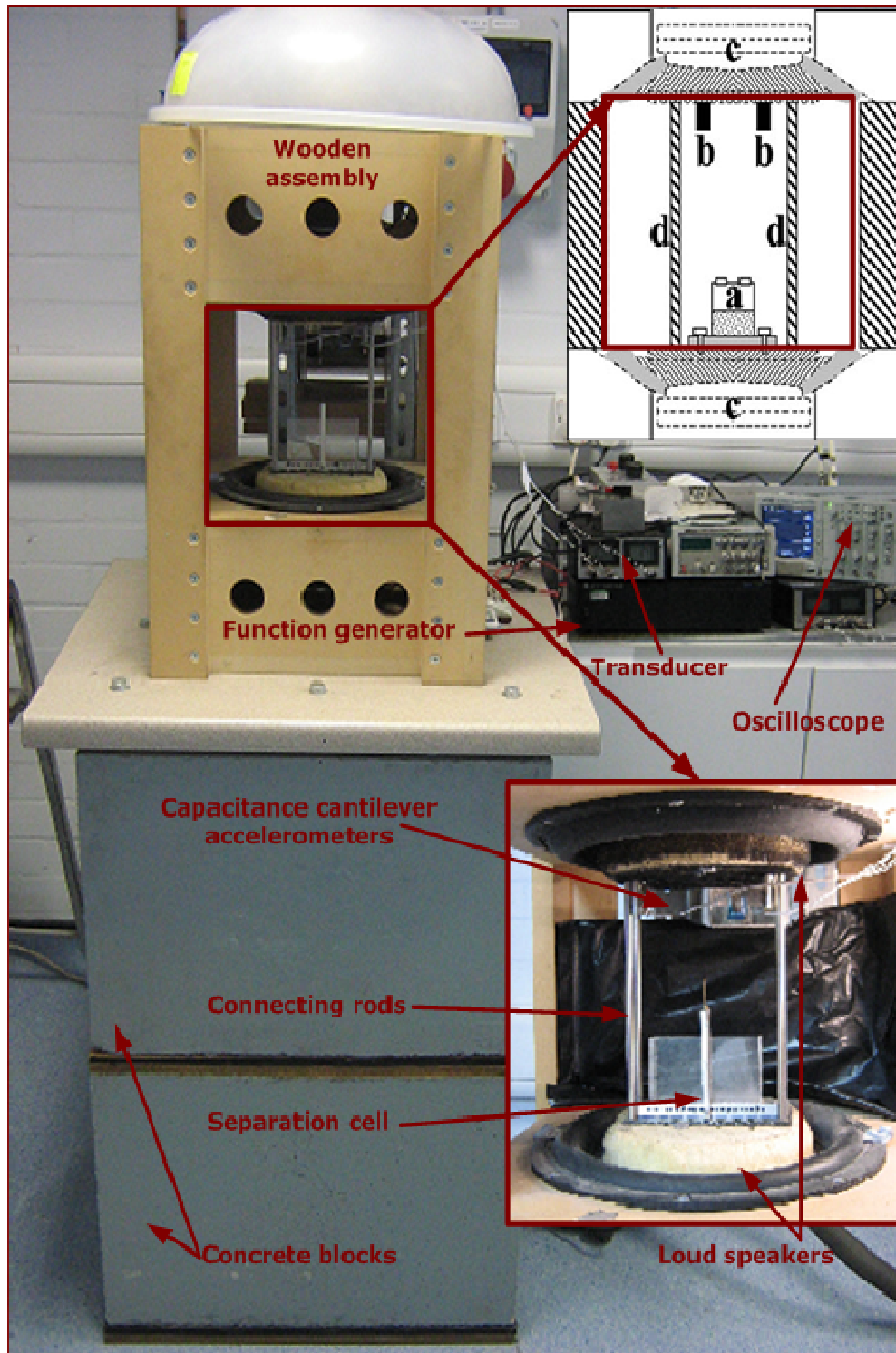


Figure 2.18: Vertical vibration setup, where, (a) is the particle segregation box, (b) accelerometers, (c) double transducer assembly and (d) is the connecting frame.

The working principle of the setup shown in Figure 2.18 is rather simple and is similar to the working rig shown in Figure 2.16 with only a few exceptions. In the later experimental setup, two interconnected and aligned vibration platforms were used without any gas supply mechanism to the vibrating box as shown in Figure 2.18. In both cases (Klein et al., 2006 (Figure 2.16) and Burtally, 2004 (Figure 2.18)) an electromechanical shaker was used to generate vertical vibration in a horizontal platform. The particle matter under investigation was placed in a transparent box on the horizontal platform. The transparent boxes were used for the ease of visualisation of particle pattern during density segregation.

The experimental conditions used by Burtally *et al*, (2002 & 2003) and Burtally, (2004) ranged from $f=10$ to 200Hz and Γ , (the ratio of peak container acceleration to that of gravity) between 1 and 18. Four different glass and bronze working particle mixtures (A, B, C & D) with three different compositions (1, 2 & 3) as shown in Table 2.2 were used in their studies.

Mixture	A	B	C	D	1	2	3
Material	Bead Diameters (μm)				Volume percentage		
Bronze	125-150	90-125	63-90	45-53	25%	50%	75%
Glass	63-90	90-125	125-150	125-150	75%	50%	25%

Table 2.2: Four distinct working particle mixtures (A, B, C & D) with three different compositions (1, 2 & 3) as used by Burtally *et al*, (2003 & 2004) and Burtally, (2004) (Adapted from Mohabuth, 2007).

The separation behaviour of each of the twelve particle mixtures as shown in Table 2.2 was visually observed and was presented as $f\Gamma$ phase diagrams. An example of their reported $f\Gamma$ phase diagrams is shown in Figure 2.19.

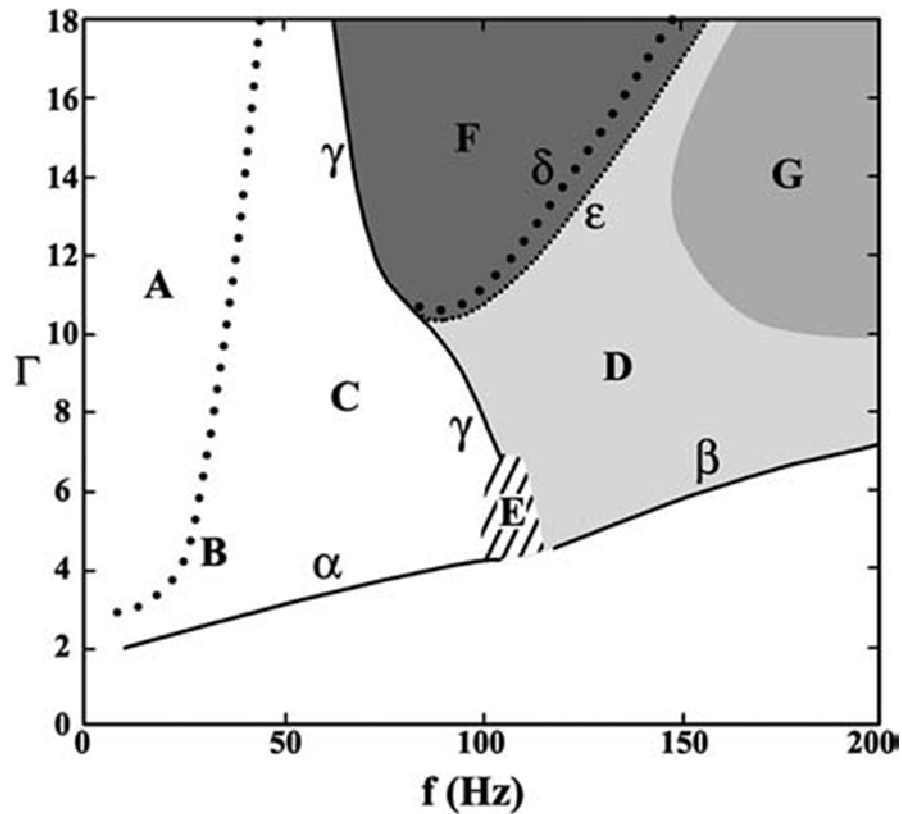


Figure 2.19: Visualized behaviour of mixture B1 in air, as a function of f & Γ showing the onset of bronze on top (α), sandwich separation (β), the transition boundary between the two (γ), onset of slow (δ) and rapid (ϵ) asymmetric inversion oscillation. Also (A) & (C) represents bronze on top, particle throwing and interface thrashing (A), tilt formation (B), sandwich formation (D), Oscillation between bronze on top and sandwich configurations (E) and continuous asymmetric oscillations (F) and the area of continuous symmetric oscillations (G) (Adapted from Burtally *et al.*, 2003).

The visually captured particle bed behaviours at different stages represented in Figure 2.19 are shown in Figure 2.20.

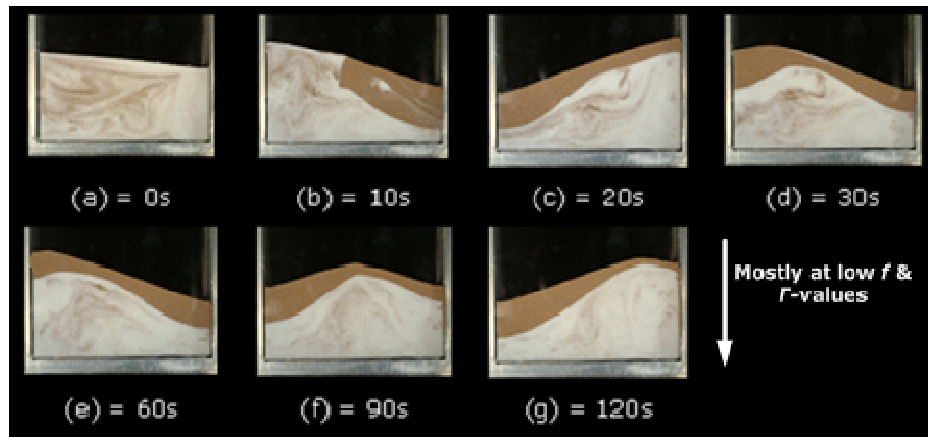


Figure 2.20: An initially well mixed bed of 90-125 μ m glass and bronze spheres separating into the bronze on top regime when vibrated at $f = 40\text{Hz}$, $\Gamma = 3.0$, in an 80mm high x 80mm wide x 10mm thick, glass lined cell with bronze at 25% and glass 75% by volume (B1). (N.B. S = seconds) (Adapted from Burtally *et al.*, 2003).

Figure 2.20 shows (a) an initially well mixed glass and bronze working particle mixture (B1). As the working particle mixture (B1) was vertically vibrated (b) a bronze on top configuration with a tilt formation in (c) left and (d) right direction was visually observed. The formation of a tilt was attributed to the generation of distinct global convection currents in each of the two particle phases that also resulted in separation of the particle mixture within the first 120 seconds of vertical vibration treatment. The formation of a stable tilt (e, f & g) was accompanied with maintaining of a clear cut separation boundary between the two particle phases.

The overall observations from their (Burtally *et al.*, 2002 & 2003; Burtally, 2004) experiments showed a number of interesting behaviours, for example, at low frequency and acceleration of vertical vibration, a number of particle mixtures were observed to form separate glass and bronze rich layers as shown in Figure 2.20. The boundary layer thickness between glass and bronze rich regions, in some instances, was observed to be only one or two

particle diameters. The high density particle layer was observed to appear on top of the particle bed surface. However, there were experimental conditions where high density particle layers formed a sandwich between two glass rich regions (Burtally *et al.*, 2002 & 2003; Burtally, 2004). Another striking observation from their (Burtally *et al.*, 2002 & 2003; Burtally, 2004) experiments was the formation of a stable particle tilt which is also reported by others (Mohabuth, 2007; Leaper *et al.*, 2005). An example of this tilt formation is shown in Figure 2.20. The observed particle separation in these experiments was quick which increased with increasing, Γ -value. Most of the particle separation was observed within the first two minutes of vertical vibration treatment. Visual observations were used to judge the “*substantially complete*” particle separation (Burtally *et al.*, 2002 & 2003; Burtally, 2004). Visual observations also showed the presence of some bronze particles in glass rich regions. However, glass particles were hardly seen in any bronze rich regions under layered particle separation regime as shown in Figure 2.20.

The change in working particle mixture composition from B2 to B3 (working particle mixture compositions given in Table 2.2) resulted in somewhat similar dry based particle separation behaviours as represented in Figure 2.19. Of particular interest was the observance of a bronze on top configuration in each case that can be possibly recovered separately. Sharp and stable separation boundaries between the glass and bronze rich regions in this case (working particle mixtures B1, B2 and B3 as given in Table 2.2) were also normally observed within the first two minutes of optimum vertical vibration treatment (Burtally *et al.*, 2002 & 2003; Burtally, 2004).

As the size ratio between the glass and bronze working particle mixtures was changed to A, C and D (working particle mixture compositions given in Table 2.2), the observed dynamics showed

the following key differences from the benchmark mixture-B (Composition given in Table 2.1) (Burtally *et al.*, 2002 & 2003; Burtally, 2004);

- In mixture-A (composition given in Table 2.2), comparatively more glass infiltration was observed in the big size bronze rich regions after vertical vibration.
- The particle bed dynamics were comparatively faster in mixture-A (composition given in Table 2.2).
- For mixture-C (composition given in Table 2.2), poor glass and bronze separation was observed. This is probably because of the fact that large particles behave rather similarly to the high density particles during vertical vibration. In the current situation (mixture-C, composition given in Table 2.2) the particle size of low density glass particles was potentially enough to entrain the small size bronze particles in their overall convective motions (mixture-C2 & 3, composition given in Table 2.2). However, considerable density segregation was still observed in mixture-C1 over a narrow range of vertical vibration frequencies ($f=25-90\text{Hz}$) and at low Γ -values. It can be observed from this situation that the relative particle concentration differential can affect particle separation behaviours under the influence of vertical vibration.
- In mixture-D (composition given in Table 2.2), the relative working particle size differences were comparatively big than all of the above cases (mixture A, B, & C; compositions given in Table 2.2). Hence, a "glass on top" configuration was mostly observed at low vertical vibration frequency, f and Γ values. At high " f " and " Γ " values, distinct and localised particle concentrates were clearly visible in the particle bed, which was far from stable.

The overall effects mentioned above can be summarized based on the definition of separation factor " S_d ", given by Equation 2.5;

- For mixture-A (composition given in Table 2.2), $S_d \approx 12$, a value which is significantly greater than 1 hence, a bronze on top configuration was observed with sharp separation boundaries.
- For mixture-B (composition given in Table 2.2), $S_d \approx 3.6$ a value still greater than one and hence resulted in good particle segregation with bronze on top configuration.
- For mixture-C (composition given in Table 2.2), $S_d \approx 1$ and this showed a weak segregation tendency in comparison to mixtures-A and B.
- For mixture-D (composition given in Table 2.2), $S_d \approx 0.4$ and a glass on top regime was observed during density segregation.

Among other things, the investigations (Burtally *et al.*, 2002 & 2003; Burtally, 2004) also highlighted the importance of interstitial fluid on particle density segregation. The large particle size of glass in mixture-C and D was possibly not sufficiently influenced by air motion during vertical vibration; this can be one of the main reasons for the poorly observed particle segregation behaviour in these cases.

2.6.3 Vertical vibration induced particle segregation and the surrounding fluid

The particle mixtures can be made to disperse in vacuum and/or in an interstitial fluid. Air and water are the most common types of interstitial fluids that are used to fill in the inter-particle spaces and/or voids in a particle mixture (Liao and Hsiao, 2010). If the interstitial fluid is a gas such as air, the particulate material is said to be in a dry state (Chou, 2000). When the particles do not adhere

to each other, the particulate material is said to be cohesion-less. Nevertheless, the dynamic behaviour of a particle mixture in the presence of an interstitial fluid can essentially be treated as a multiphase flow phenomenon (Campbell, 1990; Chou, 2000). Some examples of the multiphase flow behaviour can be seen in particle mixtures that are subject to external vertical oscillations (Burtally *et al.*, 2002, 2003; Leaper *et al.*, 2005; Majid and Walzel, 2009). In addition to the interstitial fluid effects, a distinguishing feature of the slowly deforming, or quasi-static particle flow (such as the one under the influence of vertical vibration), is the existence of direct inter-particle interactions that can play an important role in the overall flow mechanics of a particle mixture (Campbell, 1990; Chou, 2000). It has been proposed that in a closely packed finely sized particle mixture the inter particle interactions are generally dominant and are expected to play a greater role in the overall particle momentum transports in which case the interstitial fluid behaviour can be largely ignored in describing the quasi-static particle flow behaviours (Campbell, 1990; Jaeger *et al.*, 1996; Chou, 2000). However, others (Akiyama, *et al.*, 1998; Gutiérrez, *et al.*, 2005; Hsiau *et al.*, 2004; Pak *et al.*, 1995; Klein *et al.*, 2006) have stressed the importance of interstitial fluids in controlling the slowly deformed particle dynamics. Nevertheless, a significant fraction of energy and momentum transfer is expected to occur when the dynamic particles are in contact with each other and/or with a solid boundary that is neighbouring their motions (Zeilstra *et al.*, 2008).

Burtally (2004) carried out investigations to underline the importance of interstitial fluid behaviour during density segregation. To highlight the importance of particle size on density segregation, in the presence of air, glass and bronze particles of size greater than 350 μm were first used. She (Burtally, 2004) observed poorly defined glass and bronze rich regions at low vibration frequency that diminished at high values. In addition, experiments carried out at reduced air pressures with finely sized working particle mixtures A1

and B1 (composition given in Table 2.2) resulted in observing poor segregation effects. Hence, the presence of an adequate viscosity surrounding fluid was considered to be important for any density segregation to take effect.

A further investigation on density segregation in the presence of air was carried out by Burtally (2004). First, with mixtures A1 and B1 (composition given in Table 2.2) no separation was observed when the top of the particle box with a porous bottom was open to atmosphere. However, when the top of the same box was closed, density segregation with sharp separation boundaries was clearly observed. She suggested that in this case the forced air motion drawn through the vibrating particle bed bottom and forced backed into the particle mixture in a closed box was the prime cause for particle segregation. This convective air motion can be seen as an analogy to the convection currents in the vibrated particle phase, when a closed box is used, the presence of air convective currents could have been one of the motives for generating distinct convection currents in vibrated particle bed and hence resulting in particle segregation. For large size particles, investigations carried by Burtally (2004), in air failed to show any particle density segregation. This may be due to the low viscosity and powerlessness of the surrounding air medium to entrain the large size particles. Naylor *et al.*, (2003) used the same box to suggest parallel trends in particle size segregation in the presence of air. The influence of surrounding fluid on segregation of vertically vibrated working particle mixtures is also investigated in the work of Liao *et al.*, (2010) and Yan *et al.*, (2003).

Leaper *et al.*, (2005) used water as a surrounding medium in their experiments to investigate the influence of fluid viscosity on density segregation of large size spherical particles. The use of water resulted in a fifty fold increase in viscosity of the surrounding medium in comparison to air. It was assumed that this increase in

viscosity of the surrounding medium can help separate particles seven times bigger, in comparison to air alone. The use of water also offered an added advantage of eliminating static electricity among vibrating particles. Leaper *et al.*, (2005) used the same apparatus and vibration cell as reported by Burtally *et al.*, (2002 & 2003) and Burtally, (2004). An average particle bed height of 20 mm in the presence of water with vibration frequencies ranging from 0 to 200Hz and a dimensionless acceleration of 0 to 10 were used in their (Leaper *et al.*, 2005) investigations. The top of the box was closed with a rubber bung to avoid any abrupt air or water motion during vertical vibration. The air bubble free box was then placed on the loudspeaker platform in the vibratory apparatus as shown in Figure 2.18.

The separation of equal size glass and bronze particles in the size range of 90-125 μm , 150-200 μm , 300-355 μm , 600-710 μm and 1000-1180 μm , made up a 50:50 volume mixtures in all the investigated cases reported by Leaper *et al.*, 2005. In the presence of water sharp particle separations in the bronze and glass rich regions were observed for all the parallel sized particle mixtures. However, the presence of a high viscosity surrounding fluid resulted in a relatively greater resistance to particle motion. As a result, particle segregation in water was observed to occur on a time scale of several hours, much higher than that observed by Burtally, (2004) in air. The particle segregation mechanism of a 50:50 volume percentage 300-355 μm glass and bronze particles is shown as an example on an x - z plane in Figure 2.21.

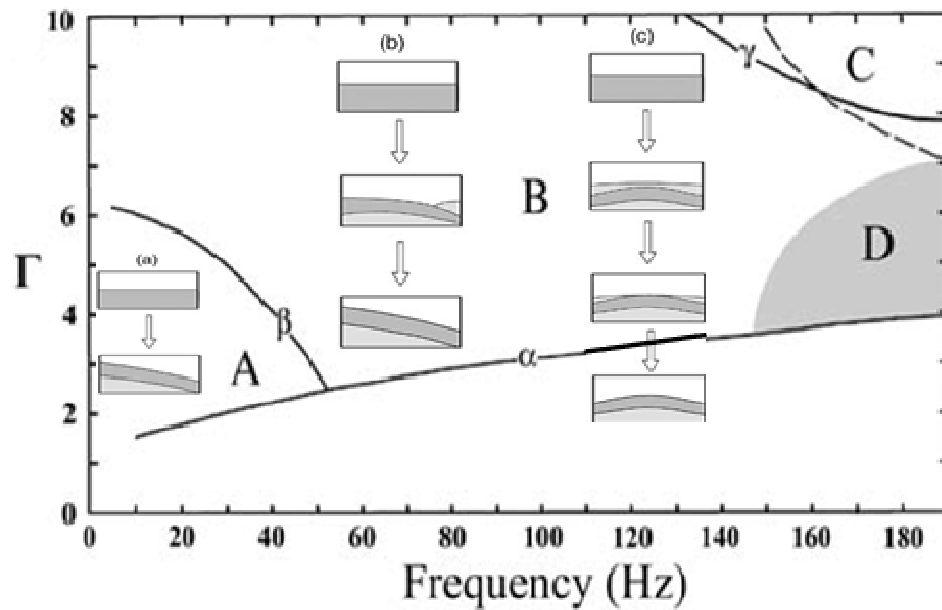


Figure 2.21: The behaviour of 50:50 volume percentage mixture of 300-355 μm glass-bronze particles submerged in water. (A) Represent a tilted bronze on top configuration, (B) tilted bronze on top via tilted sandwich configuration, (C) symmetric bronze on top via symmetric sandwich configuration, (D) represents the incomplete separation region and the line " α " represents the Γ value where cluster formation was seen in two minutes of vertical vibration. The light and dark gray colours in (a), (b) and (c) represents the low and high density materials (Adapted from Leaper *et al.*, 2005).

The particle tilt formation in the work of Leaper *et al.*, (2005) was of similar construction (zone-A in Figure 2.21) as seen in Figure 2.20. An increase in vertical vibration frequency resulted in a slightly different particle bed behaviours (zone B & C in Figure 2.21). However, even at these high frequency values all particle beds eventually resulted in a bronze on top configuration after the elapse of a sufficient stabilization time. Difficulties were encountered in separating 1000-1180 μm size particles in water; this was especially troublesome at frequencies higher than 100Hz. The formation of a global convection current at this size range actually hindered the

particle segregation affects. This resulted in a somewhat similar situation represented as D-zone in Figure 2.21. The use of 75:25 volume percentage 300-355 μm bronze and glass particles still resulted in bronze on top configurations. However, the disappearance of zone-C (Figure 2.21) in their (Leaper *et al.*, 2005) β - Γ phase map was attributed to the greater bronze population that lowered the probability of a sandwich configuration. Reversing the particle concentration of bronze and glass to 25:75 volume percentages resulted in a comparatively slower bed dynamics however; bronze on top configuration still prevailed in this case. Poor particle separation was observed when a 50:50 volume percentage bronze (200-300 μm) and glass (1000-1180 μm) working particle mixture was vertically vibrated in water. Similar situations were also encountered in other big size differential bronze and glass particle mixtures. Hsiau *et al.*, (2004) suggested that with a greater amount of water, the rising velocity of the larger beads decreases due to the viscous and liquid bridge forces between the water and beads. Akiyama *et al.*, (1998) reported that in a vertically vibrated particle bed of finely sized particles, the surrounding air and the particle bed height plays an important role in generating the convection currents that lead to particle bed heaping. Gutiérrez *et al.*, (2005) reported that an air-mediated fluidization mechanism similar to that occurring in gas-fluidised static beds is responsible for particle segregation in a vertically vibrated particle bed. Pak *et al.*, (1995) suggested that the gas trapped in the vertically vibrated particle bed is responsible for heaping. The effect of surrounding air on the segregation of particles in a shaken particle bed is also reported in the work of Yan *et al.*, (2003).

In summary, large size particles can be made to segregate in the presence of high viscosity fluids such as water. The observed density segregation behaviours with large particles in water (Leaper *et al.*, 2005) were quite similar to the ones observed in the finely sized particles in air (Burtally, 2004). However, discrepancies were

found in achievement of a total segregation time for “substantial separation”. The use of a viscous fluid such as water during the vertical vibration segregation resulted in strong buoyant forces on particles which probably reduced their settling rates. All this contributed in the slow segregation dynamics of the large sized particle mixtures in the presence of water.

2.6.4 Particle bed tilting and distinct convective motions

In the majority of the previously reported particle segregation studies (Section 2.6) some pronounced particle bed behaviours can be clearly observed. Examples include, particle bed tilting (Figure 2.22) and the formation of distinct convection currents during vertical vibration (Figure 2.22). Under suitable conditions, when a noncohesive particle bed is vertically vibrated with sufficient acceleration it tends to form a tilt. An example of this, when an initially flat pile of dry noncohesive sand is vertically vibrated with sufficient dimensionless acceleration ($\Gamma > g$), the spontaneous appearance of a slope is normally observed (Mehta, 2007). This slope forms an angle “ θ ” with the base as shown in Figure 2.22.

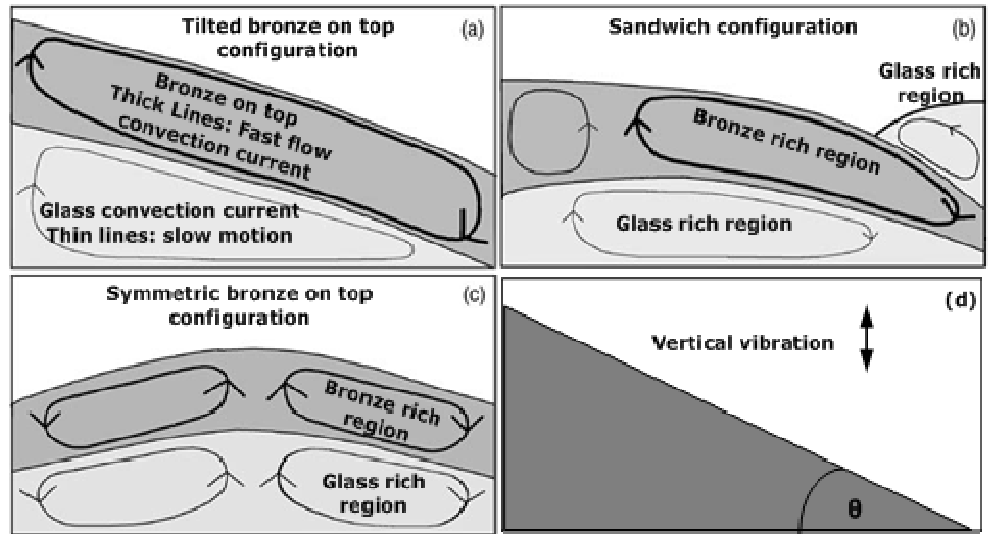


Figure 2.22: Particle convection currents in glass and bronze rich regions in the presence of water at different frequency and acceleration values (a, b & c) as reported by Leaper *et al.*, (2005).

Figure 2.22 shows bronze on top particle segregation regime along with the sketched global and local convection current patterns. In Figure 2.22, (a) represents the global convection currents in the tilted and segregated glass and bronze particle bed whereas in (b & c) a couple of local glass and bronze convection currents are shown which have reduced particle bed tilting in comparison to (a). The angle " θ " shown in Figure 2.22 is often referred to as angle of repose and is normally maintained by particle flow down the slope (Mehta, 2007). It is widely believed that the convection induced particle bed tilting behaviour was first scientifically addressed by Faraday (1831) and is therefore often referred to as "Faraday Tilting" (Kong *et al.*, 2006). Faraday, (1831) believed that vertically vibrating particles in a container will promote surrounding air currents (Milburn *et al.*, 2005). As the bed flights from surface during upward cycle in vertical vibration, a reduced air pressure beneath the particle bed will draw particles to land near the centre of the bed. The rest of the particle bed will then fall later in such a way to offset the surrounding forces, resulting in a particle tilt and/or heap formation (Thomas and Squires, 1998). Others

(Kakalios, 2005) have linked particle tilt formation to the relatively more kinetically active particles near the vibrating base. However, some believe that more kinetically active particles condense near to the top vibrating particle bed surface (Mehta, 2007).

Milburn *et al.*, (2005) carried out their particle tilting experiments in the presence of water. They observed that particle tilting can be readily seen over a wide range of conditions in fine size particle beds in comparison to the particle beds that are comprised of large size and more dense particles. They (Milburn *et al.*, 2005) reported that the horizontal fluid motion during particle bed flight under vertical vibration was mainly responsible for particle bed tilting. In the presence of air, Pak *et al.*, (1995) suggested that an increase in pressure, underneath the particle bed surface during vertical vibration, was responsible for particle bed tilting. Furthermore, Thomas and Squires, (1998) suggested that the presence of a horizontal pressure gradient caused Faraday tilting.

In vibrating particle mixtures segregation is often associated with the presence of distinct convection currents (Knight *et al.*, 1996; Kong *et al.*, 2006). The presence of particle convection currents can be considered in parallel to the presence of thermal convection currents (Hsiau *et al.*, 2002). The onset of particle convection is often related to the air motion during vertical vibration (Pak *et al.*, 1995). It has also been shown to depend on container wall characteristics (Knight *et al.*, 1993; Hsiau *et al.*, 2002; Hsiau and Chen 2000; Kong *et al.*, 2006; Zeilstra *et al.*, 2008). Aoki *et al.*, (1996) investigated particle convection mechanism in a rectangular shaped container in which the particles moved upward along the vertical side walls, and downward in the middle forming a valley. In the rectangular shaped container geometry used in their (Aoki *et al.*, 1996) work, multiple pairs of convection rolls were seen in the vertically vibrating working particle mixture. The formation of convection rolls was considered to be strongly dependent on

vibration acceleration, particle size, and to a less extent on frequency, given that the particle bed height and the container width remained constant.

Burtally, (2004) reported that in their experiments the presence of individual convection currents can be attributed to density segregation. Leaper *et al.*, (2005) observed similar convection currents in their experiments that were carried in water and are shown in Figure 2.22.

Further investigations (Leaper *et al.*, 2005; Burtally, 2004), using high speed digital photography revealed the existence of a small gap between distinct bronze and glass rich regions. The presence of this gap during particle bed flight may be the reason for the stable and distinct convection currents shown in Figure 2.22.

The direction of the convective particle motion can be controlled by altering the container geometry of the vibrating particles as demonstrated both experimentally (Kong *et al.*, 2006; Wildman *et al.*, 2005; Hsiau *et al.*, 2002; Knight, 1997; Aoki *et al.*, 1996) and with numerical simulation (Bourzutschky and Miller, 1995; Kong *et al.*, 2006, Wang *et al.*, 1996; Majid and Walzel, 2009; Ohtsuki and Ohsawa, 2003).

2.6.5 Vertical vibration induced separation of fine size particles

The previous discussions (Section 2.6) have revealed that when a mixture of distinct finely sized particles is vertically vibrated, similar size, shape or density particles usually group together. Once together, these particles tend to give a collective response to the external excitations. Under suitable conditions this response can lead to the segregation of finely sized particles (Burtally, 2004).

This particle segregation by convection mechanism can result in forming distinct particle layers of the form shown in Figure 2.22. The separate recovery of these two distinct and finely sized particle layers can form the basis for developing a new breed of vertical vibration induced particle separator.

Mohabuth (2007), Mohabuth and Miles, (2005) and Mohabuth *et al.*, (2007), based on the work of Burtally, (2004); reported the design and use of a new vertical vibration partition cell separator capable of separating two distinct particle layers in separate chambers (chamber1 & 2) as shown in Figure 2.23.

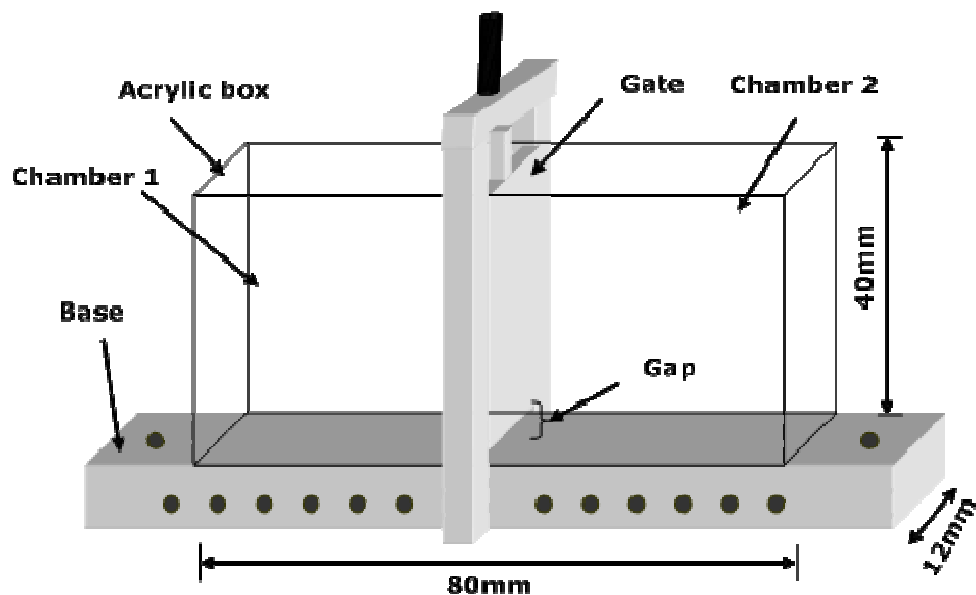


Figure 2.23: Partition cell separator (Adapted from Mohabuth, 2007).

This prototype scale partition cell separator shown in Figure 2.23 was energised by the same vibration apparatus previously used by Burtally, (2004) and Leaper *et al.*, (2005) (shown in Figure 2.18). Fine sized and spherical glass and bronze particles were first used to initially assess the separation potential of this prototype scale partition separation cell (Figure 2.23) (Mohabuth, 2007). The initial

assessment showed that the partition cell separator was capable of recovering high grades of separated glass and bronze particles into two separate chambers in the presence of air only. The importance of maintaining a suitable particle bed height and a partition gap opening between the two separate chambers were particularly highlighted (Mohabuth, 2007). With excessive and no partition gap size opening an unhindered particle flow into the next separate chamber-2 (Figure 2.23) was observed. However, distinct convection currents without tilt formation and segregation were still observed in the finely sized glass and bronze working particle mixtures. The selection of a partition gap size opening was mostly based on the working particle size and was reported to range between 3 and 5 mm. Three particle bed heights were visually investigated to map the "good separation" zones on the $T-f$ maps as shown in Figure 2.24.

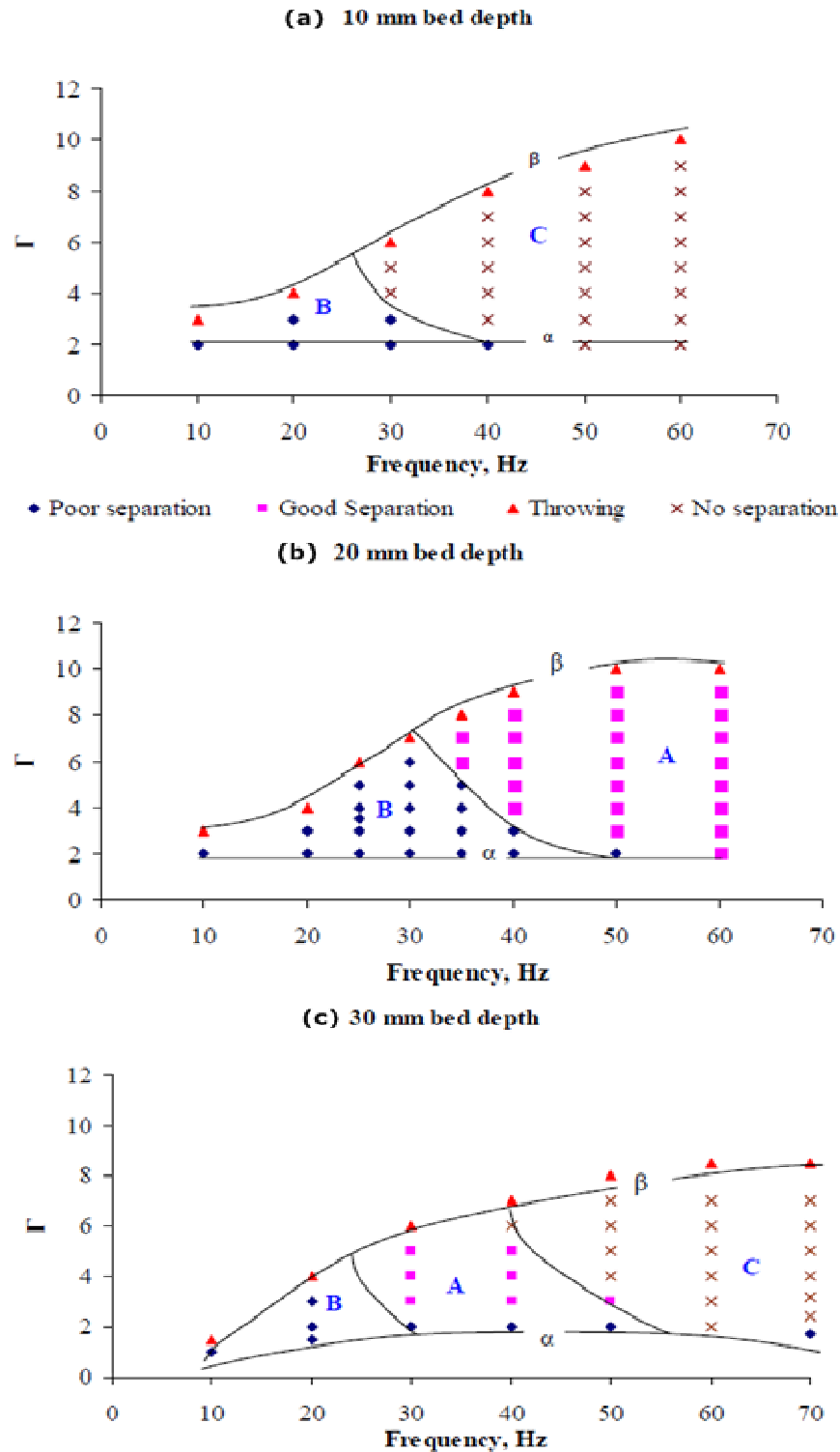


Figure 2.24: Visualized L and f phase diagrams for 75% (volume) glass and 25% (volume) bronze (90-125 μm) mixture at various bed heights. Where, A, B & C represent the good, poor and no separation zones (Adapted from Mohabuth, 2007).

The investigations carried by Mohabuth, (2007) revealed that at particle bed height of 30 mm “good separation” was only achievable in a narrow range of Γ and f values (Figure 2.24). However, when the particle bed height was decreased to 20 mm a significant increase in “good separation” zone on Γ and f map was observed (Figure 2.24). A further decrease in particle bed height to 10 mm resulted in almost no separation at any Γ and f value and the mixture looked rather homogeneous (Figure 2.24). These observations hinted towards the surrounding fluid weaknesses in starting the distinct convection currents in separating particle mixtures at high bed heights (Figure 2.24). Also, the excessive surrounding fluid motion in low particle bed heights resulted in particle motion leading to poor separation (Figure 2.24). Beside other factors, the “good separation” zone was only observed when the surrounding fluid behaviour was favourably balanced by the particle bed height (Figure 2.24).

The successful initial assessment of this prototype partition cell separator with spherical glass and bronze particles resulted in its application to separate a wide variety of fine size regular and irregular shaped particle mixtures (Mohabuth, 2007). Finely sized binary mixtures of sand/bronze, coal/glass and coal/pyrite were separated by using this technique.

Since the industrially relevant and naturally occurring particles are usually non-spherical and poly-disperse (Serero *et al.*, 2006; Castellanos, 2005), the new partition cell separator shown in Figure 2.23 was also used in separating various metallic and non-metallic fractions from waste electrical and electrical equipment (WEEE) (Mohabuth and Miles, 2003; Mohabuth *et al.*, 2007). Shredded electrical cables and multi element printed circuit boards (PCB) from end of life computers were separated into their metallic and non-metallic fractions. The dry separation of these complex and irregular shape particle mixtures in this fine size (<1000 μ m) range

is seldom reported in the literature. In some of the investigated cases (Mohabuth, 2007) metallic fraction recoveries >90% were claimed. However, high grade particle components were reported to be recovered on a prototype scale of only a few grams (Mohabuth, 2007). A photographic image of separated PCB fractions is shown in Figure 2.25.

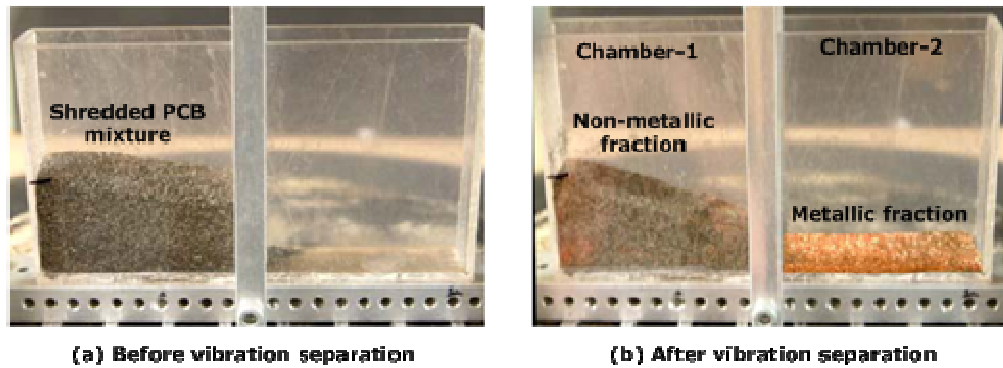


Figure 2.25: Separation behaviour of printed circuit board (PCB) fractions (150-212 μ m) (Adapted from Mohabuth, 2007).

Despite our limited understanding of vibration induced particle segregation and separation this new dry separation idea can be considered as a promising step towards developing a scaled up vibrofluidized fine particle separator. Furthermore, a preliminary effort to scale up this vibration separation system was also reported (Mohabuth, 2007). The suitable vibration induced particle segregation conditions identified from the previous prototype experiments (Mohabuth, 2007) were used in selecting a pneumatic vibrator. This pneumatic vibrator was mounted beneath a thick carbon steel plate that rested on four springs near its corners as shown in Figure 2.26. A schematic sketch of the pneumatic vibration separator is shown in Figure 2.26.

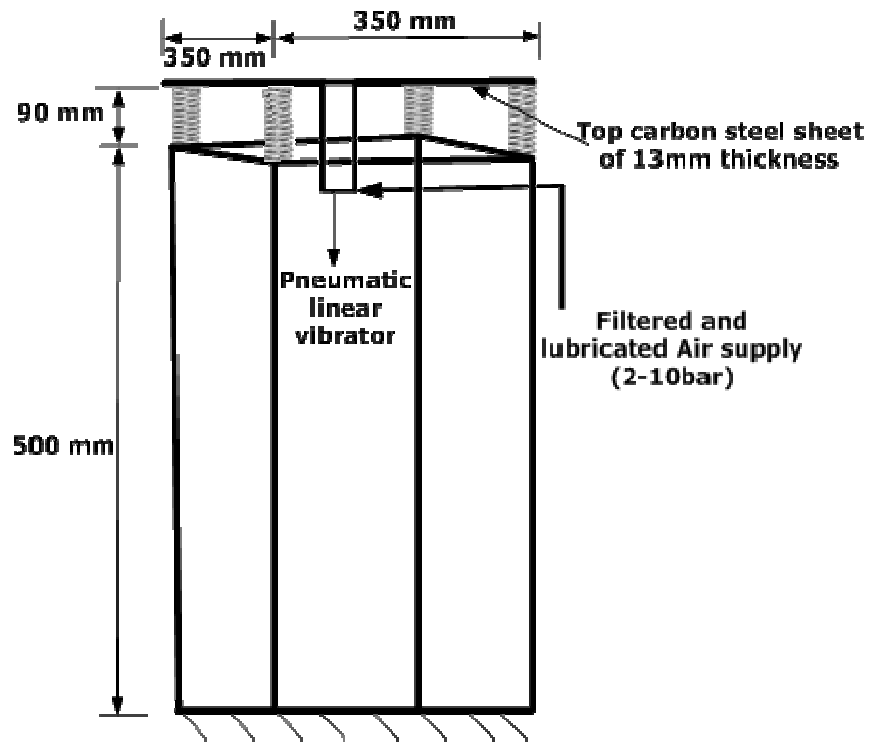


Figure 2.26: Scaled up vibration driven dry based particle separator (Adapted from Mohabuth, 2007).

All springs shown in Figure 2.26 had an outer diameter of 50 mm and 3 mm wire thickness to help resist any excessive compression from the top steel plate when stationary. These springs, however, offered no unnecessary resistance to the vibrated top plate when operated in the desired frequency and dimensionless acceleration range.

Experiments carried out on this large scale vibration separator with sand/bronze, sand/ilmenite and shredded electrical cables in big partition separation cells favoured the use of a narrow width cell. Despite the preliminary studies reported (Mohabuth, 2007) at this scaled up level, the complete assessment of this vibration separator is far from complete. More still remains to be done before this technique can be used at an industrially relevant scale.

2.7 Concluding remarks

The currently available literature on vertical vibration of particle materials can be used to deduce the following;

- ❖ Gravity separation of particulate materials is a commonly practised technique.
- ❖ Particle size is an important parameter in selecting any separation technique.
- ❖ A wide variety of particle separation choices are readily available to separate $>1000\mu\text{m}$ particles on dry basis.
- ❖ Traditional particle separation techniques rely on the generation of outer fields such as thermal, electrical, centrifugal and magnetic, which significantly increases the complexity of operation, cost and processing time.
- ❖ The particle separation choice rapidly drop as the particle size reduces below $1000\mu\text{m}$.
- ❖ Most of the finely sized particle separation processes are based on wet processing.
- ❖ Particle size segregation is a commonly observed phenomenon in industrial particle handling.
- ❖ Despite the core importance few studies have focused on investigating particle density segregation.
- ❖ The majority of the experimental and theoretical studies in particle segregation have used spherical particles in their investigations.
- ❖ No efforts have been reported in developing non-spherical particles which could be adopted as a standard for different particle investigation comparisons.
- ❖ Most of the particle segregation observations are made at the particle surface or very near to it.
- ❖ Limited efforts are reported in understanding internal particle rheology during vibration separation.

- ❖ There has been no assessment to determine if particle shapes will have an effect on vibration separation operation.
- ❖ During vertical vibration of particulate materials the fluid effects between colliding grains is principally not known.
- ❖ Unlike gas fluidisation, there are uncertainties in defining a point where a particle state can be exactly termed as vibrofluidized.
- ❖ Local pressure variations in vibrating particle beds are simply not known.
- ❖ There has been no assessment on particle laden fluid viscosity and drag forces during vibration separation.
- ❖ The majority of investigations have been carried out on prototype scales. The use of prototype scale investigations may have been drifted away from the industrial length scales and this might would have overlooked some of the other more important particle segregation features.

Materials and methods

3.1 Introduction

This chapter describes the main experimental methods that have been used to separate a range of dry and finely sized particle mixtures by controlled sinusoidal vertical vibration in a novel separator at a scaled up level. The scaled up level is defined in relation to the small scale vibration separation system shown in Figure 2.18, Figure 2.23 and Figure 2.26, reported by Mohabuth, (2007). The new vibratory setup was developed to generate the intended frequency and dimensionless acceleration of vibration in the required vertical direction only. The development of a one dimensional scaled up vertical vibration separation system formed one of the major activities in the work presented here. Of equal importance was the development of separation cells of various geometries that were used to separate various finely sized working particle mixtures. The diverse separation cell geometries, such as the ones used in this work, can help in generating and maintaining

distinct convection currents which are considered important by many (Milburn *et al.*, 2005; Knight *et al.*, 1996; Kong *et al.*, 2006; Knight *et al.*, 1993; Hsiau *et al.*, 2002; Hsiau and Chen 2000; Zeilstra *et al.*, 2008) in particle segregation via vertical vibration.

The onset of convection currents in vibrated particle beds is described in Section 2.6.4 of Chapter 2. In this work, the formations of distinct convection currents in vibrated particle beds were used to recover at least one of the separated particle layers in a semi batch mode. Once recovered, these separated particles were then analysed, by various qualitative and quantitative techniques, to determine the grade and recovery of the finally separated products. The detailed description of these qualitative and quantitative techniques will form a part of this chapter.

Vertical vibration used to separate dry fine particle mixtures by Burtally *et al.*, (2002 & 2003), Burtally, (2004), Leaper *et al.*, (2005) Mohabuth and Miles, (2005), Mohabuth *et al.*, (2007) and Mohabuth, (2007), were generated by a pair of connected loud speakers as shown in Figure 2.18. Under appropriate experimental conditions, the above mentioned prototype scale studies have shown that a vertical vibration frequency between 40 and 60Hz and dimensionless acceleration Γ , value in the range of 4 to 8 were appropriate in obtaining "good separation" for a range of finely sized working particle mixtures. The previously reported studies (Burtally *et al.*, 2002 & 2003; Burtally, 2004; Leaper *et al.*, 2005; Mohabuth and Miles, 2005; Mohabuth *et al.*, 2007; Mohabuth, 2007) have predominantly used qualitative measures (e.g. visual and photographic camera) to report the separation behaviours of fine particle mixtures. However, Mohabuth, (2007) has demonstrated the use of some quantitative measuring techniques such as heavy liquid analysis for determining the grade and recovery of separated particle products.

The separation analysis reported in this work has used qualitative as well as quantitative techniques for assessing particle separations. The main analytical techniques were readily available at the University of Nottingham, UK. The choice of an analytical technique was based on many different factors such as the availability, accuracy, precision, cost, time scale, data quality and its suitability to the materials under investigation.

In summary, this experimental work covered the development of a novel separation system for fine particle mixtures together with its assessment and application. The prototype scaled particle separation results reported by Mohabuth, (2007) were used as a basis in fine tuning of the scaled up vertical vibration induced particle separator reported in this work. The scaled up vibration separation bench (Figure 2.26) was used to generate the previously reported (Mohabuth, 2007) "good separation" range of vibration frequency and dimensionless acceleration by other more industrially applicable means (pneumatic vibrator). While ease of process integration may well be an added advantage offered by this new scaled up design, it may also help in exploring novel uses for separating finely sized multi-component solid waste particle mixtures. The detailed design description of the scaled up vibration separation system is given in the next sections.

3.2 Materials

3.2.1 Rig-1 design

In industry, vibrating troughs or plates are commonly used for transporting materials (e.g. in feeders, hoppers). A range of linear and non-linear pneumatic, electric, hydraulic, rotary, turbine, piston and ball vibrators are readily available and used to drive these metallic plates at various frequency levels (Chicago, 2009). The main initiative in developing the scale up design as Rig-1 (Figure 2.26) was to maintain the top vibrating steel plate motion in vertical direction only. The strict requirement of having this vertical motion eliminated many non-linear vibrator options from further considerations in the next selection phase. After careful consideration regarding the ease of operation, safety, costs, reliability, ease of integration, maintenance and most importantly the required range of frequency and dimensionless acceleration for “good separation”, pneumatic linear vibrators appeared on top of the final favourable list for trial experiments. Pneumatic linear vibrators (FP-series, Vibtec Ltd.) were considered most appropriate due to their wide range of pneumatic power, light weight, quiet operation, efficiency, low cost and availability with the added advantage of air pressure controlled infinitely variable frequency and amplitude range (Vibtec, 2009). The simple vibrator design also ensured their easy integration to an existing engineering structure.

The preliminary scaled up vertical vibration bench is shown in Figure 2.26 and Figure 3.1.

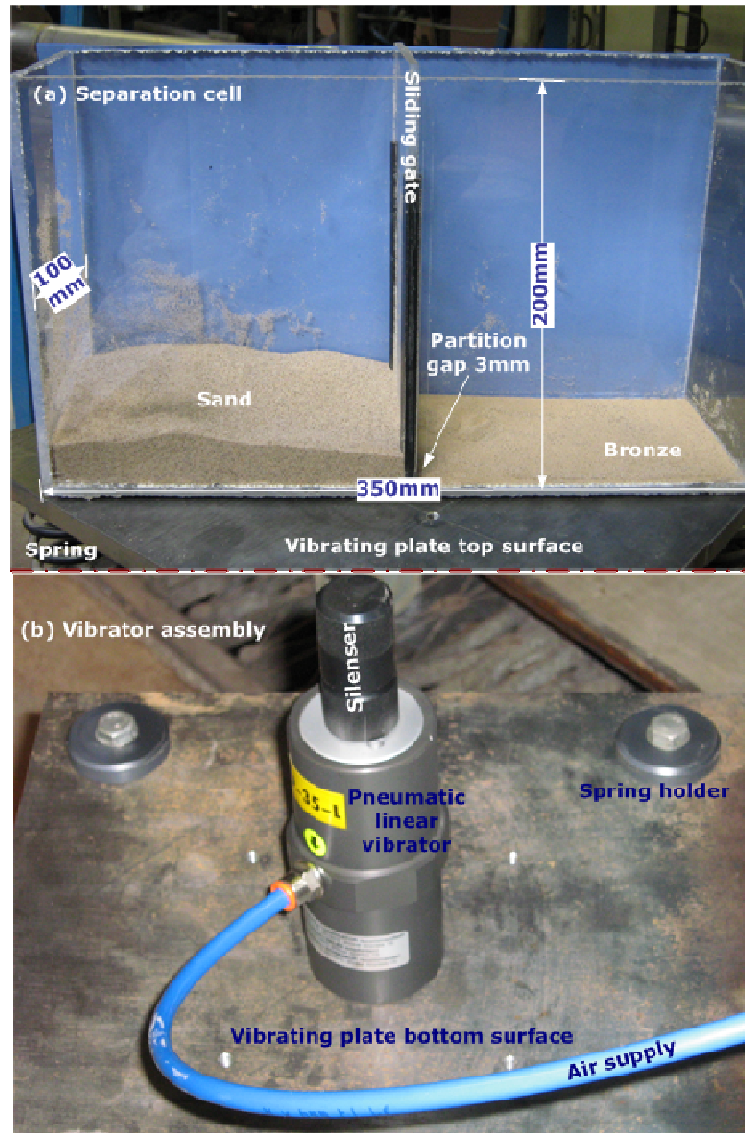


Figure 3.1: Rig-1, (a) separation cell and (b) pneumatic vibrator assembly.

Various pneumatic linear vibrators were mounted on this Rig-1 (Figure 3.1) to test their vibration power in terms of delivering the required vibration frequency and acceleration. This practice helped in selecting the most appropriate pneumatic power vibrator for the intended use in this work. In addition, other factors such as the springs and vibration plate stability with and without loads, linearity of the vibration motion and the potential carbon steel plate inclination to one end during material loadings were also observed

during the initial trial phase. These observations were used in eliminating any undesirable features from the final separator design. The major components of the scaled up vibration induced separator design are;

- ❖ A 350x350 mm² vibrating carbon steel plate of 13 mm thickness.
- ❖ 90 mm high, 60 mm outer diameter and 5 mm thick wire springs on all four corners of the carbon steel plate.
- ❖ A 500 mm high and 350 mm in width rectangular shaped metallic frame to support the above.
- ❖ A vibration driving pneumatic linear vibrator that was fixed directly beneath the centre of the oscillating carbon steel plate.
- ❖ Filtered, lubricated and pressurized air supply mechanism to the vibrator (Figure 3.2). The vibrator used an air supply pressure between 2 and 10bar, which was delivered from an already available main compressor line in the laboratory.

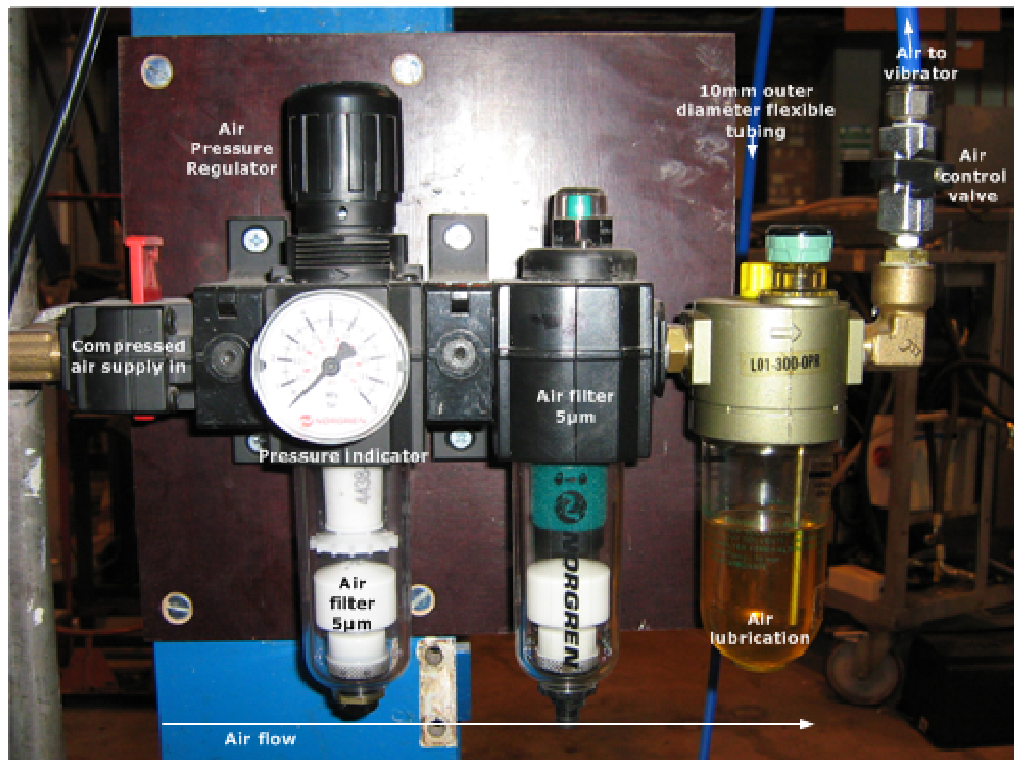


Figure 3.2: Air supply and control to the pneumatic vibrator.

The frequency and dimensionless acceleration of the top vibrating carbon steel plate was measured by means of an oscilloscope (Tektronix, TDS1002B model) that was connected through 8 and 80g accelerometers. The pneumatic linear vibrator models, FP35, FP50 and FP95 (Vibtec Ltd., 2009) were connected to the carbon steel plate as shown in Figure 3.1. These vibrators were run with varying inlet air pressures to observe the vertical vibration driven particle separation behaviours with different particulate loadings in the separation cell shown in Figure 3.1. The vertical vibration delivered by Vibtec-FP35 model were observed to be in the required frequency and dimensionless acceleration range when the top vibrating carbon steel plate was either free or had low particulate loadings in the separation cell. As the particle loadings were increased a loss in vertical vibration frequency and dimensionless acceleration was evident and the vibrator failed to work at some point during the initial trial experiments. The vibrator (Vibtec-FP35)

was then replaced with the more powerful Vibtec-FP50 and Vibtec-FP95 models. The initial trial experiments demonstrated that the added weight and power in the Vibtec-FP95 model best satisfied the required frequency and dimensionless acceleration range. Hence, it (Vibtec-FP95) was selected for further intended use in the final experimental work.

Other notable observations from the initial trial experiments on Rig-1 included the lack of control on vertical motion of the top vibrating carbon steel plate. Although, the steel plate and vibrator weights were enough to prevent any abrupt vibratory motions they were not sufficient to restrict the spring motion in other directions. This necessitated the introduction of some mechanism on all four corners alongside the springs that could restrict the vibration plate motion to vertical direction only. All of the above resulted in designing a slightly modified vertical vibration separation bench, discussed in the next section.

3.2.2 Rig-2 design

The lack of control on vertical motion can have an effect on the experimental findings where an assumption of vertical motion in one dimension is made; further modifications were therefore deemed necessary in Rig-1 design. After necessary modifications the new rig design (Figure 3.3) comprised the following essential components;

- ❖ A 500x500 mm² top vibrating carbon steel plate of 10 mm thickness. The carbon steel plate area was increased with the endeavour to accommodate large size separation cells.
- ❖ All four carbon steel plate corners with 3 mm thick wire springs of 90 mm height and 50 mm outer diameter.

- ❖ A 15 mm diameter linear motion bearing on all four corners of the carbon steel plate alongside the springs. The purpose of these linear motion bearings was to restrict the oscillating carbon steel plate motion to a vertical direction only.
- ❖ A 760 mm high and 530 mm in width rectangular shaped metallic frame fitted with anti-vibration feet. These adjustable anti-vibration feet were also used in maintaining a balanced horizontal top, vibrating surface.
- ❖ A vibration driving, pneumatic, linear vibrator (Vibtec-FP-95), which was fixed directly beneath the centre of the oscillating carbon steel plate.
- ❖ The pneumatic supply and control mechanism to Rig -2 is shown in Figure 3.2.

The detailed Rig-2 design with relevant dimensions is shown in Figure 3.3.

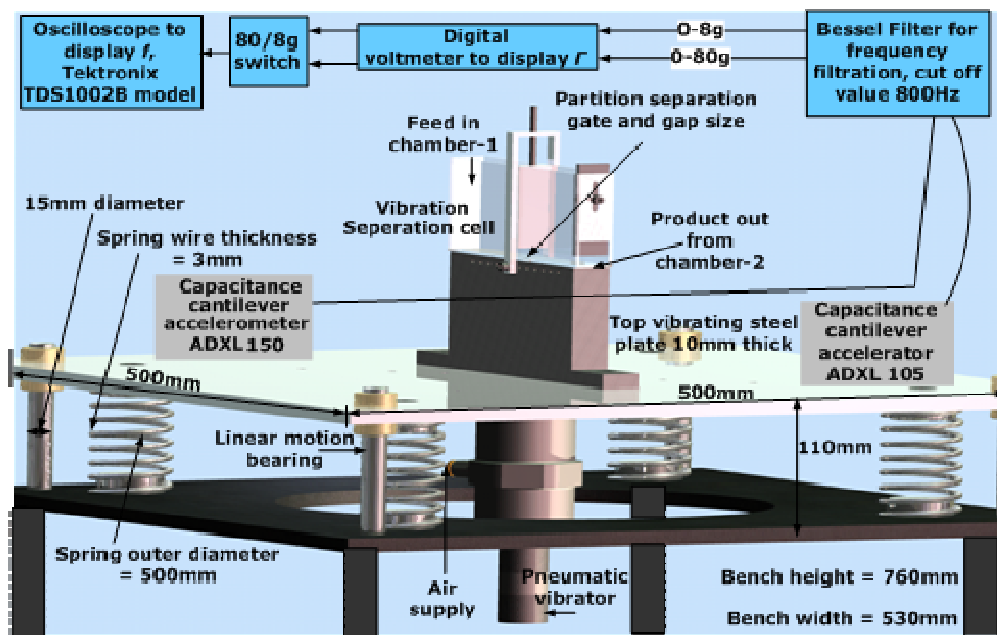


Figure 3.3: Rig-2. Scaled up vertical vibration separator.

The controlled air supply to the vibrator was delivered from a main compressor line through the pressurized air control unit shown in

Figure 3.2. It comprised an air pressure display and control followed by a filter (5 μ m) and lubricating units. The air pressure could be varied via an air pressure regulator. After filtration and lubrication the compressed air was introduced into the pneumatic linear piston vibrator via an air supply inlet shown in Figure 3.3. This compressed air supply was the prime driver for vibrating the top carbon steel plate.

The vertical vibration acceleration was displayed on a dual digital voltmeter panel connected via 8g and 80g capacitance cantilever accelerometers fixed directly onto the vibrating platform. The signals from these capacitance cantilever accelerometers to the digital voltmeter were conveyed via a Bessel filter. The Bessel filter only allowed signals up to a certain maximum frequency value and thus conveyed low frequency platform dimensionless accelerations to the dual digital voltmeter. The signals from the capacitance cantilever accelerometers passing through the dual digital voltmeter and an 80/8g switch were then used in measuring the vibration frequency by means of an oscilloscope (Tektronix TDS1002B model) (Figure 3.3).

The vibration frequency of the platform could be controlled by controlling the air supply to the pneumatic vibrator. However, no specific mechanism was in place to individually control the dimensionless acceleration. The acceleration of the vibrating platform was balanced by its weight against the stiffness of the springs. The heavy weight of the platform did not allow it to have a hasty acceleration. The dimensionless acceleration measurements conveyed by the capacitance cantilever accelerometers were found to be in the intended design range of 2 to 4. Furthermore, no significant change in the values of dimensionless acceleration was observed with varying particulate loadings in the separation cells. These observations lead us to safely believe that the minor particle loadings were insignificant in comparison to the platform weight in

controlling its dimensionless acceleration. Moreover, various holes were drilled on the vibrating platform to support the attachment of separation cells.

3.2.3 Separation cell designs

The L-type particle separation cell design is shown in Figure 3.4.

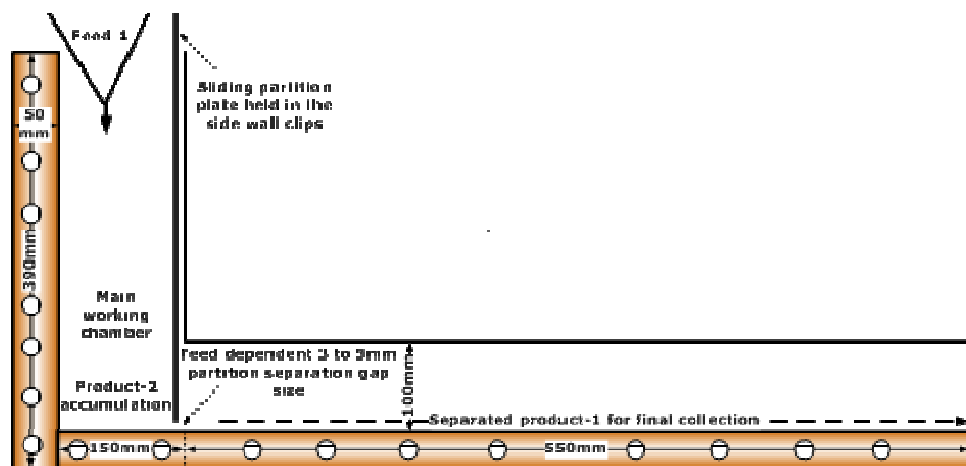


Figure 3.4: L-type particle separation cell.

The L-type particle separator construction was based on a 5 mm thick transparent Perspex[®] sheets that were glued and screwed safely on both sides of a wooden frame as shown in Figure 3.4. A distance of approximately 50 mm was maintained between the two Perspex[®] sheets. Hence, this initial cell design had a thickness of 50 mm and a long product discharge leg. The long discharge leg was provided with intention of further purifying the separating fraction as it travelled towards the exit. The transparent cell design also helped in observing the separation behaviours of various particle mixtures.

The T-type particle separation cell shown in Figure 3.5 was designed with the aim of investigating the influence of two partition

separation gap sizes on particle separation in the main working chamber.

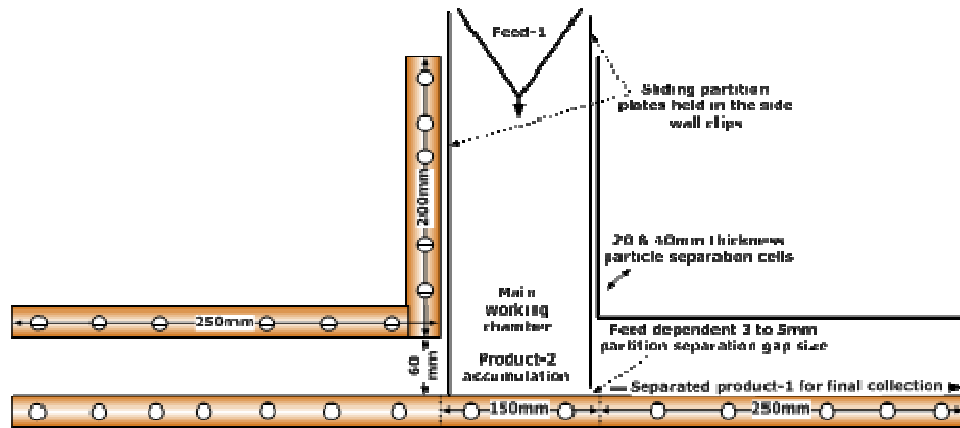


Figure 3.5: T-type particle separation cell.

The use of two partition gap sizes in the main working chamber of the T-type cell as shown in Figure 3.5 can also help in recovering the two separate fractions from the main feed stream. In the first phase of the T-type particle separation cell operation, the separating product could be recovered as product-1 while the other side remain closed. Once the recovery of one fraction is complete, the rest of the materials could be drawn from the other side as product-2. In this later form the T-type cell essentially works as L-type separation cell with an added advantage of having a separate discharge for each of the two distinct particle streams.

The two L and T-type separation cell designs could be clamped on the top surface of the vertically vibrating platform as described in Sections 3.2.1 and 3.2.2. Both the L and T-type particle separator cell designs had identical materials of construction. In these separation cells, various feed mixtures can be introduced from the top to achieve the required particle bed height in the main working chamber. Once the required particle bed height is achieved, the feeding arrangements shown in Figure 3.4 and Figure 3.5 can be removed. The open to the atmosphere particle mixtures can be

vibrated in these separation cells. Various particle bed behaviours can be observed and recorded through the transparent walls of the L and T-type separation cells.

The initial experiments carried out in the L and T-type cells showed similar particle convection and segregation trends as reported by Mohabuth, (2007) and Burtally, (2004). It was therefore decided to use these separation cells to assess their particle separation potentials with different solid waste mixtures. Further developments and refinements in the T-type design are shown in Figure 3.6.

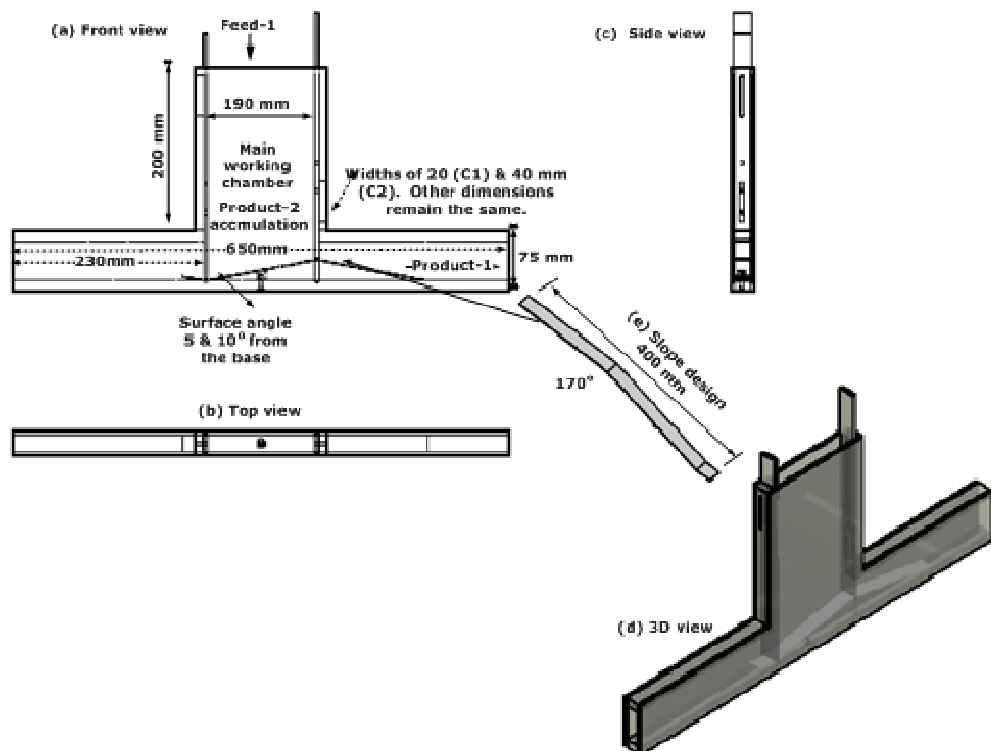


Figure 3.6: Final separation cell designs used in vibration induced particle separation experiments.

The work presented in this thesis has only looked into the particle separation behaviours in a 20 and 40 mm thickness separation cell (constructed from a Perspex[®] material and referred to as C1 and C2) with varying particle bed heights. Furthermore, no slopes as

shown in Figure 3.6 were used in this work. This is mainly due to the optimization requirements of a large number of control variables in the base particle separator cell design shown in Figure 3.6.

3.3 Methods

3.3.1 Preparation of test mixtures

In this work, size reduction was the main unit operation for the preparation of different test mixtures. It is an important and essential unit operation to reduce the bulky items to particles, the sizes of which are compatible with the vertical vibration particle separation operation. Size reduction can also bring about a degree of uniformity in terms of the maximum particle size and/or particle size distribution. This uniformity may well be a requirement for any subsequent physical separation operation.

The vertical vibration separator reported in this work used finely sized solid waste and mineral mixtures in its dry based separations. The solid waste and mineral mixtures used in this work are rarely found in a liberated form. It is therefore necessary to use size reduction equipment to bring the feed size to an acceptable liberated range, an essential prerequisite in almost all physical separation processes. The selection of a size reduction method for this purpose is governed by many different factors such as the particle physical properties, the required particle size range, degree of component liberation and the tolerable and/or on some occasions the essential final fineness of the particulates.

3.3.1.1 Retsch cutting mill (SM2000/750)

In this work a Retsch cutting mill (SM2000/750) shown in Figure 3.7 was used to shred and liberate metal fractions from the end of life (EOL) electrical cables and computer circuit boards.



Figure 3.7: Cutting mill (Adapted from Retsch, 2009).

The selection of this (Figure 3.7) size reduction method was based on consideration of material properties of the waste electrical and electronic equipment (WEEE). This technique (Figure 3.7) used a predominantly cutting mechanism to reduce the size range of WEEE components. The heat sensitive nature of the WEEE materials restricted the use of other size reduction methods that rely on impact, compression, attrition, shear and grinding in their operations.

The Retsch cutting mill (Figure 3.7) is capable of reducing a feed material from <60X80 mm to 0.25-20 mm size range (Retsch, 2009). It was operated at 60Hz with 1.5kW electrical power to generate 835 revolutions per minute. The appropriate and pre-sized WEEE materials were first introduced into the main feed chamber (Figure 3.7), they were then allowed to slide into the main cutting chamber. Once there, these WEEE materials were then comminuted

by rotating blades against the stationary cutting bars housed in the main operation chamber. The final fineness of the discharged product was mainly dependent on the discharge grid size. In this work, the size reduction was carried out in stages, for initial cutting operations, 10 and 4mm square hole discharge grids were used whereas, for fine particle size ranges, 1.5 and 0.75 mm trapezoid hole discharge grids were employed.

3.3.1.2 Retsch jaw crusher

The size reduction of various mineral ores was carried out by using a forced feed jaw crusher. The feed material entered into the crushing chamber through a no-rebound hopper. The size reduction was carried out in a wedged shaped area between the fixed and the moving arm driven by an eccentric shaft powered by a 1.5kW electric motor. The elliptical jaw motion carried out the major crushing and the resulting product was discharged under gravity. The Retsch jaw crushing unit used in this work was capable of an intake particle feed of <90 mm that can be reduced to a final finesses of less than 2 mm in size. An adjustable gap size is provided between the moving and stationary jaw to help meet the final particle size range requirements (Retsch, 2009). The size reduction processes were mainly carried out in single and/or multiple stages to best achieve the required degree of liberation and particle size ranges.

3.3.2 Sampling techniques

Sampling has always been a sensitive issue in almost all particle handling operations (Muzzio *et al.*, 2003; ParticlesCIC, 2009). Accurate and reliable particle sampling is essential for any particle

characterisation procedure. The accuracy of particle sampling is hindered both by the complex particle nature and the lack of validated and reliable sampling techniques. Sampling tools as well as sampling protocols are critically important for accurate characterisation (Muzzio *et al.*, 2003). Many sampling techniques such as; coning and quartering, scoop, table, chute and spinning riffle are commonly used (ParticlesCIC, 2009). The reliability of some particle sampling techniques according to their relative standard deviation together with some of their advantages and disadvantages are given in Table 3.1.

Sampling method	Advantages	Disadvantages	Relative standard deviation (%)
Cone and quarter	Good for powders with poor flow characteristics	Operator dependent	6.81
Scoop	Reliable for homogeneous and non-flowing powders	Possible particle segregation	5.14
Table	Separates a large material quantity	Initial feed dependent	2.09
Chute	Reduce sample by half after one pass	Operator bias	1.01
Spinning riffle	Reliable for free flowing powders	Inability to do large quantities efficiently	0.125

Table 3.1: Reliability of various sampling techniques (Adapted from ParticlesCIC, 2009).

In addition to the material properties, the scrutiny level at which a particle sample is drawn for analysis can have a significant impact on the finally reported results. It is therefore important to define the particle sampling technique for subsequent composition analysis of the feed and separated products. In this reported work small particle samples ($\approx 1\text{g}$) for Inductively Coupled Plasma-Atomic Emission Spectroscopy (ICP-AES) analysis were drawn in small increments from different locations in an initially well mixed particle mixture by using a long, small bore, glass tube. For all other analysis such as sink-float and density measurements, a laboratory

scale sampling scoop was used to incrementally draw a 20 to 30gram sample from various locations. Different sampling locations were chosen with care to avoid any biased samples that can result in accumulation of experimental errors in the final analysis. Three repeat samples from a variety of locations were drawn for each analysis to account for the acceptable levels of precision in the reported results.

3.3.3 Quantitative means of sample analysis

3.3.3.1 Sieve analysis

Particle size analysis is a commonly used method for characterising particulate samples (Perry and Green, 1999, Wills, 1997). Particle classification is important because the variations in particle size distributions can affect the physical, as well as chemical, properties of the particulates. Particle characterisation can also be used in predicting the operational performance of a sized based physical separation method. Various techniques are currently in use for characterising particulate materials according to their sizes. A wide array of particulate materials can be easily size characterised with a standard sieve analysis. Sieve analysis can be used with large and small size particles (125,000 to 5 μ m) and both wet and dry based sieving can be used. Dry sieving is generally preferred to prevent any consequent mineral ore degradation by water, which is the generally used wet medium (Wills, 1997). Dry based sieve analysis has been developed as an established, simple, most widely acceptable and proven method to ascertain the particle sizes and distributions in comparison to some of its other rivals (Table 3.2) (BS 1790-1, 1989 & ISO 2591-1, 1988).

Size characterisation method	Approximate useful size range (microns)
Test sieving	125,000-5
Microscopy (light)	50-0.25
Sedimentation (gravity)	20-1
Sedimentation (centrifugal)	5-0.25
Microscopy (electron)	1-0.005

Table 3.2: Commonly used particle size analysis methods (Adapted from BSI 1796-1, 1989 and ISO 2591-1, 1988).

This work used a tapped sieving method to classify different particle size ranges. Single layer particle materials in a standard 800 mm diameter sieve were tapped for approximately 15 minutes in a laboratory scale tapping machine. The two adjacent test sieves had an aperture width of $\sqrt{2}\mu\text{m}$. The selection of a standard $\sqrt{2}$ sieve series was considered to be more useful in preliminary indication of materials concentration by size, which was later combined with sink-float and density measurement data.

3.3.3.2 Dense media separation (DMS) and/or sink-float analysis

The visual particle segregation observations of the binary particle mixtures were confirmed by a sink-float analysis technique. In this wet based analysis technique the individual buoyancy of an insoluble particle material can be used as a basis in separating light and heavy fractions (BS7067, 1990; Mohabuth, 2007). A heavy liquid is used as a medium of separation in which the materials with density greater than that of the liquid will 'sink' to the bottom, while the materials with density less than that of the liquid will 'float' at the surface (BS7067, 1990). This technique was mainly used in the coal preparations however; it can also be adapted safely for use in separating other particle mixtures (BS7067, 1990). Sink-float analysis technique is expected to work best with large density difference particle mixtures (BS7067, 1990). A minimum of

approximately 2000 discrete particles are generally recommended for this analysis (BS7067, 1990).

The sink-float analysis technique reported in this work used a sodium poly-tungstate (SPT) powder that dissolved in deionised water to make up the medium of separation. A maximum relative density (RD) of 3.1 can be achieved in this SPT solution (Mohabuth, 2007). This separation medium was prepared and stored in plastic containers. A well-mixed 500ml SPT solution was used in various sink and float separations. The used SPT solution was then filtered from the separated particle fractions. These separated fractions were subsequently washed with deionised water and completely dried in an oven at about 50-80°C before weighing. The weight of each fraction was used in determining the particle separation efficiency in terms of grade and recovery.

Pilot tests were carried out first to establish the calibration graphs (Figures B.1 and B.2 in Appendix-B) of the known particle composition mixtures. This practise was then used to check the reliability of the obtained data from this separation analysis technique. The procedure for carrying out this analysis involved the following steps;

- ❖ Approximately 500ml of heavy medium was taken in an appropriate beaker.
- ❖ The particle mixture was weighted to make up approximately 2000 discrete particles.
- ❖ These particles were then introduced into the heavy medium with gentle agitation.
- ❖ This followed with an ultrasonic agitation for approximately 15 minutes.
- ❖ The mixture was left overnight to enable particle settlements in the heavy medium to form distinct thin particle layers.

- ❖ The sinks and floats obtained were carefully removed with a specially designed woven wire mesh strainer.
- ❖ The SPT solution was filtered to remove the light and heavy fractions with the help of a vacuum pump.
- ❖ The next step involved washing each fraction with deionised water and drying in an oven.
- ❖ Weighing each fraction finally concluded this practise (BS7067, 1990).

Care was exercised in recycling the spent SPT solution. The potential addition of very fine size particles in the spent SPT solution can alter its relative density. In this work the spent SPT solution was evaporated and diluted with deionised water to adjust its relative density.

3.3.3.3 Density measurement

Density measurement can be used as an indication of the final grade of the separated materials. The measured density can be compared to the literature/book value of the recovered particulates. The density of almost any particle can be measured by using an insoluble void filling fluid such as helium (He) gas.

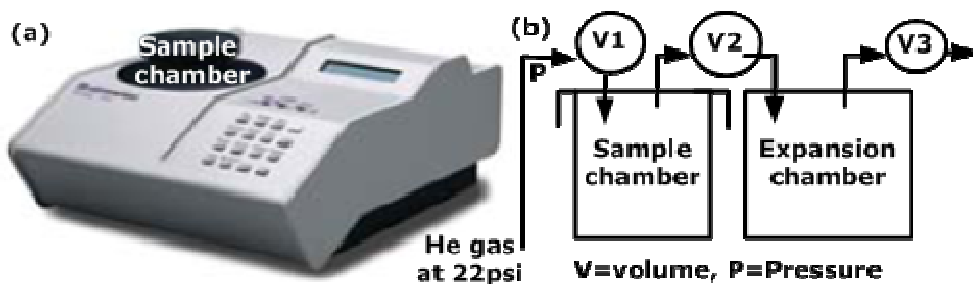


Figure 3.8: (a) He pycnometer, Accpyc 1330 model, (b) working principle.

In this work, a Helium pycnometer (Micromeritics He pycnometer, Accpyc 1330 model) capable of operating at ambient temperature and pressure was used (Figure 3.8). It contained a constant volume (100ml) chamber that could be filled with helium gas. The density measurements by this equipment involved the following steps;

- ❖ The sample free chamber was filled with helium gas to a precisely known pressure, after each filling the gas was allowed to expand (Figure 3.8). The pressure and volume variations can be related by Boyle's law. Approximately 10 repeat gas fillings and expansions were carried out in each case.
- ❖ A particulate sample of known mass was loaded into the test chamber.
- ❖ The helium gas was then filled into the sample laden chamber. The ratio of sample mass to its volume was then used in determining the true density of the particulate materials.

3.3.3.4 Inductively Coupled Plasma-Atomic Emission Spectroscopy (ICP-AES)

ICP-AES is an emission spectro-photometric technique based on the fact that the excited electrons emit energy at a given wavelength as they return to their ground state. Hence, each element will emit energy at specific wavelengths related to its chemical nature. It is quite possible for each element to emit energy at different wavelengths but normally a single (or a few) wavelength is selected for a given elemental analysis. The intensity of the energy emitted at the chosen wavelength is proportional to the concentration of that element in the analyzed sample. Hence, the determination of elemental wavelength and its intensities can result in the quantification of the elemental composition of a given sample

relative to a reference standard (Murray *et al.*, 2000; Rice, 2002; Mohabuth, 2007).

It is essential for ICP-AES analysis that a sample is present in solution, particulate samples are therefore analysed in the liquid dissolved phase. Dissolution can simply be achieved by a combined acid attack, strong concentrated acids such as hydrofluoric (HF), hydrochloric (HCl) and nitric (HNO₃) acids can be used for this purpose. These acids can be used alone or in combinations such as Aqua-Regia (concentrated HCl:HNO₃ in a 3:1 ratio by volume). The acid digestion phase can lead to a biased ICP-AES analysis if an appropriate acid is not selected for dissolving the particles e.g. silicon volatilizes in the presence of HF and titanium (Ti), chromium (Cr) and zirconium (Zr) are often difficult to dissolve. After strong acid digestion and evaporation the resulting concentrate is often diluted in HNO₃ to form a stable solution for analysis (Murray *et al.*, 2000).

3.3.3.4.1 Sample Preparation

The following steps were carried out for sample preparation;

- ❖ Great care was exercised in making sure that absolutely clean glassware, auto-sampler vials, tubes, and sample bottles were used.
- ❖ The 1±0.1gram dry sample mass (total dissolved solids, TDS) recorded up to four decimal places from each separated fraction was carefully placed in a 50ml conical flask. Care was exercised to use a homogeneous solid mix to avoid any biased elemental representation in the final solution. The selection of a conical flask for acid digestion can reduce the chances of cross contamination by condensing leachate on inner glass walls away from the heated base. Approximately

10% of all analytes were prepared identically as analytical procedural blanks to track any significant cross contamination during the sample preparation stage.

- ❖ Matrix matching is important in this type of analysis. The term “matrix”, refers to the sum of all compositional characteristics of a solution. In this work, the acid composition, calibration standards and samples were matrix matched in terms of composition, total dissolved solids and acid concentration in solution.
- ❖ Two different acid digestions were carried out in this work. A 25ml of each 70% concentrated nitric acid (HNO_3) and Aqua-Regia were used in separate digestions. HNO_3 , on the whole was used to detect silver (Ag), which can form silver chloride (AgCl) in Aqua-Regia. AgCl will form a precipitate in the solution and hence will affect dissolution. The sample laden acid solutions were carefully mixed and left overnight in a fume cupboard. The solutions were then transferred on to a hot plate where the temperature was slowly increased to 120°C . The samples were closely monitored to prevent any abrupt boiling and heated for a period of up to 12 hours until the final solution was reduced to approximately 3ml.
- ❖ These samples were then allowed to cool at room temperature. Next, a 20ml dilute HNO_3 (10% by volume) solution was added to each sample and the vessel subsequently heated for further half an hour at 120°C on a hot plate. The resulting sample was then allowed to cool at room temperature to form stable and precipitation free analytes.
- ❖ The cooled samples were transferred to 100ml volumetric flasks, and topped up with an additional 10% HNO_3 to ensure same dilution factors in all solutions.
- ❖ The presence of any un-dissolved solids in the solution can lead to a partially or completely clogged nebuliser in the ICP-

AES analyzer resulting in poor analytical precision or an analysis failure, therefore a centrifugal force was used to separate any un-dissolved solids from the solution. Approximately 40ml of solution from each 100ml flask was decanted into each of two clean 50ml polypropylene centrifuge tubes and the lids sealed. The remaining 20ml was discarded at this stage. The tubes were then centrifuged at 3000rpm for 5 minutes, resulting in solids settling at bottom. The solid free clear solutions were carefully decanted into clean and transparent plastic bottles. Duplicate sample were combined at this stage to make up a volume of approximately 80ml in each plastic bottle, ready for further ICP-AES analysis.

- ❖ The standard reference solutions were prepared with the same dilution factor and acid concentrations as those of the experimental samples to calibrate the ICP-AES equipment. ICP-AES is a comparative analytical technique; the instrument response must therefore be calibrated against standards in which the various element concentrations are known. The calibration standards can be one of the two types: (1) calibration against internationally recognized and approved standard reference materials, or (2) calibration against synthetically prepared calibration standards. In this work, synthetically prepared calibration standards were developed to closely mimic the unknown samples matrix.

3.3.3.4.2 ICP-AES analysis system

An ICP-AES analysis system normally contains three main components which are sample introduction system, plasma torch assembly and the spectrophotometers. The sample introduction system contains a peristaltic pump, Teflon tubing, a nebuliser, and a spray chamber. The fluid sample is pumped into the nebuliser to

generate an aerosol mist in conjunction with injecting the humidified argon (Ar) gas into the mist chamber. Humidification usually takes place in an Ar humidifier, where it is bubbled through the deionised water. In the mist chamber, the large mist particles are allowed to settle out as a waste stream while the finest particles are introduced in the torch assembly. Portions of the plasma torch assembly can be as hot as 1000K, enough to excite the electrons in the majority of cases. As these excited electrons return to the ground state at a certain specific position in the plasma, energy at specific wavelengths relevant to the sample's elemental composition is emitted. This energy, in the form of light, is focused through a lens and passed through a slit into the spectrophotometer. Monochromatic and/or polychromatic spectrophotometers can be used; in this case a monochromatic unit was used. Computer control ensures the detector synchronization and intensity are correlated with the emitted wavelengths. The energy intensity at each wavelength is measured in counts to provide a quantitative result that can be compared to a reference standard. The standard spectroscopic technique with back-ground corrections can provide a swift analysis of a number of chemical elements. The spectrometer is constantly flushed with nitrogen (N₂) gas to improve the detection limits of elements with the added advantage of protecting the optics from the surrounding corrosive atmosphere (Murray *et al.*, 2000).

In this reported ICP-AES analysis, Perkin Elmer[®] plasma 400 equipped with a Gilson[®] 180 position sample changer was used. The use of automatic sampler enables rapid analysis of a large number (up to 168 unknowns) of analytes. The analytical run on this instrument is controlled with software (QC Expert[®]) to enable predefined analysis parameters such as the number of repeats, wash time and quality control limits to be used. The concentration of each element was measured three times and an average value of these readings is reported in this work. The automatic calibration of

the instrument was programmed to repeat every hour with a simultaneous calibration check against the quality control solution.

The detection limit of an element was generally checked at the end of each analytical run. The detection limit of an element in solution correspond to three times the standard deviation measured when 10 analysis of the element in a blank sample are taken. The detection limit of an element in the sample solution can be defined by Equation 3.1.

$$\begin{aligned} \text{Detection limit in sample (ppm)} & \qquad \qquad \qquad \text{Equation 3.1} \\ & = \text{detection limit in solution} \\ & \times \frac{\text{sample volume (ml)}}{\text{sample mass (g)}} \end{aligned}$$

The elemental concentrations in each sample were calculated by utilizing Equation 3.2, the original sample mass and dilution factor.

$$\begin{aligned} \text{Element concentration in sample (ppm)} & \qquad \qquad \qquad \text{Equation 3.2} \\ & = \text{concentration in solution (ppm)} \\ & \times \frac{\text{sample volume (ml)}}{\text{sample mass (g)}} \end{aligned}$$

The results from this analysis are presented in subsequent chapters.

3.3.3.5 Positron Emission Tomography (PET)

Positron Emission Tomography (PET) is a well established technique in the medical profession for quantitative *in vivo* characterisation of the metabolic processes (Fan *et al.*, 2006 a & b). It involves the injection of a liquid radioactive tracer into a biological body, the pair of emitted gamma rays from this tracer are then used to obtain a three dimensional representation, using a PET scanner. PET has the

potential to be modified for use as a tool in non-destructive tracking of single and multiple particles' real time motion inside an actual engineering structure. The pioneering work in this field has been carried out at the University of Birmingham, UK, where this reported work was also carried out. The Positron Emission Particle Tracking (PEPT) system shown in Figure 3.9 can track three dimensional motion of different size and shape tracer particles such as bronze, glass, sand and ilmenite in distinct particle beds such as the ones used in this study.

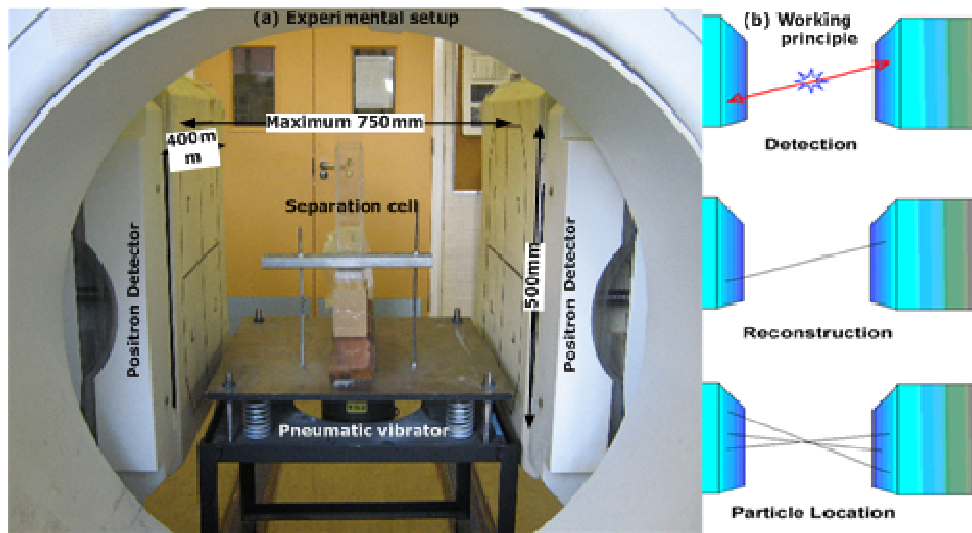


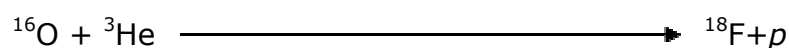
Figure 3.9: Positron Emission Particle Tracking (PEPT) setup.

The quick (within seconds) vibration driven separation of high density difference materials can help justify the assumption that; the PEPT data collected over a relatively long period of time under the same experimental conditions can pseudo represent the whole particle bed motion and velocity fields. One of the advantages offered by this technique is the use of a tracer particle with parallel physical and chemical properties to those of the bulk particle bed.

3.3.3.5.1: Radioactive labelling of a tracer particle

The tracking efficiency of PEPT is strongly dependent on the amount of radioactivity labelled on a single particle. Radioactivity can be labelled by three different techniques namely; direct activation, surface modification and ion exchange. The selection of a particular technique is generally limited by the particles' ability to withstand high temperatures experienced during the radioactive beam bombardments.

- ❖ In direct activation particles of sizes between 1 and 10 μm that are capable of withstanding high temperatures ($\sim 400^\circ\text{C}$) during 33MeV helium, ^3He , radioactive beam bombardments are normally used. The bombardment from a cyclotron (Scanditronix MC40) results in the formation of fluorine 18, ^{18}F , radioisotopes by conversion of a few oxygen atoms in the target particle by the following reaction (Fan *et al.*, 2006a & b);



- ❖ The radioisotope ^{18}F has a half-life of about 110minutes, enough for majority of the laboratory scale studies. Direct activation cannot take effect in the absence of oxygen (O) atom. Furthermore, the amount of radioactivity achieved in $<1000\mu\text{m}$ particles is too low for accurate tracking by PEPT. This is mainly limited by the fact that the amount of labelled radioactivity is directly proportional to the cross-sectional area of the particle, which is a function of its size (Fan *et al.*, 2006a).
- ❖ Smaller tracer particles ($200\text{-}600\mu\text{m}$) can be labelled by using an ion exchange technique. In ion exchange labelling the radioisotope ^{18}F is produced as a dilute solution of fluoride ions in deionised water. The ^{18}F is then made to exchange with the counter-ions in ion exchange resin beads under

specific conditions. Hence, a suitable radioactivity level (350-1000 μ Ci) in target particles can be achieved for tracking by PEPT. However, the radioactive resin beads cannot represent all of the bulk test material properties. The densities of ion-exchange organic polymer beads are close to 1g.cm⁻³. The amount of radioactivity labelled by this technique is controlled by the ion-exchange properties of the resins, anions present in the radioactive water and processing time (Fan *et al.*, 2006 a & b).

- ❖ Surface modification is another important technique that can be used to improve the selective adsorption of ¹⁸F on a particular particle surface. In this process, metallic ions form active sites on the solid surface on to which the anions bind. The commonly used metallic ions for surface modifications are Fe³⁺, Pb²⁺ and Cu²⁺. Fe³⁺ is the most chemically active and can adsorb onto most of the solid surfaces (Fan *et al.*, 2006 a & b).

Once radioactively labelled, the radionuclide in the tracer particle decays by emitting a positron as shown in Figure 3.10.

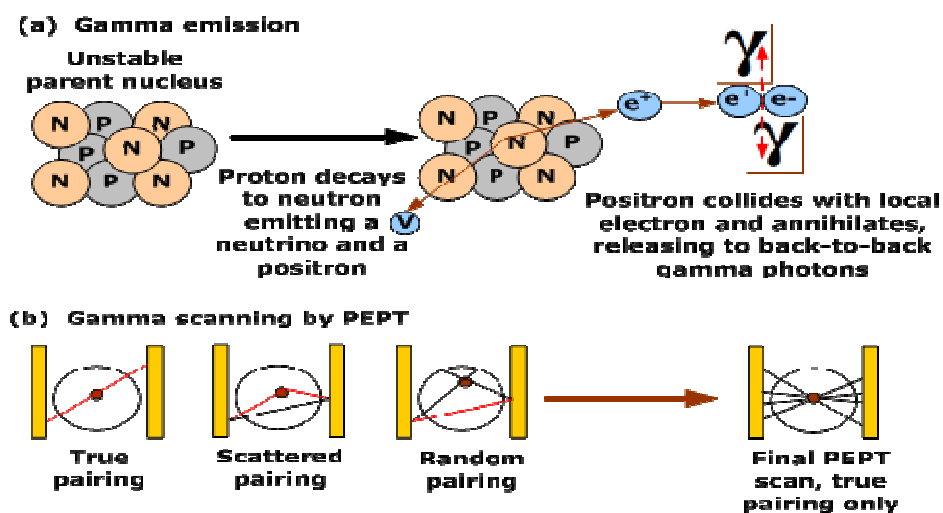


Figure 3.10: Gamma (γ) photons emission mechanism and its scanning by PEPT.

The positron rapidly annihilates with an electron, giving rise to a pair of back-to-back 511keV gamma (γ) -rays. These γ -rays are then scanned to determine the three dimensional particle positions in space as shown in Figure 3.10.

3.3.3.5.2 Positron Emission Particle Tracking (PEPT) setup

The almost collinear, very penetrating and opposite direction travelling high energy photons (γ -rays) can be detected by a scanner and/or camera as shown in Figure 3.9 and Figure 3.10. The PEPT system used in this work consisted of a pair of multi-wired chambers with an active area of 500x400 mm² that can be separated by up to 750 mm (Figure 3.9; Figure 3.10) (ADAC Forte scanner). The emitted γ -rays can be simultaneously detected in two scanner chambers and an arbitrary line of response defined. The positron camera can record up to 100k γ -ray pairs per second for subsequent analysis. The detection of a particle location resulted in <10ms by geometric triangulation, which is based on the fact that for a given set of events the individual lines of response will meet at some point in space, which is the particle location. This is carried out by collecting enough coincident pairs of γ -ray data (by a suitable resolution camera) so as to eliminate scattered and random γ -ray backgrounds with the help of an iterative algorithm run on a computer (Figure 3.10). The system can typically track particle positions with ± 1 mm error at 50-200 locations per second. Particle velocity of 10m.s⁻¹ corresponds to γ -rays detections at nearly 20 to 40 kHz (Parker *et al.*, 1993).

For accurate particle tracking separation cells must be placed away from detector edges and close to the centre of camera/scanner. Slow moving tracer particles (speed=50 mm.s⁻¹) can be located approximately 10 times per second and tracking is accurate up to

$\pm 10\%$. The particle tracking carried by a PEPT system is only limited by the particle bed thickness and the amount of activity on the tracer particle. The PEPT data acquired from this system can be stored and displayed on a computer interface which can also be used to record the 3D motion of the tracer particle. This information can then be used in computing particle occupancy, average velocity and velocity fields.

3.3.4 Qualitative means of analysis

3.3.4.1 Visual estimation of particle separation

In preliminary stages of particle separator cell design, the particle separation grades were mainly assessed visually. Particle separation at this stage was defined in terms of the separated material that moved out of the separation cell geometry. Since the ingredients of the synthetic particle mixtures were known, the separated products could simply be weighed to reveal the extent of their recovery. The visually observed particle separation behaviours were categorised as "good" when an estimated 80%wt of the separated product was recovered with little or no visible contamination. "Poor" particle separation was recorded when the separated product recovery fell below 50%wt and "no separation" was recorded when either the particle separation recoveries fell below 40%wt or considerable amounts of contamination was seen in the separated products. The above mentioned criterion was only used in the preliminary stages of particle separator cell design and the true particle separation grades and recoveries were always confirmed by other quantitative analysis techniques described in Section 3.3.3. Furthermore, the separating particles in the first few minutes of any vertical vibration treatment were recycled into the

main working chamber. This practice was followed to allow the vertical vibration induced particle separation system to reach somewhat closer to a steady state.

3.3.4.2 Digital imaging technique

A Canon power shot A430 camera with an optical sensor resolution of 4.0 mega pixel (2,272x1,704 pixels) with built in auto-focus was used to record the still and moving images. The movie recording mode could capture 640x480 pixel images at 10 frames per second with audio. The shutter speed of this camera ranged from 1/2,000 to 1 second and the camera was fixed on a tripod to steady the shot. The camera was placed at a sufficient distance away from the apparatus to clearly capture the desired area of the vibration separation cell, and used in the presence of an ultra-cool 90 Watt fluorescent light to capture good quality pictures. The vibration bench was stopped at definite time intervals to take still images to visually reflect the progress of particle separation. The pictures and movies from this camera were later transferred to a windows[®] XP based Pentium-IV Viglen computer via a universal serial port (USB).

3.3.4.3 Scanning Electron Microscope (SEM) imaging

The versatile Quanta 600 high resolution, field emission Scanning Electron Microscope (SEM) used in this work is shown in Figure 3.11.

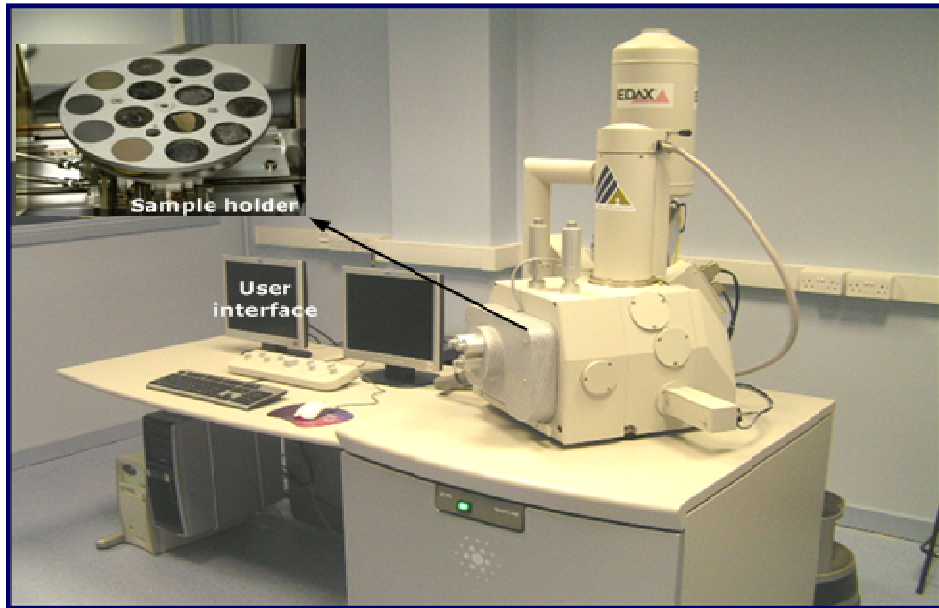


Figure 3.11: Scanning Electron Microscope (SEM), Quanta 600 (FEI company).

This SEM model could capture digital format images in three different operational modes: high vacuum (for electrically conducting materials), low vacuum (for non-conducting materials) and ESEM. The ESEM mode allows operating SEM at less than high vacuum with the introduction of a gas into the chamber. This is beneficial in imaging non-conductive and beam sensitive surfaces. The SEM model is equipped with a motorized X-Y-Z tilt-rotate stage that could provide the following movements:

X=Y=150 mm (motorized); Z=65 mm (motorized);

Tilt = +70 to -5degrees (motorized).

Magnification = 100X (at longest working distance) to 100,000X in single quadrant view of the Quanta user interface on a 19" liquid crystal display (LCD) monitor.

The SEM used Microsoft Windows XP graphical user interface to enable the images to be stored in TIFF, BMP, JPEG or AVI file formats in 8 or 16bit depth to the hard disk.

The equipment associated with SEM Quanta 600 model included: back scattered electron detector, infrared (IR) charge couple device (CCD) chamber camera, energy dispersive X-ray spectrometer (EDX (Genesis EDAX Company)) system equipped with X-ray mapping and digital imaging. The EDX can be used to gather information about the elements present within the sample.

3.4 Concluding remarks

This chapter has described the various material and methods used in this work. The particle separation experiments were carried out on a scaled up vibration separation bench. The subsequent analysis of the separated particle fractions was carried out using a range of quantitative techniques such as sink-float, sieve analysis, particle density measurement by helium pycnometer, ICP-AES analysis, positron emission particle tracking and qualitative techniques such as digital photographic imaging and scanning electron microscope imaging. The diverse particle nature dictates the use of all these techniques to accurately assess the particle separation behaviours. Calibration graphs and repeat analysis were undertaken to establish the required confidence in the reported results.

Discrete element modelling of the vertically vibrated particle bed

4.1 Introduction

As discussed in Chapter 2, most of the particulate processing knowledge remains empirical and the poor understanding of how to model particulate phenomena has resulted in the development of very few general approaches for particulate analysis. The particulate models based on kinetic theory include some constraining assumptions that limit the use of this approach to the whole range of the particulate phenomena (Campbell, 1990). There is yet no equation of particle motion analogous to the Navier-Stokes equation for fluids (Yang, 1999). The theories used for describing particulate flows contain many limiting assumptions e.g. particles are round, inter-particle collisions are instantaneous and binary, the coefficient of restitution is constant and the random motion of particles is independently distributed (Campbell, 1990; Yang, 1999). Furthermore, the laws on mechanics of interactions in particulate

materials are generally derived from the appropriate statistical averaging (Chou, 2000).

In the scenario of having many limiting assumptions for particulate theories, computer simulations and experiments provide a valuable tool to model particulate phenomena (Kruggel-Emden *et al.*, 2007). It appears that renewed interest in particulate material research is partly due to the development of powerful computer simulation tools that can now tackle thousands of particles with better reproducibility as computer processing speeds and data storage capabilities have increased since 1980s (Wassgren, 1997; Kruggel-Emden *et al.*, 2007; Asmar *et al.*, 2002). Computer simulations offer several important features for studying particulate materials such as, reduced processing times and costs, the most significant among all being that the state of particulate system is known at all times (Fazekas, 2007). Hence, the interior of a dynamic particle state can be examined and measurements can be made that may be difficult to perform during the course of any real and/or physical experiments (Zhu *et al.*, 2008). Computer simulations are not only used to replicate and validate experimental results but they are also capable of predicting the real-time dynamic particle bed behaviours in several divergent conditions such as during the course of particle segregation which is difficult or barely, if at all, accessible to detailed examination by real and/or physical experimentation (Wassgren, 1997; Fazekas, 2007; Zhu *et al.*, 2008).

The work presented in this chapter investigates the application of a DEM-fluid simulation program, developed by Langston, Fraige and Asmar (Fraige and Langston 2006; Asmar *et al.*, 2002), that was modified to model the vertically vibrating particles in a confined virtual container. The DEM-fluid simulation application in this work was aimed to replicate some of the important experiment based dynamic particle attributes such as particle bed tilting, convection currents and segregation under the influence of vertical vibration.

Furthermore, the vertical vibration induced particle segregation experiments were simulated with DEM to aid in the development of a complete DEM-fluid simulation model. The work presented in this chapter gives some background to the DEM simulations, describes the selected computational DEM model and discusses the key simulation results.

4.2 Background to DEM simulations

The highly discontinuous nature of particulate materials makes them a favourable choice for treatment by discrete methods (Fazekas, 2007; Yang, 1999; Rosato *et al.*, 2002; Zhu *et al.*, 2008; Asmar *et al.*, 2002; Fraige and Langston, 2006). The term 'discrete' refers to the fact that the DEM computer simulation models particulate materials as a system of individual particles (Wassgren, 1997). Many computational methods such as Monte Carlo techniques (Fan and Tang, 2007), Cellular Automata and the hard and soft particle models (Wassgren, 1997) including the different variants of Distinct/Discrete Element Modelling (DEM) introduced by Cundall and Strack in 1979 (Tijssens *et al.*, 2003; Fazekas, 2007), use the discrete element/particle based simulation approach (Herrmann and Ludding, 1998).

The Monte Carlo simulation techniques are statistically based where a particle assembly state is chosen based on the energy of a particle configuration (Wassgren, 1997; Fan and Tang, 2007). For each new particle state in the Monte Carlo technique, particles are given a random velocity or position within some distribution function. The configuration which gives the lowest possible system energy is chosen as the new particle state. Cellular Automata is a lattice-based kinematical approach where particles are forced to move on discrete lattice points (Wassgren, 1997). In Molecular Dynamic

(MD) simulations, the particle-particle and particle-wall interactions are modelled as binary, instantaneous collisions and the post-collision particle states are determined based on the classical particle dynamic theories (Fazekas, 2007). Hard particle models have originally evolved from the Molecular Dynamic simulations of rarefied gases and are based on the limitation that the individual particles move in the well defined trajectories until an instantaneous collision occurs with another particle or with a boundary wall (Wassgren, 1997). In hard particle simulation models, the time at which the first collision occurs is computed from particle trajectories and the positions and velocities of all the particles are then updated to that time (Fazekas, 2007). Next, the particle-particle and particle-wall collision results are computed, the time when the next collision will occur is found, and the process is repeated until a simulation end condition is satisfied (Chou, 2000).

Computer simulations based on DEM incorporate concepts from various domains of discrete geometry, theoretical physics and numerical computing (Fazekas, 2007; Wassgren, 1997). The main advantage offered by a DEM simulation is that the highly complex systems such as particle conveyers, particle mixing and segregation can be modelled with basic data without the need of any oversimplifying assumptions (Asmar *et al.*, 2002; Zhu *et al.*, 2008, Fraige and Langston, 2006). In DEM, the trajectory of each participating element/particles is calculated from its interactions with other elements/particles, interstitial fluid and with external factors such as gravity, electrical and magnetic fields (Yang, 1999; Fazekas, 2007; Zhu *et al.*, 2008). The relationship between different micromechanical properties and macroscopic particle effects can be studied in DEM simulation which makes it an extremely useful tool for testing new theoretical models, concepts and ideas (Fazekas, 2007). The capability of realistically capturing the characteristics of particulate materials makes DEM a useful tool

to design, analyse and optimize many different industrial particulate processes (Wassgren, 1997; Yang, 1999; Zhu *et al.*, 2008).

Many dynamic particle states evolving in gravity and vertical vibration influenced flow fields have multiple and long duration inter-particle and particle-wall contacts (Wassgren, 1997). To incorporate multiple and long duration particle-particle and particle-wall contacts, the DEM simulations use models based on the soft particle approach to calculate the forces acting on each particle in the system. In soft particle based DEM simulations, Newton's second law is used to calculate the acceleration of each particle and the resulting particle states are determined by numerically integrating the accelerations in small time steps, Δt to yield both velocities and positions (Yang, 1999). Next, the new forces are calculated based on the updated particle states and the procedure is repeated until some final simulation ending criteria is satisfied (Wassgren, 1997). The soft particle based DEM simulation technique determines different inter particle forces and particle states. The soft particle based DEM simulation technique however requires more computational power in comparison to its other particle simulation counterparts such as Cellular Automata and the Monte Carlo simulation techniques (Wassgren, 1997).

Biswas *et al.*, (2003) used the three dimensional soft-sphere based Molecular Dynamic technique to model the finely and parallel sized binary particle mixtures that were vertically vibrated in the presence of air which replicated most of their experimentally observed particle segregation phenomena. Zeilstra *et al.*, (2006) used a numerical simulation based hybrid particle dynamic and computational fluid dynamic models to simulate the air induced segregation of the equal sized bronze and glass particles. Their (Zeilstra *et al.*, 2006) computer simulations reproduced many of the commonly observed particle segregation behaviours such as bronze on top (in a vertical vibration time of 2.6 seconds) and bronze sandwich configurations

(in a vertical vibration time of 21 seconds) with the magnitudes of vertical vibration frequency and dimensionless acceleration in the range of 55-130 Hz and 10-11 respectively. Among others, the particle segregation behaviours simulated by Zeilstra *et al.*, (2006) with parallel particle mixtures were experimentally observed by Brutally *et al.*, (2002 and 2003). Other examples of DEM simulation technique investigating the side wall induced particle convection cells in the vertically vibrating particulate systems can be seen in the work of Gallas *et al.*, (1992); Taguchi, (1992); and Lee, (1994).

4.2.1 Soft particle based DEM simulations

The concept of soft particle simulation is straightforward however; there are many constraints that must be addressed before its application (Fazekas, 2007; Wassgren, 1997). First, the simulation environment must be addressed which includes whether the simulation is carried in two (2D) or three dimensions (3D), number of particles, types of inter-particle forces and the applicable boundary conditions. Next, the particle contact models and the physical constraints of the simulated system are addressed. Lastly, the numerical schemes for integrating the equations of particle motion are selected.

Most of the reported DEM simulations are carried in two instead of three dimensions mainly because of the need of less number of computations and memory storage requirements (Gallas *et al.*, 1992; Taguchi, 1992; Wassgren, 1997; Asmar *et al.*, 2002). The coordinate system used in the DEM simulation work reported here is shown in Figure 4.1.

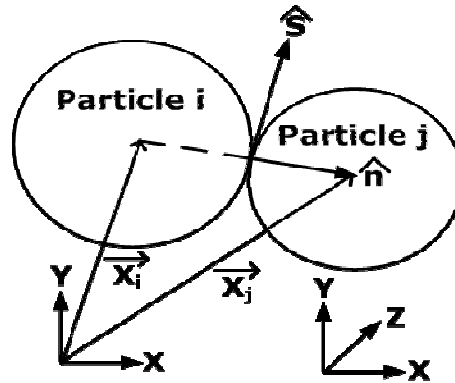


Figure 4.1: The coordinate system used in the DEM simulation.

Computer simulations carried in two dimensions have produced results that are comparable with the real system experiments for example, the shaking of particles in a container (Gallas *et al.*, 1992; Taguchi, 1992; Zhu *et al.*, 2008). The number of inter-particle contacts in three dimensions is greater than that for the same in a two dimensional simulated system which implies that there are an increased number of paths along which the forces can be transmitted and this result in consuming more computational power for a three dimensional simulated system (Gallas *et al.*, 1992; Taguchi, 1992; Wassgren, 1997; Zhu *et al.*, 2008).

The main purpose of a DEM simulation is to get some insight into the behaviour of a large assembly of discrete particles hence the use of sufficient number of particles in the computer simulation is important (Wassgren, 1997). However, what constitutes a sufficient number of particles in a computer simulation is still open to debate. The use of too few particles can result in non-representation of a real particulate system however, on occasions the use of few particles is aimed to minimize the computational costs.

The DEM simulation starts with an initial configuration of a physical particulate system (Fazekas, 2007). The usual DEM simulated systems have open boundaries however, periodic boundary conditions to imitate the large particulate systems can also be used.

Most of the particulate systems simulated by DEM consist of two dimensional circular disks in the planar and/or cylindrical walls however, more complex objects such as polygonal, polyhedral, cubical (Fraige *et al.*, 2008) and ring shaped elements can also be modelled by DEM (Fazekas, 2007; Wassgren, 1997). In DEM, the use of two dimensional circular disks can result in an easy detection of the particle-particle and particle-wall collisions, particle overlaps and the location of contact points during the inter-particle and side wall collisions. Furthermore, circular particles are used in DEM as the kinetic theories for dynamic particles have assumed spherical and/or circular shaped particles (Wassgren, 1997). Nevertheless, the resulting conclusions derived from the DEM simulations of cylindrical and/or spherical shaped particles are often considered to hold for the other kind of particle shapes (Lehon *et al.*, 2003).

A particular advantage of using a soft particle model based DEM simulation approach is that the many different types of forces can be simulated to act on different particles (Fazekas, 2007). The forces are generally classified as either body or contact forces (Wassgren, 1997). Body forces such as gravitation and/or electromagnetic fields typically act on all dynamic particles. However, the contact forces such as cohesive, elastic, friction and damping forces are event driven and act only when the particles are in a contact (Wassgren, 1997; Asmar *et al.*, 2002; Fraige and Langston 2006). In a 2D simulation system, the contact forces are usually modelled in the normal and tangential directions (Asmar *et al.*, 2002). Interstitial fluid forces are the third type of force that can also be included in the soft particle based DEM simulations (Wassgren, 1997). In DEM, the interactions of particles are usually explicitly computed (Fazekas, 2007). In simple particle systems, only elasto-plastic contact forces are usually considered however, in complex systems, cohesive, hydrodynamic, electric, and magnetic interactions can also be modelled. The force calculations in DEM are based on the principle that during a small time step, the particle

forces and accelerations can be assumed constant, while the particle velocities are allowed to vary linearly hence, the selection of a simulation time step is crucial to maintain the stability and accuracy of the simulation algorithm (Asmar *et al.*, 2002; Fraige and Langston 2006). In DEM, particles are moved to new locations by solving the Newton's equation of particle motion (Fazekas, 2007). The force calculation and integration procedure is repeated several times and the data can either be processed during the course of a simulation run to create the computer animations or can be stored for later evaluation.

4.3 The applied DEM model

The DEM simulation work reported here has modelled circular shaped particles with linear interactions as these particle shapes were considered to best represent the spherical shape features of the particles used in the real and/or physical experiments reported in this work and in the experiments reported by Burtally *et al.*, (2002 and 2003) and Mohabuth, (2007). Note that instead of simulating circular disks, the DEM simulation models particles as spheres constrained to move in two dimensions. The difference between using the disks or spheres appears only in the moment of inertia of the particles (Wassgren, 1997). The moment of inertia for a circular disk is $\frac{1}{2}mr^2$ and that for a sphere is $\frac{2}{5}mr^2$ where m , is the mass of the particle and r is the particle radius. The equations representing the moment of inertia of a particle shows that the spheres rotate more easily in comparison to disks. The mass, m of a spherical particle can be represented by Equation 4.1,

$$m = \rho \frac{4}{3} \pi r^3 \quad \text{Equation 4.1}$$

where, ρ represents the particle density, r is a particle radius and $\pi = 3.141593$ is a mathematical constant. If the DEM simulations are modelled to consider only the inter-particle and body forces, the mass and density of a spherical and/or disk shaped particle will not affect the simulation results. However, if other forces such as electrostatic and/or interstitial fluid forces are considered then the mass of a spherical particle (Equation 4.1) could potentially become important as it would significantly affect the momentum of the individual particles (Wassgren, 1997).

Variants of DEM simulations differ mainly in the way in which the inter-particle interactions (hard and soft-body) are calculated (Fazekas, 2007). In this DEM work, a soft body inter particle interaction approach was used.

4.3.1 Construction of a discrete geometry

Handling the high level of discreteness in the particulate system makes DEM simulation an algorithmically complex problem (Fazekas, 2007). Finding the particle pairs which are close to each other is a computationally challenging problem (Asmar *et al.*, 2002). Solving this purely geometrical problem, which is mostly independent of the way in which the inter-particle and particle-wall interactions are calculated, does not affect the outcome of a DEM simulation (Fazekas, 2007). The overall performance of a DEM simulation program depends on building, as fast as possible, a sufficiently tight set of possibly interacting particle pairs and applying the interaction model only on those particle pairs that are in contact. The simplest way to find the particles that are close to each other is to divide the simulation space into cells of a given size and assign each particle to the cell in which its centre point is

located. Different geometric constructs that are used to speed up the detection of the interacting particles are shown in Figure 4.2.

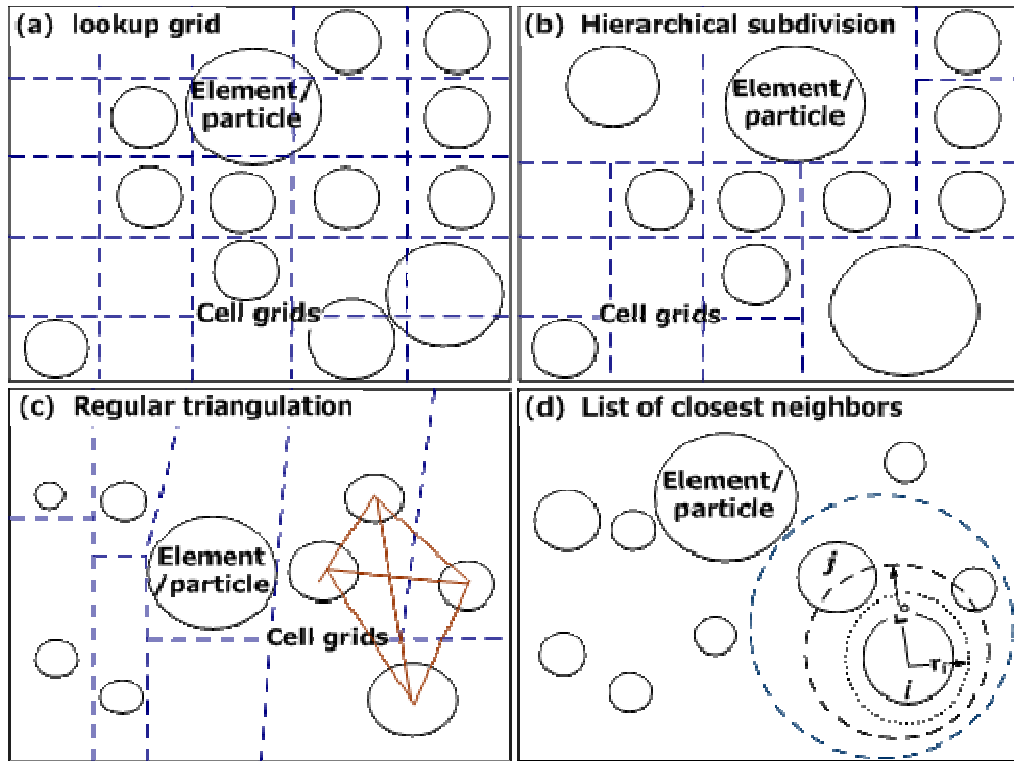


Figure 4.2: Geometric constructs/grids which are used to speed up the detection of the interacting particle pairs (Adapted from Fazekas, 2007).

In DEM, it is assumed that in a single time step the disturbances cannot propagate further than the immediate neighbour of a single particle (Asmar *et al.*, 2002). Nevertheless, this assumption has proved less defective in DEM simulations in comparison to the other usual assumptions of using the spherical shaped particles and not modelling the dynamic particle breakages (Asmar *et al.*, 2002). Nevertheless, finding the possibly interacting particles in a geometric construct/grid (Figure 4.2) is done by checking the neighbouring cells. If the particles and the cells have a more or less same size then each geometric cell and/or grid is expected to contain a single particle and the lookup grid construct shown in Figure 4.2 gives a solution close to optimum. However, if particle

size differentials are present in the simulation system, the lookup type grid selection becomes less efficient.

In case of a finely sized geometric grid, having a grid cell size close to the smallest particle size, not only the adjacent cells but the second and/or higher order neighbours are also considered in the force calculation models (Fazekas, 2007). In a region where the particles are mostly small size, this is needless. The use of a course grid size, having a grid cell size close to the size of the largest particle, can result in accommodating many small sized particles in a single grid cell which may not be in contact with any other particles in the adjacent cells. These conditions will lead to the wastage of CPU time. However, the problems can be solved by using an adaptive cell size approach, as shown in Figure 4.2, which results in a hierarchically grid structure. In a hierarchical grid structure, each box which contains more than one particle is further divided into even smaller size grid cells and this procedure is repeated until each box contains no more than one particle (Fazekas, 2007). Other grid designs include regular triangulation and the list of close neighbouring particles as shown in Figure 4.2. The DEM work reported here used the list of close neighbours (Figure 4.2) geometric construct and/or grid structure to speed up the detection of the interacting particle pairs.

The dynamic time scale of a particulate system is difficult to predict in the DEM simulation conditions where a slowly deforming particulate system (such as the one under the influence of vertical vibration) suddenly moves rapidly in an avalanche (Fazekas, 2007). If the refresh rate is not chosen correctly some interacting particle pairs might be omitted from detection and hence some forces might go without calculation and this can lead to particles going too close to each other, producing huge overlaps resulting in huge forces, and the simulation system can virtually explode (Fazekas, 2007). Extending the geometric algorithms outlined in Figure 4.2 to three

dimensions incorporating spherical shaped particles is usually straight forward however, working with non-spherical shape particles in three dimensions has proved troublesome to some extent.

4.3.2 Particle contact models

The physical essence of a DEM simulation is given by the models that define the contact interactions of the participating particles (Fazekas, 2007). The particle contact models are used to measure the geometrical overlaps and the relative velocity of the particles in a contact. The contact models and their parameters are the main factors which determine the outcome of a DEM simulation program. In engineering DEM simulation applications, particle stiffness, restitution coefficient of particle collisions and the internal frictions are carefully calibrated in order to match the experimental results as close as possible. Even though the contact model, its parameters, and the size of a simulated sample cannot exactly replicate the experimental situation, the outcome of a simulation should be comparable with the experiments.

The widely used soft sphere contact model in DEM is the so called linear spring-dashpot model (Fazekas, 2007; Wassgren, 1997). The selection of a soft sphere model, as used in this work, was based on the fact that most of the real particles used in the vertically vibrating particulate systems experience the multiple and long duration particle-particle and particle-wall contacts, at-least for part of an oscillation cycle. This point rules out the use of a hard sphere contact model in this work. Also, it was expected that the inter-particle forces play an important role in the formation of different particulate phenomena such as segregation (as discussed in Chapter 2) hence, a soft particle based contact model was expected to best

replicate the experimental particulate phenomena. Nevertheless, the soft sphere based linear spring dashpot contact model is based on the idea that when a contact relative to the surface orientation is established between the two particles, a normal and tangential spring is created at the initial contact point (Fazekas, 2007). The motion of particles is then assumed to govern by the elongation of these imaginary springs and the springs act until the particles separate from each other. The schematic of a soft sphere based linear dashpot contact force model is shown in Figure 4.3.

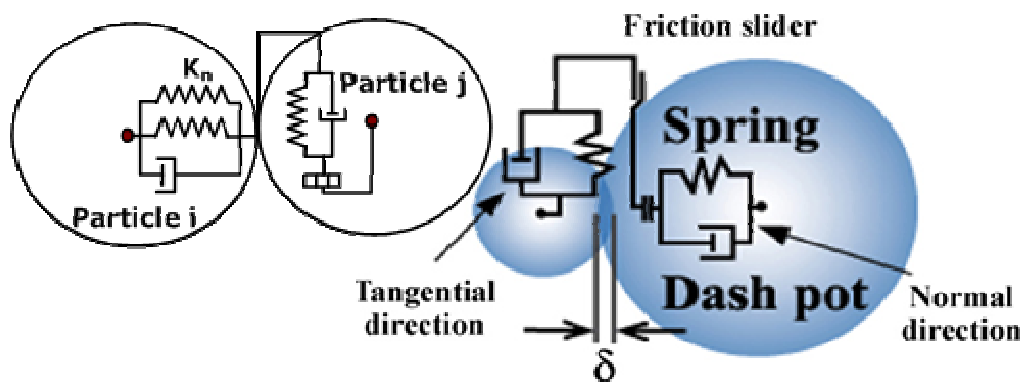


Figure 4.3: Schematic diagram of contact forces that are modelled by using a soft sphere based linear spring-dashpot model (Fazekas, 2007; Asmar *et al.*, 2002; Wassgren, 1997).

In the soft sphere based linear spring-dashpot contact model as shown in Figure 4.3, the springs provide a restoring force that tries to push the particles apart, and the dashpot provides the dissipation energy that makes the collisions inelastic (Wassgren, 1997). In addition, a friction slider with an associated friction coefficient μ_f is added in series with the tangential-direction spring and dash-port so that there is no tangential slippage between the particles as long as the tangential force is smaller than μ_f times the normal force (Figure 4.3). If this value is exceeded, the particles will slip with a force equal to μ_f times the normal force, F_n (Wassgren, 1997).

4.3.3 Particle contact forces

In a DEM simulation, each equation of particle motion relates the change in a particle's position to its velocity and the forces to which it is subjected (Wassgren, 1997). The total force on a particle consists of a constant gravitational acceleration and the forces exerted over the points of contact with its immediate neighbours and the boundary walls of the simulation (Fazekas, 2007). In the linear spring-dashpot contact model as used in this DEM simulation, the normal and tangential components of force (F_n and F_t respectively) which the particles in contact exert on each other, were calculated by using Equation 4.2 and Equation 4.3,

$$F_n = -K_n u_n - \gamma_n v_n \quad \text{Equation 4.2}$$

$$F_t = -K_t u_t - \gamma_t v_t \quad \text{Equation 4.3}$$

where $K_{n,t}$ and $\gamma_{n,t}$ are the normal and tangential stiffness and damping coefficients, u_n and u_t are the normal and tangential displacements relative to the initial contact point (elongation point of the spring), and v_n and v_t are the relative velocities at contact point of the arbitrarily translating and rotating particles (Fazekas, 2007). The normal displacement, measured along the direction perpendicular to the surface of the particles in contact, depends on the relative position, size, and shape of the particles (Fazekas, 2007), for example, in case of two spheres this is represented by Equation 4.4,

$$u_n = R_{r1} + R_{r2} - \|r_{c1} - r_{c2}\| \quad \text{Equation 4.4}$$

where $R_{r1,2}$ are the radii of the spheres and $r_{c1,2}$ are the centre points of the spheres. Equation 4.4 is non-negative as long as the spheres overlap (Fazekas, 2007). When u_n becomes negative, the bodies do not touch each other and no contact force should act between them (Fazekas, 2007).

The tangential displacement u_t was calculated by integrating the tangential velocity v_t in the contact plane during the lifetime of contact by using Equation 4.5.

$$u_t(t) = \int v_t(t)dt \quad \text{Equation 4.5}$$

In two dimensions the tangential displacement, u_t and the tangential velocity, v_t in Equation 4.5 can be represented as scalars and hence the vector integral in Equation 4.5 reduces to a simple scalar integral (Fazekas, 2007). In three-dimensions the situation is a bit more complex and care must be taken in order to keep u_t in the contact plane. The physical relevance of computing a tangential force lies in the fact that it can model static and sliding friction between the particles (Fazekas, 2007). Care must be taken to avoid the ghost forces, instabilities and spurious dissipation (Fazekas, 2007). According to Coulomb's rule, any friction force which act in the tangential direction, F_t must obey the constraint given in Equation 4.6,

$$\|F_t\| \leq \mu_f \|F_n\| \quad \text{Equation 4.6}$$

where μ_f is the coefficient of friction between the two sliding surfaces (Fazekas, 2007). In order to satisfy the Coulomb's rule (Equation 4.6), F_t was shortened when its magnitude becomes too large, while its direction was kept the same. For modelling sliding contacts, the elongation of the tangential spring F_t was relaxed to $\mu_f \|F_n\|/k_t$ accordingly.

A simple and computationally efficient model of friction is obtained by assuming viscous damping at small relative velocities and by using the largest friction force allowed by the Coulomb's rule (Fazekas, 2007). In linear dashpot model, care must be taken in choosing the friction model and setting its parameters in order to avoid the anomalies originating from the different time scale characteristics of the normal and tangential forces. Further

extensions in the base friction model can incorporate rolling friction, viscous friction with the interstitial medium and the coupling between sliding and spinning motions (Fazekas, 2007).

In the linear spring dashpot model, exact relation between the model parameters (e.g., stiffness and damping coefficients), collision time and the restitution coefficient of an individual collision is usually found analytically (Fazekas, 2007). Other models estimate friction parameters on numerical basis however their application in a real DEM environment is challenging. Nevertheless, the details regarding the contact models other than the linear spring dashpot model are not discussed in detail as this goes beyond the scope of the limited work reported here.

In this work, a linear spring dashpot model as shown in Figure 4.3 was used to calculate the particle-particle and particle-wall contact forces. The normal contact force F_n in the DEM-fluid model used in this work was calculated by using Equation 4.7

$$F_n = F_{ne} + F_c + F_{nd} \quad \text{Equation 4.7}$$

where F_{ne} is the normal elastic force, F_c is the cohesion force and F_{nd} is the normal damping force. The tangential contact force F_t is limited by the Coulomb's frictional limit to the point where the surface contact shears and the particles begin to slide over each other (gross sliding). The tangential contact force F_t in the DEM-fluid model used in this work was calculated by Equation 4.8 and Equation 4.9

$$F_t = F_{fbgs} + F_{td}, \text{ below the Coulomb's frictional limit} \quad \text{Equation 4.8}$$

and

$$F_t = F_{fags}, \text{ above the Coulomb's frictional limit} \quad \text{Equation 4.9}$$

where, F_{fbgs} is the elastic component of friction force prior to gross sliding, F_{td} is the tangential damping force, and F_{fags} is the friction force at and after gross sliding (Asmar *et al.*, 2002; Fraige and Langston, 2006).

4.3.3.1 Normal elastic force

In this DEM simulation, the normal elastic force F_{ne} which represents the repulsive force between any two particles was calculated by using Hook's linear spring relationship as given by Equation 4.10,

$$F_{ne} = K_n u_n \quad \text{Equation 4.10}$$

where K_n is the spring stiffness in the normal direction and u_n is the displacement between particles i and j as shown in Figure 4.3. The maximum particle overlap is desired around 0.1 to 1.0% which requires spring stiffness K_n to be in the order of 10^6 - 10^7 N.m⁻¹ (Asmar *et al.*, 2002).

4.3.3.2 Normal damping force

The normal damping force F_{nd} is modelled as a dashpot that dissipates a portion of the relative kinetic energy (Asmar *et al.*, 2002; Fraige and Langston, 2006). In this DEM simulation the F_{nd} was estimated by Equation 4.11,

$$F_{nd} = \gamma_n v_n \quad \text{Equation 4.11}$$

where v_n is the normal component of relative velocity and γ_n is the normal damping coefficient, which can be chosen to give a required coefficient of restitution ε which is defined as the ratio of the normal component of relative velocities before and after collision. In this

work the normal damping coefficient γ_n was estimated by Equation 4.12,

$$\gamma_n = 2\gamma_c \sqrt{m_{ij}K_N} \quad \text{Equation 4.12}$$

where γ_c is the coefficient of critical damping and was calculated by Equation 4.13.

$$\gamma_c = \frac{\ln(\varepsilon)}{\sqrt{\pi^2 + \ln^2(\varepsilon)}} \quad \text{Equation 4.13}$$

where m_{ij} in Equation 4.12 represents the mass of particles i and j which was estimated by Equation 4.14,

$$m_{ij} = \frac{m_i m_j}{m_i + m_j} \quad \text{Equation 4.14}$$

Although each particle can have a different coefficient of restitution however, in the general DEM modelling practice a sole value for all particles is used (Asmar *et al.*, 2002).

4.3.3.3 Friction force

In this DEM simulation, the variation in friction force prior to gross sliding F_{fbgs} was calculated by using the Hook's linear spring relationship as given by Equation 4.15,

$$F_{fbgs} = K_t u_t \quad \text{Equation 4.15}$$

where K_t is the tangential stiffness coefficient and u_t is the total tangential displacement between the two particle surfaces since their initial contact (Asmar *et al.*, 2002). As mentioned, the total tangential force is limited by the Coulomb's frictional limit. If u_t

exceeds $u_{t\max}$ then sliding occurs and u_t does not increase. In this DEM simulation, the friction force after gross sliding F_{fags} was calculated by using Equation 4.16,

$$F_{fags} = \mu_f F_{ne} \quad \text{Equation 4.16}$$

where μ_f is the coefficient of friction and F_{ne} is the normal elastic force. In this work the $u_{t\max}$ was calculated by using Equation 4.17,

$$u_{t\max} = \delta_r u_n \quad \text{Equation 4.17}$$

where δ_r is a constant and u_n is the total normal displacement. It has been shown that δ_r , which couples the tangential displacement to normal displacement, can be calculated as a function of Poisson's ratio ν_p and the coefficient of friction μ_f of the particles (Asmar *et al.*, 2002).

4.3.3.4 Tangential damping force

In this DEM simulation, the tangential damping force F_{td} (Equation 4.18) was modelled as a dashpot that dissipates energy as a result of the tangential particle motion.

$$F_{td} = \gamma_t v_t \quad \text{Equation 4.18}$$

where v_t is the tangential component of relative velocity between the particles and γ_t is the tangential damping coefficient. The tangential damping coefficient γ_t , calculated by Equation 4.19, can be chosen to give a specified coefficient of restitution ε_r which is defined as the ratio of post- to pre-collision tangential component of the relative velocity.

$$\gamma_t = 2\gamma_c \sqrt{m_{ij} K_t} \quad \text{Equation 4.19}$$

In Equation 4.19, γ_c and m_{ij} are the same as represented in Equation 4.13 and Equation 4.14. When gross sliding occurs then the value of $K_t = 0$ and in this situation the gross sliding F_{fags} (Equation 4.16) is the total force that dissipates energy from the tangential motion (Asmar *et al.*, 2002).

4.3.3.5 Particle-wall contacts

In this DEM simulation, the interaction of a particle with the vessel wall was modelled in a similar manner as a particle-particle contact. Even when the particle is in contact with two walls, only one contact is generally simulated in DEM (Asmar *et al.*, 2002). This assumption has proven to be less significant in comparison to the other assumptions that are routinely made in a DEM simulation.

4.3.4 DEM simulation parameters

The DEM simulation parameters used in this work were classified into two major categories which were based on the method in which they are chosen (Fazekas, 2007; Wassgren, 1997; Asmar *et al.*, 2002). The first category was for parameters that were taken directly from the experiments such as gravitational acceleration g ($\text{m}\cdot\text{s}^{-2}$), vertical vibration frequency f that is given by Equation 4.20,

$$f = \frac{\omega}{2\pi} \quad \text{Equation 4.20}$$

where in Equation 4.20, ω is the angular frequency, Hz, π is a mathematical constant, dimensionless vertical vibration acceleration given by Equation 4.21,

$$\Gamma = \frac{a\omega^2}{g} \quad \text{Equation 4.21}$$

where in Equation 4.21, a (m) is the oscillation amplitude, g ($\text{m}\cdot\text{s}^{-2}$) is the gravitational acceleration and ω is the angular frequency (Hz) that is given by Equation 4.20, container width, particle bed depth and/or height, mean particle diameter d , particle density ρ , particle-particle coefficient of restitution, particle-wall coefficient of restitution, particle-particle sliding friction coefficient and particle-wall sliding friction coefficient while the second is for parameters that were based on the force calculation contact models such as particle-particle and particle wall dashpot coefficient, tangential particle-particle and particle-wall spring constant and the DEM simulation time (Fazekas, 2007).

4.3.5 Modelling of external forces in DEM

4.3.5.1 Gravitational force

The gravitational force g was introduced into this DEM simulation model as a constant linear force, of magnitude $9.8 \text{ m}\cdot\text{sec}^{-2}$, acting at the centre of each particle.

4.3.5.2 Vibration force

In DEM, the vibration force can be introduced by oscillating the container (Asmar *et al.*, 2002). In this DEM model, the vibration force on the particle container was limited and/or confined to act in z-direction only. The particles moved as a result of a contact between the moving base wall and the particles. The particle's container movement was defined relative to the vessel base, which at any time was represented by Equation 4.22 and Equation 4.23,

$$\text{for } t < t_{start}, Z_{base} = 0 \quad \text{Equation 4.22}$$

$$\text{for } t > t_{start}, Z_{base} = a \sin (f(t - t_{start})) \quad \text{Equation 4.23}$$

where a is the vibration amplitude, f is the vibration frequency, t is the vibration time, and t_{start} is the time when the vibration first starts.

4.3.6 Air drag calculation

In this DEM simulation, the vertical vibration induced air drag on each particle was calculated by using Equation 4.24,

$$F_d = -\frac{\Delta P_p}{\Delta x} \left(\frac{V}{(1 - \varepsilon_v)} \right) \quad \text{Equation 4.24}$$

where ΔP was estimated in the lean particle phase (for particle void fraction $\varepsilon_v > 0.8$) by Equation 4.25 which was first proposed by Wen and Yu in 1966 (Fraige and Langston, 2006),

$$\beta = \frac{\Delta P_{lp}}{\Delta x} = \frac{3(1 - \varepsilon_v)}{4} \frac{C_d \rho_f \varepsilon_v^{-2.7}}{\bar{d}} |u_g - \bar{v}| (u_g - \bar{v}) \quad \text{Equation 4.25}$$

(Wen and Yu, 1966)

where ΔP_{lp} is the pressure drop in the lean particle phase, Δx is the length of the particle container, C_d is the coefficient of drag acting on a single particle, u_g is the interstitial gas velocity, \bar{v} is the average particle velocity and ε_v is the particle void fraction.

The pressure drop induced due to the presence of particles in the dense phase (for particle void fraction, $\varepsilon_v < 0.8$) was estimated by Equation 4.26 which was first proposed by Ergun in 1952 (Fraige and Langston, 2006),

$$\beta = \frac{\Delta P_{dp}}{\Delta x} = \frac{(1 - \varepsilon_v)}{\bar{d}\varepsilon_v^3} \left[150 \frac{(1 - \varepsilon_v)}{\bar{d}} \mu_{fv} \varepsilon_v (u_g - \bar{v}) + 1.75 \rho_f \varepsilon_v^2 |u_g - \bar{v}| (u_g - \bar{v}) \right] \quad \text{Equation 4.26}$$

(Ergun, 1952)

where ΔP_{dp} is the pressure drop in the dense particles phase and μ_{fv} is the interstitial fluid viscosity. In this work, the particle void fraction ε_v for each grid cell was estimated using the list of close neighbors (Figure 4.2) method.

The gas phase motion in this DEM-fluid model was predicted by the Euler's equation of motion which assumes the surrounding gas to be incompressible and in-viscid with no gravity and turbulence effects (Limtrakul *et al.*, 2007). The gravity effect on the surrounding gas was assumed negligible due to its lean density and the viscosity of the gas was made negligible due to the in-viscid gas assumption. The density of a gas can vary in the presence of pressure differentials that are generally generated in the vertically vibrated particle systems however, this change was assumed negligible and a constant density assumption was made for the whole of the vertically vibrated DEM simulated particulate systems. In this DEM work, the flow of the interstitial gas was fixed with the Euler's grid. In this work the equation of interstitial gas motion was based on the continuity and conservation of gas momentum relationship as given by Equation 4.27,

$$\frac{\partial(\varepsilon \bar{u})}{\partial t} + \nabla \cdot (\varepsilon_v \bar{u}_g \bar{u}_g) = -\frac{\varepsilon_v \nabla p}{\rho} + \bar{f}_s \quad \text{where } \bar{f}_s = \frac{\beta}{\rho} (\bar{v}_p - \bar{u}_g) \quad \text{Equation 4.27}$$

where \bar{u}_g is the interstitial fluid velocity, \bar{f}_s is the force exerted by particles on the interstitial fluid, \bar{v}_p is the particle velocity vector and β is the same factor as given in Equation 4.25 and Equation 4.26 for the lean and dense particle phases.

4.3.7 Integration of Particle motion in DEM

The general position of an arbitrary object and/or particle can be given with the prediction of a combination of the translational and rotational particle movements (Fazekas, 2007). The particle motion is generally described with translation of the particle's centre of mass and a rotation around an axis passing through this point. In soft body DEM simulations, the particle's translational motions are normally computed first and later the rotational integrations are solved.

The solution of Newton's equation of particle motion through a numerical scheme moves the particles to a new position from simulation step to the simulation step. By considering the total and/or net force F acting on a body of mass m the acceleration a_p of a particle was calculated by Equation 4.28.

$$a_p = F/m \quad \text{Equation 4.28}$$

With Euler's method, the new position and/or displacement and velocity of the particle was calculated by using Equation 4.29 and Equation 4.30,

$$r(t + \delta t) = r(t) + v(t)\delta t \quad \text{Equation 4.29}$$

$$v(t + \delta t) = v(t) + a_p(t)\delta t \quad \text{Equation 4.30}$$

where δt is a small time step. The new positions (Equation 4.29) and velocities (Equation 4.30) were used to update the forces by repeating the procedure as many times as needed. The integration time scale δt can be either fixed or adapted to the dynamic time scale of the simulated system (Fazekas, 2007). Euler's method tends to produce kinetic energy as a result of the integration errors however, in particulate systems this is generally not critical as the energy gained through the numerical integration errors is balanced

by the energy dissipated in particle collisions. Other models (e.g. Runge-Kutta, Predictor-Corrector and Verlet's Leap-Frog method) exist that can follow an accurate integration scheme but at the expense of enhanced computational power (Fazekas, 2007).

In this two dimensional DEM-fluid simulation work, the orientation of an arbitrarily shaped particle was described by the rotation angle relative to the fixed direction and Euler's method for computing the translational particle motion was used to compute the particle's rotational motions.

4.3.7.1 Translational particle motion

The translational particle motion in this DEM work was calculated by using Newton's law of motion as given by Equation 4.31,

$$m_i \frac{dv}{dt} = F_g + \sum F_n + \sum F_t \quad \text{Equation 4.31}$$

where m is the mass of a single particle i , F_g is the gravitational force, $\sum F_n$ and $\sum F_t$ are the respective sums of all the normal and tangential forces (particle-particle and particle-wall) acting on a single particle and v is the linear particle velocity. In this DEM work, the acceleration of a single particle was computed from the net force (Equation 4.28) which was then integrated for particle velocity (Equation 4.29) and displacement (Equation 4.30).

4.3.7.2 Rotational particle motion

The rotational particle motion in this work was calculated by using Equation 4.32,

$$I_i \frac{d\bar{\omega}_a}{dt} = \sum M \quad \text{Equation 4.32}$$

where I is the moment of inertia of a particle, $\bar{\omega}_a$ is the angular velocity, and M is the particle's momentum which was calculated by

$$M = R \times F_t \quad \text{Equation 4.33}$$

where R is a radial vector which extends from the particle's centre to the point of contact and \times is a vector cross product. In this DEM work, the trajectories of all particles were traced by integrating Equation 4.31 and Equation 4.32. The simulation time step Δt is a constant value that is chosen to ensure the stability and accuracy of the numerical integration system (Asmar *et al.*, 2002). The value of simulation time step Δt was determined on the basis of maximum particle stiffness k , and the smallest particle mass m as shown in Equation 4.34.

$$\Delta t \propto \sqrt{\frac{m}{k}} \quad \text{Equation 4.34}$$

In Equation 4.34, several values of proportional constant are suggested in literature such as 0.1, 2 and $2\pi/10$ (Asmar *et al.*, 2002). However, it is sometimes necessary to conduct some simulation trial runs to evaluate the most appropriate time step value for use in a simulation system. The selection of an inappropriate time step value can lead to the propagation of rounding error, artificial oscillations and unnecessarily long runtimes.

4.3.8 DEM input parameters

The input variables needed to run this DEM simulation were divided into three main groups and/or categories; the geometric data of the vertically vibrating particle container, the particle physical properties and the required simulation output.

4.3.8.1 Group-1 input variables

Group-1 DEM input variables included the geometric vessel data such as the size and shape of the particle container and/or vessel. It also included the number of container sections, height and width. In each DEM model, the position of the walls was defined with respect to the global coordinate system shown in Figure 4.1.

4.3.8.2 Group-2 input variables

These included the particle's physical properties such as the size, shape and density which in this work were chosen to closely mimic the experimental particles.

4.3.8.3 Group-3 output variables

Depending on the objectives of the computer simulation study, a TRUE/FALSE Boolean value was assigned to each possible output variable of the DEM simulation program.

4.3.9 The DEM implementation code

The DEM simulation code used in this work was written in Visual Basic-6 and was divided into several logical subroutines. The DEM simulation flow chart is shown in Figure 4.4

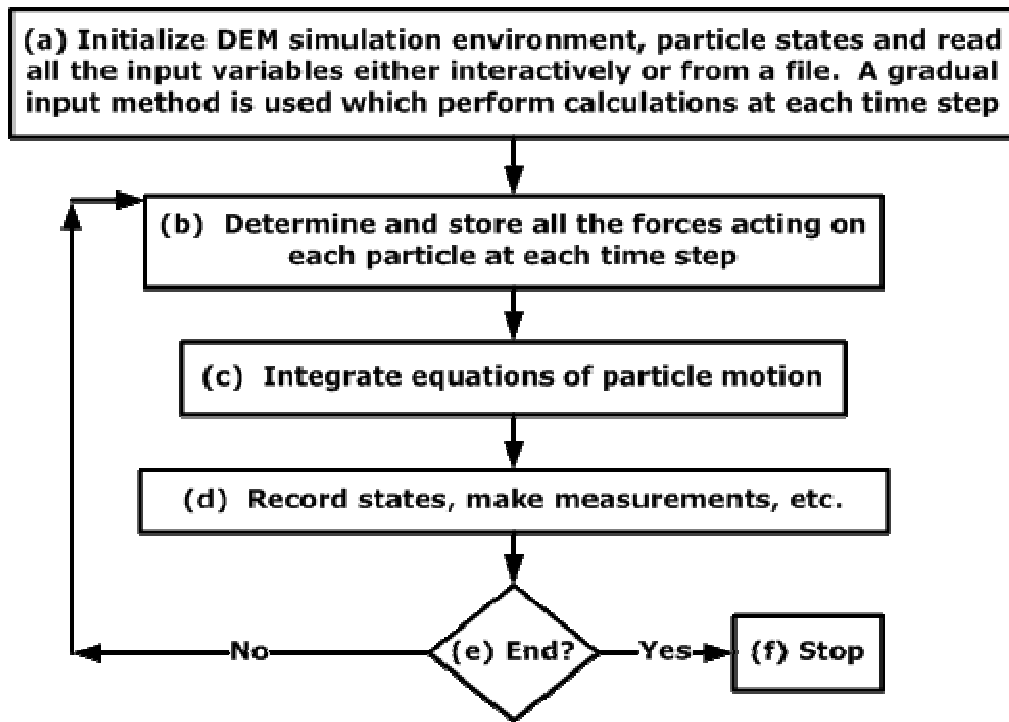


Figure 4.4: The DEM simulation flowchart.

The DEM simulation flowchart as shown in Figure 4.4 demonstrates that during the course of any computer simulations, the particle and simulation environment data is first read and after that the particle initial conditions are determined. Next, the preliminary routines are called in from the DEM program and the main simulation loop begins. In the main simulation loop, the forces acting on each particle in the system are determined based on the selected particle contact model (soft particle method in this case). Once the force subroutine is finished, the particle equations of states are integrated and the appropriate measurements are made. Next, the particle states are recorded to an output file. The loop repeats until an

ending condition, which is usually the maximum allowable simulation time, is reached.

All the DEM simulations reported in this work were run on a Viglen desktop personnel computer with an Intel Pentium (R)D 3.4GHz processor with a 2GB RAM and a Microsoft XP professional version 2002 service pack 3 operating system.

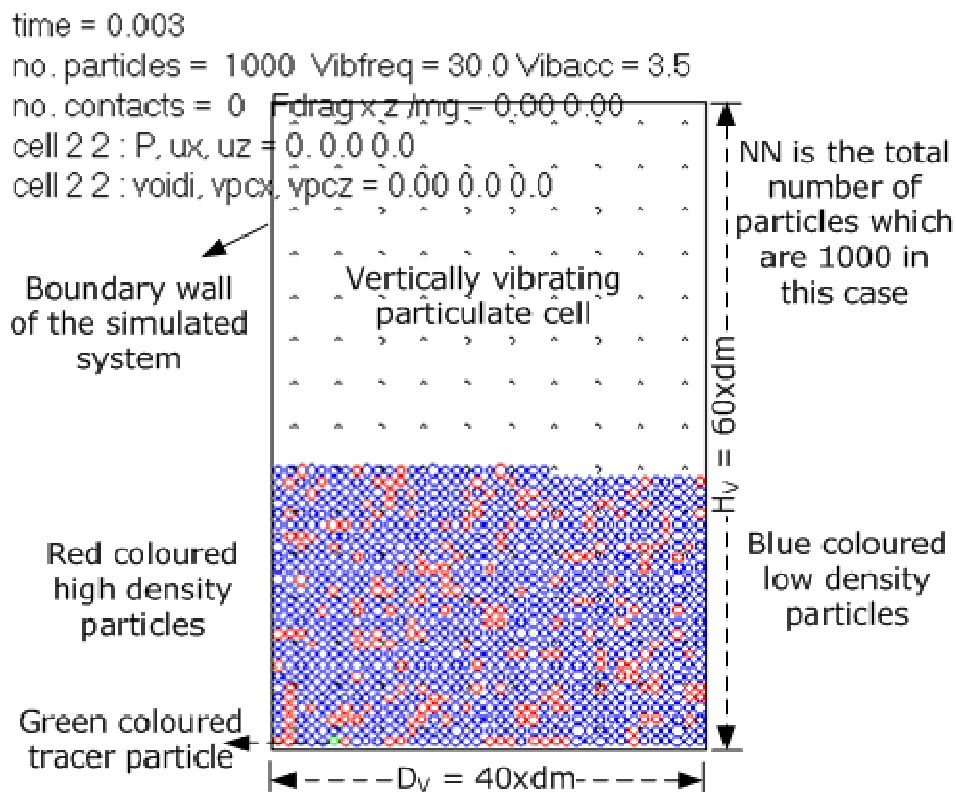
4.3.9.1 DEM validation tests

Before the full scale running of the DEM simulation program, several validation tests were performed on the DEM simulation program to increase the confidence that the code has no mistakes.

- ❖ Large runs to inspect the overall running of the program.
- ❖ Manual calculations to check the small test runs.
- ❖ Inspection of the graphical output for the above mentioned steps to see if they look sensible.

4.3.10 DEM simulation setup

The rectangular shaped container box representing the DEM simulation setup as used in this work is shown with dimensions in Figure 4.5.



H_v is the cell height, and D_v is the width of the simulated particle container and d_m is the diameter of a sole particle.

Figure 4.5: DEM simulation setup.

The main simulation parameters as used in the DEM simulation setup (Figure 4.5) reported in this work are summarised in Table 4.1.

Parameter	Values
Number of particles, N	1000
Dimensionless acceleration, Γ	2.0, 3.0, 3.5, 4.0
Vertical vibration frequency, f (Hz)	6, 7, 9, 30, 35, 40, 45
Simulation boundaries	Walls
Particle density, ρ (kg.m^{-3})	(a) Glass (2500), Bronze (8900) and (b) Particles with the density of 1000 and 2500
Diameter of the particles, d_m (μm)	500 and 250
Maximum simulation time, t sec.	30 s
Average CPU time for 1 s of simulation run	20hrs
Interstitial gas	Air
Air viscosity ($\text{kg.m}^{-1}.\text{s}^{-1}$)	0.000018
Air density, (kg.m^{-3})	1.2
Gravity force (m.s^{-2})	9.8
Particle-particle stiffness coefficient, K_{np} (kg.s^{-2})	250
Particle-wall stiffness coefficient, K_{nw} (kg.s^{-2})	250
Particle-particle tangential stiffness coefficient, K_{tp} (kg.s^{-2})	250
Particle-wall tangential stiffness coefficient, K_{tw} (kg.s^{-2})	250
Particle-particle friction coefficient, μ_{fp}	0.3
Particle wall friction coefficient, μ_{fw}	0.3
Rolling friction, μ_{fr} ($\text{N}=\text{kg.m}^{-1}.\text{s}^{-2}$)	0.0005
Particle-particle displacement ratio, u_p	0.36
Particle wall displacement ratio, u_w	0.36
Particle-particle normal damping coefficient, γ_{np}	0.3
Particle-wall normal damping coefficient, γ_{nw}	0.3
Time step, Δt , sec.	0.001

Table 4.1: The parameters used in the DEM-fluid simulations.

4.4 DEM simulation of the vertically vibrating particle mixtures

The simulation procedure in this DEM work was initiated by assigning random positions to the simulated working particles within the rectangular shaped virtual container as shown in Figure 4.5. The simulated particles were allowed to fall under gravity until a stable particle structure as shown in Figure 4.5 was obtained. In this DEM work, several experiments were performed to investigate the density segregation behaviour of the different spherical shaped particles that were subject to simulated vertical vibration.

4.4.1 Preliminary density segregation simulations

The simulated working particle mixture used in the preliminary density segregation investigation is shown in Table 4.2.

Bead diameter (μm)	Density $\rho(\text{kg.m}^{-3})$	Number ratio of particles
500	1000	0.3
500	2500	0.7
Total number of particles used in the DEM simulations		600 and 1000

Table 4.2: The size and density of the simulated working particle mixture used in the preliminary density segregation investigation.

The time averaged progression of vertical vibration induced particle segregation in the particle mixture shown in Table 4.2 at a vertical vibration frequency of 6.3Hz and with a dimensionless acceleration magnitude of 1.6 is snapshot and shown in Figure 4.6.

Chapter-4 Discrete element modelling of the vertically vibrated particle bed

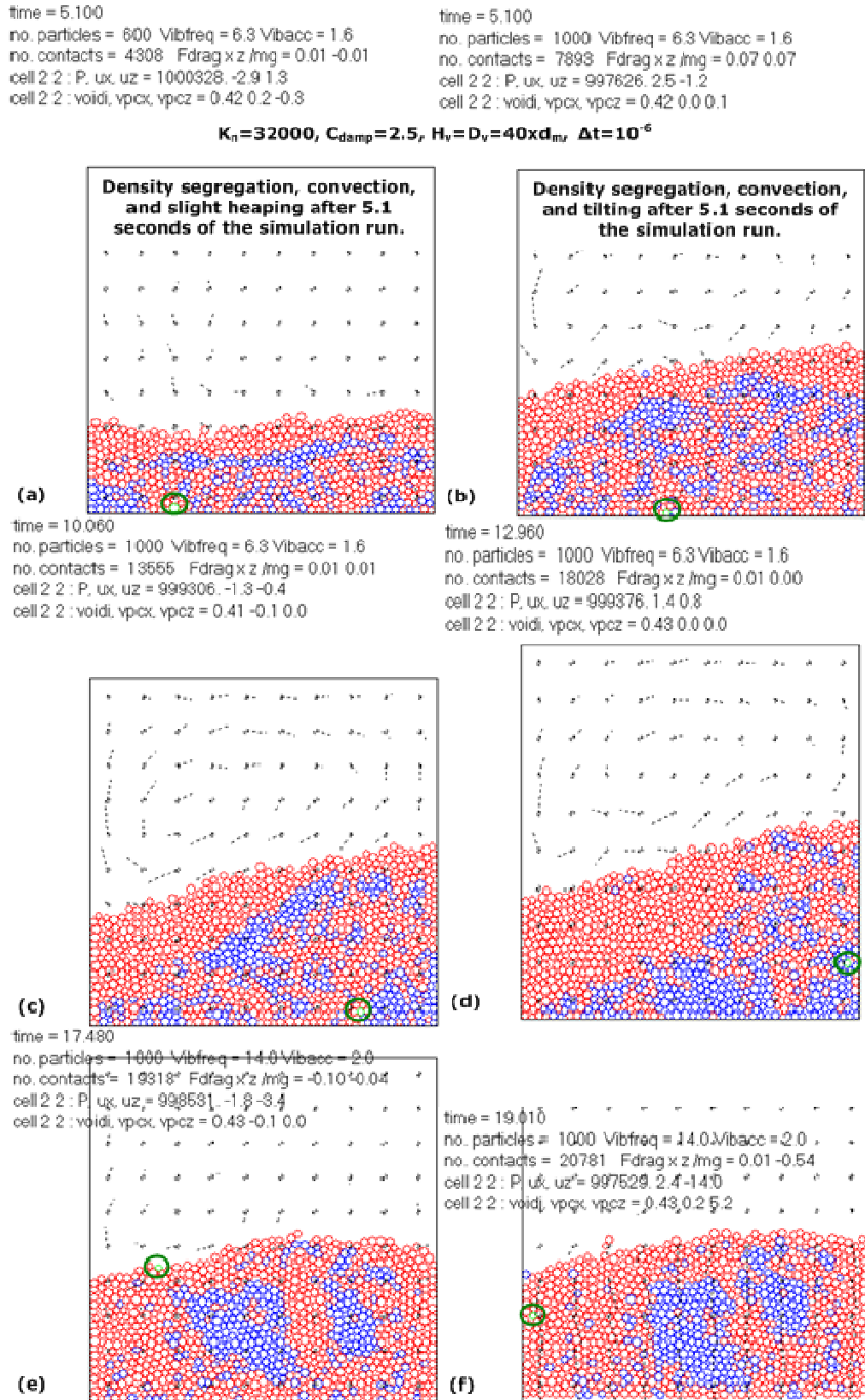


Figure 4.6: DEM simulation of segregation progression in the 70:30% high and low density particle mixture (Table 4.2).

The green particle shown in Figure 4.6 simulated a high density tracer particle that was introduced into the simulation system to capture and highlight the distinct movements of the high density particles. The tracer particle shown in Figure 4.6 is encircled in green for the ease of its detection. Nevertheless, the DEM simulation experiment (Figure 4.6) carried out with particle mixtures (Table 4.2) that contained 600 particles showed (a) density segregation coupled with convective particle motions and slight heaping and/or tilting of the working particle bed in nearly 5 seconds of a simulation run. The DEM simulation results shown in Figure 4.6 were considered encouraging enough to simulate a further increase in the number of working particles. With everything else remaining the same, the increase in the number of working particles to 1000 (Table 4.2) showed (b) similar particle segregation trends as seen in the simulation of 600 particles with the addition of a tilt formation that continued to remain stable even after (c) 10, (d) 13, (e) 17, and (f) 19 seconds of the simulation run. In addition to tilt formation interstitial fluid currents on top of the vertically vibrated particle bed in clockwise direction can also be seen in Figure 4.6 (b, c, d and e).

Of particular interest in the simulation run (Figure 4.6) carried out with 1000 particles was the distinct movement of the green tracer particle which was initially housed in the bottom layer of the simulated particles. As the vertical vibration was started, the green tracer particle started to move towards the top of the tilted particle bed surface. However, during the course of this motion the tracer particle was observed to follow a trajectory that was very close to the boundary walls of the rectangular shaped cell. Once on top, the tracer particle was observed to slide downhill from top of the tilted particle bed surface. This observation is especially in-line with the experimental observations reported in the Positron Emission Particle Tracking (PEPT) experiments (Chapter 6). Although the DEM simulations reported here replicated some of the experimentally

observed density segregation attributes, however the use of a very low vertical vibration frequency and dimensionless acceleration magnitude as well as the use of a very low density differential particle mixture (Table 4.2) was considered far from agreement with most of the experimental results reported in literature such as the ones reported by Burtally *et al.*, (2003) in Figure 2.19 and Mohabuth, (2007) in Figure 2.24. Nevertheless, in an effort to simulate some of the experimentally observed particle segregation conditions such as the ones reported by Burtally *et al.*, (2002 and 2003), the next set of DEM simulation was carried at the high vertical vibration frequency and dimensionless acceleration magnitudes and with particle mixtures that had a high density differential and which reflected the properties of the finely sized glass and bronze particles.

4.4.2 DEM simulation of density segregation in the glass and bronze particle mixture

The particulate material used in this DEM simulation work replicated the properties of the finely sized glass and bronze particles. The size and composition of the simulated glass and bronze working particle mixtures is given in Table 4.3.

Mixture			A	B	C
Material	Bead diameter (μm)	Density $\rho(\text{kg.m}^{-3})$	Number ratio of particles	Number ratio of particles	Number ratio of particles
Glass	500	2500	0.8	0.7	0.5
Bronze	500	8900	0.2	0.3	0.5
Total number of particles used in the DEM simulations			1000	1000	200

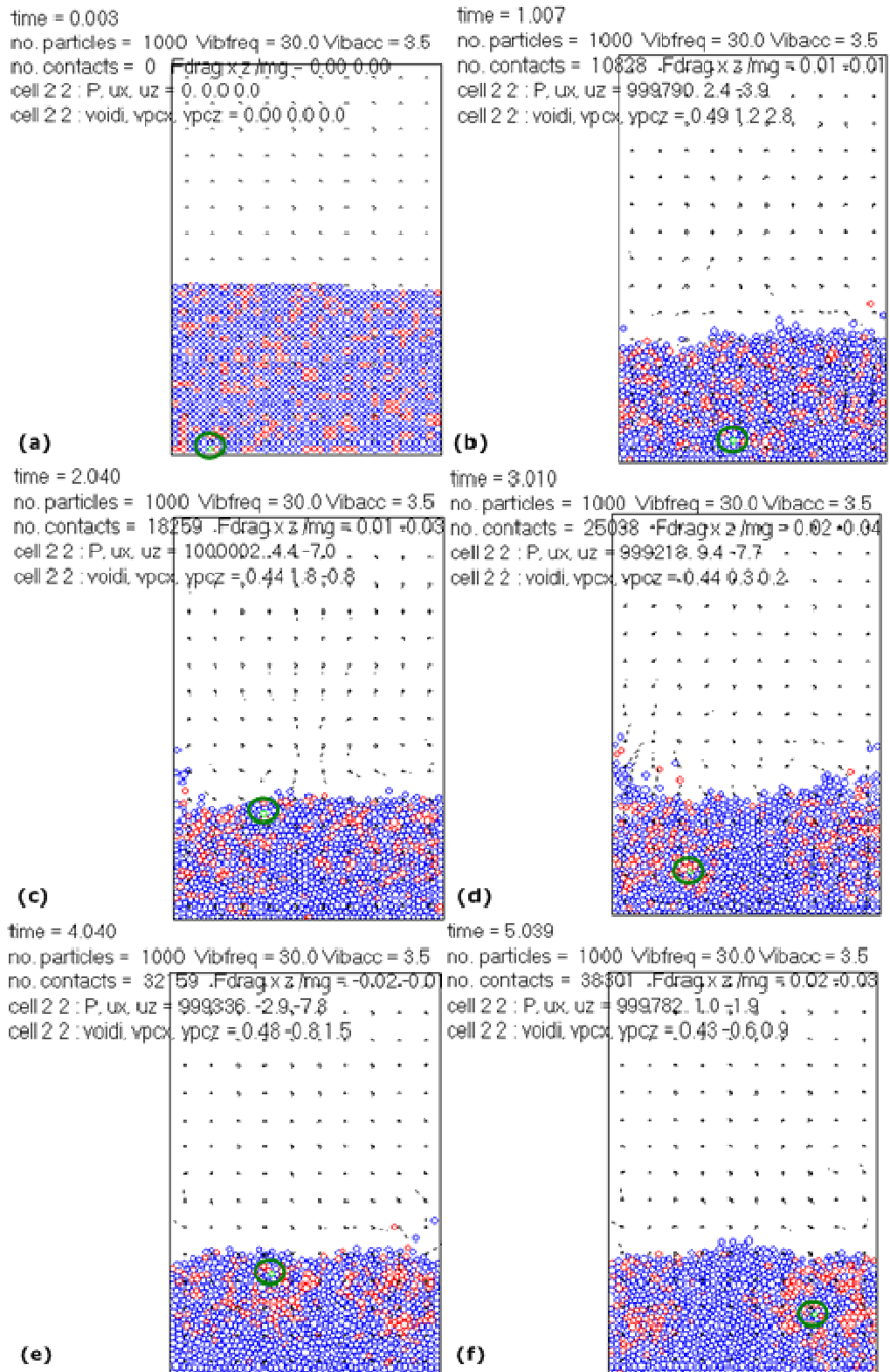
Table 4.3: The size and composition of the simulated working particle mixtures used in the DEM simulations.

4.4.2.1 DEM simulation of density segregation in the glass and bronzer particle mixture-A

The DEM simulations carried with particle mixture-A (Table 4.3), which was comprised of spherical shaped glass (70% by number and are shown in blue colour) and bronze (30% by number and are shown in red colour) particles at the vertical vibration frequency of 20 and 30Hz and with the dimensionless acceleration magnitudes of 2 and 3 failed to show any significant density segregation potential. This was in disagreement with the experimental segregation results reported by Burtally *et al.*, (2003) in Figure 2.19 and Mohabuth, (2007) in Figure 2.24.

The time averaged progression of vertical vibration induced particle segregation in mixture-A at a vertical vibration frequency of 30Hz and with a dimensionless acceleration magnitude of 3.5 is snapshot and shown in Figure 4.7. The green particle in Figure 4.7 simulates a bronze density tracer particle that is introduced into the simulation system to capture and highlight the distinct movements of the high density particles. The tracer particle in Figure 4.7 is encircled in green for the ease of its detection.

Chapter-4 Discrete element modelling of the vertically vibrated particle bed



Chapter-4 Discrete element modelling of the vertically vibrated particle bed

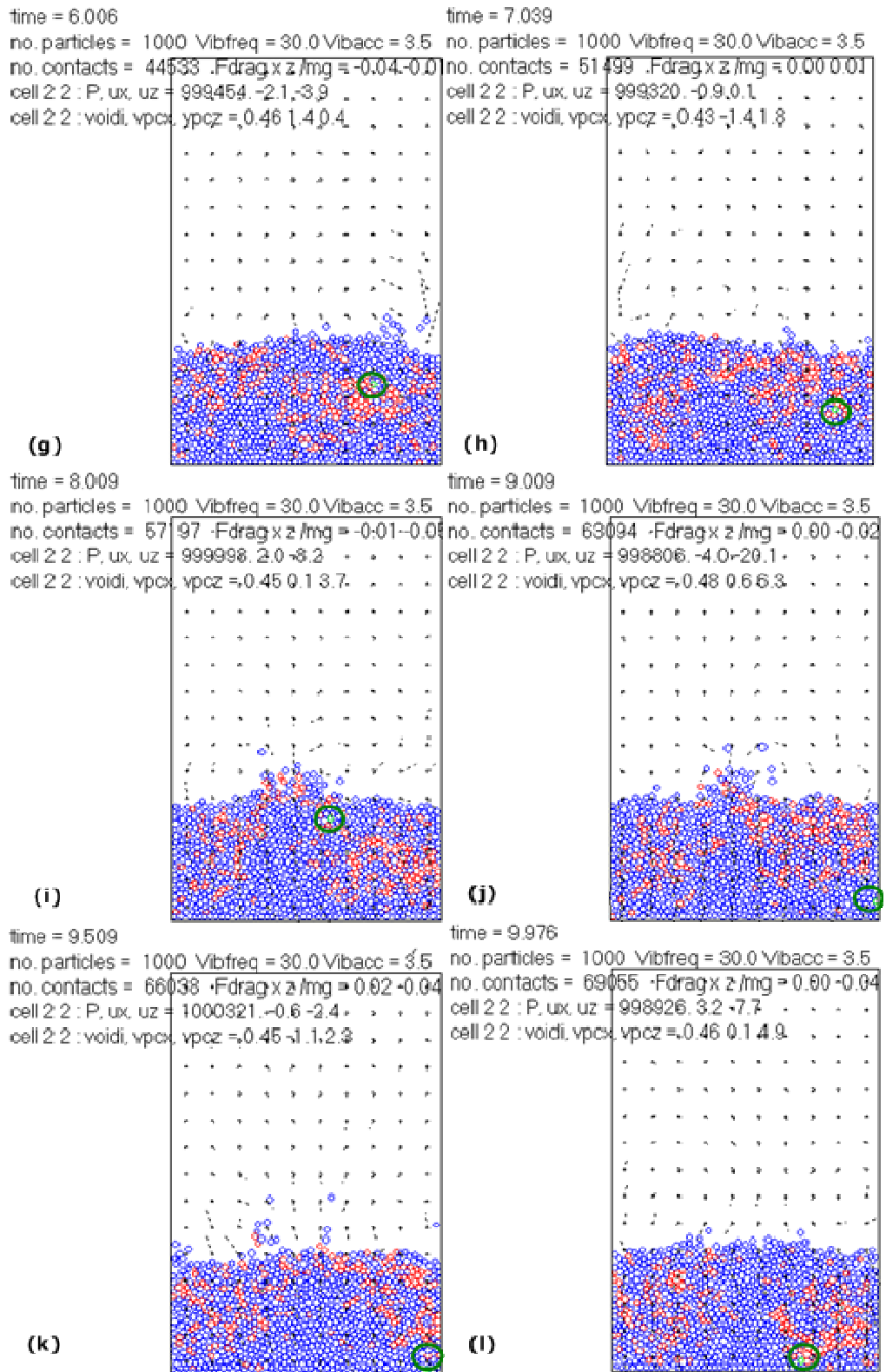


Figure 4.7: DEM simulation of time averaged (from a to l, ~10 second) segregation progression in an 80:20 % number glass and bronze particle mixture-A (Table 4.3).

The snapshots shown in Figure 4.7, (a) shows a randomly well mixed particle mixture-A (Table 4.3) that is placed in a rectangular cell and/or container. The vertical vibration is introduced into this container by the up and down movement of the whole container in z-direction as shown in Figure 4.5. Once all the particles of mixture-A (Table 4.3) were randomly in-placed in the rectangular shaped container and/or cell which took nearly 0.03 seconds of the simulation time, the particle mixture was vertically vibrated.

The vertical vibration of particle mixture-A (Table 4.3) resulted in (b) dynamic particle movements which, in this simulation, lead to the development of the identical particle concentration zones. The less stable particle concentration and/or segregation zones (c, d, e and f) were mostly observed in the initial simulation stages however, as the simulation time then progressed (g, h, i, j, k and l) the stable local bronze concentrates, as opposed to the experimental clear cut distinct particle layers reported by Burtally *et al.*, (2003) in Figure 2.19 and Mohabuth, (2007) in Figure 2.24 were clearly observed. One of the main reasons for the non observance of the clear cut and distinct particle layers in this simulation may be the use of a limited simulation time (10 seconds). In this DEM simulation, the simulation time of only 10 seconds or less was used because of the high levels of CPU demand. This was probably due to the use of a less computational power computing system for 1000 particles. Nevertheless, even within 10 seconds of the DEM simulation run (Figure 4.8) some interesting particle segregation behaviours were readily observed.

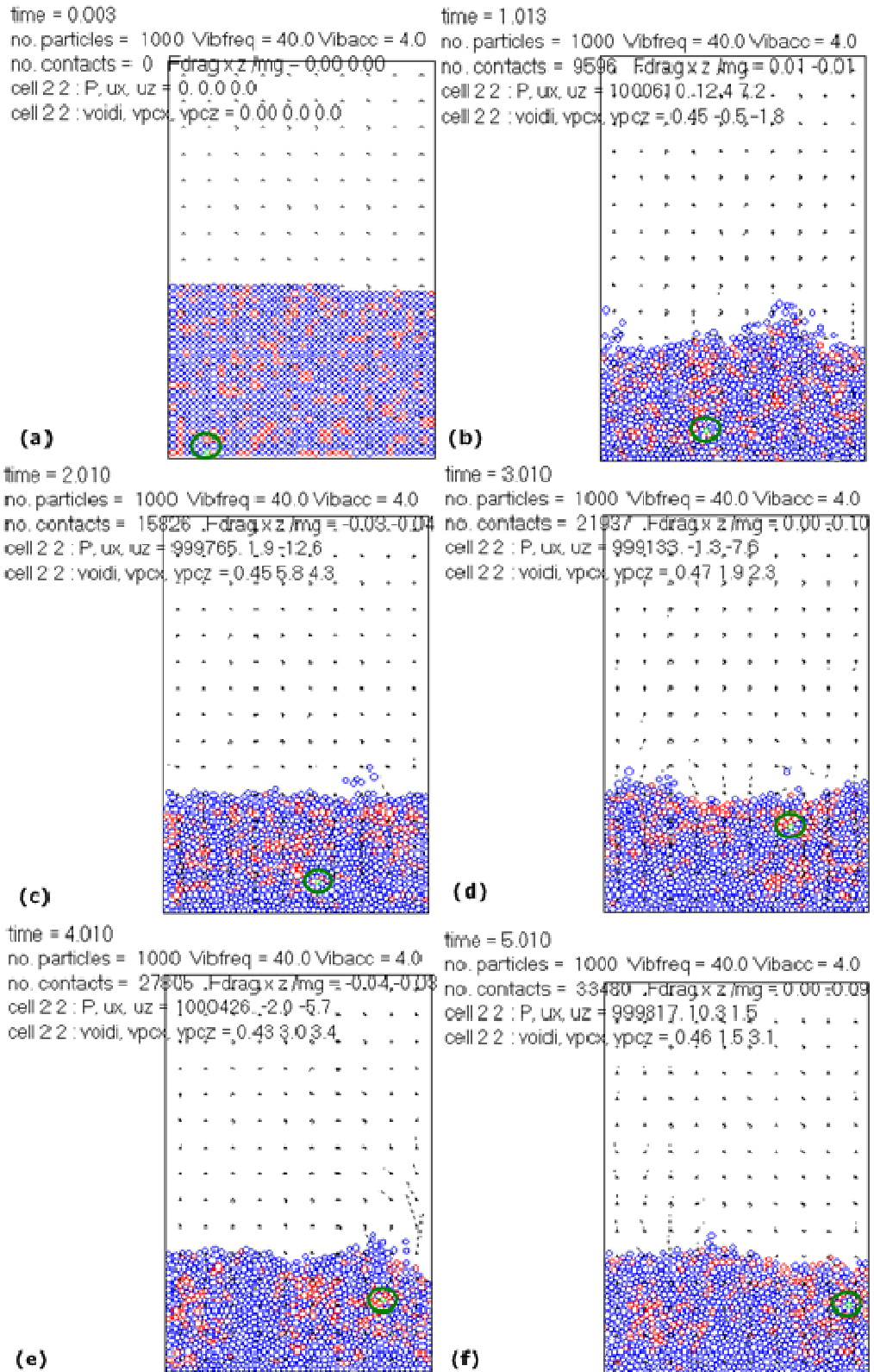
Of particular interest in this DEM simulation case was the tracked movement of the high density green tracer particle which nearly replicated the parallel particle movements as were experimentally observed in the PEPT of the high density bronze tracer particle as shown in Section 6.3.1. The green tracer particle (Figure 4.7) was initially housed in the bottom layer (a) of the particle mixture-A and

as the vertical vibration of the particulate container was started (b, c and d) the green tracer particle was observed to move towards the local high density particle concentrates and gradually started to rise to the vibrated particle bed surface. Once it reached the top particle bed surface, it continued to maintain its motion with the local high density particle concentrates which were mostly developed there because of the vertical vibration of the whole particulate system. Overall, the green tracer particle movements showed that it nearly moved to all locations in the vertically vibrated rectangular cell however, the majority of the green tracer particle movements were observed very close to the container boundaries. This observation is particularly in-line with the experimental and PEPT as discussed in Section 6.3.1.

Other notable observation from the DEM simulation reported here was the distinct interstitial gas (air in this case) movement that was introduced in grid from various locations in the vertically vibrated rectangular cell. The air moved through the vibrating particle mixture and showed some distinct convective displacements that were mostly near to the top particle bed surface as shown in Figure 4.7. The air movement patterns observed in this DEM simulation had some similarities to the experimentally observed air movement patterns reported in the smoke blanket visualization experiments (Section 5.4.4). Furthermore, a limited tendency towards the particle bed tilting was also observed in this DEM simulation however, a stable particle bed tilt formation, as observed in the parallel material experimentation reported by Burtally *et al.*, (2003) in Figure 2.19 and Mohabuth, (2007) in Figure 2.24, was never achieved.

The time averaged progression of density segregation in the working particle mixture-A (Table 4.3) which was vertically vibrated at the vertical vibration frequency of 40Hz and with a dimensionless acceleration magnitude of 4.0 is snapshot and shown in Figure 4.8.

Chapter-4 Discrete element modelling of the vertically vibrated particle bed



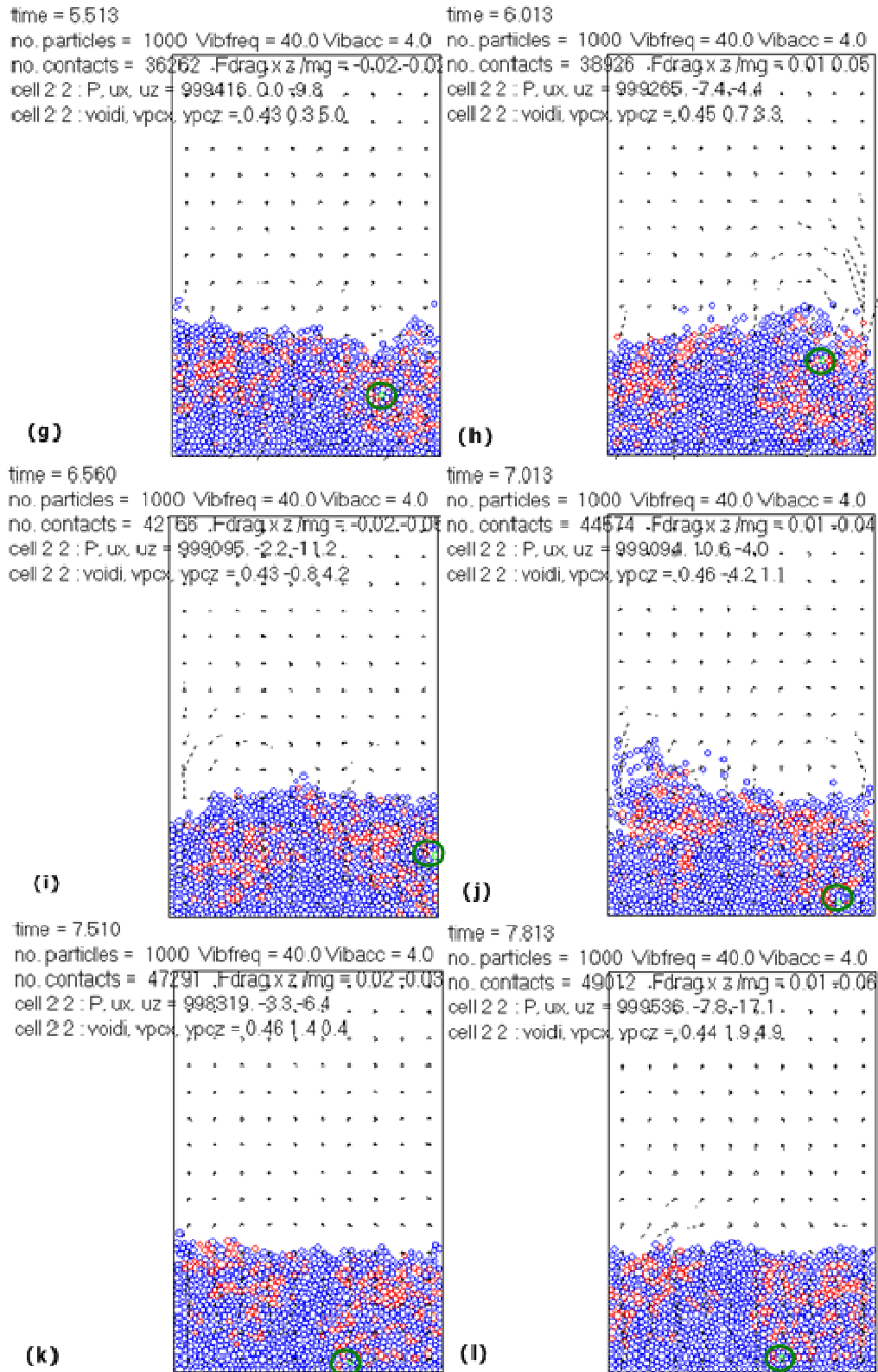


Figure 4.8: DEM simulation of time averaged (from a to l, ~7.8 second) segregation progression in an 80:20 % number glass and bronze particle mixture-A (Table 4.3).

The DEM simulation results reported in Figure 4.8 showed similar patterns as seen in Figure 4.7. The green tracer particle was observed to join the local high density particle concentrates and it moved in a distinct trajectory that was mostly near to the container walls and on top of the particle bed surface. The air currents in this simulation (Figure 4.8) were observed to be of somewhat stronger magnitude in comparison to that observed in the simulation reported in Figure 4.7. Nevertheless, a stable tilt formation and clear-cut particle layer segregation was never observed in this simulation however, stable high and low density particle concentrates were readily observed.

4.4.2.2 DEM simulation of density segregation in the glass and bronzer particle mixture-B

The time averaged progression of density segregation in the working particle mixture-B (Table 4.3) which was vertically vibrated at the vertical vibration frequency of 30Hz and with a dimensionless acceleration magnitude of 3.0 is snapshot and shown in Figure 4.9.

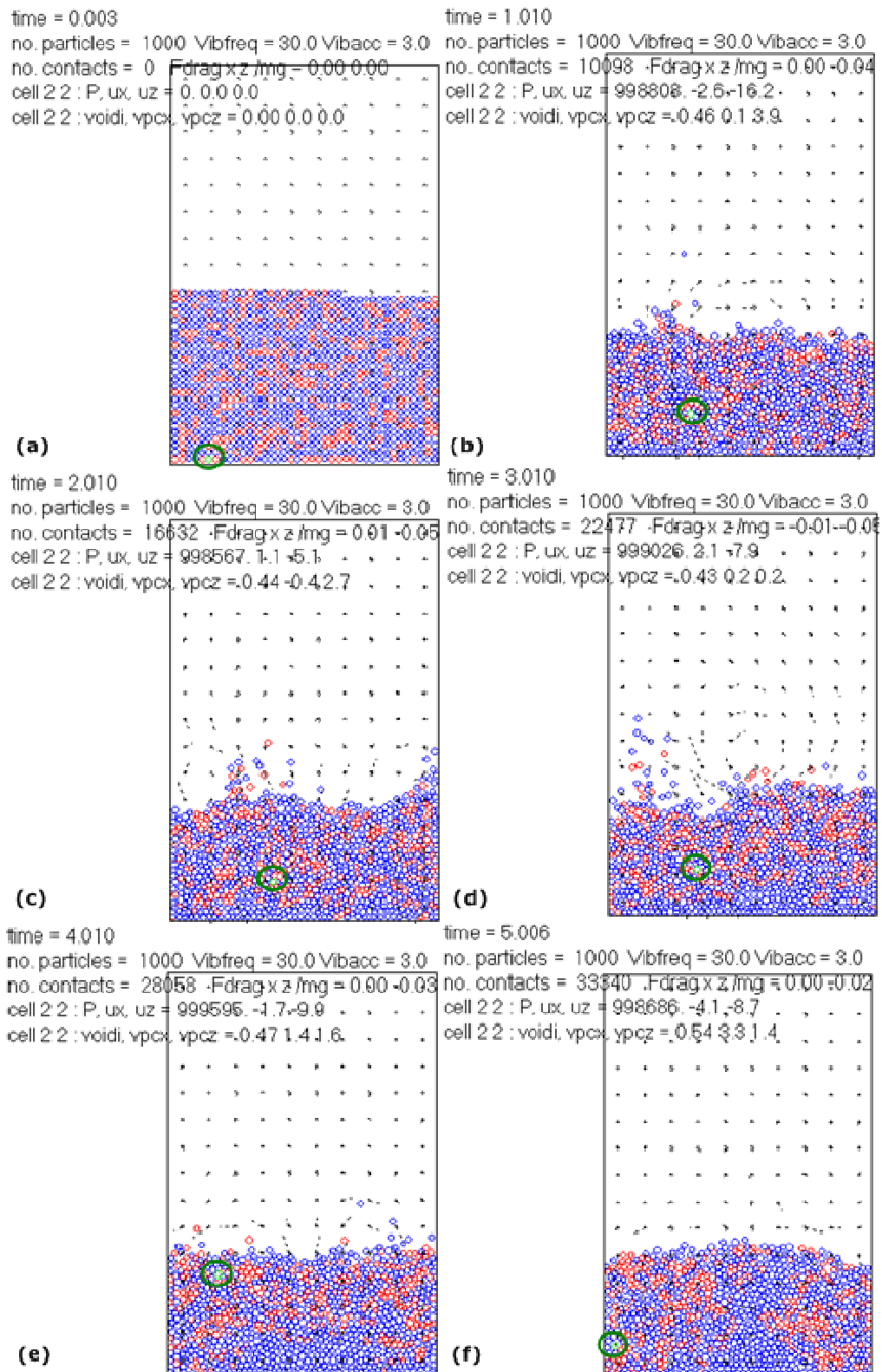


Figure 4.9: DEM simulation of time averaged (from a to f, ~5.0 second) segregation progression in a 70:30 %number glass and bronze particle mixture-B (Table 4.3).

The DEM simulation results reported in Figure 4.9 showed that by increasing the number of high density particles to 30% by number, the particle segregation behaviour did not improve in nearly 5.0 seconds of the simulation run. The segregation trends seen in Figure 4.9 remained somewhat identical to the patterns reported in Figure 4.7 and Figure 4.8.

In the DEM simulation reported in Figure 4.9, the green tracer particle was observed to join the local high density particle concentrates and moved to the top of the particle bed surface however, in this simulation run (Figure 4.9) the tracer particle did not patrol the outer particle bed trajectory close to the rectangular cell walls. This tracer particle behaviour may be due to the presence of a large number of high density particles that could have affected the vibrated particle bed dynamics.

4.4.2.3 DEM simulation of density segregation in glass and bronzer particle mixture-C

In Section 4.4.1, the DEM simulations revealed some exciting particle segregation attributes however, when the experimental particle conditions were investigated in the DEM simulation program (Section 4.4.2.1 and 4.4.2.2), poor particle segregation patterns were revealed. Beside other things, one of the main reasons for the observance of poor particle segregation behaviours may be the use of a large number of simulating particles. In light of the observations made in Sections 4.4.1, 4.4.2.1 and 4.4.2.2, it was considered to simulate the glass and bronze working particle mixture-C (Table 4.3) with the lesser number of simulating particles (200 and 600). Reducing the number of particles to 200 and 600 in the DEM simulation program resulted in showing some clear-cut

high density particles on top and bottom density segregation regimes as shown in Figure 4.10.

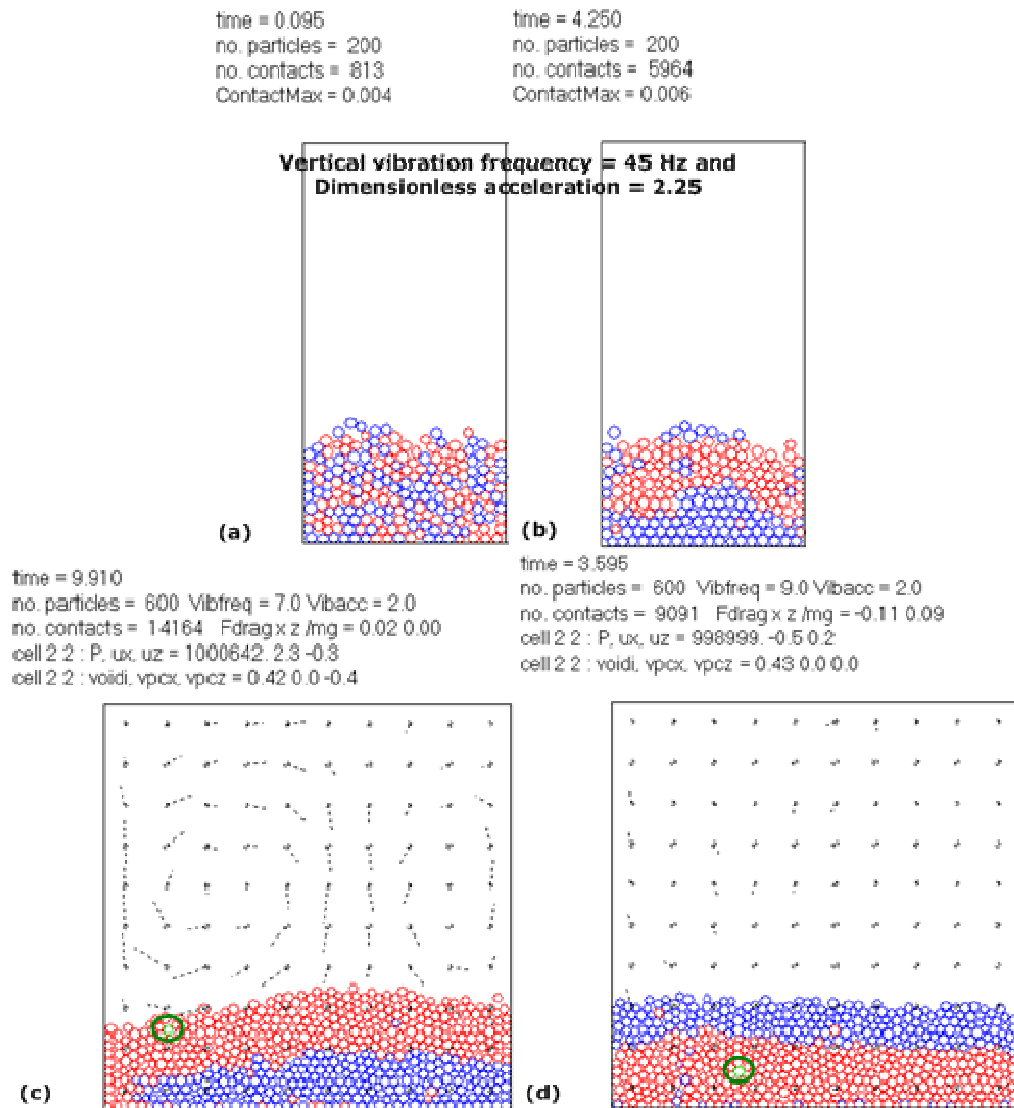


Figure 4.10: DEM simulation of particle mixture-C (Table 4.3).

In Figure 4.10, density segregation in 200 working particles (Figure 4.10) was observed in nearly four seconds of the simulation run. This high density particles on top density segregation regime was achieved when the particle mixture-C (Table 4.3) was vertically vibrated (a, b) at the vertical vibration frequency of 45Hz and with a dimensionless acceleration magnitude of 2.25. Under the same conditions of vertical vibration frequency and dimensionless

acceleration (45Hz and 2.25) the increase in the number of particles to 600 did not result in showing any appreciable density segregation. However, (c, d) when the vertical vibration frequency and dimensionless acceleration were dropped to <10Hz and 2.0 respectively (c) the formation of high density particle on top and (d) bottom particle segregation regimes as shown in Figure 4.10 were clearly observed. However, the simulated frequency and dimensionless acceleration values were still found to be in disagreement with the experimental values reported by Burtally *et al.*, (2003) in Figure 2.19 and Mohabuth, (2007) in Figure 2.24.

4.4.2.4 DEM simulation of density segregation in the partitioned separation cell

The work presented in Sections 4.4.1, 4.4.2, 4.4.2.1, 4.4.2.2, and 4.4.2.3 has mainly looked into the segregation behaviours of the working particle mixtures in a rectangular shaped boxed and/or container. However, the experimental work reported in this thesis has used a partitioned particle separation cell as shown in Figure 3.4, Figure 3.5, and Figure 3.6. At this development stage of the DEM simulation program, the simulation of the full scale partitioned particle separation cells as shown in Figure 3.4, Figure 3.5, and Figure 3.6 was considered difficult however, an attempt was made to simulate the prototype scaled partition separation cell (Figure 2.23) reported by Mohabuth, (2007).

The working particle mixture used in this work comprised 40 % by number of simulated glass (250 μ m) particles and 60 % by number of bronze (500 μ m) particles. The time averaged progression of density segregation in the working particle mixture that was vertically vibrated at the vertical vibration frequency of 45Hz and

with a dimensionless acceleration magnitude of 2.25 is snapshot and shown in Figure 4.11.

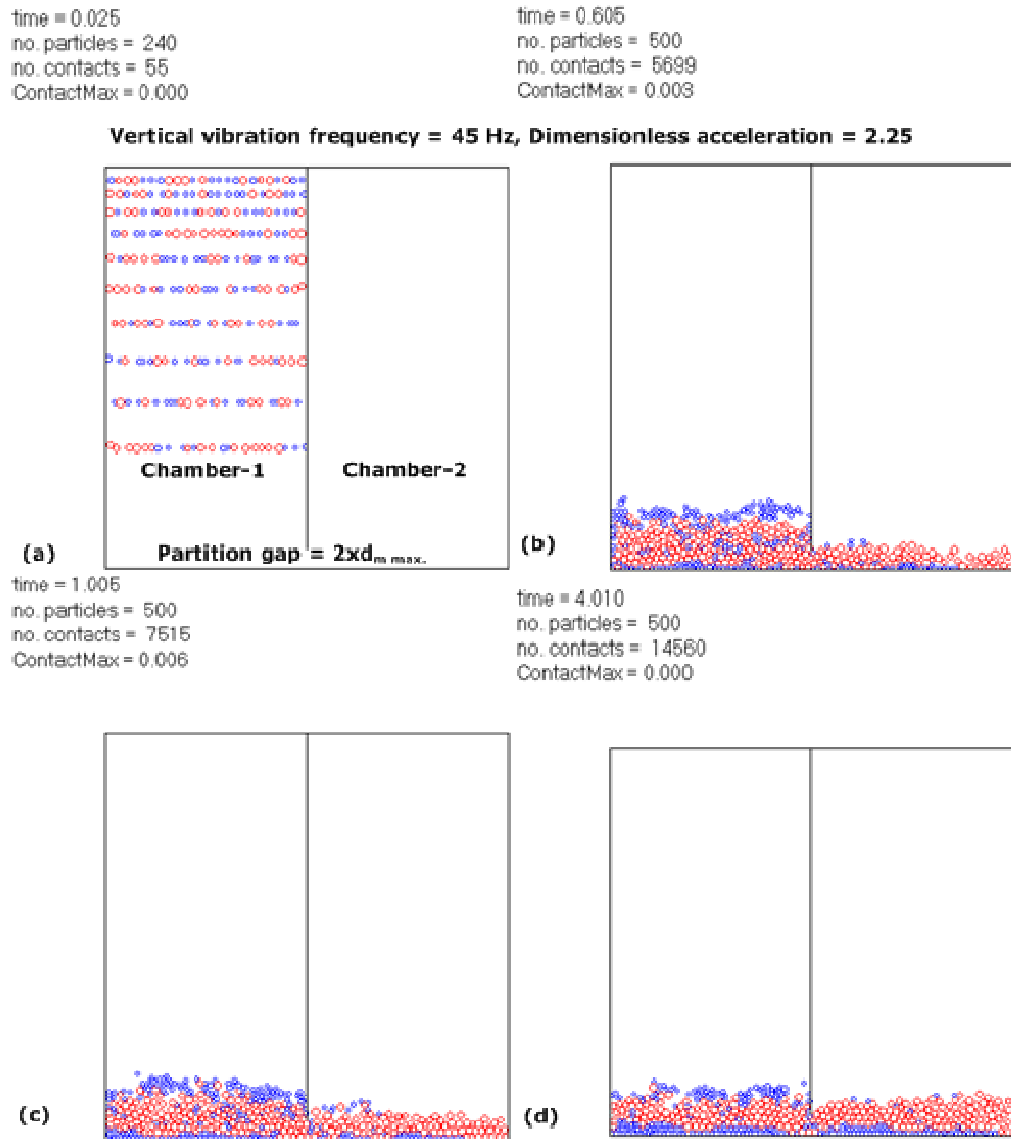


Figure 4.11: DEM simulated segregation in a glass (40 % by number) and bronze (60 % by number) working particle mixture.

The DEM simulation run is snapshot and shown in Figure 4.11 (a) shows the initial particle charging in chamber-1 of the partitioned container and the particle segregation in chamber-1 and 2 after (b) 0.6, (c) 1.0 and (d) 4.0 seconds of the simulation run. It is important to note that although particle segregation was clearly observed in almost all the DEM simulation runs reported in this

investigation, including the partitioned DEM simulation system shown in Figure 4.11, however, the observed particle segregation mechanism was predominantly fluidisation especially at the top particle bed surface and it was not purely convective which is proposed in many experimental investigations including the ones reported by Burtally *et al.*, (2003) in Figure 2.19 and Mohabuth, (2007) in Figure 2.24. The frequency and dimensionless acceleration values used in this simulation were in agreement with the experimental results reported by Burtally *et al.*, (2003) in Figure 2.19 and Mohabuth, (2007) in Figure 2.24. Furthermore, increasing the number of working particles and by using an identical particle size working mixture in the simulation run shown in Figure 4.11, poor particle separation was simulated.

4.5 Concluding remarks

Based on the work presented in this chapter the following conclusions can be deduced;

- ❖ The complete theoretical description of particulate dynamics is still in infancy.
- ❖ In the absence of complete theoretical models, the computer simulations provide a valuable tool to determine the static and dynamic particle properties.
- ❖ Discrete element modelling offers a flexible approach that can be used to bridge the static and dynamic particle characteristics.
- ❖ In DEM, the velocities and accelerations of all dynamic particles in the chosen coordinates can be calculated and this can be used to map out the individual particle dynamics.
- ❖ In this work, an analysis of two dimension particle dynamics in a vertically vibrated container is presented.
- ❖ The DEM model used in this work has shown some elements of convection, tilting, segregation and partitioned particle separation however, significant differences with the experimental results can still be observed.
- ❖ The DEM simulations presented here has used a maximum of 1000 particles and the particle tracking trends in a high density differential particle mixture are mostly consistent with the experimental work presented in this thesis.
- ❖ The work presented in this Chapter has provided a useful insight to aid in the further development of the full scale DEM-fluid simulation program. The key aspects that are especially encouraging in the development of a future model that can tackle an enhanced number of particles are, modelling in three dimensions and the incorporation of a more detailed fluid motion model.

- ❖ The DEM simulation program reported here is still under development and is therefore unable to predict all the important dynamic particle characteristics in a vertically vibrated container.

Separation of particle mixtures in the scaled up vertical vibration separator

5.1 Introduction

The vibration driven movements of particles in a closed geometry box will produce collisions and friction between the particles and with the walls of the container. The inter-particle collisions and boundary wall friction will generate many different kinds of particle motions (Kakalios, 2004). The particle motions in a vibrated particle bed can be simply controlled by changing the parameters of vibration (frequency, amplitude and acceleration), vibrated container, and the characteristics of the working particles. In a vertically vibrated particle bed, particle motions generally take place when the amplitude of vertical vibration acceleration is recorded above a certain threshold value i.e. $1.2g$ where, g is the gravitational acceleration (Hsiau *et al.*, 2002). Below this threshold

value the particle bed generally behaves like a solid mass. Nevertheless, experiments have shown that by controlled vertical oscillations of finely sized particle mixtures, in a closed geometry box, a number of interesting phenomena (Section 1 of Chapter 1) can be readily observed. The major driving mechanisms behind such particle bed behaviours are presently under vigorous investigations and conclusive evidence is still lacking as to the major cause of these phenomena. However, some (Taguchi, 1992; Knight *et al.*, 1993) believe that convection is an important driving mechanism that can be attributed to the distinct particle bed behaviours. In this work, some evidence of convective particle motion in a vertically vibrated particle bed has also been identified, and is presented in Chapter-6, where a Positron Emission Particle Tracking (PEPT) system has been used to track the real time motions of various solo particles in diverse particle mixtures. Nevertheless, the quest for fundamental understanding of dynamic particle bed behaviour under the influence of vertical vibration still continues. At present, this work is mainly undertaken by the physics community which is also evident from the review of currently published literature, presented in Chapter 2.

Physicists at the University of Nottingham, UK have identified that through careful control of frequency and acceleration during vertical vibration, different types of finely sized particles can be positioned, or segregated, in a small rectangular cell (Figure 2.20) (Burtally *et al.*, 2002, 2003). The preliminary investigations reported by Burtally *et al.*, (2002, 2003) were aimed at acquiring some basic understanding of the dynamic particle bed behaviours under the influence of vertical vibration. However, the formation of distinct and stable concentration zones in different regular shaped particle mixtures was quickly identified as a potential new method for separating a range of finely sized particle mixtures, preferably on a dry basis (Mohabuth, 2007). These investigations therefore sparked

the interest to explore and develop a potential new breed of vertical vibration induced particle separators.

An extension of the work reported by Burtally *et al.*, (2002, 2003) resulted in the design of a new prototype scale batch separator that was capable of recovering separated particle layers in two different chambers (Mohabuth and Miles, 2005 and Mohabuth *et al.*, 2007; Mohabuth, 2007). This prototype scaled partition cell separator was used to separate a wide variety of regular and irregular shaped finely sized particle mixtures with reported particle separation grades as high as >90% in almost all cases (Mohabuth, 2007). Despite our limited understandings of vertical vibration induced particle segregation, the prototype scale work reported by Mohabuth, (2007) can be considered as a promising step forward towards designing an industrially relevant scaled up version of the vertical vibration induced particle separator for separating a range of industrially relevant finely size particle mixtures on a dry basis. The development of such a unit is presented in this work and like many of its previous counterparts, will be predominantly based on an empirical approach. The prototype designs will be assessed in their ability to separate various particle mixtures on a dry basis.

5.2 The scaled up design development of a new vertical vibration induced particle separator

Dry based particle separation techniques are gaining popularity due to their decreased economic and environmental impacts (Macpherson *et al.*, 2009). Recent attempts in designing new dry based particle separation techniques are reported in the work of Vasconcelos *et al.*, (2009); Hirajima *et al.*, (2010) and Macpherson *et al.*, (2009). Nonetheless, the discussions made in Chapter 2 strongly indicate in favour of extending the preliminary stage

vertical vibration induced particle separation work to develop it as a potential new method for separating a range of finely sized particle mixtures at a scaled up level. However, scaling up of a particle separation system, like many of its other counterparts, has the potential to be seriously undermined by the unpredictable particle nature if a careful and incremental scale up approach is not exercised in any design process. This is partly because of the fact that, despite a large body of work on separating various particle mixtures, size length scales in particle processing are not fully developed yet (Jaeger, 1997). The absence of even a simple scale up design correlation and the relevant experimental data dictates the use of experience and heuristics, derived from the initial trial runs, to develop the new vertical vibration induced particle separator design at each incremental scaled up level. Nevertheless, the work presented here is designed to form the basis for identifying any operational difficulties that can be avoided in future design developments, modifications and/or final tuning of this novel vertical vibration induced particle separation technique. This knowledge can also be of significance in determining any additional potential applications of this technique in separating various industrially relevant particle mixtures.

5.2.1 The development of scaled up vertical vibration bench

The detailed development description of the new scaled up vertical vibration bench design is previously presented in Section 3.2 of Chapter-3.

5.2.2 The development of scaled up separation cell design

The development of a prototype scaled partitioned particle separator (Figure 2.23 of Chapter 2) cell design is previously reported in the work of Mohabuth, (2007), Mohabuth *et al.*, (2007) and Mohabuth and Miles (2005). Based on this prototype scaled particle separator cell design, the first scaled up semi continuous separation cell geometry with an open end in one direction is shown in Figure 5.1.

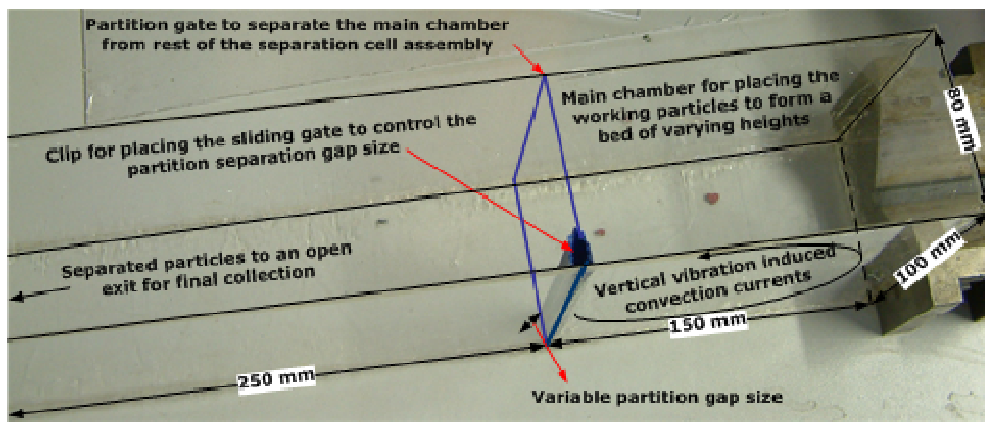


Figure 5.1: Design of a semi-continuous vertical vibration induced particle separation cell with an open end in one direction.

The transparent one millimetre thick Perspex[®] material construction of this rectangular shaped scaled up particle separator cell design, as shown in Figure 5.1, was fairly simple. The selection of a rectangular shaped geometry used in this work was based on the previously reported findings described by Mohabuth, (2007) which demonstrated a lack of segregation and convection current control in other non-rectangular shaped separation cell geometries. The role of container geometry and the influence of a boundary wall roughness in controlling the vertical vibration induced particle convection currents is also investigated in the work of Knight, (1997), Kong *et al.*, (2006) and Zeilstra *et al.*, (2008). Nevertheless, the rectangular shaped separation cell geometry,

shown in Figure 5.1, was mainly comprised of a working chamber which was constructed by placing a sliding gate into the side wall clips. The clips for holding the sliding gate were readily adhered to the side walls. The sliding gate was placed into the clips so that it only allowed a small, variable, partition gap size of 3 to 5 mm at its bottom. Once the main working chamber was all set, the finely sized particles of the working mixture were gradually poured into it to form a static particle bed. The composition of a synthetic working mixture used in this investigation, along with the mass mean diameters of the glass and bronze particles, and an “ S_d ”-factor value calculated by using Equation 2.5 is given in Table 5.1.

Mixture	A				
Material	Bead diameters range(μm)	Mass mean diameters (μm)	Density, $\rho(\text{kg.m}^{-3})$	%wt	“ S_d ”-value (Eq. 2.7)
Glass particles	38-106	123.15	2500	80%	5.84
Bronze particles	38-300	157.67	8900	20%	

Table 5.1: Composition of the synthetic glass and bronze particle mixture used in the preliminary investigations.

The spherical glass (80%wt) and bronze (20%wt) particles of the synthetic mixture shown in Table 5.1 had an average mass mean diameter of 123.15 μm and 157.67 μm respectively. The “ S_d ”-factor value of 5.84 as shown in Table 5.1 suggested a strong density segregation potential for this spherical shaped working particle mixture. The spherical shape features of the working glass and bronze particles are highlighted in the SEM images shown in Figure 5.2.

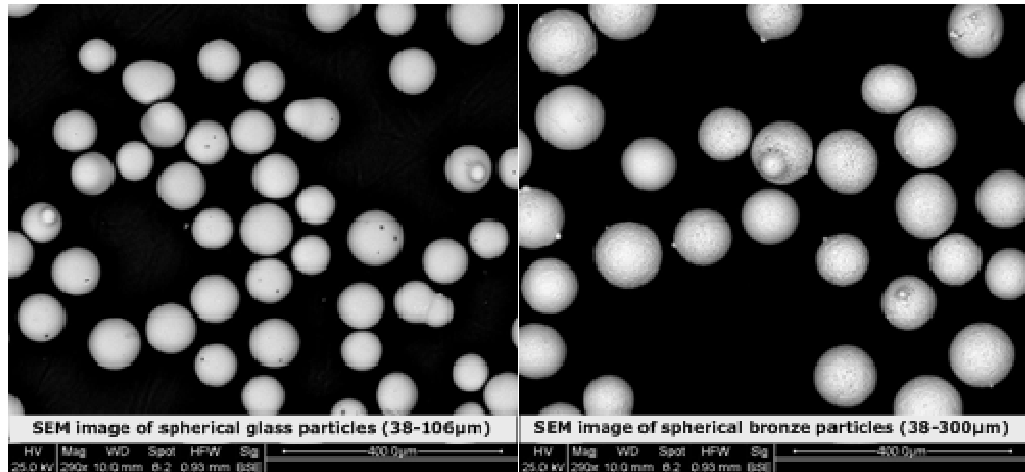


Figure 5.2: SEM images of the spherical glass and bronze working particles.

The complete size characterisation of the working particle mixture is given in Figure 5.3.

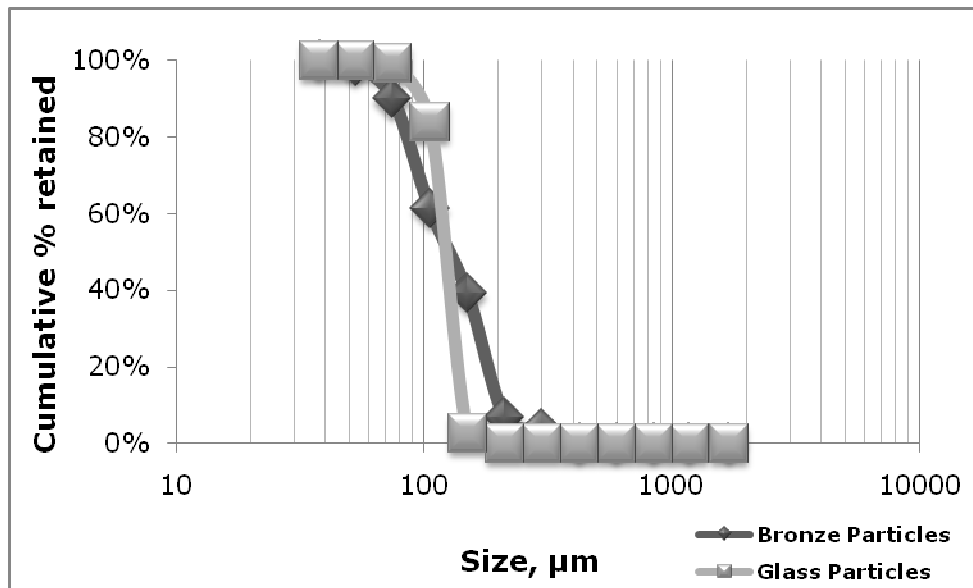


Figure 5.3: Particle size characterisation of glass and bronze particles used in the preliminary investigations.

The selection of a finely sized glass and bronze particle mixture with a high density differential ($\rho_{\text{bronze}}(8900\text{kg.m}^{-3})/\rho_{\text{glass}}(2500\text{kg.m}^{-3}) = 3.56$) was important in investigating a density segregation phenomenon in the vertically vibrated particle bed. The selection of a glass and

bronze working particle mixture also offered ease of visualisation in any transparent structure. The average particle bed height of the working mixture in the separation cell geometry shown in Figure 5.1 could be varied according to the requirements of a particle separation investigation. Once the desired particle bed height was achieved in the working chamber, the separation cell geometry was clamped on top surface of the vibrating platform (Figure 2.26 of Chapter 2). Next, the working particle mixture was vertically vibrated at different frequency levels in an effort to find the optimum vibration separation frequency value. The optimum value of vertical vibration frequency was only recorded when a "good particle separation" criterion, as described in Section 3.3.4.1 of Chapter 3, was achieved.

At an optimum vibration separation frequency value, the onset of a distinct convection current was observed in each of the two particle phases and the vibrated particle bed formed a stable right angled tilt in one direction. The formation of this right angled tilt is also reported in the work of Milburn *et al.*, (2005) and Leaper *et al.*, (2005) and is previously discussed in Section 2.6.4 of Chapter 2. Nevertheless, on most occasions the formation of a particle bed tilt was in an exact opposite direction to the sliding partition separation gate. The other important prerequisite for the observance of an optimum vertical vibration separation frequency value was considered to be the non-observance of any abrupt particle throwing from the tilted particle bed surface during the course of convective particle motions.

The start of a vertical vibration treatment was marked by the generation of local convection currents in each of the two particle phases. It was visually observed that there was a greater probability of the generation of a local convection current in the higher particle bed height working mixtures. Nevertheless, in case of particle bed height investigations reported here, the localized

convection currents were observed to quickly and steadily merge with each other in the individual particle phases. The merger of these localised convection currents resulted in generation of a distinct global convection current in each of the two particle phases. The global convection currents were observed to form within the first few seconds of any vertical vibration treatment. This was especially true in the low particle bed height working mixtures. The onset of a visually observed global convection current in each of the two particle phases was considered to be the main driver for the vertical vibration induced particle separation behaviour of the high density particles.

The low density particles were observed to move in a global convection current which was largely confined to the inner regions of the vibrated particle bed. The high density particles were observed to move in a distinct global convection current which was predominantly patrolling in the outer periphery of the tilted particle bed. During the course of this manoeuvre the high density particles were observed to concentrate in close proximity of the partition separation gap. There, the partition separation gap was placed to separate the working chamber from the rest of the separation cell assembly. The small partition separation gap size only allowed the high density and/or high momentum particles to pass through and reach the other side of the main working chamber. Once the separated particles passed through the partition separation gap and reached the other side of the working chamber, their collective convective motions were mostly observed to cease. However, the external vertical vibration treatment still imparted enough momentum into these separated particles that they continued to move towards the exit for their final collection as a separated material.

In this work, the arbitrarily selected particle bed heights of 20 mm and 40 mm and a partition separation gap size of ~5 mm was used.

The use of a partition gap size below 5 mm was observed to hinder the distinct particle motions of the separated particles from the main working chamber. Nevertheless, selection of the 20 mm and 40 mm particle bed heights and ~ 5 mm partition gap size was solely based on the previously reported prototype scale investigations of Mohabuth, (2007). For an initial vertical vibration induced particle separation assessment in the newly designed separation cell geometry, shown in Figure 5.1, a working mixture of spherical glass (80%wt) and bronze (20%wt) particles was vertically vibrated for a continuous period of 15 minutes in each investigation. The initial trial runs with various combinations of frequency and dimensionless acceleration revealed that the vertical vibration frequency value of $\sim 30 \pm 10$ Hz and a dimensionless acceleration value of $\sim 3 \pm 10\%$ were optimum for the dry based separation of the synthetic particle mixture (Table 5.1). In the scaled up particle separation cell, the separated products were first visually assessed for the extent of their separation. The visually assessed particle separation criterion used in this work was based on the guidelines given in Section 3.3.4.1, of Chapter 3.

The particle segregation experiments reported here were performed under atmospheric temperature and pressure. All the experiments reported were repeated at-least five times under the same operating conditions to estimate an average particle separation time. The representative samples of the separated products were drawn by using the procedure described in Section 3.3.2 of Chapter 3. The acquired representative samples were later analysed by the standard sink and float analysis technique described in Section 3.3.3.2, of Chapter 3, to reveal the true grades and recoveries of the separated fractions. The percentage recovery of the separated fraction was calculated by using Equation 5.1.

Equation 5.1

$$\% \text{ Recovery of fraction A in the mixture} = \frac{\text{Mass fraction A in the finally separated product}}{\text{Mass fraction A in the initial particle mixture}} \times 100$$

The percentage grade of the separated fraction was calculated by using Equation 5.2.

Equation 5.2

$$\% \text{ Grade of fraction A in the mixture} = \frac{\text{Mass fraction A in the finally separated product}}{\text{Total mass of the finally separated material}} \times 100$$

Based on Equation 5.1 and Equation 5.2, the final grades and recoveries of the separated bronze particles at the average particle bed heights of 20 and 40 mm are shown in Figure 5.4.

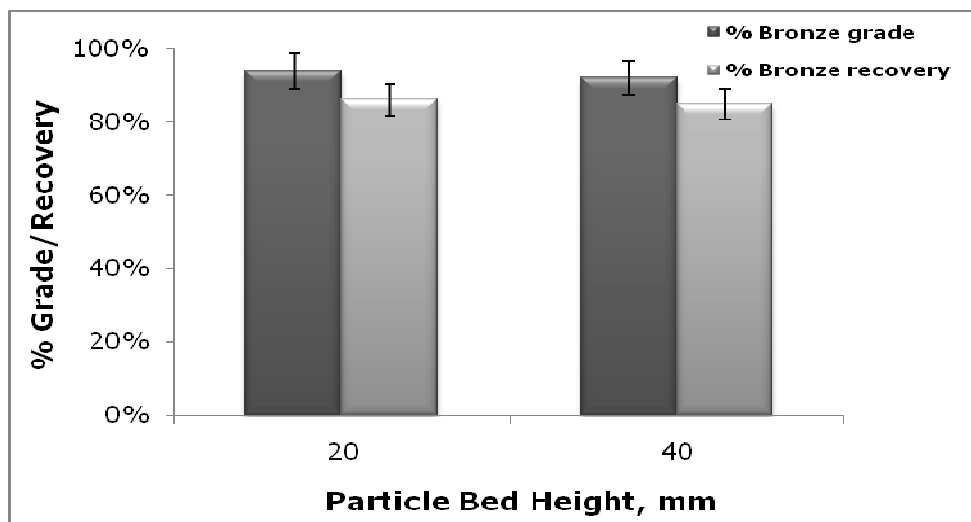


Figure 5.4: Grade and recovery of the separated bronze particles in the first scaled up separation cell geometry.

An analysis of Figure 5.4 shows that the separated products had the separation grades >90% with excellent recovery values >80% in almost all the optimum particle separation cases reported here. The particle separation grades and recoveries reported in this investigation were nearly the same at both 20 and 40 mm particle bed heights. Overall, the particle separation behaviour in the newly

designed separation cell (Figure 5.1) geometry showed very little, or no, deviation from the basic particle separation mechanism previously described in the work of Mohabuth, (2007), on a prototype scale. The percentage grades of the recovered bronze particles which stayed nearly constant over the full length of an estimated particle separation time are shown in Figure 5.5.

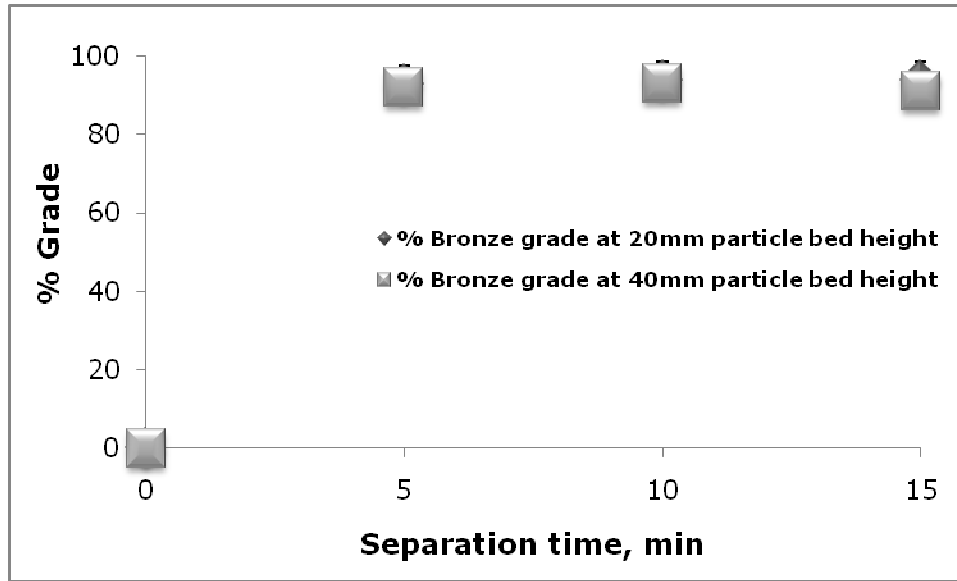


Figure 5.5: % Grade of the separated bronze particles in product-1 in relation to the average particle separation time.

The particle separation geometry (Figure 5.1) reported in this section was basically a trial design that was used to gain some insight into the dry based particle separation behaviour of a binary particle mixture at a scaled up level. The experimental experience of particle separation in this geometry (Figure 5.1) and the results from the previously reported work of Mohabuth, (2007) hinted that a more precise control of the convective particle motions to impart an effective particle separation may be achieved in the smaller width separation cell geometries. The effective control of convection currents in the narrow width separation cell geometry may be due to the enhanced wall frictional effects that could help generate somewhat stronger distinct convection currents in the vibrating

particle mixtures. The size and shape influence of a container on the vibration induced particle dynamics of a binary particle mixture is also reported in the work of Jaeger *et al.*, (1996). Nevertheless, the acquired experimental know-how from the first scaled up particle separator cell design was put into practical use by designing the L and T shaped particle separation cells.

5.2.3 Particle segregation in the L-type separation cell geometry

The design of an L-type particle separation cell (shown in Figure 3.4, Chapter 3) was largely based on the experimental observations, described in Section 5.2.2. To date, the majority of vertical vibration induced particle segregation behaviours are explored with particle mixtures that predominantly have a high density differential. Despite the core importance of a size segregation phenomenon, only a limited number of investigations addressing this research area have been reported in the literature. Some, worth mentioning, size segregation investigations are reported by Brone and Muzzio, (1997); Cooke *et al.*, (1996); Duran *et al.*, (1993); Duran *et al.*, (1994); Hong *et al.*, (2001); Hsiau *et al.*, (2002); Knight *et al.*, (1993); Kudrolli, (2004); Moysey and Baird, (2009); Naylor *et al.*, (2003); Ohtsuki *et al.*, (1995); Rapaport, (2001); Rosato *et al.*, (1987) and Sanders *et al.*, (2004). The majority of the above mentioned investigations have tried to explore the size segregation effects of a single intruder particle in finely sized particle mixtures. In the vertically vibrated finely sized particle mixtures, the size segregation investigations have also claimed that a big size intruder particle will behave identically to a small size but high density intruder particle. Nevertheless, the work reported by Sanders *et al.*, (2004) is an exception and has explored the size segregation

potential of the multiple intruder particles in the vertically vibrated finely sized particle mixtures.

In an effort to extend the work carried out by Sanders *et al.*, (2004) and to explore the segregation potential of the size differential particle mixtures, experiments reported here were performed by using two different sized, but equal density and identical shape, (spherical) glass particles. The separation dynamics of the working particle mixtures, used in this investigation, were explored in the scaled up 50 mm width L-type separation cell geometry, as shown in Figure 3.4 of Chapter 3. The L-type particle separation cell was vertically vibrated by using Rig-2. The construction and working of Rig-2 is previously described in Section 3.2.2 of Chapter 3. The size characterization of the glass particles used in this investigation is shown in Figure 5.6.

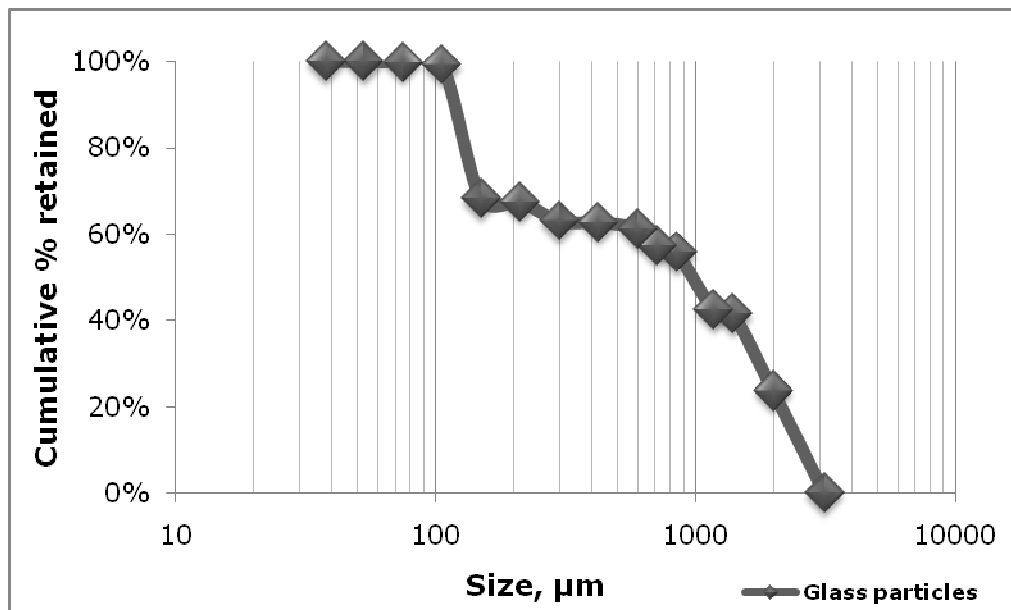


Figure 5.6: Particle size distribution of the glass particles (mixture A and B combined) used in the size segregation experiments.

Among the full particle size characterisation given in Figure 5.6, the particle size ranges that were chosen to make the synthetic working particle mixtures A and B are shown in Table 5.2.

Mixture	A			B			1
Material	Bead dia.* (µm)	Mass mean dia.* (µm)	S_d -value	Bead dia.* (µm)	Mass mean dia.* (µm)	S_d -value	%wt
Small size glass particles	38-106	89.54	52.12	38-106	89.54	133	80%
Big size glass particles	355-710	646.43		850-1180	1032.52		20%

Table 5.2: Composition of the spherical glass particle mixtures A and B used in the size segregation investigations carried in an L-type particle separator. (* dia.= diameter)

The selection of working particle mixtures A and B, as shown in Table 5.2, was solely based on the initial visual investigations. The initial visual investigations showed very little, or no, segregation potential for the very close size range glass particles in the L-type separation cell geometry. Nevertheless, the finally selected 355-710µm and 850-1180µm size range glass particles were spray painted in blue and green to help visualise their distinct convective motions in the predominantly small size, but naturally transparent, 38-106 µm glass particles. In all the investigated size segregation cases reported here, the 80:20%wt mixtures of small and big size glass particles were vertically vibrated for a continuous period of 20 minutes. The estimation of an average particle separation time was based on the visually observable “good particle separation” criterion described in Section 3.3.4.1, of Chapter 3. In addition to the visual observations, digital images were also recorded by using a digital imaging device/camera of the type described in Section 3.3.4.2. Finally, the separated products were quantitatively analysed by using the standard sieve analysis technique, described in Section 3.3.3.1, to reveal the true grades and recoveries of the separated products.

The working particle mixtures A and B, as shown in Table 5.2, were initially well mixed in a two litre plastic beaker using a standard

laboratory scoop. Next, the working particle mixtures were gradually poured into the main working chamber of the L-type separation cell geometry (Figure 3.4, Chapter 3) by using a suitably sized plastic funnel. Size segregation in the initially well mixed working particle mixtures was readily observed at this particle pouring stage. Nevertheless, before the start of any vertical vibration treatment it was always ensured that the working particle mixtures remain confined to the main working chamber. An average particle bed height of 60 mm was used in this investigation. This particular particle bed height was selected to explore the size segregation potential of the low density particles at the higher than previously explored particle bed heights of 20 mm and 40 mm. Nevertheless, in this case the identification of an optimum vertical vibration frequency and dimensionless acceleration value for effective particle segregation was based on the visual observations made through the transparent walls of the L-type particle separator. The visually observed vertical vibration induced particle size segregation behaviours of particle mixtures A and B showed virtually similar trends. The size segregation behaviour of mixture-A (Table 5.2) is shown in Figure 5.7(a-d) to highlight some of the observed size segregation trends in the scaled up L-type separation cell geometry.

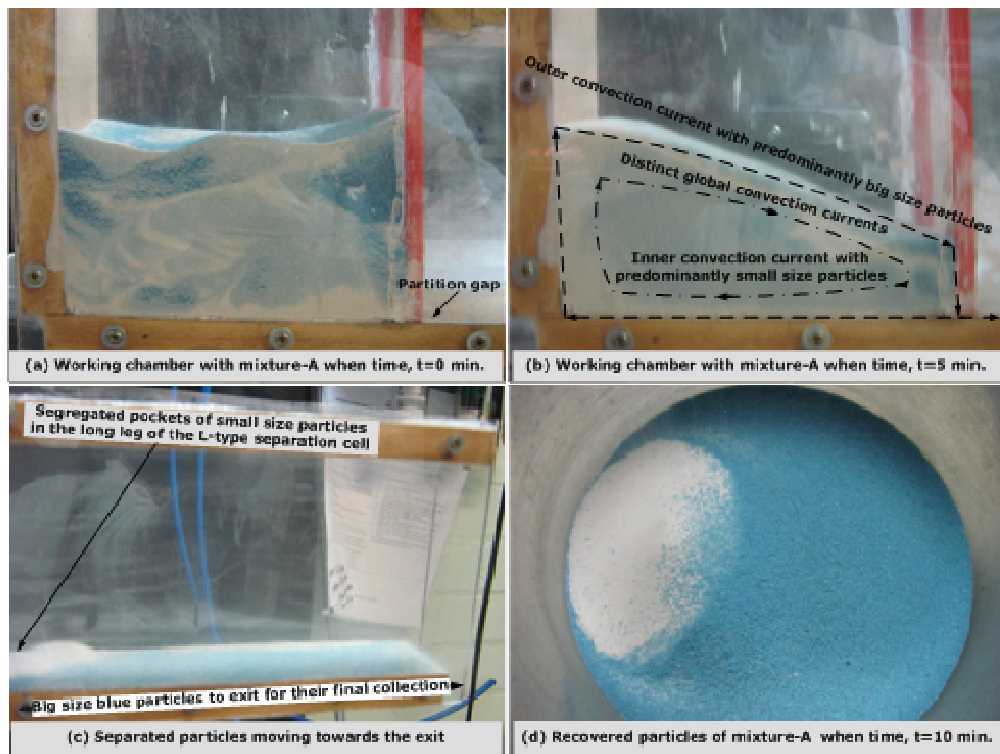


Figure 5.7: Size segregation behaviour of mixture-A in the L-type particle separation cell.

In Figure 5.7, (a) shows an initially well mixed working mixture-A in the main working chamber of the L-type separation cell. Once the mixture that formed an average particle bed height of 60 mm in this case was vertically vibrated, it dilated largely near to the top particle bed surface and formed a stable right angled tilt. The formation of this right angled tilt is shown in Figure 5.7(b). Besides maintaining a right angled tilt, the vertically vibrated particle mixture also supported the formation of a distinct global convection current in each of the two particle phases. The approximate trajectories of the two visually observed global convection currents are shown in Figure 5.7(b). The outer convection current, as shown in Figure 5.7, (b) predominantly contained the big size particles while the small size particles were mostly observed to move in the inner regions of the tilted particle bed.

The big size particles, during the course of their convective manoeuvres, were observed to move into the next separate chamber through a small partition gap size of ~ 5 mm. There, the partition gap size was provided to separate the main working chamber from rest of the separation cell assembly. The partition gap size was used to control the type of particles that can actually move out and reach the next, separate, chamber. The actual working of the partition gap size in controlling and limiting the particle flows is still not completely understood. However, a strong contribution from the surrounding fluid, inter-particle and side wall frictional effects coupled with the individual momentum of the vertically vibrated mobile particles are suspected to play an important role in controlling the flow of particles through the partition gap size. Once the predominantly big size particles were through the partition gap size and reached the long leg of the L-type separation cell geometry, secondary particle segregation was observed to start in the separated material. In most of the cases, reported here, the secondary particle segregation in the long leg of L-type separation cell geometry was responsible for further purification of the separated blue particles. During the course of this purification the localised pockets of small size glass particles were observed to form (Figure 5.7(c)). These pockets were mainly observed to form near the transparent side walls of the L-type separation cell. Once enough small size particles were gathered in these pockets, the commencement of a localised convection current was readily observed. Nevertheless, the presence of small size particles in the long leg of the L-type particle separator did not hinder the distinct movements of the big size blue particles that continued to separate out from the main working chamber. The blue particles were finally collected as product-1 in the bucket (Figure 5.7(d)) that was purposefully placed at the long leg exit of the L-type particle separator. Once a significant amount of big size

particles moved out of the main working chamber, the residual small size particles were recovered from the main chamber as product-2.

Parallel particle segregation trends, as described for mixture-A, were readily observed in the segregation of particle mixture-B. An illustration of the size segregation progression is shown in Figure 5.8.

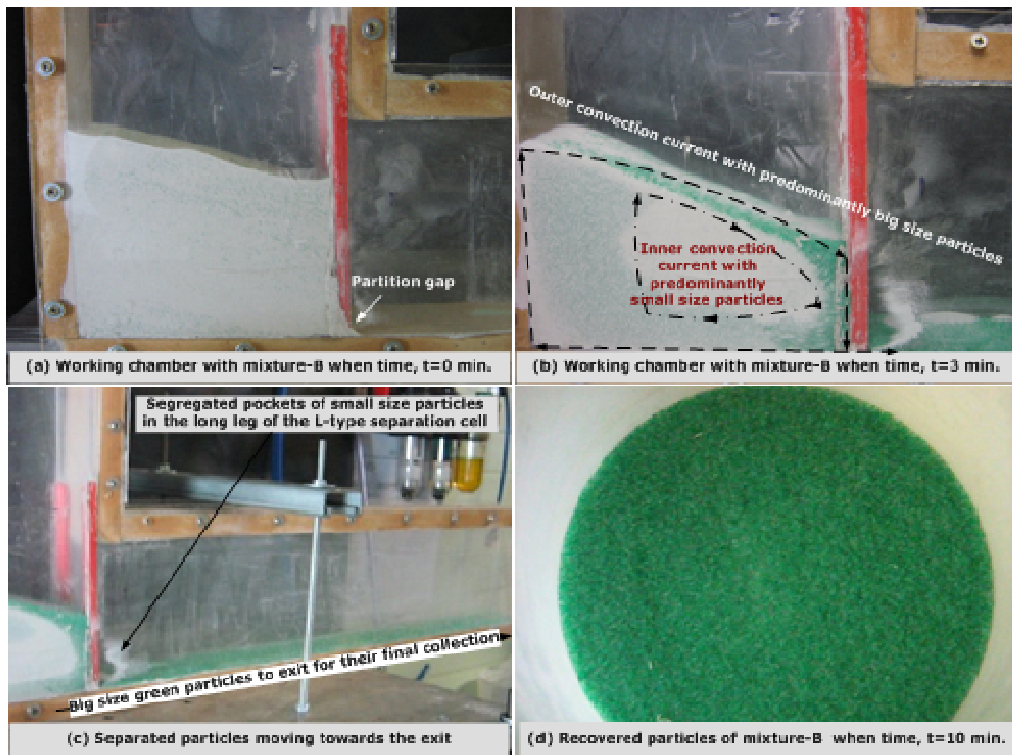


Figure 5.8: Size segregation behaviour of mixture-B in the L-type particle separation cell.

The visual particle separation investigations, reported here, have shown that, at 60 mm particle bed height, the vertical vibration frequency and dimensionless acceleration values of $\sim 30 \pm 10\%$, Hz and $3 \pm 10\%$ were optimum in separating particle mixtures A and B. Nevertheless, once the optimum particle separation conditions were visually identified, the size segregation experiments reported here were repeated at least five times to estimate an average particle separation time, which was ~ 20 minutes in almost all the

investigated cases reported here. The representative samples from the feed and segregated products were drawn by following the procedure described in Section 3.3.2, of Chapter 3. The acquired representative samples were sieve analysed for size based grading by using Equation 5.3 and Equation 5.4 to report the final big size (Table 5.2) particle separation grades and recoveries of mixtures A and B.

% Grade of big size particles in mixture A & B -

Equation 5.3

$$\frac{\text{Mass fraction of big size particles in the finally separated product}}{\text{Total Mass of the finally separated material}} \times 100$$

% Recovery of big size particles in mixture A & B -

Equation 5.4

$$\frac{\text{Mass fraction of big size particles in the finally separated material}}{\text{Mass fraction of big size particles in feed}} \times 100$$

The average big size particle separation grades of mixtures A and B were nearly constant at full length of an average particle separation time as shown in Figure 5.9.

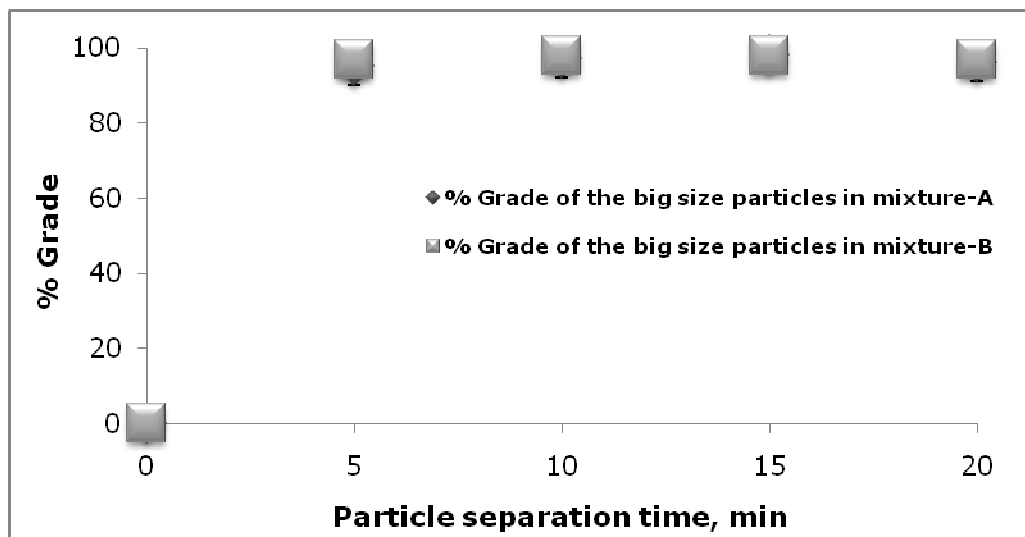


Figure 5.9: Separation grades of big size particles in product-1 in relation to an average particle separation time.

The final sieve analysed grades and recoveries of the separated big size particles are shown in Figure 5.10.

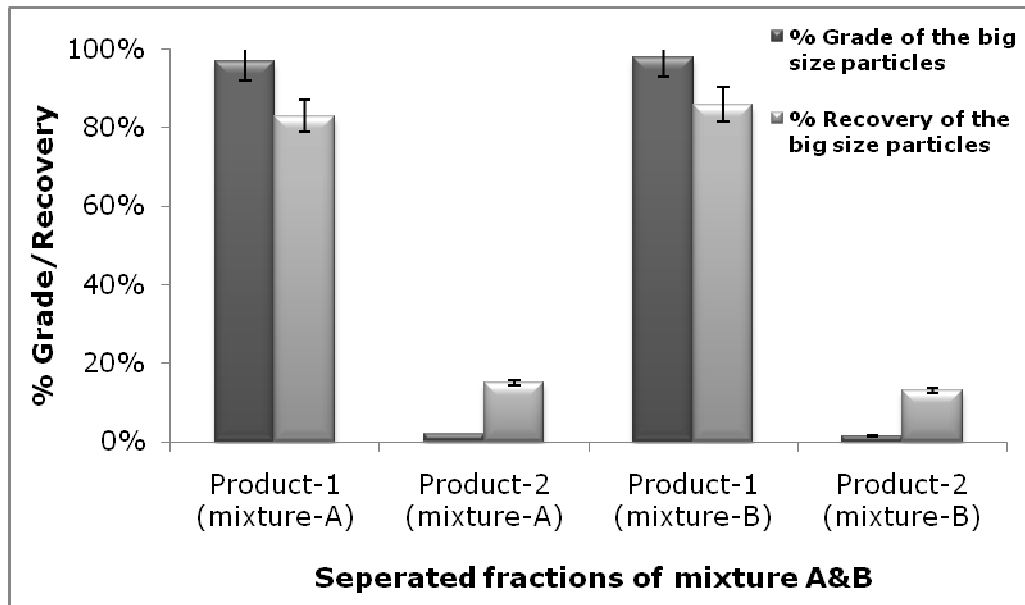


Figure 5.10: Grades and recoveries of the big size particles in mixture A and B at a particle bed height of 60 mm in the L-type particle separator.

Figure 5.10 reveals that the particle separation grades and recoveries of both mixture A and B were nearly the same at an identical particle bed height of 60 mm. The preliminary particle separation investigations, reported here, have mainly relied on the semi-continuous operation of the L-type particle separation cell. In an effort to reach a step closer to a continuous particle separator cell design, the L-type particle separation cell geometry was further modified. This resulted in design of a T-type particle separation cell.

5.2.4 Particle segregation in the T-type separation cell geometry

5.2.4.1 Separation of a glass and bronze particle mixture

The detailed design assembly of a T-type particle separation cell is shown in Figure 3.5, of Chapter 3. This design comprised a working chamber which was equipped with two adjustable partition gap sizes. During the course of any particle bed flights under the influence of vertical vibration, this particular partition gap size positioning was designed to draw-in the surrounding fluid from both ends of the main working chamber. Among others, the role of a surrounding fluid in enhancing the vertical vibration induced particle dynamics is reported in the work of Burtally, (2004), Naylor *et al.*, (2003), Klein *et al.*, (2006) and Leaper *et al.*, (2005). The predictive enhanced surrounding fluid flow into the main working chamber of the T-type separation cell was targeted to result in generating rather strong convection currents for particle segregation.

The working mixture used in this preliminary investigation comprised 80:20%wt glass and bronze particles (Table 5.1). The complete size characterisation of this working particle mixture is given in Figure 5.3. The investigations, reported here, were carried with varying particle bed heights of 60, 80 and 100 mm in the 20 and 40 mm width T-type separation cells. A partition gap size of ~5 mm was used in this investigation. The investigations reported here have shown parallel particle segregation behaviours in the finely sized glass and bronze particle mixtures which were vertically vibrated in the main working chambers of the 20 and 40 mm width T-type separation cells having an active partition gap size of ~5 mm on both ends. Also, the use of two partition gap sizes in the main

working chambers of the 20 and 40 mm width T-type separation cells showed that the observed particle segregation behaviours were nearly the same at the particle bed heights of 60, 80 and 100 mm. The particle segregation behaviour at a particle bed height of 100 mm in a 40 mm width T-type separation cell is shown as an example in Figure 5.11.

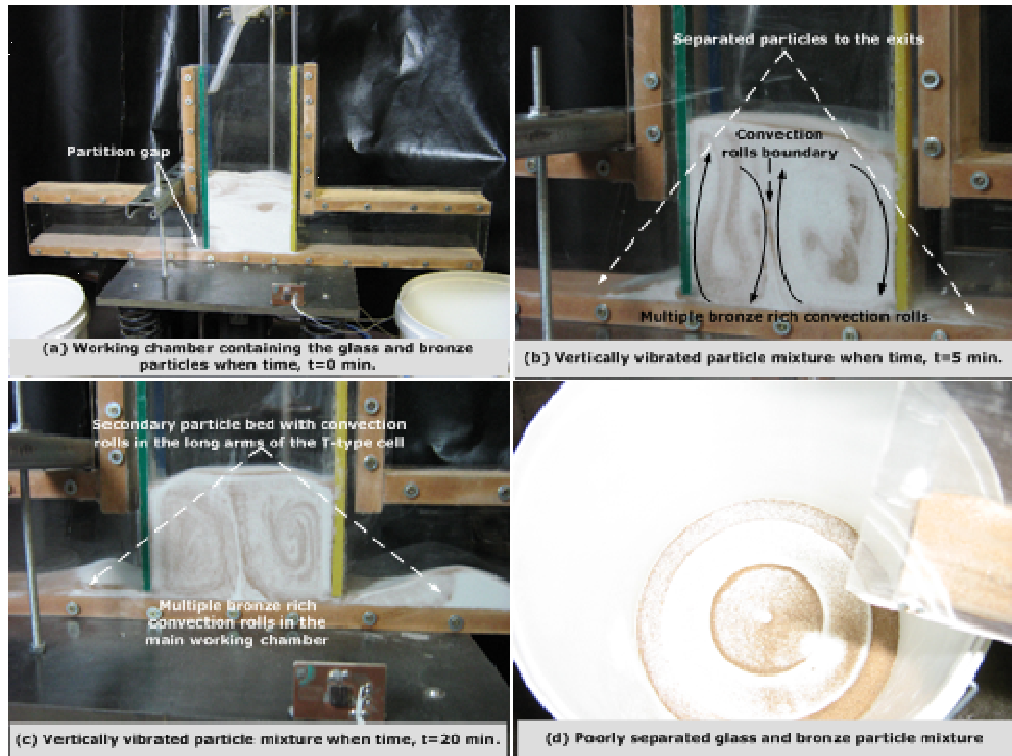


Figure 5.11: Density segregation behaviour of a finely sized 80:20%wt glass and bronze particle mixture at a particle bed height of 100 mm in the 40 mm width T-type separation cell.

In Figure 5.11, (a) shows an initially well mixed working particle mixture that was placed in the main working chamber of the 40 mm width T-type particle separation cell. As the vertical vibration treatment of the working particle mixture was carried out at the visually identified optimum frequency and dimensionless acceleration values of $30 \pm 10\%$ Hz and $3 \pm 10\%$, the onset of multiple convection currents as shown in Figure 5.11(b) was readily observed. Any increase or decrease in the optimum frequency and

dimensionless acceleration value was observed to diminish the global convection currents that were deemed necessary for particle segregation. At higher than optimum magnitudes of vertical vibration frequency and dimensionless acceleration, the particle bed was observed to show particle throwing from the top vertically vibrating particle bed surface in the main working chamber. At lower than optimum magnitudes of vertical vibration frequency and dimensionless acceleration, the convective particle motions were mostly observed to seize.

The onset of strong and distinct fluid motions in the main working chambers of the T-type separation cells was considered to be the main driver for the multiple convection currents observed in the working particle mixtures. During the course of vibration driven particle bed flights, the surrounding fluid was considered to be drawn in from both ends of the main working chamber. Nevertheless, the generation of multiple convection currents, as shown in Figure 5.11(b), was not helpful in separating the finely sized working particle mixtures. An example of particle separation hindrance that arose due to the use of two partition gap sizes can be seen in Figure 5.11(c) where the poorly separated particle mixtures exiting from both ends of the main working chamber were observed to group together and form the secondary particle beds in the long legs of T-type separation cell. Once the substantial amounts of particles were grouped together in the long legs of the T-type separation cells, varying magnitudes of secondary particle segregation was readily observed. This situation can also be seen in Figure 5.11(c) where the secondary particle bed occupied the full width of the long leg outside the main working chamber.

The uncontrolled and complex particle segregation situation observed in this investigation resulted in a poorly separated particle mixture (Figure 5.11(d)). The particle segregation situation in this investigation did not improve even after an hour of continuous

vertical vibration treatment. The particle segregation described in this work was similar to the other (Mohabuth, 2007; Burtally *et al.*, 2002 and 2003) investigated cases in this category. The “poor particle separation” reported here was assessed based on criterion described in Section 3.3.4.1, of Chapter 3. Although, the investigations described in this section did not result in any good particle separation, the practice however was considered valuable in identifying the poor particle separation configurations that can be avoided in future design endeavours.

5.2.4.2 Separation of shredded electrical cable particles

The particle separation failure (Section 5.2.4.1) in the main working chamber of the T-type separation cell (Figure 3.5), where two partition gap sizes could be opened concurrently, resulted in exploring the other possibilities for operating the 20 and 40 mm width T-type separation cells. This resulted in using a new strategy where only a single partition gap size of ~5 mm was used in the main working chambers of the 20 and 40 mm width T-type separation cells. Once the desired particle fraction was separated out from the operational partition gap size opening, the remaining particles in the main working chamber were drawn out separately from the other end. This operational strategy was nearly similar to one used in the operation of the L-type particle separation cell (Section 5.2.3) with the exception of recovering the separated particles from two different ends at different time intervals.

The previously reported investigations, in this chapter, have mainly looked into the segregation behaviours of the regular shaped synthetic particle mixtures. Although the use of a regular shaped particle mixture is useful in gaining some insight into the separation behaviour of the finely sized particle mixtures, the majority of the

industrially relevant particle mixtures are irregular and complex shapes. In an effort to explore the particle segregation behaviour of the irregular and complex shaped particle mixtures, the investigations reported here were performed using shredded electrical cable particles. The electrical cables used in this work originated from personal computers (PCs) and were acquired from the Information Services Department, of the University of Nottingham, UK. The electrical cables were initially cut in to ~200 mm long pieces with pliers. These ~200 mm long electrical wire pieces were then cut in stages of -10 mm, -4 mm and -1.5 mm particle size ranges by using a Retsch® cutting mill (Section 3.3.1.1 of Chapter 3) to get a final particle size range below -0.75 mm. The minus (-) sign used here represents the material passing through each discharge grid size of the cutting Retsch® mill. The final particle size range from the -0.75 mm Retsch® mill cut resulted in generating long copper wire pieces along with complex and irregular shaped plastic particles. The SEM image of the -0.75 mm shredded PC electrical cable particles is shown in Figure 5.12.

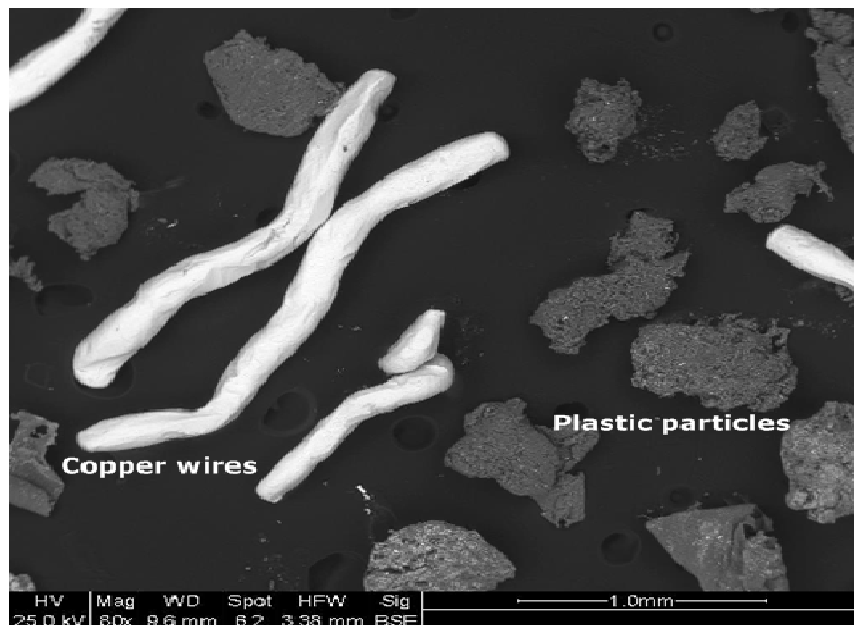


Figure 5.12: SEM image of the shredded electrical cable particles.

The shredded electrical cable particles used in this work were specifically chosen to represent a high density differential ($\rho_{\text{copper wires}}/\rho_{\text{plastic coating}}=8300\text{kg.m}^{-3}/930\text{kg.m}^{-3}=8.92$) binary working particle mixture. The selection of this mixture also offered easy particle visualisation through the transparent walls of the T-type separation cells. The working particle mixture used here was size characterised using the standard sieve analysis technique described in Section 3.3.3.1, of Chapter 3. The size characterisation of the -0.75 mm working particle mixture is shown in Figure 5.13.

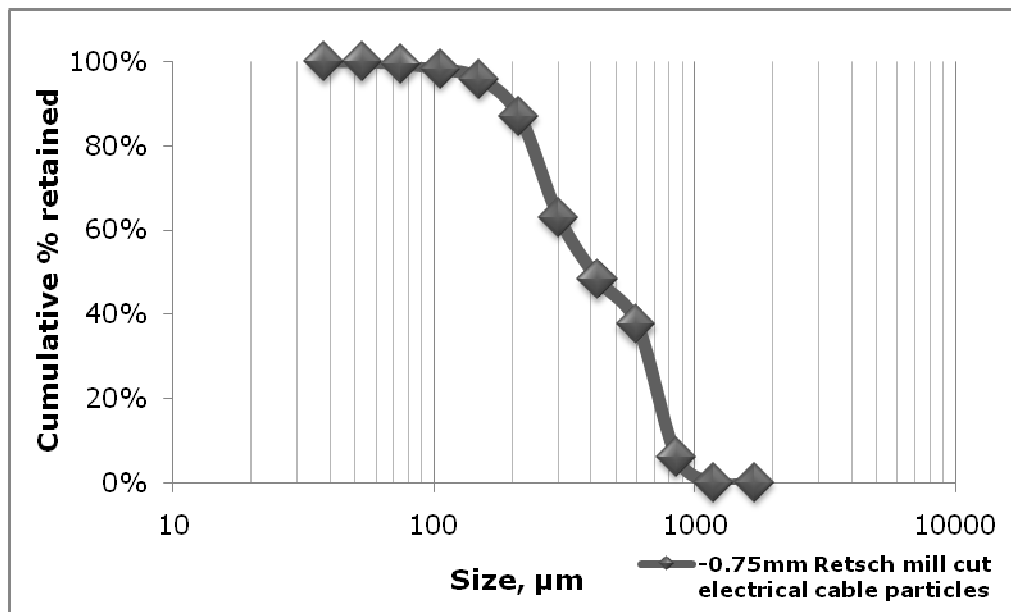


Figure 5.13: Particle size characterisation of the shredded electrical cable particles used in the T-type cell.

Among the full particle size characterisation, given in Figure 5.13, only a 250-425µm size range particle mixture was used in this preliminary investigation. This particular particle size range was favoured to avoid the excessive presence of any finely sized particles in the working particle mixture. The excessive presence of finely sized particles can increase cohesiveness and potentially leads to the compaction of the vertically vibrated particle mixture. It may be due to this that the 250-425µm size range particles were also preferred in the work of Mohabuth (2007). The initially well mixed

shredded electrical cable particles were poured into the main working chamber of the 20 mm width T-type separation cell. In this preliminary investigation a sole particle bed height of 80 mm was used with a single partition gap size of ~ 5 mm in the main working chamber of the T-type separation cell. The particle separation behaviour of the shredded electrical cable particles under the influence of vertical vibration in a 20 mm width T-type separation cell is shown, as an example, in Figure 5.14.

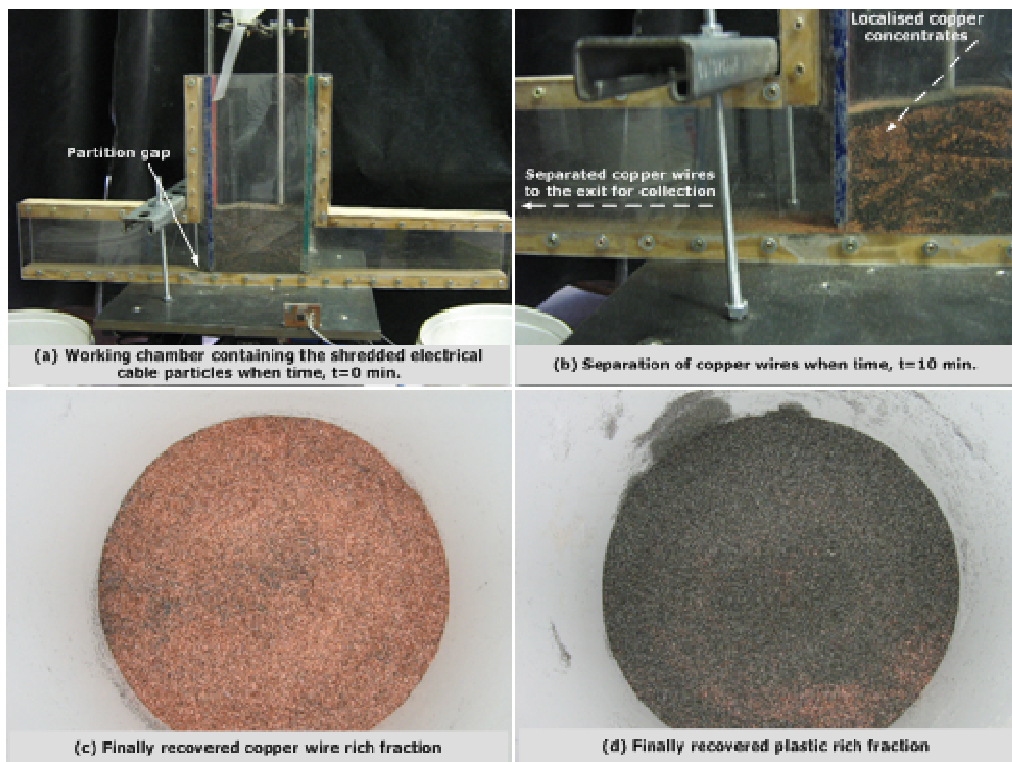


Figure 5.14: Particle separation behaviour of the shredded electrical cable particles in a 20 mm width T-type separation cell.

In Figure 5.14, (a) shows the initially well mixed particle mixture in the main working chamber of the 20 mm width T-type separation cell. When this working particle mixture was vertically vibrated at the visually identified optimum frequency and dimensionless acceleration magnitudes of $30 \pm 10\%$ Hz and $3 \pm 10\%$, localised copper concentrates, as shown in Figure 5.14(b), were readily observed. These copper concentrates were mainly developed as a

result of the convective particle motions in the working mixture. The distinct particle bed behaviour showing the formation of localized concentrates, as shown in Figure 5.14, can be attributed to the complex shaped features of the working particles. Nevertheless, the generation of local concentrates in the working particle mixture did not hinder in the convection induced separation of the high density particles. Furthermore, entanglement of the copper wire particles was not an issue with the particle size range used in this work. The free flowing copper wire particles were readily observed to emerge from the main working chamber and move in the long leg of the T-type cell. It took nearly 45 minutes to get a finally separated copper wire particle product which is shown in Figure 5.14(c). Once the copper wire particles were separated out, the remaining plastic material was recovered from the other end of the separation cell and is shown in Figure 5.14(d). In this investigation “good particle separation” with a relatively long separation time can be attributed to the distinct size, shape and density effects of the working particles. Nevertheless, the separated particle fractions were later analysed by using a sink and float analysis technique, described in Section 3.3.3.2 of Chapter 3, to reveal the copper separation grades which are shown in Figure 5.15.

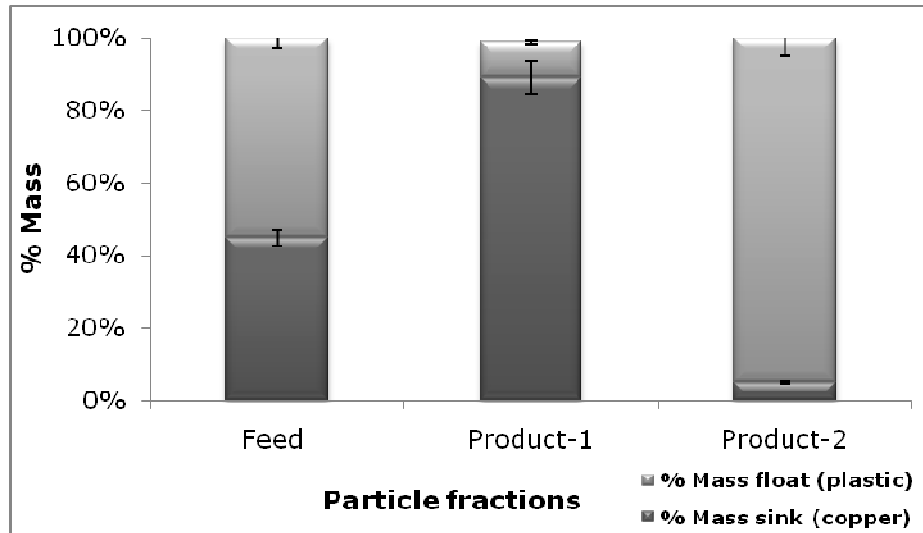


Figure 5.15: Grades of the separated shredded electrical cable particles in a 20 mm width T-type separation cell.

Figure 5.15 show that the working particle mixture comprised ~45wt% copper wire particles. The initial copper wire grade was finally concentrated to ~88wt% in about 45minutes of continuous vertical vibration treatment. The separated copper grades of product-1 at different intervals of an average particle separation time are shown in Figure 5.16.

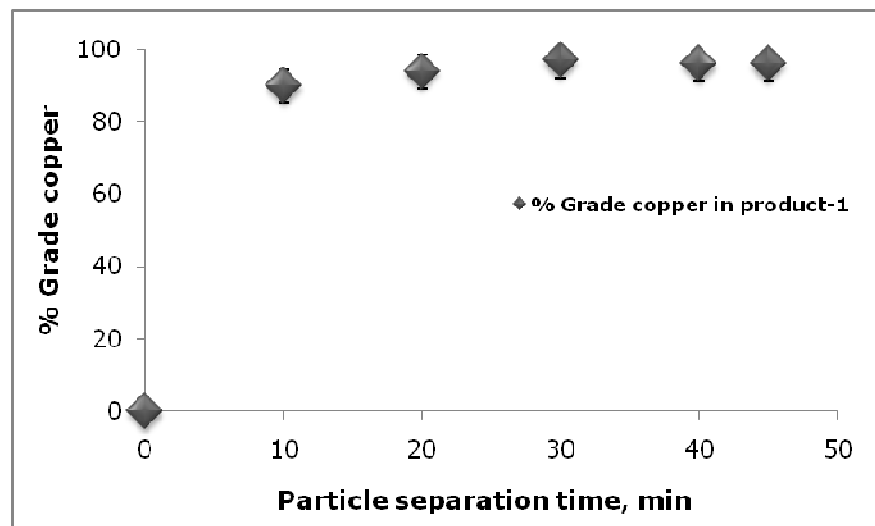


Figure 5.16: Grades of separated copper in product-1 at different intervals of an average particle separation time.

Figure 5.16 show that the copper wire separation grades were nearly constant during the full length of an average particle separation time.

In summary, the preliminary investigations reported above have looked into the possibilities of scaling up a vertically vibrated particle separation system. These investigations have shown some interesting particle separation behaviours in various semi-continuous separation cell geometries. Although an initial attempt at a continuous particle separation operation failed in the flat based T-type particle separation cell however, the use of a slightly tilted bottom separation cell surface as explored in the prototype scale work of Webster, (2009) and the use of distinct size partition gaps in the main working chamber of the T-type particle separator could potentially lead to the continuous separation of the binary particle mixtures. It is mainly due to the anticipated possibilities of improved operational performance that further modifications in the T-type separation cell design, as shown in Figure 3.6 of Chapter 3, were carried out. Investigations exploring the continuous particle separation in the T-type separation cell were considered beyond the scope of this preliminary stage research work. The continuous particle separation options were therefore not taken into further consideration at this stage. Instead, a semi continuous particle separation operation, as described in Section 5.2.4.2, was explored in detail by assessing the particle separation behaviours of various synthetic working particle mixtures.

5.3 Detailed particle segregation assessment in the T-type separation cell

The detailed design description of the modified T-type particle separation cell is given in Figure 3.6. In this work the controlled segregation of irregular shaped particles, as discussed in Section 5.2.4.2, was used as a basis to explore the detailed segregation potential of a variety of dry and non-cohesive finely size (<500 μm) particle mixtures with varying particle sizes and densities. During the course of vertically vibrating a working particle mixture, important vibration separation parameters such as particle bed height, partition gap size and the effects of varying particle concentration, in the synthetic working mixtures, were explored in an effort to determine the optimum vibration separation conditions. Furthermore, smoke blanket visualizations to mimic the interstitial fluid behaviours during the course of vertically vibrating a synthetic glass and bronze particle mixture were also carried out.

5.3.1 Segregation of the glass and bronze particle mixtures

The first detailed assessment and application of the novel vertical vibration induced particle separation technique was carried out to separate the, so called, ideal glass and bronze working particle mixture. The complete size characterisation of this working particle mixture is given in Figure 5.3. Various concentration combinations of this predominantly well-defined spherical shape (Figure 5.2) particle mixture were investigated to establish, and understand, the important vertical vibration particle separation parameters in the new scaled up particle separation system (shown in Figure 3.3 and Figure 3.6). The understanding of particle separation developed here was designed to form the basis for separating a variety of

industrially relevant particle mixtures. The important vertical vibration induced particle separation parameters and their effective ranges were predominantly identified from the previously reported work in literature (Chapter 2) and from the initial trial experiments, reported in Section 5.2 and are listed in Table 5.3.

Experimental parameters		Ranges
1.	Vibration frequency, f , (Hz)	25, 30 and $40 \pm 10\%$
2.	Average static particle bed height, mm	20, 40, 60, 80, 100
3.	Vertical vibration acceleration, dimensionless	$2.0-3.0 \pm 10\%$
4.	Weight percentage of glass and bronze particles	90:10, 80:20, 70:30
5.	Partition gap size, mm	5 and 10
6.	Average particle separation time, minutes	0 to 20

Table 5.3: Experimental parameters and their ranges used in the vertical vibration induced separation of a glass and bronze particle mixture.

The glass and bronze particles used in this investigation had an average mass mean diameters of $123.15\mu\text{m}$ and $157.67\mu\text{m}$ respectively. The weight percentages of the particle mixtures used in this investigation are shown in Table 5.4.

Material	Mixture			A	B	C	“ S_d ”-value (Eq.2.7)
	Bead Dia. (μm)	Mass mean Dia. (μm)	Density $\rho(\text{kg.m}^{-3})$	% wt	% wt	% wt	
Glass	38-106	123.15	2500	90	80	70	5.84
Bronze	38-300	157.67	8900	10	20	30	

Table 5.4: Synthetic glass and bronze particle mixtures used in the detailed vertical vibration induced particle separation assessment.

Selection of the naturally transparent glass and coloured bronze particles used in this work offered ease of distinct particle visualization, through the transparent walls of the T-type particle separation cell. During the course of vertical vibration treatment the transparent T-type separation cell walls also enabled ease of digitally imaging the real time particle motions. The digital imaging

device/camera used to record the photographic images of dynamic particle motions is previously described in Section 3.3.4.2. The ease of particle visualization during the course of vertical vibration treatment was particularly useful in the initial experimental phase where it was regularly used to decide on the values of various operating parameters such as those listed in Table 5.3. Here, the initial visual assessment of particle separation was based on the criterion described in Section 3.3.4.1, of Chapter 3.

The vertical vibration induced particle separation work reported by Mohabuth (2007) used volume percentages of particles mixtures. This selection was preferred due to the ease of particle separation comparison between the different working particle mixtures. Nonetheless, the work reported here has used weight percentages of the working particle mixtures. This selection was considered to be in line with many of the parallel practices in the industrial particle separation processes.

5.3.1.1 The effect of vertical vibration frequency on particle separation

Work reported by Mohabuth, (2007) demonstrated that under appropriate conditions, in a prototype scale partitioned separation cell, the magnitude of vertical vibration frequency below ~50 Hz can be used to impart good separation in different regular, and irregular, shaped working particle mixtures. In addition to the magnitude of vertical vibration frequency and acceleration (Azéma *et al.*, 2006), the dynamic behaviour of a particle mixture is also dependent on the individual particle properties (Zang and Rosato, 2004) such as size and shape.

In an effort to investigate the influence of vertical vibration frequency on particle separation at a scaled up level, the work

reported here has used four different frequency values of 25, 30, 35 and $40 \pm 10\%$ Hz. The separate control of dimensionless acceleration magnitude was not possible in this new scaled up vertical vibration particle separation system. However, the desired dimensionless acceleration range in this work was mostly controlled by the massive weight (30kg) of the top vibrating platform at different vertical vibration frequency levels. At the frequency values used in this work, the dimensionless acceleration magnitudes mostly varied in the range of $2-4 \pm 10\%$. The effect of varying frequency values was investigated on glass and bronze particle mixtures with varying bronze concentrations of 10, 20 and 30wt% (Table 5.4) in 20 mm(C-1) and 40 mm(C-2) width separation cells (Figure 3.6 in Chapter 3). The glass and bronze particle concentration mixtures used in this investigation were selected based on the consideration of the industrially relevant solid waste particle mixtures that normally have a high density differential with somewhat matching constituent weight percentages.

The glass and bronze particles used in this investigation were initially well mixed in a four litre plastic beaker. The resulting particle mixture was carefully poured into the working chambers of the separation cells (C-1 and 2) to form the desired particle bed height. Once this was completed, the whole separation cell assembly was clamped on the top platform of the vertical vibration bench (Figure 3.3). Next, the pneumatically driven vertical vibration was started at the desired frequency level. At this stage, the vertical vibration driven particle bed behaviours were visually observed. The visual observations in this investigation have shown that in all cases a vertical vibration frequency in excess of $40 \pm 10\%$ Hz resulted in visible throwing of the top particle bed surface. Particle throwing from the top particle bed surface is shown as an example in Figure 5.17 (glass (70%wt) and bronze (30%) with 60 mm particle bed height vibrated at $40 \pm 10\%$ Hz).

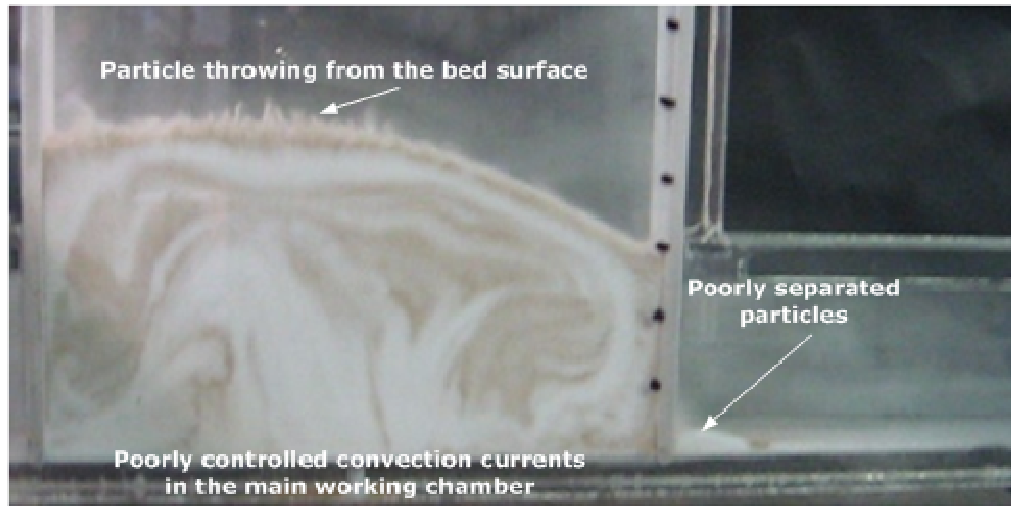


Figure 5.17: Particle throwing from the tilted bed surface at a vertical vibration frequency value of $40\pm 10\%$ Hz in a 20 mm width separation cell. Initial particle bed height of 60 mm, glass and bronze concentration of 70:30%wt (mixture-C) and a partition gap size of ~ 5 mm were used in this investigation.

In addition to the particle bed throwing, the formation of an undefined and mixed convection current, as shown in Figure 5.17, was also observed. Throwing of the mixed glass and bronze particles was not just limited to the top tilted particle bed surface, it was also observed to occur through the partition gap sizes of 5 mm and 10 mm. Nevertheless, in almost all the investigated cases reported here, the undefined, uncontrolled and unstable particle bed behaviours at the frequency levels above $40\pm 10\%$ Hz were strongly observed to contribute in the final collection of a poorly separated material. The reduction of the vertical vibration frequency value to below 40 ± 10 Hz resulted in seizure of visible particle throwing from the top particle bed surface. However, on occasions at vertical vibration frequency values of $\sim 35\pm 10\%$ Hz, the formation of an inverted particle bed tilting as shown in Figure 5.18 was observed.

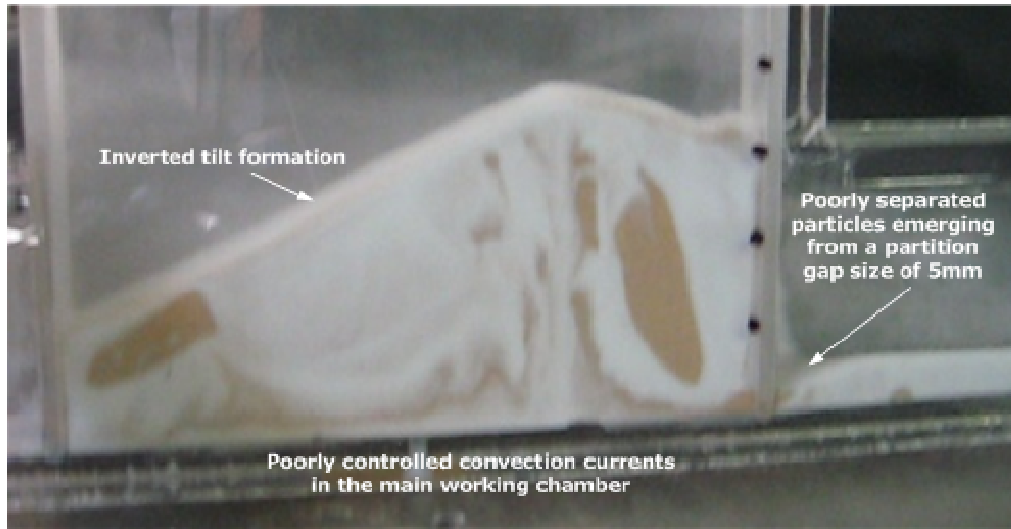


Figure 5.18: Inverted tilt formation at a vertical vibration frequency value of 35 ± 10 Hz. The image shown here shows a glass and bronze (70:30%wt) working mixture-C with an initial particle bed height of 40 mm in separation cell C-1 and with a partition gap size of ~ 5 mm.

The formation of an inverted particle bed tilt as shown in Figure 5.18 was observed to halt the generation of favourable distinct convection currents for particle separation. However, in the majority of the vertically vibrated particle beds with inverted tilting, the formation of localised convection currents and local particle concentrates, as shown in Figure 5.18, were observed to form and proceed in a normal fashion. The onset of inverted particle bed tilting was visually observed to be more pronounced in the particle bed heights above 40 mm. Nevertheless, at high levels of vertical vibration frequency (>35 Hz) the generation of mixed convection currents and an inverted tilt formation resulted in the final collection of a poorly separated material in almost all the investigated cases in separation cells C-1 and 2.

Low values of vertical vibration frequency ($<25\pm 10\%$) resulted in slow convective motions of the vertically vibrated particles. The slow convective particle motions resulted in slow recovery of the

desired bronze particles in the low particle bed height (20 and 40 mm) working mixtures. In the majority of the cases that involved high particle bed height working mixtures (>40 mm), the magnitude of vertical vibration frequency <25 Hz was observed to be insufficient in starting and sustaining any distinct particle convection motions/currents. It was visually observed that a vertical vibration frequency value of $\sim 30 \pm 10\%$ Hz with a corresponding dimensionless acceleration value of $3 \pm 10\%$ at an inlet vibrator air pressure of $2.5 \pm 10\%$ bar were optimum in separating the desired bronze particles at 20 and 40 mm particle bed heights. The particle separation dynamics were mostly observed to be parallel in the 20 and 40 mm width separation cells C-1 and 2 with the partition separation gap sizes of 5 and 10 mm in the working chambers. In the high particle bed height (>40 mm) working mixtures, poor particle separation was visually recorded in all the investigated cases. These observations were later confirmed by the standard sink and float analysis technique described in Section 3.3.3.2 of Chapter 3 and will be discussed in detail in the subsequent sections. The visually observed particle separation behaviours investigated in this work are summarised in Table 5.5.

Particle bed height, mm	Vertical vibration frequency, Hz $\pm 10\%$							
	25	30	35	40	25	30	35	40
	Dimensionless acceleration, $\pm 10\%$				Dimensionless acceleration, $\pm 10\%$			
	2	2.5	3.0	4.0	2	2.5	3.0	4.0
	Visually observed separation in C-1 with working mixtures A, B and C.				Visually observed separation in C-2 with working particle mixtures A, B and C.			
20	X*	X	$\sqrt{}$ *	X	X	X	$\sqrt{}$	X
40	X	X	$\sqrt{}$	X	X	X	$\sqrt{}$	X
60	X	X	X	X	X	X	X	X
80	X	X	X	X	X	X	X	X
100	X	X	X	X	X	X	X	X

Table 5.5: Particle separation behaviour at different frequency and dimensionless acceleration values in the separation cells C-1 and 2. (N.B: * X represent poor and $\sqrt{}$ represent good particle separation).

The visually observed particle separation behaviours summarised in Table 5.5 show only a narrow range of vertical vibration frequency and dimensionless acceleration conditions where an appreciable bronze separation was observed in an average particle separation time of 20 minutes.

5.3.1.2 The effect of partition gap size on particle separation

If the controlled partition gap size is removed from the main working chambers of the 20 and 40 mm width separation cells the visual observations have shown that an unhindered and mixed particle flow will creep to the exits of the separation cells. This situation was observed to result in diminishing tilt formation which is normally thought to be sustained by the side walls of the main rectangular shaped working chamber. In the absence of any flow restrictions from the main working chamber a somewhat even distribution of the particle bed was seen in the whole separation cell assembly. This situation also resulted in generating a number of small heaps with local and uncontrolled convection currents. Overall, in all the investigated cases reported here (Table 5.3) the absence of any controlled partition gap size in the main working chambers resulted in collection of the un-separated particles from the final exits of the separation cells.

Although no particle separation was observed in the un-partitioned working chambers, the exercise highlighted the importance of maintaining an effective partition gap size to impart particle separation at a scaled up level. The importance of maintaining an effective partition gap size is also stressed by Mohabuth, (2007). In this investigation the visual observations have shown that a partition gap size below 5 mm resulted in hindering the flow of separated

bronze particles from the main working chambers. On the other hand the use of a partition gap size above 10 mm failed to regulate the controlled flow of the separated bronze particles and a mixed flow of glass and bronze particles was observed to emerge from the main working chambers in all cases. To-date the role of a partition gap size in controlling the flow of separated particles is not completely understood. Nevertheless, the visual observations made in this work and based on the findings reported by Mohabuth (2007), two partition gap sizes of 5 and 10 mm were selected for further investigation at a scaled up level. Visual observations at this stage have shown that, in case of a glass and bronze particle mixture the particle separation tendencies were nearly the same in the main working chambers of C-1 and 2 with distinct partition gap sizes of 5 and 10 mm. However, the same visual observations revealed that the particle bed heights/particle loadings in the main working chambers of separation cells had an obvious influence on the particle separation tendencies. This observation is also evident from Table 5.5 where poor particle separations in all cases were recorded at high (>40 mm) particle bed heights.

5.3.1.3 The effect of varying particle bed height on vertical vibration induced particle separation

As discussed earlier, in Section 5.3.1.2, the onset of global convection currents to impart an effective particle separation in a glass and bronze particle mixture was observed to be strongly dependent on the particle loadings in the main working chambers of the 20 and 40 mm width separation cells C-1 and 2. Detailed photographic descriptions of particle separation behaviours with varying particle bed heights in the main working chamber of a 20 mm width separation cell are presented, as example, in Figures 2, 3, 4, 5 and 6 of Appendix-A. The subsequent investigations presented

were all carried out with the previously identified optimum vertical vibration frequency and dimensionless acceleration magnitudes of $30 \pm 10\%$ Hz and $3 \pm 10\%$ respectively. After the initial visual assessment the separated particles were finally analysed by using the sink and float technique, described in 3.3.3.2 of Chapter 3. The quantitative assessment of particle separation efficiency reported in this work was based on the expression (Equation 5.5) proposed by Vesilind and Rimer, (1981);

$$E(x, y) = \left(\frac{x_1}{x_o} - \frac{y_1}{y_o} \right) 100 = \left(\frac{x_2}{x_o} - \frac{y_2}{y_o} \right) 100 = \left(\frac{x_1}{x_o} \right) \left(\frac{y_2}{y_o} \right) 100 \quad \text{Equation 5.5}$$

where the variables x and y represent the individual component concentrations at the corresponding separator inlet and outlet as shown in Figure A.1, of Appendix-A. In addition to reporting the particle separation efficiencies, the particle separation grades and recoveries were also calculated based on Equation 5.1 and Equation 5.2. The calculated grades and recoveries of the desired bronze particles are shown in Figures A.10, A.11, A.12, A.13, A.14 and A.15 of Appendix-A. The particle separation efficiencies calculated by using Equation 5.3 were plotted against the average particle bed heights and are shown in Figure 5.19 and Figure 5.20.

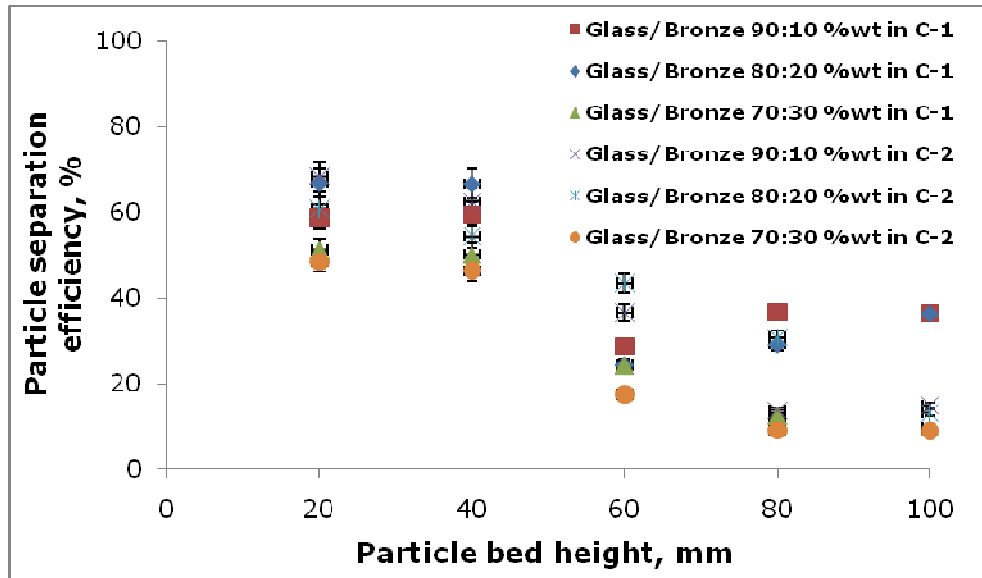


Figure 5.19: Bronze separation efficiency vs particle bed height in separation cells C-1 and C-2. A partition gap size of 5 mm and the vertical vibration frequency and dimensionless acceleration magnitudes of $30 \pm 10\%$ Hz and $3 \pm 10\%$ were used in this investigation.

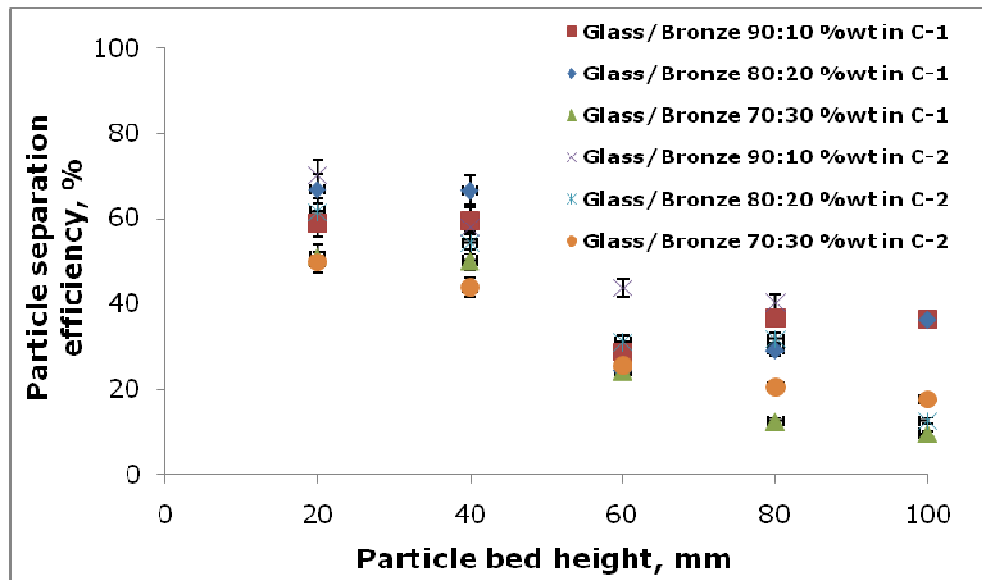


Figure 5.20: Bronze separation efficiency vs particle bed height in separation cells C-1 and C-2. A partition gap size of 10 mm and the vertical vibration frequency and dimensionless acceleration magnitudes of $30 \pm 10\%$ Hz and $3 \pm 10\%$ were used in this investigation.

Figure 5.19 and Figure 5.20 represent some interesting particle separation behaviours in the working chambers of 20 and 40 mm width separation cells. The detailed description of the particle separation behaviours, as evident from the Figure 5.19 and Figure 5.20, are presented in the subsequent sections.

5.3.1.3.1 Separation at 20 and 40 mm bed heights

When the glass and bronze particle mixture (Table 5.4) was vertically vibrated at low particle bed heights (20 and 40 mm), interesting particle motions were observed. The distinct particle motions in the main working chambers of C-1 and 2 were considered to be the prime drivers for the onset of distinct convection current in each of the two glass and bronze particle phases. The applied optimum vertical vibration frequency and dimensionless acceleration magnitudes of $30 \pm 10\%$ Hz, and $3 \pm 10\%$ resulted in a stabilised tilt formation within the first 30 seconds in almost all the investigated cases. The observed tilt formation as shown in Figures A.2 and A.3 of Appendix-A was in an exact opposite direction to the sliding partition gate of the working chambers. The time averaged change of the particle bed behaviours in a 20 mm width separation cell was digitally photographed and is shown as an example in Figures A.2 and A.3 of Appendix-A. The visually observed convective particle motions in the tilted particle beds of C-1 and C-2 are mapped out in Figure A.7, of Appendix-A.

As discussed, the distinct particle motions in the vertically vibrated bed resulted in high density particles to concentrate and a give collective convective response. The high density particles were observed to start a clockwise global convection current in the outer periphery of the tilted particle bed. The bronze particle concentration and the onset of their distinct global convection current was observed in the first few seconds of the vertical

vibration treatment. The bronze rich convection current was predominantly observed to move in the outer periphery of the main working chamber and formed a distinct boundary layer of only a few particle diameters thick with predominantly glass rich regions. The inner regions of the tilted particle bed were predominantly occupied by the glass particles that also moved in a distinct global convection current. The onset of a distinct global convection current in each of the two particle phases was observed to help in grouping/concentrating of the similar particles while maintaining a clear separation boundary between the two distinct particle phases.

The visual observance of distinct global convection currents also revealed differences in the accelerations of the glass and bronze particles. This observation was later confirmed by tracking the identical solo particles by using the positron emission particle tracking technique, presented in Chapter 6. The differences in particle accelerations observed here can be attributed to the individual momentums of the glass and bronze particles in the presence of a surrounding fluid. The influence of surrounding fluid/media on particle dynamics and segregation is also identified in the work of Leaper *et al.*, (2005), Burtally *et al.*, (2002), Akiyama *et al.*, (1998), Gutiérrez *et al.*, (2005) and Klein *et al.*, (2006). In the investigations reported here the clock-wise convective particle motions were thought to be sustained by the distinct surrounding air currents, which was later confirmed by the smoke blanket visualizations and are shown in Figure A.7 of Appendix-A. The horizontal component of the surrounding air near to the partition gap was considered to move beneath the vertically vibrated particle bed as a result of a pressure differential that developed during the particle bed flights. The proposed air movements in this fashion (Figure A.7 of Appendix-A) also acted as a filter to stop the low momentum glass particles moving out of the main working chamber. In contrast the high momentum bronze particles sliding at high speeds from the top of the tilted particle bed were

considered to overcome this surrounding air barrier (currents) and were observed to steadily move out of the main working chamber and reach the exit for their final collection.

The particle acceleration magnitude was also observed to differ with particle locations in the main tilted particle bed. Bronze particles rising from the base of the tilted particle bed were observed to have a comparatively lower acceleration magnitude in comparison to their sliding down hill counterparts from the top of the tilted particle bed surface. The differences in acceleration magnitudes of the vibrating particles can be attributed to the frictional resistances the particles experience at different locations in the tilted particle bed. The low particle bed height of 20 mm resulted in the formation of a very thin particle layer in close proximity of the partition separation gap. The formation of a thin particle layer offered lower friction and collision resistance to the separating bronze particles that were steadily moving downhill with the aid of a distinct global convection current. The bronze particles coming downhill had higher momentum and thus greater probability of moving out of the main working chamber by passing through the partition gap size. When the particle bed height was increased to a level of 40 mm the particle layer thickness, in close proximity to the partition gap was also observed to increase. However, the particle thickness in the lower end of the tilted particle bed was still allowing the separating bronze particles to move out of the main working chamber and reach the final exit for their collection.

The finally separated particles from the main chambers of the separation cells C-1 and 2 were analysed by using a sink and float technique to reveal the particle separation efficiency, using Equation 5.5. Figure 5.19 and Figure 5.20 shows that the particle separation efficiencies were maximum at low particle bed heights of 20 and 40 mm in separation cells C-1 and 2. Nevertheless, in low bronze concentration particle mixtures (10%wt and 20%wt) no significant

bronze contamination was visually observed in the glass rich regions. However, in the high bronze concentration mixtures (30%wt) some bronze particles were observed to penetrate into the glass rich regions.

The analysis of separation grade and recovery results presented (Figures A.10, A.11, A.12, A.13, A.14 and A.15 of Appendix-A) revealed that the bronze purity/grade of >90% can be achieved in the separation cells C-1 and 2. The recoveries of bronze particles were >50% at particle bed heights of 20 and 40 mm in all the investigated cases reported in this work.

5.3.1.3.2 Separation at 60 mm bed height

An increase in particle bed height to 60 mm resulted in the formation of a thick particle layer at the lower end of the tilted particle bed. The formation of this thick particle layer in close proximity to the partition separation gap resulted in an enhanced resistance to the downhill moving bronze particles. The downhill bronze particle motion resulted in increased inter-particle collisions and collisions with the partition gate. The presence of a thick particle layer in close proximity to the partition gap was observed to hinder the surrounding air currents that were considered to play a vital role in generating, and sustaining, the distinct convection currents for particle separation. At high particle bed height the formation of an effective tilt was also suffered. The absence of an effective tilt resulted in a decrease in the momentum of the downhill travelling particles. The entire particle separation situation at 60 mm bed height is highlighted in Figures A.4 and A.8 of Appendix-A. Overall, the excessive resistance to the separating bronze particles affected their recovery from the exits of the separation cells C-1 and 2. Hence, a decrease in the separation efficiency was recorded at a particle bed height of 60 mm, as shown in Figure 5.19 and Figure

5.20. The results also showed a substantial decrease in the recovery and grade of the separated bronze particles, evident from Figures A.10, A.11, A.12, A.13, A.14, and A.15 of Appendix-A.

5.3.1.3.3 Separation at 80 and 100 mm bed heights

At particle bed heights of 80 and 100 mm, the onset of distinct global convection currents in each of the two glass and bronze rich particle phases was observed to diminish. However, mixed and multiple convection current as shown in Figures A.5, A.6 and A.9, of Appendix-A, were observed at these particle bed heights. The effective particle bed tilting was never observed at these particle bed heights. This entire situation resulted in seizure of any particle separation and mixed glass and bronze particles were observed to emerge from the working chambers of the separation cells C-1 and 2 which were finally collected at the exits. Hence, low grades and recoveries of the separating bronze particles were recorded and are shown in Figures A.10, A.11, A.12, A.13, A.14 and A.15 of Appendix-A. Separation efficiencies below 40% were recorded at these particle bed heights (80 and 100 mm) as shown in Figure 5.19 and Figure 5.20. The particle separation efficiencies were especially low in the high bronze concentration working particle mixtures which can be attributed to the high particle loading/weight and excessive inter-particle collisions among the high density particles in these mixtures.

5.3.2 Separation of the shredded glass and bronze particle mixtures

Since the majority of particle mixtures used in the process industries are of irregular and complex shapes, a particle separation

investigation was performed with the irregular shaped shredded glass and bronze particle mixtures. The shredded glass and bronze particle mixtures were vertically vibrated in separation cells C-1 and 2 with a sole partition gap size of ~ 5 mm in the working chambers. The compositions of the synthetic shredded glass and bronze particle mixtures used in this investigation are given in Table 5.6.

Material	Mixture			A	B	C	“ S_d ”-value (Eq.2.7)
	Bead Dia. (μm)	Mass mean Dia. (μm)	Density $\rho(\text{kg.m}^{-3})$	% wt	% wt	% wt	
Glass	38-600	537	2500	90	80	70	5.84
Bronze	38-850	424	8900	10	20	30	

Table 5.6: Synthetic shredded glass and bronze particle mixtures used in the detailed vertical vibration induced particle separation assessment.

The particle size characterisation of the mixture in which the glass and bronze particles had an average mass mean diameters of $537\mu\text{m}$ and $424\mu\text{m}$ respectively is given in Figure 5.21.

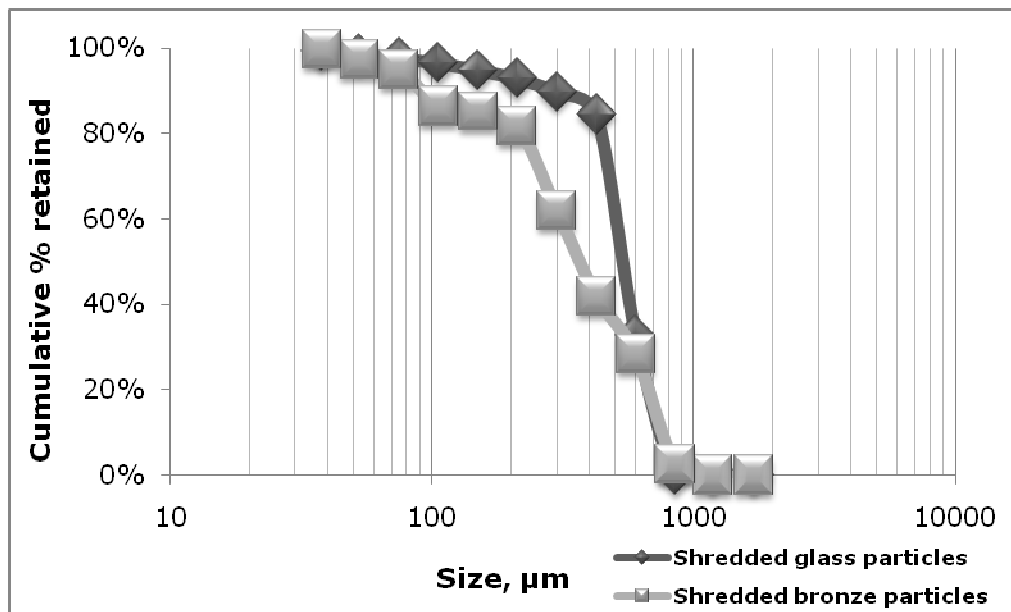


Figure 5.21: The size characterisation of the shredded glass and bronze particles.

The Scanning Electron Microscope (SEM) image highlights some irregular shape features of the shredded glass and bronze particles and is shown in Figure 5.22.

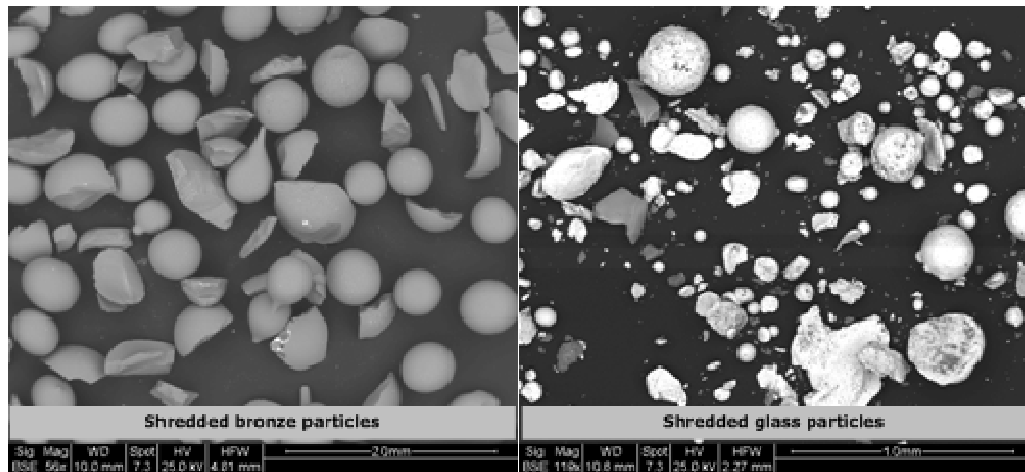


Figure 5.22: Scanning Electron Microscope (SEM) images of the shredded glass and bronze particles.

The investigations reported here were identical to the ones presented in Section 5.3.1 except that they were only carried with a sole partition gap size of ~ 5 mm in the working chambers of separation cells C-1and2. The particle separation efficiency of the working particle mixtures used in this investigation is shown in Figure 5.23.

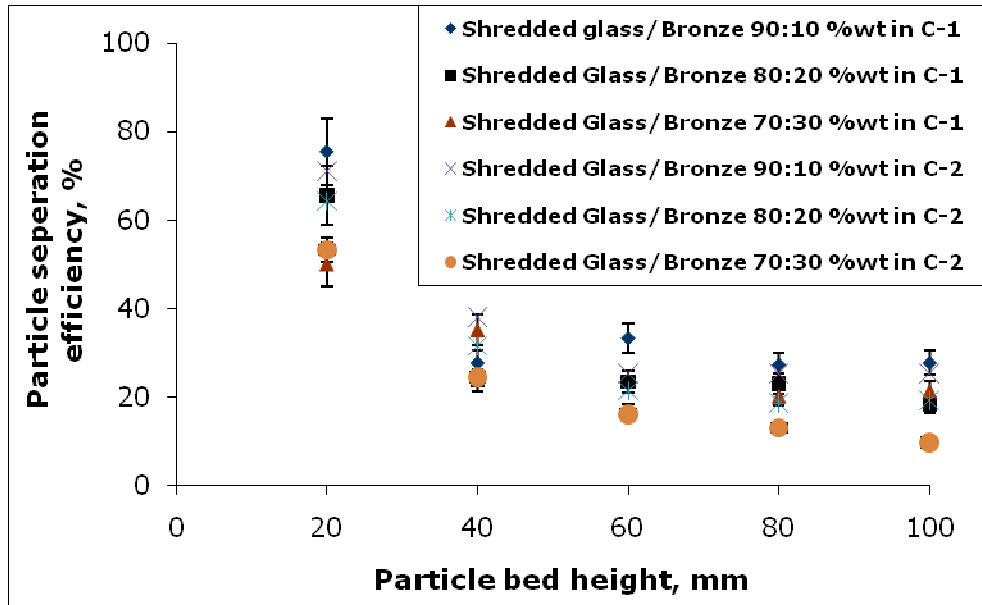


Figure 5.23: Bronze separation efficiency vs particle bed height in separation cells C-1 and C-2. A partition gap size of ~ 5 mm and the vertical vibration frequency and dimensionless acceleration magnitudes of $30 \pm 10\%$ Hz and $3 \pm 10\%$ were used in this investigation.

Visual observations and the bronze particle separation efficiency results, shown in Figure 5.23, revealed some interesting particle separation behaviours. In this case the high particle separation efficiency was only observed at a particle bed height of 20 mm. The particle separation efficiency was observed to fall substantially as the particle bed height was increased to 40 mm and above. This fall in particle separation efficiency at high particle bed heights (40 mm and above) can be attributed to the enhanced inter-particle collisions, friction between particles, and the side wall frictional effects in the irregular shaped working particle mixtures. The vertical vibration of these irregular shaped particles was thought to generate excessive inter-particle frictions which led to the recovery of very low grade bronze particles at high particle bed heights as shown in Figures A.16, A.17 and A.18, of Appendix-A. The investigations reported here were valuable in demonstrating that the

same material particles with different shapes can behave quite differently in vertical vibration induced particle separation systems.

5.3.3 Separation of the sand and bronze particle mixtures

Compositions of the sand and bronze particle mixtures used in this investigation are given in Table 5.7.

Mixture				A	B	C	“ S_d ”- value (Eq.2.7)
Material	Bead Dia. (μm)	Mass mean Dia. (μm)	Density* $\rho(\text{kg.m}^{-3})$	% wt	% wt	% wt	
Sand	38-300	155	1780	90	80	70	5.2
Bronze	38-300	158	8900	10	20	30	

Table 5.7: Synthetic sand and bronze particle mixtures used in the detailed vertical vibration induced particle separation assessment. (*N.B. the density of particles used in this work was measured by Helium Pycnometer (Section 3.3.3.3)).

The sand and bronze particle mixtures used in this investigation had a large density differential ($\frac{\rho_{\text{bronze}}}{\rho_{\text{sand}}} = \frac{8900\text{kg.m}^{-3}}{1780\text{kg.m}^{-3}} = 5.0$). The complete size characterisation of the particle mixture is given in Figure 5.24.

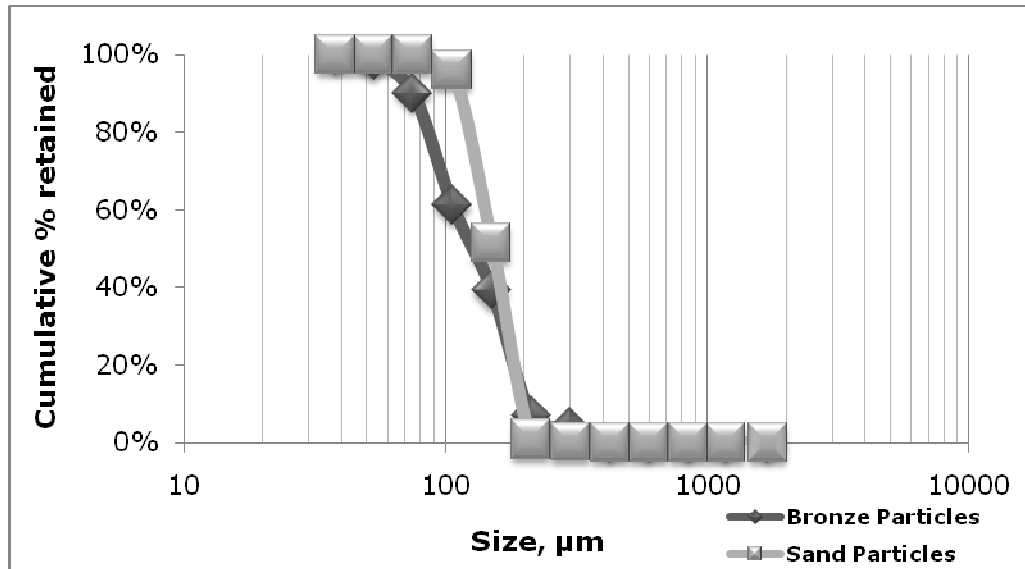


Figure 5.24: The size characterisation of the white beach sand and bronze particles.

The SEM image of the working particle mixture representing some of the irregular shape features of sand and regular shape features of the bronze particles is shown in Figure 5.25.

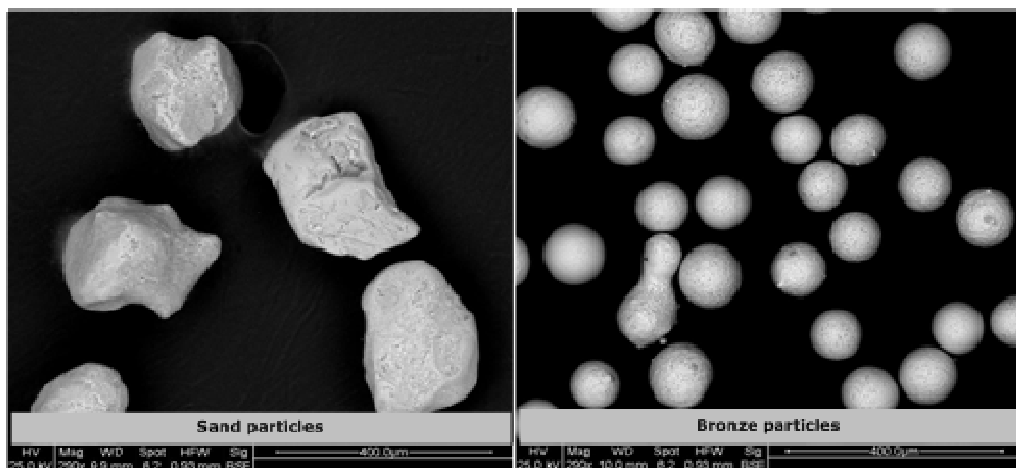


Figure 5.25: SEM image of the working sand and bronze particles.

The working mechanism behind the vertical vibration induced separation of this (Table 5.7) working particle mixture was fairly simple. In this case the start of a vertical vibration separation treatment was marked by the generation of distinct convection

currents and with an immediate tilting of the particle bed. The particle separation behaviour observed in this case was similar to the one described in Section 5.3.1, a high grade bronze product was recovered within 20 minutes of continuous vertical vibration treatment. The particle separation efficiency of the bronze particles is shown in Figure 5.26.

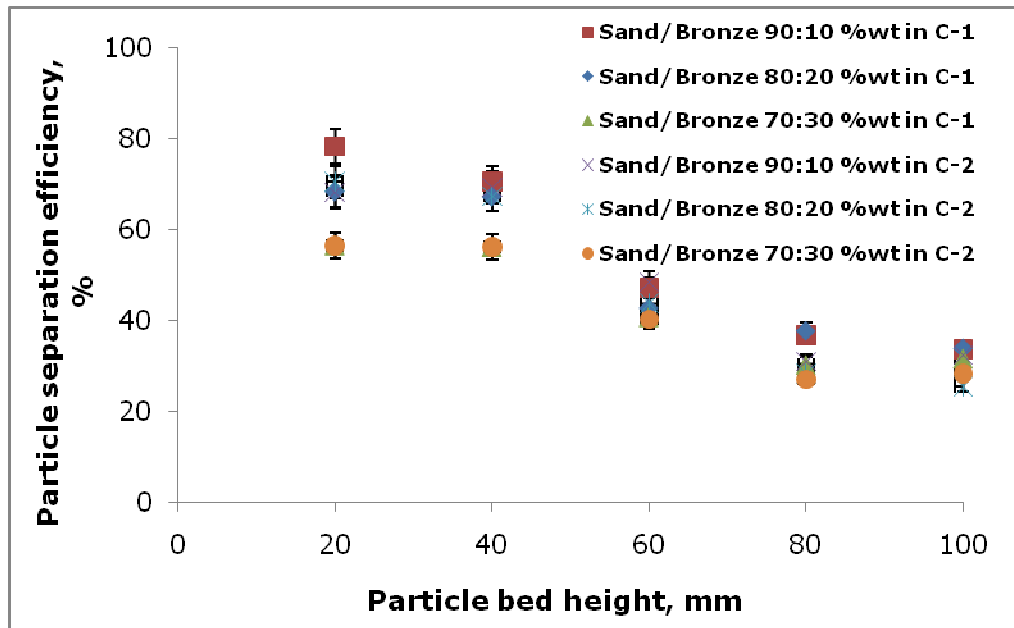


Figure 5.26: Bronze separation efficiency vs particle bed height in separation cells C-1 and C-2. A partition gap size of 5 mm and the vertical vibration frequency and dimensionless acceleration magnitudes of $30\pm 10\%$ Hz and $3\pm 10\%$ were used in this investigation.

The particle separation efficiencies, reported in Figure 5.26, revealed excellent separation of the bronze particles in the low particle bed height working mixtures. This investigation has shown that a substantial amount of separation can still be achieved at a particle bed height of 60 mm in separation cell C-1 and 2. This may be due, largely, to the use of a high density differential particle mixture in this case. Nevertheless, at high particle bed heights of 80 and 100 mm poor particle separation efficiencies, as shown in Figure 5.26, were readily observed as the formation of particle bed tilting and the

onset of a global convection current, in each of the two distinct particle phases, was mostly observed to seize.

5.3.4 Interstitial fluid visualisation via smoke blanket motions

The patterns of the surrounding medium, such as air, are central to many dry based particle separation processes such as air classification (Hirajima, *et al.*, 2010). However, since these patterns are normally invisible, it is difficult to predict how the surrounding medium is behaving and the possibility of an error in the predictions is significant (Settles, 1997). In the majority of vertical vibration induced particle segregation studies no attempt is made to visualise the dynamic surrounding medium behaviours and only some conceptual sketches are drawn of how it is thought to behave. This is partly due to the traditional difficulty of clearly visualizing air currents and, unfortunately, many of the surrounding airflow phenomena cannot be seen in photographs. Most traditional air flow visualization methods involve seeding the air with tracer particles, smoke, fog, and neutrally-buoyant soap bubbles have been used for this purpose.

The role of a surrounding fluid in controlling the vertical vibration induced particle segregation is stressed in the work of Leaper *et al.*, (2005), Burtally *et al.*, (2002), Akiyama *et al.*, (1998), Gutiérrez *et al.*, (2005) and Klein *et al.*, (2006). However, air flow visualizations were not performed in their work and majority of the surrounding fluid behaviours were sketched based on the behaviour of a vertically vibrated bed in the presence of air, water and in vacuum. In an effort to visualize the surrounding air behaviours during the vertical vibration separation of a finely sized glass and bronze

particle mixture at a scaled up level, a smoke blanket visualization technique was used in this work.

The smoke/aerosol generator used in this work was supplied by the S and M Electronics Limited, UK, and it used a mixture of pure cosmetic grade Shell Ondina oil EL and carbon dioxide, as an inert gas, to generate smoke particles of $\sim 3\mu\text{m}$ which were harmless, non-irritant, non-flammable and left no contamination on surfaces with which it came in contact under normal calibrated operation. The smoke/aerosol released from the generator diffused in air with little tendency to either rise or fall in the stagnant surrounding air. Hence, the smoke/aerosol released in an enclosed environment such as on the top surface of a stationary particle bed in the working chambers of the T-type particle separation cells (C-1 and 2) was observed to remain there for several hours. However, when the separation cell assembly, comprising the particle mixture and the stagnant smoke particles, was vertically vibrated the smoke particles were observed to move in distinct motions along with the surrounding air currents. The distinct movements of smoke particles along with surrounding air currents were used as a basis to determine the surrounding airflows during the vertical vibration separation of the working particle mixtures. A simplified design assembly of the smoke/aerosol generator is shown in Figure 5.27.

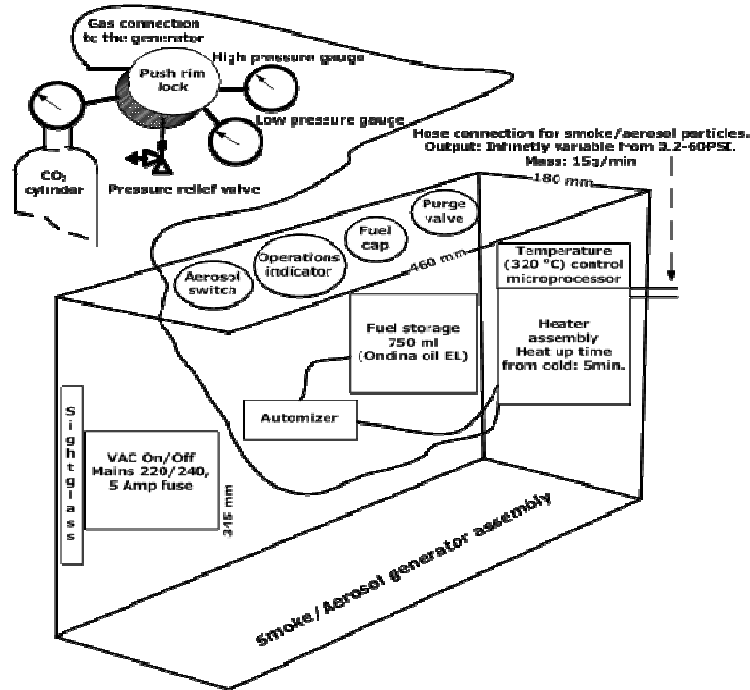


Figure 5.27: A simplified design assembly of the smoke/aerosol generator.

The smoke/aerosol generator shown in Figure 5.27 basically comprised a fuel compartment to house the Shell Ondina oil EL and its delivery system to the main heater. The Shell Ondina oil EL and the carbon dioxide gas were heated to a temperature of $\sim 320^{\circ}\text{C}$ to get a variable output supply of smoke/aerosol from the main hose (Figure 5.27). The complete experimental setup for the smoke blanket visualization investigations is shown in Figure 5.28

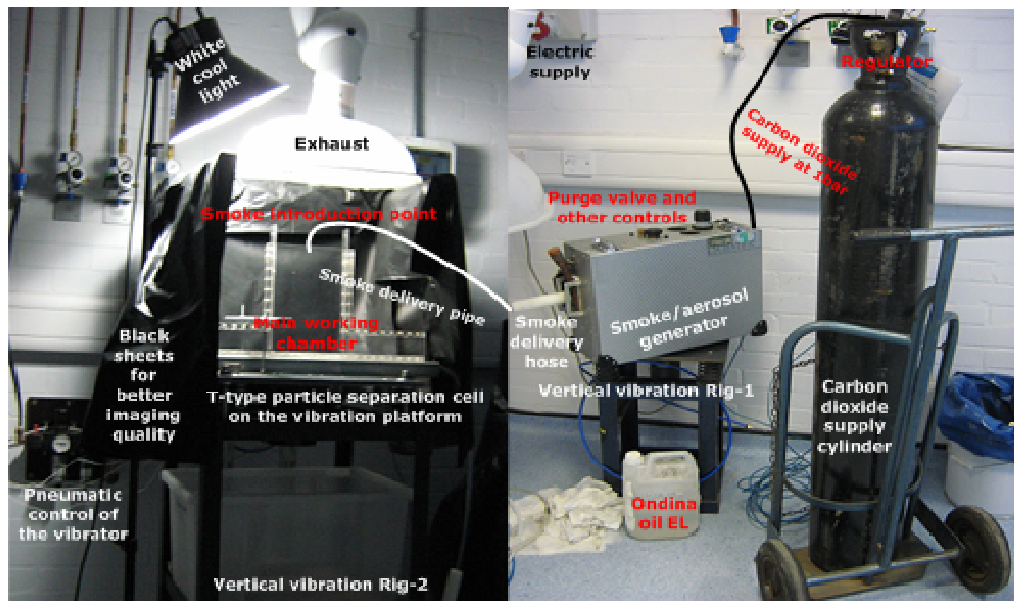


Figure 5.28: Experimental setup for the smoke blanket visualization investigations.

The smoke/aerosol produced from the generator filled the main working chambers of the separation cells C-1 and 2 with the help of a 5 mm diameter flexible plastic pipe connected to the main hose as shown in Figure 5.28. The smoke temperature in the main working chamber was $\sim 19^{\circ}\text{C}$ which was measured by using a thermometer. The position of an exhaust above the separation cell assembly was positioned so that it did not disturb the stagnant smoke blanket in the main working chamber.

Before visualizing any smoke blanket movements with a particle mixture in the main working chamber of the separation cell assembly some baseline investigations were made without the presence of any particle mixture. It is worthwhile noting that the investigations carried in separation cells C-1 and 2 with the partition gap sizes of 5 and 10 mm were nearly the same. Here, the investigations carried in separation cell C-1 are reported as a representative example of C-2. For baseline investigations the main working chamber of the separation cell C-1 was completely filled-in

with smoke particles. The baseline investigations were carried out in the main working chamber of C-1 with closed partition gap sizes and a sole partition gap size of 5 mm in one direction. The vertical vibration treatment was carried out at the, previously identified, optimum frequency and dimensionless acceleration magnitudes of $30 \pm 10\%$ Hz and $3 \pm 10\%$ respectively. The visually observed smoke blanket movements in the working chamber without a partition gap size and with a sole partition gap size of 5 mm is shown in Figure 5.29.

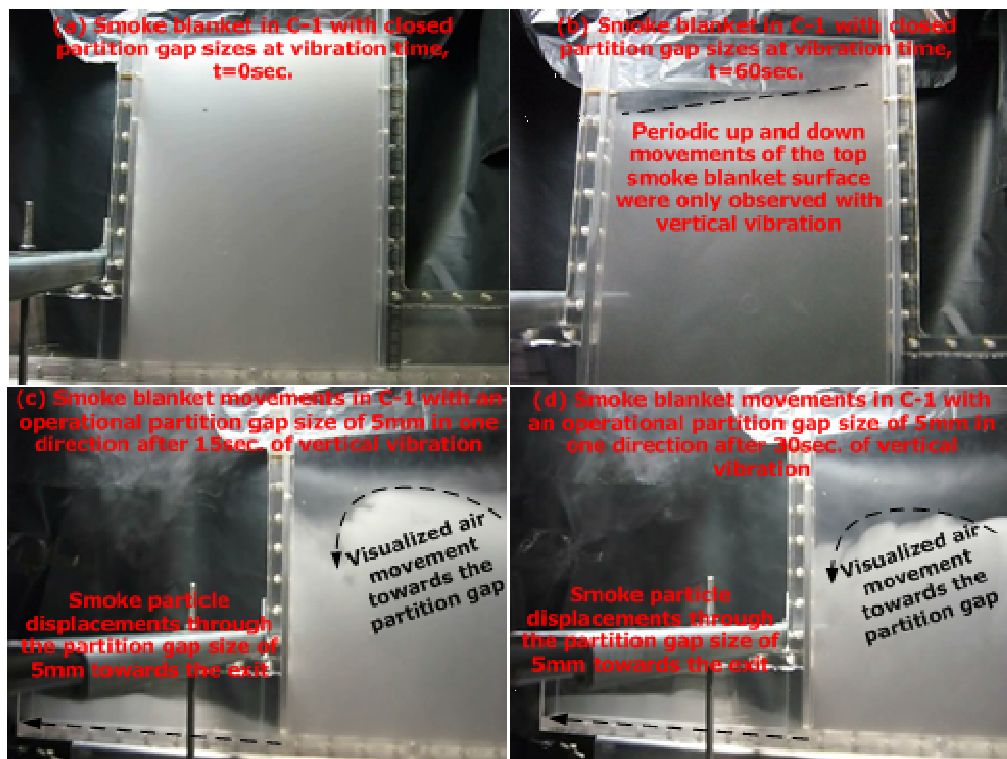


Figure 5.29: Visualized smoke blanket movements in the main working chamber of C-1 with closed partition gap sizes (a and b) and with a partition gap size of 5 mm in one direction (c and d). The recorded observations are presented as Smoke-Video-D15 in the provided Compact Disk (CD), No.15 in Appendix-D.

In Figure 5.29, (a) shows a working chamber without any partition gap that was completely filled with the smoke particles. The vertical vibration of this main working chamber did not show any distinct

displacements of the smoke particles. These observations were recorded and are included in this thesis as Smoke-Video-D15 in the provided Compact Disk (CD) (No.15 Appendix-D). Nevertheless, the vertical vibration induced periodic up and down displacements of the top smoke blanket surface was visually observed, as shown in Figure 5.29(b) and Smoke-Video-D15 (No.15 in Appendix-D) however, the rest of smoke blanket in the main working chamber largely remained stagnant. However, the smoke blanket in the main working chamber was observed to dilate and become less thick with the passage of time as smoke particles continued to escape from the open top end of the working chamber (Figure 5.29c). The situation completely changed when the same smoke blanket was visualized in a working chamber with a partition gap size opening in one direction. Soon after the start of vertical vibration treatment the smoke blanket moved in distinct clockwise convection currents as shown in Figure 5.29 (c and d). It is interesting to note that the smoke particles moved towards the partition gap size opening and from there they moved into the next separate chamber towards the exit. Once the smoke particles were out from the exit they were observed to rise freely towards the exhaust opening. However, the smoke particles were not observed to move out from the top open end of the main working chamber. These distinct smoke blanket displacements can be attributed the distinct air circulation currents in the main working chamber that were powered by the vertical vibration treatment. In summary, the baseline investigations reported here have shown that the clockwise distinct air circulation currents compelling the smoke particles through the partition gap size opening can be attributed to the special geometrical effects of the separation cell design with a small partition gap size opening in one direction. These distinct smoke particle movements were thought to be in the direction of the least external resistance under the influence of a dynamic environment. The above smoke

circulations currents were next tested in the presence of a working particle mixture.

The composition and size characterisation of the particle mixture used in this work is given in Table 5.1 and Figure 5.3 respectively. The mixture filled the main working chambers of the separation cell C-1 and 2 to form the average particle bed heights of 20 and 40 mm. Once a desired particle bed height was achieved the space above the stationary particle bed was filled with the smoke particles to form a blanket. Next, the vertical vibration treatment of the working particle mixture was carried at the, previously identified, optimum frequency and dimensionless acceleration magnitudes of $30 \pm 10\%$ Hz and $3 \pm 10\%$ respectively. Due to the similar nature of the outputs from the investigations carried in separation cells C-1 and C-2 with the partition gap sizes of 5 mm and 10 mm, the dynamic smoke blanket visualisations in separation cell C-1 with a partition gap size of 5 mm in one direction were chosen as a representative example for the rest of the studies. Nevertheless, the time averaged visualized smoke blanket displacements in the main working chamber of C-1, with a partition gap size of 5 mm in one direction, are shown in Figure 5.30.

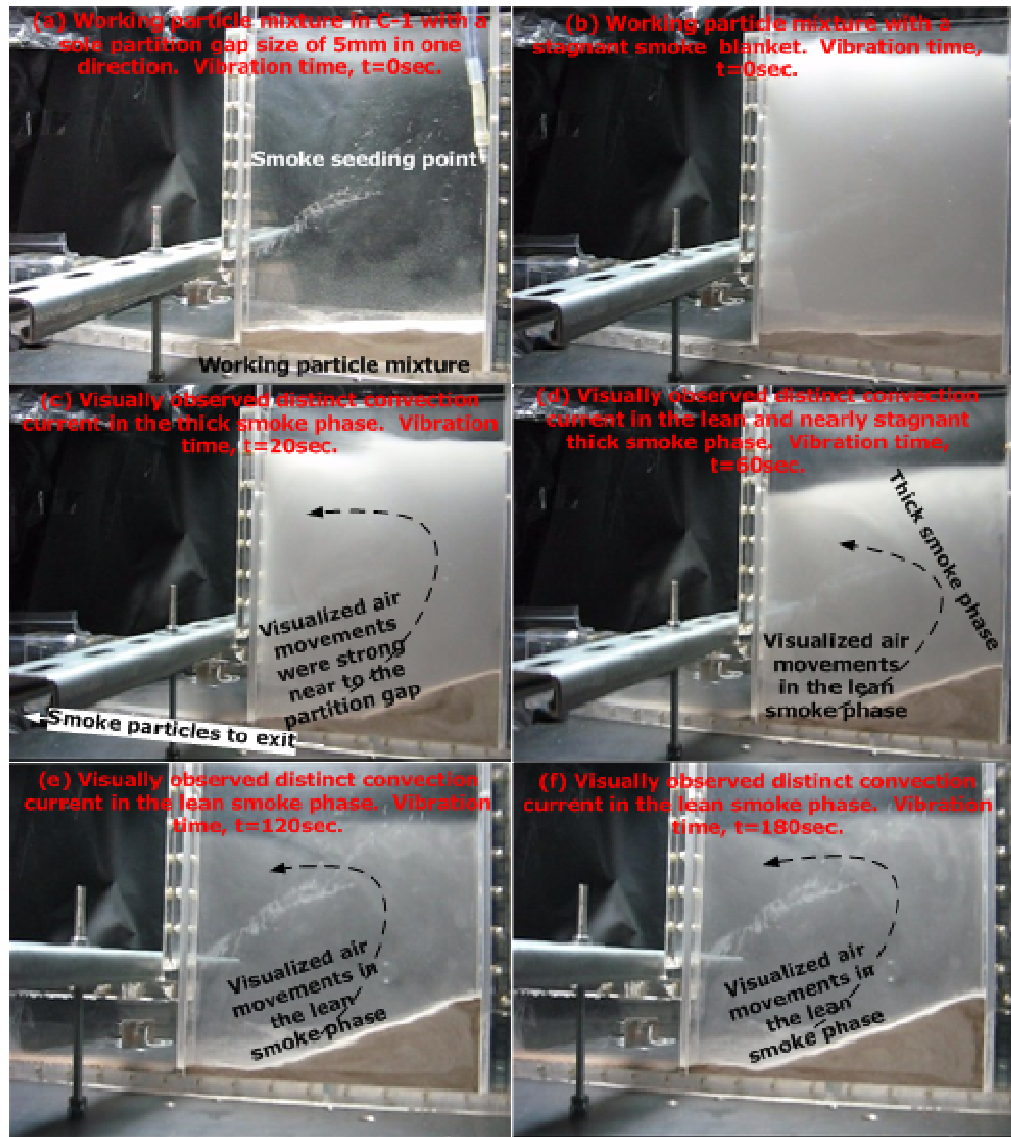


Figure 5.30: Visualized smoke blanket displacements in the main working chamber of C-1 with a partition gap size of 5 mm in one direction. The recorded observations are presented as Smoke-Video-D13 and D14 in the provided CD, No.13 and 14 in Appendix-D

In Figure 5.30, (a) shows the initially well mixed working particle mixture in the main working chamber of C-1 that formed an average static particle bed height of 20 mm. The space above the working particle mixture was filled with the smoke blanket, as shown in Figure 5.30(b). Next, the vertical vibration was started and the distinct convection currents were observed in the thick smoke phase (Figure 5.30c). The convection current near to the partition gap size

was observed to be more dynamic and this resulted in dilation of the area near to the partition gap size where the smoke particles continued to move out into the next separate chamber via a partition gap size of 5 mm. All this resulted in the generation of a lean and thick smoke phase in the main working chamber (Figure 5.30d). The dynamic displacements of the smoke particles were then sustained in this fashion that gradually resulted in diminishing the thick smoke phase as more smoke particles moved out of the main working chamber (Figure 5.30 e and f). These observations were recorded and are included in this thesis as Smoke-Video-D13 and Smoke-Video-D14 in the provided Compact Disk (CD) (No.13 and 14 in Appendix-D). In summary, the smoke blanket visualizations presented here confirmed the trajectories of the, previously proposed and sketched, surrounding air currents which are discussed in Section 5.3, and presented in Figures A.7, A.8 and A.9 of Appendix-A.

5.4 Concluding remarks

In an effort to design and assess a new type of vertical vibration induced particle separator, we have observed a glimpse of associated challenges with the particulate materials. The results presented in this chapter can be used to deduce the following;

- ❖ Both regular and irregular, shaped particle mixtures were separated by using this novel technique. Separation grades as high as >90% were achieved for some cases in this separator.
- ❖ In this work, increased particle loading above a certain level for majority of the cases showed an adverse effect on particle separation efficiency.

Tracking particle dynamics in the vibration separator

6.1 Introduction

Dry based separation of finely sized particles (Chapter 2) find increasingly new uses in emerging areas of particle processing such as solid waste processing. However, in many new and old applications the lack of basic inside knowledge regarding the specific particle behaviours has resulted in poor performances of these devices due to the unpredictable particle nature (Ottino and Khakar, 2000). This is considered to have seriously undermined many of their potential applications in different particle processing and handling unit operations.

The development of a simple particle flow theory which is normal in fluid mechanics still remains a challenging problem in the case of particulate materials (Yu, 2003; Götzendorfer, 2007; Goldhirsch, 2003; Ottino and Khakar, 2000). Currently, two particle flow

approaches are in common use; first the quantum approach which deals with particles at a macroscopic level, and a discreet approach which is mainly concerned with the particle behaviours at a microscopic level (Yu, 2003). A comprehensive understanding of quantum particle flows and discreet particle motions are important prerequisite for gaining insight into any particle separation system. This knowledge is not only of practical importance in any process design but also has scientific significance attached to it and thus can lead to the understanding of many unanswered particulate phenomena. In addition, this knowledge can also be used to help optimise a particle separation system against many different dynamic operating conditions.

Despite a large body of work (Wills, 1997; Perry and Green, 1999) on separating particulate materials, the underpinning simple design correlations are not yet fully developed. Hence, phenomenological assumptions are routinely made which have resulted in very limited and narrowly scoped applications of particle separation in practice. In the absence of any consensus based theoretical and mathematical models for separating particulate materials, many (Mohabuth, 2007) have used experience and heuristics derived from the experiments in designing any new particle separation system. In addition for scaling up an existing particle separator size length scales are simply not present (Wassgren *et al.*, 1996; Jaeger, 1997; Ottino and Khakhar, 2002). In the absence of any reliable design and assessment tools, a large body of currently available literature (Mohabuth, 2007; Burtally, 2004; Burtally *et al.*, 2002 and 2003) in this field is based on the observations made at the particle bed surfaces, or very near to them. Hence, much of the events inside an actual engineering structure are poorly understood. This is potentially hampered by the difficulty in employing non-invasive particle tracking techniques to a non-opaque and finely sized particle bed which is normally resident inside an engineering structure such as a particle separator.

As scientific knowledge has flourished with time so new ways of understanding peculiar particle behaviours have emerged. Tracking of real time particle motion can be used as an effective tool to better understand the working of a particulate separation system and this can assist in identifying any potential operational difficulties. In addition, particle tracking can also be used in optimising any new particle separator design developments and to evaluate computer modelling and simulation work. Nevertheless, the principle behind particle tracking is simple: a distinguishably seeded particle is introduced into the system and its location is tracked through time (Parker *et al.*, 1993; Parker and Fan, 2008; Parker *et al.*, 2009).

In this work, a three dimensional (3D) Positron Emission Particle Tracking (PEPT) technique which was initially developed at the University of Birmingham, UK, has been used to track a single particle's real time dynamics, occupancies and velocity field vectors inside the newly designed (Section 5.2) scaled up vibration driven particle separator. These investigations were carried out with a range of finely sized working particle mixtures and with varying particle bed conditions.

6.2 Particle tracking: A review

Particle tracking is a sophisticated problem and as a result many solutions have been produced for it. These solutions range from the versatile computational simulations to Particle Image Velocimetry (PIV), Particle Tracking Velocimetry (PTV) (Jesuthasan *et al.*, 2006), laser deflection particle tracking, X-ray tomography, magnetic resonance imaging, radioactive tracers, resin freeze, layering of different colour particles, high speed video particle tracking (Lueptow *et al.*, 2000) and a relatively new entrant 3D-PEPT (Parker *et al.*, 1993; Parker and Fan, 2008). The above mentioned

popular particle tracking techniques find the majority of their applications in a multiphase environment e.g., particles within different fluids. Each of the above mentioned techniques has certain drawbacks attached to their potential applications. Some of the most notable among them are cost, spatial resolution, temporal resolution, and invasiveness (Lueptow *et al.*, 2000). However, due to the limited scope of the work presented in this chapter, which mainly looked into a slowly deforming or quasi-static particle flow under vertical vibration, a complete review of the entire particle tracking techniques mentioned above is not presented. The subsequent discussions are therefore restricted to the tracking of particles in the parallel phase only.

Optical methods have long been used to study particle flows in-between two narrowly-spaced plates. Though PIV is normally employed to study dynamic fluid behaviours in a transparent multiphase environment, its use has also been demonstrated in investigating particle flows between two narrowly-spaced boundary plates. One such example is the use of PIV to investigate particle displacements and velocity fields in vertically vibrated particle flows (Lueptow *et al.*, 2000). Others (Jesuthasan *et al.*, 2006) have used it to track quasi-static and rapid particle flows. PIV is an optical tracking technique with certain limitations; it requires a mix of light and dark particles and stroboscopic illuminations. Even with all these arrangements; PIV application is restricted to tracking particle displacements next to a clear wall surface in only two dimensions (2D). Furthermore, maintaining a clear and transparent wall surface for PIV imaging is an important prerequisite for its successful application to any particle flow (Lueptow *et al.*, 2000; Jesuthasan *et al.*, 2006).

The technique of Positron Emission Particle Tracking (PEPT) has been under development at the University of Birmingham, UK, since 1990 (Parker *et al.*, 2009). The PEPT technique enables accurate

tracking of a single, or multiple, radioactive tracer particles moving at speeds up to 2000 mm.s^{-1} inside any piece of equipment that can fit in its scanner and/or camera geometry (Parker *et al.*, 2009). The PEPT camera geometry with dimensions is shown in Figure 3.9. The working and equipment description of PEPT has previously been discussed in Section 3.3.3.5. PEPT has remained a subject of great interest and many have reported on its full working details (Parker *et al.*, 1997; Parker and Fan, 2008; Fan *et al.*, 2006; Stellema *et al.*, 1998) and also on a new modular positron camera (Parker *et al.*, 2009).

PEPT can be considered as a distinct particle investigation tool, principally due to the non-invasive nature of its particle visualization and measurement that can be used for rapid diagnostics and development studies. The engineering use of PEPT in exploring the particle flow problems in fairly opaque engineering structures has been popular since its introduction (Hsiau *et al.*, 2008; Wildman *et al.*, 2000; Wildman and Parker, 2002). As a result, many investigations (Hsiau *et al.*, 2008; Wildman *et al.*, 2000; Wildman and Parker, 2002) tracking complex particle flows such as the ones driven by vertical vibration have been carried out by using this technique. Experimental investigations employing PEPT have been used to explore the existence of two different particle temperatures (i.e. specific fluctuation kinetic energy of the moving particles) in a binary vibro-fluidised particle bed (Wildman and Parker, 2002) and more exclusively in the vertically vibrated particle beds (Hsiau *et al.*, 2008; Wildman *et al.*, 2000). Different particle temperatures are believed to exist due to the distinct particle energy transportation and its subsequent dissipation in the binary vibro-fluidised particle beds (Wildman and Huntley, 2003).

The use of PEPT is not just limited to the study of particle temperatures in a vibrated particle bed, other particulate phenomena such as particle convection in a vibrated annular particle

assembly have also been explored (Wildman *et al.*, 2005). The study of particle dynamics in vertically vibrated particle beds by employing PEPT has also revealed the existence of a strong particle rotational movement in the horizontal plane (Wong *et al.*, 2001). The rotational particle motion was observed to increase with increasing the vibration amplitude and also resulted in enhanced particle dispersion. The enhanced particle dispersion in turn was observed to be stronger in the horizontal plane. Furthermore, the study of particle bed instabilities at a single particle scale by employing PEPT has also being carried out and these studies have suggested a close link between the particle displacements and the vertically oscillating platform (Wong *et al.*, 2006).

PEPT has also found applications in exploring particle flow regimes in other more complex engineering structures such as the horizontally positioned and slowly rotating opaque cylinder (Lim *et al.*, 2003). In addition, particle tracking in e.g., rotating drums (Parker *et al.*, 1997; Seville *et al.*, 2005), high solid fraction laden solid-liquid pipe flows (Fairhurst *et al.*, 2001), horizontal mixer (Laurent *et al.*, 2001), mechanically stirred vessel (Fangary *et al.*, 2000; Barigou, 2004), pulp and froth phases (Waters *et al.*, 2008), vertically stirred mill (Barley *et al.*, 2004), high shear mixer granulator (Ng *et al.*, 2007) and in a fluidised bed (Stein *et al.*, 1998) has also been undertaken.

The PEPT system used in this work has relied on the assumption that the PEPT data collected over a relatively long period of time under the same experimental conditions can pseudo represent the whole particle bed motion and velocity fields. This assumption was also used in the work of Wildman *et al.*, (2000).

6.3 Positron Emission Particle Tracking (PEPT) experiments

The experiments reported in this section were concerned with the use of PEPT to investigate the trajectories, occupancies and velocity field vectors of individual glass, bronze, sand and ilmenite particles. The particles were tracked in their respective binary mixtures that were driven dynamically by vertical vibration.

The labelling and maintenance of a sufficiently high radioactivity on a tracer particle is both challenging and important (Fan *et al.*, 2006a). In this work the tracer particle was made radioactive by the use of a cyclotron. In PEPT, the radioactive particle labelling is predominantly carried out by direct activation, ion exchange and by surface modification techniques. The detailed discussions on irradiating a finely sized particle are presented in Section 3.3.3.5.1. The selected tracer particle was loaded with the radioactive isotope of Fluorine (^{18}F) which has a half-life of about 110 minutes. The radioactive half-life of a particle is defined as the time during which half of its original radioactivity level will decay. The radioactive loading on a single particle at this stage was aimed to impart a suitable activity level that can be accurately detected in the PEPT camera. The tracer activity levels between 300 to 1000 μCi are considered to be sufficient for majority of applications (Fan *et al.*, 2006a). The accomplished radioactivity level in any single particle is a function of its physical properties. Once irradiated, the tracer particle could be used for nearly two hours before the activity level is decreased to such a value that is below the detection limit of the PEPT system (Fan *et al.*, 2006b).

Once a particle is irradiated the resulting radioisotopes will endure a natural decay. During the course of this decay some of the nuclei in the tracer particle will undergo a positive β -decay, whereby a proton in the nucleus will convert into a neutron by the emission of a

positron. The emitted positron travels approximately 1 to 2 mm until it annihilates with an electron, forming two 511keV gamma (γ) rays which are emitted back to back (Fan *et al.*, 2006a). The detection of these two γ -rays can locate the tracer particle somewhere between the annihilation lines of the two detection points as shown in Figure 3.9 and Figure 3.10. The detection point in principle will be the one where a large number of annihilation lines will intersect. This particle detection choice is expected to result in offsetting any inaccurate measurements that can result due to the false annihilation line intersections. The particle location can thus be located many times per second by using an iterative algorithm with the help of a computer that discarded the γ -rays passing away from the centroid (Fan *et al.*, 2006b). In this work the particle locations were mapped out after six repeat measurements at a single tracked point.

In the PEPT experiments reported here, the choice of particle bed height, vibration frequency and dimensionless acceleration was based on the investigations reported in Chapter 5. The main objective of the investigations reported here is to demonstrate the dynamic particle behaviours in a vertically vibrated environment. Therefore, only a single particle mixture from each material category with the previously (Chapter 5) identified good particle separation configurations was used in this work. The experiments reported in this section were carried out in the PEPT facility located at the University of Birmingham, UK.

6.3.1 Glass and bronze particle tracking

The tracer particle used in the experiments reported here comprised a sole glass and bronze particle that was tracked in the distinct working particle mixtures. This particle selection was designed to represent the parallel physical and chemical properties of the tracer particle, identical with that of the bulk material under the PEPT investigations. The synthetic glass and bronze working particle mixture was investigated to gain the basic vibration separation knowledge and to mimic the particle separation behaviour of finely sized, but relatively high density differential, solid waste particle mixtures, such as various WEEE fractions.

The complete size characterisation of the glass and bronze particles used in this work are shown in Figure 6.1.

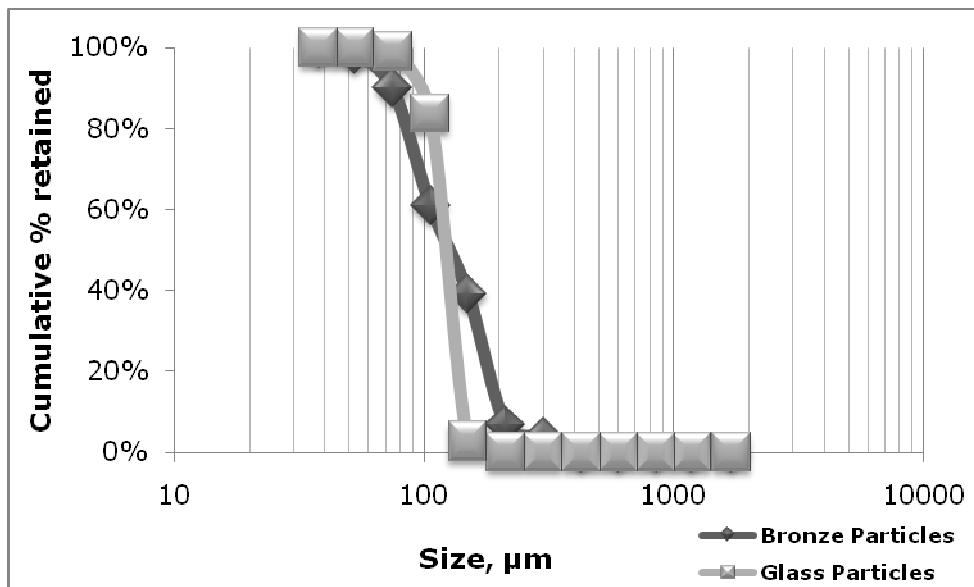


Figure 6.1: Particle size characterisation of the glass and bronze particles used in the PEPT investigations.

The average mass mean diameter of the glass and bronze particles was found to be $123.15\mu\text{m}$ and $157.67\mu\text{m}$ respectively. The selection of a glass and bronze particle mixture for the PEPT

investigations is important when it is considered that most of the available literature, in the vertical vibration field, is devoted in understanding their vibration driven particle behaviours at different sets of operating conditions. The other main reason for selecting the glass and bronze particles is their predominantly regular spherical shapes. A fairly narrow glass and bronze particle size distribution was used to eradicate any size segregation effects in this study. In addition to the other factors, previous investigations involving the use of parallel particle mixtures (Chapter 5) have shown good particle separation efficiencies at low particle bed heights, this knowledge was used here to determine the particle bed heights, in addition to fixing the vibration frequency, dimensionless acceleration and the partition gap size opening. The operating conditions used in the PEPT experiments reported here are shown in Table 6.1.

Operating parameters	Set values
Particle mixture	Glass and bronze
Mass fraction	80:20wt% glass and bronze respectively
Vertical vibration frequency, f	30±10% Hz
Dimensionless acceleration value, Γ	3±10%
Separation cells	C-1 and C-2
Particle bed height	30 mm in C-1 and 60 mm in C-2 respectively
Partition separation gap	5 mm
Tracking time	From 15 to 60 minutes, depending on the tracer location in the separation cell, its size and the type of material

Table 6.1: Operating parameters used in the PEPT experiments.

The radioactive bronze tracer particle was introduced on top surface of the glass (80wt) and bronze (20wt) mixture that formed an average particle bed height of 60 mm in C-1 (Figure 3.6) and 30 mm in C-2 (Figure 3.6). These two particle bed heights were selected to mimic the particle separation behaviour of the parallel mixtures that have been discussed in Chapter 5. The previous

investigations with the glass and bronze working particle mixtures in Chapter 5 have shown that the particle separation efficiency falls appreciably at 60 mm bed height and thereafter at 80 and 100 mm in both C-1 & 2. However, for the same particle mixtures the previously defined "good particle separation" can be observed at 20 and 40 mm particle bed heights. Hence, the particle bed selection reported here was able to represent both good and poor particle separation conditions. Furthermore, the previously observed particle separation behaviours with 10, 20 and 30% mass bronze and glass particles were not much different from each other. Hence, a 20% mass bronze and glass mixture was selected to demonstrate the dynamic particle behaviours triggered by vertical vibration at 60 and 30 mm particle bed heights in separation cell C-1 and C-2 respectively.

6.3.1.1 Bronze tracer in a 20 mm width separation cell, C-1

The real time change in the position of a bronze tracer particle with respect to X (horizontal), Y (vertical) and Z-axis is mapped out in Figure 6.2.

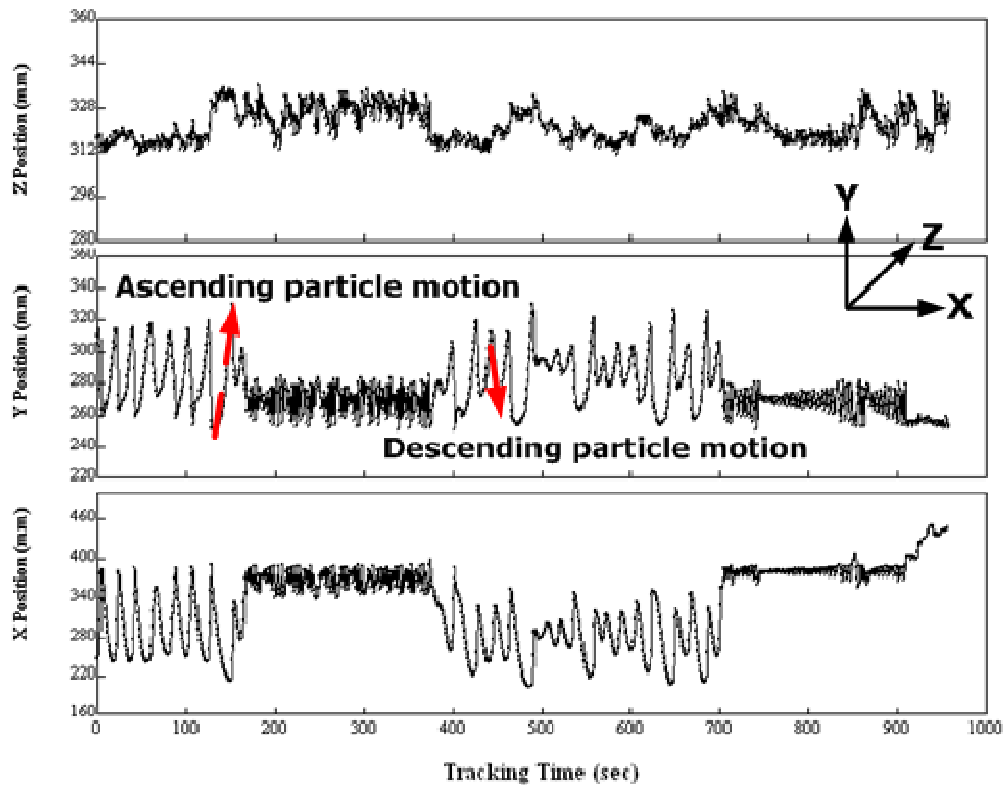


Figure 6.2: The real time change in the position of a bronze tracer particle with respect to X (horizontal), Y(Vertical) and Z-axis in separation cell, C-1.

A little change in the initial location of a bronze tracer particle between 200 to 400 and 700 to 950 seconds in Figure 6.2 give some indication about the tracer location which, at that time, may be deep inside the vibrated particle bed. Figure 6.2 also shows the ascending and descending particle motions in the vertical plane (y-axis). The large ascending peaks in the vertical direction (y-axis) in Figure 6.2 give an indication of the maximum average particle bed height. These large ascending peaks in the vertical direction (Y-axis) were recorded when the tracer particle was caught in the outer

convection current and it was transported upward to the top of the tilted particle bed under the influence of vertical vibration. The descending peak slopes in Figure 6.2 appear less steep and represent the tracer segregation at this stage.

The tracer particle motions were also recorded in the horizontal plane (X-axis) as shown in Figure 6.2. These motions represent a gradual tracer particle shift towards the opposite end of the tilted particle bed. During the course of this manoeuvre the tracer particle finally moved to the exit through a partition separation gap size of 5 mm for final collection.

The tracer particle was released on top surface of the tilted particle bed that was vertically vibrated. As the tracking time moved on, the real time complex bronze tracer motions were recorded in 3D alongside their average tracer speeds. This data is mapped out in Figure 6.3 where the end of tracking time is recorded when the tracer particle moves into the next chamber through a partition separation gap size of 5 mm.

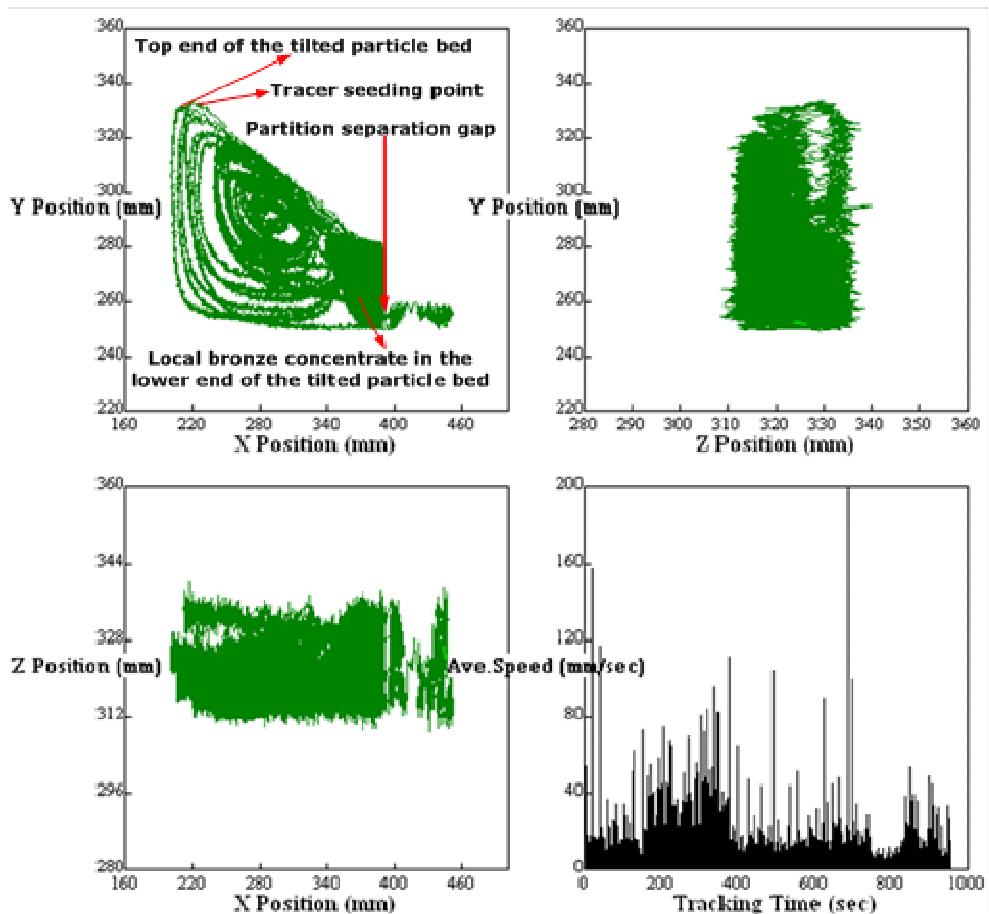


Figure 6.3: The three dimensional bronze tracer location and average speed at the end of the PEPT experiment when time, $t=980$ sec. The recorded real time observations are presented as PEPT-Video-D01 at 10X speed in the provided CD (No.1 in Appendix-D).

Figure 6.3 reveals an interesting tracer particle trajectory that can be readily observed. Soon after the release of tracer particle in the vibrated particle bed, it started to move in a distinct trajectory. The initial tracer motion was mainly recorded in the outer periphery of the tilted particle bed. On average the tracer particle took ~ 20 seconds to complete a single circulation loop in the outer periphery of the vibrated particle bed, this tracer circulation time was calculated from the tracking plot shown in Figure 6.3. Nevertheless, as the tracking time moved on, the bronze tracer particle was engaged in the localised convection currents. One of the most

sustained localised convection currents was visually observed to form in close proximity to the partition separation gap where a bunch of predominantly bronze particles was able to develop within the first 200 seconds of the vertical vibration treatment.

The tracer particle was observed to use most of the tracking time in the global and localised convection currents; however this vibration driven tendency did not prevent it from entering into the main particle bed. On many occasions the tracer particle moved out of the bronze rich convection currents and entered into the glass rich inner regions. In reality, the tracer particle moved everywhere (Figure 6.3) within the vibrated particle bed, however most of its tracking time was spent close to the partition separation gap. This tracked tracer particle behaviour via PEPT is in agreement with the previously explained visual observations, reported in Chapter 5, with the use of parallel materials. The vibrating bronze particles continued to segregate and concentrate in close proximity to the partition separation gap and eventually the bronze tracer particle moved to the next separate chamber after 980 sec of vertical vibration treatment.

In addition, the plot of average speed against the tracking time, shown in Figure 6.3, reveals that higher values of the tracer speeds were recorded when the tracer particle had the chance to slide down freely from the top end of the tilted particle bed. The tracer particle speeds were reduced when it moved deep inside the vertically vibrated particle bed. Similar velocity profiles in an un-tilted particle bed can also be found in the work of Wildman *et al.*, (2000). The average speed of the bronze tracer particle mostly varied in range of 0 to 60 mm.s⁻¹, which on some occasions reached as high as 100 mm.s⁻¹ as shown in PEPT-Video-D01 in the provided Compact Disk (CD) (No.1 in Appendix-D). The PEPT-Video-D01 shows the real time dynamics of bronze tracer particle which was recorded 10 times faster than the normal tracer speed. Higher values of the

average speed generally represent the motion of the tracer particle that is very close to, or is completely on, the top surface of the tilted particle bed.

In addition to mapping of tracer flow trajectory and average particle speeds, the velocity profile of a tracer particle can also be calculated from the data acquired by PEPT. The above mentioned observations are further confirmed when the time averaged velocity vector profile of the tracer particle is placed in the separation cell geometry as shown in Figure 6.4.

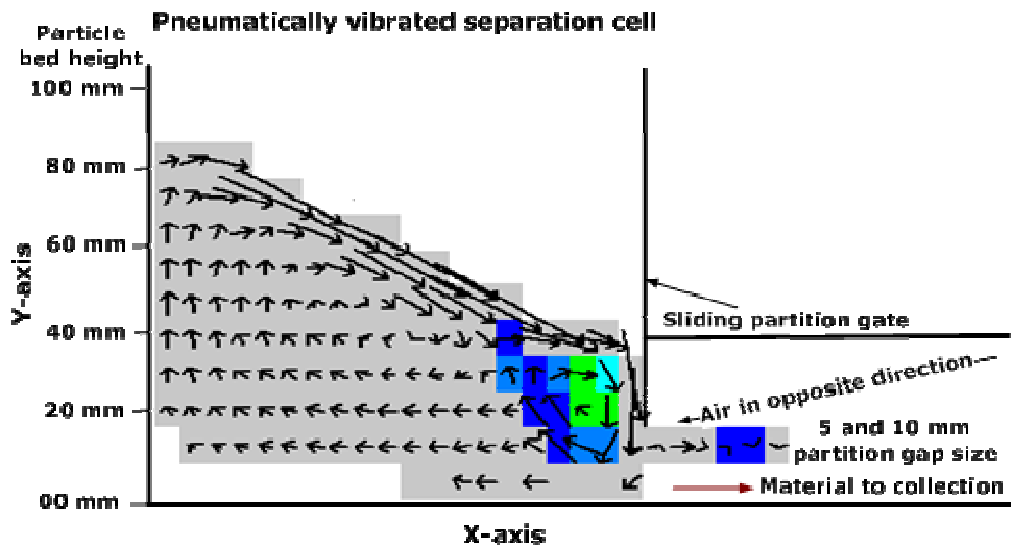


Figure 6.4: The occupancy and velocity field vectors of a bronze tracer particle in relation to the separation cell (C-1) geometry.

In Figure 6.4, a single arrow shows the distance that is travelled by a tracer particle within each 50 milli-seconds. Different colours in Figure 6.4 represent the occupancy of the tracer particle in each pixel. Here the occupancy is defined in terms of time that the tracer particle spends in each individual pixel divided by the total tracking time. The detailed description of the colours used in Figure 6.4 are given in Figure 6.5 where a three dimensional occupancy and velocity vector profile of the tracer particle is also mapped out.

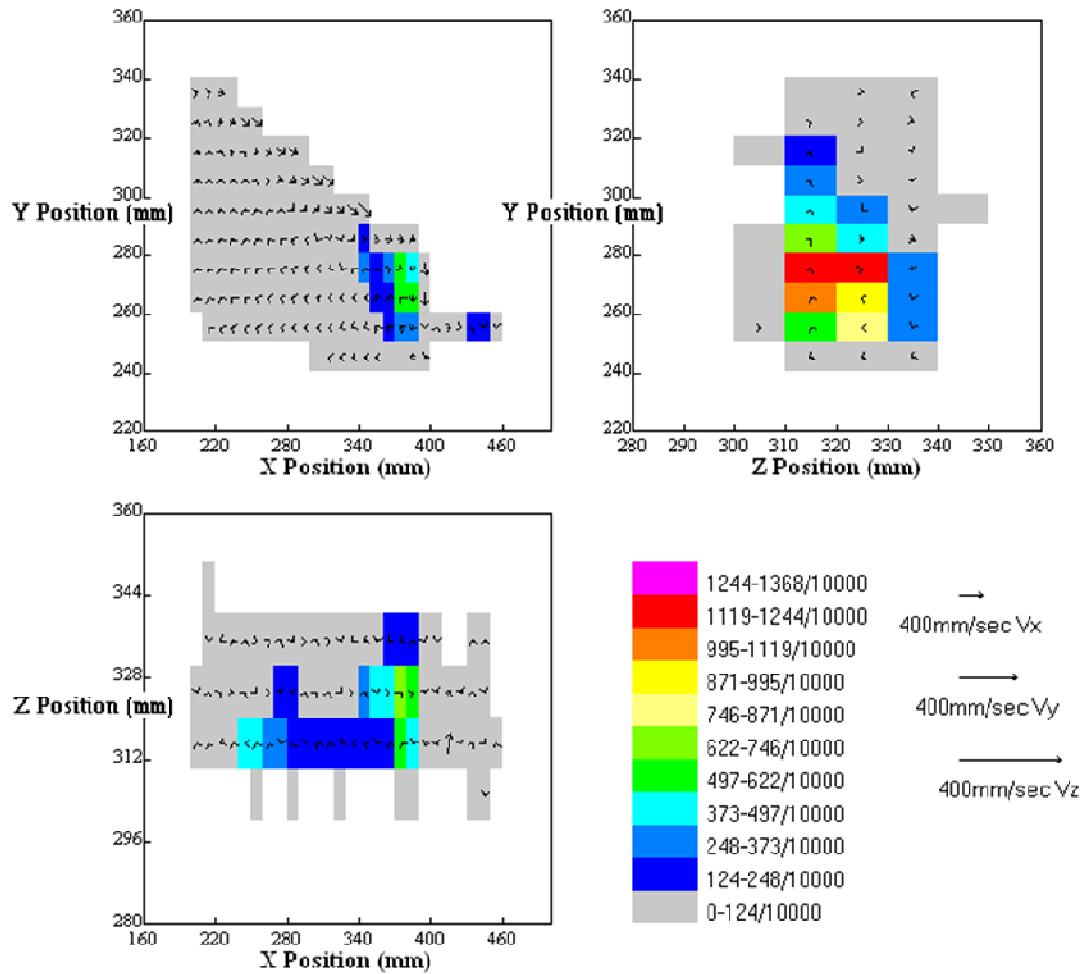


Figure 6.5: The three dimensional motion and occupancy mapping of a bronze tracer particle in separation cell, C-1.

Figure 6.4 and Figure 6.5 reveal a striking difference in the magnitude of the tracer velocity that can be readily seen at different particle bed locations. The tracer velocity was of high magnitude in the particle bed locations that are very close to the top surface of the tilted particle bed and also close to the partition separation gap. In comparison to the above, the recorded tracer velocity is of low magnitude in locations that are deep inside the main vertically vibrated particle bed.

In Figure 6.4 and Figure 6.5, the higher magnitude of the recorded tracer velocity in close proximity to the partition separation gap can be explained by considering the actual particle bed structure. The

vertically vibrated and tilted particle bed contained far less particle layers in close proximity to the partition separation gap (lower end) in comparison to the middle and top end of the tilted particle bed. The particles in the lower end were therefore less loaded and enjoyed a comparatively high magnitude of individual momentum which was injected, mainly, by the vertical vibration and, in part, by the inter-particle collisions. Furthermore, the role of surrounding fluid on the individual particle motion and velocity cannot be understated. The surrounding air had more circulation influence in the lower end of the tilted particle bed. This resulted in enhancing the velocity of the bronze tracer particle in close proximity to the partition separation gap.

Although the high density bronze tracer particle demonstrated long presence in the local bronze rich convection current in close proximity to the partition separation gap its transfer to the next chamber was mainly restricted by the inter-particle collisions and collisions with the sliding partition wall as shown in Figure 6.4 and Figure 6.5. Other possible explanations could be the opposite direction motion of the surrounding fluid that is drawn into the vertically vibrated particle bed to offset the effects of negative fluid pressure (Zeilstra *at al.*, 2006) that is expected to form during the particle bed flights. This air motion in the opposite direction to the separating particles can also act as a filter by returning the low momentum particles into the main particle bed.

Generally, in a well tilted particle bed there is minimum particle bed thickness very close to the partition separation gap. This minimum bed thickness provides an excellent opportunity for the surrounding fluid to take this route that, theoretically, has a minimum resistance and penetrate deep into the bottom of the particle bed to offset the effects of the negative fluid pressure that is formed during vertical vibration. This situation can result in an increased fluid motion next to the partition separation gap and as a result could add an extra

amount of energy to the adjacent vertically vibrating particles. The fluid motion near to the partition gap can also act as a momentum filter for moving back the low density particles into the main vibrated bed. The fluid induced filtration effect may be one of the main reasons that predominantly bronze particles, with comparatively high values of inherent momentum energy, were able to cross the partition separation gap. In addition to the bronze particles, some glass particles were also observed to cross the partition gap but they were mostly considered to be driven by the inter-particle collisions with high momentum particles.

On occasions, the bronze tracer particle was observed to cross the partition gap but it returned back to the main particle bed after a very short period of time. The possible explanation for this behaviour may be the inter-particle collisions and the opposite direction motion of the surrounding fluid. Nonetheless, the bronze tracer particle was observed to find a stable transfer into the next chamber after 980 sec of vertical vibration treatment for the final collection.

6.3.1.2 Glass tracer in a 20 mm width separation cell, C-1

The real time change in the position of a glass tracer particle with respect to X (horizontal axis), Y (vertical axis) and Z-axis is illustrated in Figure 6.6.

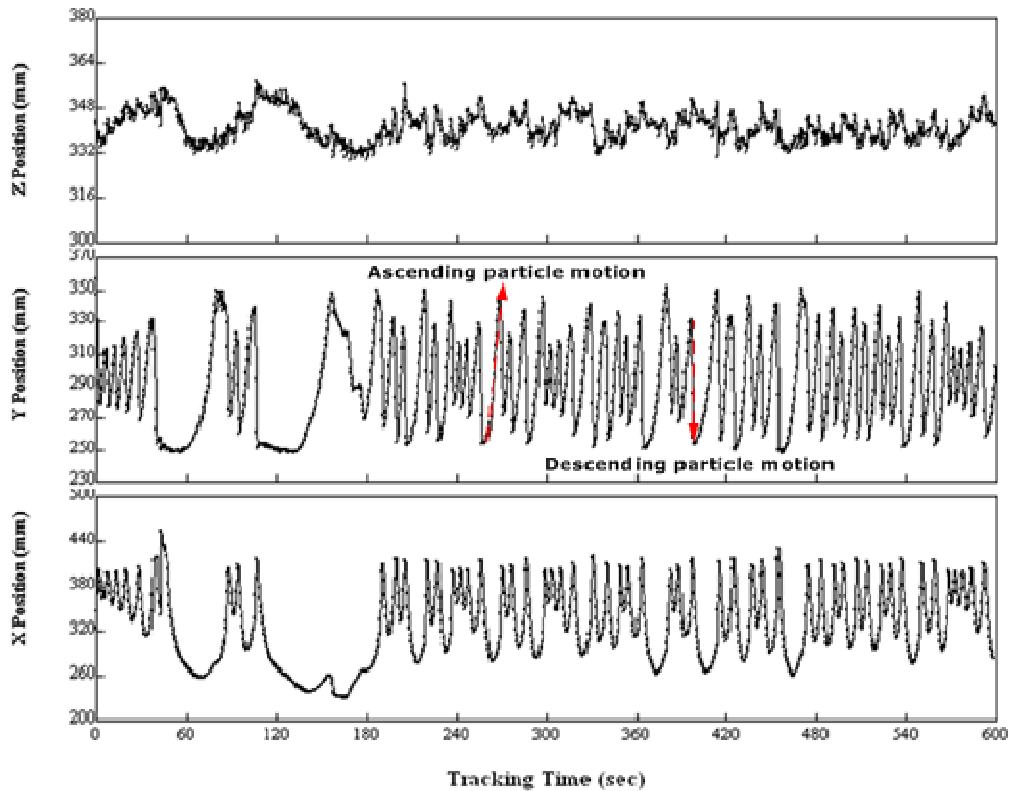


Figure 6.6: The real time change in the position of a glass tracer particle with respect to X (horizontal), Y(Vertical) and Z-axis in separation cell, C-1.

The comparatively stagnant zones between the tracking times of 55-65 and 100-180 seconds in Figure 6.6 represent a less mobile tracer particle in the X and Y-directions. This drop in tracer motion can be attributed to its location which at that time appeared to be deep inside the tilted particle bed. Nevertheless, in Figure 6.6 the large ascending peaks in the vertical direction (Y-axis) were recorded when the glass tracer particle moved close to the top surface of the tilted particle bed. These ascending peaks in the Y-direction can be used to get an indication of the maximum particle bed height.

Furthermore, in Figure 6.6 the X-axis denotes the tracer particle motions in the horizontal plane.

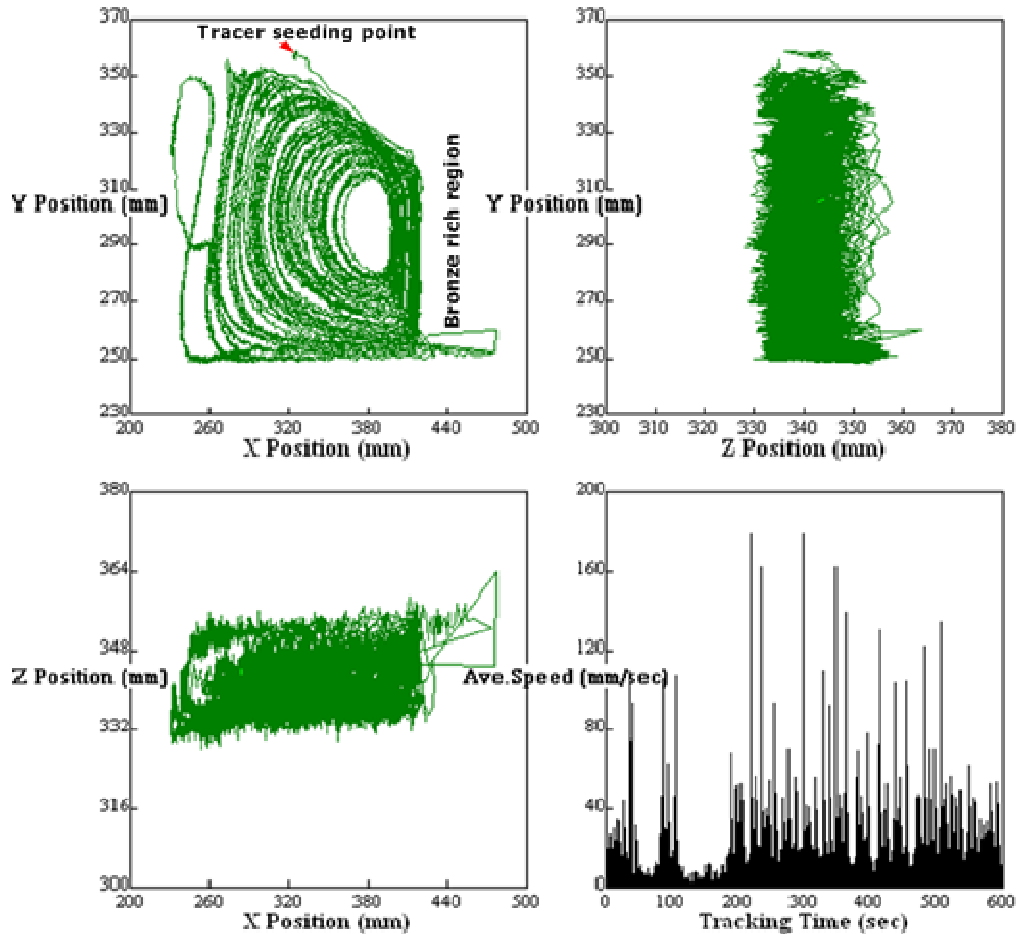


Figure 6.7: The three dimensional glass tracer location and average speed from the start to the end of the PEPT experiment. The recorded real time observations are presented as PEPT-Video-D02 at 10X speed in the provided CD (No.2 in Appendix-D).

The Figure 6.7 reveals a complete real time trajectory of the irradiated glass tracer particle. The glass tracer particle was released on the top surface of the vertically vibrated particle bed. The tracer seeding point is shown in Figure 6.7. Soon after the release of the tracer particle into the vibrated particle bed it started to move in a distinct trajectory. Initially, the glass tracer motions were confined to a local convection current that distinctly developed predominantly in the lower end of the tilted particle bed, in close

vicinity to the local bronze concentrate that has been shown previously in Figure 6.3 and is also marked in Figure 6.7. However, the glass tracer particle did not sustain this local convective motion for long periods of time. Presumably, once the glass tracer particle was able to gain enough momentum it started to move gradually outward i.e. towards the global convection current in the outer periphery of the tilted particle bed. This tracer trajectory trend was then maintained for the rest of the tracking time during which the motion of the glass tracer particle was seldomly recorded in the bronze rich local convection current. On an average, the glass tracer particle took ~40 seconds to complete a single loop in the outer periphery of the tilted particle bed. This circulation time was calculated from the trajectory measurements shown in Figure 6.7. Nevertheless, there was not much difference in the average tracer speeds of the glass and bronze particles (Figure 6.7). The recorded average speed of the glass tracer particle was mostly in the range 0-60 mm.s⁻¹, which on some occasions reached as high as 100 mm.s⁻¹ as shown in PEPT-Video-D02 in the provided Compact Disk (CD) (No.2 in Appendix-D). The PEPT-Video-D02 shows the real time dynamics of glass tracer particle which was recorded 10 times faster than the normal tracer speed. Nevertheless, one of the possible reasons for the recorded glass tracer behaviour may be the mixed convective motion of the glass and bronze particles due to their limited separation tendency at particle bed heights above 40 mm. Hence, a parallel particle speed can be expected from the glass tracer particle due to the frequent exchange of the individual kinetic energies between the glass and bronze particles.

The understanding of the tracer trajectory can be further enhanced by considering the occupancy and velocity field vectors in relation to the separation cell geometry as shown in Figure 6.8 and Figure 6.9.

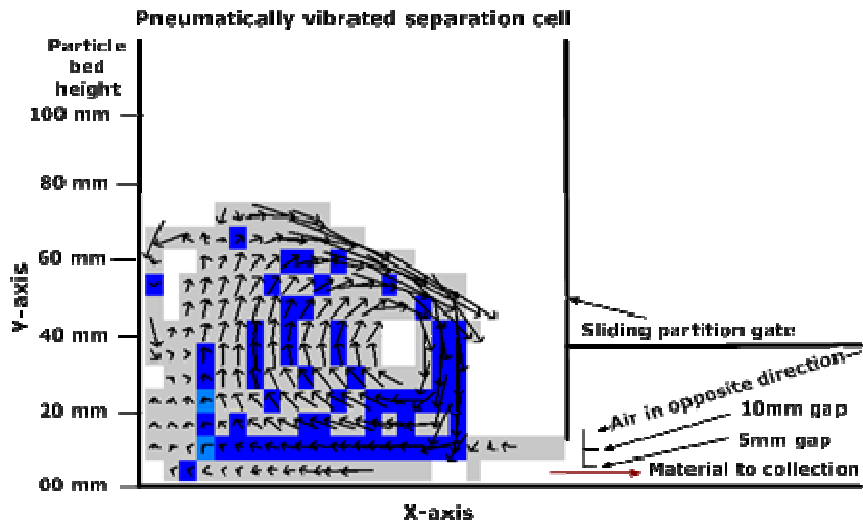


Figure 6.8: The occupancy and velocity field vectors of the glass tracer particle in relation to the separation cell (C-1) geometry.

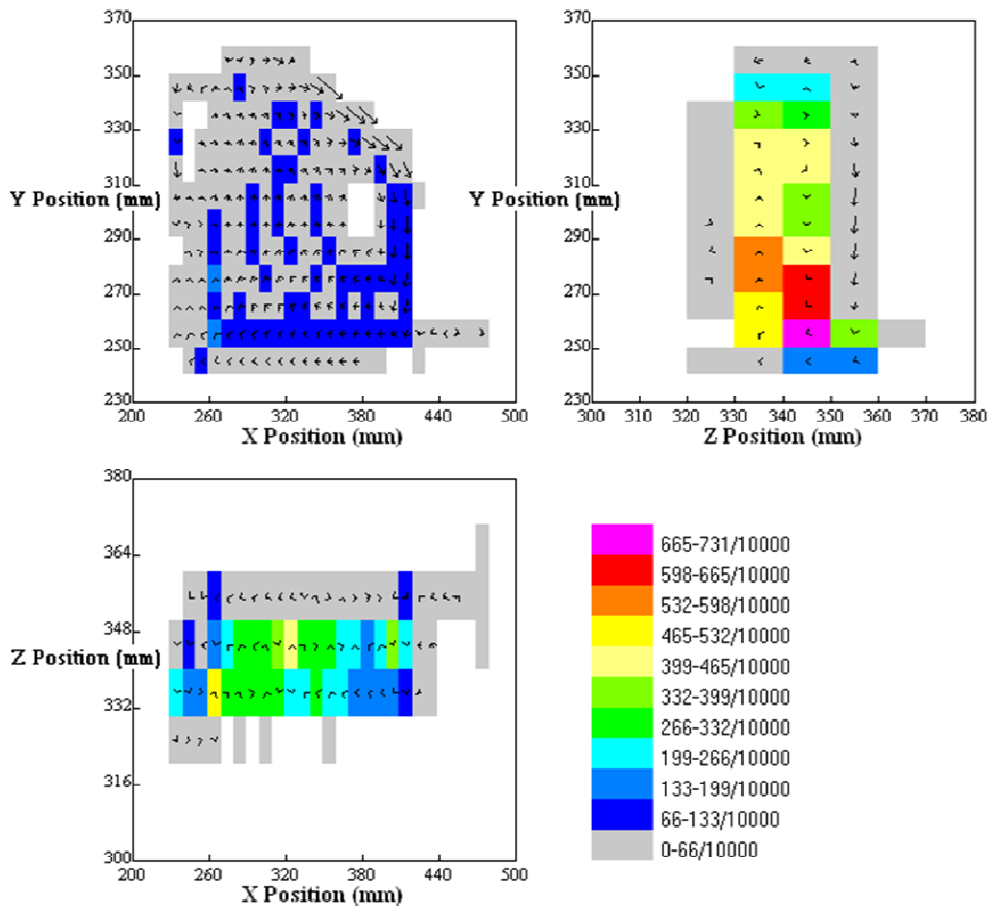


Figure 6.9: The three dimensional motion and occupancy mapping of a glass tracer particle in separation cell, C-1.

An ordered convective motion of the glass tracer particle can be readily observed from Figure 6.8 and Figure 6.9. The magnitude of the mapped velocity field vectors is high close to the top surface of the vertically vibrated particle bed, as shown in Figure 6.8 and Figure 6.9. This is in agreement with the previous observations and further supports the comments reported in Section 6.3.1.1. However, a striking difference between the occupancy of the glass and bronze tracer particle can be readily observed. The mapped occupancy of the bronze tracer particle (Figure 6.4 and Figure 6.5) was recorded mostly in close vicinity to the partition separation gap. On the other hand the glass tracer particle mostly resided in the main particle bed during most of its tracking time. This is marked with blue colours in Figure 6.8 and Figure 6.9. Another important observation from the occupancy mapping is the inability of the glass tracer particle to enter the bronze rich stronghold in close vicinity to the partition separation gap. This may be due to the strong inter-particle collisions and distinct rheology of the glass and bronze particles. Presumably, the glass and bronze particles were having strong inter-particle collisions at the boundary of these two distinct and opposite direction convection currents. The recorded velocity field vectors of the glass tracer particle are of higher magnitude in close vicinity to the local bronze concentrates in comparison to other places in the vibrated particle bed. This may be a result of a rapid momentum transfer between the glass and bronze particles with each other on their convection current boundaries. Furthermore, the glass tracer motions were mostly recorded away from the separation cell geometries, an indication of its motion in a distinct convection current. Nevertheless, the tracer motions were finally stable in the predominantly glass rich convection currents and the tracking time was stopped after 600 seconds of vertical vibration treatment.

6.3.1.3 Bronze tracer in a 40 mm width separation cell, C-2

The real time change in the position of an irradiated bronze tracer particle with respect to X (horizontal), Y (vertical) and Z-axis is mapped out over a tracking time of 360 seconds in Figure 6.10. As previously discussed, the choice of the final tracking time was based on the individual particle motions in each experiment. The final tracking time in each experiment was recorded when the tracer particle either separated out into the next chamber or it started to move in a stable convection current in the vertically vibrated particle bed.

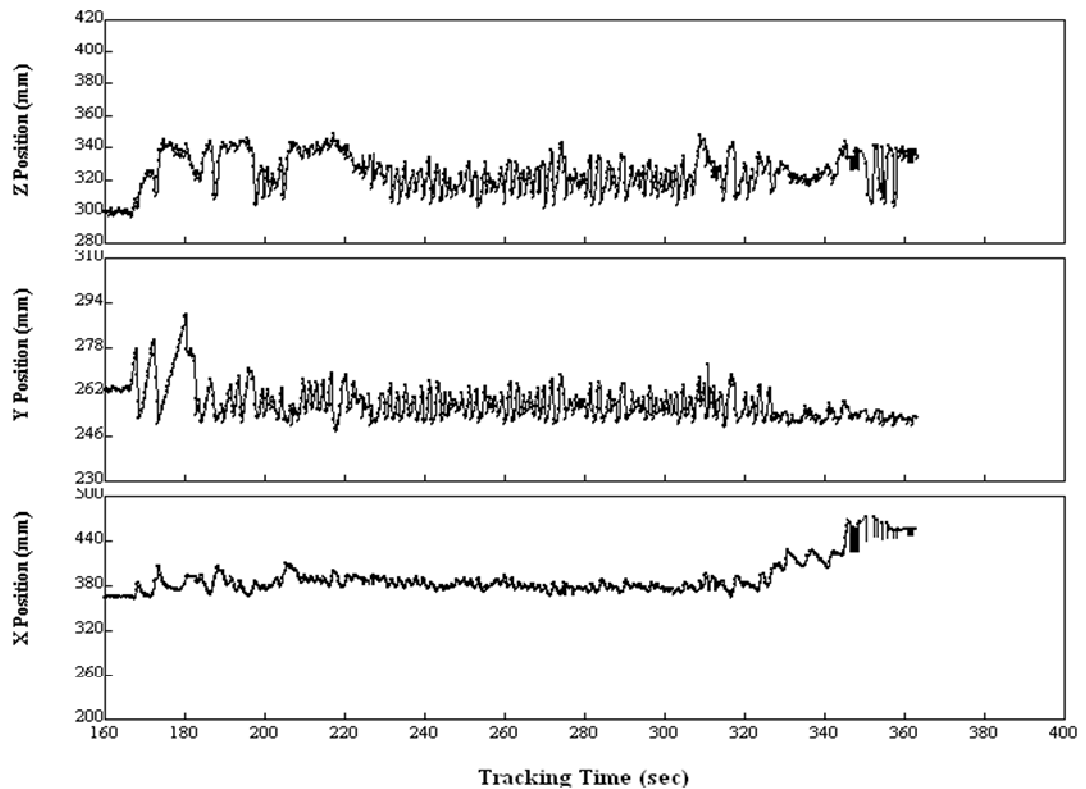


Figure 6.10: The real time change in the position of a bronze tracer particle with respect to X (horizontal), Y (vertical) and Z-axis in separation cell, C-2.

In Figure 6.10, the comparatively steep ascending and descending motions of bronze tracer particle in the horizontal (X) and vertical (Y) directions demonstrates that the particle rheology was of a

different nature at lower particle bed heights in comparison to that previously recorded with parallel materials at a particle bed height of 60 mm (Section 6.3.1.1).

The change in particle dynamics, of the bronze tracer particle, at particle bed height of 30 mm in separation cell C-2, mostly resulted due to the lower particle bed loading. The lower particle bed loading offered comparatively less resistance to the surrounding fluid currents which entrained the particle bed during the course of vertical vibration, this resulted in quick segregation of the bronze particles. The segregated bronze particles were observed to concentrate in close vicinity to the partition separation gap from where they were gradually transferred into the next chamber for collection. These observations are further confirmed by the three dimensional tracking map of the single bronze particle as shown in Figure 6.11.

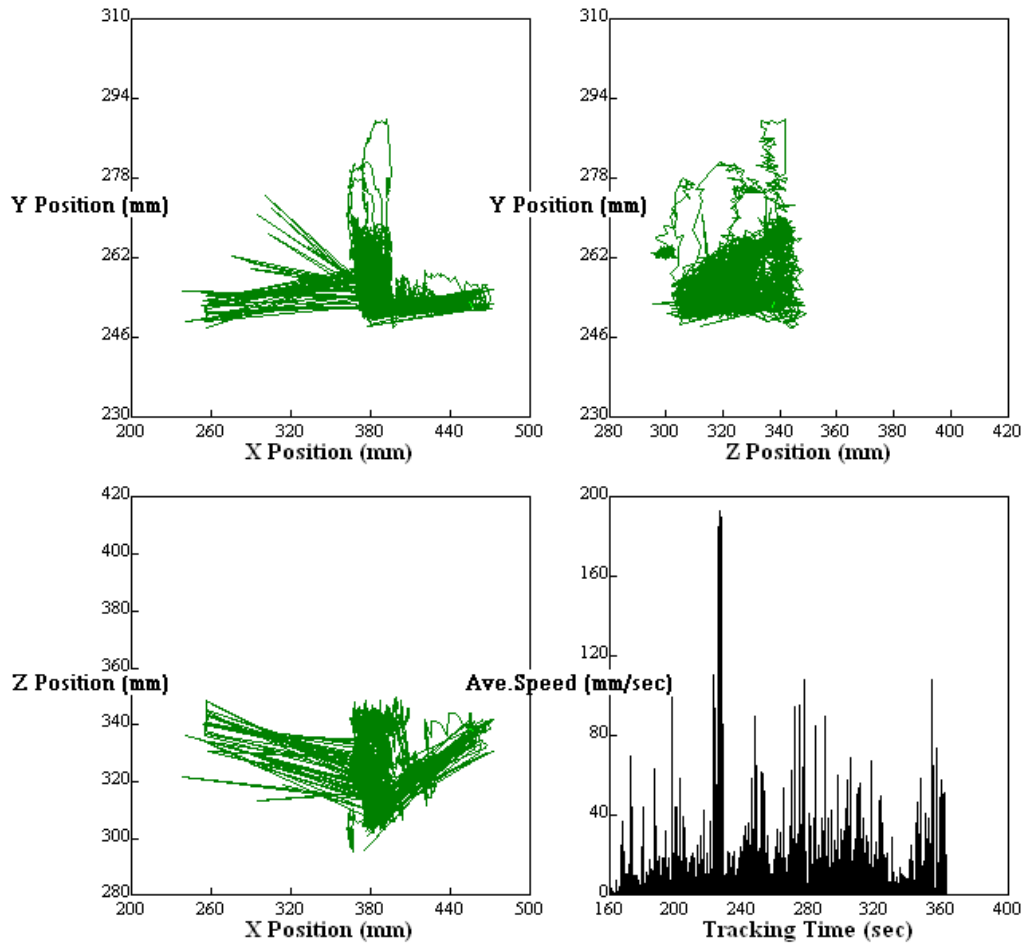


Figure 6.11: The three dimensional bronze tracer location and average speed from start to the end of the PEPT experiment in a 40 mm width separation cell, C-2. The recorded real time observations are presented as PEPT-Video-D03 at 10X speed in the provided CD (No.3 in Appendix-D).

Figure 6.11 shows that, the tracer motion was mostly abrupt but it did actually spend some time in the local convection currents. However, the tracer motion was never recorded in a global convection current, this may be due to the formation of an inverse tilt in the vertically vibrated particle bed. This is in contrast to what was previously recorded at 60 mm particle bed height, reported in Section 6.3.1.1. Nevertheless, soon after the release of the tracer particle into the vibrated particle bed it started to move in a local convection current close to the partition separation gap where most

of its motion was recorded. On occasions the tracer particle travelled towards the other end of the vibrated particle bed, but only for a very short period of time. The tracer mostly stayed in close vicinity of the separation gap and finally moved out into the separate chamber after 360 seconds of vertical vibration treatment. These observations are shown in PEPT-Video-D03 in the provided Compact Disk (CD) (No.3 in Appendix-D). The average speed of the bronze tracer particle was of a similar order to that previously recorded in the case of a 60 mm particle bed height in separation cell, C-1 (Section 6.3.1.1).

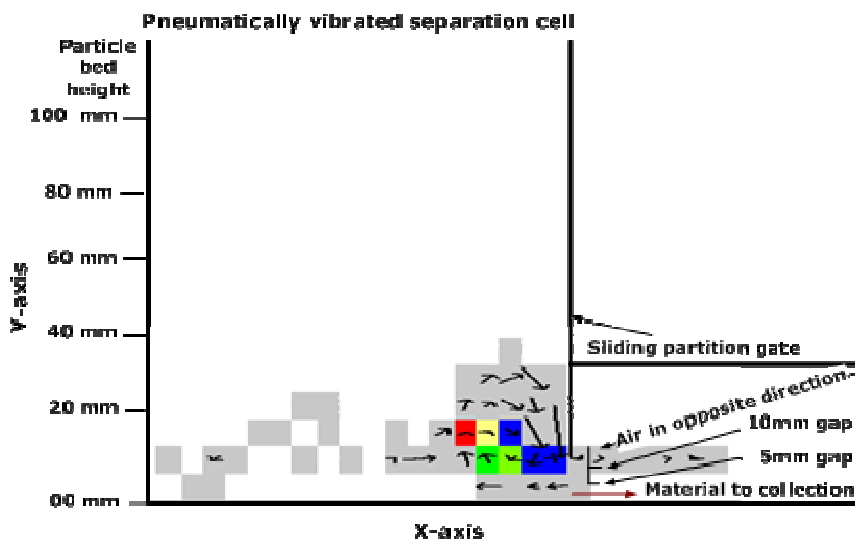


Figure 6.12: The occupancy and velocity field vectors of a bronze tracer particle in relation to the separation cell (C-2) geometry.

The above observations are further confirmed when we plot the occupancy and tracer velocity vectors in relation to the separation cell (C-2) geometry, as shown in two dimensions in Figure 6.12 and in three dimensions in Figure 6.13.

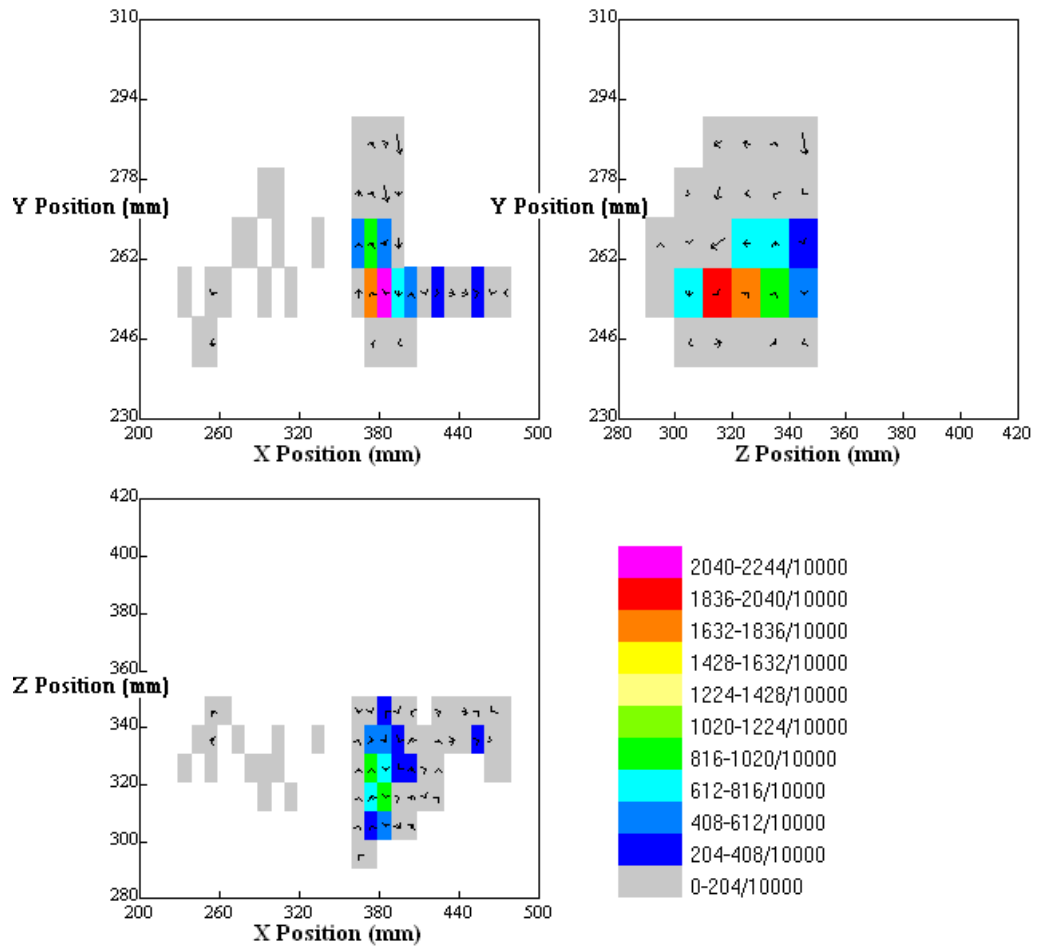


Figure 6.13: The three dimensional motion and occupancy mapping of a bronze tracer particle in separation cell, C-2.

The velocity field vectors are of strong magnitude on top surface of the particle bed and close to the partition separation gap (Figure 6.12 and Figure 6.13), in agreement with previous observations (Section 6.3.1.1 and 6.3.1.2).

6.3.1.4 Glass tracer in a 40 mm width separation cell, C-2

The real time change in the position of an irradiated glass tracer particle with respect to X (horizontal), Y (vertical) and Z-axis is mapped out in Figure 6.14.

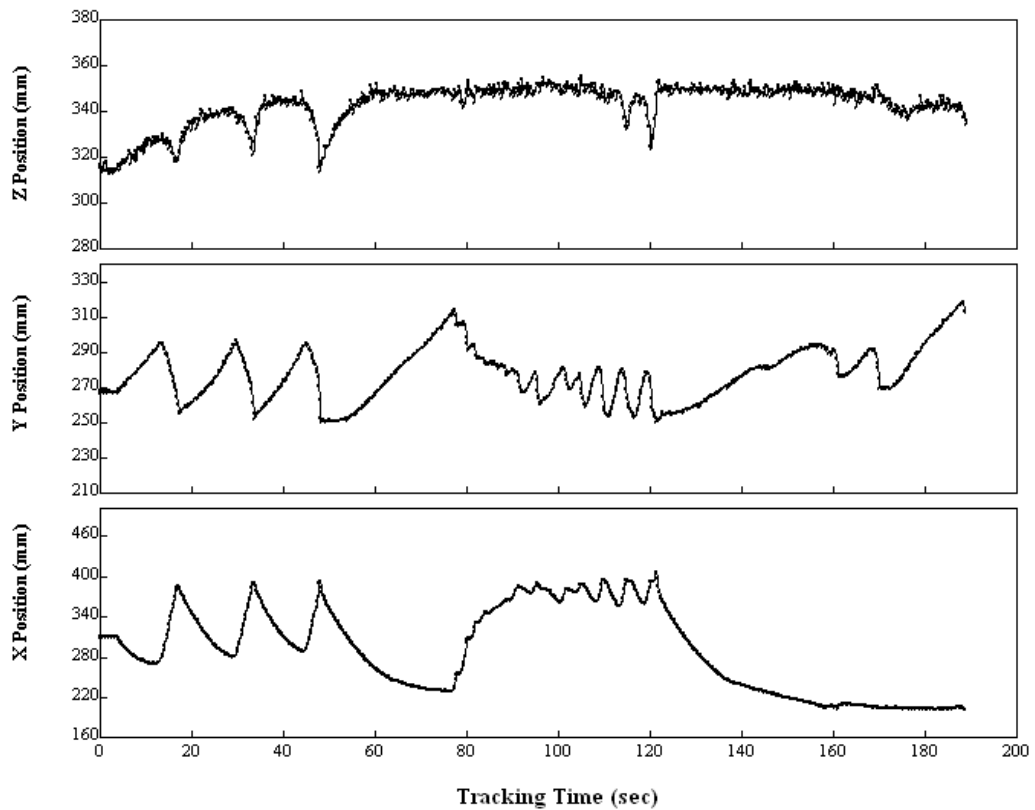


Figure 6.14: The real time change in the position of a glass tracer particle with respect to X(horizontal), Y(Vertical) and Z-axis in separation cell, C-2.

In Figure 6.14, the first 80 seconds of the tracking time represent ordered ascending and descending motions of the tracer particle in the horizontal (X) and vertical (Y) directions. During this time the tracer particle was tracked to move in a clockwise global convection current. In this experiment, the tracer's joining of the global convection current was found to be relatively smooth. This behaviour is further supported by the real time mapping of the glass tracer particle in three dimensions, shown in Figure 6.15.

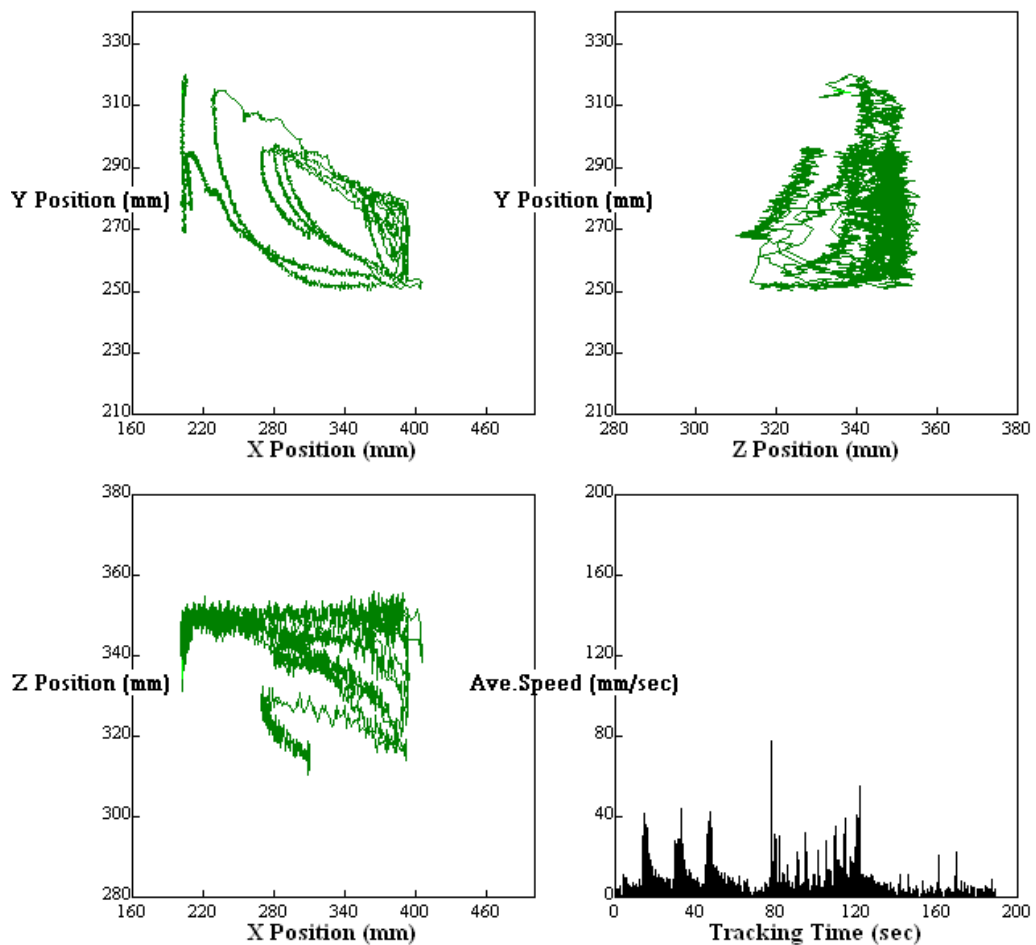


Figure 6.15: The three dimensional glass tracer location and average speed from start to the end of the PEPT experiment in a 40 mm width separation cell, C-2. The recorded real time observations are presented as PEPT-Video-D04 at 10X speed in the provided CD (No.4 in Appendix-D).

In Figure 6.15, the tracer motions were mostly recorded in the glass rich regions. The circulation time of the tracer particle in the outer periphery was found to be ~ 25 seconds. Here, when the same glass tracer particle as used in the experiments reported in Section 6.3.1.4, was tracked in a parallel mixture but at a low particle bed height of 30 mm in separation cell C-2, a striking difference in the average speeds of the two tracer particles was recorded. The drop in average speed of the tracer particle at 30 mm particle bed height was found to be significant, this could be as a result of many

different factors. However, the principal factor behind this behaviour was observed to be the relatively quick formation of distinct glass and bronze rich zones which appeared within first few seconds of the vertical vibration treatment. As the matching particles started to move in distinct convection currents and the high density ones segregated out sharply into the next chamber, the exchange of inter particle kinetic energy between the dissimilar particles was decreased. Hence, lower values of average speeds were recorded as a result. On most instances the average speed of the tracer particle was found to be below 40 mm.s^{-1} . The recorded real time glass tracer dynamics are shown in PEPT-Video-D04 in the provided Compact Disk (CD) (No.4 in Appendix-D).

In Figure 6.15, a further decrease in average speed of the tracer particle can be seen after 100 seconds of vertical vibration, a time when the bulk of bronze particles had already moved into the next chamber. At this stage, only glass particles were present in the vertically vibrated separation cell and the glass tracer particle by no means tried to move into the next chamber. The glass tracer velocity field vectors and occupancies are mapped out in Figure 6.16 and Figure 6.17.

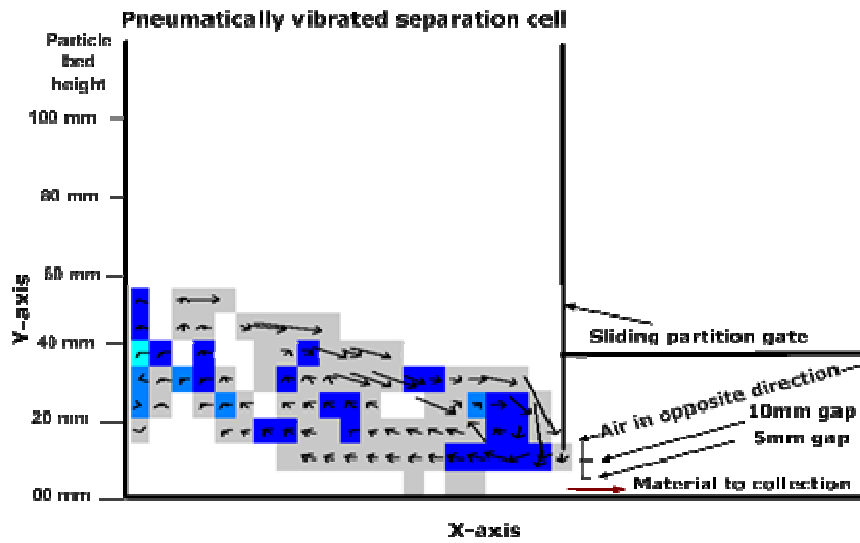


Figure 6.16: The occupancy and velocity field vectors of a glass tracer particle in relation to the separation cell (C-2) geometry.

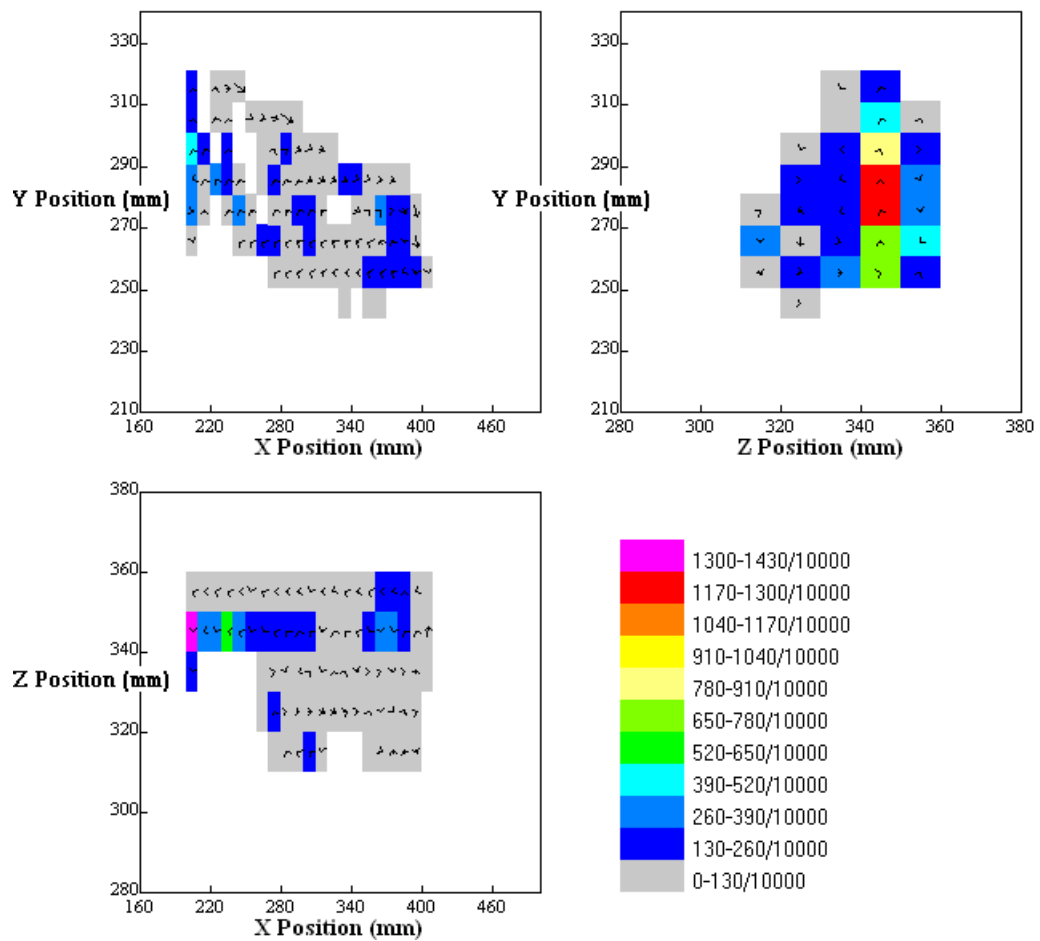


Figure 6.17: The three dimensional motion and occupancy mapping of a bronze tracer particle in separation cell, C-2.

In Figure 6.16 and Figure 6.17, the glass tracer velocity vectors were found to be of higher magnitude near to the top surface of the tilted particle bed and next to the partition separation gap. On top surface of the tilted particle bed, the enhanced velocity field vectors can be attributed to the downhill sliding motion of the tracer particle. However, the increased velocity field vectors next to the partition separation gap may be as a result of the inter-particle collisions with predominantly bronze particles in the surrounding area.

6.3.2 Glass (53-150 μm) and glass (300-600 μm) particle tracking

The particle segregation phenomenon is not just limited to diverse density particle mixtures. The existence of this phenomenon is also well established in particle mixtures incorporating different sizes. Particle size separation is an important problem that is encountered in many different areas of Process and Environmental Engineering, however it can be used to an advantage for separating different finely sized non-cohesive particle mixtures. In this work, size segregation via vertical vibration has been used to separate identical particle mixtures. As reported earlier (Chapter 2), some researchers have suggested that in parallel particle mixtures the large size particles behave in similar fashion to the high density particles, however, much of the insight into the peculiar size segregation behaviour is still lacking.

In the work presented here, an effort has been made to improve our understanding of the peculiar particle dynamics of two different sized but equal density glass particles in a particle bed subjected to vertical vibration. The particle size distribution of the two different size glass particles is given in Figure 6.18.

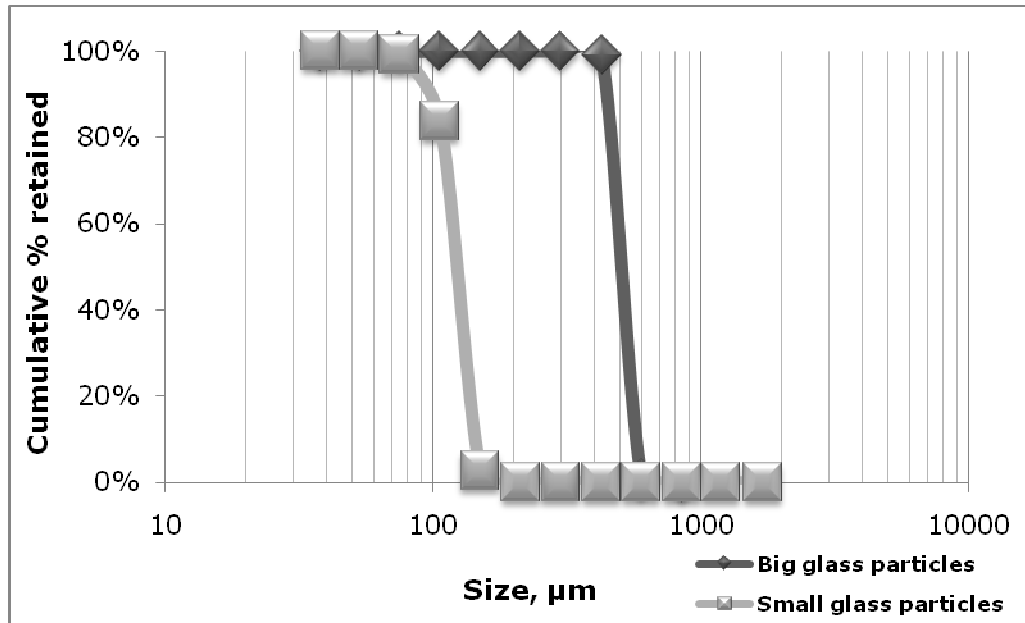


Figure 6.18: Particle size characterisation of two distinctly sized glass particles used in the PEPT investigations.

Figure 6.18, shows the average mass mean diameter of the small and large size glass particles to be 123.15µm and 512.80µm respectively. The small glass particles formed 80%, by weight, of the whole particle mixture whereas the rest was comprised of all large size glass particles. The tracer particle was subjected to the same tracking conditions as previously outlined in Table 6.1. Furthermore, the distinctly sized glass particle mixture formed an average particle bed height of 80 mm in separation cell C-1 and 40 mm in separation cell C-2. Since the particle dynamics in the separation cells C-1 and C-2 has been shown not to be different, the selection of an 80 mm particle bed height was chosen to investigate the tracer motions in a poorly separating particle mixture. Whereas the 40 mm particle bed height was used to track the tracer motion in a particle mixture that mimicked the good particle separation behaviour.

6.3.2.1 PEPT of the large glass tracer particle in a 20 mm width separation cell, C-1

The three dimensional motion and average speeds of the large size glass tracer particle within 800 seconds of tracking time is completely mapped out in Figure 6.19.

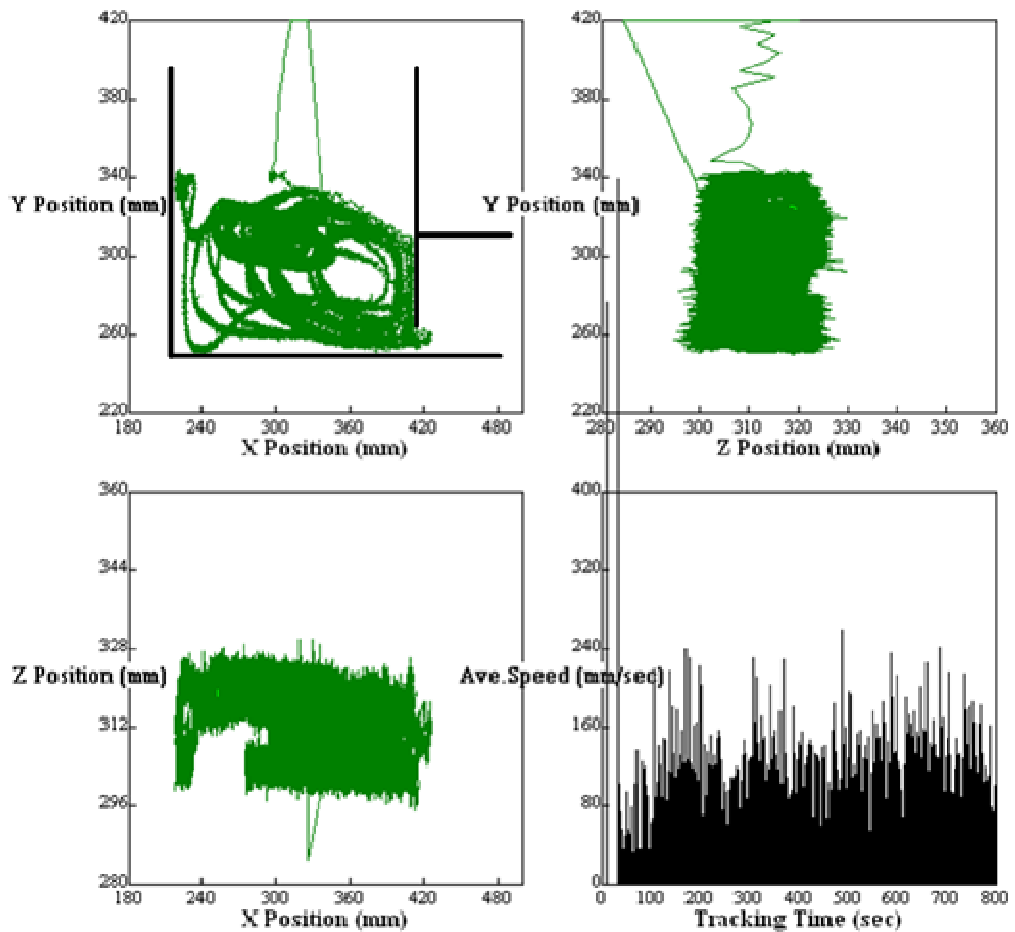


Figure 6.19: The three dimensional large glass tracer location and average speed from start to the end of PEPT experiment in a 20 mm width separation cell, C-1. The recorded real time observations are presented as PEPT-Video-D05 at 10X speed in the provided CD (No.5 in Appendix-D).

An interesting motion of the large size glass tracer particle can be seen in Figure 6.19. Soon after the release of the tracer particle on top surface of the tilted particle bed it started to move in a local

convection current that was able to develop in close vicinity of the partition separation gap. The tracer particle remained there for an initial 200 seconds of the tracking time before it gradually started to move away and joined the main global convection current that patrolled the outer periphery of the tilted particle bed. However, the motion of the tracer particle in the global convection current was only for a limited amount of time and soon it was able to join a second local convection current that developed near to the top surface of the vibrating particle bed. The tracer particle spent nearly 250 seconds of the total tracking time in this second local convection current. Besides moving in local and global convection currents the tracer particle also on occasions moved into the next separate chamber, but only for a very short period of time. A stable transfer of the tracer particle into the next separate chamber was never recorded. The average speed of the tracer particle in this case was mostly recorded in the range of 100-160 mm.s⁻¹, which on some occasions reached as high as 200 mm.s⁻¹ as shown in PEPT-Video-D05 in the provided Compact Disk (CD) (No.5 in Appendix-D). The PEPT-Video-D05 shows the real time dynamics of large glass tracer particle which was recorded 10 times faster than the normal tracer speed.

The recorded velocity field vectors and occupancies of the large glass tracer particle via PEPT are shown in Figure 6.20. The maximum occupancy of the large size glass tracer particle was recorded on top surface of the poorly tilted particle bed.

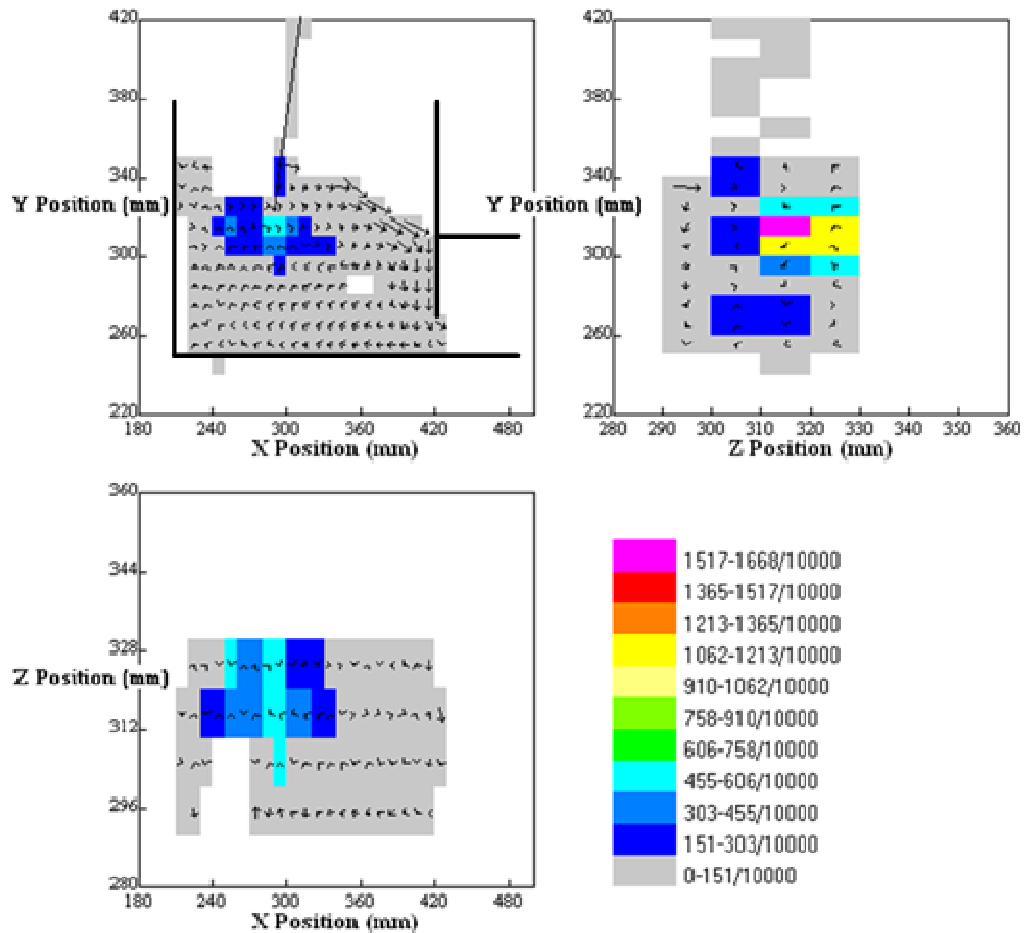


Figure 6.20: The three dimensional motion and occupancy mapping of a large glass tracer particle in separation cell, C-1.

In Figure 6.20, the recorded velocity field vectors of the tracer particle are of higher magnitude on the lower end of the poorly tilted particle bed. The recorded velocity field vectors tend to decrease in magnitude as the tracer particle moves deep into the vertically vibrated particle bed. These observations are in agreement with the previously reported discussions in Section 6.3.1.1.

In this work, the main reasons behind the poorly observed particle bed behaviour and especially the poorly formed particle bed tilt can be linked to the excessive particle loadings and the surrounding fluid circulations during the vertical vibration. In a controlled geometry box when a particle bed undergoes vertical vibration a negative fluid pressure is usually developed very close to its bottom surface during

the particle bed flights (Zeilstra *et al.*, 2006). To offset the effects of this negative fluid pressure the surrounding fluid tends to move in from the areas that offer minimum resistance to its motion. In this case the area offering minimum resistance to fluid motion seems to be the one closest to the partition separation gap. As the fluid moves into the particle bed from the opposite direction it tends to reverse the direction of the separating large size glass particles. The surround fluid motion offered more resistance to the separating large size glass particles and hence those having less momentum were reversed and carried back into the main particle bed. The fluid resistance is expected to increase with an increase in the particle bed height. This may be due to the formation of a thick particle layer with fewer perforations for the surrounding fluid motions close to the partition separation gap. The formation of a thick particle layer close to the partition separation gap can be one of the main reasons for observing the poor particle separation efficiency at particle bed heights above 40 mm.

6.3.2.2 PEPT of the small glass tracer particle in a 20 mm width separation cell, C-1

Figure 6.21 shows the three dimensional motion mapping and average speed of the small glass tracer particle within 1000 seconds of the PEPT time.

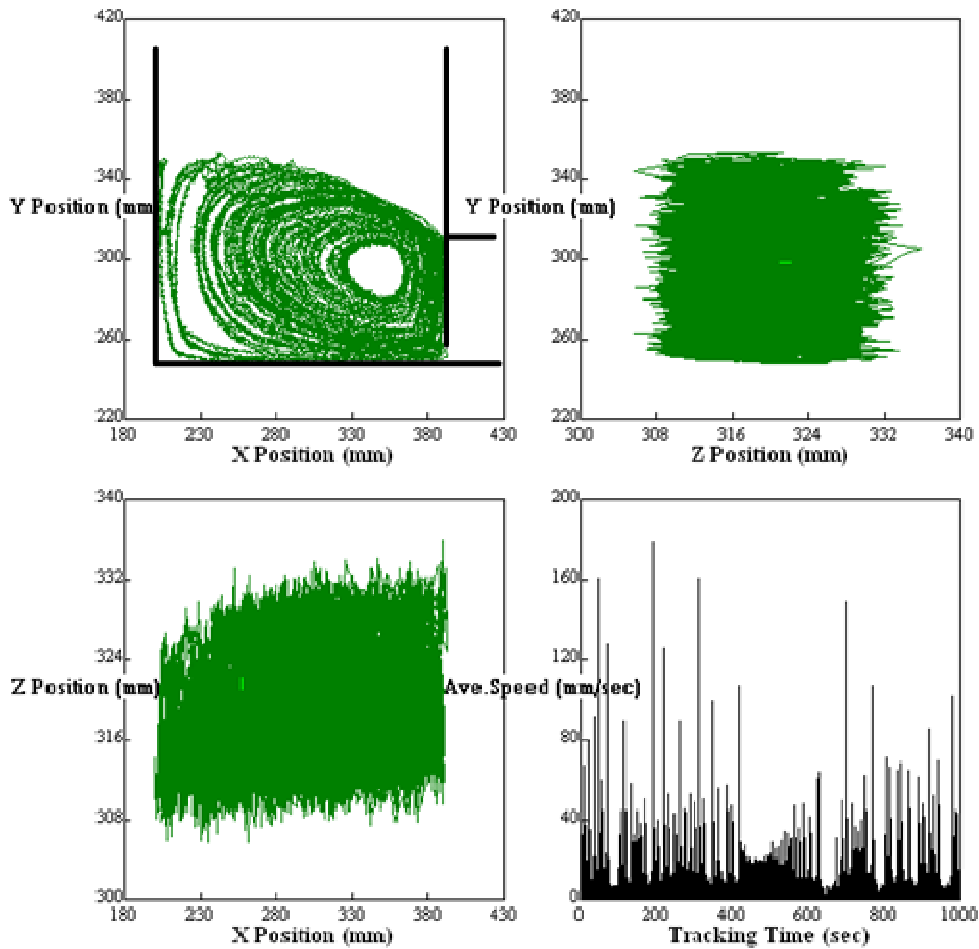


Figure 6.21: The three dimensional small glass tracer location and average speed from start to the end of PEPT experiment in a 20 mm width separation cell, C-1. The recorded real time observations are presented as PEPT-Video-D06 at 10X speed in the provided CD (No.6 in Appendix-D).

The tracer dynamics, represented by Figure 6.21, show an ordered particle motion. Soon after the release of the tracer particle into the

vibrated particle bed it started to move in a clockwise convection current in the inner periphery which gradually expanded to the outer boundaries of the tilted particle bed. In this case, smooth tracer particle motions were observed at all times and no abrupt change in the motion of the tracer particle was recorded. The recorded average speeds of the tracer particle were slightly lower in magnitude in comparison to the large size glass particle tracked in Figure 6.19. The average speed of the small glass tracer particle mostly varied between 20 and 40 mm.s⁻¹, which on some occasions reached as high as 80 mm.s⁻¹ as shown in PEPT-Video-D06 in the provided Compact Disk (CD) (No.6 in Appendix-D). The PEPT-Video-D06 shows the real time dynamics of tracer particle which was recorded 10 times faster than the normal tracer speed. Higher values of the average tracer particle speeds were recorded when the tracer particle slid downhill from the top surface of the tilted particle bed.

The velocity field vectors and occupancy map of the small glass tracer particle in three dimensions is shown in Figure 6.22.

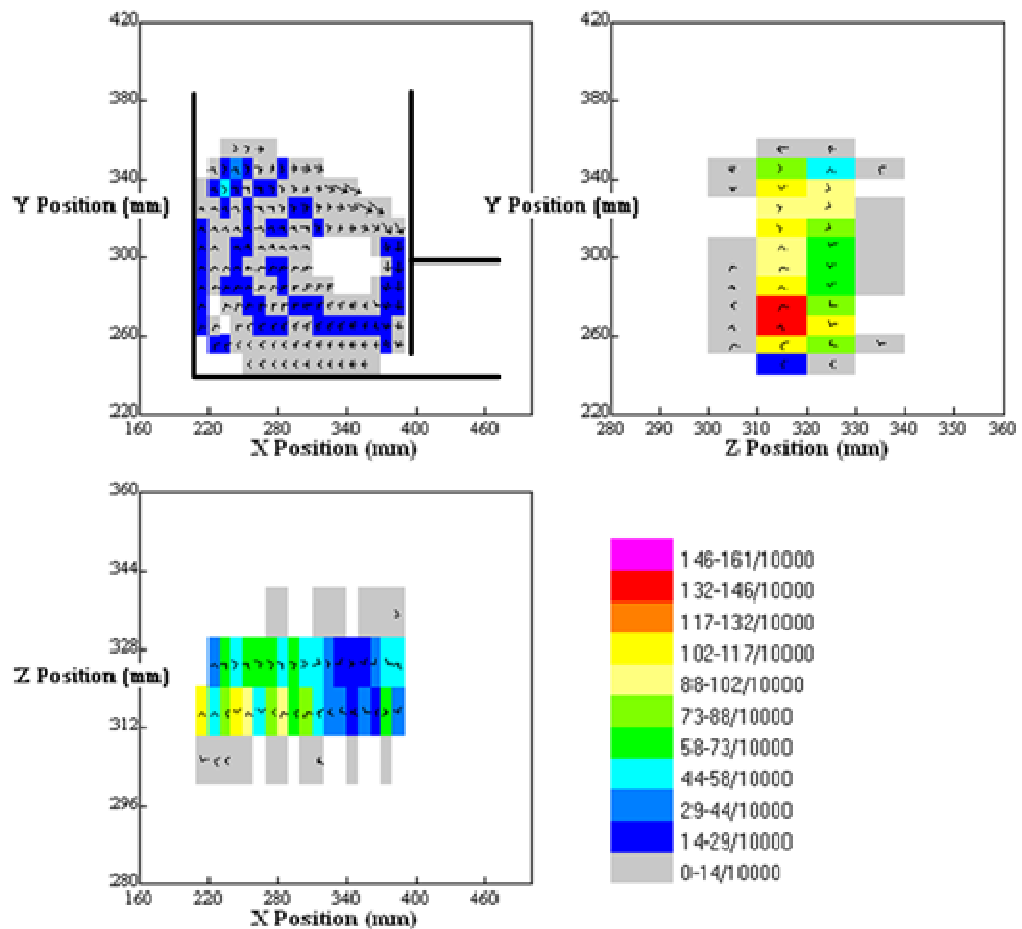


Figure 6.22: The three dimensional motion and occupancy mapping of a small glass tracer particle in separation cell, C-1.

Analysing Figure 6.22 reveals that for most part of the tracking time the tracer particle remained inside the main particle bed, close to the partition separation gap and close to the outer edges of the tilted particle bed. The tracer particle was never seen to show any tendency to move toward the next separate chamber. The length of the velocity field vectors, in Figure 6.22, are of small magnitude which represent a short tracer particle displacement in any direction during 50ms, the standard time over which the velocity field vectors are recorded in each case.

6.3.2.3 PEPT of the large glass tracer particle in a 40 mm width separation cell, C-2

The three dimensional motion mapping and average speed of the large size glass tracer particle at a reduced particle bed height of 40 mm in separation cell, C-2, is shown in Figure 6.23.

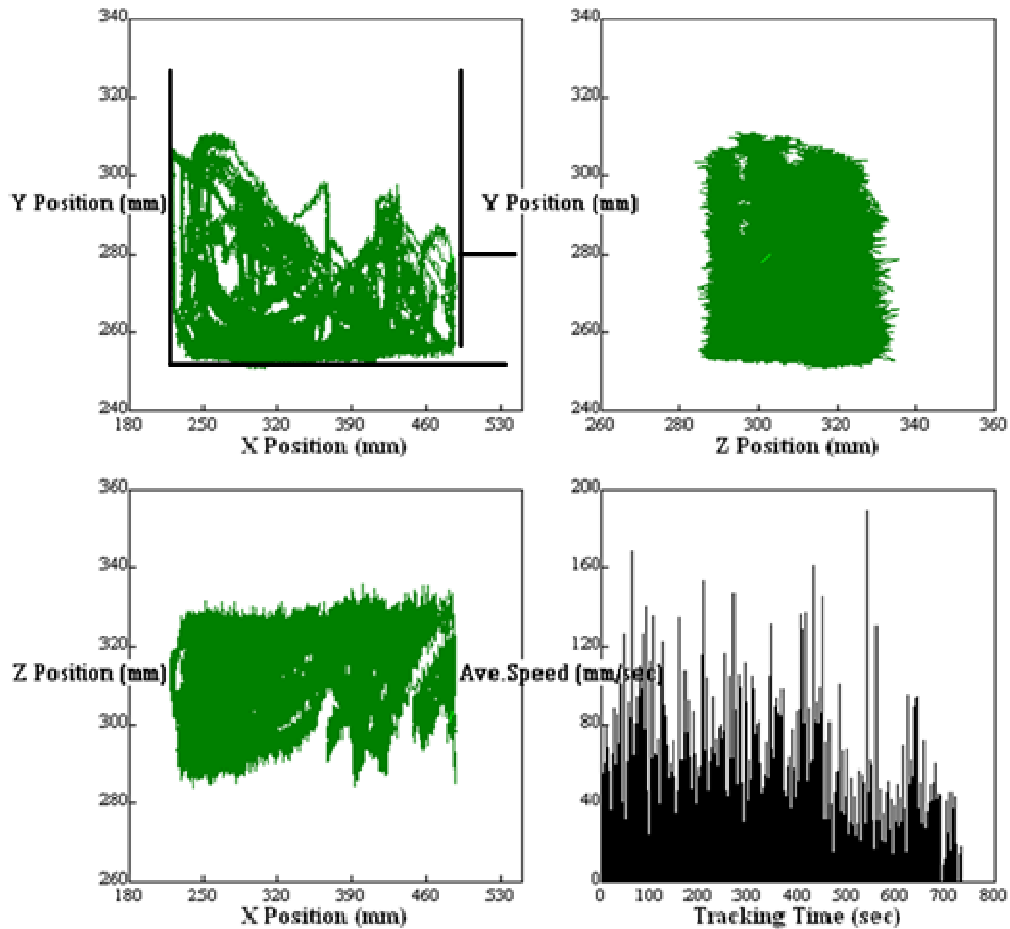


Figure 6.23: The three dimensional large glass tracer location and average speed from start to the end of PEPT experiment in a 40 mm width separation cell, C-2. The recorded real time observations are presented as PEPT-Video-D07 at 10X speed in the provided CD (No.7 in Appendix-D).

The large glass tracer particle reported in this section was tracked over a time period of 750 seconds. Here the tracer tracking revealed an interesting particle motion which was mostly restrained

to a valley shaped particle bed as shown in Figure 6.23, this valley shaped particle bed behaviour has been reported previously in the work of Mohabuth (2007). Nevertheless, soon after the release of the tracer particle into the vertically vibrated particle bed it started to move with the main clockwise convection current which was developed on the opposite side of the vertically vibrated particle bed. For most part of the tracking time (~ 550 seconds) the tracer particle stayed in the main clockwise convection current. However, the tracer particle did showed some tendency to join the local convection current that was moving in the anti-clockwise direction, in close proximity to the partition separation gap. The particle motions in the opposite direction are important to keep a stable valley shape particle bed structure. On occasions the large size glass tracer particle was observed to move in the anti-clockwise direction even within the main convection current. The large glass tracer particle eventually moved into the anti-clockwise local convection current after the initial 600 seconds of the vertical vibration treatment. The tracer motions were, however, still confined to the main particle bed and the tracer did not show any tendency to move towards the next separate chamber, even on a single occasion, within 750 seconds of the vertical vibration treatment. The recorded values of the average speed mostly varied in the range of $60\text{-}80\text{ mm}\cdot\text{s}^{-1}$, which on some occasions reached as high as $100\text{ mm}\cdot\text{s}^{-1}$ as shown in PEPT-Video-D07 in the provided Compact Disk (CD) (No.7 in Appendix-D). The PEPT-Video-D07 shows the real time dynamics of tracer particle which was recorded 10 times faster than the normal tracer speed.

The tracked velocity field vectors and occupancies of the large size glass tracer particle in three dimensions are shown in Figure 6.24.

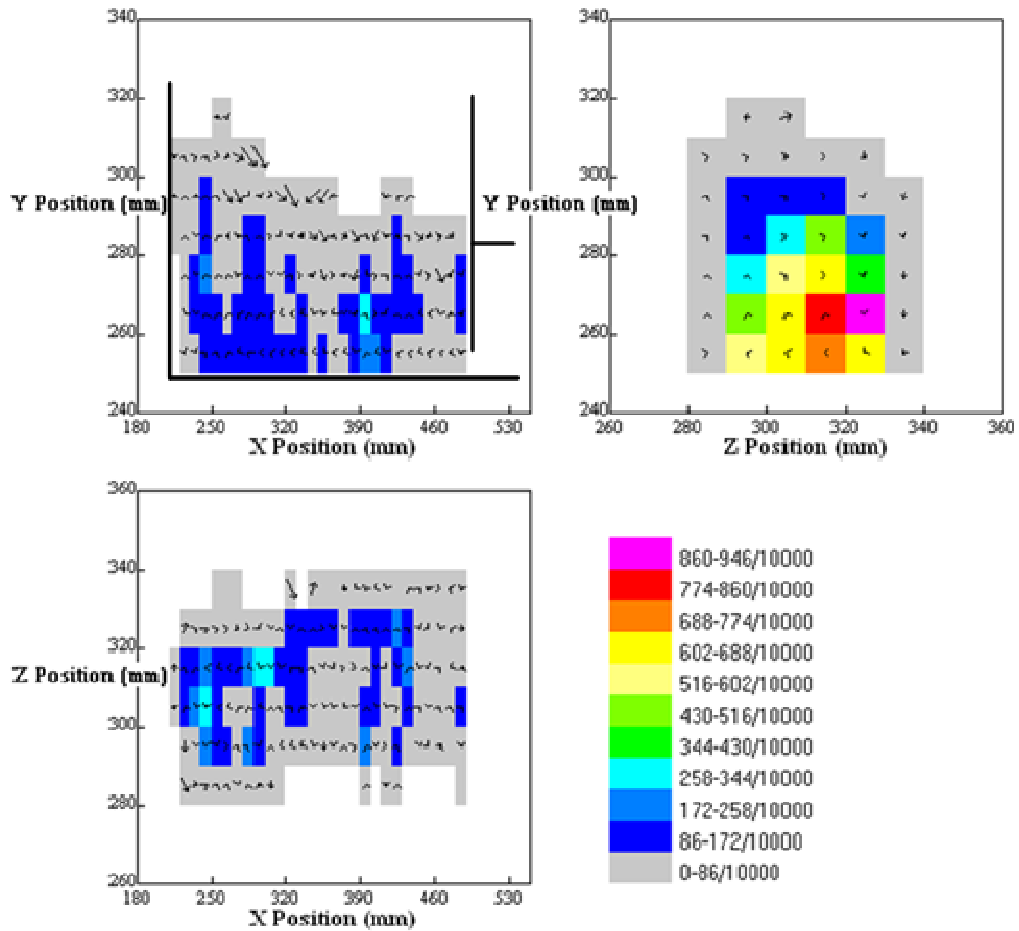


Figure 6.24: The three dimensional motion and occupancy mapping of a large glass tracer particle in separation cell, C-2.

Figure 6.24 shows that for most part of the tracking time the large size glass tracer particle stayed deep inside the vertically vibrated particle bed. This was probably due to the formation of a valley shaped particle bed that contained two distinct convection currents which were moving in opposite directions and were suppressing the tracer particle motions. This suppression eventually resulted in non-separation of the large size glass tracer particle. In line with the previous studies, the velocity field vectors of the tracer particle were stronger on top surface of the particle bed which eventually decreased as the tracer particle moved deep in to the vertically vibrated particle bed.

6.3.2.4 PEPT of the small glass tracer particle in a 40 mm width separation cell, C-2

The three dimensional motion mapping and average speed of the small size glass tracer particle at a reduced particle bed height of 40 mm in separation cell, C-2 is shown in Figure 6.25.

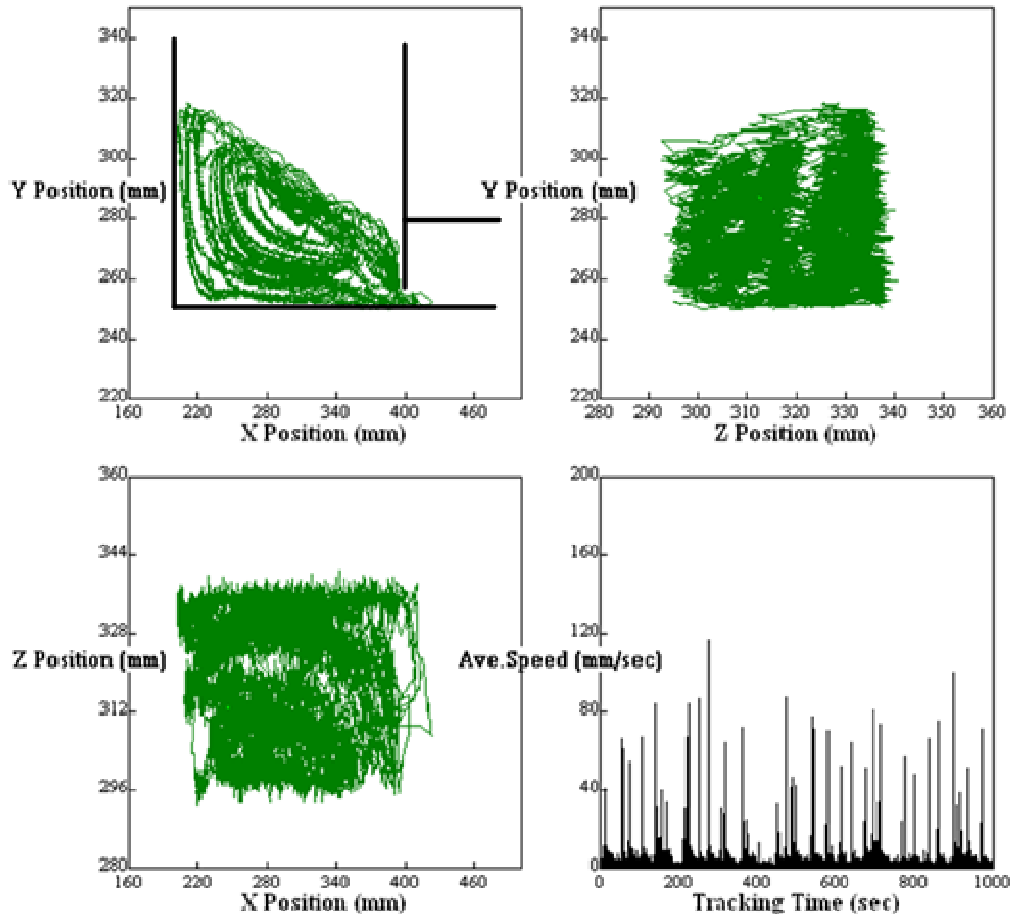


Figure 6.25: The three dimensional small glass tracer location and average speed from start to the end of PEPT experiment in a 40 mm width separation cell, C-2. The recorded real time observations are presented as PEPT-Video-D08 at 10X speed in the provided CD (No.8 in Appendix-D).

In Figure 6.25, a steep tilt formation in comparison to the 80 mm particle bed height (Figure 6.21) can be readily observed. The small glass tracer particle showed a distinctive and well defined convective

motion as is reflected in Figure 6.25. Soon after the release of the tracer particle into the vertically vibrated particle bed it started to move in the outer periphery of the tilted particle bed. However, the tracer motion in the outer periphery of the tilted particle bed did not last for long and soon it entered into the main particle bed. This behaviour is also reflected by the recorded average speeds of the tracer particle which mostly stayed below 30 mm.s^{-1} and seldom increased above 40 mm.s^{-1} . The real time dynamics of the small glass tracer particle is shown in PEPT-Video-D08 in the provided Compact Disk (CD) (No.8 in Appendix-D). The PEPT-Video-D08 shows the real time dynamics of tracer particle which was recorded 10 times faster than the normal tracer speed.

The recorded velocity field vectors and occupancies of the small glass tracer particle are shown in Figure 6.26.

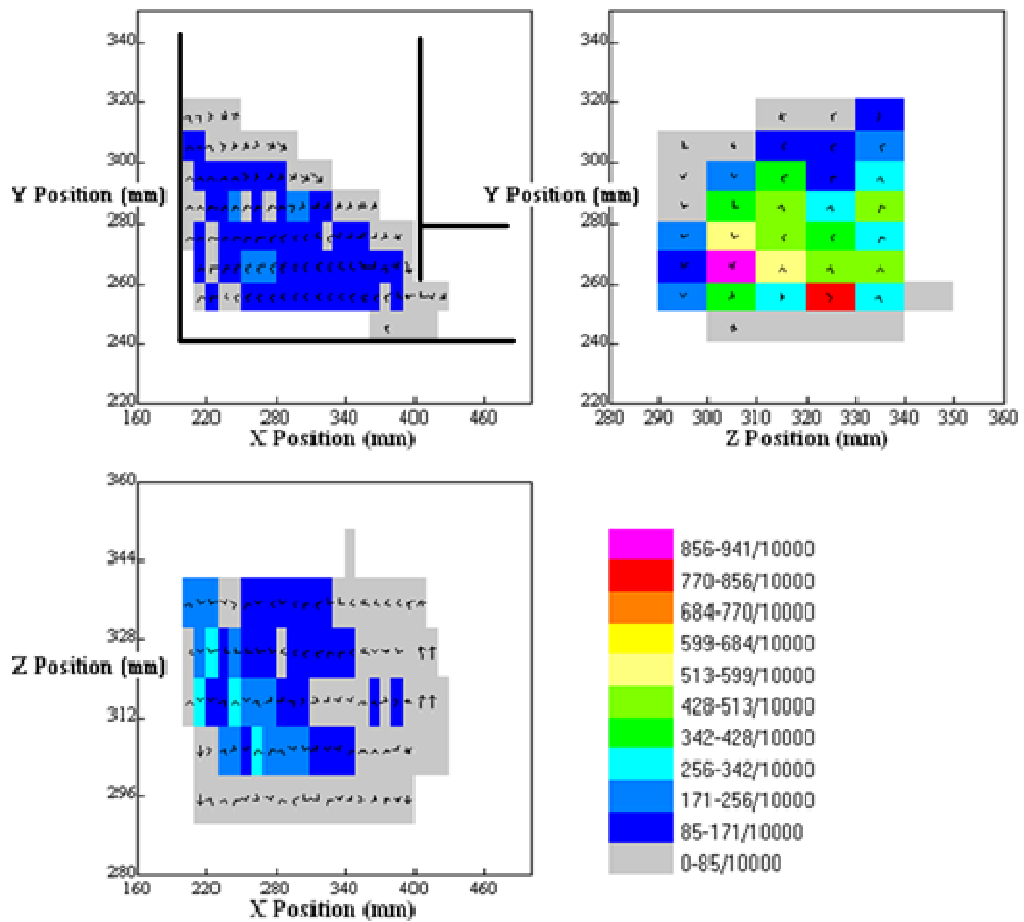


Figure 6.26: The three dimensional motion and occupancy mapping of a small glass tracer particle in separation cell, C-2.

The tracer occupancies were mostly recorded deep inside the particle bed (Figure 6.26) where it predominantly stayed with the parallel type of particles. Owing to the low average speed of the small glass tracer particle, low magnitude of the velocity field vectors were also recorded which, on occasions, were comparatively stronger near to the top surface of the vertically vibrated particle bed.

6.3.3 Sand and ilmenite particle tracking

As discussed in Chapter 2, the density segregation phenomenon in regular shape and parallel size but distinct density particle mixtures is well explored in the literature (Mohabuth, 2007; Burtally *et al.*, 2002 and 2003; Burtally, 2004; Leaper *et al.*, 2005). One such example is the investigations that have focused on the glass and bronze particle mixtures. The use of a regularly shaped particle mixture is important in gaining insight and extending the existing knowledge of a vertically vibrated particle bed. However, the fact that majority of the industrially relevant particle mixtures are of irregular shape has resulted in a renewed interest by many investigations to focus on these particles (Mohabuth, 2007). It is due to this renewed interest that this work investigated the peculiar particle behaviour of an irregular shaped particle mixture which was subjected to the externally driven vertical vibration.

The selection of a sand and ilmenite particle mixture is important considering that both particle species have an inherent complex particle shape and are largely non-cohesive in the fine particle size range that was selected for this work. The sand and ilmenite particle mixture used in this work had a measured density ratio of $\rho_{\text{ilmenite}}(4.79\text{gm.cm}^{-3})/\rho_{\text{sand}}(1.7\text{gm.cm}^{-3})=2.82$. The particle mixture contained ~80% by weight of sand particles while the rest was made up with the ilmenite particles. The particle size distribution of the ilmenite and sand particles is given in Figure 6.27.

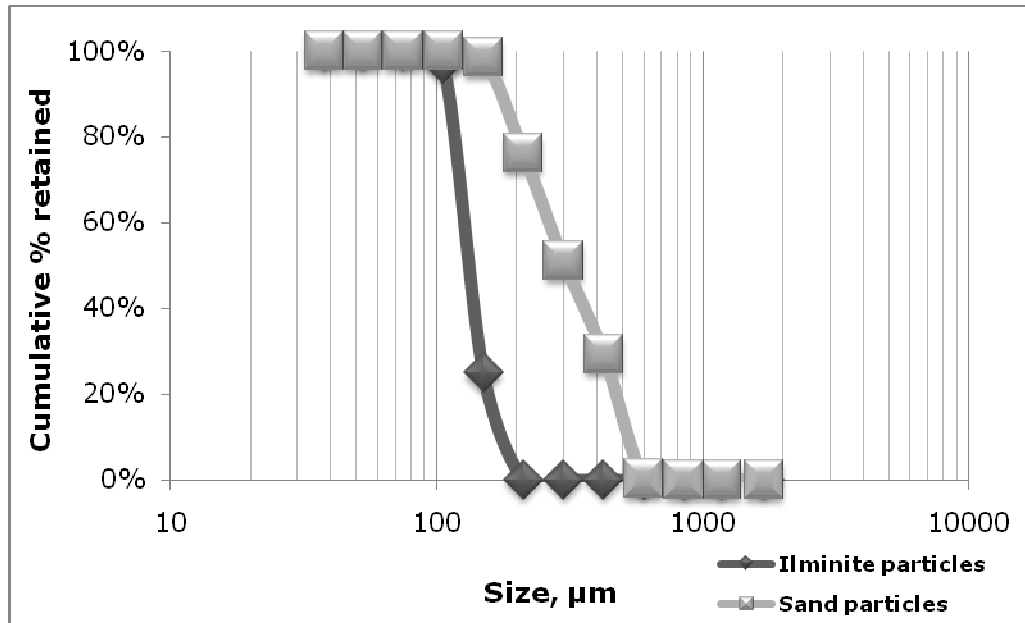


Figure 6.27: Particle size characterisation of the ilmenite and sand particles used in the PEPT investigations.

Figure 6.27 shows the average mass mean diameter of the ilmenite and sand particles to be $137.52\mu\text{m}$ and $336.74\mu\text{m}$ respectively. The selection of these particle sizes was based on consideration that in real particle mixtures the valuable ilmenite fraction is normally distributed in a broad size range of sand particles. Hence, this work is attempted to mimic the preliminary mineral concentration behaviour of the ilmenite and sand particles. A higher than normal weight percentage of the ilmenite particles is only used to visualize the ilmenite concentration behaviour during vertical vibration. Nevertheless, a single ilmenite and sand particle was tracked separately in the individual PEPT investigations. The tracer particle was subjected to the same tracking conditions as previously outlined in Table 6.1. Furthermore, the ilmenite and sand particle mixture formed an average particle bed height of 80 mm in separation cell, C-1 and 40 mm in C-2.

6.3.3.1 PEPT of the ilmenite tracer particle in a 20 mm width separation cell, C-1

The three dimensional motion and average speed of the ilmenite tracer particle within 1000 seconds of tracking time is mapped out in Figure 6.28.

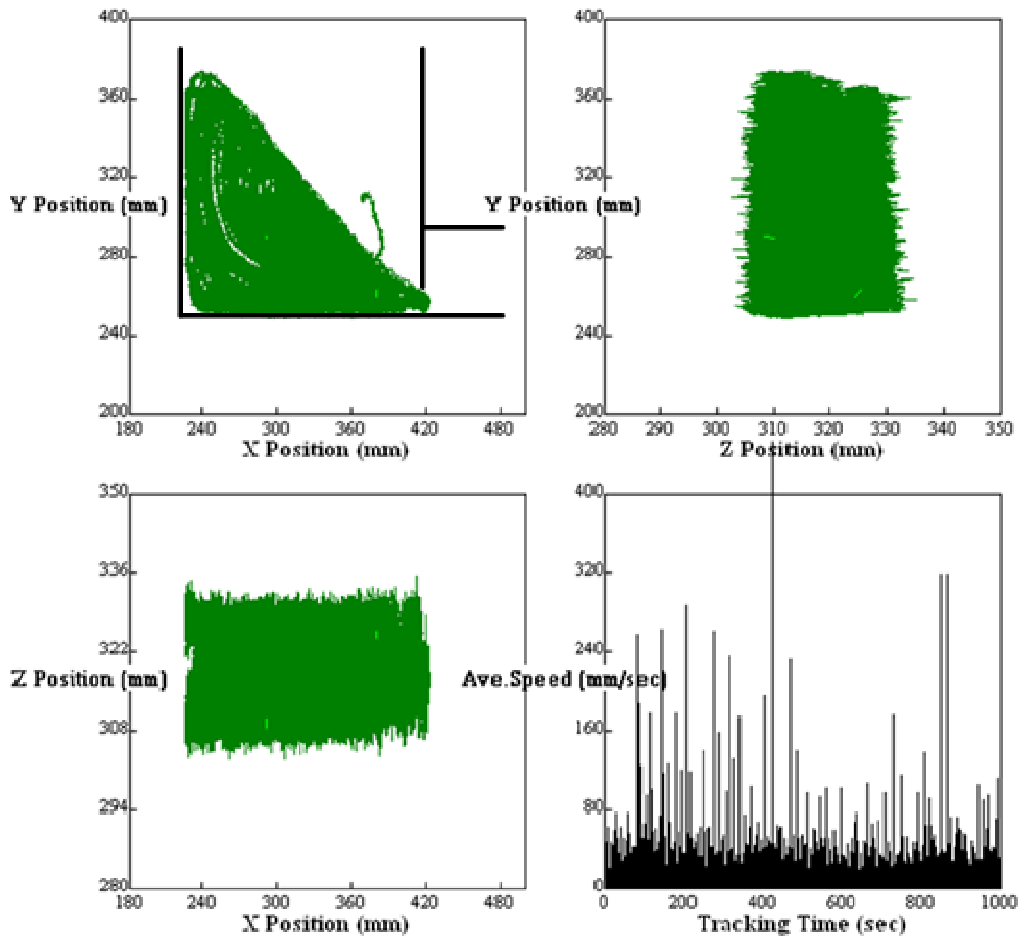


Figure 6.28: The three dimensional ilmenite tracer location and average speed from start to the end of PEPT experiment in a 20 mm width separation cell, C-1. The recorded real time observations are presented as PEPT-Video-D09 at 10X speed in the provided CD (No.9 in Appendix-D).

On an average the tracer particle took ~ 25 seconds to complete a single circulation in the outer periphery of the tilted particle bed. Nevertheless, Figure 6.28 reveals an interesting motion of the

ilmenite tracer particle. Soon after its release on the top surface of the tilted particle bed it started to move in a global convection current that was predominantly moving in the outer periphery of the tilted particle bed. The initial tracer particle motion in the outer periphery did not limit its reach to the inner most parts of the tilted particle bed. The tracer particle entered into the inner regions within the first 50 seconds of vertical vibration. On occasions the motion of the tracer particle was recorded close to the lower end of the tilted particle bed that was in close proximity of the partition separation gap. The tracer particle did show some tendency to move into the next separate chamber but it returned back into the main particle bed after a very short period time. The recorded average speeds of the ilmenite particle were of comparatively higher magnitude when it was sliding downhill from the top surface of the titled particle bed. This is also reflected by the Figure 6.28 where the higher peak measurements represent the higher particle speeds.

The average speed of the tracer particle mostly varied in the range of 40-60 mm.s^{-1} , which on some occasions reached as high as 200 mm.s^{-1} as shown in PEPT-Video-D09 in the provided Compact Disk (CD) (No.9 in Appendix-D). The PEPT-Video-D09 shows the real time dynamics of tracer particle which was recorded 10 times faster than the normal tracer speed. The lower values of ilmenite average speeds were probably recorded due to its inter-particle collision with the large size sand particle that offered more resistance to its motion in the tilted particle bed. Nevertheless, the tracer particle showed a well-constructed convection current motion which was largely due to the existence of a well tilted bed, in this case. Although the circulation path of the tracer particle shrank and expanded within the boundaries of the tilted particle bed it was able to maintain a constant presence in the area that was very close to the top tilted particle bed surface. This tracer particle behaviour is further confirmed by Figure 6.29 where the occupancies and velocity field vectors of the ilmenite tracer particle are mapped.

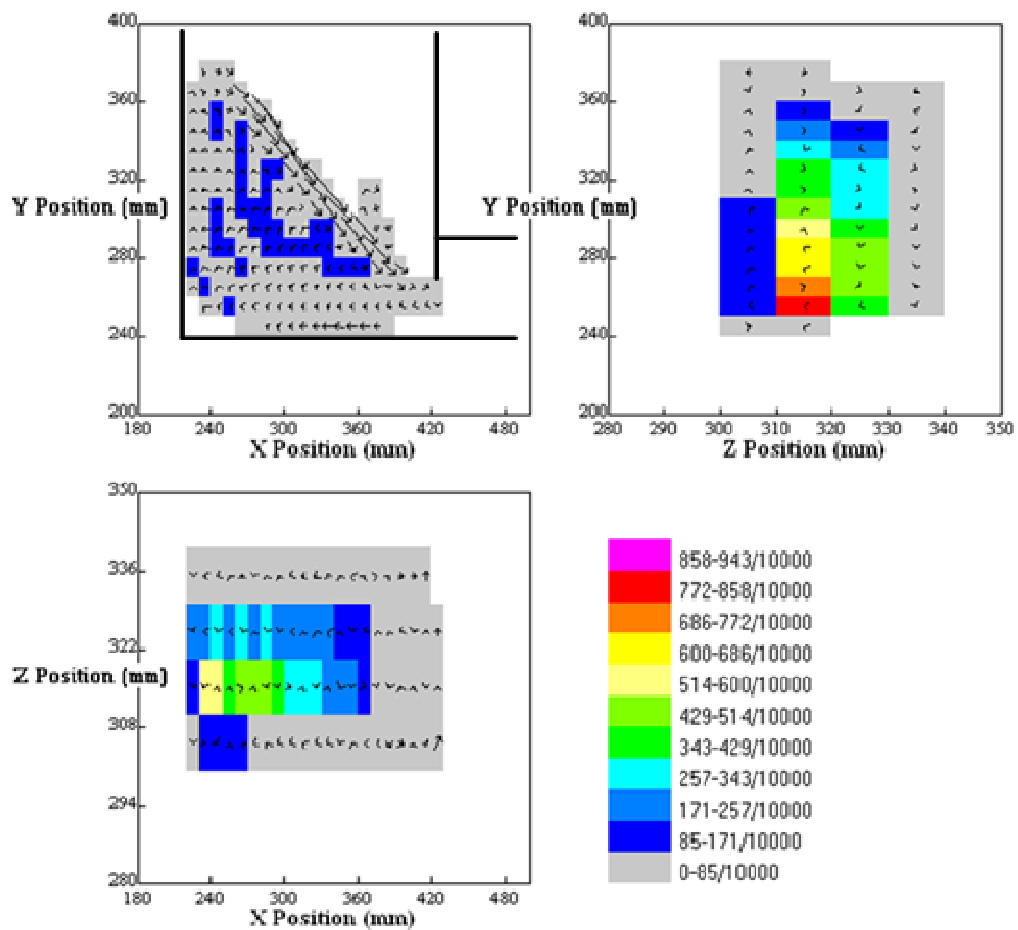


Figure 6.29: The three dimensional motion and occupancy mapping of an ilmenite tracer particle in separation cell, C-1.

Figure 6.29 shows the areas where the maximum occupancy of the ilmenite tracer particle was recorded. The recorded velocity field vectors are of higher magnitude in close proximity to the tilted particle bed surface. The magnitude of the recorded velocity field vectors decreases as the tracer particle moves into the inner regions of the tilted particle bed. These observations are in agreement with the previously reported investigations presented in this work.

6.3.3.2 PEPT of the sand tracer particle in a 20 mm width separation cell, C-1

Figure 6.30 shows the three dimensional motion mapping and average speeds of the sand tracer particle within 1000 seconds of PEPT time.

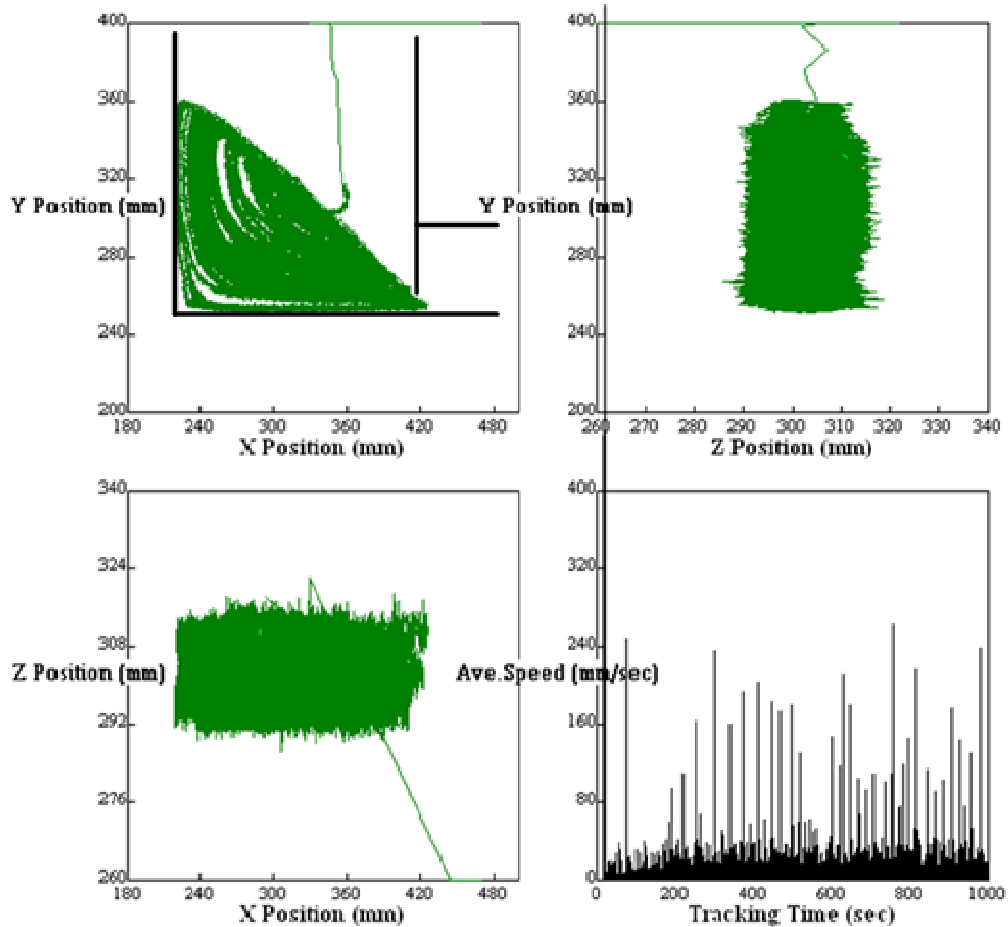


Figure 6.30: The three dimensional sand tracer location and average speed from start to the end of PEPT experiment in a 20 mm width separation cell, C-1. The recorded real time observations are presented as PEPT-Video-D10 at 10X speed in the provided CD (No.10 in Appendix-D).

Figure 6.30 shows almost parallel sand tracer particle motions as were previously exhibited by an ilmenite tracer particle discussed in section 6.3.3.1. Nevertheless, in this study, the tilted particle bed

was able to develop within first few seconds of the vertical vibration. One of the striking differences observed here was the development of a steep tilted particle bed in comparison to a glass and bronze particle mixture under a parallel set of operating conditions. This may be due to the existence of greater inter-particle frictional forces in the sand and ilmenite particle mixture. The steep tilt formation also ensured that a very thin particle layer was developed in close proximity to the partition separation gap, as can be seen in Figure 6.30. The sand tracer particle was not observed to exhibit a stable transfer into the next separate chamber and stayed mostly in the tilted particle bed of the main chamber. The sand tracer particle took almost 10 seconds to complete one single circulation in the outer periphery of the tilted particle bed.

Soon after its introduction the sand tracer particle started to move to the outer periphery of the tilted particle bed where it spent the first 200 seconds of the tracking time. However soon after the initial phase in the outer territory the tracer particle started to move into the inner regions of the vibrated particle bed and stayed there in a sand rich local convection current. However, the inner and outer convection currents were observed to overlap occasionally and the tracer particle was able to smoothly switch between the two. During the course of this convection current switching the sand tracer particle was observed to end up on the top surface of the tilted particle bed and moved downhill with high speed. The average speed of the tracer particle varied largely in the range of 20-40 mm.s⁻¹, which on some occasions reached as high as 200 mm.s⁻¹ as shown in PEPT-Video-D10 in the provided Compact Disk (CD) (No.10 in Appendix-D). The PEPT-Video-D10 shows the real time dynamics of tracer particle which was recorded 10 times faster than the normal tracer speed. Low magnitudes of the recorded average speeds of the tracer particle in this case give some indication regarding the tracer location which was probably deep inside the tilted particle bed.

The velocity field vectors and an occupancy map of the sand ilmenite particle in three dimensions is shown in Figure 6.31.

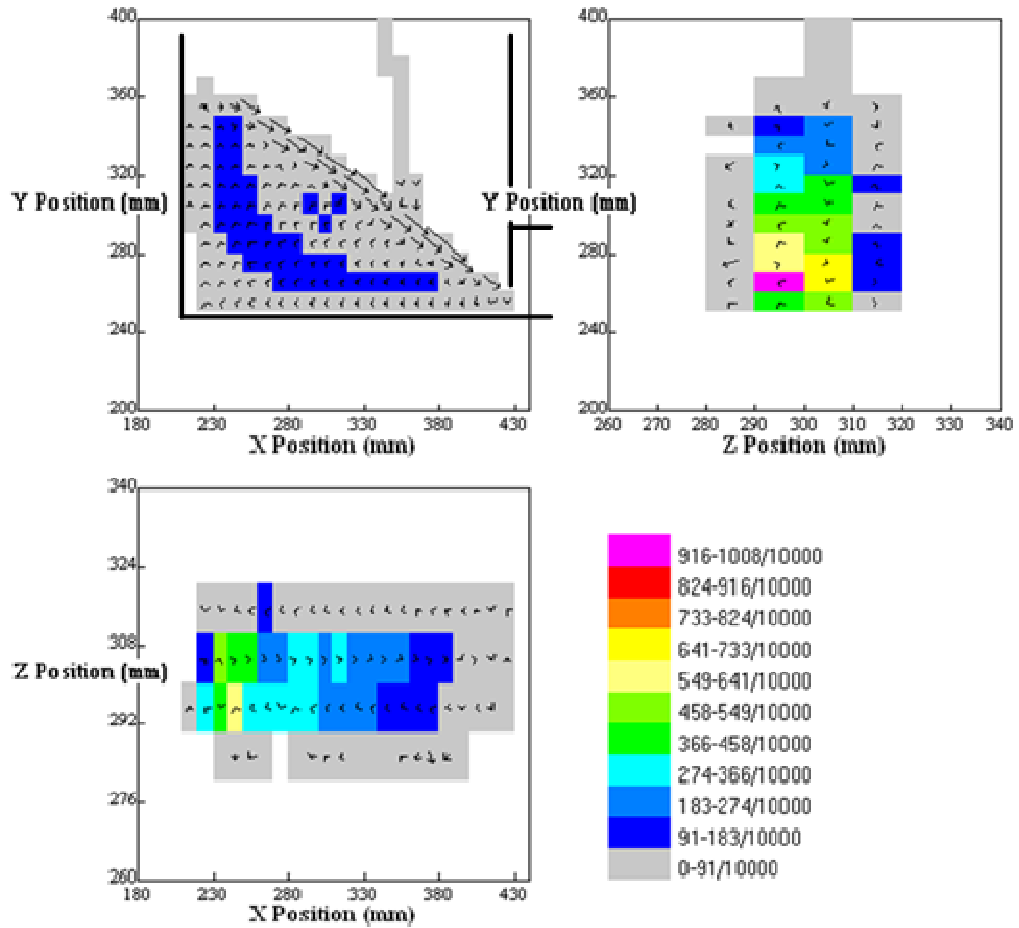


Figure 6.31: The three dimensional motion and occupancy mapping of a sand tracer particle in separation cell, C-1.

Figure 6.31 confirms the observations made previously where a maximum occupancy of the sand tracer particle is found to be in middle of the tilted particle bed. Furthermore, the maximum values of the velocity field vectors are found to be on top surface of the tilted particle bed which is in agreement with the previous reported investigations in this work.

6.3.3.3 PEPT of the ilmenite tracer particle in a 40 mm width separation cell, C-2

The three dimensional motion mapping and average speed of the ilmenite tracer particle at a reduced particle bed height of 40 mm in separation cell, C-2, is shown in Figure 6.32.

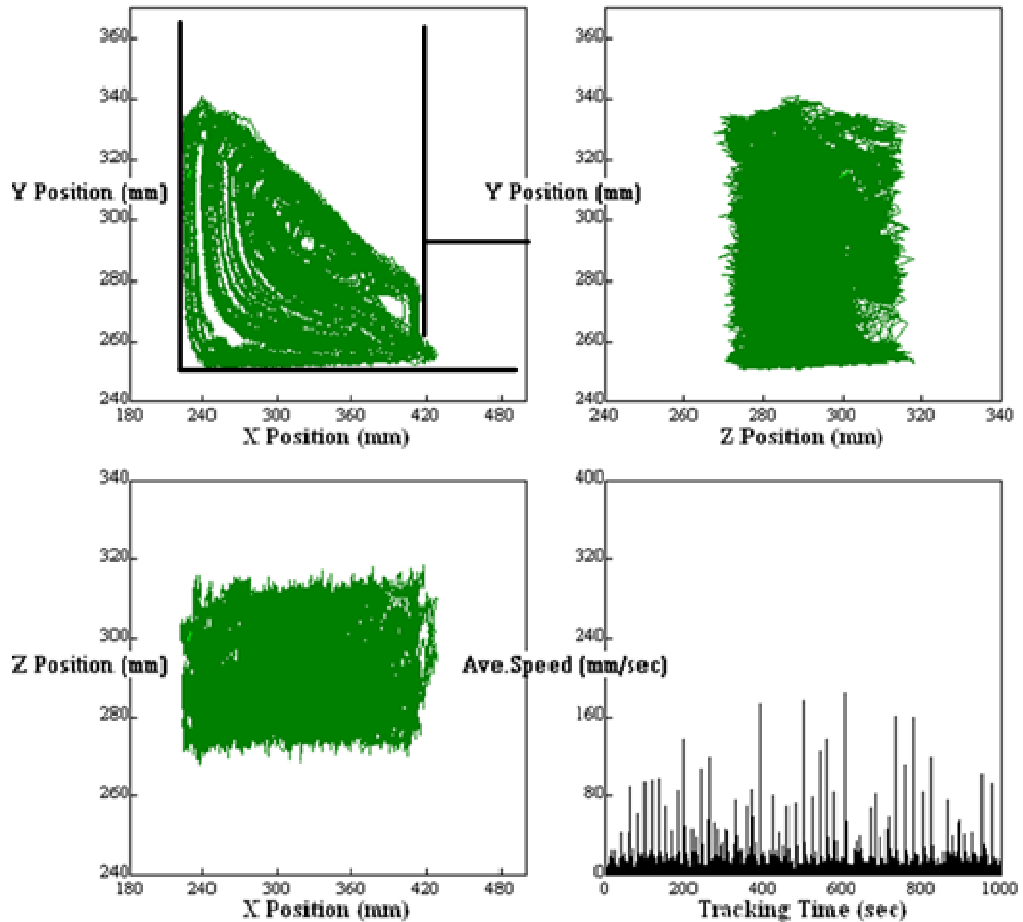


Figure 6.32: The three dimensional ilmenite tracer location and average speed from start to the end of PEPT experiment in a 40 mm width separation cell, C-2. The recorded real time observations are presented as PEPT-Video-D11 at 10X speed in the provided CD (No.11 in Appendix-D).

In this set of experiments the ilmenite tracer particle showed similar behaviour as discussed in Section 6.3.3.1. Soon after the release of the ilmenite tracer particle it started to move in the outer territory

of the tilted particle bed. However its motions were not just limited in the outer periphery, it also occupied the inner regions of the tilted particle bed, as shown in Figure 6.32. The tilted bed formation was not as steep as was observed in the previous cases that involved the sand and ilmenite particle mixtures. The recorded average speeds of the tracer particle were of low magnitude and mostly varied in the range of 20-30 mm.s⁻¹, which on some occasions reached as high as 80 mm.s⁻¹ as shown in PEPT-Video-D11 in the provided Compact Disk (CD) (No.11 in Appendix-D). The PEPT-Video-D11 shows the real time dynamics of tracer particle which was recorded 10 times faster than the normal tracer speed. The ilmenite tracer particle nearly took 25 seconds to complete a single circulation in the outer periphery of the tilted particle bed. Despite the high density of the ilmenite tracer particle it was unable to move into the next separate chamber.

Figure 6.33 shows the occupancy and velocity field vectors of the ilmenite tracer particle.

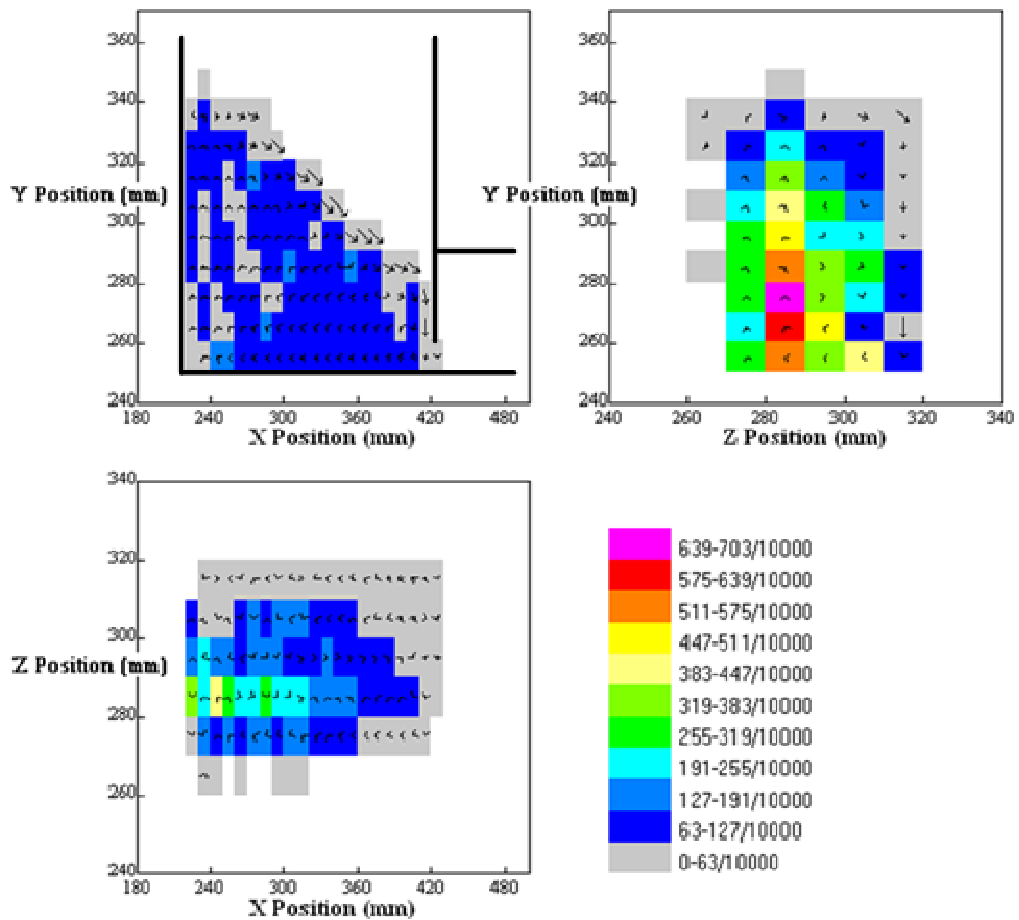


Figure 6.33: The three dimensional motion and occupancy mapping of an ilmenite tracer particle in separation cell, C-2.

The occupancy map of the ilmenite tracer particle, Figure 6.33, illustrates that the tracer particle was mostly trapped in the inner regions of the main particle bed. The maximum occupancy of the ilmenite particle is shown to be deep inside the tilted particle bed. This behaviour is different to the previous observations where a high density particle, such as bronze, was observed to stay in close proximity of the partition separation gap and steadily move into the next separate chamber at a reduced particle bed height of 40 mm. The ilmenite behaviour observed here is may be due to its high density but small size in comparison to the other sand particles in the mixture.

6.3.3.4 PEPT of the sand tracer particle in a 40 mm width separation cell, C-2

The three dimensional motion mapping and average speed of the ilmenite tracer particle at a reduced particle bed height of 40 mm in separation cell, C-2 is shown in Figure 6.34.

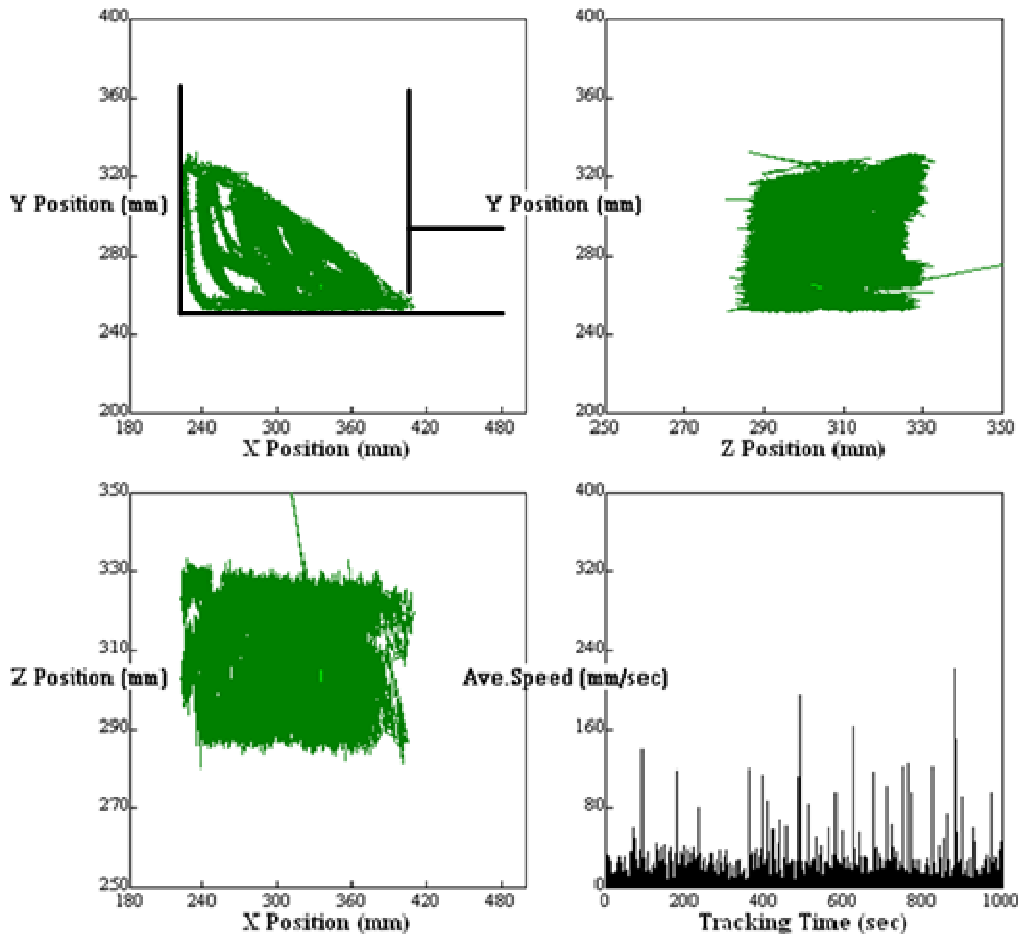


Figure 6.34: The three dimensional sand tracer location and average speed from start to the end of PEPT experiment in a 40 mm width separation cell, C-2. The recorded real time observations are presented as PEPT-Video-D12 at 10X speed in the provided CD (No.12 in Appendix-D).

The PEPT investigations at a reduced particle bed height of 40 mm, in Figure 6.34, showed the occasional trapping of the sand tracer particle in a local convection current of predominantly sand particles

that was able to develop near to the top of the tilted particle bed. The tracer particle remained trapped there for the initial 50 seconds of the tracking time. However, soon after the release of the tracer particle from this local convection current it started to move in a global convection current that was patrolling the outer periphery of the tilted particle bed. The tracer particle was mostly observed to move in the areas that were deep inside the tilted particle bed. A well-constructed and steep particle bed surface was able to develop however it still did not allowed the tracer particle to move into the next separate chamber. The average speed of the tracer particle mostly varied in the range of 20-30 mm.s⁻¹, which on some occasions reached as high as 60 mm.s⁻¹ as shown in PEPT-Video-D12 in the provided Compact Disk (CD) (No.12 in Appendix-D). The PEPT-Video-D12 shows the real time dynamics of tracer particle which was recorded 10 times faster than the normal tracer speed. The tracer particle took nearly 20 seconds to complete a single circulation in the outer periphery of the tilted particle bed.

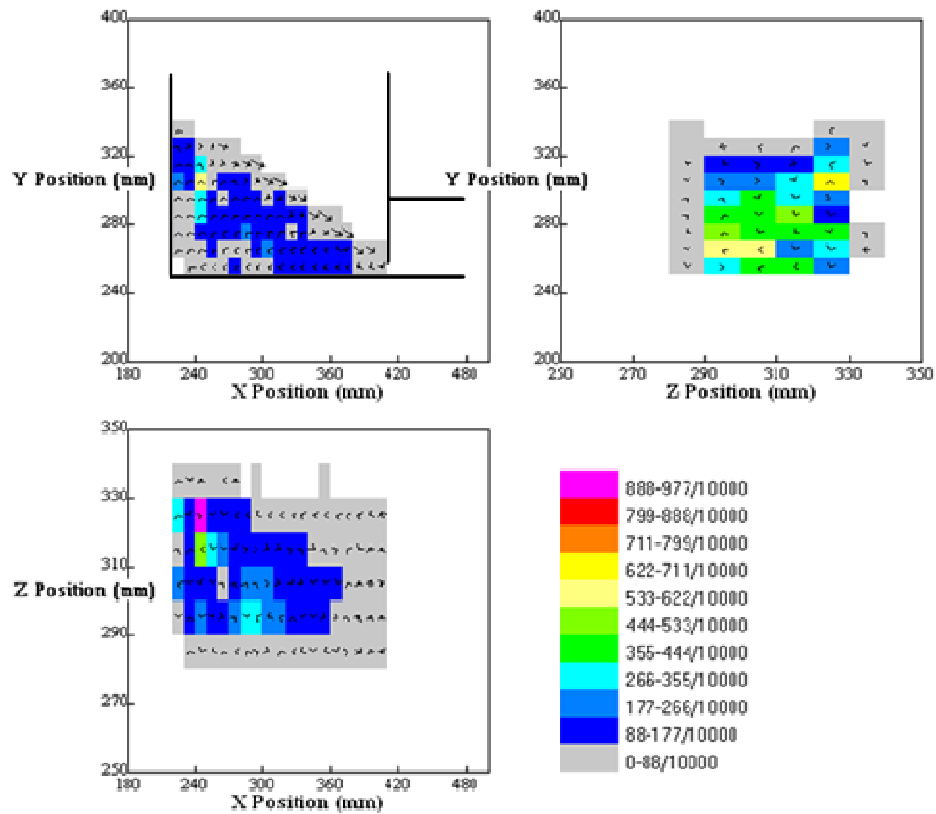


Figure 6.35: The three dimensional motion and occupancy mapping of a sand tracer particle in separation cell, C-2.

The above observations are further confirmed when the occupancy and velocity field vectors of the tracer particle are observed, as shown in Figure 6.35. The maximum occupancies of the tracer particle are recorded in the inner regions of the tilted particle bed. The velocity field vectors are stronger on top surface of the tilted particle bed and their magnitude decreases as the tracer particle moved deep into the tilted particle bed.

6.4 Concluding remarks

Based on the explored particle dynamics of various tracer particles via PEPT in this chapter the following conclusions can be deduced;

- ❖ PEPT is a non-invasive technique in which a tracer particle emits pair of gamma photons and the detection of these enables tracer trajectory to be followed in three dimensions (X, Y and Z-axis) inside an actual engineering structure.
- ❖ In this work identical tracer particles, as that of the bulk material, were used.
- ❖ Tracer production was done via a cyclotron.
- ❖ In this work, PEPT was used to examine the particle motion behaviour in the vertically vibrated beds of different working particle mixtures.
- ❖ Particle tracking was done in low as well as high particle bed height working mixture in the 20 (C1) and 40mm (C2) width separation cells.
- ❖ Regular as well as irregular shaped working particle mixtures were investigated in this work.
- ❖ The PEPT study reported here agrees well with the segregation experiments reported in Chapter 2.
- ❖ In this study the tracked tracer particle motions confirmed that particle segregation is a strong function of particle bed height and convection currents.

Dry separation of solid waste mixtures

7.1 Introduction

Previous chapters have focussed on the operational aspects of vibration induced dry separation behaviours of synthetic working particle mixtures of varying compositions. Many researchers (Burtally *et al.*, 2002, 2003, & 2004; Leaper *et al.*, 2005; Naylor *et al.*, 2003) have used narrowly sized and spherical shaped glass and bronze synthetic mixtures in their vertical vibration induced particle separation investigations. The use of a synthetic mixture is important in gaining greater understanding of a particle separation process and has remained popular despite the fact that majority of industrially relevant particle mixtures are of varying size, shape and composition (Serero *et al.*, 2006; Castellanos, 2005).

Often, the variations in bulk physical properties of different particulate materials, before any physical separation operation, are

in direct relation to their initial processing such as crushing, grinding, tabling and screening (Wills, 1997). The un-liberated and complex particle mixtures encountered in mineral, chemical, pharmaceutical and recycling industries are normally passed through various size reduction steps to increase their degree of component liberation. These operations often result in production of a continuous size range and liberated particle mixtures of varying shapes.

Mohabuth *et al.*, (2005 & 2007) demonstrated the use of vertical vibration in separating the certain size range WEEE particle mixtures of complex shapes. However, instead of using a narrow size range (as used by Mohabuth *et al.*, 2005 & 2007) WEEE particle mixture, the use of continuous and broader size range WEEE particle mixtures could result in reduction of initial feed preparation stages such as, particle pre-sizing, before any vertical vibration induced particle separation operation. A wider particle size range could be defined as one without any particle pre-sizing. Nevertheless, the predominantly idealised nature of feed materials used in the previously reported work (Burtally, 2004; Burtally *et al.*, 2002 and 2003; Leaper *et al.*, 2005; Mohabuth, 2007) has determined the scope for this work to explore the potential application of a scaled up vertical vibration separation technique to separate different industrially relevant finely sized solid waste mixtures having continuous size distributions.

7.2 Solid waste WEEE mixtures

According to the Waste Framework Directive (WFD) (European Directive (WFD) 2006/12/EC as amended by new WFD Directive 2008/98/EC), waste is defined as;

“Any substance or object the holder discards; intends to discard or is required to discard”.

The Environment Agency in the UK considers waste to remain waste until fully recovered in an un-harmful way to the environment and/or human health (Wrap, 2009). The proactive recovery and recycling of valuable resources from waste streams should result in enhanced environmental sustainability of the planet. Solid waste can be generated in a number of ways, for example, as “scrap” from a mechanical manufacturing process or from End of Life (EOL) Waste Electrical and Electronic Equipment (WEEE) originating from a variety of consumers.

Electrical and Electronic Equipment (EEE) have infiltrated almost every aspect of our modern daily lives. It has provided us with the comfort of easy information acquisition and exchange. It has also resulted in bringing health and security into our routine daily lives (Hannequart, 2003). However, all these benefits are at the risk of being offset with the increased generation of WEEE which has the potential to harm our environment. There is an increase in WEEE due to an ever increasing EEE replacement frequency which in turn is triggered by the quality, quantity and intensity of human activities that are increasing at an exponential rate (Huisman *et al.*, 2008). During 2007-2010, the projected total WEEE arising in India were estimated to be 2.5 million metric tons which included waste from computers (30% of total units of WEEE generated), televisions refrigerators and washing machines (Dwivedy and Mittal, 2010). In Chile, it is estimated that about 10,000 to 20,000 tons of end of life computer waste will be generated in the years 2010 and 2011 (Steubing *et al.*, 2010). The global production of E-waste in 2006 was estimated to be 20-25 million tonnes per year (Robinson, 2009). However, the exact figure remains controversial and others (UNEP, 2005) have estimated the global E-waste production amount to be around 20-50 million tonnes.

The increasing WEEE volumes recorded each year are due to technological innovation, market expansion, shorter product life cycles, market expansion, falling prices, switchover from analogue to digital broadcasting and improvements in the economy (Huisman *et al.*, 2008). This has resulted in electrical and electronic equipment (EEE) to have an increasing market penetration in developing countries and replacement market in developed countries. The European Union (EU) expansion from EU15 to EU27 has resulted in an increased amount of WEEE. In EU, WEEE amounts were estimated to be in excess of 9.1 million tonnes in 2005 and this amount is expected to increase at a rate of 2.7% each year, possibly reaching a figure of 12.3 million tonnes in 2020 (Huisman *et al.*, 2008; Robinson, 2009). The average compositional breakdown of WEEE in EU is shown in Figure 7.1.

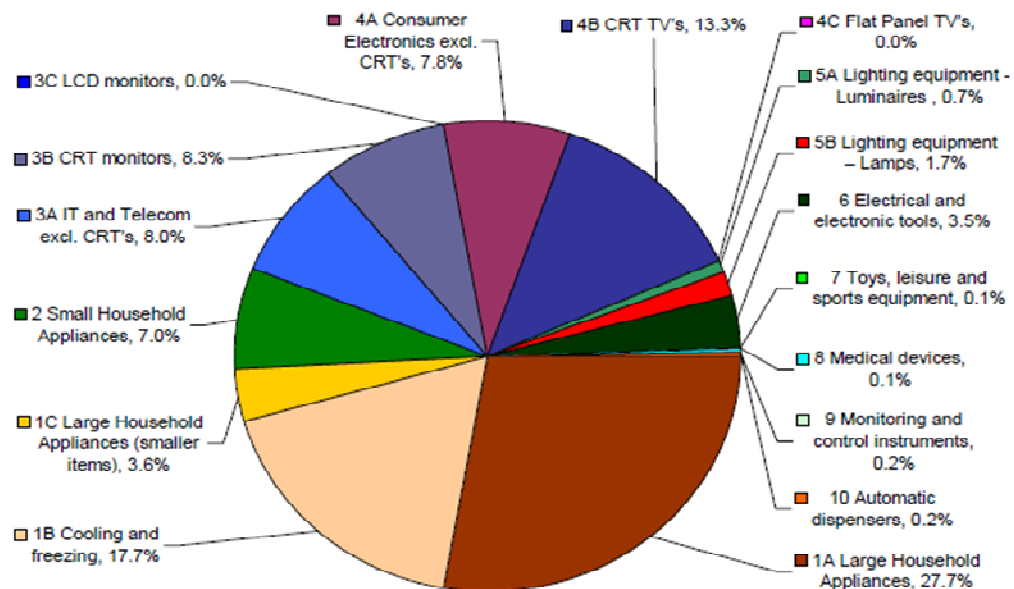


Figure 7.1: Breakdown of EC WEEE arising in 2005 (Adapted from Huisman *et al.*, 2008).

Among all, Consumer Electronic Devices (CED), IT and telecom forms a significant 16% of all arising (Huisman *et al.*, 2008). There is an obligation to safely dispose of WEEE to protect our environment and society. This obligation is enforced by the

European Commission (EC) through various environmental regulations such as Waste Framework Directive, (2003). In addition, customer, politicians and Non-Governmental Organisations (NGOs) perception on various environmental issues also play an important role on E-waste recycling strategies (Robinson, 2009). All these combined efforts have resulted in introducing an Environmentally Conscious Manufacturing (ECM), End of Life (EOL) Product Recovery Obligation (ECMPRO), Zero Waste (ZW) and E-Waste Recycling System based on product design (Schaik and Reuter, 2010) concepts among many different industrial and environmental concerns (Gungor and Gupta, 1998; Jofre and Morioka, 2005). Due to the limited scope of this work these concepts will not be discussed in detail here.

The UK WEEE arising in 2009 were estimated at 1.18million tonnes, with an annual growth rate of ~4% in the subsequent years, possibly reaching a figure of 1.61million tonnes in 2017 (Defra, 2009). The Restricting of the Use of Certain Hazardous Substances in Electrical and Electronic Equipment Regulations (RoHS) 2008, restricted the use of certain hazardous substances, such as lead, mercury, cadmium, chromium, poly-brominated bi-phenyls and poly-brominated di-phenyl ethers (Table 7.1) (Bigum and Brogaard, 2009; Robinson, 2009) in WEEE and promoting the collection and recycling of these materials has been enforced in European Commission (EC) since February 2003 (Category 3 dealing with IT and Telecommunication equipment in Waste Framework Directive, 2003).

Banned compounds in RoHS, 2002
Lead
Mercury
Cadmium
Hexavalent Chromium
Poly-brominated biphenyls (PBB)
Poly-brominated di-phenyl ethers (PBDE)

Table 7.1: Banned compounds in the RoHS (Restriction of Hazardous Substances) directive, 2002 (Adapted from Bigum and Brogaard, 2009).

The WEEE Directive (Waste Framework Directive, 2003) also aims to improve the environmental performance of all EEE stakeholders and sets requirements relating to the criteria for collection, treatment, recycling and recovery of WEEE. It obligates producers to financing most of the above activities while retailer/distributors are required to take back all WEEE. This directive became law in the UK in January, 2007. The directive encourages member states to collect and recycle at least 4kg of WEEE per inhabitant each year (Science Daily, 2007; Waste Framework Directive, 2003).

Despite all waste framework directives and associated legislation the fate of WEEE is of concern as only one third of it is reported to be appropriately treated in the EC (Science Daily, 2007). The other two thirds are potentially going to landfill or ending up in sub-standard treatment sites in and/or outside EU. The use of low tech manual recycling technologies such as burning, acid dissolution and reuse poses a significant risk to the human health and global environment (Robinson, 2009). One of the major reasons for mismanaging WEEE is its inherently complex and multi-faceted nature. Complete WEEE management requires many technical, economic and educational questions to be answered (Science Daily, 2007). However, in the absence of any survey based data on estimates of stockpiled e-waste, it has been necessary to use statistics based on industry sale data, estimated product lifespan

and assumptions regarding the consumer behaviours. These data have shown that for all white goods arising, 40% of large appliances (e.g. refrigerators, washing machines, air conditioners, electric stoves, water heaters), 25% of medium devices (e.g., toys, microwaves, electronic cooker) and close to zero for most small scale brown products (e.g. mobiles, DVD players, laptops, MP3 players, hand held games computers, televisions) are being collected for recycling in EC (Science Daily, 2007). Nevertheless, an increased public demand to curb WEEE exports to developing countries is putting pressure on policymakers and recyclers to expand their existing infrastructures to treat WEEE. The EC has therefore proposed a mandatory collection target equal to 65% of the average weight of all EEE placed on the market over the two previous years (EUROPA, 2009).

The improper discarding of waste Consumer Electronic Devices (CED) poses a threat to public and environmental health (Dimitrakakis, *et al.*, 2009; Tsydenova and Bengtsson, 2010). The investigation carried by Tang *et al.*, (2010) has reported alarming levels of heavy metal and organic compound deposition in soil in Wenling (an emerging e-waste recycling city in China). Despite the obligation for separate collection and recycling of CED, 0.4-1.5wt% can still be found in the household residual waste streams. Waste CED are strongly believed to contribute to the hazardous pollution loads as they contain many leach-able toxic elements such as lead, cadmium and bromine. However, in new CED there has been an increasing trend to use less hazardous materials (Dimitrakakis, *et al.*, 2009). This observation is also reflected in Table 7.2. However, the reported values in Table 7.2 are still subjected to arguments as they refer to many different methodological approaches and diverse sampling conditions.

Element	RoHS Limit (ppm)	Literature data (concentrations in mg.kg ⁻¹)							
		Dimitrakakis <i>et al.</i> , (2009)		Morf <i>et al.</i> , (2001)	Vehlow & Mark, (1997)	APME & VKE (1997)	Fink <i>et al.</i> , (2000)	Rotter <i>et al.</i> , (2006)	Nnorom & Osibanjo, (2009)
		HXRAF	AAS						
Pb	1000	34	17.41	1900	100-2100	127-165	500-1000	40-196	5-340
Cd	100	38	5.71	160	30-240	115-186	200-2000	2.3-56	4.6-1005
Hg	1000	53	-	0.31	-	0.3-1.4	-	0.29-15	-
Cl	-	-	-	8600	1900-11,000	6300-6400	-	Not detected (N.D)	-
Br	1000	5300	-	-	4300-41,000	4200-6800	150-250,000	N.D	-
Ni	-	480	-	1300	90-800	299-703	-	19-30	5-11,000
Zn	-	360	-	2300	620-5100	361-520	120-5000	187-269	-
Cu	-	570	-	18,000	80-105,000	-	-	391-406	-
Cr	1000	100	8.38	900	60-380	34-71	-	-	-
Sb	-	2000	-	3500	2000-13,000	-	1000-80,000	-	-
Fe	-	780	-	11,000	440-3300	1483-1673	-	-	-
Sn	-	140	-	2300	60-2100	139-267	500-3000	-	-
V	-	430	-	-	35-900	-	-	-	-
Ti	-	8000	-	-	1500-18,400	4187-4767	300-90,000	-	-
As	-	21	-	-	9-46	Up to 10	-	-	-

Table 7.2: Change in elemental concentrations (mg.kg⁻¹) of CED with time (Adapted from Dimitrakakis, *et al.*, 2009).

In EEE, a Printed Circuit Board (PCB) forms a platform upon which microelectronic components such as semiconductor chips and capacitors are mounted. The PCB provides the electrical interactions between components and is an integral part of all EEE such as mobiles, computers, televisions and more (Lincoln *et al.*, 2007). It's components contain numerous toxic materials, such as lead, zinc, copper, antimony, cadmium, brominated flame retardants and mercury, which if discarded improperly, have the potential to contaminate groundwater and soil (Lincoln *et al.*, 2007; Robinson, 2009). Hence, this represents a significant probable risk.

Contrary to the above, WEEE might well be considered as a valuable resource. The recovery and recycling of various valuable fractions from it could result in significant savings of energy, virgin resources and environment (Cui and Forssberg, 2003). In any developing and developed country, resource recovery forms an integral part of overall economic growth. The use of recycled copper and plastics alone could result in an energy saving of >80% over the virgin materials (Cui and Forssberg, 2003). Beside legislations, the major economic force for recycling PCBs is the value of metallic fractions (Table 7.3); a typical PCB with un-mounted electronic parts will contain ~28% metals (mainly copper) and ~72% non-metallic materials (Guo *et al.*, 2009).

Metal	WEEE	g/tonne of ore
Gold	22.2 g/tonne	≤9
Silver	313 g/tonne	22
Palladium	7.2 g/tonne	7
Copper	43,510 g/tonne	7,973
Silver	313.32 g/tonne	-
Iron	401.92 kg/tonne	-
Aluminium	33 kg/tonne	-
Nickel	3 kg/tonne	-
N.B: g = gram, kg = kilograms and tonne in metric units		

Table 7.3: Comparison of average metal contents of some valuable metals in high grade WEEE and ore (Adapted from Bigum and Brogaard, 2009).

PCBs are a mixture of glass fibre, plastics and multiple kinds of metals (Sommer and Edward, 2005). The typical composition of PCBs as reported by Guo *et al.*, (2003) is shown in Table 7.4.

Element	Content	Element	Content
Silver, Ag	3300g/t	Gallium, Ga	35g/t
Aluminium, Al	4.7%	Manganese, Mn	0.47%
Arsenic, As	<0.01%	Molybdenum, Mo	0.0003%
Gold, Au	80g/t	Nickel, Ni	0.47%
Sulphur, S	0.10%	Zinc, Zn	1.5%
Barium, Ba	200g/t	Antimony, Sb	0.06%
Beryllium, Be	1.1g/t	Selenium, Se	41g/t
Bismuth, Bi	0.17%	Silicon dioxide, SiO ₂	15%
Bromine, Br	0.54%	Tin, Sn	1.0%
Carbon, C	9.6%	Tellurium, Te	1g/t
Cadmium, Cd	0.015%	Titanium, Ti	3.4%
Chlorine, Cl	1.74%	Scandium, Sc	55g/t
Chromium, Cr	0.05%	Iodine, I	200g/t
Copper, Cu	26.8%	Mercury, Hg	1g/t
Fluorine, F	0.094%	Zirconium, Zr	30g/t
Iron, Fe	5.3%	Strontium, Sr	10g/t
g/t = gram/metric ton		% = wt%	

Table 7.4: Typical composition of printed circuit boards from EOL computers (Adapted from Guo *et al.*, 2003).

The complex physical and/or chemical characteristics (e.g., unliberated metallic fractions and brominated plastics) of PCBs make them somewhat difficult to recycle (Guo *et al.*, 2009; Liu *et al.*, 2009; Yang *et al.*, 2009). However, the presence of great intrinsic material value (metals) in PCB makes it a favourable option for smelting (Menad *et al.*, 1998; Lee *et al.*, 2004; Vehlow *et al.*, 1997; Quan *et al.*, 2009), vacuum pyrolysis (Zhou and Qiu, 2010; Zhou *et al.*, 2010) and/or chemical leaching (Goosey and Kellner, 2002; Xie *et al.*, 2009) to recover precious metals such as copper, gold and silver (Guo *et al.*, 2009; Liu *et al.*, 2009).

The current PCB recycling practices include the following essential steps (Cui and Forssberg, 2003);

- ❖ Pre-treatment, involving the removal of hazardous components such as batteries.

- ❖ Disassembly, involving the removal of major elements such as aluminium heat sinks.
- ❖ Size reduction is primarily targeted at liberating various metallic and non-metallic fractions for subsequent physical and/or chemical separation.
- ❖ Physical and/or chemical separation is done to purify different material fractions.
- ❖ Recycling of metallic and non-metallic fractions.

It has been reported (Bigum and Brogaard, 2009) that shredding WEEE increases the risk of precious metal-rich materials ending up in wrong fractions e.g. dust resulting from shredding WEEE can contain nearly 5% of the Palladium. Nevertheless, size reduction is an important unit operation for component liberation (Veasey, 1997). The degree of achieved component liberation, in the size reduction phase, is a key factor for the efficiency and effectiveness of any subsequent physical and/or chemical separation process in terms of yield, quality of the recovered material and energy consumption of the process (Das *et al.*, 2009; Veasey, 1997). An investigation reported by Cui and Forssberg, (2003) has shown the PCB component liberation to be in the range of 95.6% to 99.5% for a two stage comminuted -5 mm fractions. However, a recent investigation (Das *et al.*, 2009) has claimed the PCB metal liberation to be only 23% for -5 mm comminuted PCB fractions. In the study carried by Das *et al.*, (2009) complete metal liberation was reported to be achieved in <100µm particle size fractions. Moreover, this investigation (Das *et al.*, 2009) has also highlighted the difficulties in separating finely sized and flat metal pieces (resulting from the comminution step) by conventional gravity separation techniques.

In addition to the recycling of valuable metals from WEEE, some efforts (Biddle *et al.*, 2009; Guo *et al.*, 2009) have also been extended to recycle different plastics by depolymerisation (APME, 1997), bioleaching (Wang *et al.*, 2009) and froth flotation (Daniels,

2009). Guo *et al.*, (2010) have reported the use of recovered PCB plastic in their wood plastic composites. Zheng *et al.*, (2009) used a combination of fluidised bed and cyclone separators to recover valuable glass fibres from waste PCBs. Others (Boerrigter, 2000) have worked to extract different hazardous elements such as bromine and antimony from WEEE plastics. Lou *et al.*, (2009) recommended the use of the Ferrite process in combination with the Fenton method to recover different metallic ions and organic matter from the wastewater generated in the production of PCBs. The next section will investigate the different recycling practices to recover valuable components from waste PCBs.

7.3 Current practices to separate PCB

Separation of different valuable assets from waste PCBs has remained a topic of great interest among many different resource efficiency oriented enterprises, environmentalists, governments, public and researchers (Das *et al.*, 2009; Daniels, 2009; Zheng *et al.*, 2009). Recycling oriented characterisation of WEEE can give an indication of the recovery potential from different recycling processes (Chancerel and Rotter, 2009). Recycling of PCBs not only reduces the amount of WEEE heading for landfills but it can also provide revenues to maintain a financially viable recycling programme. At present, a well liberated PCB feed can be separated by a combination of dry and wet physical beneficiation processes (Veasey, 1997). Some of the most common physical separation processes have been discussed in Chapter 2.

In 2002, an estimated 50,000 tonnes per annum of WEEE scrap was generated in the UK alone and nearly 80% of this amount was PCBs (Goosey and Kellner, 2002). However, the lack of accurate predictions on a stable PCB scrap supply in the future (Chancerel

and Rotter, 2009) coupled with the uncertainties involved in the demand of recycled materials in international markets has resulted in increased investigation into low cost technology options for recycling WEEE (Goosey and Kellner, 2002). In the low cost particle separation technology scenario, Kang and Schoenung, (2005) presented a review of technology options for recovering valuable fractions from WEEE in USA. Viet *et al.*, (2005) used a combination of magnetic and electrostatic techniques to separate different metallic and non-metallic fractions from waste PCBs. They reported the achievement of metal fraction enrichment values as shown in Table 7.5

Elements	Feed wt%	Enrichment wt%
Copper, Cu	12.5	50
Tin, Sn	4.0	25
Lead, Pb	2.7	7.0

Table 7.5: PCB metal fraction enrichment values as reported by Viet *et al.*, (2005).

Zang and Forssberg, (1998) reported the use of an electro-dynamic separation technique to upgrade 11%Cu and 7%Al to a value of 34%Cu and 22% Al with a respective 87% and 99% Cu and Al-metal recovery. Jiang *et al.*, (2009) used a two-roll electrostatic separator for recycling metallic fractions originating from waste PCBs. Veit *et al.*, (2005) has reported the use of magnetic and electrostatic separation techniques for recycling PCBs. Niu and Li (2007) have proposed a compaction and cementation method for PCB disposal. Recovery of valuable fractions from PCB has also been reported by Yoo *et al.*, (2009) with the average metal contents in their waste printer PCBs reported in Table 7.6.

Elements	Content (wt%)
Copper, Cu	19.19
Aluminium, Al	7.06
Nickel, Ni	5.35
Iron, Fe	3.56
Tin, Sn	2.03
Lead, Pb	1.01
Zinc, Zn	0.73
Cobalt, Co	0.04
Titanium, Ti	0.04
Silver, Ag	0.01
Gold, Au	0.007
Total	39.09

Table 7.6: Average metal content in PCBs disassembled from obsolete printers (Adapted from Yoo *et al.*, 2009).

Researchers (Jiang *et al.*, 2009; Yoo *et al.*, 2009; Zang and Forsberg, 1998) have shown that various dry physical concentration techniques such as an electrostatic separation can be used effectively to separate a coarse particle size range originating from a feed comprising comminuted PCB. However, it has been discussed previously (Chapter 2) that for the majority of dry separation processes the separation efficiency decreases with decreasing particle size range. It is mainly due to this reason that many different wet concentration techniques such as wet tabling and flotation are commonly used to separate different finely sized PCBs fractions. Das *et al.*, (2009) used a combination of wet and dry separation techniques to report ~93% grade and ~54% recovery of the metallic PCB fractions. Their work also demonstrated a decrease in grade (~54%) with increasing recovery (~95%) of the metallic fractions. The chemical composition of waste PCBs used in their work is given in Table 7.7.

Elements	Feed, (%)	Concentrate-1, (C1) wt%	Concentrate-2, (C2) wt%	Overall concentrate, (C1+C2) wt%
Cu	12.58	51.12	40.11	47.47
Pb	2.44	10.38	5.12	8.64
Sn	1.41	6.67	4.42	5.93
Fe	3.24	13.09	7.69	11.3
Al	2.38	9.33	6.48	8.39
Ni	0.39	2.39	0.69	1.83
Total	22.5	93.1	64.6	83.7

Table 7.7: Chemical analysis of the two concentrates with feed for the EOL-PCBs generated from the obsolete computers (Adapted from Das *et al.*, 2009).

Goosey and Kellner, (2003) reported the elemental composition of PCBs and material specific gravities shown in Table 7.8 and Table 7.9 respectively. A large specific gravity difference between many different material fractions that comprise a typical PCB can be readily seen in Table 7.9. These large density differences among many different PCB fractions can be used to an advantage to form a basis for their dry based physical separation, possibly in a very fine particle size range.

Element	% weight
Non-metallic e.g., glass reinforced polymer	70%
Copper, Cu	16%
Solder	4%
Iron, ferrite (for transformer cores)	3%
Nickel, Ni	2%
Silver, Ag	0.05%
Gold, Au	0.03%
Palladium, Pd	0.01%
Other (bismuth, antimony, tantalum etc.)	<0.01%

Table 7.8: Elemental composition of PCB sourced from EOL computers (Adapted from Goosey and Kellner, 2002).

Materials	Specific gravity range (g.cm ⁻³)
Gold, Tungsten, platinum group	19.3-21.4
Lead, silver, molybdenum	10.2-11.3
Magnesium, aluminium, titanium	1.7-9.0
Copper, nickel, iron, zinc	7.0-9.0
Glass reinforced plastic	1.8-2.0

Table 7.9: Specific gravity of different materials in PCBs obtained from EOL computers (Adapted from Goosey and Kellner, 2002).

The elemental composition of PCBs is also reported by Mohabuth *et al.*, (2007) and Mohabuth, (2007), shown in Table 7.10.

Main constituents (wt%)	>600 μm	425-600 μm	300-425 μm	212-300 μm	150-212 μm	<150 μm
Copper, Cu	23.20	24.20	18.80	17.30	23.30	5.69
Tin, Sn	8.47	6.22	6.66	6.14	4.86	3.36
Lead, Pb	3.70	3.35	3.49	3.64	2.67	1.93
Aluminum, Al	4.41	4.69	6.39	5.21	4.23	3.56
Nickel, Ni	0.18	0.21	0.31	0.31	0.18	0.32
Iron Fe	0.18	0.18	0.20	0.18	<0.09	0.64
Zinc, Zn	2.72	2.41	1.03	0.85	0.69	0.93
Gold, Au	0.010	0.012	0.008	0.007	0.006	0.020

Table 7.10: Chemical composition of PCB originating from EOL computers (Adapted from Mohabuth, 2007).

Most of the studies to date have focused on the selected PCB elemental concentrations which are subjected to different methodological approaches and diverse sampling procedures. Table 7.4, Table 7.6 and Table 7.8 clearly show the diversity of an individual component concentration in PCBs that was sourced from different EOL-computers. In common with other WEEE fractions a complete PCBs component concentration profile looks far from agreement. The change in component concentration in PCBs contents is probably linked to different PCB designs produced by different manufacturers, and changes in composition from the same manufacturer over time (Robinson, 2009). This is usually triggered by the new production trends and/or due to the introduction of new, increasingly stringent legislation on the use of hazardous materials.

Nevertheless, the reported PCB composition values in the literature can still be used in future investigations for comparison purposes.

Currently, no single treatment approach can handle the diverse and varying waste PCB streams. The majority of the current dry based WEEE recycling techniques such as screening, magnetic separation, eddy current separation and nail roll separation have limitations of a minimum working WEEE particle size range of ~ 5 mm. In the case of waste PCBs however, the complete metallic asset liberation is achieved in very fine particle size range, normally $< 1000 \mu\text{m}$. Greater than 90% of all the intrinsic material value of a waste PCB is the value of its gold and palladium content (AEA, 2006). Size classification of comminuted PCBs prior to any physical separation process could result in loss of precious metal contents as they are normally believed to reside in the very fine particle size range (AEA, 2006). Estimated precious metals loss during size classification can range upwards from $\sim 10\text{wt}\%$ (AEA, 2006). On the other hand, the use of populated PCB assemblies can help in an enhanced yield of the metallic fractions (AEA, 2006). Most of the literature in this field has focused on physical recycling routes to recover valuable components from waste PCBs. This trend is promoted due to the fact that a hydrometallurgical approach (i.e. using water and/or other solvents) in practise can potentially result in a significant environmental impact.

In light of the discussions presented above, it can be deduced that there is increasing demand for a dry based physical separation technique employing a continuous size range of finely sized WEEE particles. The need for a dry based physical separation process to treat WEEE has also been discussed in the work of Cui and Forssberg, (2003). Hence, the development of a cost effective and efficient separation process that can handle varying compositions of WEEE and PCB scrap would result in a significant resource recovery improvement and additional environmental benefits.

The work presented in the next section (7.3.1) will therefore look into the application of a novel vertical vibration driven fine particle separator to recover valuable fractions from comminuted waste PCBs. In this work (Chapter 5), the separator has been used initially to assess the separation behaviours of varying compositions of finely sized glass and bronze mixtures. Here, the performance of this separator will be judged by employing it to separate various continuous and finely sized WEEE and solid waste particle mixtures on a dry basis.

7.3.1 Application-1: Vibration induced separation of WEEE mixtures

7.3.1.1 WEEE sample-1: waste electrical cables

Worldwide, an estimated one billion Personal Computers (PC) were in use by the end of 2008 (Forrest research, 2007). This figure is projected to reach a value of two billion PCs by the end of 2015. The life span (time from its introduction to obsolescence) of a PC had decreased from 4-6 years in 1997 to 2 years in 2005 and is further decreasing with time (Kang and Schoenung, 2006). Electrical cables (EC) form an integral part of all PCs and contain a valuable copper asset in the form of wires, normally surrounded by plastic coatings. The electrical cables are generated as solid waste along with EOL (end of life) PCs. Since, these electrical cables are un-liberated; the liberation of copper from the surrounding plastics forms an important initial step before any subsequent physical separation operation.

In this work, the selection of waste electrical cables for their component separation via vertical vibration separator was based on many different considerations such as;

- ❖ The size reduction of electrical cables results in a binary mixture of copper and plastic.
- ❖ This non synthetic binary mixture has very complex particle shapes and sizes (Figure 7.1).
- ❖ The significant colour difference between copper and plastic could help visualize different particle motions under the influence of vertical vibration.
- ❖ A continuous size range of this material can be used in vertical vibration separator.
- ❖ Sink-float analysis can be used to reveal the final grades of the separated products.

7.3.1.1.1 Sample preparation

A well liberated and complex shape copper and plastic mixture preparation from the scrap electrical cables originating from the EOL PCs for their onward separation by vertical vibration treatment included the following essential steps:

- ❖ Step-1: EOL-PC electric cables were acquired from the IT Department, Information Services, University of Nottingham, UK.
- ❖ Step-2: The electrical cables were manually freed from their connecting ends with the help of pliers (Figure 7.2). The odd shapes and hard construction of the connecting ends were considered unsuitable for feeding in a cutting mill.

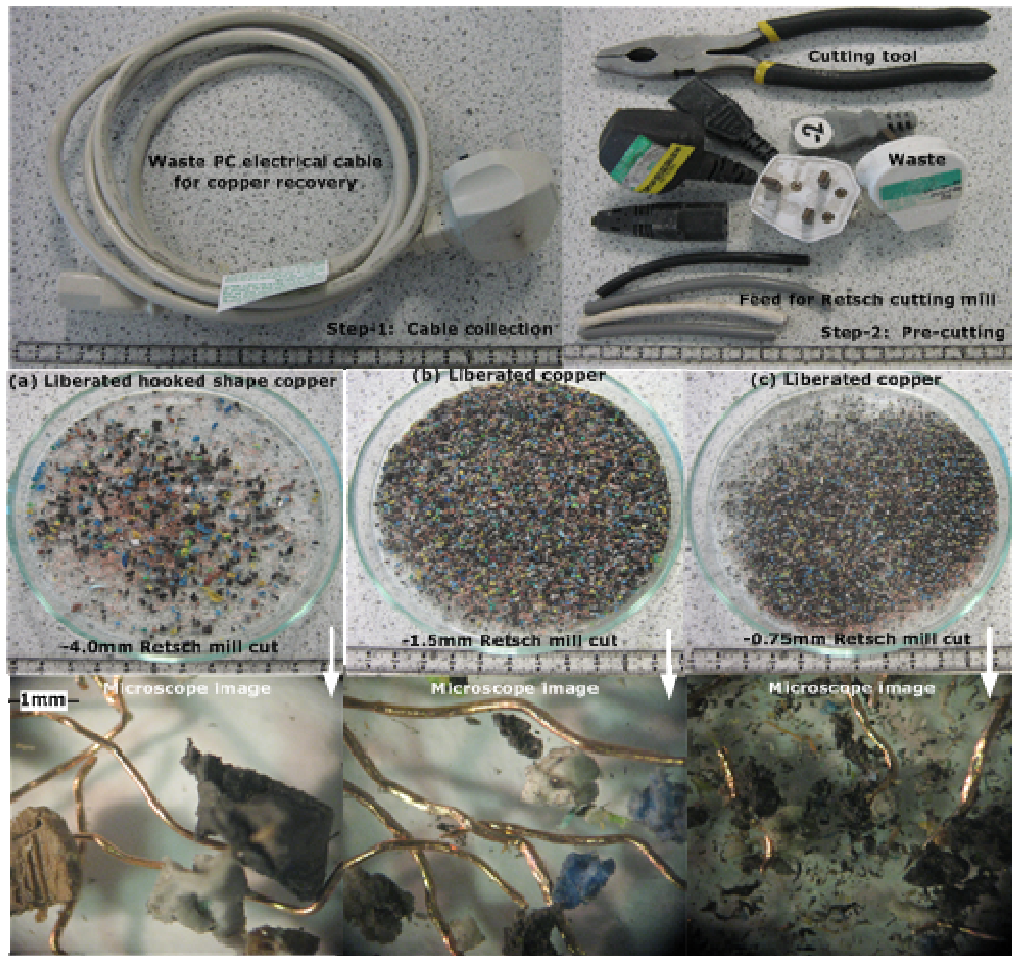


Figure 7.2: Feed preparation steps for vibration separation of waste PC electrical cables.

- ❖ Step-3: The cables were cut in approximately 10 mm length pieces so as to ease their feeding in a Retsch mill (Figure 7.2).
- ❖ Step-4: The size reduction of electrical cables was carried out in stages using a Retsch cutting mill (Figure 3.7). A staged cutting strategy was employed to avoid any excessive heat build-up that could potentially degrade the plastic coatings during Retsch cutting operations. The Retsch mill used in this work predominantly relied on a cutting effect which is normally generated between its moving (3-blade rotor) and stationary sharp edges. The cutting action imparted by this machine is particularly suitable for the preliminary sized

reduction of soft, medium-hard, elastic and fibrous materials. The first stage in cutting waste electrical cables involved the use of a 10 mm square hole grid at the exit from the main cutting chamber in the Retsch mill. This was followed by a separate material passes through a 4 mm square, 1.5 mm and -0.75 mm trapezoid aperture discharge grids in the Retsch mill. The minus (-) sign represents the material passing through each grid size. The final -0.75 mm and -1.5 mm particle sizes are shown under a laboratory microscope in Figure 7.2.

- ❖ Step-5: The final products from -1.5 and -0.75 mm discharge grids were size characterised by using a standard sieve analysis technique described in Section 3.3.3.1. It is a general perception that the energy requirement increases sharply for particle size reductions below 10 mm. While, size reduction is energy and maintenance intensive unit operation, two different particle sizes of -0.75 and -1.5 mm were selected for vibration separation trials to investigate if any reduction in the cutting stage can be achieved in this work. The particle size distributions of -1.5 and -0.75 mm Retsch mill cut fractions are shown in Figure 7.3.

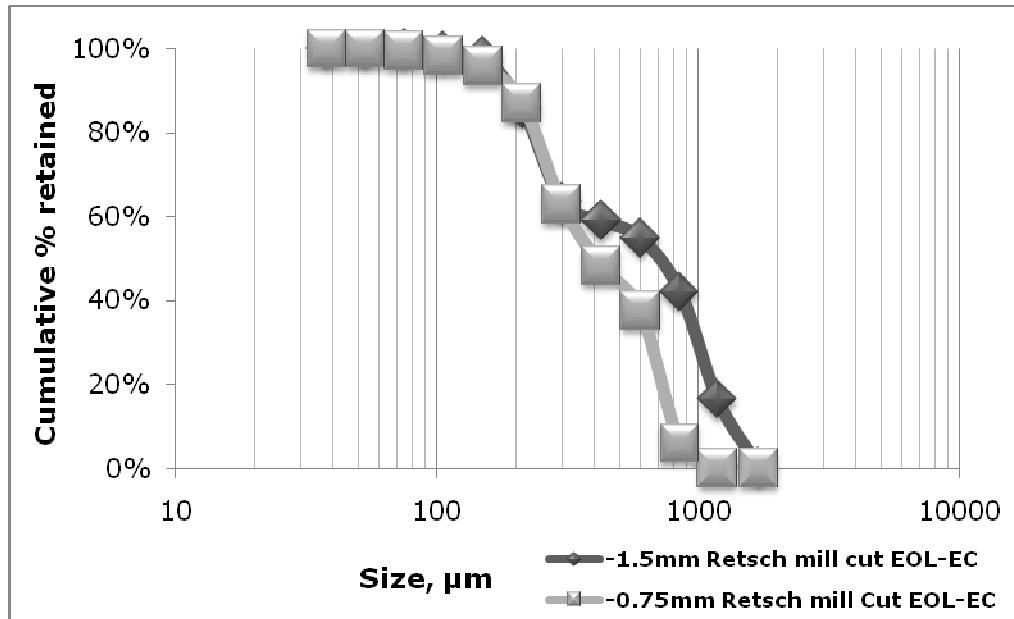


Figure 7.3: Size characterisation of waste electrical cables from - 0.75 and -1.5 mm Retsch mill cut.

The -1.5 and -0.75 mm size range material was selected for separation in the vertical vibration separator. Figure 7.3 reveals that the particle size distributions for -1.5 and -0.75 mm cut electrical cables are not significantly different below 300µm particle size range. However, particle size distributions change significantly above 300µm, probably due to the existence of comparatively long copper wires in a -1.5 mm cut (Figure 7.2). A large length to diameter ratio of copper wires can enhance the possibility of escape through the small discharge grid openings of the cutting machine before they are adequately cut into the desired particle size range.

7.3.1.1.2 Initial experiments on the separation of waste electrical cables

The initial experiments to recover the copper wires from the waste electrical cables were carried out in an L-type separation cell assembly as shown in Figure 3.4. First, the vibration bench

reported as Rig-1 (Figure 2.23) in Section 3.2.1 was used to visually assess the particle separation behavior. This was followed by the detailed vibration separation investigations being carried by the use of Rig-2 (Figure 3.3). The detailed vertical vibration bench assembly of Rig-2 is described in Section 3.2.2.

The work carried by Mohabuth, (2007) has reported a failure in dry based separation of 250-425 μm size range shredded electrical cable particles in the prototype separation cell assembly shown in Figure 2.23. The 250-425 μm size range shredded electrical cable particles used in their work (Mohabuth, 2007) were prepared by using a staged -0.5 mm Retsch mill cut. However, the vertical vibration separation of the same 250-425 μm shredded electrical cable particulate material was reported in the presence of water. In an effort to investigate the dry separation potential of the 250-425 μm size range shredded electrical cables at a scaled up level, the initial experiments reported here were performed in the L-type separation cell. Three different particle bed heights of 50, 100 and 150 mm with a fixed partition gap size of 5 mm was used in the L-type separation cell assembly in each of the investigated cases.

Copper wires have a density of $\sim 8.3\text{g}\cdot\text{cm}^{-3}$ whereas the majority of low density polyethylene plastics, used in the electrical cables, are in the density range of $0.91\text{-}0.93\text{g}\cdot\text{cm}^{-3}$ (Frontier Recycling, 2009). A large density differential between copper wires and plastics has the potential to make them an excellent mixture for investigating the density segregation of irregular shape particles. A sink-float analysis technique (described in Section 3.3.3.2) carried out on comminuted electrical cable feed materials revealed a copper to plastic ratio of 65:45wt% in this solid mixture.

The vibration separation experiments reported here were conducted at ambient conditions of temperature and pressure. Vertical vibration frequency (f) in the range of 30-50Hz and dimensionless

acceleration (Γ) value in the range of 3-5 were used in this work. A range of values is reported based on the fact that at any inlet air pressure to the vibrator the displayed values fluctuated in a certain range. The vertical vibration frequency (f) in the range of 30-50Hz and dimensionless acceleration (Γ) value in the range of 3-5 corresponds to an inlet air gauge pressure of \sim 2-3bar. Nevertheless, the choice of these values was based on the previously reported work of Mohabuth and Miles, (2005) and Mohabuth *et al.*, (2007) and Mohabuth, (2007).

The initially well mixed binary particle mixtures placed in the separation cells were vertically vibrated for nearly an hour in each case. The mixture components gradually formed distinct layers/regions. However, the overall group movements of the high density copper wires were insignificant in comparison to combined group motions of the bronze particles in the previously discussed glass/bronze mixtures. In later case, the majority of the bronze particles were seen to patrol the outer periphery of the whole particle bed. The differences in bulk particle motion may be attributed to the individual and distinct particle shapes. The local convective motions of copper wires and plastic particles were comparatively slow and hence took a long time to form distinct particle zones. A distinct copper on top layer was never observed. Instead, local pockets of copper wires were consistently observed in the overall particle bed motions as can be seen in Figure 7.4.

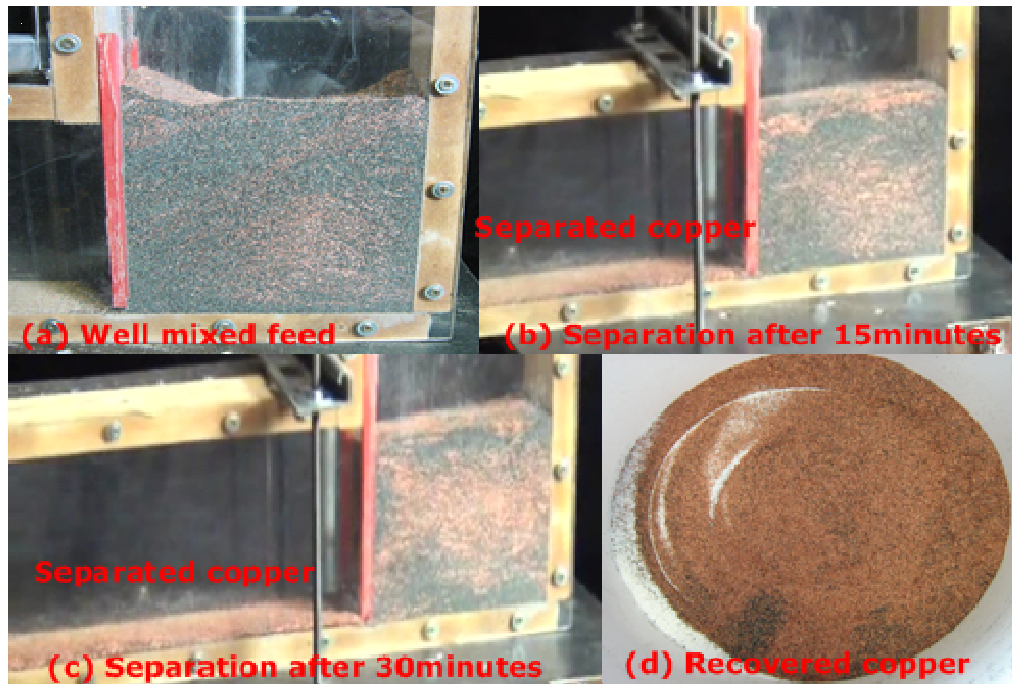


Figure 7.4: Separation 250-425 μ m shredded electrical cables in a L-type separation cell (Bed height = 150 mm and Partition gap size = 5 mm).

The vertical vibration of 250-425 μ m shredded electrical cable feed mixtures (Figure 7.4), at the stated conditions of f and Γ , resulted in quick (~ 1 minute) formation of a lean global convection current. The outer periphery of this global convection current contained some high density copper particles along with majority of plastic particles. When the global convection current was near to the partition separation gap it encouraged the transfer of copper wires into the next chamber (Figure 7.4) which probably was due to their higher individual momentum values, in comparison to the plastic particles. Other factors could include their shape which could have helped them to easily slide through the separation gap and into the next chamber. Once in the next chamber, they were triggered to flow to the exit under the influence of vertical vibration. The separated copper wires were finally collected (Figure 7.4) at the exit of the long arm shown in Figure 7.4. The plastic particles on the other hand were seen to concentrate in the short arm of the L-type

separation cell and were collected separately at the end of each separation batch (Figure 7.4).

In all investigated cases, the grades of the recovered copper wires were found to be in excess of 95wt% which was determined by three repeat sink-float analysis of each fraction. However, the material loadings did affect the recovery of the separated particles. Even after vertical vibration treatment of one hour, at 100 and 150 mm particle bed heights, significant amounts of high density material ($\sim 25\%$ wt) were still observed. Thus investigating the influence of particle bed height on final grades of the separated copper wires was required and is discussed in the next two sections (7.3.1.1.3 and 7.3.1.1.4).

7.3.1.1.3 Separation of -1.5 mm Retsch mill cut electrical cables in separation cell C-1 & 2

WEEE material used in the experiments reported here comprised a continuous particle size range of copper wires and plastic particles derived from shredded electrical cables. The average mass mean diameter of this continuous size range sample was found to be $703.65\mu\text{m}$. The complete particle size characterisation of this sample is given in Figure 7.3. The use of a continuous size range mixture is dissimilar to a definite particle size range ($250\text{-}425\mu\text{m}$) mixtures which were used in the initial experiments described in section 7.3.1.1.2. Nonetheless, experiments carried out on -1.5 mm continuous size range (Figure 7.3) Retsch mill cut did not show any significant component separation of the shredded electrical cables at any of the investigated particle bed heights (20, 30, 40, 60, 80 and 100 mm). The existence of excessively oversize copper wires (in terms of their length in comparison to plastic particles) potentially hindered the individual convective motions of the separating particles during the vertical vibration treatment. Since, the

individual convective motions were not fully developed; a change in partition gap size from 5 mm to 10 mm did not help in improving any particle separation behaviours. Zero separation efficiency was therefore recorded in both separation cells (C-1 & 2, Figure 3.6). This experiment however demonstrated the importance of having a parallel size and shape particles for their separation by vertical vibration treatment.

7.3.1.1.4 Separation of -0.75 mm Retsch mill cut electrical cables in separation cell C-1 & 2.

Visual observations demonstrated that copper liberation was not an issue with a -1.5 mm Retsch mill cut. However, reduced particle mobility was strongly attributed to the existence of long copper wires in this sample. Further, a descending particle size reduction step can help overcome this issue. Hence, a -0.75 mm Retsch mill cut was selected for the next trial phase which resulted in significant size reduction of big size particles. The complete particle size characterisation of -0.75 mm Retsch mill cut electrical cables is shown in Figure 7.3. The average mass mean diameter of this continuous size range sample is found to be 480.52 μ m. The size reduction step principally targeted 400-800 μ m particle size range (Figure 7.3) whereas the particle sizes below 400 μ m remained parallel to the -1.5 mm Retsch mill cut.

A 100 mm diameter polypropylene funnel was used to introduce the mixed feed material into the short arm of the separation cell C-1 and C-2 (Figure 3.6). Once the desired particle bed height of the material was reached in the separation cell, it was clamped on top surface of the vibrating steel plate (Rig-2, Figure 3.3). The loaded separation cells were vertically vibrated for approximately one minute to obtain a stable bed formation and to check if the set vibration parameters had not drifted. The separated materials

collected over this period of time were recycled into the main particle bed in the short arm of C-1 & 2. Once everything was set, vertical vibration recommenced and a convective particle motion could be readily seen in the particle bed. Local copper concentrates were seen to form quickly which patrolled around the outer periphery of the tilted particle bed in the short arm of C-1 & 2. During the course of this convective motion the high density particles were observed to find their way into the next separated chamber through a small partition gap. The small partition gap size was provided in-between the two separate chambers that helped controlled the flow of the separating particles. A 10 mm gap size allowed some plastic particles to accompany the separated copper wires. However, a 5 mm gap size served the desired purpose of restricting majority of the plastic particles from ending up in the next chamber. The separated copper wires were collected at the end of long arm for subsequent sink-float and helium (He) pycnometer analysis to determine the grades of the separated products. The analysed copper grades at different particle bed heights are reported in Figure 7.5 and Figure 7.6.

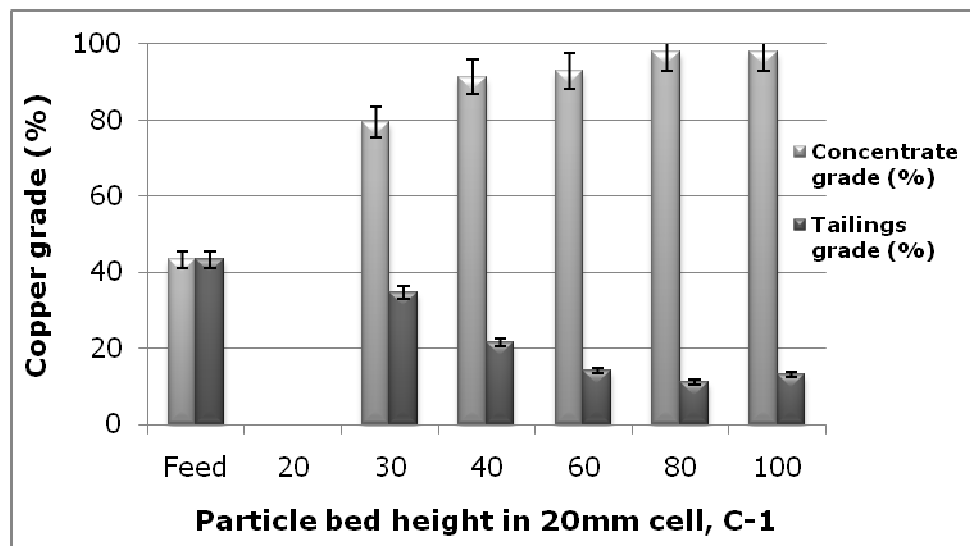


Figure 7.5: Copper grade (wt%) vs particle bed height (mm) of the separated electrical cables in a 20 mm width separation cell (C-1).

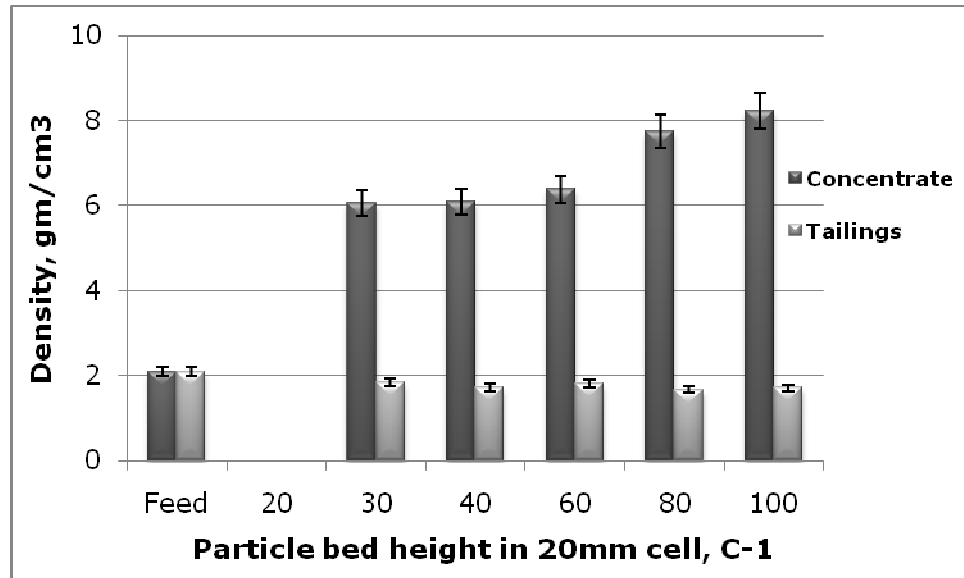


Figure 7.6: True density ($\text{g}\cdot\text{cm}^{-3}$) vs particle bed height (mm) of the separated electrical cables in a 20 mm width separation cell (C-1).

Figure 7.5 shows that the feed material comprised $\sim 43\text{wt}\%$ copper wires. Separation did not take effect at the low particle bed height of 20 mm (Figure 7.5 and Figure 7.6). The importance of maintaining an adequate particle bed height for vibration separation was evident from non-commencement of particle segregation at low particle bed heights. The separated copper grades did improve once the average particle bed height was increased to 30 mm and above (Figure 7.5). Low copper grades were recorded at 30 mm particle bed height however the grades improved substantially at 40, 60, 80 and 100 mm particle bed heights. However, all this came at the cost of an increased separation time which was assessed visually (Figure 7.7).

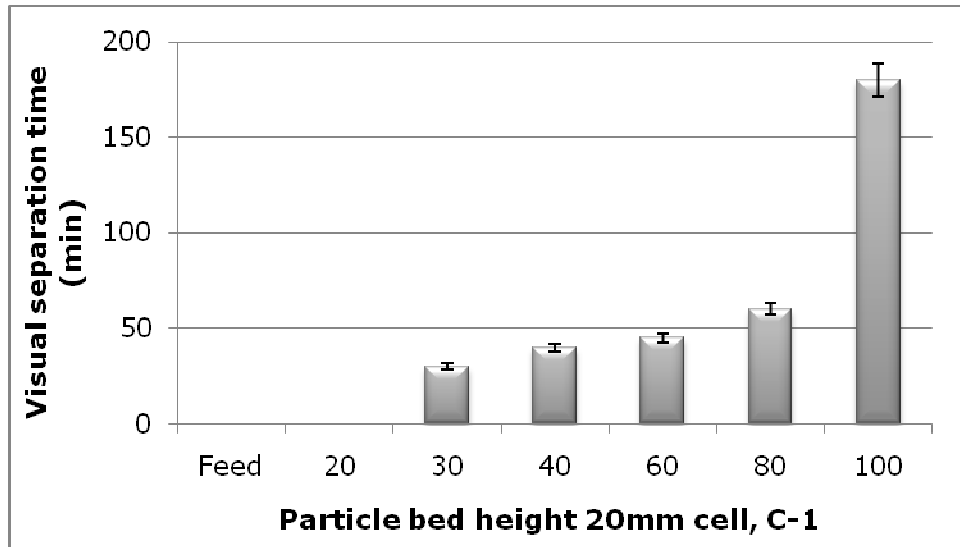


Figure 7.7: Visually assessed separation time (min.) vs particle bed height (mm) in a 20 mm width separation cell (C-1).

The copper grades were not significantly different at 40, 60, 80 and 100 mm bed heights as shown in Figure 7.5 and Figure 7.6. However, the copper grades in tailings were low for 60, 80 and 100 mm particle bed heights. The 60 mm particle bed height had the lowest separation time of 45 minutes (Figure 7.7). Parallel copper grades in terms of its measured density by the helium (He) Pycnometer are reported in Figure 7.6. On occasions, the measured density values of the separated products were observed to be very close to the literature/book density of pure copper.

An increase in separation cell thickness to 40 mm (C-2) resulted in an improved copper grade which was above 90wt% at 40 and 60 mm particle bed heights (Figure 7.8).

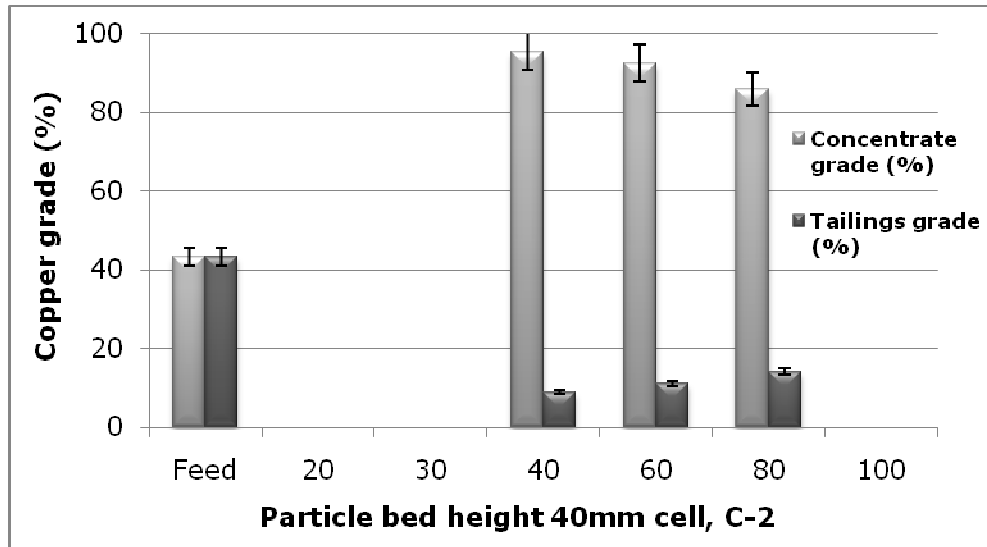


Figure 7.8: Copper grade (%) vs particle bed height (mm) in a 40 mm width separation cell (C-2).

Also, the copper grades in the corresponding tailings were $\sim 10\text{wt}\%$ (Figure 7.8). Similar trends were observed when the He-pycnometer density measurements of the separated products were carried out, which are shown in Figure 7.9.

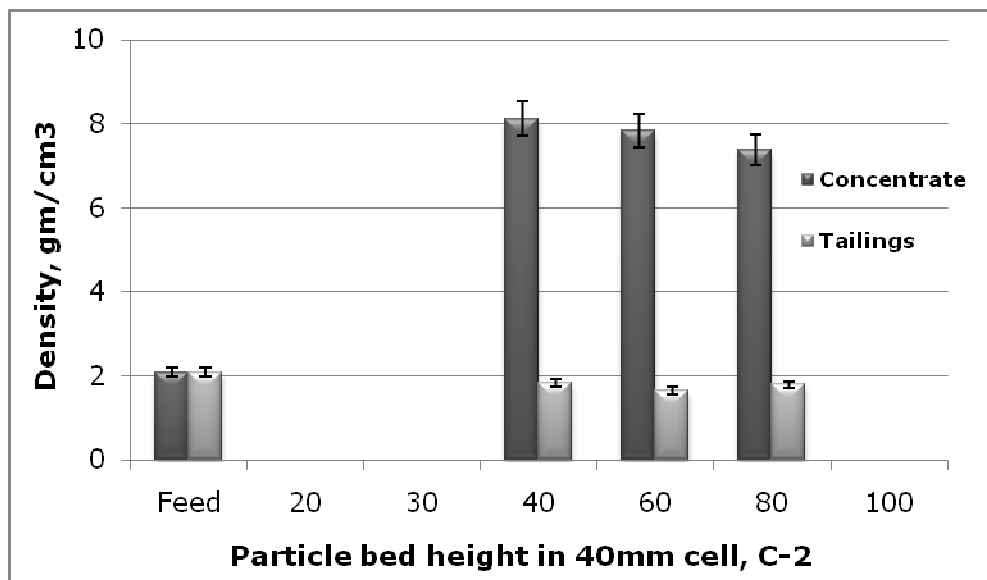


Figure 7.9: True density ($\text{g}\cdot\text{cm}^{-3}$) vs particle bed height (mm) of the separated electrical cables in a 40 mm width separation cell (C-2).

Furthermore, the visually assessed separation time of the separated products is shown in Figure 7.10.

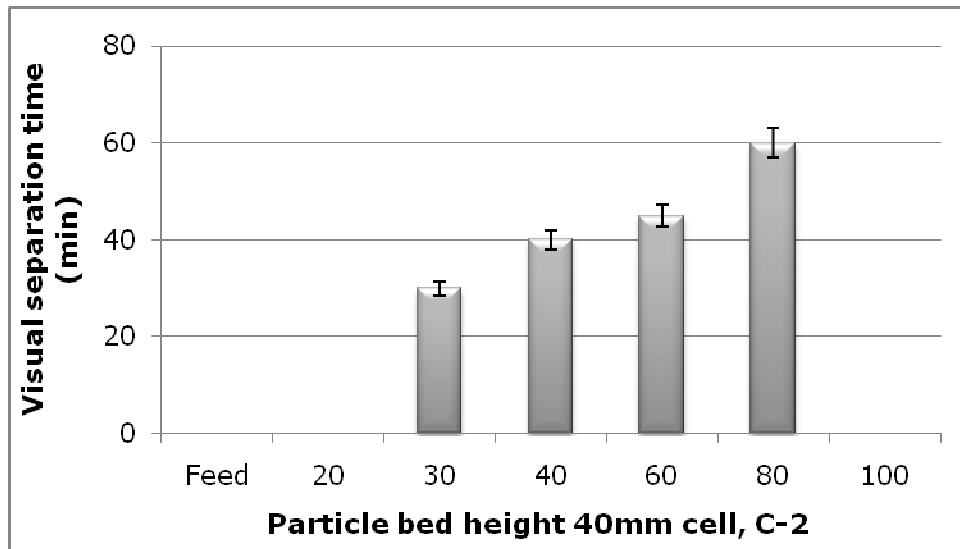


Figure 7.10: Visually assessed separation time (min.) vs particle bed height (mm) in 40 mm width separation cell (C-2).

The separation cell C-2, had more particle loadings at any particular particle bed height in comparison to C-1. It may be one of the reasons for high copper grades of the separated materials in C-2. The presence of more material could have resulted in enhanced grouping of the high density material during the course of convective particle motions. In addition, the non-cohesive particle nature of the material used in this study could have allowed strong air currents to flow through the vertically vibrating particle beds, as a result, segregation was possible at high particle bed heights.

7.3.1.2 WEEE sample-2: printed circuit boards (PCBs)

The majority of discarded WEEE materials such as shredded electrical cables and PCBs have certain characteristics in common. Basic processing principles such as size reduction, screening and physical separation are usually non-specific with respect to the

material in any category. However, the details of equipment design, degree of complexity, size and processing costs can be strongly influenced by the nature and utilization of the material to be recovered and the extent and degree of component separation.

The separation of copper from end of life shredded electrical cables has many similarities to the physical separation of PCB fractions. The complete component liberation of both materials can be achieved in a sub-micron particle size range via size reduction in a Retsch cutting mill. However, the size reduction of PCBs would result in generation of complex particle mixtures. The ability to achieve a complete component characterisation of these comminuted PCB mixtures is still in doubt (Table 7.4, Table 7.7, and Table 7.8). The key components in comminuted PCB mixtures are listed in Table 7.9 where significant differences in different particle densities can be readily seen. These mixtures can be easily characterised as high and low density fractions on the basis of their density differences. In a typical comminuted PCB mixture, the high density or heavy fraction is generally a mixture of different metallic particles. On the other hand, the low density fraction normally contains different polymeric materials in addition to various additives (e.g. flame retardants, stabilizers), ceramics and glass.

The main objective of the work reported in this section is to investigate the vertical vibration particle separation behaviour of comminuted PCB mixtures. In this context, the next section (7.3.1.2.1) will explain various PCB feed sample preparation steps.

7.3.1.2.1 Sample preparation

- ❖ Step-1: PCBs originating from different end of life personal computers were acquired from Reclaimed Appliances Ltd., UK. The acquired PCB samples were air blown to remove any contaminants such as dust articles.
- ❖ Step-2: They were manually freed from large aluminium heat sinks with the help of pliers (Figure 7.11). The odd shapes and hard construction of the heat sinks was considered unsuitable for feeding directly into a Retsch cutting mill. The electronic batteries were also removed at this stage.
- ❖ Step-3: The populated PCBs were cut into approximately 15-20 mm length strips, approximately 2-4 mm in width, by using an electric saw. This size selection helped ease their feeding in a Retsch cutting mill (Figure 7.11).
- ❖ Step-4: Further size reductions of PCB strips carried out in descending size stages using a Retsch cutting mill (Figure 3.7). Staged cutting was preferred to avoid any excessive heat build-up that potentially would have degraded the PCB polymeric materials during Retsch mill cuttings, as reported by Dimitrakakis *et al.*, (2009). The first cutting stage in this work used a 10 mm square hole grid at discharge from the cutting mill, followed by separate material passes through a 4 mm square, 1.5 mm and 0.75 mm trapezoid aperture discharge grids in the Retsch mill (Figure 7.2).
- ❖ Step-5: PCB particle size from -4.0 mm Retsch mill cut did not result in complete metal liberation. However, adequate liberation was visually assessed for samples resulting from -0.75 mm and -1.5 mm Retsch mill cut. The final products from -0.75 mm & -1.5 mm discharge grids were size characterised using a standard sieve analysis technique, described in Section 3.3.3.1. The particle size characterisation of -0.75 mm & -1.5 mm PCB Retsch mill cut are shown in Figure 7.12.

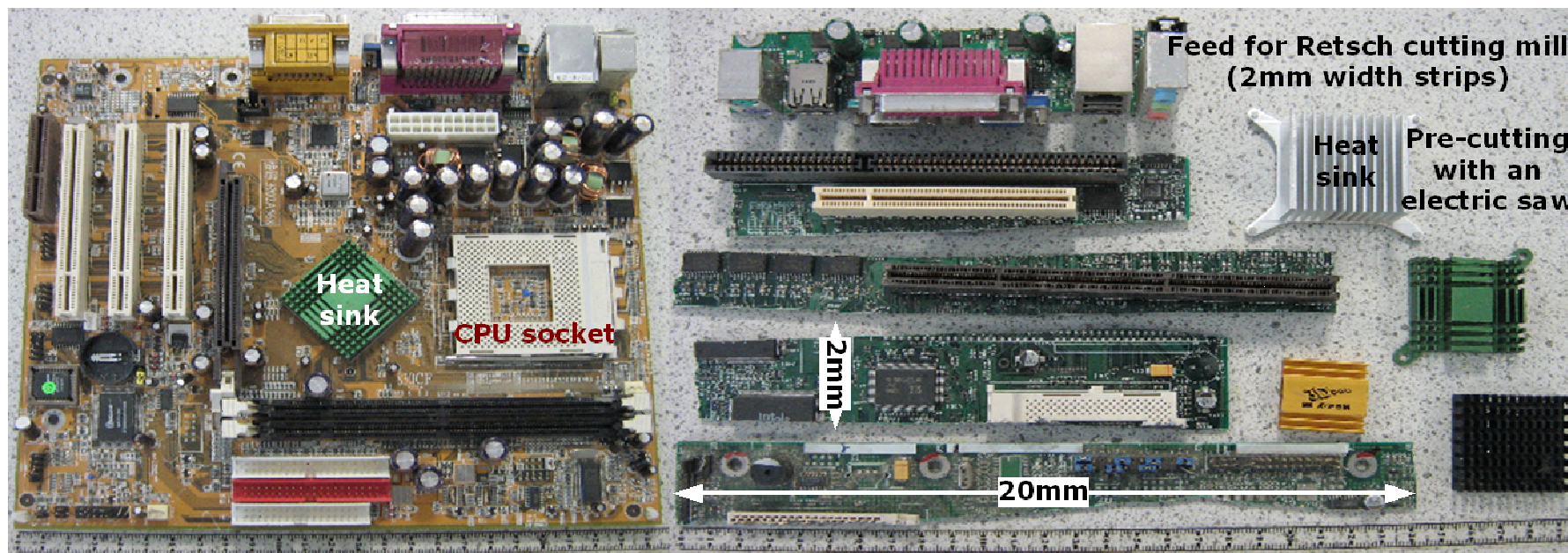


Figure 7.11: PCB feed preparation for cutting in Retsch mill.

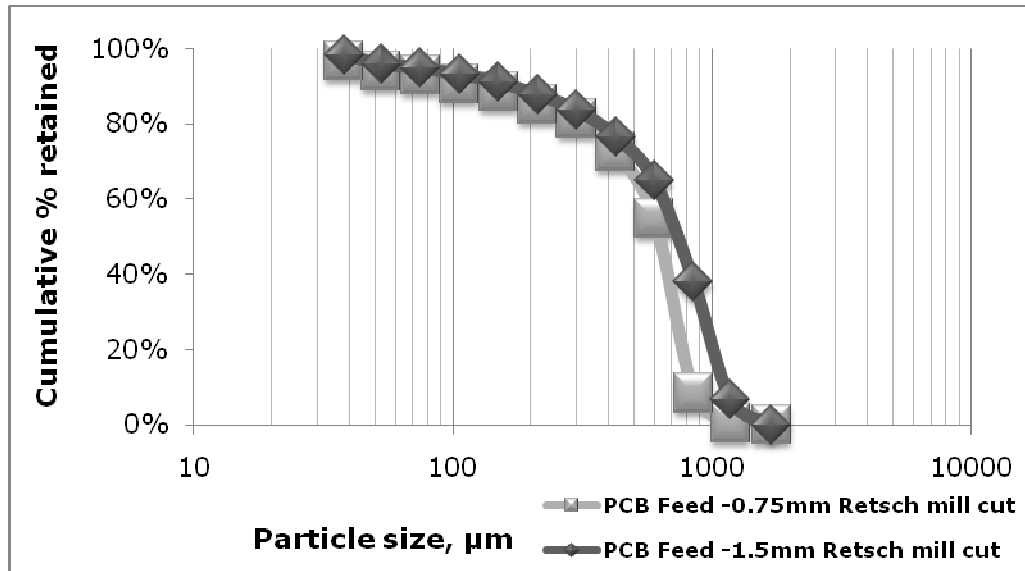


Figure 7.12: Particle size characterisation of PCB -0.75 and -1.5 mm Retsch mill cut.

From Figure 7.12 the average mass mean diameter of -0.75 mm and -1.5 mm PCB particles was found to be 472µm and 774µm. A continuous size range -0.75 mm and -1.5 mm Retsch mill cut PCB samples were used in the experiments reported here. Initially, visual analysis was used to determine the component liberation of the comminuted PCB samples. As the liberation of metallic and non-metallic fractions is an essential pre-requisite prior to any physical separation operation, the liberation of feed mixtures were confirmed by Scanning Electronic Microscope (SEM) images as shown in Figure 7.13 and Figure 7.14.

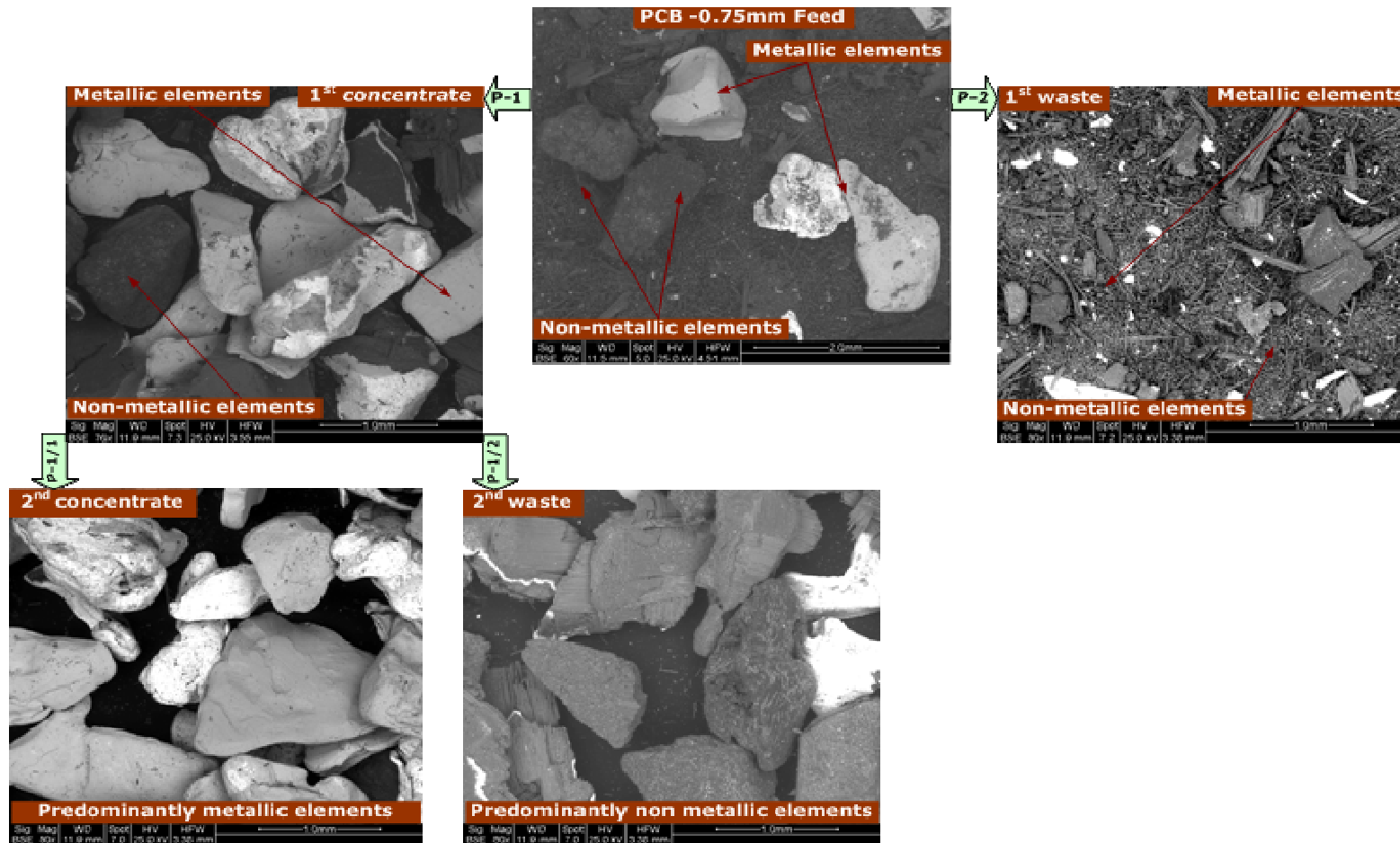


Figure 7.13: Scanning electron microscope (SEM) images of -0.75 mm PCB feed and separated fractions.

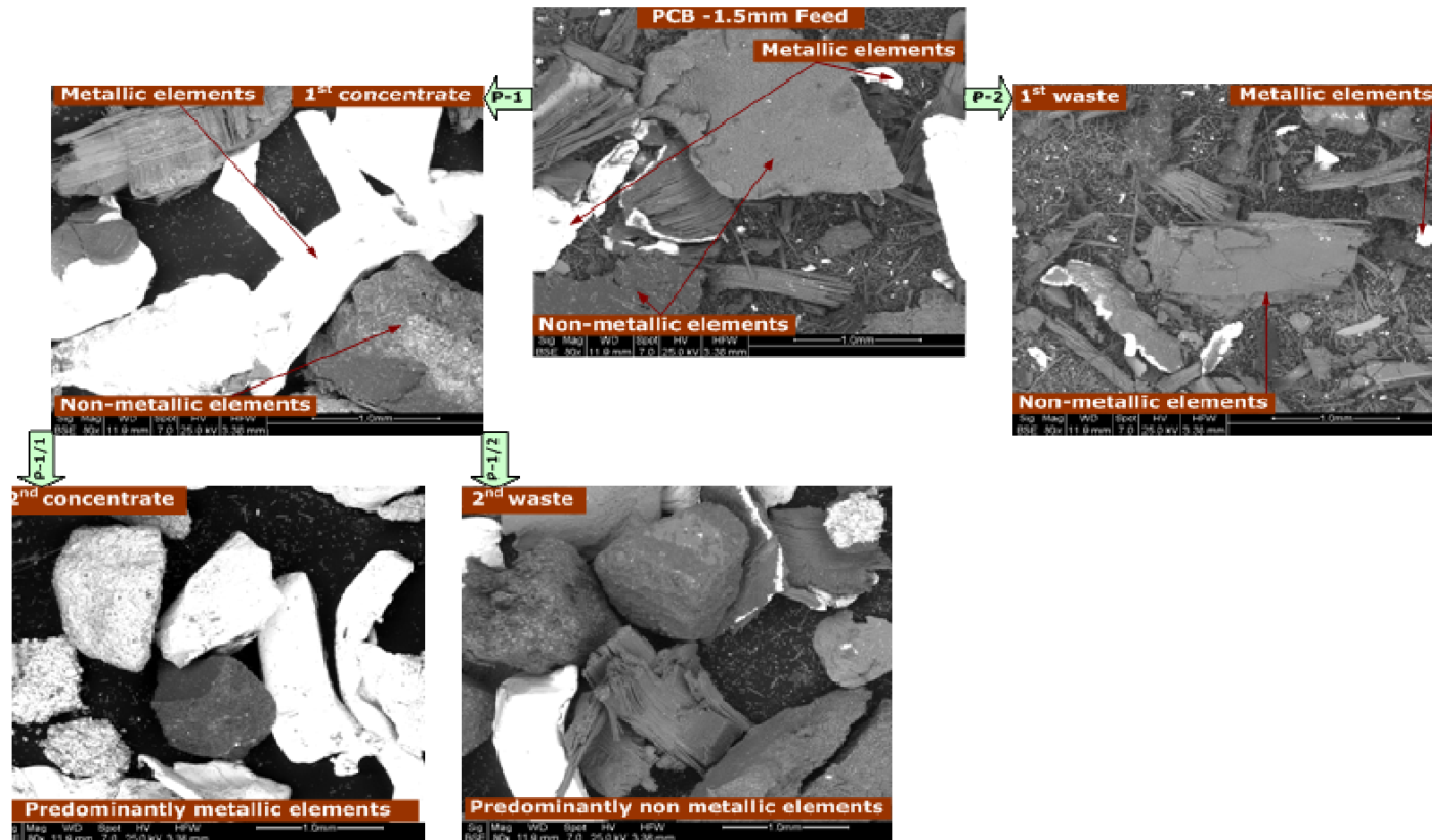


Figure 7.14: Scanning electron microscope (SEM) images of -1.5 mm PCB feed and separated fractions.

Vertical vibration separation experiments reported here used a 2.0-2.5 bar inlet air pressure to the vibrator. This resulted in top metallic platform to vibrate at a frequency and acceleration of 30-35±10%Hz and 3.5-4±10% respectively. A fixed vibration separation time of 45±10% minutes was used in each case.

Visual observations from the experiments, carried out in 20 and 40 mm separation cells, showed poor component separation at particle bed heights above 40 mm. However at 20, 30 and 40 mm particle bed heights good separation was observed. A partition gap size of 3 mm was maintained in each investigated case, the partition gap values above this did not result in good separation. The visually observed separation trends were not much different for 20, 30 and 40 mm particle bed heights except in their separation times, which were visually assessed and ranged between 30-45minutes for each case. A series of vertical vibration separation operations that employed both 20 and 40 mm separation cells was used in the experiments reported here. The initial and/or phase-1 vibration separation of PCB feed was carried out in a 40 mm separation cell. Phase-1 vibration separation resulted in two separate particle streams that are reported as product-1(P-1) and product-2 (P-2) (reference to Figure 3.5) in Figure 7.13 and Figure 7.14.

The first phase of vertical vibration treatment for both -0.75 and -1.5 mm resulted in predominantly size segregation coupled with density. The above observation was also confirmed by sieve analysis of the separated products (Figure 7.15 and Figure 7.16) and in SEM images (Figure 7.13 and Figure 7.14).

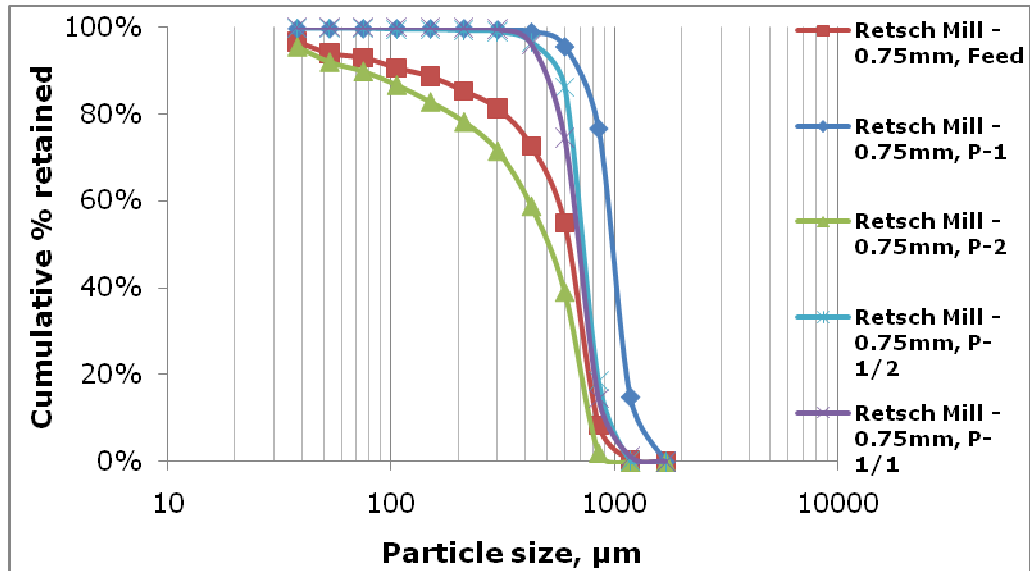


Figure 7.15: Particle size characterisation of -0.75 mm PCB cut separated products.

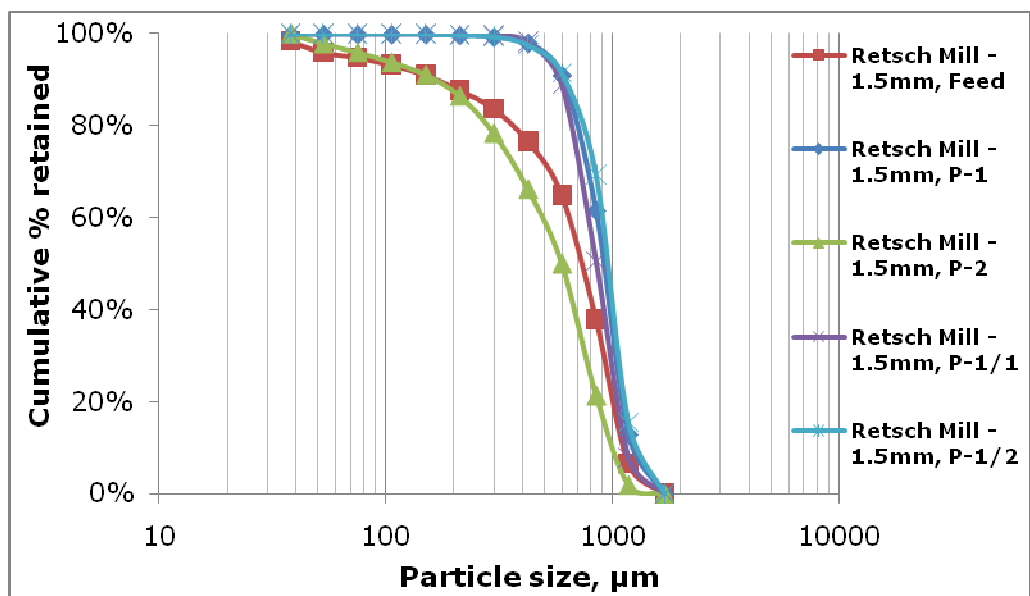


Figure 7.16: Particle size characterisation of -1.5 mm PCB cut separated products.

The separation in 40 mm cell therefore served two purposes: classification and pre-concentration of the separated materials. Particle classification from this stage can be an advantage as many physical separation techniques such as flotation are known to work

well with a consistent pre-sized feed (Das *et al.*, 2009). The majority of P-1 comprised consistent big size metallic particles and hence formed a valuable feed for the next separation stage. The separated PCB streams (P-1 and P-2) from two different passes in a 40 mm separation cell (stage one) were of sufficient magnitude for it (P-1) to be processed in a 20 mm separation cell as a feed. The presence of somewhat consistent particle sizes in P-1 resulted in density segregation in the second vibration separation phase. Furthermore, vertically vibrating P-2 mixtures did not show any significant separation in any case which may be due to the existence of very low metallic concentrations and their very fine sizes in those mixtures.

Metallic and non-metallic fractions of a separated product can be determined by sink float analysis as described in Section 3.3.3.2. This was used to track the metallic grades in the feed and in the different product fractions and are shown in Figure 7.17.

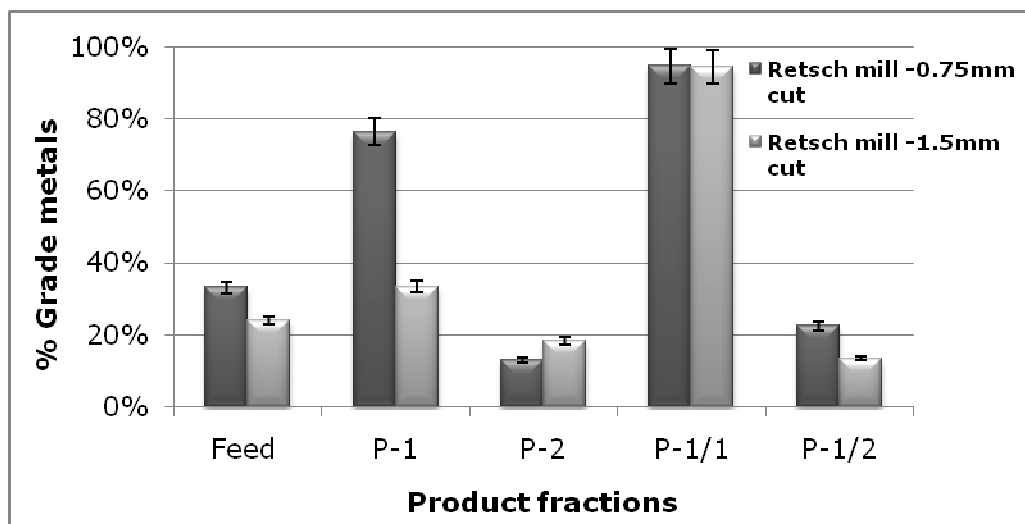


Figure 7.17: Sink-float analysis of the separated PCB fractions.

In Figure 7.17, it is interesting to note that metallic grades are of higher value for -0.75 mm in comparison to the -1.5 mm Retsch mill cut. This suggests enhanced liberation of -0.75 mm Retsch mill cut.

However, the P-1/1 fraction grades are of equal magnitude for both -0.75 and -1.5 mm cuts. Similar results were also seen by measuring the true density of the separated PCB fractions, shown in Figure 7.18.

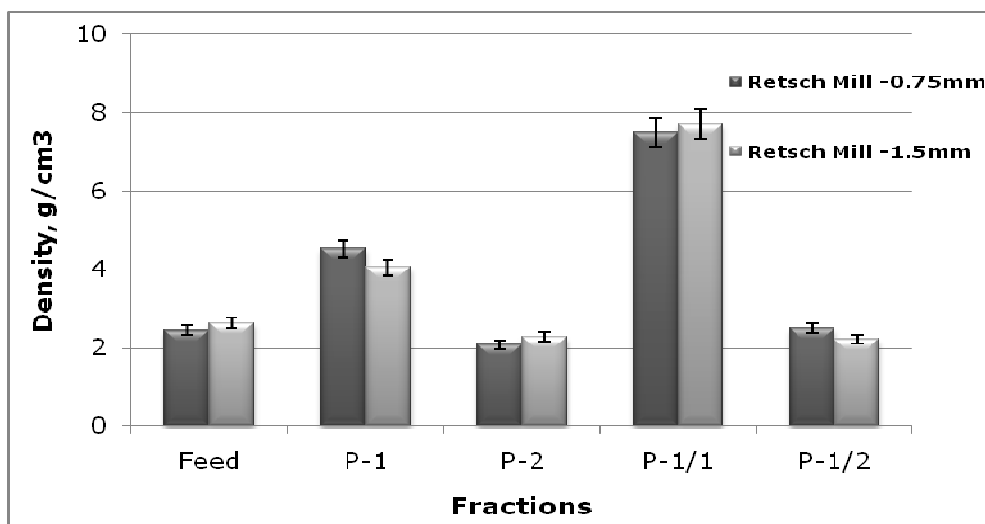


Figure 7.18: Helium pycnometer density measurements of the separated PCB fractions.

The diverse nature of PCB does not allow float-sink, SEM and density measurements to represent changes in individual elemental concentrations of the separated products. Nevertheless, a chemical analysis technique such as Inductively Coupled Plasma-Atomic Emission Spectrometer (ICP-AES), described in Section 3.3.3.4 can be utilized as a useful mean in determining the individual metal concentrations of feed and different separated fractions. The advantages of this technique for PCB element analysis is also stressed in the work of Wienold *et al.*, (2010). ICP-AES technique relies on total acid digestion of a very small sample (~1g) hence true representative sampling is of paramount importance in this type of analysis. In this work, great care was exercised in acquiring each representative sample using a laboratory sampling scoop. Three repeat samples were taken from each separated fractions which were separately digested in aqua-regia and nitric acid. Ten

repeat measurements of each sample were made in the subsequent ICP-AES analysis. The results originating from ICP-AES analyser were statistically analysed to look for any inconsistencies in the measurements.

Statistical analysis such as coefficient of variance (CV) can be used as a valuable tool for boosting confidence on the ICP-AES measurements. A precise method of analysis would result in close to zero CV values; however, in practise %CV values varying in the range of 0 to 5 are generally acceptable. The small and acceptable variations in CV values may be due to the existence of inherent experimental errors.

In this work, the major elements analysed by ICP-AES are outlined in Table 7.11 and Table 7.12 with their corresponding CV and wavelengths. The %CV value for each measurement is below 1% representing very reliable elemental composition measurements by this technique. A small elemental composition difference can be seen by comparing -0.75 and -1.5 mm particle size fractions however no major discrepancy is evident. A slightly lower elemental composition values for -0.75 mm PCB cut may have resulted from the greater material loss in very fine particle size range.

Major elements	Density, g.cm ⁻³	Wavelength	CV (%)	-0.75 mm PCB feed (wt%)
Copper, Cu	8.96	327	0.1	21.72
Tin, Sn	7.31	190	0.12	3.7
Lead, Pb	11.35	220	0.2	2.0
Zinc, Zn	7.13	206	0.15	3.7
Iron, Fe	7.87	238	0.16	4.0
Nickel, Ni	8.9	232	0.12	0.4
Silver, Ag	10.5	328	0.18	0.002
Titanium, Ti	4.54	335	0.21	0.1
Aluminium, Al	2.7	396	0.02	3.2
Gold, Au	19.32	268	0.7	0.02

Table 7.11: Major elements in -0.75 mm PCB feed as analysed by ICP-AES alongside their corresponding wavelengths and CVs. All

elements digested in aqua-regia except silver Ag, which was digested in nitric acid.

Major elements	Density, g.cm ⁻³	Wavelength	CV (%)	-1.5 mm PCB Feed (wt%)
Copper, Cu	8.96	327	0.1	23.3
Tin, Sn	7.31	190	0.23	4.3
Lead, Pb	11.35	220	0.3	2.3
Zinc, Zn	7.13	206	0.22	4.2
Iron, Fe	7.87	238	0.4	4.4
Nickel, Ni	8.9	232	0.4	0.5
Silver, Ag	10.5	328	0.13	0.001
Titanium, Ti	4.54	335	0.4	0.1
Aluminium, Al	2.7	396	0.1	4.21
Gold, Au	19.32	268	0.24	0.011

Table 7.12: Major elements in -1.5 mm PCB feed as analysed by ICP-AES alongside their corresponding wavelengths and CVs. All elements digested in aqua-regia except silver Ag, which was digested in nitric acid.

The elemental concentrations reported in Table 7.11 and Table 7.12 differs slightly from each other. However these figures, when compared with other literature values reported in Table 7.4, Table 7.7, Table 7.8 and Table 7.10, reveal large scale discrepancies in individual elemental concentration values. This is in agreement with the previously reported arguments in section 7.3. Nevertheless, Table 7.13 and Table 7.14 show complete elemental concentration behaviour of -0.75 mm and -1.5 mm Retsch mill cut via vertical vibration separation.

Major element	-0.75 mm feed, % (wt/wt)	First concentrate (P-1), % (wt/wt)	First Tailings (P-2), % (wt/wt)	Second concentrate (P-1/1) % (wt/wt)	Second tailings (P-1/2), % (wt/wt)
Copper, Cu	21.72	48.62	10.47	52.74	24.25
Tin, Sn	3.7	12.28	1.36	12.1	2.45
Lead, Pb	1.97	6.5	0.73	6.25	1.4
Zinc, Zn	3.66	10.46	0.87	13.038	1.8
Iron, Fe	3.963	9.4	1.44	11.56	0.17
Nickel, Ni	0.401	0.88	0.1828	1.0	0.1
Silver, Ag	0.001	0.0015	0.0009	0.002	0.0009
Titanium, Ti	0.08	0.19	0.07	0.13	0.03
Aluminium, Al	3.19	1.1	4.4	0.54	4.23
Gold, Au	0.02	0.0284	0.0063	0.01	0.02

Table 7.13: Elemental composition change in complete vibration separation cycle for -0.75 mm PCB cut.

Major element	-1.5 mm feed, % (wt/wt)	First concentrate (P-1), % (wt/wt)	First Tailings (P-2), % (wt/wt)	Second concentrate (P-1/1) % (wt/wt)	Second tailings (P-1/2), % (wt/wt)
Copper, Cu	23.3	38.55	15.49	50.11	20.83
Tin, Sn	4.3	7.3	2.62	10.7	1.45
Lead, Pb	2.3	3.8	1.51	5.46	0.72
Zinc, Zn	4.2	8.29	1.87	12.09	2.17
Iron, Fe	4.38	7.71	2.44	14.77	0.24
Nickel, Ni	0.5	0.63	0.41	1.34	0.21
Silver, Ag	0.001	0.0015	0.0009	0.002	0.0009
Titanium, Ti	0.01	0.01	0.077	0.042	0.067
Aluminium, Al	4.22	3.0	4.97	0.52	4.73
Gold, Au	0.011	0.01	0.011	0.0036	0.06

Table 7.14: Elemental composition change in complete vibration separation cycle for -1.5 mm PCB cut.

Copper, one of the major constituent of all comminuted PCBs, is concentrated from ~21% (wt/wt) to ~52.74% (wt/wt) in merely two vibration stages. Other elements of notable presence in comminuted PCB feed reported here include, Al, Fe, Pb, Sn and Zn while, Ag, Au, Ni and Ti are only found in very small quantities. Ag and Au are widely regarded as precious earth metals and hence complete recovery of these metals is always a requirement of any separation operation.

Vibration separation of -0.75 mm PCB feed (Table 7.13) showed an increase in all metal concentration values except Al. Low density Al-metal was found to concentrate in the tailings. The PCB tailings were predominantly comprised of different polymeric materials of low density, they also contained significant amounts of Cu, Sn, Zn, Fe and Pb. However SEM images, presented in Figure 7.13 and Figure 7.14, show that the metals present in tailings were generally un-liberated and were in very fine particle size range. The legacy regarding Al concentration in tailings is in alignment with the previously reported separation mechanism of vibration induced separator. The vibration induced separator is mainly reliant on particle size and density differentials to drive any physical separation. In addition similar separation trends were also seen in separating -1.5 mm PCB feed, shown in Table 7.14.

7.3.2 Application-2: Dry separation of iridium and aluminium oxide mixtures

7.3.2.1 Introduction

During the course of many mechanical manufacturing processes, cutting, drilling and grinding operations are in common use (Kalpakjian and Schmid, 2006). These operations normally result in considerable quantities of fine metal chips and/or metal dust particles, which form mixtures with other particles that result due to the abrasion of cutting, drilling and/or grinding tools. The average particle size originating from any grinding and/or shear cutting operation is usually found to be less than 1000 μm . These finely sized metallic dust mixtures are of higher intrinsic value if they originate from precious metals such as iridium.

Pure iridium is a silvery-white and precious transition earth metal of platinum family. It has a density of 22.42g.cm⁻³ (second only to osmium by 0.1%) and melts at 2410°C (Patnaik, 2003). Due to its high melting temperatures iridium has been used as an alloy in many different mechanical components exposed to environments of high temperature, pressure and concentrations. It is chemically inert and can help resist chemical attacks and corrosion at temperatures as high as 2000°C (Patnaik, 2003). However, some molten salts such as sodium and potassium cyanide and halogens particularly fluorine can attack this metal at higher temperatures (Patnaik, 2003). It has the lowest coefficient of expansion among all metals making it a suitable material for its use in the human body such as a platform for broken bones.

The mechanical processing of iridium metal such as extrusion and/or drawing requires its cutting and grinding at some stage. These operations can form a finely sized (<500 μm) particle mixture of

iridium and aluminium oxide. The aluminium oxide particles are believed to originate from the grinding and/or cutting wheel abrasions. The aluminium oxide has a density of 3.89g.cm^{-3} and melts at 1750°C (Patnaik, 2003). Separation of this metallic mixture based on melting point differentials can be accomplished however; this requires considerable amounts of energy due to the high melting point of both metals. Although, other physical separation techniques, such as the ones briefly described in Chapter 2 (e.g. gravity, setting, sieving, electrostatic and hydro-cyclones), are considered well developed however, their particular application in this case look troublesome. Noticeable constraints for this working particle mixture separation operation include; very high density differential material, its greater intrinsic value and the existence of its very fine particle size range. Other noticeable considerations include; a very small scale production of waste mixtures over a relatively long period of time and maximum product recovery with minimal losses and waste generation during its physical separation.

Recycling, recovery and reuse of precious iridium metal is of paramount importance to many manufacturing concerns due to the ever increasing value of this metal in the international market. The work presented in this section will primarily investigate the application of a scaled up vertical vibration separation technique to separate industrially relevant iridium and aluminium oxide solid waste mixtures of varying compositions. Four iridium and aluminium oxide batches were processed in this work and the separation method was optimised for the recovery of nearly pure iridium metal. A particle bed height between 20-30 mm was maintained in each case. The previous work (Chapter 5) regarding the dry separation of fine particle mixtures via vertical vibration was applied to determine the different vibration separation parameters. Once the optimum separation conditions were identified in the trial phases, all samples were processed in identical ways.

7.3.2.1.1 Separation of iridium/aluminium oxide sample-1

The particle size characterisation of iridium/aluminium oxide working particle mixtures (the source of these sample will remain anonymous in this work) (sample-1) is given in Figure 7.19.

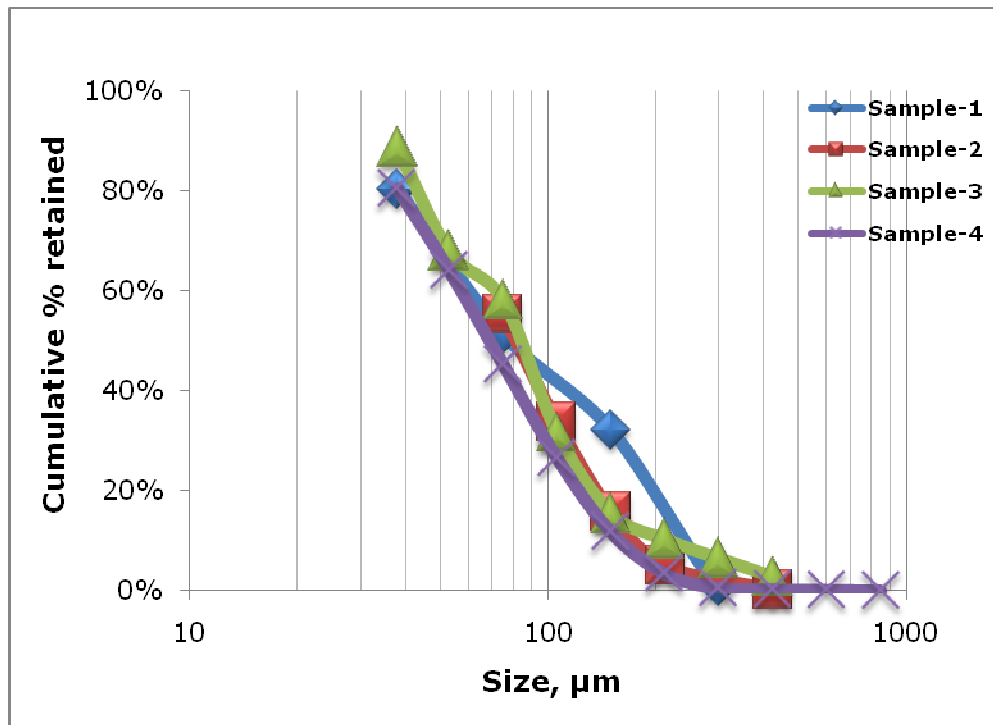


Figure 7.19: Particle size characterisation of iridium and aluminium oxide mixtures.

This sample was acquired from a mechanical grinding batch-1. The average mass mean diameter of this 2kg sample was measured to be 111.58µm by standard sieve analysis. As noted earlier, the Ir/Al₂O₃ mixture has a large density differential ($\rho_{\text{Iridium}}/\rho_{\text{Aluminium oxide}}=8.3$), it was therefore considered to use close size fractions of, 300-425µm, 150-300µm, 75-150µm and 38-75µm, for separation. These size fractions were used in initial experiments to avoid any size segregation that might have coupled with the strong density segregation potential of this mixture during vertical vibration separation. Fractions above 425µm and below 38µm were only present in small amounts (few grams); therefore they were not

considered for vibration separation. In all reported Ir/Al₂O₃ mixture separations hereafter, each mixture was vertically vibrated in separation cell, C-1 (Section 3.2.3, Figure 3.6) for ~20-30 minutes, the time during which most of the Ir was visually observed to separate out into the next chamber, moving through the fixed partition gap size of 5 mm.

Density measurements were used as a mean to record the grades of separated fractions. The feed and separated material samples were taken to avoid any biased representation in the final measurements. A non-destructive density measurement technique employing He-Pycnometer (Micromeritics He Pycnometer" AccPyc 1330 model) was used in this work. The measured densities were then compared with book values to assess the extent of dry separation and purity of the separated materials. The measured densities of sample-1 are shown in Figure 7.20; the measured density on occasions reached as high as 20g.cm⁻³ for 150-300µm & 75-150µm particle size fractions.

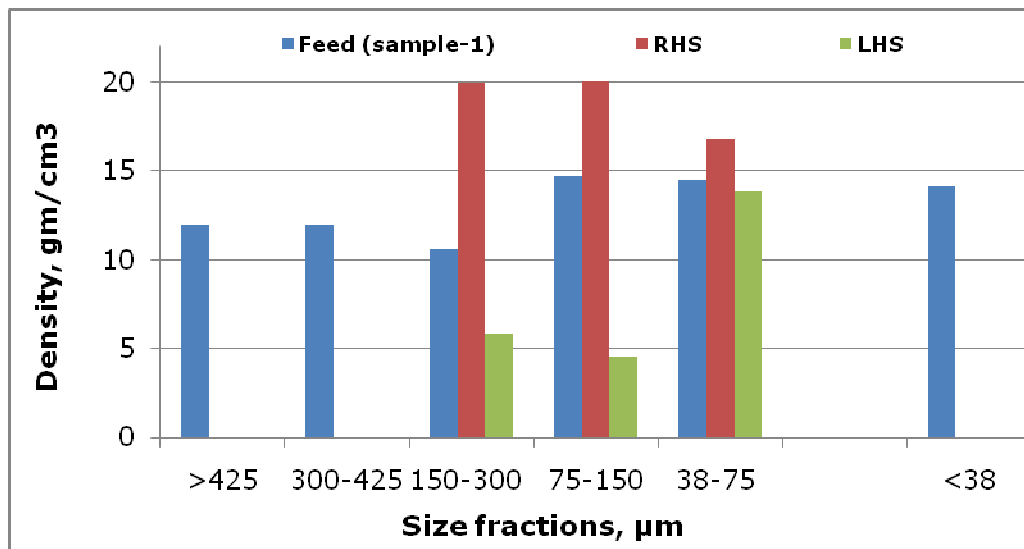


Figure 7.20: Grades of the separated Ir/Al₂O₃ fractions (sample-1).

The high purity values of the separated iridium metal obtained in coarse particle size range can be attributed to the enhanced air

circulation in the coarse particle size range during vertical vibration. Since a large density differential is present in these mixtures, dense particles were expected to achieve higher momentum magnitudes during their global convection current motions. Even the acquired momentum of the iridium particles was enough to drag some of the aluminium oxide particles towards the exit, unfortunately, this leads to the presence of impurities in the separated materials.

Two distinct particle zones were clearly seen within the vibrating particle mixture. The high density iridium particles were seen to dominate the global convection current and were concentrated near to the partition gap. The global convection current was seen to aid in transferring the high density particles into the next chamber. Once there, the vibration force was enough to throw them towards the exit where they were finally collected for analysis. The low density aluminium oxide particles were allowed to concentrate in the main vibrating chamber. Once the vibration separation time was approximately 20-30minutes, the aluminium oxide particles were collected separately.

SEM images were used to confirm the visually observed excellent component liberation of this sample. The images were acquired before and after any vibration separation treatment. The SEM images of feed, iridium and aluminium oxide rich fractions are shown in Figure 7.21.

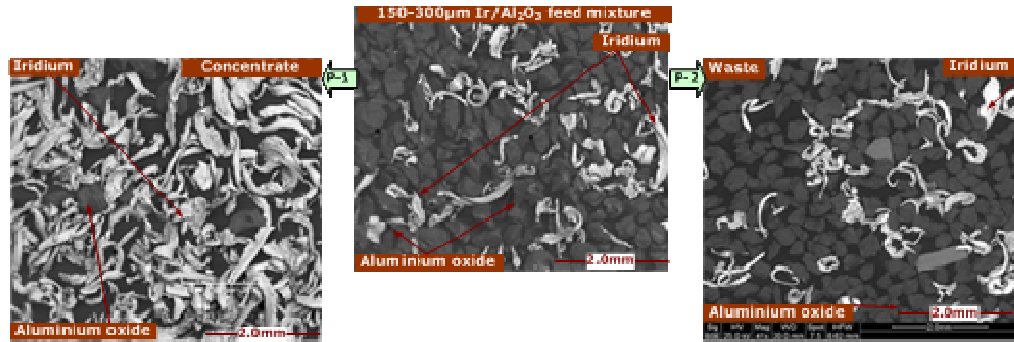


Figure 7.21: SEM Images of the feed and separated 150-300µm Ir and Al₂O₃ fractions (sample-1).

7.3.2.1.2 Separation of iridium/aluminium oxide sample-2

Particle size characterisation of grinding sample-2, shown in Figure 7.19, represents an average mass mean diameter of 78.11µm. This sample-2 had a slightly finer average particle size in comparison to the sample-1. This could be exploited by trying to separate a relatively continuous particle size range of this material. However, good separation did not result when this sample was vibro-separated without any particle sizing. The reason for observing poor separation in particles mixtures having very fine and very large particle sizes can be linked to particle cohesion between fine particles and to the onset of size segregation in the presence of large particles. However, the vibration separation did improve when a particle size range of 75-425µm was used. The purity of feed and separated particles was determined by measuring their densities. The measured density of the separated iridium was observed to reach as high as 21g.cm⁻³, representing very good iridium separation. The measured densities are shown in Figure 7.22.

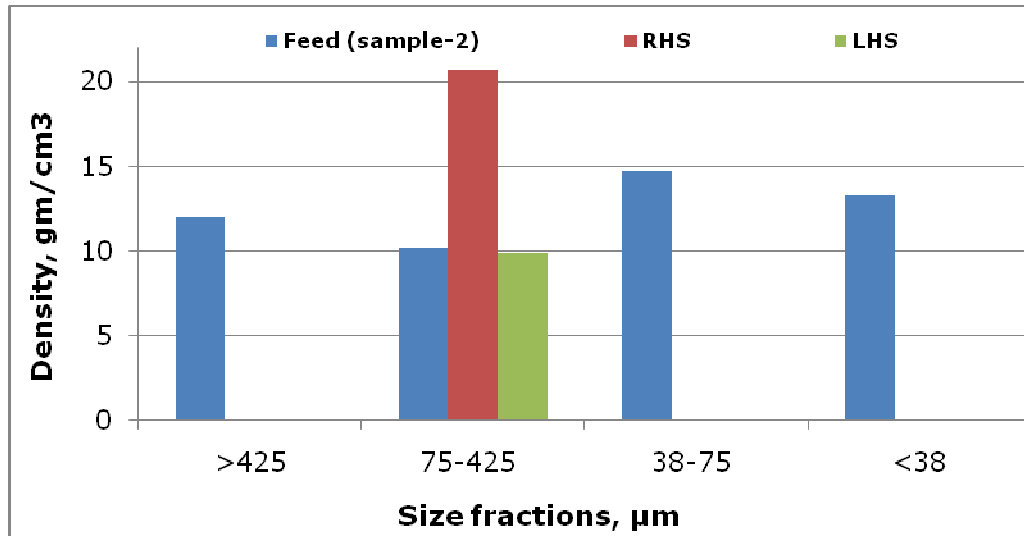


Figure 7.22: Grades of the separated Ir/ Al_2O_3 fractions (sample-2).

SEM images (Figure 7.23) revealed a well liberated feed, aluminium oxide rich and iridium rich products. Little amounts of size fraction above $425\mu\text{m}$ and very fine below $75\mu\text{m}$ restricted their detached vertical vibration separation treatment.

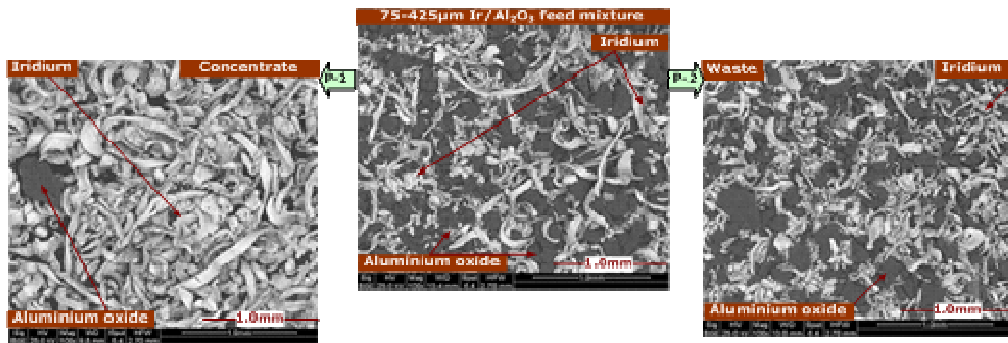


Figure 7.23: SEM Images of the feed and separated $75\text{-}425\mu\text{m}$ Ir and Al_2O_3 separated fractions (sample-2).

7.3.2.1.3 Separation of iridium/aluminium oxide sample-3

In comparison to sample-1 & 2, sample-3 was acquired from a different mechanical cutting source. The complete particle size characterisation of this sample is given in Figure 7.19 and it had an average mass mean particle diameter of $98.77\mu\text{m}$ measured by a standard $\sqrt{2}$ sieve analysis. This sample comprised very fine iridium particles which were not well liberated (Figure 7.25 & Figure 7.26). Aluminium oxide was observed to be present with some fluffy form of material which also had adhered to most of the fine iridium particles around them (Figure 7.26). All of this resulted in reduced particle liberation and hence free motion of the individual particles in distinct convection currents. Hence little and/or no separation, which is also reflected in the reported density measurements of different fractions, was observed. The particle separation behaviour of this sample is shown in Figure 7.24.

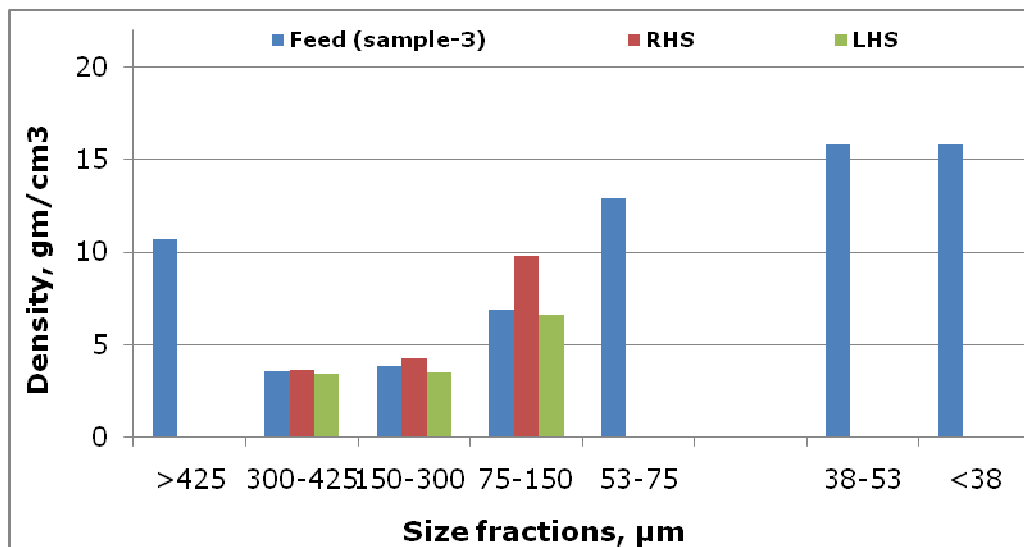


Figure 7.24: Grades of the separated Ir/Al₂O₃ fractions (sample-3).

Due to the limited liberation and very fine particle size range of this sample, the measured densities of the separated products varied between 10 and 15 g.cm^{-3} which seldom increased above 10 g.cm^{-3} for any vibration separated fraction.

In addition to the fluffy material, iridium particles were present in the form of wires which were easy to hook with other particles. The fluffy material was believed to originate from the fibrous base upon which the aluminium oxide particles are adhered to form a cutting wheel. Nonetheless, SEM images confirmed the iridium particle shapes and their adhesion to the fluffy material as shown in Figure 7.25 and Figure 7.26 respectively.

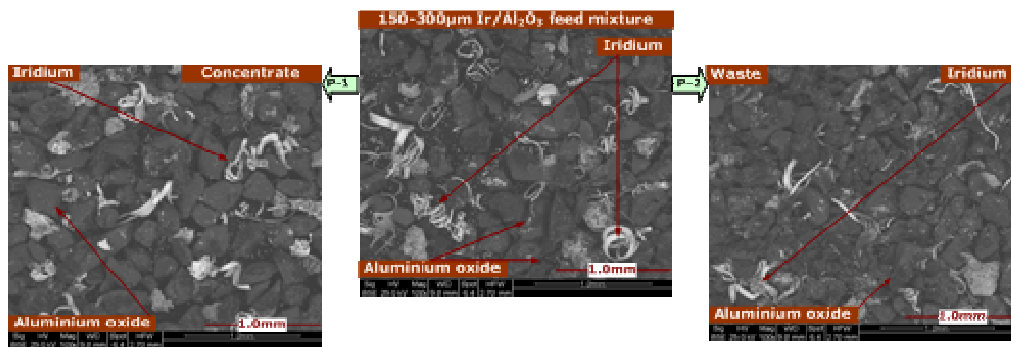


Figure 7.25: SEM Images of the feed and separated 150-300µm Ir and Al₂O₃ separated fractions (sample-3).

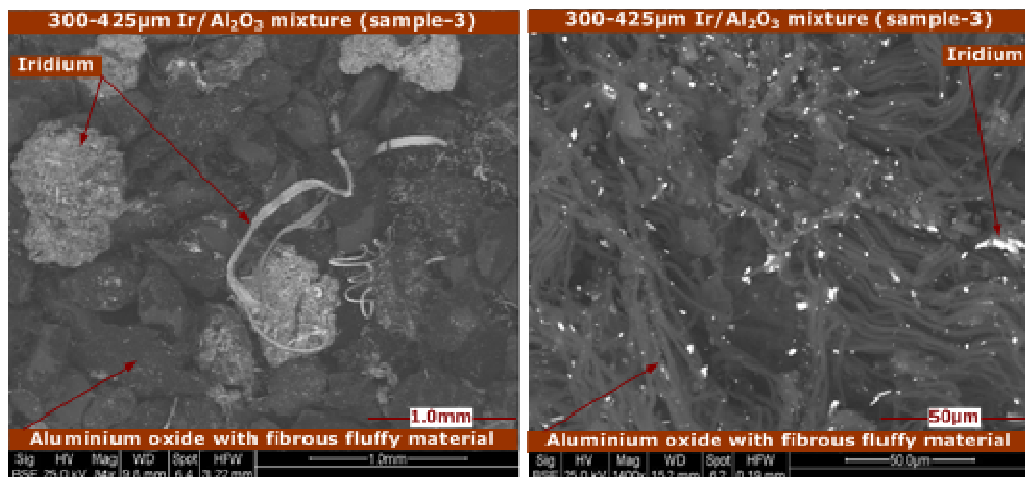


Figure 7.26: SEM Image of 300-425µm Ir/Al₂O₃ mixture.

7.3.2.1.4 Separation of iridium/aluminium oxide sample-4

The complete particle size characterisation of sample-4 is given in Figure 7.19. This size characterisation reveals an average mass mean particle diameter of $51.55\mu\text{m}$ which was measured by a standard $\sqrt{2}$ sieve analysis. This sample had the finest particle size range of all the samples used and was nearly half the value of an average mass mean particle diameter of both sample-1 & 2. Due to the presence of a very tight particle size range, this sample was subjected to vibration separation without any particle pre-sizing. However, the mixture failed to show good separation behaviour with a continuous particle size range. During these initial trial experiments, the presence of very fine particles ($<53\mu\text{m}$, Figure 7.29) resulted in particle bed compactions during vertical vibration. This resulted in restricted particle flows during vibration induced convection motions. As a result, poor and/or undeveloped particle convection patterns were observed. However, $53\text{-}425\mu\text{m}$ particle size range did result in good particle separation which is also represented by their density measurements in Figure 7.27 and SEM images in Figure 7.28.

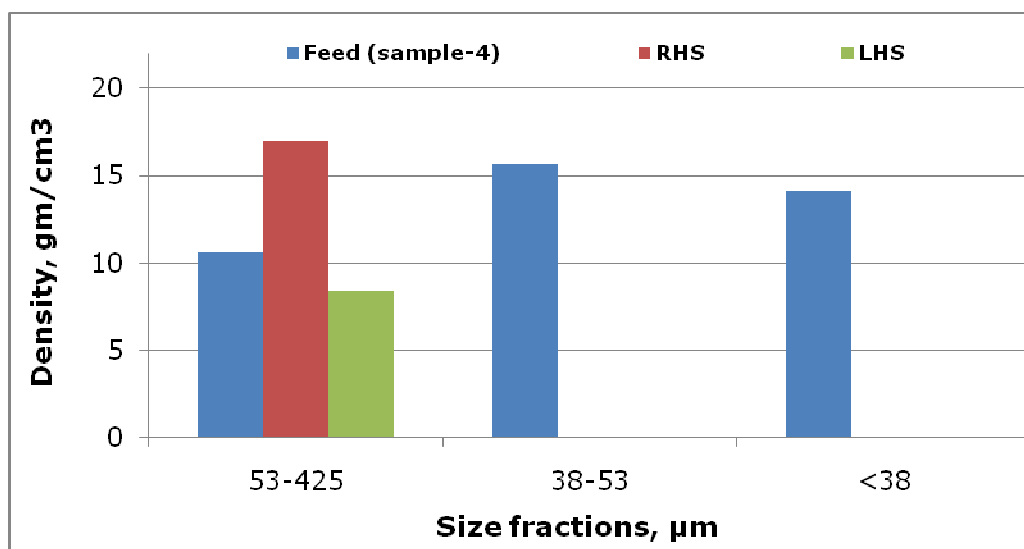


Figure 7.27: Grades of the separated Ir/ Al_2O_3 fractions (sample-4).

The 53-425 μm particle size range mixture achieved a density concentration value of 17.0g.cm⁻³ for the separated concentrate.

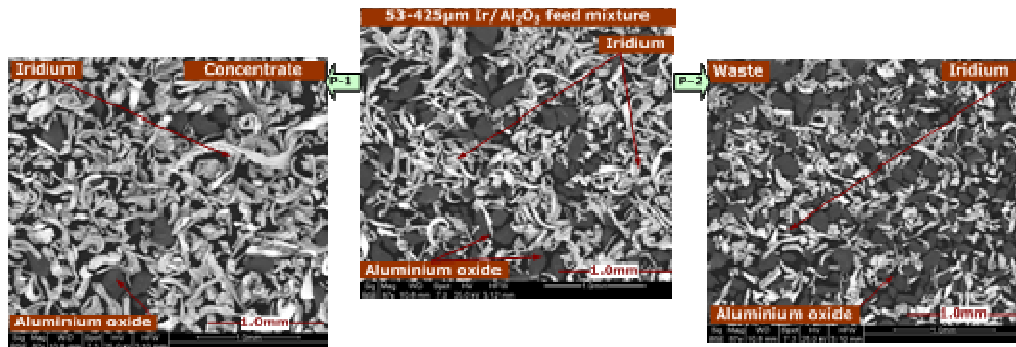


Figure 7.28: SEM Images of the feed and separated 53-425 μm Ir and Al₂O₃ separated fractions (sample-4).

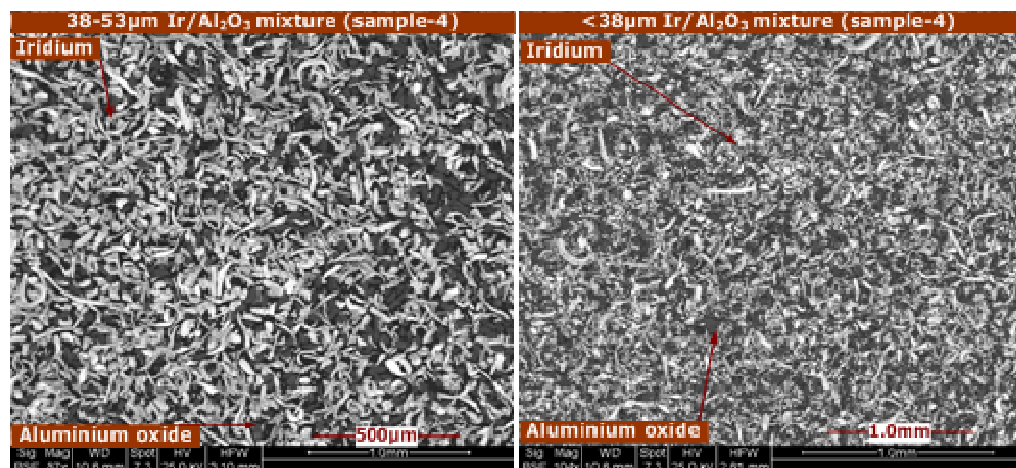


Figure 7.29: 38-53 μm and <38 μm Ir and Al₂O₃ grinding mixture (sample-4).

7.4 Concluding remarks

Based on the work presented in this chapter, the following conclusions can be deduced;

- ❖ High density difference fine particle materials of industrial relevance can be separated by vertical vibration treatment in their dry state.
- ❖ The observed controlling separation factors in vertical vibration treatment are;
 - ♣ Degree of liberation.
 - ♣ Size and shape of the materials.
 - ♣ Density differential in a mixture.
- ❖ The presence of fine particles will result in an increased separation time with decreased grade of the recovered product. However, this can be balanced by employing a series particle separation operation.
- ❖ Care should be exercised in selecting a continuous particle size range as it may result in size segregation coupled with density segregation.

Conclusions and future work

8.1 Conclusions

The main objective of this research was to develop a scaled up vertical vibration driven particle separator and to assess its potential application for dry based separation of a range of particle mixtures. Based on this objective the investigations reported in this thesis have focused on four major particulate system attributes; first, the DEM modelling of segregation in density differential binary particle mixtures that were vertically vibrated in confined virtual containers; second, the development of vertical vibration induced particle separator and its application in exploring the size and density segregation of various synthetic experimental particle mixtures; third, the Positron Emission Particle Tracking of solo particles in the vertically vibrating synthetic binary particle mixtures and fourth, the application of vertical vibration induced particle segregation technique to separate the industrially relevant particle mixtures (iridium and aluminium oxide, shredded PCBs and shredded

computer electrical cables). The principal conclusions deduced from this investigation are summarised as follows;

Finely sized particles are often generated, e.g. as a result of a process requirement such as component liberation, from many different particle processing industries. However, the finely sized particles are often discarded as a waste stream since the recovery of valuable components in this size range is considered uneconomic, inefficient and/or technically challenging. However, increased pressure on world resources has driven the requirement for the extraction of valuable components from the increasingly finely sized particulate materials.

One approach to the dry based separation of the finely sized particle mixtures is the application of a novel vertical vibration technique which causes the size and density differential particle mixtures to segregate. It has been reported (Burtally *et al.*, 2002 and 2003) that vertical vibration can be used to separate and/or position the various components of a size and density differential particle mixture to different regions and/or locations in a prototype scaled rectangular container. However, a clear understanding of the underlying particle segregation mechanism is still lacking and there remains a scope for this work to explore the potential application of this technique to separate the industrially relevant particle mixtures in a semi-continuous mode at a scaled up level.

The absence of complete theoretical models and detailed experimentation in the area of vertical vibration induced particle segregation has resulted in the application of a DEM simulation tool to get an insight into the dynamic particle bed behaviours and acquire an understanding of particle segregation phenomena. A DEM-fluid model has been used in this work to simulate major elements of convection, tilting, segregation and partitioned particle separation in a density differential particle mixture. The DEM-fluid

simulations reported in this work have used a maximum of 1000 particles and the high density particle tracking trends in the density differential particle mixtures were mostly found to be consistent with the Positron Emission Particle Tracking investigations. Some of the worth mentioning particle segregation phenomena replicated by the DEM-fluid simulations reported in this work included layered particle separation, high density particles ending on top and bottom of the particle bed, convection currents, particle bed tilting and partitioned particle separation.

The experimental work reported in this thesis is concerned with the apparatus and methods that were developed to separate the finely sized (1000 μm) particulate materials such as glass and bronze, shredded glass and bronze, shredded printed circuit boards and computer electrical cables and iridium and aluminium oxide particle mixtures. The mixtures used in this work had different particle densities, sizes and shapes. Experimentation has shown that a scaled up, durable, simple and mechanically reliable particle separator capable of vertically vibrating various particle mixtures with sufficient accelerations to impart density and size segregation can be constructed from a combination of pneumatic vibrator, springs, rectangular plate and iron bars as shown in Figure 3.3. The use of a pneumatic control valve (Figure 3.2) with particle separator provided many different options for controlling the frequency and dimensionless acceleration of vertical vibration induced particle separation process.

Experiments and visualizations established that the individual particle properties such as size, shape and density and that of the bulk such as concentration were of prime importance in imparting the effective dry based particle segregation in different synthetic and/or industrially relevant particle mixtures. Of equal importance for an effective particle separation were the geometric construct arrangements of the separation cell assemblies and the amount of

finely sized particle loadings in separation cells that were observed to control the overall dynamics of the vertically vibrating particles and helped in the formation of distinct global convection currents which were deemed necessary to impart segregation in various working particle mixtures.

In line with the layered particle separation reported by Mohabuth, (2007); Burtally *et al.*, (2002 and 2003) in the prototype scaled vertical vibration induced particle separation studies, the investigations reported in this thesis, with a semi-continuous scaled up particle separator design, showed that the layered particle separation can be controlled so as to get high density particles to move out of the main working chamber by passing through a partition gap. Once separated and moved out into the next separate chamber, the valuable separated material can be collected from the open end of the separation cell. Measurements showed that a narrow width (20 and 40mm) particle separation assembly, in which the vertically vibrating working particle mixtures were forced to move in convection currents across the breadth of the working chamber, was best suited for separating the desired components.

In comparison to the prototype scale studies reported by Mohabuth (2007) which mostly used a specific size range particle mixtures, the particle mixtures used in this work were mostly comprised of a continuous particle size range and took longer to segregate at a scaled up level. Convection currents, as noted in the previously reported studies (Mohabuth, 2007; Burtally *et al.*, 2002 and 2003), were considered the prime driving mechanism (as measured by PEPT and shown in Figure 6.2, Figure 6.6, Figure 6.10, Figure 6.14, Figure 6.19, Figure 6.21, Figure 6.23, Figure 6.25, Figure 6.28, Figure 6.30, Figure 6.32, and Figure 6.34) to impart segregation in the vertically vibrating working particle mixtures.

In the investigated vertically vibrated particle mixtures, the formation of two clear-cut and/or distinct particle layers via convection were comparatively less pronounced in the irregular shaped working particle mixtures in comparison to what was clearly observed in the spherical shaped glass and bronze working particle mixtures. However, the formation of distinct and/or clear-cut particle layers in the irregular shaped working particle mixtures was not deemed necessary for particle separation via convection at a scaled up level.

Measurements showed that the use of large particle loadings (e.g. particle bed height $\geq 60\text{mm}$) in the vertically vibrating separation cell assemblies led to changes in the properties of the convective particle motions. In majority of the investigations reported in this work it was found that distinct global convection currents were stronger in the low particle bed height (20 and 40mm) working mixtures and hence resulted in excellent separation (Figure 5.4, Figure 5.19, Figure 5.20, Figure 5.23, and Figure 5.26). When particle bed height was increased above a certain level ($\geq 60\text{mm}$), the formation of distinct global convection currents was observed to cease. At high particle bed heights, the distinct global convection currents were observed to be replaced by the localised convection currents and particle concentrates which in some cases resulted in good separation even at high particle bed heights (as shown in Figure 5.10, Figure 5.15, Figure 7.4, Figure 7.5, Figure 7.6, Figure 7.8, and Figure 7.9).

Measurements showed that the use of a small partition gap (5 and 10mm) size is important in controlling the flow of valuable components from the main working chamber. Measurements also showed that the vertical vibration frequency of $30 \pm 10\%$ Hz and the dimensionless acceleration magnitude of $3 \pm 10\%$ were optimum for the experimental segregation of the particle mixtures however, in DEM simulations performed with glass and bronze mixtures,

segregation was best simulated at low (6Hz) as well as high (45Hz) magnitudes of vertical vibration frequency with nearly the same dimensionless acceleration (2 and 2.25) magnitudes.

The optimum experimentally measured particle separation conditions of vertical vibration frequency and dimensionless acceleration magnitudes reported in this work were based on the successful particle separation efficiencies, recoveries and grades which were mostly assessed through the heavy liquid analysis and helium pycnometry. The recovery of valuable components from the complex shaped multi-component particle mixtures were assessed by the ICP-AES analysis. Particle separation recoveries and grades as high as $\geq 50\%$ and $\geq 95\%$ were reported for some investigations.

In this work, the scaled up particle separator was not only used to separate the high density differential particle mixtures but measurements also showed that it was capable of separating the size differential particle mixtures (big and small size glass particles) of parallel shapes and densities with high grades and recoveries. Since, particles as well the interstitial fluid is thought to play an important role in particle segregation, a Positron Emission Particle Tracking as well as a smoke blanket visualisation was carried out to report the individual particle trajectories and interstitial gas movements during the course of vertical vibration induced particle segregation. The visualization of interstitial gas dynamics via smoke blanket movements on top of a vertically vibrating particle bed showed some distinct fluid motions which were mostly observed to be moving in an anti-clock wise direction, opposite to the convention current movements of the vibrating particles.

PEPT measurements showed that the high and low density particles followed distinct trajectories when they were vertically vibrated in a particle mixture. Measurements also confirmed that the tracking particle trajectories were different at different particle bed heights.

Also, the tracked particle accelerations were different at different locations in a vibrated particle bed. In comparison to the tracer particle location deep inside the particle bed, the average tracer particle speeds were significantly higher near to the top of the tilted particle bed and when it slide downhill from the top of the tilted particle bed surface. Convective motions of the individual high density particles in this fashion were thought to be the prime factor for particle separation via vertical vibration.

The experiments on the scaled up semi-continuous particle separator confirmed what was identified previously in that good particle separation could be achieved through careful control of the frequency and acceleration during vertical vibration. This information lays the foundations for a new breed of low cost, dry separator for fine particulate mixtures.

8.2 New scientific contributions

Based on the work presented in this thesis the following contributions to the scientific knowledge were made;

- ❖ By means of DEM simulations, an analysis of the vertically vibrated particle bed was carried out. Of particular interest was the modelling of particle segregation in a prototype scaled two compartment separation cell.
- ❖ By means of experimentation, the design of a novel vertical vibration induced particle separation cell was presented and optimised for the separation of various regular and irregular shaped particle mixtures.
- ❖ Tracking of various solo particles and the interstitial fluid dynamics during the course of vertical vibration induced particle segregation was performed to report some distinct particle and interstitial fluid behaviours.
- ❖ By means of experimentation, comminuted printed circuit board complex shape particle mixtures were separated on dry basis.

8.3 Future work

Based on the work reported in this thesis the following recommendations are made for future work;

- ❖ The DEM work presented in this thesis has provided a useful insight to aid in the further development of a full scale DEM-fluid simulation program. The especially encouraging aspects that can be included in future model developments are; the development of a model that can tackle an enhanced number of particles, modelling in three dimensions and the inclusion of a more detailed fluid motion model.
- ❖ There are possibilities for this technique to be used in series whereby several narrow width separation cells can be attached to the same vibration plate.
- ❖ There are plenty of possibilities to explore vertical vibration induced particle separation to design a separator that can be operated in a continuous mode.
- ❖ The simple particle separator presented in this thesis can be combined with other particle separation techniques to best achieve particle separation in a continuous mode. The process combination scheme is stressed because too often different separation processes are seen as individual solutions without looking for a possibility to combine the best parts of the two different processes.
- ❖ A more systematic approach is needed in treating the application of this novel vertical vibration induced particle separation technique for example in application of a parallel and/or series operation.
- ❖ The application of vertical vibration induced particle separation technique need to be explored with other industrially relevant mineral and solid waste particle mixtures.

References

- 1 AEA Technology, (2006), "WEEE and hazardous waste: part 2", A report produced for Department for Environment, Food and Rural Affairs (DEFRA), London, UK.
- 2 Akiyama, T., Aoki, K.M., Yamamuro, K. and Yoshikawa, T., (1998), "Experimental study on vibration-induced convection and heaping in granular beds", *Granular Matter*, Vol.**1**, pp.15-20.
- 3 Akiyama, T., Yamamuro, K. and Okutsu, S., (2000), "A solid-solid extraction", *Powder technology*, Vol.**110**, pp.190-195.
- 4 Answer, (2009), available online at www.answers.com/topic/mechanical-classification, retrieved on 25/04/2009 at 11:40GMT.
- 5 Aoki, K.M., Akiyama, T., Maki, Y. and Watanabe, T., (1996), "Convective roll patterns in vertically vibrated beds of granules", *Physical Review, The American Physical Society*, Vol.**E54**, No.1, pp.874-883.
- 6 Aoki, K.M., and Akiyama, T., (1995), "Simulation studies of pressure and density wave propagation in vertically vibrated bed of granules", *Physical Review E., The American Physical Society*, Vol.**52**, No.3, pp.3288-3291.
- 7 APME, (1997), "Feedstock recycling of electrical and electronic plastic waste, depolymerisation and conversion into syncrude", A technical paper by the Association of Plastic Manufacturers in Europe, A joint APME and VKE Project.
- 8 Aranson, I.S. and Tsimring, L.S., (2006), "Patterns and collective behaviour in granular media: Theoretical concepts", *Reviews of Modern Physics*, Vol.**78**, pp. 641-692.
- 9 Asmar, B.N., Langston, P.A., Matchett, A.J., and Walters, J.K., (2002), "Validation tests on a distinct element model of vibrating cohesive particle systems", *Computers and Chemical Engineering*, Vol.**26**, pp.785-802.

-
- 10 Azéma, E., Radjaï, F., Peyroux, R., Dubois, F., and Saussine, G., (2006), "Vibrational dynamics of confined granular materials", *Physical Review E, The American Physical Society*, Vol.**74**, pp.031302/1-10.
- 11 Barigou, M., (2004), "Particle tracking in opaque mixing systems: An overview of the capabilities of PET and PEPT", *Chemical Engineering Research and Design, Trans IChemE, Part A*, Vol.**82**, No.A9, PP.1258-1267.
- 12 Barley, R.W., Baker, J.C., Pascoe, R.D., Kostuch, J., McLoughlin, B., and Parker, D.J., (2004), "Measurement of the motion of grinding media in a vertically stirred mill using positron emission particle tracking (PEPT) Part II", *Minerals Engineering*, Vol.**17**, pp.1179-1187.
- 13 Barsky, E., (2004), "Conditions providing optimum separation", *Physical Separation in Science and Engineering*, Vol.**13**, Issue, 3-4, pp.153-163.
- 14 Baumann, G., Janosi, I. M., & Wolf, D. E., (1994), "Particle trajectories and segregation in a two-dimensional rotating drum", *Euro phys. Lett.*, Vol.**27**, no.3, pp. 203-208.
- 15 Biddle, M.B., Dinger, P., and Fisher, M.M., (2009) "An overview of recycling plastics from durable goods: Challenges and opportunities", Identiplast II Conference Reprint, available online at http://www.americanchemistry.com/s_plastics/doc.asp?CID=1588&DID=6044, Retrieved on 28/08/2009 at 09:30GMT.
- 16 Bigum, M., and Brogaard, L.K-S., (2009), "LCA Modelling of metal recovery from WEEE, Waste Electrical and Electronic Equipment", M.Sc Thesis, DTU Environment, Technical University of Denmark. Available online at <http://www.affaldsinfo.dk/files/Filer/Litteratur/Rapporter%20til%20hjemmesiden/LCA%20modelling%20of%20metal%20recovery%20from%20WEEE.pdf>, retrieved on 14/04/2010 at 21:30GMT.
- 17 Biswas, P., Sánchez, P., Swift, M.R. and King, P.J., (2003), "Numerical simulations of air-driven granular separation",
-

-
- Physical Review, The American Physical Society*, Vol.**E68**, pp.050301/1-4.
- 18 Boerrigter, H., (2000), "Implementation of thermal processes for feedstock recycling of bromine and antimony, with energy recovery, from plastics waste of electrical and electronic equipment (WEEE), Phase-1, Unit ECN Biomass of the Netherlands Energy Research Foundation (ECN), Project No. 8.20183. Available online at <http://www.ecn.nl/docs/library/report/2000/c00114.pdf> and phase-2 report on http://ec.europa.eu/environment/waste/stakeholders/industry_assoc/ebfrp/annex7.pdf, retrieved on 28/08/2009 at 08:14GMT.
- 19 Bougie, J., Moon, S.J., Swift, J.B. and Swinney, H.L., (2002), "Shocks in vertically oscillated granular layers", *Physical Review Letters, The American Physical Society*, Vol.**E66**, No.5, pp.051301/1-9.
- 20 Bourzutschky, M. and Miller, J., (1995), "'Granular' convection in a vibrated fluid", *Physical Review Letters, The American Physical Society*, Vol.**74**, No.12, pp.2216-2219.
- 21 Breu, A.P.J., Ensner, H.M., Kruelle, C.A. and Rehberg, I., (2003), "Reversing the Brazil nut effect: competition between percolation and condensation", *Physical Review Letters, The American Physical Society*, Vol.**90**, pp.014302-1-3.
- 22 Brey, J.J., Ruiz-Montero, M.J. and Moreno, F., (2005), "Energy partition and segregation for an intruder in a vibrated granular system under gravity", *Physical Review Letters, The American Physical Society*, Vol.**95**, No.9, pp.098001/1-4.
- 23 Bridgwater, J., (2003), "The dynamics of granular materials – towards grasping the fundamentals", *Granular matter*, Vol.**4**, pp175-181.
- 24 Brone, D., and Muzzio, J., (1997), "Size segregation in vibrated granular systems: A reversible process", *Physical*
-

-
- Review E, The American Physical Society, Vol.56, No.1, PP.1059-1063.*
- 25 BS 1796-1, (1989) and ISO 2591-1, (1988), "Test sieve manual", Endecotts Ltd. Publishers, London.
- 26 BS 7067, (1990), "Guide to determination and presentation of float and sink characteristics of raw coal and of products from coal preparation plants", British Standard Institution, London.
- 27 Buell, (2010)," Introduction to air classification", Buell Classifier, Fisher-Klosterman Inc., available online at http://www.buellclassifiers.com/intro_air.htm, retrieved on 09/04/2010 at 12:25GMT.
- 28 Burtally, N., (2004), "Dynamical behaviour of fine binary mixtures in the presence of air", Ph.D. Thesis, School of Physics and Astronomy, University of Nottingham, UK
- 29 Burtally, N., King, P.J. and Swift, M.R., (2002), "Spontaneous air-driven separation in vertically vibrated fine granular mixtures" *Science*, Vol.**295**, pp.1877-1879.
- 30 Burtally, N., King, P.J., Swift, M.R. and Leaper, M., (2003), "Dynamical behaviour of fine granular glass/bronze mixtures under vertical vibration", *Granular Matter*, Vol.**5**, pp.57-66.
- 31 Campbell, C.S., (1990), "Rapid granular flows," *Annual Review of Fluid Mechanics*, Vol.**22**, pp.57-90.
- 32 Campbell, C.S., (2006), "Granular material flows – An overview", *Powder Technology*, Vol.**162**, pp.208-229.
- 33 Castellanos, A., (2005), "The relationship between attractive inter particle forces and bulk behaviour in dry and uncharged fine powders", *Advances in Physics*, Vol.**54**, No.4, pp. 263-376.
- 34 Catherall, A.T., López-Alcaraz, P., Sánchez, P., Swift, M.R. and King, P.J., (2005), "Separation of binary granular mixtures under vibration and differential magnetic levitation force", *The American Physical Society*, Vol.**71**, Issue.2, pp.021303/1-8.
-

-
- 35 Chancerel, P., and Rotter, S., (2009), "Recycling-oriented characterisation of small waste electrical and electronic equipment" *Waste Management*, Vol.**29**, pp.2336-2352.
- 36 Chicago, (2009), "Chicago vibrator products flow and compaction", Available online at <http://www.chicagovibrator.com/Default.aspx?tabid=58> retrieved on 10/06/2009 at 16:17GMT.
- 37 Chou, C-S., (2000), "Research on rapid granular flows of highly inelastic particles", *Proc. Natl. Sci. Counc. ROC(A)*, Vol.**24**, No.5, pp.317-329.
- 38 Cleary, P.W., Sinnott, M.D., Morrison, R.D., (2008), "DEM prediction of particle flows in grinding processes", *International Journal for Numerical Methods in Fluids*, Wiley Inter Science, Vol.**58**, pp.319-353.
- 39 Clément, E. & Rajchenbach, J., (1991), "Fluidization of a bi-dimensional powder", *Europhys. Lett.*, Vol.**16**, no.2, pp. 133-138.
- 40 Clément, E. & Rajchenbach, J., (1992), "Experimental study of heaping in a two-dimensional sandpile", *Physical Review Letter*, Vol.**69**, pp. 1189-1192.
- 41 Clément, E., Duran, J., and Rajchenbach, J., (1992), "Experimental study of heaping in a two dimensional "sandpile"", *Physical Review Letters, The American Physical Society*, Vol, **69**, No.8, pp.1189-1192.
- 42 Coniglio, A. & Herrmann, H. J. (1996), "Phase transitions in granular packings". *Physica A*, Vol.**225**, pp. 1-6.
- 43 Cooke, W., Warr, S., Huntley, J.M and Ball, R.C., (1996), "Particle size segregation in a two-dimensional bed undergoing vertical vibration" *Physical Review, The American Physical Society*, Vol. **E53**, No.3, pp.2812-2822.
- 44 Couper, J.R., Penney, W.R., Fair, J.R., Walas, S.M., (2010), "Disintegration, agglomeration, and size separation of particulate solids", Chaper-12 in *Chemical Process Equipment Selection and Design*, Revised Second Edition, Butterworth-Heinemann Publishers Oxford, OX2 8DP, U.K, pp.364.
-

-
- 45 Cui, J. and Forssberg, E., (2003), "Mechanical recycling of waste electric and electronic equipment: a review", *Journal of Hazardous Materials*, Vol.**B99**, pp.243-263.
- 46 Cui, J., (2005), "Mechanical recycling of consumer electronic scrap", Ph.D Thesis, Luleå University of Technology, Sweden.
- 47 Cui, J., and Forssberg, E., (2003), "Mechanical recycling of waste electric and electronic equipment: a review", *Journal of Hazardous Materials*, Vol.**B99**, pp.243-263.
- 48 Daniels, E., (2009), "Froth-Flotation, An innovative plastics recycling process developed by Argonne National Laboratory", University of Chicago, USA, Available online at http://www.es.anl.gov/Energy_Systems/Process_Engineering/Current_Projects/Documents/FROTH.pdf, retrieved on 28/08/2009 at 08:48GMT.
- 49 Das, A., Vidyadhar, A., and Mehrotra, S.P., (2009), "A novel flowsheet for the recovery of metal values from printed circuit boards", *Resources, Conservation and Recycling*, Vol.**53**, pp.464-469.
- 50 David and Janets's collections, available online at http://images.google.co.uk/imgres?imgurl=http://lh4.ggpht.com/_WglGCzgzMg/R05rzNt1cI/AAAAAAAAAQ/rDICA6hI7iA/IMG_0411.JPG&imgrefurl=http://picasaweb.google.com/lh/photo/a3uZUmSsP2nMkRzC70w2Lw&usg=__KVZLYhNOzmYWVuMTwzNq40bPZmA=&h=1200&w=1600&sz=26&hl=en&start=6&sig2=XDmxngi7FpsYWo5Scu_8lw&tbnid=6D0JLuCnU1ZT8M:&tbnh=113&tbnw=150&prev=/images%3Fq%3Dstony%2Bdesert%26hl%3Den%26rlz%3D1T4ADBF_en-GBGB245GB247&ei=N1_WScK-MMagjAeiuYX_Dg, retrieved on 03/04/09 at 10:00GMT.
- 51 de Gennes, P.G., (1999), "Granular matter: A tentative view", *Reviews of Modern Physics, The American Physical Society*, Vol.**71**, No.2, pp.S374-S382.
- 52 De jong, T.P.R., Fabrizi, L. and Kuilman, W., (2005), "Dry density separation of mixed construction and demolition waste", Presentation for the 2005 sortierkolloquium, TU
-

-
- Berlin, available online at (http://www.kringbouw.nl/kringbouw/data/publiek/nieuws/bestand_CDWRecSortierKollBerlin05.pdf) and retrieved on 27/05/2009 at 11:34 GMT.
- 53 Deanne, T., (2004), "See n sort: optical sorting equipment helps recycles to sort diverse materials into relatively homogeneous commodity streams", News publications, BNET, U.K., available online at, http://findarticles.com/p/articles/mi_m0KWH/is_5_42/ai_n6080226, retrieved on 17/06/2008 at 10:30GMT.
- 54 Defra, (2009), "Waste Electrical and Electronic Equipment", Available online at <http://www.defra.gov.uk/environment/waste/strategy/strategy07/pdf/waste07-annex-c10.pdf>, retrieved on 10/07/2009 at 17:03GMT.
- 55 Delgado, C and Stenmark, A., (2005), "Technological reference paper on recycling plastics", Virtual European Recycling Centre, Available online at http://www.wastexchange.co.uk/documenti/H%20Medio_Ambiente_PROYECTOS_Z5008_verc_clara_WP2_refpaper_Refpaper_plastic_v2.pdf, retrieved on 12/04/09 at 10:00GMT.
- 56 Deng, R., and Wang, C-H., (2003), "Instabilities of granular material undergoing vertical vibrations: a uniformly driven layer", *Journal of Fluid Mechanics*, Cambridge University Press, Vol.**492**, pp.381-410.
- 57 Density separation, (2009), available online at http://209.85.229.132/search?q=cache:05QxeTZfMRAJ:www.femp.org/info/Recycling/10_Sifting_DryDensity/10_DryDensity.pdf+SIFTING+%26+DRY+DENSITY+SEPARATION&cd=2&hl=en&ct=clnk&gl=uk, retrieved on 05/06/2009 at 19:43GMT.
- 58 Dimitrakakis, E., Janz, A., Bilitewski, B., and Gidaracos, E., (2009), "Determination of heavy metals and halogens in plastics from electric and electronic waste", *Waste Management*, Vol.**29**, pp.2700-2706.
-

-
- 59 Dolgunin, V.N., Ukolov, A.A. and Ivanov, O.O., (2006), "Segregation kinetics in the rapid gravity flow of granular material", *Theoretical Foundations of Chemical Engineering*, Pleiades Publishing, Inc., ISSN 0040-5795, Vol.**40**, No.4, pp.393-404.
- 60 Duran, J., (2000), "Sands, powders and grains: an introduction to the physics of the granular materials", Springer-Verlag Inc., N.Y, USA.
- 61 Duran, J., Mazozi, T., Clément, E. and Rajchenbach, J., (1994), "Size segregation in a two-dimensional sand pile: Convection and arching effects", *Physical Review*, *The American Physical Society*, Vol.**E50**, pp.5138-5141.
- 62 Duran, J., Rajchenbach J. & Clément, C., (1993). "Arching effect model for particle size segregation", *Phys. Rev. Lett.*, Vol.**70**, no.16, pp. 2431-2434.
- 63 Dwivedy, M., and Mittal, R.K., (2010), "Estimation of future outflows of e-waste in India", *Waste Management*, Vol.**30**, pp.483-491.
- 64 Eisenmann, M, D., (2005), Elutriation technology in heavy mineral separations", *M.Sc Thesis*, Virginia Polytechnic Institute and State University, Blacksburg, Virginia, USA. Available online at <http://scholar.lib.vt.edu/theses/available/etd-11152001-101926/unrestricted/Thesis-Eisenmann.pdf>, retrieved on 09/04/2010 at 12:39GMT.
- 65 Eswaraiah, C., Kavitha, T., Vidyasagar, S. and Narayanan, S.S., (2006), "Classification of metals and plastics from printed circuit boards (PCB) using air classifier", *Chemical Engineering and Processing: Process Intensification*, Vol.**47**, Issue-4, pp.565-576.
- 66 EUROPA, (2009), "Waste electrical and electronic equipment", available online at http://ec.europa.eu/environment/waste/weee/index_en.htm, retrieved on 10/07/2009 at 20:20GMT.
-

-
- 67 Evesque, P., and Rajchenbach, J., (1989), "Instability in a sand heap", *Physical Review Letter*, Vol.**69**, pp.44-46.
- 68 Fairhurst, P.G., Barigou, M., Fryer, P.J., Pain, J.-P., and Parker, D.J., (2001), "Using positron emission particle tracking (PEPT) to study nearly neutrally buoyant particles in high solid fraction pipe flow", *International Journal of Multiphase Flow*, Vol.**27**, pp.1881-1901.
- 69 Falcon, È., Fauve, S. and Laroche, C., (1999), "Cluster formation, pressure and density measurements in a granular medium fluidised by vibrations", Rapid Note in Euro physics, *The European Physical Journal B*, EDP Sciences, Springer Verlag, Vol.**9**, pp.183-186.
- 70 Falconer, A., (2003), "Gravity separation: Old technique/New methods", *Physical Separation in Science and Engineering*, Taylor and Francis Group, Vol.**12**, No.1, pp.31-48.
- 71 Fan, X., Parker, D.J., and Smith, M.D., (2006a), "Enhancing ¹⁸F uptake in a single particle for positron emission particle tracking through modification of solid surface chemistry", *Nuclear Instruments and Methods in Physics Research A*, Vol.**558**, PP.542-546.
- 72 Fan, X., Parker, D.J., and Smith, M.D., (2006b), "Labelling a single particle for positron emission particle tracking using direct activation and ion-exchange techniques", *Nuclear Instruments and Methods in Physics Research, Section A*, Vol.**562**, No.1, PP.345-350.
- 73 Fang, X., and Tang, J., (2007), "A direct simulation Monte Carlo approach for the analysis of granular damping", *Journal of Computational and Nonlinear Dynamics, Transactions of the ASME*, Vol.**2**, pp.180-189.
- 74 Fangary, Y.S., Barigou, M., Seville, J.P.K., and Parker, D.J., (2000), "Fluid trajectories in a stirred vessel of non-Newtonian liquid using positron emission particle tracking", *Chemical Engineering Science*, Vol.**55**, pp.5969-5979.
- 75 Faraday, M., (1831), " On a peculiar class of acoustical figures; and on certain forms assumed by groups of particles
-

-
- upon vibrating elastic surfaces”, *Corr. Mem. Royal Academy of Sciences*, Paris, pp.299-340.
- 76 Fazekas, S., (2007), “Distinct element simulations of granular materials”, *Ph.D. Thesis*, Budapest University of Technology and Economics, Hungary.
- 77 Feitosa, K and Menon, N., (2002), “Breakdown of energy equipartition in a 2D binary vibrated granular gas”, *Physical Review Letter, The American Physical Society*, Vol.**88**, No.19, pp.198301/1-4.
- 78 Feitosa, K. and Menon, N., (2002), “Breakdown of energy equipartition in a 2D binary vibrated granular gas”, *Physics Review Letters, The American Physical Society*, Vol.**88**, No.19, pp.198301/1-4.
- 79 Fluent, (2009), available online at <http://www.fluent.com/solutions/metals/cycloneseparator.htm>, retrieved on 21/04/2009 at 22:22GMT.
- 80 Ford, K.J., Gilchrist, J.F., and Caram, H.S., (2009), “Transition to vibro-fluidization in a deep granular bed”, *Powder Technology*, Vol.**192**, pp.33-39.
- 81 Forest Research, (2007), “One billion PCs in use by the end of 2008”, A press Release by Forrester, available online at <http://www.forrester.com/ER/Press/Release/0,1769,1151,00.html>, retrieved on 14/07/2009 at 21:16GMT.
- 82 Fraige, F.Y., and Langston, P.A., (2006), “Horizontal pneumatic conveying: a 3d distinct element model”, *Granular Matter*, Springer-Verlag, Vol.**8**, No.2, pp.67-80.
- 83 Fraige, F.Y., Langston, P.A., and Chen, G.Z., (2008), “Distinct element modelling of cube particle packing and flow”, *Powder Technology*, Vol.**186**, pp.224-240.
- 84 Frontier recycling, (2009), available online at <http://www.frontierrecycling.co.uk/products/>, retrieved on 28/07/2009 at 13:40GMT.
- 85 Gallas, J.A.C., Herrmann, H.J., and Sokolowski, S., (1992), “Convection cells in vibrating media”, *Physical Review Letter, The American Physical Society*, Vol.**69**, No.9, pp.1371-1374.
-

-
- 86 Galvin, J.E., Dahl, S.R. and Hrenya, C.M., (2005), "On the role of non-equipartition in the dynamics of rapidly flowing granular mixtures", *Journal of Fluid Mechanics*, Cambridge University Press, U.K, Vol.**528**, pp.207-232.
- 87 Garzó, V. and Dufty, J.W., (2002), "Hydrodynamics of a granular binary mixture at low density", *Physics of Fluids*, American Institute of Physics, Vol.**14**, No.4, pp.1476-1490.
- 88 Garzó, V., (2008), "Segregation in granular binary mixtures: Thermal diffusion", Available online at http://arxiv.org/PS_cache/cond-mat/pdf/0603/0603232v3.pdf retrieved on 14/05/2009 at 11:42GMT.
- 89 Ghadiri, M., Yuregir K.R., Pollock, H.M., Ross, J.D.J. & Rolfe, N., (1991), "Influence of processing conditions on attrition of NaCl crystals", *Powder Tech.*, Vol.**65**, pp 311-320.
- 90 GM Engineering, (2010), "Post consumer PET bottles washing lines", available online at http://www.ledarecycling.it/menu/pet_bottles_recycling.htm, retrieved on 31/03/2010 at 15:35GMT.
- 91 Goldhirsch, I. (2001), "Kinetic and continuum descriptions of granular flows", *Mechanics for a new millennium*, *Kluwer academic publishers*, Netherlands, pp-345-358.
- 92 Goldhirsch, I., (2003), "Rapid granular flows", *Annu. Rev. Fluid Mech.*, Vol.**35**, pp.267-293.
- 93 Goldshtein, A., Shapiro, M., and Gutfinger, C., (1996), "Mechanics of collisional motion of granular materials. Part 4. Expansion wave", *J. Fluid Mechanics*, Vol.**327**, pp.117-138.
- 94 Goosey, M., and Kellner, R., (2003), "A scoping study end-of-life printed circuit boards", *Circuit World*, Vol.29, No.3, pp.33-37, Intellect, Shipley Europe Limited, Department of Trade and Industry, UK, available online at http://www.intellectuk.org/component/option,com_docman/task,cat_view/gid,262/?mosmsg=You+are+trying+to+access+from+a+non-authorized+domain.+%28www.google.co.uk%29.
-

-
- 95 Götzendorfer, A., (2007), "Vibrated granular matter: transport, fluidisation and patterns", *Ph.D. Thesis*, Von der Universität Bayreuth, Germany.
- 96 Götzendorfer, A., Tai., C-H., Kruelle, C.A., Rehberg, I., and Hsiau, S-S., (2006), "Fluidisation of a vertically vibrated two-dimensional hard sphere packing: A granular meltdown", *Physical Review E*, Vol.**74**, pp.011304/1-9.
- 97 Gungor, A., Gupta, S.M., (1998), "Issues in environmentally conscious manufacturing and product recovery: a survey", *Computers and Industrial Engineering*, Vol.**36**, pp.811-853.
- 98 Guo, J., Guo, J., and Xu, Z., (2009), "Recycling of non-metallic fractions from waste printed circuit boards: A review", *Journal of Hazardous Materials*, Vol.**168**, pp.567-590.
- 99 Guo, J., Tang, Y., and Xu, Z., (2010) "Performance and thermal behaviour of wood plastic composite produced by nonmetals of pulverized waste printed circuit boards", *Journal of Hazardous Materials*, Vol.**179**, pp.203-207.
- 100 Gutiérrez, G., Reyes, L.I., Sánchez, I., Rodríguez, K., Idler, V., Paerdes, V.R., (2005), "Vibration induced airflow through granular beds and density-dependent segregation", *Physica A*, Vol.**356**, pp.83-87.
- 101 Hanesian, D. and Rankell, A., (1968), "Elutriation from a multi-size particle fluidised bed", *Industrial Engineering Chemical Fundamentals*, Vol.**7**, No.3, pp.452-458, available online at <http://pubs.acs.org/doi/pdf/10.1021/i160027a017?cookieSet=1> retrieved on 19/04/2009, at 15:30GMT.
- 102 Hanesian, D. and Rankell, A., (1968), "Elutriation from a multisize particle fluidised bed", *Industrial Chemical Engineering Fundamentals*, Vol.**7**, No.3, pp.452-458. Available online at <http://dx.doi.org/10.1021/i160027a017> retrieved on 19/04/2009 at 19:00GMT.
- 103 Hannequart, J-P., (2003), "The management of waste electrical and electronic equipment", A guide for local and
-

-
- regional authorities, The Association of Cities and Regions for Recycling (ACRR), EU, ACRR-Gulledelle 100 -B-1200 Brussels, Belgium. www.acrr.org, E-mail: acrr@acrr.org.
- 104 Herminghaus, S., (2005), "Dynamics of wet granular matter", *Advances in Physics*, Taylor and Francis Group, Vol.**54**, No.3, pp.221-261.
- 105 Herrman, H.J., and Luding, S., (1998), "Modelling granular media on the computer", *Continuum Mech. Thermodyn.*, Springer-Verlag, Vol.**10**, pp.189-231.
- 106 Herrmann, H.J., (1995) "Some new results on fracture". *Physica A*, Vol.**221**, pp 125-133.
- 107 Hirajima, T., Petrus, H.T.B.M., Oosako, Y., Nonaka, M., Sasaki, K., and Ando, T., (2010), "Recovery of cenospheres from coal fly ash using a dry separation process: separation estimation and potential application", *International Journal of Mineral Processing*, Vol.**95**, No.1-4, pp.18-24.
- 108 Hong, D.C., Quinn, P.V. and Luding, S., (2001), "Reverse Brazil nut problem: Competition between percolation and condensation", *Physical Review Letter*, The American Physical Society, Vol.**86**. No.15, pp.3423-3426.
- 109 Hopkins, M.A. & Louge, M.Y., (1991), "Inelastic microstructure in rapid granular flows of smooth disks", *Phys. Fluids*, Vol.**A3**, pp. 47-57.
- 110 Hsiau, S.S. and Chen, C.H., (2000), "Granular convection cells in a vertical shaker", *Powder Technology*, Vol.**111**, pp.210-217.
- 111 Hsiau, S.S. and Hunt, M.L., (1996), "Granular thermal diffusion in flows of binary-sized mixtures", *Acta Mechanica*, Springer Wien, Vol.**114**, No.1-4, pp.121-137.
- 112 Hsiau, S.S., Lu, L.S. and Tai, C.H., (2008), "Experimental investigations of granular temperature in vertical vibrated beds", *Powder Technology*, Vol.**182**, pp.202-210.
- 113 Hsiau, S.S., Wang, P-C. and Tai, C-H., (2002), "Convection cells and segregation in vibrated granular bed", *AIChE*, Vol.**48**, no.7, pp.1430-1438.
-

-
- 114 Hsiau, S-S., Tai, C-H., and Chiang, M-C., (2004), "Effect of moisture content on the Convective motion of powders in a vibrated bed", *Advanced Powder Technology*, VSP and Society of Powder Technology, Japan, Vol.**15**, No.6, pp.673-686.
- 115 Huan, C., Yang, X., Candela, Mair, R.W. and Walsworth, R.L., (2004), "NMR experiments on a three-dimensional vibrofluidised granular medium", *Physical Review*, The American Physical Society, Vol.**E69**, pp.041302/1-13.
- 116 Huerta, D.A. and Ruiz-Suárez, J.C., (2004), "Vibration induced granular segregation: A phenomenon driven by three mechanisms", *Physical Review Letters*, The American Physical Society, Vol.**92**, No.11, pp.114301/1-4.
- 117 Huisman, Jaco, Magalini, Federico, Kuehr, Ruediger, Maurer, Claudia, Ogilvie, Steve, Poll, Jim, Delgado, Clara, Artim, Eniko, Szlezak, Josef, Stevels and Ad, (2008), "2008 Review of Directive 2002/96 on Waste Electrical and Electronic Equipment (WEEE), Final Report, United Nations University, UN Campus, Bonn, Germany, available online at http://ec.europa.eu/environment/waste/weee/pdf/summary_unu.pdf, retrieved on 10/07/2009 at 16:22GMT.
- 118 Ichiki, K. & Hayakawa, H., (1995), "Dynamical simulation of fluidized beds: Hydrodynamically interacting granular particles". *Phys. Rev. E.*, Vol.**52**, no.1, pp 658-670.
- 119 Ishii, T. & Matsushita, M., (1992), "Fragmentation of long thin glass rods", *Journal of the physical society of Japan*, Vol.**61**, no.10, pp 3474-3477.
- 120 Jaeger, H.M. and Nagel, S.R., (1992), "Physics of the granular state", *Science*, Vol.**255**, No.5051, pp.1523-1531. www.sciencemag.org
- 121 Jaeger, H.M., (1997), "Chicago experiments on convection, compaction, and compression", in Proceedings of the NATO/ASI Workshop on Dry Granular Materials, Cargese 1997, available online at
-

-
- <http://jfi.uchicago.edu/granular/Papers/cargese.pdf>,
retrieved on 18/03/2010 at 12:22GMT.
- 122 Jaeger, H.M., Nagel, S.R. and Behringer, R.P., (1996), "Granular solids, liquids, and gases, *Reviews of Modern Physics*, The American Physical Society, Vol.**68**, pp.1259–1273.
- 123 Jain, N., Ottino, J.M. and Lueptow, R.M., (2005), "Combined size and density segregation and mixing in noncircular tumblers", *Physical Review*, The American Physical Society, Vol.**E71**, No.5, pp.05130/1-10.
- 124 Jesuthasan, N., Baliga, B.R., and Savage, S.B., (2006), "Use of particle tracking velocimetry for measurements of granular flows: Review and application", *Particle Tracking Velocimetry for Granular Flow Measurements*, KONA, Japan, Vol.**24**, pp.15-26.
- 125 Jha, A. K., and Puri, V. M., (2009), "Percolation segregation of binary mixtures under periodic movement", *Powder Technology*, Vol.**195**, pp.73-82.
- 126 Jiang, W., Jia, L., and Ming, X. Z., (2009), " A new two-roll electrostatic separator for recycling of metals and non-metals from waste printed circuit board", *Journal of Hazardous Materials*, Vol.**161**, pp.257-262.
- 127 Jofre, S., and Morioka, T., (2005), "Waste management of electric and electronic equipment: Comparative analysis of end-of-life strategies", *J Mater Cycles Waste Manag.* Springer-Verlag, Vol.**7**, pp.24-32.
- 128 Johanson, K., (2007a), "Understanding segregation mechanisms", *Powder Pointers*, Fall 2007, Vol.1, No.C, pp.1-4. Available online at <http://www.matflowsol.com/2007-c.pdf>, retrieved on 16/03/10 at 14:48GMT.
- 129 Johanson, K., (2007b), "Why is understanding segregation mechanisms so important", Available online at <http://matflowsol.com/seghints.pdf>, retrieved on 16/03/10 at 14:50GMT.
-

-
- 130 Jullien, R., Meakin, P. and Pavlovitch, A., (1992), "Three-Dimensional model for particle-size segregation by shaking" *Phys. Rev. Lett.*, Vol.**69**, pp.640-643.
- 131 Kadanoff, L.P., (1999), "Build upon sand: Theoretical ideas inspired by granular flows", *Reviews of Modern Physics*, The American Physical Society, Vol.**71**, No.1, pp.435-444.
- 132 Kakalios, J. (2005), "Granular physics or nonlinear dynamics in a sand box", *American Journal of Physics*, *American Association of Physics Teachers*, Editor. Stuewer R.H., Vol.**73**, No.1, pp.8-22.
- 133 Kalpakjian, S., and Schmid, A., (2006), "Part IV, Chapter 21 in Manufacturing engineering and technology", *Prentice Hall Publishers*, N.Y.
- 134 Kang, H.Y., and Schoenung, J.M., (2005), "Electronic waste recycling: A review of U.S. infrastructure and technology options", *Resources, Conservation and Recycling*, Vol.**45**, No.4, pp.368-400.
- 135 Kang, H.Y., and Schoenung, J.M., (2006), "End of life personnel computer systems in California: analysis of emissions and infrastructure needed to recycle in the future", *Proceedings of the 2006 IEEE International Symposium on Electronics and Environment*, *IEEE*, available online at <http://ieeexplore.ieee.org/stamp/stamp.jsp?tp=&arnumber=1650084&isnumber=34595>, retrieved on 14/07/2009 at 21:30GMT.
- 136 Katayama, T., Sugiyama, T., and Yamamoto, K., (2003), "2-Component mixing using the vertical vibration mixing mechanism caused by the container wall pressure", *Journal of Materials Processing Technology*, Vol.**143-144**, pp.901-904.
- 137 Klein, M., Tsai, L.L., Rosen, M.S., Pavlin, T., Candela, D. and Walsworth, R.L., (2006), "Interstitial gas and density segregation of vertically vibrated granular media", *Physical Review*, The American Physical Society, Vol. **E74**, pp.010301/1-4.
-

-
- 138 Knelson, 2009, available online at www.knelson.com, retrieved on 24/04/2009 at 18:00GMT.
- 139 Knight, J.B., (1997), "External boundaries and internal shear bands in granular convection", *Physical Review*, The American Physical Society, Vol.**E55**, No.5, pp.6016-6023.
- 140 Knight, J.B., Ehrichs, E.E., Kuperman, V.Y., Flint, J.K., Jaeger, H.M., Nagel, S.R., (1996), " Experimental study of granular convection", *Physical Review E*, The American Physical Society, Vol.**54**, No.5, pp.5726-5738.
- 141 Knight, J.B., Jaeger, H.M. and Nagel, S.R., (1993), "Vibration-induced size separation in granular media: The convection connection", *Physical Review Letters*, The American Physical Society, Vol.**70**, No.24, pp.3728-3731.
- 142 Kong, X.Z., Hu, M.B., Wu, Q.S. and Wu, Y.H., (2006), "Effects of bottleneck on granular convection cells and segregation", *Granular Matter*, Springer-Verlag, Vol.**8**, pp.119-124.
- 143 Kruggel-Emden, H., Simsek, E., Rickelt, S., Wirtz, S., and Scherer, V., (2007), "Review and extension of normal force models for the discreet element method", *Powder Technology*, Vol.**171**, pp.157-173.
- 144 Kudrolli, A., (2004), "Size separation in vibrated granular matter", *Reports on Progress in Physics*, Institute of Physics Publishing, UK, Vol.**67**, pp.209-247.
- 145 Kuo, H.P., and Chen, Y.W., (2008), "Determination of state transition of granular materials in a vibrating bed using a novel optical signal analysing method", *Advanced Powder Technology*, Vol.**19**, pp.61-71.
- 146 Laurent, B.F.C., Bridgewater, J., and Parker, D.J., (2001), "Convection and segregation in a horizontal mixer", *Powder Technology*, Vol.**123**, PP.9-18.
- 147 Leaper M.C., Smith A.J., Swift M.R., King P.J., Webster H.E., Miles N.J., Kingman S.W., (2005), "The behaviour of water-immersed glass-bronze particulate systems under vertical vibration", *Granular Matter*, Vol.**7**, pp57-67.
-

-
- 148 Lee, C.H., Chang, C.T., Fan, K.S., and Chang, T.C., (2004), "An overview of recycling and treatment of scrap computers", *Journal of Hazardous Materials*, Vol.**114**, No.1-3, pp.93-100.
- 149 Lee, J. & Leibig, M., (1994), "Density waves in granular flow: a kinetic wave approach", *J. Phys. I., France*, Vol.**4**, pp. 507-514.
- 150 Lee, J., (1994), "Heap formation in two-dimensional granular media" *Journal of Physics A.*, Vol.**27**, pp.L257-L262.
- 151 Lee, J., (1994), "Heap formation in two-dimensional granular media", *Letter to the Editor, J. Phys. A: Math. Gen.*, Vol.**27**, pp.L257-L262, IOP publishing Ltd. U.K.
- 152 Lehon, C.N., Cambou, B., and Vincens, E., (2003), "Influence of particle shape and angularity on the behaviour of granular materials: a numerical analysis", *International Journal for Numerical and Analytical Methods in Geomechanics*, John Wiley and Sons, Ltd., Vol.**27**, pp.1207-1226.
- 153 Li, H., (2005), "Impact of cohesion forces on particle mixing and segregation". *PhD Thesis*, University of Pittsburgh. U.K.
- 154 Li, J., Nakazato, T., and Kato, K., (2004), "Effect of cohesive powders on the elutriation of particles from a fluid bed", *Chemical Engineering Science*, Vol.**59**, pp.2777-2782.
- 155 Liao, C-C and Hsiao, S-S., (2010), "Experimental analysis of dynamic properties in wet sheared granular matter", *Powder Technology*, Vol.**197**, pp.222-229.
- 156 Liffman, K., Metcalfe, G. and Cleary, P., (1997), "Granular convection and transport due to horizontal shaking", *Physical Review Letters*, The American Physical Society, Vol.**79**, No.23, pp.4574-4576.
- 157 Lim, S.-Y., Davidson, J.F., Forster, R.N., Parker, D.J., Scott, D.M., and Seville, J.P.K., (2003), "Avalanching of granular material in a horizontal slowly rotating cylinder: PEPT studies", *Powder Technology*, Vol.**138**, pp.25-30.
- 158 Limtrakul, S., Rotjanavijit, W., and Vatanatham, T., (2007), "Lagrangian modelling and simulation of effect of vibration
-

-
- on cohesive particle movement in a fluidised bed”, *Chemical Engineering Science*, Vol.**62**, pp.232-245.
- 159 Lincoln, J.D., Ogunseitan, O.A., Shapiro, A.A., Saphores, J.-D., (2007), “Leaching assessments of hazardous materials in cellular telephones”, *Environmental Science & Technology*, American Chemical Society, Vol.**41**, pp.2572–2578.
- 160 Liu, R., Shieh, R.S., Yeh, R.Y.L., and Lin, C.H., (2009), “The general utilization of scrapped PC board”, *Waste Management*, Vol.**29**, No.11, pp.2842-2845.
- 161 Losert, W., Cooper, D.G.W., Delour, Kudrolli, A. and Gollub, J.P., (1999), “Velocity statistics in excited granular media”, *Chaos, The American Institute of physics*, Vol.**9**, No.3, pp.682-690.
- 162 Lou, J-C., Huang, Y-J., and Han, J-Y., (2009), “Treatment of printed circuit board industrial wastewater by Ferrite process combined with Fenton method”, *Journal of Hazardous Materials*, Vol.**170**, pp.620-626.
- 163 Luding, S., Clément, E., Blumen, A., Rajchenbach, J. & Duran, J., (1994), “Onset of convection in molecular dynamics simulations of grains”, *Phys. Rev. E*, Vol.**50**, No.3, pp. R1762-R1765.
- 164 Lueptow, R.M., Akonur, A., and Shinbrot, T., (2000), “PIV for granular flows”, *Experiments in Fluids*, Springer-Verlag, pp.183-186.
- 165 Macpherson, S.A., Iveson, S.M., and Galvin, K.P., (2009), “Density based separations in the reflux classifier with an air-sand dense-medium and vibration”, *Minerals Engineering*, Vol.**23**, No.2, pp.74-82.
- 166 Majid, M. and Walzel, P., (2009), “Convection and segregation in vertically vibrated granular beds”, *Powder Technology*, Vol.**92**, No.3, pp.311-317.
- 167 McCarthy, J.J., (2009), “Turning the corner in segregation”, *Powder Technology*, Vol. 192, pp.137-142.
- 168 Mehta, A., (2007), “Introduction” Chapter-1 in *Granular Physics*, Cambridge University Press, U.K.
-

-
- 169 Menad, N., Björkman, B., and Allain, E. G., (1998), "Combustion of plastics contained in electric and electronic scrap", *Resources, Conservation and Recycling*, Vol.**24**, pp.65-85.
- 170 Midi, G.D.R., (2004), "On dense granular flows", *The European Physical Journal E*, Vol.**14**, pp.341-365.
- 171 Miettinen, T., Ralston, J., and Fornasiero, D., (2010), "The limits of fine particle flotation", *Minerals Engineering*, Vol.**23**, pp.420-437.
- 172 Milburn, R.J., Naylor, M.A., Smith, A.J., Leaper, M.C., Good, K., Swift, M.R. and King, P.J., (2005), "Faraday tilting of water immersed granular beds", *Physical Review*, The American Physical Society, Vol.**E71**, pp.011308/1-10.
- 173 Möbius, M.E., Lauderdale, B.E., Nagel, S.R. and Jaeger, H.M., (2001), "Brazil-nut effect: Size separation of granular particles", *Nature*, Vol.**414**, pp.270.
- 174 Modderman, L. collections (2009), www.scienceart.nl, Retrieved on 03/04/2009 at 22:00GMT.
- 175 Mohabuth, N. & Miles, N. J., (2005), "The Recovery of Recyclable Material from Waste Electrical and Electronic Equipment (WEEE) by using Vertical Vibration Separation", *Resources, Conservation and Recycling*, Vol.**45**, pp 60-69.
- 176 Mohabuth, N., (2007), "The design of a new vertically vibrated particle separator", *PhD thesis*, University of Nottingham, UK.
- 177 Mohabuth, N., Hall, P., & Miles, N., (2007), "Investigating the use of vertical vibration to recover metal from electrical and electronic waste", *Minerals Engineering*, Vol.**20**, pp.926-932.
- 178 Moon, S.J., Swift, J.B., and Swinney, H.L., (2004), "Steady state velocity distributions of an oscillated granular gas", *Physical Review*, The American Physical Society, Vol.**E69**, pp.011301/1-8.
- 179 Moysey, P.A., and Baird, M.H.I., (2009), "Size segregation of spherical nickel pellets in the surface flow of a packed bed:
-

-
- Experiments and Discrete Element Method Simulations”, *Powder Technology*, Vol.**196**, pp.298-308.
- 180 Mullin, T., (2002), “Mixing and De-mixing”, *Science*, Vol.**295**, pp.1851. www.sciencemag.org.
- 181 Mullin, T., (2005), “Coarsening of self-organised clusters in binary mixtures of particles”, *Physical Review Letters*, The American Society of Physics, Vol. **84**, No.20, pp.4741-4744.
- 182 Murray, R.W., Miller, D.J., Kryc, K.A., (2000), “Analysis of major and trace elements in rocks, sediments, and interstitial waters by inductively coupled plasma–atomic emission spectrometry (ICP-AES)”, ODP Tech. Note, 29 Available online from <http://www-odp.tamu.edu/publications/tnotes/tn29/INDEX.HTM> retrieved on 25/06/2009 at 23:21GMT.
- 183 Muzzio, F.J., Goodridge, C.L., Alexander, A., Arratia, P., Yang, H., Sudah, O., and Mergen, G., (2003), “Sampling and characterization of pharmaceutical powders and granular blends”, *International Journal of Pharmaceutics*, Vol.**250**, No.1, pp.51-64.
- 184 Naylor, M.A., Swift, M.R. and King P.J., (2003), “Air-driven Brazil nut effect”, *Physical Review*, The American Physical Society, Vol.**E68**, pp.012301/1-4.
- 185 Neederman, R.M., (1992), “Introduction”, Chapter-1 in the Statics and kinematics of granular materials, Cambridge University Press, UK, pp.1.
- 186 Ng, B.H., Kwan, C.C., Ding, Y.L., Ghadiri, M., and Fan, X.F., (2007), “Solids motion of calcium carbonate particles in a high shear mixer granulator: A comparison between dry and wet conditions”, *Powder Technology*, Vol.**177**, pp.1-11.
- 187 Nicodemi, M., Fierro, A. and Coniglio, A, (2002), “Segregation in hard-sphere mixtures under gravity. An extension of Edwards approach with two thermo-dynamical parameters”, *Euro-physics Letters*, Vol.**60**, No.5, pp.684-690.
-

-
- 188 Ning, Z. & Ghadiri, M., (1996), "Computer simulation of attrition in a shear cell", *The 1996 IChemE Research Event*, Vol.**2**, pp 323-325.
- 189 Niu, X., and Li, Y., (2007), "Treatment of waste printed wire boards in electronic waste for safe disposal", *Journal of Hazardous Materials*, Vol.**145**, pp.410-416.
- 190 Nwafor, O.F., (2009), "Development of pneumatic dry jigging for waste treatment", *Ph.D. Thesis*, University of Nottingham, UK.
- 191 Ohtsuki, T. and Ohsawa, T., (2003), "Hydrodynamics for convection in vibrating beds of cohesionless granular materials", *Journal of the physical society of Japan*, Vol.**72**, No.8, pp.1963-1967.
- 192 Ohtsuki, T., Kinoshita, D., Takemoto, Y. and Hayashi, A., (1995), "Segregation by shaking in cohesion less granular: Effect of particle size and density", *Journal of the Physical Society of Japan*, Vol.**64**, No.2, pp.430-434.
- 193 Oshitani, J., Franks, G.V., and Griffin, M., (2010), "Dry dense medium separation of iron ore using a gas-solid fluidized bed", *Advanced Powder Technology*, Vol.**21**, No.5, pp.573-577.
- 194 Ottino, J.M. and Khakhar, D.V., (2002), "Scaling of granular flow processes: from surface flow to design rules", *Particle Technology and Fluidization*, AICHE Journal, Vol.**48**, No.10, pp.2157-2166.
- 195 Ottino, J.M., (2006), "Granular matter as a window into collective systems far from equilibrium, complexity, and scientific prematurity", *Chemical Engineering Science*, Vol.**61**, pp.4165-4171.
- 196 Ottino, J.M., and Khakhar, D.V., (2000), "Mixing and segregation of granular materials", *Annu. Rev. Fluid Mechanics*, Vol.**35**, pp.55-91.
- 197 Pak, H.K., and Behringer, R.P., (1993), "Surface waves in vertically vibrated granular materials", *Physical Review*
-

-
- Letters*, The American Society of Physics, Vol.**71**, No.12, pp.1832-1835.
- 198 Pak, H.K., Van Doorn, E. and Behringer, R.P., (1995), "Effects of ambient gases on granular materials under vertical vibration", *Physical Review Letters*, The American Physical Society, Vol.**74**, No.23, pp.4643-4646.
- 199 Parker, D.J., Allen, D.A., Benton, D.M., Fowles, P., McNeil, P.A., Tan, M., and Beynon, T.D., (1997), "Developments in particle tracking using the Birmingham positron camera", *Nuclear Instruments and Methods in Physics Research*, Vol.**A392**, pp.421-426.
- 200 Parker, D.J., and Fan, X., (2008), "Positron emission particle tracking-Application and labelling techniques", *Particuology*, Vol.**6**, pp.16-23.
- 201 Parker, D.J., Broadbent, C.J., Fowles, P., Hawkesworth, M.R. and McNeil, P., (1993), "Positron emission particle tracking—a technique for studying flow within engineering equipment", *Nuclear Instruments and Methods in Physical Research A*, Vol.**326**, No.3, pp.592-607.
- 202 Parker, D.J., Dijkstra, A.E., Martin, T.W., and Seville, J.P.K., (1997), "Positron emission particle tracking studies of spherical particle motion in rotating drums", *Chemical Engineering Science*, Vol.**52**, No.13, pp.2011-2022.
- 203 Parker, D.J., Leadbeater, T.W., Fan, X., Hausard, M, N, Ingram, A., and Yang, Z., (2009), "Positron emission particle tracking using a modular positron camera", *Nuclear Instruments and Methods in Physics Research A*, Vol.**604**, pp.339-342.
- 204 Particles CIC, (2009), available online at www.particlescic.com, retrieved on 18/06/2009 at 00:22GMT.
- 205 Patnaik, P., (2003), "Handbook of Inorganic Chemicals", McGraw-Hill, NY, London, pp.409.
- 206 Perry, R.H. and Green, D.W., (1999), editors, "Solid-solid operations and equipment", Section-19 in Perry's Chemical
-

-
- Engineering Handbook, 7th ed., McGraw-Hill Companies Inc. N.Y., pp.19-3.
- 207 Poms, do it., (2009), available online at http://www.doitpoms.ac.uk/tlplib/recyclingmetals/eddy_current.php, retrieved on 25/04/2009 at 22:00GMT.
- 208 Poschel, T. & Buchholtz, V., (1993), "Static friction phenomena in granular materials: Coulomb law versus particle geometry", *Phys. Rev. Lett.*, Vol.**71**, no.24, pp.3963-3966.
- 209 Qingfan, S., Xuequn, Y., Meiyang, H., Xiaojuan, N., and Kunquan, L., (2003), "Experimental study of segregation patterns in binary granular mixtures under vertical vibration", *Chinese Science Bulletin*, Vol.**48**, No.7, pp.627-629.
- 210 Quan, C., Li, A., and Gao, N., (2009), "Thermogravimetric analysis and kinetic study on large particles of printed circuit board waste" *Waste Management*, Vol.**29**, pp.2353-2360.
- 211 Rapaport, D.C., (2001), "Mechanism for granular segregation", *Physical Review*, The American Physical Society, Vol.**64**, pp.061304/1-4.
- 212 Retsch, (2009), available online at <http://www.retsch.co.uk/uk/products/milling>, retrieved on 17/06/2009, at 17:08GMT.
- 213 Rhodes, M., (1998), "Introduction to particle technology", John Wiley and Sons Ltd., Great Britain.
- 214 Rice, G. E., (2002), "The Characterization and recycling of incinerated tyres", *Ph.D Thesis*, University of Nottingham, U.K.
- 215 Richardson, J.F., Harker J.H. and Backhurst J.R., (2002) "Particulate solids", Chapter-1 in Coulson and Richardson's Chemical Engineering, Butterworth Heinemann, London, Vol.**2**, 5th edition, pp.1-29.
- 216 Ristow, G.H., (1994), "Particle mass segregation in a two-dimensional rotating drum", *Europhys. Lett.*, Vol.**28**, no.2, pp.97-101.
-

-
- 217 Robinson, B., (2010), "E-Waste: An assessment of global production and environmental impacts", *Science of the Total Environment*, Vol.**408**, pp.183-191.
- 218 Rosato, A., Strandburg, K.J., Prinz, F. and Swendsen, R.H., (1987), "Why the Brazil nuts are on top: Size segregation of particulate matter by shaking", *Phys. Rev. Lett.*, Vol.**58**, pp.1038-1040.
- 219 Rosato, A.D., Blackmore, D.L., Zhang, N. and Lan, Y., (2002), "A perspective on vibration-induced size segregation of granular materials", *Chemical Engineering Science*, Vol.**57**, pp.265-275.
- 220 Rosato, A.D., Lan, Y. and Wang, D.T., (1991), "Vibratory particle size sorting in multi-component systems", *Powder Technology*, Vol.**66**, pp.149-160.
- 221 Sanders, D.A., Swift, M.R., Bowley, R.M. and King, P.J., (2004), "Are Brazil nuts Attractive", *Physical Review Letters*, The American Physical Society, Vol.**93**, No.20, pp.208002/1-4.
- 222 Sarkar, S. and Khakhar, D.V., (2008), "Experimental evidence for a description of granular segregation in terms of the effective temperature", *EPLA*, EDP Sciences, France, Vol.**83**, No.5, Article No.54004, pp.54004/1-6.
- 223 Schaik, A. V., Reuter, M.A., (2010), "Dynamic modelling of E-waste recycling system performance based on product design", *Minerals Engineering*, Vol.**23**, pp.192-210.
- 224 Schlesinger, M.E., (2006), "Beneficiation technology Chapter-5 in Aluminum recycling, CRC Press, Taylor & Francis Group, ISBN 084939662X, pp-62-71.
- 225 School for champions, (2009), "Friction types", available online at http://www.school-for-champions.com/science/friction_equation.htm, retrieved on 10/05/2009, at 19:36GMT.
- 226 Schröter, M., Ulrich, S., Kreft, J., Swift, J.B. and Swinney, H.L., (2006), "Mechanisms in the size segregation of a binary
-

-
- mixture", *Physical Review*, The American Physical Society, Vol.**E74**, pp.011307/1-14.
- 227 Science Daily, (2009), "Recycling of Europe's electronic waste needs improvements, UN report urges", available online at <http://www.sciencedaily.com/releases/2007/11/071115113338.htm>, retrieved on 10/07/2009 at 23:14GMT.
- 228 Scott, A.M. and Bridgewater, J., (1975), "Inter-particle percolation: a fundamental solids mixing mechanism", *Industrial Engineering Chemical Fundamentals*, Vol.**14**, No.1, pp.22-27.
- 229 Serero, D., Goldhirsch, I., Noskowicz, S.H., and Tan, M.-L., (2006), "Hydrodynamics of granular gases", *Journal of Fluid Mechanics*, Vol.**554**, pp.237-258.
- 230 Settles, G. S., (1997), "Visualizing full-scale ventilation airflows", *Ashrae Journal*, American Society of Heating, Refrigerating and Air-Conditioning Engineers, pp.19-26, Available online at <http://www.mne.psu.edu/psgdl/Full-ScaleVentilation.pdf>, retrieved on 25/03/2010 at 11:45GMT
- 231 Seville, J.P.K., Ingram, A., and Parker, D.J., (2005), "Probing processes using positrons", *Chemical Engineering Research and Design*, Trans IChemE, Part A, Vol.**83**, No.A7, pp.788-793.
- 232 Shapiro, M. and Galperin, V., (2004), "Air classification of solid particles: a review", *Chemical Engineering and Processing*, Vol.**44**, Issue.2, pp-279-285.
- 233 Shinbrot, T. and Muzzio, F.J., (1998), "Reverse buoyancy in shaken granular beds", *Physics Review letter*, The American Physical Society, Vol.**81**, Issue.20, pp.4365-4368.
- 234 Shishodia, N. and Wassgren, C.R., (2001), "Particle segregation in vibrofluidized beds due to buoyant forces", *Physical Review Letter*, The American Physical Society, Vol.**87**, No.8, pp.084302/1-4.
-

-
- 235 Somerfield, C. (2009), "Private communication", Division of Process and Environmental Engineering Research, University of Nottingham, UK.
- 236 Sommer, Jr., and Edward, J., (2005) "Identification and sorting of Printed Wiring Boards (PWBs) within and E-waste Recycling Stream", National Center for Environmental Research, U.S. Environmental Protection Agency, available online at http://cfpub.epa.gov/ncer_abstracts/index.cfm/fuseaction/display.abstractDetail/abstract/7484, retrieved on 23/07/2009 at 14:48GMT.
- 237 Sort-O-Mat, (2009), "Sort-O-Mat Ballistic Separator", available online at <http://www.brt.biz/BASEP.htm>, retrieved on 19/04/2009 at 19:30GMT.
- 238 Soto, R., Marescha, M. and Risso, D., (1999), "Departure from Fourier's law for fluidized granular media", *Physical Review*, The American Physical Society, Vol.**83**, pp.5003-5006.
- 239 Squires, A.M., (2004), "Chemical process opportunities for vibrated powders 2. In the field", *Powder Technology*, Vol.**147**, pp.10-19.
- 240 Stein, M., Seville, J.P.K., and Parker, D.J., (1998), "Attrition of porous glass particles in a fluidised bed", *Powder Technology*, Vol.**100**, pp.242-250.
- 241 Steinert systems, (2009), "Products page", available online at <http://www.steinert.de/40.0.html?&L=1>, retrieved on 14/04/2009 at 17:38GMT.
- 242 Stellema, C.S., Vlek, J., Mudde, R.F., de Goeij, J.J.M., van den Bleek, C.M., (1998), "Development of an improved positron emission particle tracking system", *Nuclear Instruments and Methods in Physics Research A*, Vol.**404**, pp.334-348.
- 243 Steubing, B., Böni, H., Schluep, M., Silva, U., Ludwig, C., (2010), "Assessing computer waste generation in Chile using

-
- material flow analysis", *Waste Management*, Vol.**30**, pp.473-482.
- 244 Sun, Q., Wang, G., and Hu, K., (2009), "Some open problems in granular matter mechanics", *Progress in Natural Science*, Vol.**19**, pp.523-529.
- 245 Taguchi, Y.H. (1992), "New origin of convective motion: Elastically induced convection in granular materials", *Physical Review Letters*, The American Physical Society, Vol.**69**, No.9, pp.1367-1370.
- 246 Tai, C.H. and Hsiau, S.S., (2004), "Dynamic behaviors of powders in a vibrating bed", *Powder Technology*, Vol.**139**, pp.221-232.
- 247 Tai, S.C. and Hsiau, S.S., (2009), Movement mechanisms of solid-like and liquid-like motion states in a vibrating granular bed", *Powder Technology*, Vol.**194**, pp.159-165.
- 248 Tang, X., Shen, C., Shi, D., Cheema, S.A., Khan, M.I., Zhang, C., and Chen, Y., (2010), "Heavy metal and persistent organic compound contamination in soil from Wenling: An emerging e-waste recycling city in Taizhou area, China", *Journal of Hazardous Materials*, Vol.**173**, pp.653-660.
- 249 Tarzia, M., Fierro, A., Nicodemi, M. and Coniglio, A., (2004), "Segregation in fluidized versus tapped packs", *Physical Review Letters*, The American Physical Society, Vol.**93**, No.19, pp.198002/1-4.
- 250 Tarzia, M., Fierro, A., Nicodemi, M., Ciamarra, M.P. and Coniglio, A., (2005), "Size segregation in granular media induced by phase transition", *Physical Review Letters*, The American Physical Society, Vol.**95**, No.7, pp.078001/1-4.
- 251 Taylor, J.B., (1988), "Dry electrostatic separation of granular materials", IEEE-88CH2565, pp-1741-1759. (Available online <http://ieeexplore.ieee.org/iel5/726/952/00025295.pdf?tp=&isnumber=&arnumber=25295>, retrieved on 17/06/2008, 11:38GMT).
-

-
- 252 Thomas, B., and Squires, A.M., (1998), "Support for Faraday's view of circulation in a fine-powder Chladni heap", *Physical Review Letters*, The American Physical Society, Vol.**81**, No.3, pp.574-577.
- 253 Thomas, G., (2000), "Segregation effects in processes handling powder mixtures", *Chem. And Ind. Confrence*, Paris-13-15 September, 2005, available online at <http://hal.archives-ouvertes.fr/docs/00/12/52/81/PDF/GT-ChemInd0905.pdf>, retrieved on 16/03/2010, 20:30GMT.
- 254 Thornton, A.R., Gray, J.M.N.T. & Hogg, A.J., (2006), "A three phase mixture theory for particle size segregation in shallow granular free surface flows", *Journal of Fluid Mechanics*, Cambridge University Press, U.K., Vol.**550**, pp.1-25.
- 255 Tijskens, E., Ramon, H., and Baerdemaeker, J.D., (2003), "Discreet element modelling for process simulation in agriculture", *Journal of Sound and Vibration*, Vol.**266**, pp.493-514.
- 256 Tohka, A. and Lehto, H., (2005), "Mechanical and thermal recycling of waste from electric and electrical equipment", Helsinki University of Technology Department of Mechanical Engineering, Energy Engineering and Environmental Protection Publications, Espoo, available online at <http://eny.tkk.fi/library/publications/tkk-eny/TKK-ENY-25.pdf>, retrieved on 09/06/2009, at 16:21GMT.
- 257 Trujillo, L., Alam, M. and Herrmann, H.J., (2003), "Segregation in a fluidised binary granular mixture: competition between buoyancy and geometric forces", *Euro-physics Letters*, Vol.**64**, Issue.2, pp.190-196.
- 258 Tsuji, Y., Tanaka, T. and Ishida, T., (1992), "Langrangian numerical simulation of plug flow of cohesionless particles in horizontal pipe", *Powder Technology*, Vol.**71**, pp.239-250.
- 259 Tsydenova, O., Bengtsson, M., (2010) "Chemical hazards associated with treatment of waste electrical and electronic equipment" *Waste Management*, Accepted Manuscript, Article in Press, DOI:10.1016/j.wasman.2010.08.014.
-

-
- 260 Ulrich, S., Schröter, M. and Swinney, H.L., (2007), "Influence of friction on granular segregation", *Physical Review*, The American Physical Society, Vol.**E76**, No.4, pp.042301/1-3.
- 261 UNEP, (2005), "E-waste, the hidden side of IT equipments' manufacturing and use", Environment Alert Bulletin, United Nations Environment Programme, DEWA/GRID-Europe. Available online at http://www.grid.unep.ch/product/publication/download/ew_ewaste.en.pdf, retrieved on 14/02/2011 at 20:30GMT.
- 262 Vasconcelos, T.F., Morais, A.F., Cisne Jr, R.L.C, Parteli, E.J.R., Andrade Jr, J.S., (2009), "Particle separation in a ramified structure", *Chemical Engineering Science*, Vol.**65**, No.4, pp.1400-1406.
- 263 Veasey, T.J., (1997), "An overview of metals recycling by physical separation methods", *Proc Instn Mech Engrs., Journal of Process Mechanical Engineering*, IMechE, Vol.**211**, No.1, Part E. pp.61-64.
- 264 Vehlow, J., Karlsruhe, F., and Mark, F.E., (1997), "Electrical and electronic plastics waste co-combustion with municipal solid waste", *A technical paper from Association of Plastics Manufacturers in Europe (APME)*, Dow Europe.
- 265 Veit, H.M., Diehl, T.R., Salami, A.P., Rodrigues, J.S., Bernardes, A.M., and Tenório, J.A.S., (2005), "Utilization of magnetic and electrostatic separation in the recycling of printed circuit boards scrap", *Waste Management*, Vol.**25**, pp.67-74.F
- 266 Vesilind, P.A. & Rimer, A.E., (1981), "Chapter-4 & 5 in Unit operations in resource recovery engineering", Prentice Hall, INC, N.Y.
- 267 Vibtec Ltd. (2009), available online at <http://www.vibtec.com/> retrieved on 10/06/2009 at 19:51GMT.
- 268 Wagner, D and Mitchell, C.J., (2007), "Waterless fines removal; Technical feasibility of using air classification to
-

-
- separate fines from sand and gravel”, *British Geological Survey, Economic Minerals Programme, Commissioned Report CR/07/010N*, available online at <http://nora.nerc.ac.uk/7488/1/CR07010N.pdf>, retrieved on 09/04/2010 at 12:30GMT.
- 269 Walton, K., Zhou, J., and Galvin, K.P., (2010), “Processing of fine particles using closely spaced inclined channels”, *Advanced Powder Technology*, Vol.**21**, No.4, pp.386-391.
- 270 Wang, D.W., Chou, Y.C. and Hong, T.M., (1996), “Possible origin of convection flow in granular systems”, *Euro-physics Letters*, Vol.**35**, No.5, pp.333-336.
- 271 Wang, J., Bai, J., Xu, J., and Liang, B., (2009), “Bioleaching of metals from Printed wire boards by *Acidithiobacillus ferrooxidans* and *acidithiobacillus thiooxidans* and their mixtures”, *Journal of Hazardous Materials*, Vol.**172**, pp.1100-1105.
- 272 Wang, X., (2006), “Numerical and experimental study of centrifugal fluidized bed separation”, *Ph.D thesis*, University of Nottingham, UK.
- 273 Wassgren, C.R., (1997), “Vibration of granular materials”, Ph.D Thesis, California Institute of Technology, USA, available online at http://thesis.library.caltech.edu/4504/1/Wassgren_cr_1997.pdf, retrieved on 11/07/2009 at 20:46GMT.
- 274 Wassgren, C.R., Brennen, C.E., and Hunt, M.L., (1996) “Vertical vibration of a deep beds of granular material in a container”, *Journal of applied Mechanics*, Vol.**63**, pp.712-719.
- 275 Waste Framework Directive, (2003), “Directive 2002/96/EC of the European Parliament and of the Council of 27 January 2003 on waste electrical and electronic equipment, *Official Journal of the European Union*, available online at <http://eur-lex.europa.eu/LexUriServ/LexUriServ.do?uri=OJ:L:2003:037:0024:0038:EN:PDF>, retrieved on 10/07/2009 at 19:46GMT.
-

-
- 276 Waste Framework Directive, (2006), "Directive 2006/12/EC of the European Parliament and of the Council of 5 April 2006 on waste", *Official Journal of the European Union*, Available online at http://eur-lex.europa.eu/LexUriServ/site/en/oj/2006/l_114/l_11420060427en00090021.pdf , retrieved on 09/07/2009 at 14:51GMT.
- 277 Waste Framework Directive, (2008), "Directive 2008/98/EC of the European Parliament and of the Council of 19 November 2008 on waste and replacing certain Directives", Available online at <http://eur-lex.europa.eu/LexUriServ/LexUriServ.do?uri=OJ:L:2008:312:0003:0030:EN:PDF> , retrieved on 09/07/2009 at 14:54GMT.
- 278 Water Act, (2003), available online at www.opsi.gov.uk/acts/acts2003/20030037.htm, retrieved on 09/04/10 at 12:48GMT.
- 279 Webster, H., (2009), *Private communications*, Division of Process and Environmental Engineering Research, University of Nottingham, UK.
- 280 Weitkämper, L., Wotruba, H., and Steinberg, M., (2009), "Development of a new dry density separator for fine-grained materials", *Minerals Engineering Physical Separation Conference 09*, June 16-17, Falmouth, Cornwall, UK. Details of conference available on <http://www.min-eng.com/physicalseparation09/paps.html>, retrieved on 17/03/2010 at 15:00GMT.
- 281 Wen, C-Y. and Hashinger, R.F., (1960), "Elutriation of solid particles from a dense phase fluidized bed", *AIChE Journal*, Vol.6, Issue 2, pp.220-226, available online at <http://www3.interscience.wiley.com/cgi-bin/fulltext/109072385/PDFSTART> retrieved on 19/04/2009, at 15:45GMT
- 282 Wen, C-Y., and Hashinger, R.F., (1960), "Elutriation of solid particles from a dense phase fluidized bed", *A.I.Ch.E. Journal*, Vol.6, No.2, pp.220-227.
- 283 Wiegardt, K., (1975), "Experiments in granular flow", *Annual review of fluid mechanics*, Vol.7, pp.89-114.
-

-
- Available online at <http://arjournals.annualreviews.org/doi/abs/10.1146/annurev.fl.07.010175.000513?prevSearch=granular+matter+and+vertical+vibration&searchHistoryKey=> and retrieved on 08/06/2009 at 16:40GMT.
- 284 Wienold, J., Recknagel, S., Scharf, H., Hoppe, M., and Michaelis, M., (2010), "Elemental analysis of printed circuit boards considering the ROHS regulations", *Waste Management*, Corrected proof, Article in Press, doi:10.1016/j.wasman.2010.10.002.
- 285 Wildman, R.D and Huntley, J.M., (2003), "Scaling exponents for energy transport and dissipation in binary vibro-fluidized granular beds", *Physics of Fluids*, American Institute of Physics, Vol.**15**, No.10, pp.3090-3098.
- 286 Wildman, R.D., and Parker, D.J., (2002), "Coexistence of two granular temperatures in binary vibrofluidized beds", *Physical Review Letters*, The American Physical Society, Vol.**88**, No.6, pp.064301/1-4.
- 287 Wildman, R.D., Huntley, J.M., Hansen, J.-P, Parker, D.J., and Allen, D.A., (2000), "Single-particle motion in three-dimensional vibrofluidized granular beds", *Physical Review E*, The American Physical Society, Vol.**62**, No.3, pp.3826-3835.
- 288 Wildman, R.D., Martin, T.W., Krouskop, P.E., Talbot, J., Huntley, J.M., and Parker, D.J., (2005), "Convection in vibrated annular granular beds", *Physical Review E*, The American Physical Society, Vol.**71**, pp.061301/1-9.
- 289 Williams, J.C. (1963), "Vertical vibration of a bed of granular material in a container", *Fuel Society Journal*, Vol.**14**, pp.29-34.
- 290 Williams, J.C. (1976), "The segregation of particulate materials, A review", *Powder Technology*, Vol.**15**, pp.245-251.
- 291 Wills, B.A., (1997), "Chapter-8 & 14, in Mineral Processing Technology: An introduction to the practical aspects of ore
-

-
- and mineral recovery”, 6th ed., Butterworth-Heinemann, Oxford, UK.
- 292 Wong, Y.S., Gan, C.H., and Wang, C.-H., (2001), “Study of granular dynamics in vertically vibrated beds using tracking technique”, Available online at http://dspace.mit.edu/bitstream/handle/1721.1/7495/MEBC_S024.pdf?sequence=1, retrieved on 16/08/2009 at 14:56GMT.
- 293 Wong, Y.S., Gan, C.H., Wang, C.H., Fan, X., Parker, D.J., Ingram, A., and Seville, J.P.K., (2006), “Instabilities in vertically vibrated granular beds at the single particle scale, *Physics of Fluids*, American Institute of Physics, Vol.**18**, pp.043302/1-15.
- 294 Wrap, (2009), “Definition of waste”, Material change for a better Environment, Available online at http://www.aggregain.org.uk/waste_management_regulations/background/definition_of.html, retrieved on 09/07/2009 at 15:14GMT.
- 295 Xie, F., Li, H., Ma, Y., Li, C., Cai, T., Huang, Z., and Yuan, G., (2009)., “The ultrasonically assisted metals recovery treatment of printed circuit board waste sludge by leaching separation”, *Journal of Hazardous Materials*, Vol.**170**, pp.430-435.
- 296 Xing, W. and Hendriks, C., (2006), “Decontamination of granular wastes by mining separation techniques”, *Journal of Cleaner Production*, Vol.**14**, pp.748-753.
- 297 Xu, C and Zhu, J., (2006), “Parametric study of fine particle fluidization under mechanical vibration”, *Powder Technology*, Vol.**161**, pp.135-144.
- 298 Yan, X., Shi, Q., Hou, M., Lu, K., and Chan, C.K., (2003), “Effects of air on the segregation of particles in a shaken granular bed”, *Physical Review Letters*, The American Physical Society, Vol.**91**, No.1, pp.014302/1-4.
- 299 Yang, J., Xiang, D., Wang, J., Duan, G., Zhang, H-C., (2009), “Removal force models for component disassembly
-

-
- from waste printed circuit board", *Resources. Conservation and Recycling*, Vol.**53**, pp.448-454.
- 300 Yang, S.C., (2006), "Density effect on mixing and segregation processes in a vibrated binary granular mixture", *Powder Technology*, Vol.**164**, pp.65-74.
- 301 Yang, S-C., (1999), "Dynamic behaviour of cohesive granular materials in a vibrated bed", *Ph.D. Thesis*, National Central University, Taiwan, Available online at http://thesis.lib.ncu.edu.tw/ETD-db/ETD-search/view_etd?URN=85343006, retrieved on 10/06/2009 at 16:17GMT.
- 302 Yoo, J.M., Jeong, J., Yoo, K., Lee, J.C and Kim, W., (2009), "Enrichment of the metallic components from waste printed circuit boards by a mechanical separation process using a stamp mill", *Waste Management*, Vol.**29**, pp.1132-1137.
- 303 Young, A.C., (2009), "Selecting and sizing process screening equipment", Rotex news article, available online at http://www.rotex.com/05newsevents/article_selectingscreens.aspx, retrieved on 15/04/2009 at 21:30GMT.
- 304 Yu, A.B., (2003), "Discreet particle simulation of granular flow", *Third International Conference on CFD in the Minerals and Process Industries*, CSIRO, Melbourne, Australia, 10-12 December, 2003.
- 305 Zeilstra, C., Collignon, J.G., Hoef, M.A.V.D., Deen, N.G., and Kuipers, J.A.M., (2008), "Experimental and numerical study of wall-induced granular convection", *Powder Technology*, Vol.**184**, pp.166-176.
- 306 Zeilstra, C., Hoef, M.A.V.D., & Kuipers, J.A.M., (2006), "Simulation study of air-induced segregation of equal-size bronze and glass particles", *Physical review E*, The American Physics Society, Vol.**74**, pp.010302-1 to 4.
- 307 Zhang, N., and Rosato, A.D., (2004), "Analysis of instantaneous dynamic states of vibrated granular materials", *Mechanics Research Communications*, Vol.**31**, pp.525-544.
-

-
- 308 Zhang, S., and Forsberg, E., (1999), "Intelligent liberation and classification of electronic scrap", *Powder Technology*, Vol.**105**, No.1-3, pp.295-301.
- 309 Zheng, Y., Shen, Z., Ma, S., Cai, S., Zhao, X., and Xing, Y., (2009), "A novel approach to recycling of glass fibres from non-metal materials of waste printed circuit boards", *Journal of Hazardous Materials*, Vol.**170**, pp.978-982.
- 310 Zhou, Y., and Qiu, K., (2010), "A new technology for recycling materials from waste printed circuit boards", *Journal of Hazardous Materials*, Vol.**175**, pp.823-828.
- 311 Zhou, Y., Wu, W., and Qiu, K., (2010) "Recovery of materials from waste printed circuit boards by vacuum pyrolysis and vacuum centrifugal separation", *Waste Management*, Vol.**30**, pp.2299-2304.
- 312 Zhu, H.P., Zhou, Z.Y., Yang, R.Y., and Yu, A.B., (2008), "Discreet particle simulation of particulate systems: A review of major applications and findings", *Chemical ngineering Science*, Vol.**63**, pp.5728-5770.
- 313 Zivkovic, V., Biggs, M.J., Glass, D.H., Pagliai, P., and Buts, A., (2008), "Particle dynamics in a dense vibrated fluidized bed as revealed by diffusing wave spectroscopy", *Powder Technology*, Vol.**182**, pp.192-201.